UNIVERSIDADE FEDERAL DE SÃO CARLOS
CENTRO DE CIÊNCIAS EXATAS E DE TECNOLOGIA
DEPARTAMENTO DE QUÍMICA
PROGRAMA DE PÓS-GRADUAÇÃO EM QUÍMICA

"Multicomponent Reactions in the Discovery of Organocatalysts and the Diversification of Organocatalytic Approaches"

Alexander Fernández de la Torre

Tese apresentada como parte dos requisitos para obtenção do título de DOUTOR EM CIÊNCIAS, área de concentração: QUÍMICA ORGÂNICA

Orientador: Prof. Dr. Márcio Weber Paixão
Co-orientador: Prof. Dr. Daniel Gracía Rivera

*bolsista CNPq

São Carlos - SP
2015

Folha de Aprovação

Assinaturas dos membros da comissão examinadora que avaliou e aprovou a Defesa de Tese de Doutorado do candidato Alexander Fernández de La Torre, realizada em 19/06/2015:

Prof. Dr. Márcio Weber Paixão
UFSCar

Prof. Dr. Carlos Kleber Zago de Andrade
UnB

Prof. Dr. Antonio Luiz Braga
UFSC

Prof. Dr. Igor Dias Jurberg
UNICAMP

Prof. Dr. Marco Antonio Barbosa Ferreira
UFSCar

``O propósito de nossa vida é acrescentar valor à vida das pessoas desta geração e das gerações seguintes.´´

Buckminster Fuller

Dedicated to my Family!

Acknowledgements

Firstly, I´m proud to express the majority of acknowledgements to my family! In special to my mom: Pilar Maritza de la Torre Armenteros, my son: Alexander Fernández Concepción and my wife: Odette Concepción González.

I´m indebted to Prof. Dr. Marcio Weber Paixão, my PhD supervisor, who spent his time teaching me. His passion and skill for chemistry is, without doubt, the best I have ever seen. Besides providing an exciting educational work environment, he has showed true concern and extraordinary lab experience for which I will always be very grateful. I also owe a debt of gratitude to Prof. Daniel Garcia Rivera, who believe in me at the beginning. I have to mention that I am here due him because my first contact with Brazil was through Prof. Daniel four years ago. In addition, he has remained an awesome inspiration to chemistry, and I will always keep in mind that. Important! They are superb academic advisors, and I could not be more pleased with my decision to work for both. Thanks for this opportunity!

I would like to thank all the professors of Chemistry Department at Federal University of São Carlos (UFSCar) for the wonderful class and seminaries. Also, thank to my friends in and outside of the lab of LSPN among the years 2011-2015. I appreciate those with whom I have worked most closely, including, Odette (my wife), Sandrina Silva, Karla Santos Feu, Julia Monteiro, Rodrigo Cesar, Lucas Possi, Marcelo de Pavia (Montana), Akabar Ali (Ali-Baba), Senthil Naraperunemal, Deborah Araujo, Floyd etc... In addition, I would like to express my full aknowledgemnt to all my friends and professors in CUBA!

Thanks to Gabriel dos Santos Scatena (Guerra), who is my Brazilian brother, for his patient and ability to live with me in the lab and out.

Also to the agencies CAPES, CNPq and FAPESP for the financial support of the project.

Abreviatures

AC	Asymmetric catalysis
AIBN	Azobisisobutyronitrile
Aib	Aminoisobutyric acid
BA	Brønsted acid
COSY	Correlation spectroscopy
dr.	Diastereoisomeric ratio
DMF	Dimethylformamide
DMSO	Dimethylsulfoxide
ee	Enantiomeric excess
er.	Enantiomeric relation
Gly	Glycine
HB	Hydrogen bonding
HSQC	Heteronuclear single-quantum correlation
HMBC	Heteronuclear multiple bond correlation
I-MCR	Isocyanide multicomponent reaction
Ile	Isoleucine
Leu	Leucine
LB	Lewis base
Met	Methionine
MCR	Multicomponent reaction
MM	Molecular mechanics
NOE	Nuclear overhauser effect
NMR	Nuclear magnetic resonance
P-3CR	Passerini three component reaction
Pro	Proline
RCM	Ring closing metathesis
ROESY	Rotating frame nuclear overhauser effect spectroscopy
SI	Steric interactions
TS	Transition states
TBTU	2-(1H-Benzotriazole-1-yl)-1,1,3,3-tetramethyluronium tetrafluoroborate
TGA	Termogravimetric analysis
Trp	Tryptophan
Ugi-4CR	Ugi four component reaction
Ugi-5C-3CR	Ugi five center three component reaction
Ugi-5C-4CR	Ugi five center four component reaction
Val	Valine

List of Tables

List of Figures

List of Schemes

List of Charts

Resumo

"Multicomponent Reactions in the Discovery of Organocatalysts and the Diversification of Organocatalytic Approaches"

Esta tese reporta o desenvolvimento de reações multicomponentes tendo como objetivos específicos: a) a descoberta de um novo e eficiente catalisador para transformações assimétricas e b) a síntese de compostos cíclicos analogos de produtos naturais a partir de uma reação *tandem* organocatalítica seguida de uma reação multicomponente.

No Capítulo 1 foi implementada uma abordagem MCR com base na reação de Ugi-4C para o desenvolvimento de novos organocatalisadores pseudo-peptídeos derivados de Prolina. Uma série de *pseudo*-peptídeos com a sequência genérica Pro-N-R^1-Xaa-NHR^3, sendo Xaa = Gly (R^2 = H) ou Aib (R^2 = gem-Me), R^1 e R^3 cadeias alquílicas ou aminoácidos foram obtidos com rendimentos na faixa de 61-93%. As características conformacionais dos catalisadores também foram estudadas, dentre os quais, selecionados os catalisadores **67** e **69** para modelagem molecular e estudos de RMN. A maioria dos catalisadores mostraram grande eficácia na reação de adição conjugada assimétrica, obtendo adutos de Michael com boa a excelente enantio- e diastereosseletividade. No entanto, quando os catalisadores foram empregados em reações de aldol, apenas moderados resultados foram obtidos. Além disso, uma nova estratégia via reação multi-componente seguida de polimerização foi desenvolvida para síntese dos novos catalisadores. Nesta estratégia foi utilizado álcool furfurílico como monômero derivado de matéria-prima renovável. Os catalisadores **89** e **90** foram examinados como organocatalisadores heterogêneos na adição conjugada de aldeídos a nitroolefinas, obtendo os adutos de Michael em 84% e 29% de ee, respectivamente. Além disso, este sistema catalítico foi avaliado sobre condições de fluxo contínuo utilizando uma *syringe pump* e uma coluna de HPLC previamente carregada com catalisador **89** em uma velocidade de fluxo de 2,5 µL min^{-1}, obtendo-se o produto desejado em 42% de rendimento, com uma produtividade de 0,28 durante 22 horas de reação, com boa diastereosseletividade (*dr.* 95: 5 (*syn: anti*)) e moderada enantiosseletividade, 72% ee.

O Capítulo 2 descreve novas sequências reacionais baseadas em reações organocatalíticas seguidas de reações multicomponentes. Vários procedimentos de adição conjugada organocatalisados foram desenvolvidos para o preparo de hemiacetais quirais, os quais foram utilizados em varias reações multicomponentes tipo Ugi. Estas sequências incluem: a) a adição de Michael de nitroetanol com aldeídos α,β-insaturados, seguido por uma reação de Ugi levando a um *depsi*-peptídeo mimético cíclico; b) a adição de Michael de compostos 1,3-dicarbonílicos com aldeídos α,β-insaturados seguida por uma nova reação estereoselectiva de Ugi-Smiles levando a hexa quinolina-6-onas; e c) a adição de Michael, de aldeídos a nitroolefinas fenólicas, seguida de um novo tipo de reação multicomponente levando à formação de novos ciclopentenos penta-sustituídos. O sucesso destas sequências provaram o potencial de combinar reações organocatalíticas e reações multicomponentes para obtenção de novos (hetero)cíclicos derivados de produtos naturais.

Abstract

"Multicomponent Reactions in the Discovery of Organocatalysts and the Diversification of Organocatalytic Approaches"

This thesis reports the development of multicomponent approaches directed to specific objectives: a) the discovery of new and efficient peptide-based catalyst for asymmetric transformations and b) the synthesis of (hetero)cyclic natural products-like compounds derived from organocatylic/multicomponent reaction sequences.

Chapter 1 describes the utilization of the Ugi-4CR reaction for the development of new prolyl *pseudo*-peptides capable to act as aminocatalysts in asymmetric conjugate addition reactions. Thus, a series of *pseudo*-peptides having the generic sequences Pro-N-R^1-AA-NHR^3, being AA an amino acid and R^1 and R^3 either alkyl or amino acids, were obtained in moderate to excellent yields. The prolyl *pseudo*-peptides were screened for their catalytic efficacy, most of them proving great efficiency and good to excellent enantio- and diastereoselectivity in the asymmetric conjugate addition of aldehydes to nitroolefins. However, only moderate results were obtained in the asymmetric organocatalytic aldol reaction. A molecular modeling and NMR study were performed for catalysts **67** and **69**, aiming to understand their different organocatalytic behavior based on the conformational features. A similar multicomponent process followed by a polymerization step was developed to obtain two new polyfurfuryl alcohol polymers bearing the prolyl *pseudo*-peptide motif anchored to polymer chain. The prolyl peptide-containing polymers were utilized in the heterogeneous organocatalytic conjugate addition of aldehydes to nitroolefins under bath and flow conditions, producing Michael adducts in moderate yield and enantioselectivity but in excellent diastereoselectivity.

Chapter 2 describes the development of new reaction sequences based on consecutive organocatalytic and multicomponent reactions. Several aminocatalytic conjugate addition procedures were implemented to prepare chiral hemiacetals, which were next used in varied Ugi-type multicomponent reactions. These sequences include: a) the Michael addition of nitroethanol to α,β-unsaturated aldehydes followed by an Ugi reaction leading to cyclic depsipeptide mimics; b) the Michael addition of 1,3-cycloalkanediones to α,β-unsaturated aldehydes followed by a new stereoselective Ugi-Smiles-type reaction leading to hexahydroquinolin-6-ones; and c) the Michael addition of aldehydes to phenolic nitroolefins

followed a new type of multicomponent reaction, leading to pentasubstituted cyclopentenes. The success of these sequences proved the potential of combining organocatalytic asymmetric transformations with follow-up multicomponent reactions for accessing natural product-like cyclic compounds.

Summary

Chapter 1

1 Introduction: Chapter 1

``We live in a world of duality: up and down, light and dark, hot and cold, in and out, fast and slow, right and left. These are but a few examples of the thousands of opposite poles. For one pole to exist, the other pole must also exist.´´ [1] Is it possible to have a right side without a left side? Can Chemistry do it?

In chemistry, many molecules are chiral, meaning they exist in two forms that are mirror images of each other-like left and right hands. [2]

In chemical synthesis, much effort has been directed towards the development of asymmetric transformations that yield the products with a significant excess of either the left-handed or the right-handed enantiomer. This could be achieved by the use of chiral auxiliaries or catalysts that influence the course of reactions, with the enantiomeric excess (ee) of the product related to the ee of the auxiliary or catalyst used.

The enantioselective construction of stereogenic C-C bonds is a fundamental goal of Organic Synthesis. As we know, there are strict regulations for the employment of enantiopure compounds in Pharmaceuticals, Agrochemicals and in other sectors of fine chemical industry. Then, new improvements over the known methodologies to obtain enantiopure compounds are done continuously. The methods to generate enantiomerically pure compounds from achiral starting materials are: chiral auxiliary, chiral pool and asymmetric catalysis (AC) (FIGURE 1.1). Of the above mentioned methods, ``Asymmetric Catalysis´´ is the most desirable. The AC employs a chiral catalyst for the formation of a new chiral compound. During this process, the catalyst is not consumed and may be used in little amounts (economically friendly); often they are reused, improving efficiency and avoiding waste. The preferences for AC are in agreement with both low cost and environmental concerns.

At first, two distinct AC methods have been used (FIGURE 1.1); 1) Biocatalysis: where enzymes, which possess high molecular weight, are employed, and 2) Metal catalysis: using transition metals and organic chiral ligands to induce asymmetry. Nowadays, a new class of catalysis using small organic molecules without presence of metal trace is recognized to be a great potential in AC. This new class is known as `Organocatalysis´.
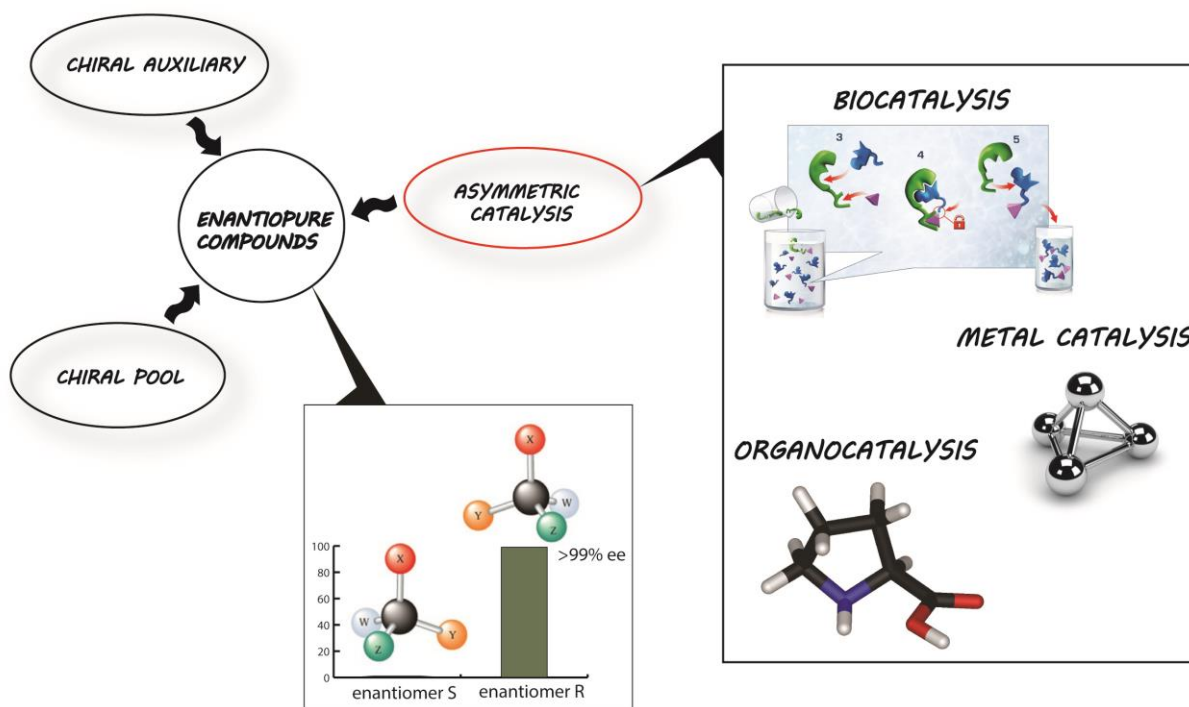
FIGURE 1.1- Methods to obtain enantiopure compounds.

The first example using small organic molecules as catalysts was reported in the early 70s by the group of Hajos-Parrish and the Wiechert group [3,4,5]. In this case, the enantioselective version of Robinson annulation in the construction of steroids skeletons were done in presence of Proline (Pro) as organocatalyst. Both groups employed *S*-Pro to produce, through an enamine intermediate, an intramolecular aldol cyclization of Wieland–Miescher ketones **1** and **2** (SCHEME 1.1). Even using the same catalyst, the efficiency and stereoselectivity of both studies show to be dependent on the solvent, for Hajos-Parrish study in DMF the yield was 100% and 93% ee. For Wiechert study in CH_3CN the yield obtained was 87% and a small decrease of ee was observed (84%) (see **3**, **4**, **5** and **6**, SCHEME 1.1). This comparison let the author to conclude that a possible hydrogen bonding (HB) of the carboxylic acid is what induce the enantioselectivity of the final product.
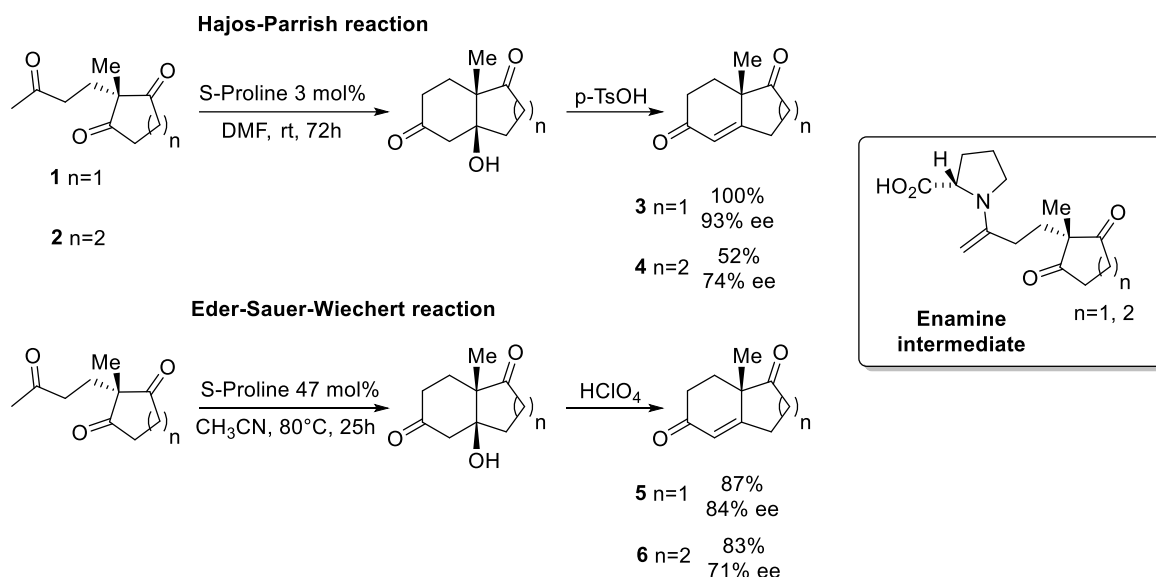
SCHEME 1.1 - Asymmteric Hajos-Parrish-Eder-Sauer-Wiechert version of Robinson annulation.

Actually, these relevant results using Pro as catalyst were interesting but the field was under the shadow of Lewis acid catalysis. As few examples of specific catalysts mitigating single transformations appeared in the 1970s, the value of organocatalytic chemistry was largely unrealized until 2000, when MacMillan mentioned for the first time the term ``Organocatalysis´´. [6] By the same time, Barbas, Lerner and List,[7,8] highlighted the use of Pro and its derivatives as useful tools in AC in terms of economic, environmental and other benefits for the scientific community, by the fact that these classes of compounds are generally easily handled to construct C-C bonds in an efficient and stereoselective way. In Chart 1.1, we can observe clearly an exponential increase with the time of the references published with the concept ``organocat´´ as found in Scifinder.
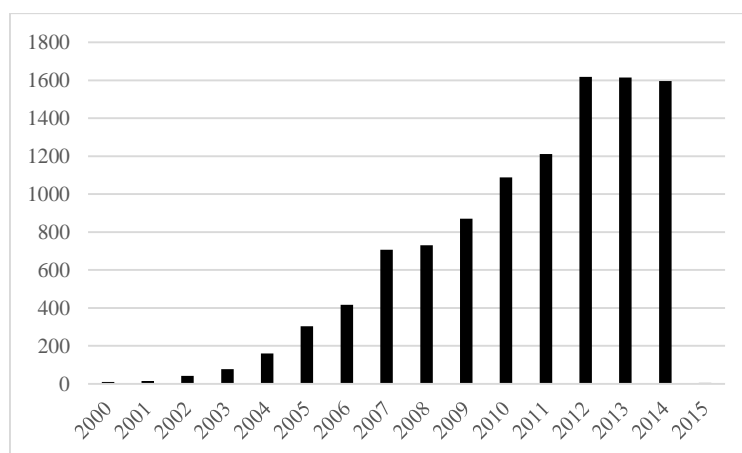
CHART 1.1- Exponential increase of publications containing the concept ``organocat´´ between 2000 and 2015.

4

The inspiration for the development of the organocatalysis field began with the ability to activate aldehydes or ketones and catalyze aldol reactions via an enamine type mechanism as much as larger aldolase type I can do.

As known, the term aldolase is related to a type of enzyme that forms and/or cleaves carbon-carbon bonds. There are many different types of aldolases with different substrates and products. In order to avoid confusion we are referring here to two different types of aldolases that form C-C bonds. Type I: where enzymes are only found in plants and animals; and type II: enzymes are usually found in bacteria, protists, and fungi. The action of these two types of aldolases are completely unrelated. In the case of aldolase type I; it is found that it plays a pivotal role in ``Gluconeogenesis´´, pathway of glucose biosynthesis. In SCHEME 1.2 is represented how aldolase type I catalyze the formation of a new C-C bond, via enamine activation. The substrates are glyceraldehyde 3-phosphate and dihydroxyacetone phosphate and the product is fructose 1,6-*bis*phosphate.
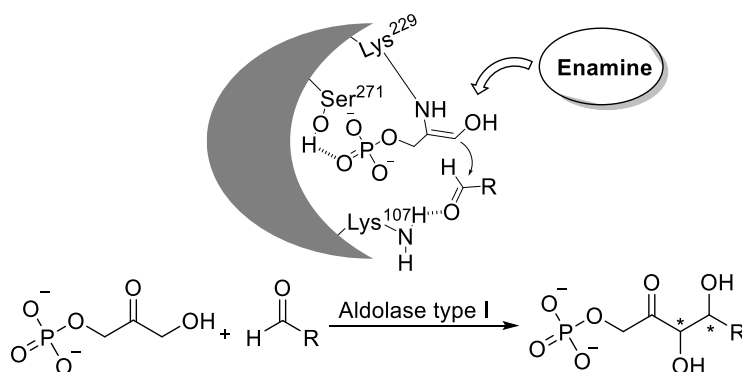
SCHEME 1.2 - Representation of aldolase type I acting as enamine in Aldol reaction.

Proline also works via an enamine intermediate with a considerable acceleration rate of a given transformation. This is possible due to the synergistic action between Brønsted acid (BA) and Lewis base (LB) sites in the structure of Pro. This special characteristic allows Pro to function as a bifunctional catalyst: as a nucleophile catalyst and as a chiral proton source. The secondary amine of Pro (pyrrolidine core) having a pKa of 10.47 (α-amino), undergoes nucleophilic additions to the carbonyl groups (aldehydes or ketones) to form enamine intermediates (also iminium ions can be formed), with a consequent increment of the density of the highest occupied molecular orbital (HOMO) of the enamine. The acid residue of Pro with pKa = 1.95 (α-carboxylic acid) directs the electrophilic species over one fase of the enamine, lowering the unoccupied molecular orbital (LUMO) of the electrophile. The orientation of the new stereogenic center generated will depend on the relative configuration of Pro (*S* or *R*).

This natural amino acid is cheap, abundant, and accessible in both enantiomeric forms. However, there are certain disadvantages and/or limitations associated with the use of Pro as catalyst. In particular, Pro is poorly soluble in many ordinary organic solvents. In some transformations, it provides moderate stereoselectivities and when aldehyde is used as substrate, self-condensation or polymerization may occur. These limitations have motivated scientists to search for modified catalysts to develop and improve new catalysts based on the sense of rational design. The development of numerous efficient new organocatalysts was based on those limitations of Pro. The vast majority of organocatalytic motifs discovered so far are based on rational design, an approach that requires a fine understanding of the nature, strength, and dimensionality of the interactions –e.g., covalent, hydrogen-bonding, electrostatic, etc…taking part in the catalyst-substrates association process.[9] Then, many organocatalysts based on pyrrolidine core have been synthesized (FIGURE 1.2). [10,11,12,13,14,15,16,17,18,19,20,21]

The disadvantage on the synthesis of these catalysts remains on the multip-step linear synthesis and the drastic reaction conditions required. Those conditions provides low atom economy and global yield, with tedious purifications. Significant challenges remains in this area, including optimization, simplicity, and green synthetic routes to obtain new efficient organocatalysts.
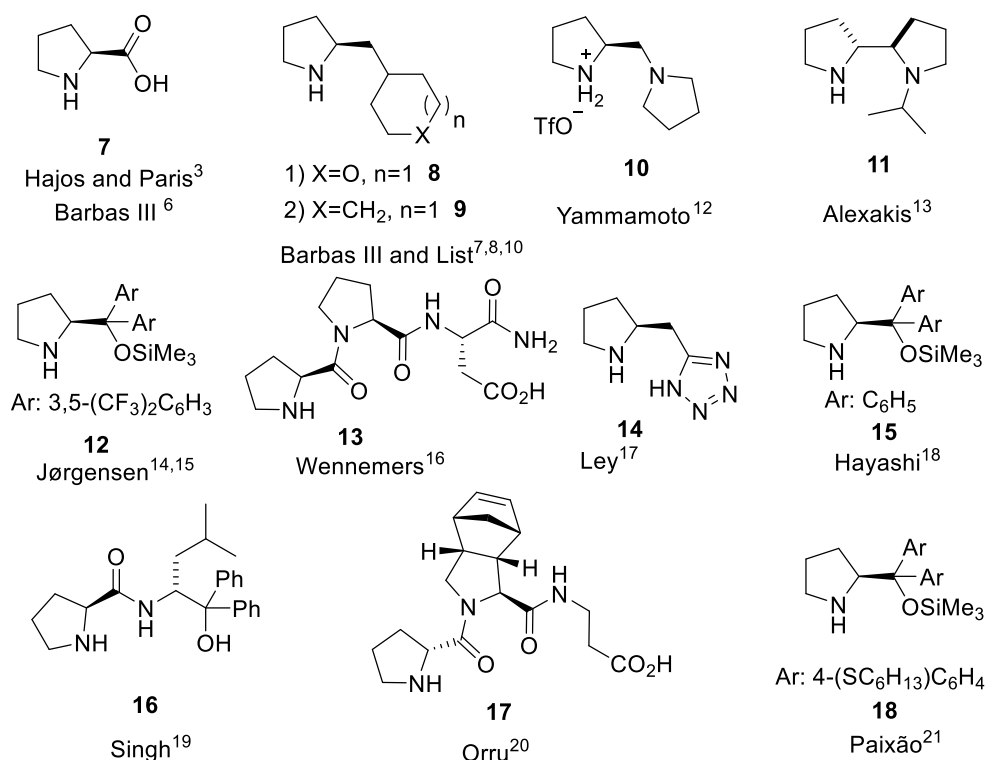
FIGURE 1.2 - Some known synthesized pyrrolidine-type organocatalysts.

6

1.1 Enamine catalysis

The application of secondary amines (i.e., pyrrolidine-type catalyst) to catalyze the direct asymmetric Aldol, Michael and Mannich reactions has been extensively exploited in the last decade. In general, this type of catalysts can activate aldehydes and ketones in a covalent way via enamines formation, which react with a determined electrophile **E** to form C-C, C-S, C-N, C-X (X=F, Cl, Br) bonds with good efficiency and stereoselectivity (SCHEME 1.3). [11, 22,23,24,25,26]
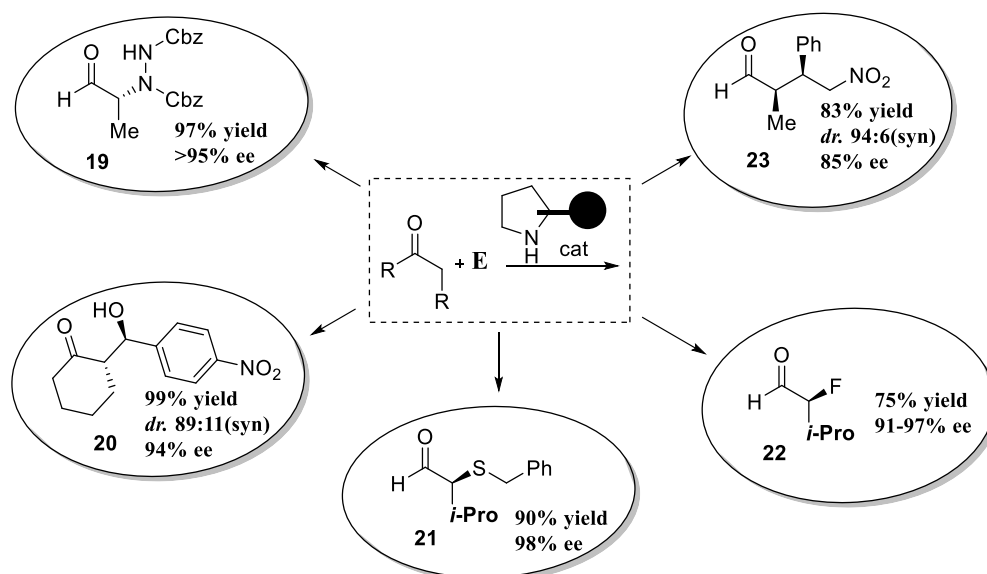
SCHEME 1.3 - Some α-functionalization of aldehydes or ketones promoted by pyrrolidine-type catalysts via enamine.

A rational design is usually an enormous challenge and depends directly on the chosen asymmetric reaction to do. Rarely, the discovery of potential catalysts is successful. The process often involves a separate synthesis of many catalysts and testing their catalytic properties in individual reaction, like test-error. The development of an effective organocatalyst usually needs further optimization process in which both the substituents and position of the catalytic functions are varied and examined towards the reaction of interest.

However, how the pyrrolidine-type catalysts induce stereoselectivity?

Let´s explain the enamine activation mechanism, the insights of the stereochemistry induction for the substituents and catalytic function.

It is important to understand the basic principles of enantioselectivity induction in order to design a new catalyst.

1.1.1 Mechanistic aspects

The enamine formation is produced between pyrrolidine ring and the correspondent aldehyde or ketone as shown in the catalytic cycle (SCHEME 1.4), where the enamine formed has two possible configurational isomers (E and Z), in a thermodynamic equilibrium. Unless other general and specific interactions favors the enamine Z, the enamine E is energetically most favored and always the formation of this conformation is predominantly. Two rotational isomers (*s-trans* and *s-cis*) exist in the enamine E, where by steric interactions the most favorable is the *s-trans*-enamine E (SCHEME 1.4). It is generally accepted that the *s-trans*-enamine is the most stable conformer, where the double bond is situated in the opposite direction to the bulky group located in the 2-position of the pyrrolidine ring.
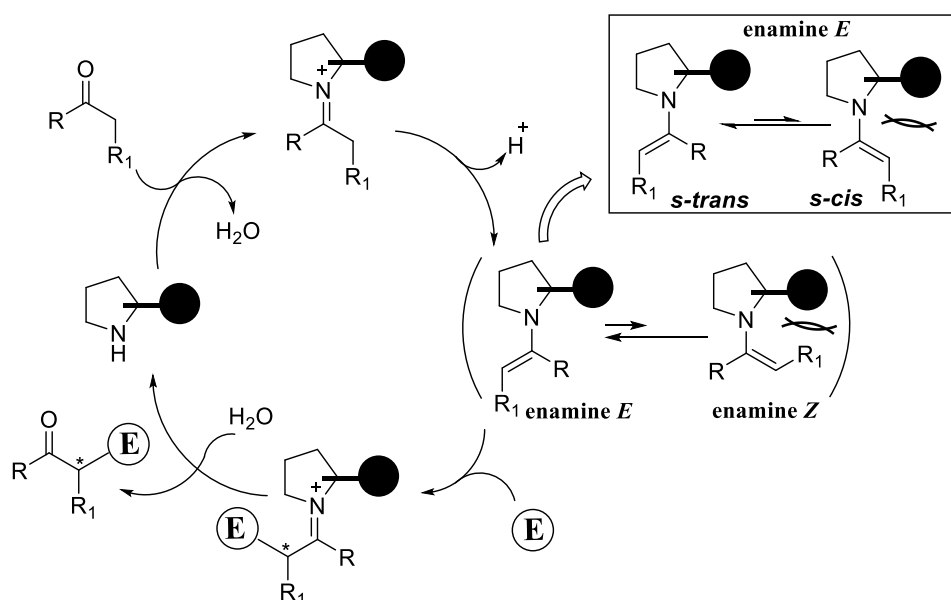
SCHEME 1.4 - Pyrrolidine-catalyzed activation cycle of enamine.

The *s-trans* conformer has also been considered as the most reactive intermediate until now (*vide infra*). So far, the role of the pyrrolidine ring is to activate the oxo component increasing the energy of the HOMO of the substrate when the enamine is formed but not in the trajectory of the electrophile in the formation of the new stereogenic C-C bond. The trajectory of the electrophile depends of the side group attached to the pyrrolidine ring.

The trajectory of the incoming electrophile has traditionally been proposed to follow either of the two different models (A and B, FIGURE 1.3) based on the nature of catalysts. Model A shows the induction of stereoselectivity by an HB interaction, and model B shows the approach of the electrophile ruled by steric interaction (SI).

8
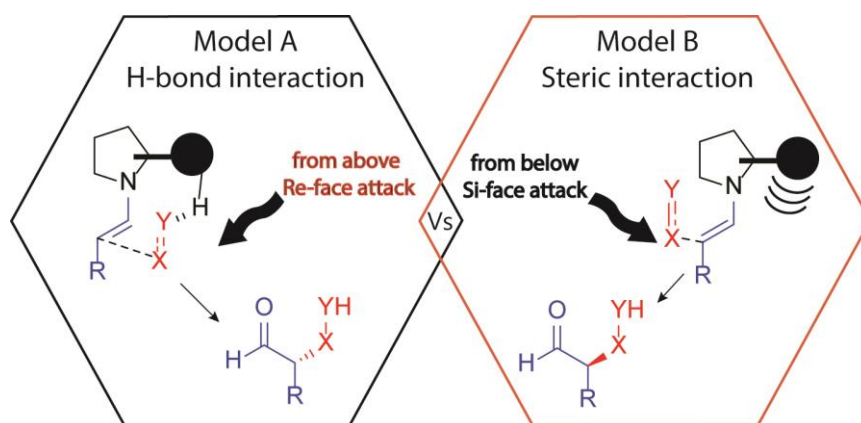
FIGURE 1.3 - Stereocontroller models A and B. Hydrogen Bonding vs. Steric Hindrance.

In general, catalysts with a HB directing group (i.e. -CO$_2$H, -OH, -CONH$_2$, etc…) at the position 2 of the pyrrolidine ring, follows model A (see **7**, **13**, **14**, **16**, FIGURE 1.4). In contrast, bulky substituents in the position 2 of pyrrolidine ring (i.e. -2Ph, -2PhCF$_3$, etc…) where the steric hindrance blocks one face of the enamine, are in agreement with model B of induction of stereoselectivity (see **12**, **15**, **18**, FIGURE 1.4). Some pyrrolidine-type catalysts are illustrated again in FIGURE 1.4 for better understanding; the red color in the structures refers to the respective HB or SI groups.
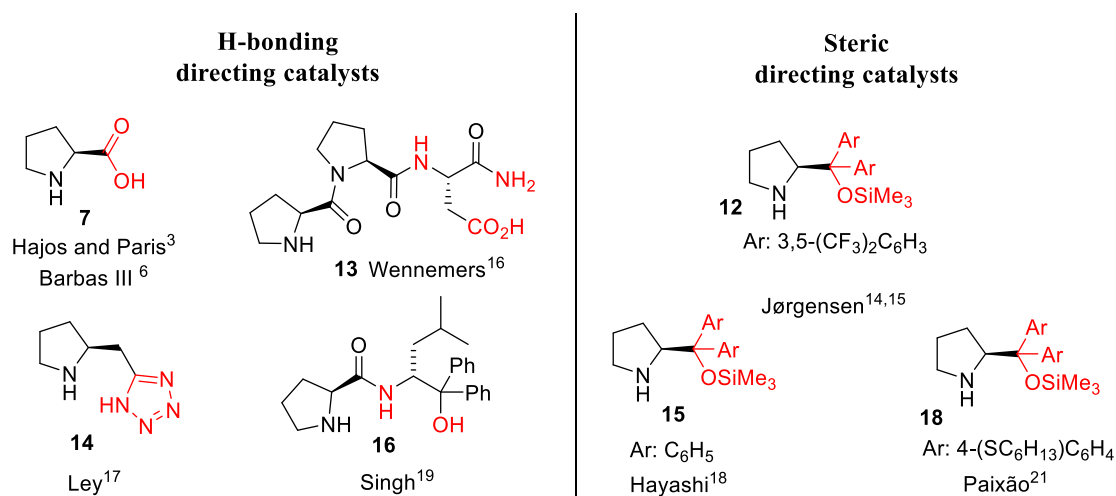
FIGURE 1.4 - Some pyrrolidine-type catalysts with Hydrogen Bonding or Steric directing groups.

Interestingly, models A and B produce opposite stereoisomers even if the catalysts have the same absolute stereochemistry. To better understand, let´s compare model A with B in conjugate additions, in specific the Michael reaction between *n*-propanal and *β*-nitrostyrene (SCHEME 1.5) with Pro and catalyst **15** with the same configuration in the position 2 of the pyrrolidine ring with a different directing group.

The Michael reaction is one of the most useful methods for the mild formation of C–C bonds that follows an enamine mechanism. It is, among other asymmetric reactions, used to test new catalysts based on enamine activation.
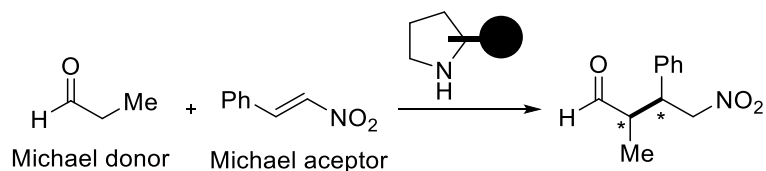
SCHEME 1.5 - Model organocatalized Michael reaction between *n*-propanal and *β*-nitrostyrene.

In SCHEME 1.6 it can be noted that the substituent attached to the pyrrolidine core is important in the direction of the induction in both enantio- and diastereoselectivity of the formed compounds. Four possible transition states (TS) can be drawn for both models (model A and model B, SCHEME 1.6). These TS show that even with the possibility to form the *s-cis-* enamine *E* (TS III, IV, VII and VIII), the equilibrium is displaced to the formation of the most stable *s-trans*-enamine E (TS I, II, V and VI) of both models, and therefore, the difference in terms of energy between these TS determines the course of stereoselectivity. Model A, also known as Houk-List model,[27,28] (SCHEME 1.6, TS I-IV) shows an HB between the proton of the carboxylic acid and the nitro group of *β*-nitrostyrene. This HB directs the *β*-nitrostyrene to the **Re** face of the enamine by a like approach, thus forming the *S,R*-diastereomer as the major product. However, model B is determined by SI, the bulky group attached to pyrrolidine core produces a steric hindrance capable of approaching the **Si** face of enamine to *β*-nitrostyrene and thus produce the inversed *R,S*-configuration of Michael product (see model B in SCHEME 1.6). In either case, model A or model B lead to the formation of the major diasteromer *syn*.

Two factors are important for good stereoselection: 1) one face of the enamine must be less accessible; 2) the equilibrium between the enamine rotamers must be well displaced to the one side.

According to SCHEME 1.6, model A and B having the pyrrolidine-type catalyst with the same configuration produce different stereoisomers. The **Re**-**Re** approach is favored for model A and **Si-Si** for Model B. This makes us to conclude that the stereoselection is totally influenced by the linked functional group in the backbone of catalyst.
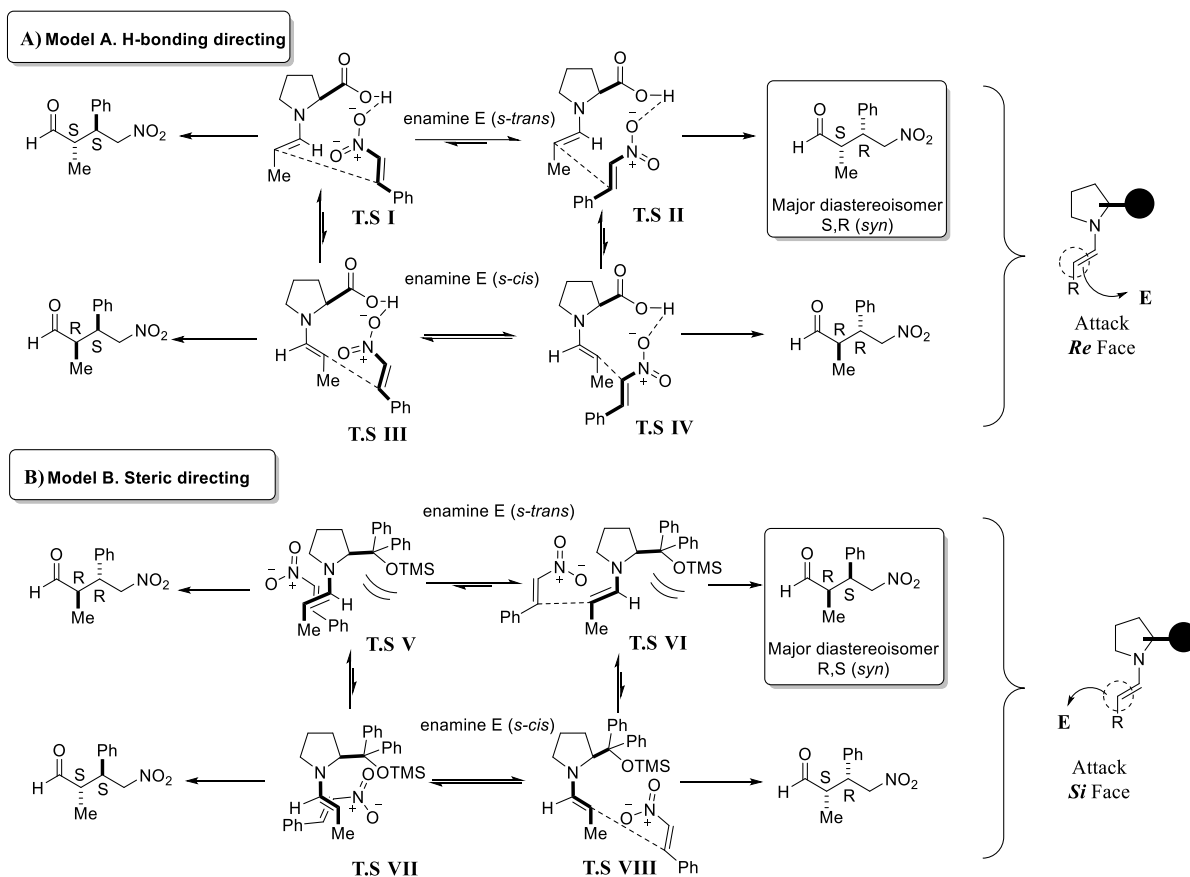
SCHEME 1.6 - Transition states by HB and SI control in Michael addition: A) HB with S-Proline as catalyst, B) SI with Hayashi´s catalyst.

Interestingly, the peptide-based catalyst develop by Wenemers (H-L-Pro-L-Pro-L-Asp-NH$_2$)[29] acts as HB and is an exception of Houk´s model. According to model A (SCHEME 1.6) this class of catalyst should give *S,R*-isomer of Michael adduct instead of *R,S*-isomer as shown in FIGURE 1.5. The author justified this exception by Molecular Mechanics (MM) studies. The optimized structure for the enamine *E* with peptide catalyst shows an specific conformation where the HB directs the electrophile to the *Si* face of enamine (FIGURE 1.5), producing the 1,4 addition and consequently the opposite configuration *R,S* as should be expected for model A.
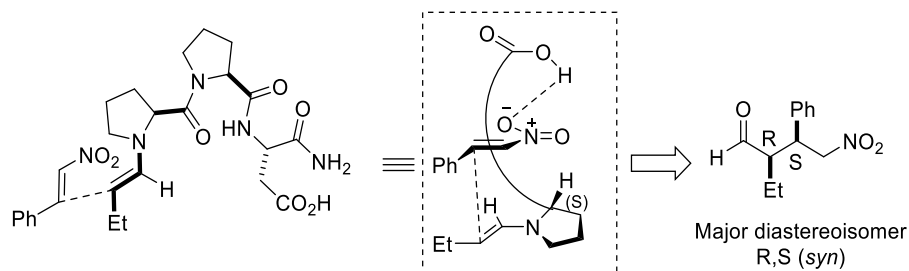
FIGURE 1.5 - Proposed transition state for Michael reaction with catalyst **13**. Inversion of the model A.

Not only the adopted model of the catalyst and/or backbone of catalysts, but also the intermediates structures formed in the catalytic system can affect the stereoselectivity of the final product. Thereafter, the tridimensional intermediates structure of catalysts and substrates (Transitions States), as well as parasitic intermediates should also be taken in consideration. Blackmond and co-workers[30] reported a kinetic study of the Michael reaction, where they found a parasitic intermediated which influences the stereoisomers of the final product. In this work, the conjugate addition of *n*-propanal to *β*-nitrostyrene, catalyzed by diarylprolinol silyl ether, reveals that the formation of the product (iminium species, SCHEME 1.7) is the rate-determining step of the reaction, and not the enamine formation as mentioned before. The formation of the cyclobutane intermediate (SCHEME 1.7), called as `parasitic intermediate´ during the catalytic cycle, is very important to keep the high stereoselectivity in the final product. Interestingly, this parasitic intermediate, which should delay the reaction, is considered to be important in the stereoselectivity.
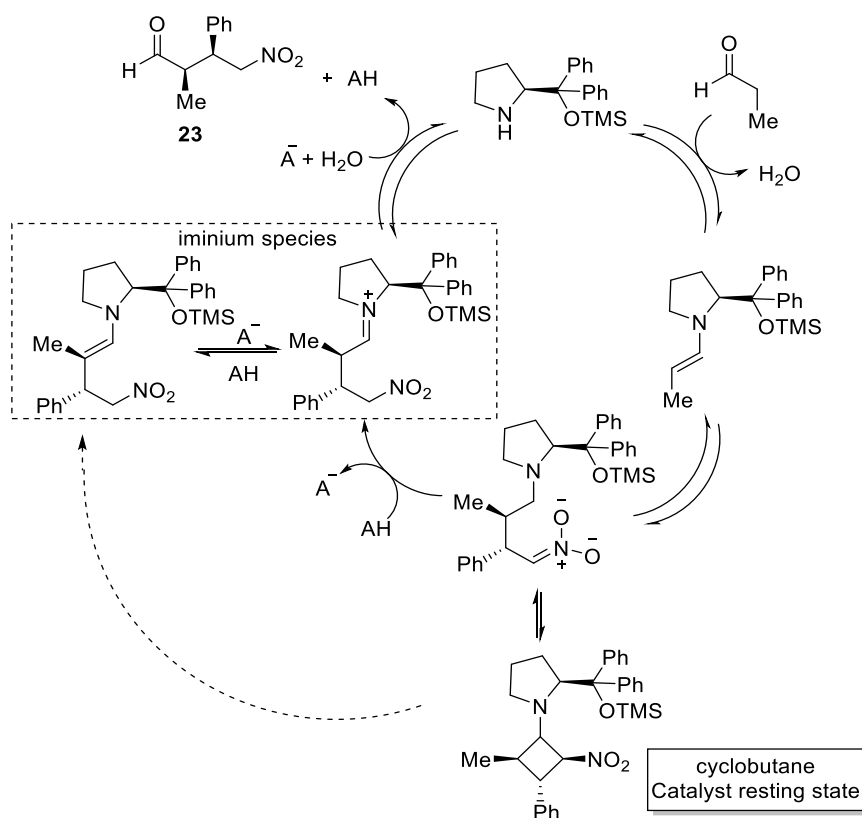
SCHEME 1.7 - Catalytic system for Michael reaction proposed by Blackmond.

Therefore, the intermediates, the backbone structure, and the conformation for determined pyrrolidine-type catalysts prove to be important in the selected asymmetric reaction. The side chain of the catalyst has effect in the asymmetric induction and is important to produce asymmetric catalysis. Besides, it is important to know that the system of reaction and the

backbone of catalyst may affect the stereoselectivity of the final product. This is the case of a new class of pyrrolidine-type catalyst developed by Barbas III in 2006. [25] They rationalized that these new catalysts (SCHEME 1.8) are capable to act as aldolase type I (enamine intermediate) without the presence of acidic pathway in the structure. The asymmetric Aldol reaction tested between cyclohexanone and *p*-nitrobenzaldehyde in water shows that compound **30** having long hydrophobic chains results to be good in efficiency and stereoselectivity (98%, *dr*. 89:11, 94% ee). This was possible due to the possibility of micelle formation in aqueous system. Therefore, the system of reaction plus the side chain attached to the pyrrolidine ring produces the best combination to induce high stereoselectivity in the reaction.
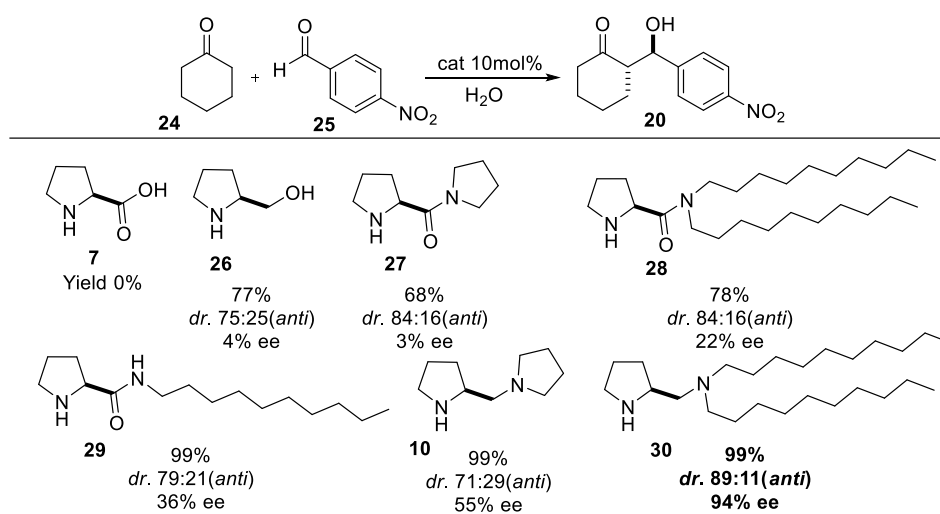
SCHEME 1.8 - Screening of various catalysts, developed by Barbas III, in the asymmetric Aldol reaction between cyclohexanone and *p*-nitrobenzaldehyde.

Independently of the model of induction (model A or B) the catalyst hold, the conformation and catalytic functions, the backbone, the reaction system, and the intermediates formed during the catalysis are important in the asymmetric induction.

These mechanistic principles help us to design new organocatalysts based in covalent enamine activation. Although a rational design is usually an enormous challenge, major is to develop new ecofriendly and economic route to access a library of catalysts to test.

1.2 Peptides catalysts. A rational design

The invention of peptide synthesis in the 50th stimulated the development of different application areas in which synthetic peptides are now used, including the development of specific antibodies against pathogenic proteins, the study of protein functions, study of enzyme-substrate interactions and catalysis. Every year it is being more evident that combinatorial

chemistry can face the synthesis and analysis not only of analogous entities (focused libraries) of previously identified leads but also of truly new catalytic systems based on novel dissimilar chemical functionalities.

Small peptides employed as organocatalysts have molecular weights often comparable to that of typical synthetic catalysts, and they provide the same and in some cases better results in asymmetric enamine reactions. [31]

How can we design a new peptide (or focused library) catalyst?

In the same way, the first step is: thinking of the target reaction (e.g., Aldol, Michael, Mannich reaction, etc…), the mechanism and the reaction conditions. Second: selecting the mode of activation (e.g., enamine, iminium…). This step is very dependent of the first step where the peptide in point should carry a secondary or primary amine depending on the asymmetric reaction selected. Third: improving the backbone in the structure of the peptide catalyst taking into account model A or B explained in SCHEME 1.6. Some structural motifs of peptides [32] are represented in FIGURE 1.6; α-helix and β-turn are the major motifs adopted by small-synthesized peptide catalysts. Forth: screening peptide catalysts, the catalytic efficiency, stereoselectivity and the scope of catalysts are followed in this step.
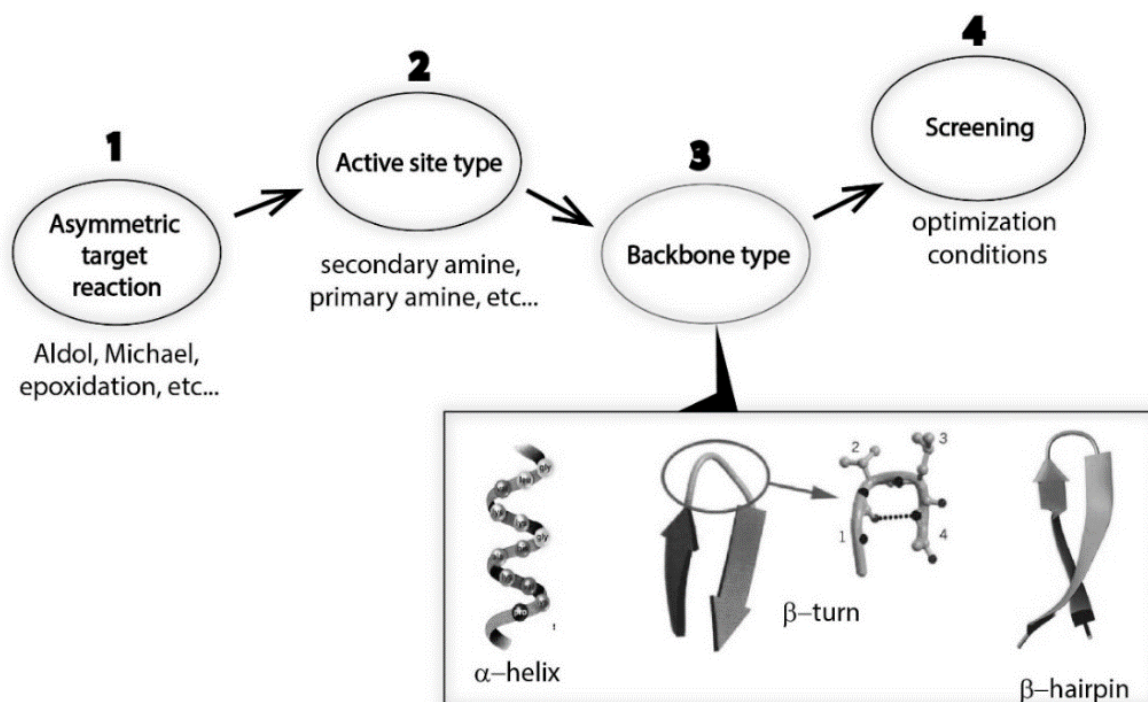
FIGURE 1.6 - Rational design of a new peptide catalyst.

In 2003, Reymond and co-workers [33] reported for the first time the rational design of peptide catalysts based on the active site of an enzyme. This study was divided in two different classes of peptides (Class I and II, SCHEME 1.9). Class I: based on a primary amine as catalytic

group, as seen in aldolases type I (Class IA and IB). Class IA contains a quaternary ammonium salt to lower the pKa of the amine to pKa=7, to mimic enzymes. Class II: based on secondary amines catalysts, comprises peptides with either acyclic (Class IIA) or cyclic secondary amine (pyrrolidine ring, Class IIB). Classes IA, IB, and IIA, peptides containing either a primary amino group (Class IB) or an acyclic secondary amine (Class IIA) (SCHEME 1.9), did not catalyze the Aldol reaction of acetone and compound **25**. However, peptides with pyrrolidine ring (Class IIB) gave high conversions (97%), confirming that pyrrolidine ring is important in the structure of peptide catalysts to act through enamine activation.
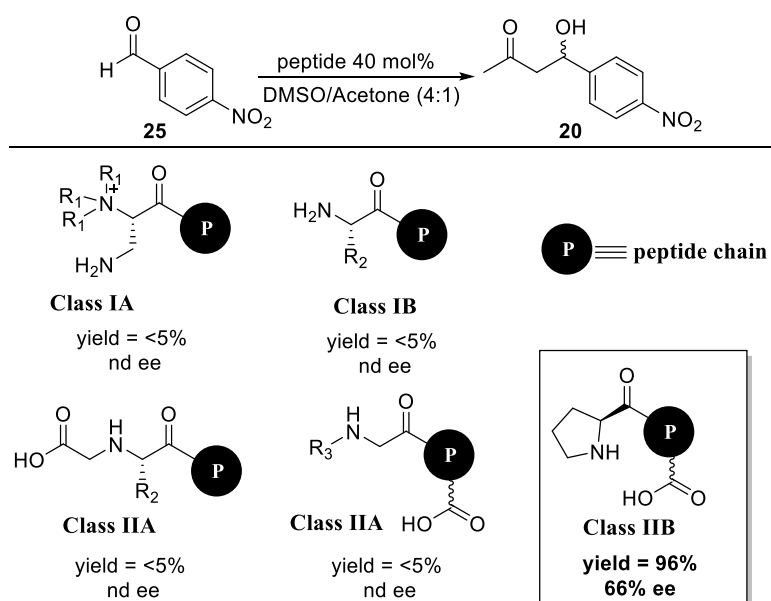
SCHEME 1.9 - Screening of the activity of various peptide catalysts in the asymmetric Aldol reaction.

As known, the enamine mode of activation is produced by the active site of peptide catalyst but the stereoselectivity is dependent on the conformational structure adopted by the catalyst.

In the next pages, some examples where secondary structures of peptides influence the stereoselectivity of the final product will be shown.

Secondary structure in peptides is the ordered arrangement or conformation of amino acids in localized regions of the molecule. The preferred peptide chain conformation under physiological conditions is dominated by the energetically favored torsion angles, together with additional stabilizing factors such as HB and hydrophobic contacts. A hydrogen bonding is formed between the NH group (hydrogen bond donor) and the carbonyl oxygen atom (hydrogen bond acceptor) of peptide bonds. The energy of a single HB is quite low (20 kJmol^{-1}), compared

to a covalent bond (200–400 kJmol^{-1}). However, in most secondary structure elements stabilized by HB it is multiple rather than single hydrogen bonds that are formed, and it is these multiple interactions of such a cooperative system that result in considerable stabilization. These interactions cause three different motifs: α-helix, β-sheet and coil. [32,34] Among these secondary structures, α-helix and β-turn motifs are the major structures employed as catalysts.

The α-helix comprises a spiral arrangement of the peptide backbone with 3.6 amino acid residues per turn (n = 3.6). It is stabilized by hydrogen bonds directed backwards from a C-terminal NH to an N-terminal CO (NH^{i+4} → CO^i) forming a 13-membered ring (FIGURE 1.7). Among the types of local structure in proteins, α-helix is the most regular and the most predictable from sequence, as well as the most prevalent.
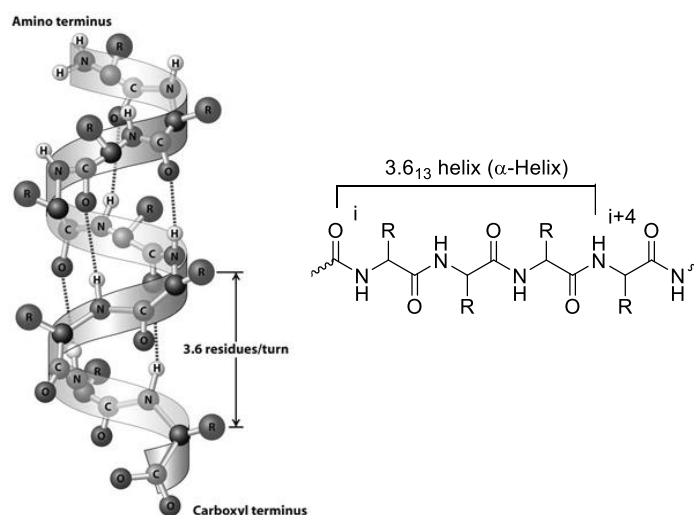
FIGURE 1.7 - Hydrogen bond pattern in α-helical peptides and schematic representation.

A turn (loop) is an element of secondary structure in polypeptide or protein where the chain reverses its overall direction. Often, but not necessarily, they are stabilized by an HB between a C-terminal amino group and an N-terminal carboxy group. Turns are classified according to the number of amino acid residues involved as γ-turns (three amino acids), β-turn (four amino acids), α-turn (five amino acids), or π-turn (six amino acids). β-turn are very common motifs. A general criterion for the existence of a β-turn is that the distance of the atoms C (i) and C (i + 3) is smaller than 7 Å. It is stabilized by hydrogen bonds directed backwards from a C-terminal NH to an N-terminal CO (NH^{i+3} → CO^i). Also, it could be stabilized by certain alkyl residues presented in position i+2 such as (α,α)-dialkylglycines such as aminoisobutyric acid (Aib) (FIGURE 1.8). [32]
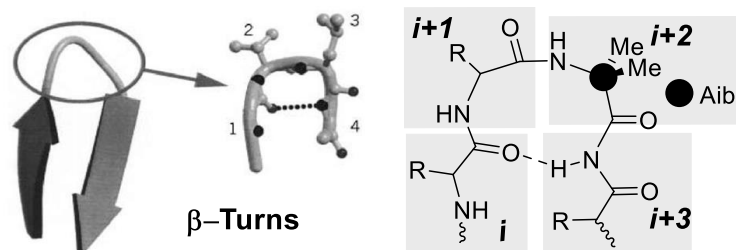
FIGURE 1.8 - Hydrogen bond representative of *β*-turns. Schematic representation.

Peptides catalysts having the sequence H-Pro-(Phe)n-OCH$_3$ (n= 1–5) proved to be efficient catalysts for the asymmetric direct Aldol reactions of hydroxyacetone **31** and aldehydes to obtain chiral 1,4-diols **33** in high ee (>96%). [35] Catalyst **32** does not have the free acidic group (SCHEME 1.10); however, this catalyst induces chirality as model A previously discussed. This occurs due to the amide NH group that produce HB. With the increment of lengths of the chain of peptide, it was also observed that there is an increase in the stereoselectivity. This effect was observed in Barba´s study [25] for the catalysts with hydrophobic chains. Possibly, the length of the peptide may produce several HB with the increase of the number of NH amide including the secondary structure adopted of peptide. No further study to prove this was done.
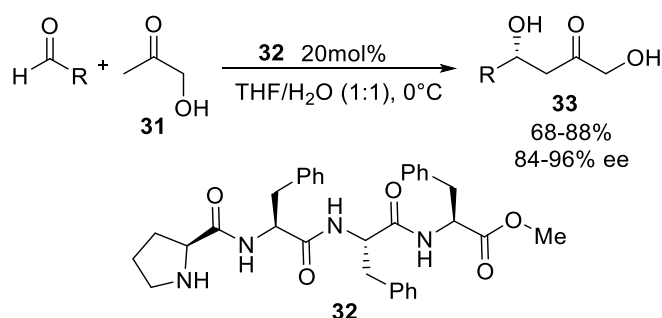
SCHEME 1.10 - Aldol reaction between hydroxyacetone **31** and different aldehydes catalyzed by peptide **32**.

In 1983, Juliá-Colona and co-workers[36] reported an enantioselective epoxidation of chalcones using *α*-helical peptides **35** as catalysts (SCHEME 1.11). Polypeptides with more than 10 amino acids produce epoxidation in high chemical yield and 96% ee. The results can be attributed to the *α*-helix adopted structure of these polypeptides, which increases the stereoselectivity in the epoxidation reaction.
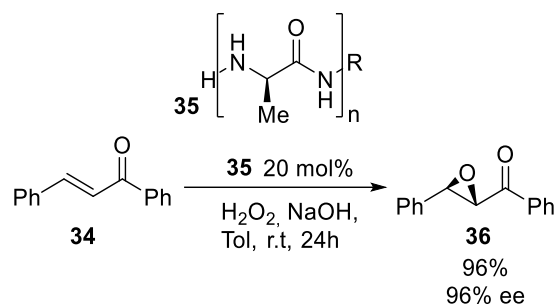
SCHEME 1.11 - Juliá-Colona epoxidation of chalcone **34**.

In the same way, Tanaka and co-workers [37] developed α-helical peptides as catalysts. The asymmetric epoxidation of chalcone was done with α-helical secondary structure of peptide containing chiral cyclic amino acid in the peptidic sequence (**37**) (see (A), SCHEME 1.12). An X-ray crystallographic analysis for a dodecamer (see (B), (SCHEME 1.12) with dimethylformamide (DMF) shows an α-helical structure, where DMF molecules connect to amide NH protons by HB. In this case, the chalcone might show HB with the amide NH protons of the helical peptide as well as DMF does, giving high stereoselectivity.
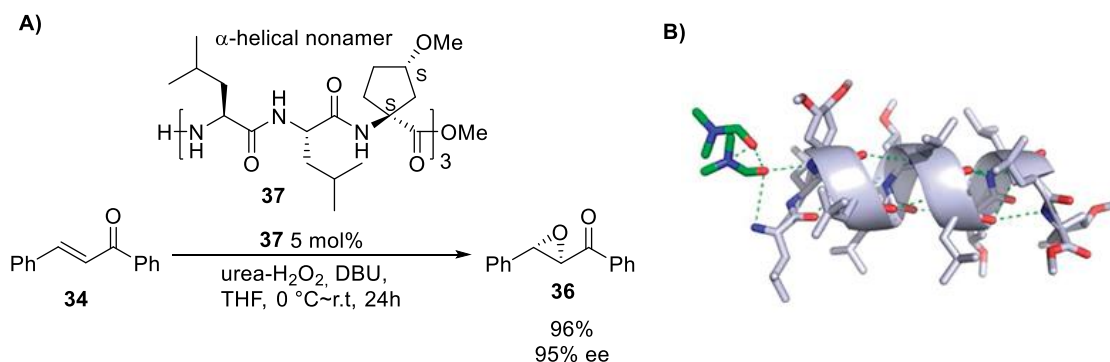
SCHEME 1.12 - A) Epoxidation of chalcone **34** with α-helical nonamer **37**. B) X-ray crystallographic analysis of the reaction.

In 2004, Miller [38] designed a range of peptide catalysts having β-turn conformation. Kinetic resolution of *trans*-1,2-acetamidocyclohexanol (**38**) was the target in this study (SCHEME 1.13). Catalyst **41** with Pro-Aib β-turn motifs in the dipeptide sequence showed a selectivity factor $k_{rel} = 17$. However, catalyst **42**, lacking the β-turn motifs afford only $k_{rel} = 1$. Furthermore, comparing peptides **43** and **44**; compound **43** with Pro residue in i+1 position, exhibit only a modest selectivity ($k_{rel} = 3$), however compound **44** containing D-Pro at i+1 gave higher selectivity ($k_{rel} = 28$) (see SCHEME 1.13). Then, different conformations offer a strikingly different reactivity. The initial results of compounds **43** and **44** stimulated the author to synthesize an octapeptide catalyst **45** to form β-hairpins. Indeed, the β-hairpins structure of **45** affords the best result (k_{rel}=51).

18
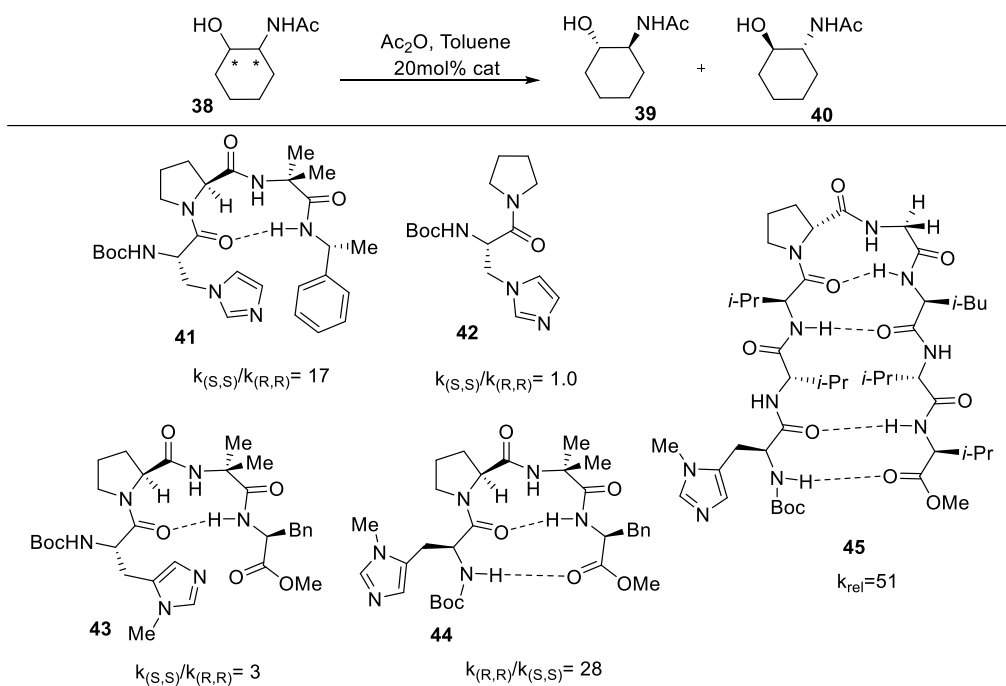
SCHEME 1.13 - Kinetic resolution of *trans*-1,2-acetamidocyclohexanol (**38**).

Peptides containing β-turn motifs can also promote asymmetric conjugate addition. [39] Pentapeptides with D-Pro-Aib turn element were utilized to provide the structural rigidity and consequently facial selectivity in Michael reaction. High efficiency (64-99%) with ee up to 74% was observed in the nitroalkanes addition to α,β-unsaturated aldehydes. The β-turn motifs were not the only target modification in the design of pentapeptides. A histidine residue was also incorporated to serve as a mild base to deprotonate the nitroalkane and additional HB functionality was included (e.g. guanidine, urea and thiourea). These three elements together increase the stereoselectivity and efficiency of the catalyst.

After obtaining the different peptide catalysts, their catalytic efficiency is screened in order to identify the best catalyst synthesized. Wennemer and co-workers [40] used a smart screening method, for the fast identification of active peptide catalysts (SCHEME 1.14). The smart screen method consist in a 'catalyst–substrate co-immobilization' in a one-bead–one-compound, where one of the peptide catalysts is immobilized on a resin that is linked via a spacer to one reactant (see **46** in SCHEME 1.14). The other reactant has been incorporated to a colored fluorescent tag (Dispersed Red 1 dye) (see **47** in SCHEME 1.14) to allow for the easy identification of a "hit" catalyst. This methodology permits the identification of one highly active peptidic catalyst **13**, among $15^3=3375$ different tripeptides screened. Interestingly, the best tripeptide catalyst identified, having a sequence H-L-Pro-L-Pro-L-Asp-NH$_2$ presents a β-

19

turn motif. This combination of two amino acids Pro-Pro increases the rigidity in the catalyst enabling to employ amounts of 1 mol% (SCHEME 1.14).
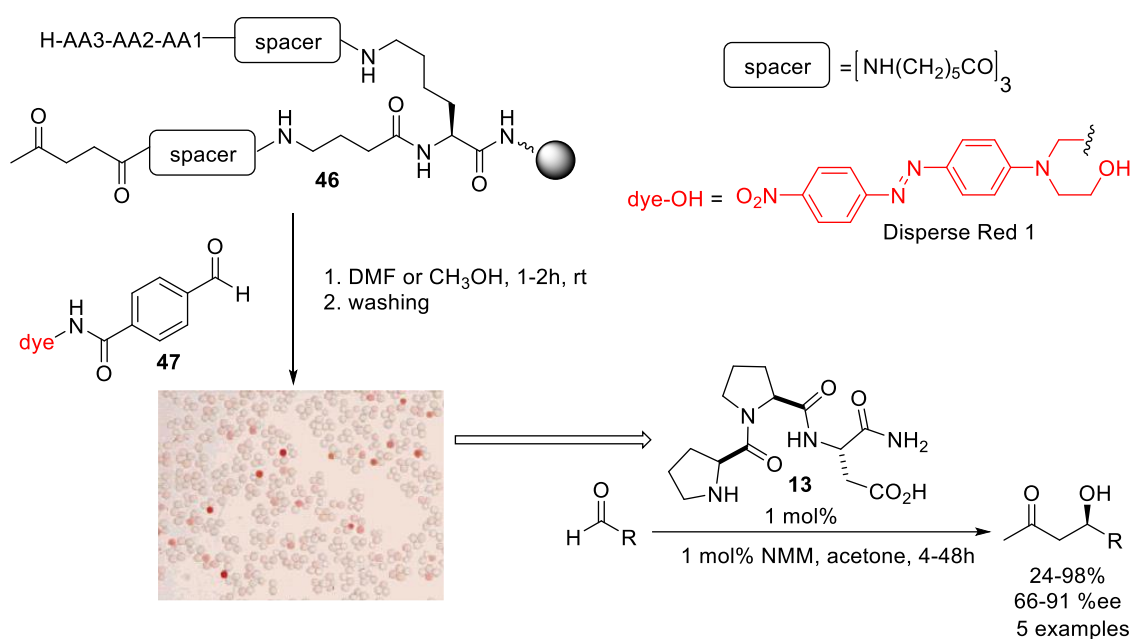
SCHEME 1.14 - Peptide Catalyst–substrate co-immobilization to identify catalytically active peptides in a one-bead–one-compound method. Enamine-based asymmetric Aldol reaction with catalyst **13**.

Interestingly, catalyst **13** with sequence H-L-Pro-L-Pro-L-Asp-NH$_2$ that was good in Aldol reaction was not efficient in Michael addition.[29] Here, again it is noted that the D-Pro epimer of catalyst **13** (H-D-Pro-L-Pro-L-Asp-NH$_2$) produces better results in Michael addition than in Aldol reaction. The adopted conformation in a determinate catalyst is crucial to improve efficiency and enantioselectivity.

Based on these observations, pyrrolidine-type peptides can be considered as very useful organocatalysts for direct AC. The major disadvantages of this peptide catalysts remain in the linearity of the synthesis. Peptide synthesis most often occurs by coupling the carboxyl group of the incoming amino acid to the *N*-terminus of the growing peptide chain. The growing peptide chain follows the step-wise method to add amino acids one-at-a-time to the growing peptide chain. This produces low yields and atom economy. Peptide coupling requires the activation of the *C*-terminal carboxylic acid of the incoming amino acid using carbodiimides such as dicyclohexylcarbodiimide (DCC) or diisopropylcarbodiimide (DIC). Carbodiimides form such a reactive intermediate that racemization of the amino acid can occur. Therefore, reagents to avoid or reduce racemization are often added, including 1-hydroxybenzotriazole (HOBt) and 2-(1H-benzotriazol 1-yl)-1,1,3,3-tetramethyluronium hexafluorophosphate

(HBTU). These coupling reagents, resin and additives are expensive and some times are unrecovered.

1.3 Multicomponent reactions

Multicomponent Reactions (MCRs) are procedures in which more than two building blocks react in one pot to afford a structure including moieties from all the reactants.[41] These processes are considered as a subclass of domino reactions, as all transformations are performed in one pot under similar reaction conditions and in a time-resolved manner (i.e., one after each other). The MCRs have many advantages compared with conventional techniques, in which the final product is obtained using a multi-step sequence with the formation of a single bond in each step. By contrast, MCRs are convergent and therefore very convenient in terms of efficiency (SCHEME 1.15).

A) Multi-Step Synthesis

85% 80%

overall yield
in three steps
65%

95%

B) Multicomponent Synthesis

overall yield
in one step
95%

product
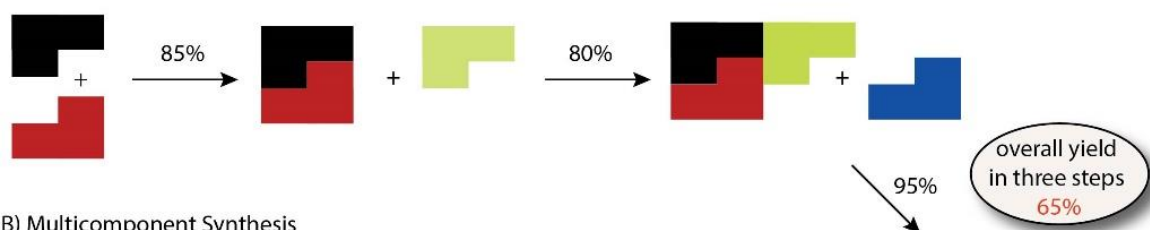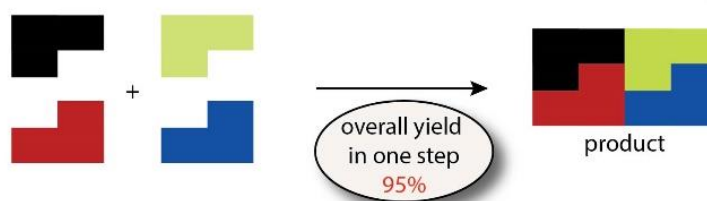
SCHEME 1.15 - A) General multi-step synthesis, B) General multicomponent synthesis.

MCRs generally have perfect atom economy and thus represent suitable synthetic tools for addressing the Green Chemistry criterion. Usually, the starting materials of MCRs are readily available, or can easily be prepared. In special, in the isocyanide multicomponent reaction (I-MCR), the `isocyanide´ reagent has been hated because of the notoriously and terrible smell of volatile isocyanides, which suggests toxicity similar to cyanides. However, in the 1960s Ivar Ugi and co-workers [42] made a comprehensive investigation of isocyanides synthesis, where they conclude that there is not a general toxicity for this class of compounds. I-MCRs in unconventional solvents have been comprehensively studied.[43] The vast list of I-MCRs running in water, ionic liquids, polyethylene glycol (PEGs), bio-derived solvents (p-cymene, glycerol,

Me-THF and others), and neat systems is impressive. However, some I-MCRs like the Ugi four-component reaction (Ugi-4CR) prefer a specific polar protic solvent such as methanol.

Accordingly, in I-MCRs several chemical bonds are formed with high chemical efficiency, and generating high levels of structural diversity and complexity such as: *pseudo*-peptidic (e.g; depsipeptides [44], peptoids [45,46,47]) and peptidomimetic (e.g., oxa-[48], dihydroimida-[49], thia-[50] and tetrazoles[51]) motifs (see SCHEME 1.16) in a diversity-oriented manner without utilization of coupling agents or additives like in peptide chemistry.
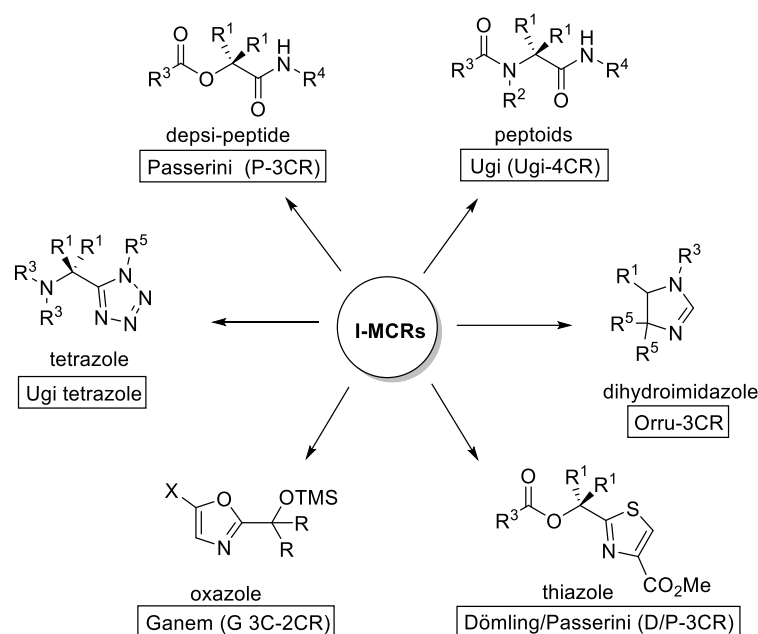
SCHEME 1.16 - Some I-MCRs reactions in the formation of: depsipeptides, peptoids, oxazoles, tetrazoles, thiazoles and dihydroimidazoles.

When the pharmaceutical industry 'discovered' combinatorial chemistry about 30 years ago, the solid-phase approach, pioneered by Merrifield for multistep synthesis of large biopolymers, was adapted for multistep syntheses of drug-like molecules. Only recently, the drug-discovery community has realized the power of Ugi's vision for quickly generating molecular diversity through robust, yet simple, reaction cascades that assemble Multiple Components in solution as one of the best methods for generating *N*-substituted peptides named Ugi-4CR. Most chemical reactions have their own scope and limitation, whereas the Ugi-4CR can convert almost all combinations of starting materials into their products. It was in 1959, when Ivar Ugi develop the Ugi-4CR, [52] with the combination of an amine, an aldehyde or ketone, a carboxylic acid and an isocyanide (SCHEME 1.17).
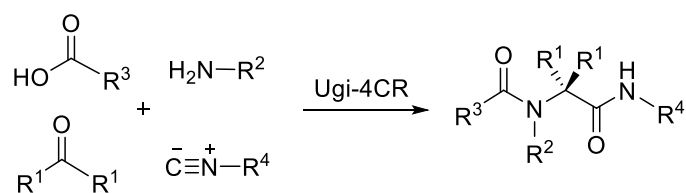
SCHEME 1.17 -The Ugi four-component reaction (Ugi-4CR).

This reaction consists of an ionic mechanism developed in polar protic solvents (such as methanol). The mechanism of Ugi-4CR is shown in SCHEME 1.18. [53,54] In the first step, the amines and carbonyl compounds (aldehyde or ketone) condensed to the imine. The imine is protonated by the carboxylic acid. Depending on the solvent, the ion can be as salt pair or separately. Then, both ions react with the isocyanide component to form an imidate intermediate. The last step is the Mumm rearrangement, consisting in an intramolecular acylation and subsequent rearrangement forming a (C=O) double bond and consequently the Ugi product.
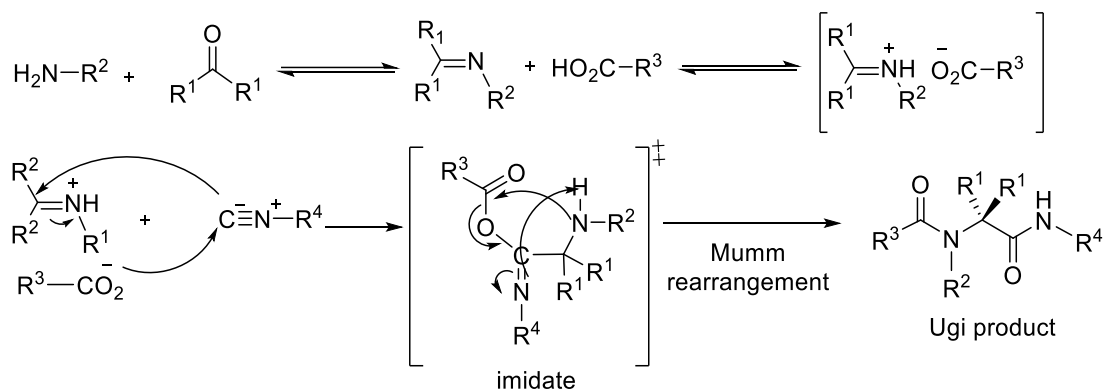
SCHEME 1.18 - General mechanism of the Ugi-4CR.

In accord with the ever-increasing demand for `atom economic´ processes and efficient methods to obtain compounds capable inducing good enantioselectivity, I-MCRs are an unexploited and elegant field that deserve to be studied.

Could it be possible to apply I-MCRs, specifically Ugi-4CR, to generate a new class of versatile compounds capable to catalyze chemical reactions? Might it be an easy and green way to mix more than one component to get a library of *pseudo*-peptide organocatalysts?

During the preparation of this PhD project, no work was reported with the aim to apply Ugi-4CR to add a new class of prolyl *pseudo*-peptides in the area of organocatalysis.

In 2010, Orru and co-workers [20] published an article with the Ugi type 3CR for the straightforward synthesis of catalyst **17** (SCHEME 1.19) resembling the structure and catalytic behavior of Wennemer´s catalyst **13**.
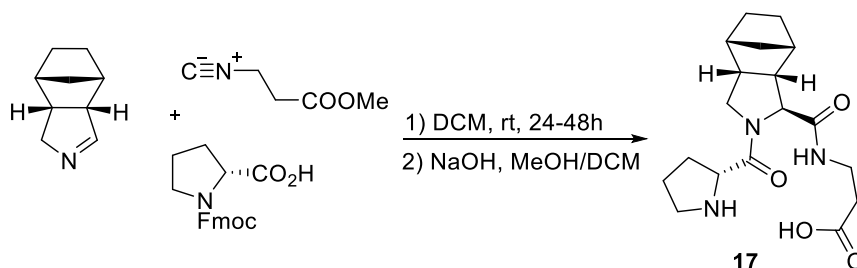
SCHEME 1.19 - Ugi-type 3CR reaction developed by Orru and co-workers.

Recently, Nenajdenko and co-workers [55] synthesized new tetrazole-derived organocatalysts **50** via azido-Ugi reaction with cyclic ketimines **48** (SCHEME 1.20). The principal focus was not the organocatalytic methodology but the use of I-MCRs of azido-Ugi reaction to develop a new class of compounds (**49**). However, after racemate resolution of **49**, 10 mol% of **50** was tested in the asymmetric reaction of α-amination of aldehydes obtaining high ee (>99%).
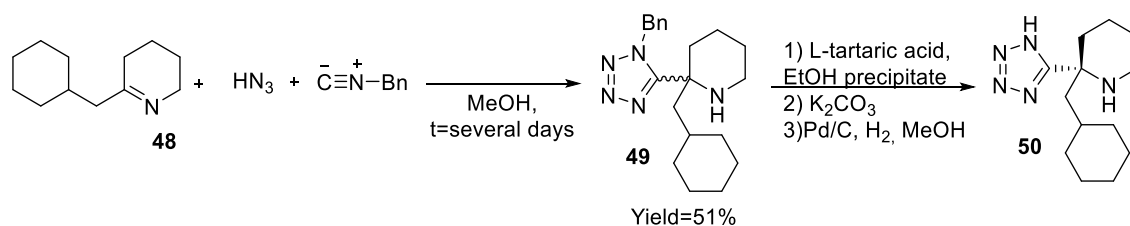
SCHEME 1.20 - Synthesis of tetrazole-derived compound **50** via Azido-Ugi tetrazole reaction.

The application of Ugi-4CR in the field of organocatalysis could be useful to generate versatility in combinatorial approaches to rapidly and efficiently generate peptide derivatives with possible catalytic potential in the area of asymmetric catalysis. Then, our first interest is directed to I-MCRs (Ugi-4CR) that allow a one-pot synthesis of prolyl *pseudo*-peptides with promissory potential in organocatalysis, which will enable application in combinatorial approaches in the discovery of new small libraries of organocatalysts.

1.3.1 Application of I-MCRs in polymer science

I-MCRs have only recently introduced into polymer science. The combination of Passerini three component (P-3CR) to obtain **52** and post acyclic diene metathesis (ADMET) was used to form new polyesters[56]. This new class of polymer (**53**) is considered as a new

contribution to the sustainable development because of the utilization of reagents from renewable resources such as ricinoleic acid **51** (SCHEME 1.21).
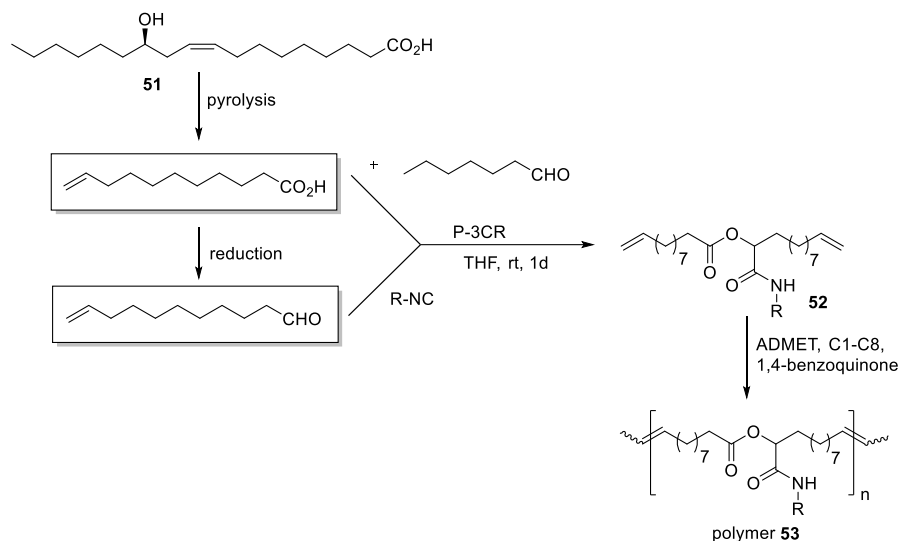
SCHEME 1.21 - Synthesis of new class of polyesters **53** with the combination of P-3CR and ADMET.

More recently, the Ugi-4CR was also employed in the synthesis of polymers following the same methodology for ADMET polymerization. In this case, highly functionalized polyamides were obtained. [57] The initial examples only describe the methodology to obtain polymers using I-MCRs, but no applications of these new materials have been described.

Photocatalysts polymer Ruthenium complexes (Ru-CPs) obtained via P-3CR is the first application of polymers obtained via I-MCRs. Ruthenium complexes **54** (Ru-CPs) were the target molecules to be introduced into the polymeric matrix (SCHEME 1.22). Polymer **55** is shown to be a highly effective and recyclable heterogeneous photocatalyst for oxidation of thioanisole (Yield 55-92%) and benzylamine (Yield 90%). [58]
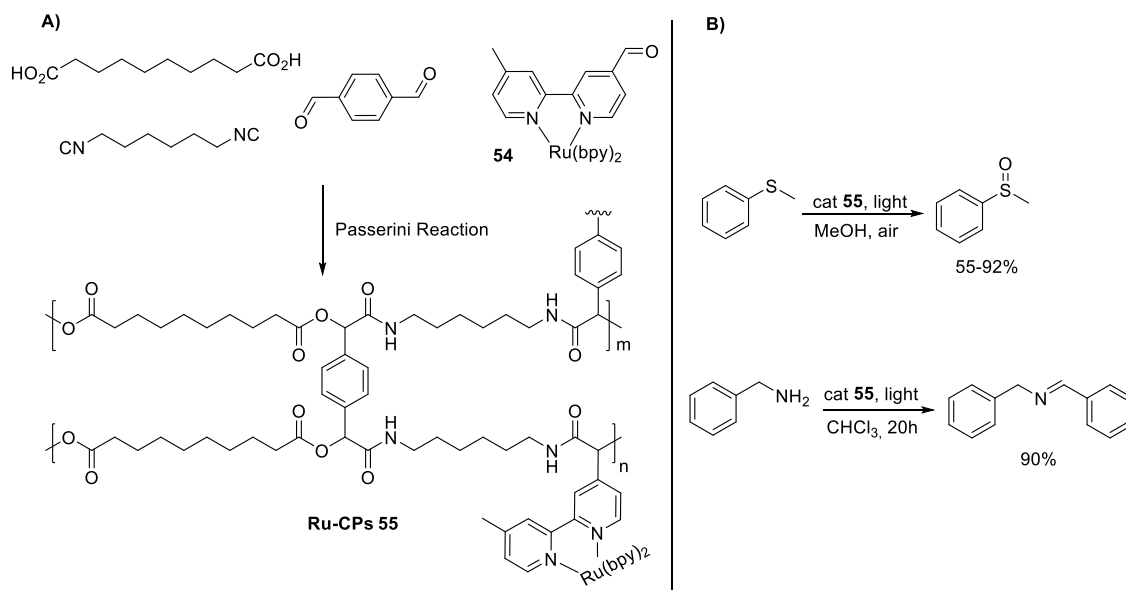
SCHEME 1.22 - A) Synthesis of Ruthenium complexes (Ru-CPs) polymer via P-3CR, B) Aplication of polymer **55** as photoacatalyst.

This new combination of I-MCRs and polymer science is an interesting, non-explored field, and a promising avenue for applications in asymmetric catalysis.

Up to now, there are no reports using Ugi-4CR to make branched or cross-linked polymers with pyrrolidine ring (as functional group for organocatalysis) pendant in the backbone of the polymer. Due to its valuable applications shown in the above literature, our interest is to develop a one-pot Ugi-4CR followed by a cationic co-polymerization to immobilize a new chiral prolyl *pseudo*-peptide organocatalyst into a polymer support for further applications in asymmetric reactions.

1.4 Immobilized organocatalysts

Employing organocatalysis under homogeneous conditions, a tedious workup procedure is often required to purify the product. Thereafter, immobilizing homogeneous organocatalysts onto a solid support provides easy manipulation, simple workup, scale-up of reaction, and recyclability. These are the main reason that prompted chemists to immobilize organocatalysts.

Different types of supports have been used to immobilize organocatalysts, the most popular being inorganic materials (like silica), insoluble polymeric resins (Merrifield) and soluble organic polymers (polyethylene glycols).

Takemoto reported [59] the first polymer-supported proline-type catalysts (**56**). Trans-4-hydroxy-L-proline was immobilized onto polymer and this material was applied directly to the Robison annulation reaction, where, low yield and ee were obtained (53% yield, 18% ee) (SCHEME 1.23).
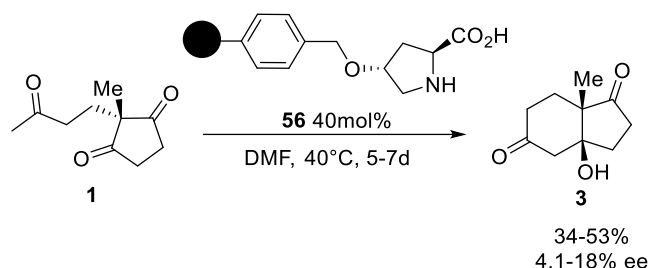
SCHEME 1.23 - Robinson annulation reaction using catalyst **56**.

After this unsuccessful result, the immobilization of organocatalysts into polymers re-started a decade after improving the efficiency and stereoselectivity. Then, many pyrrolidine-type catalysts supported into polymers were reported (FIGURE 1.9). [60, 61, 62, 63]
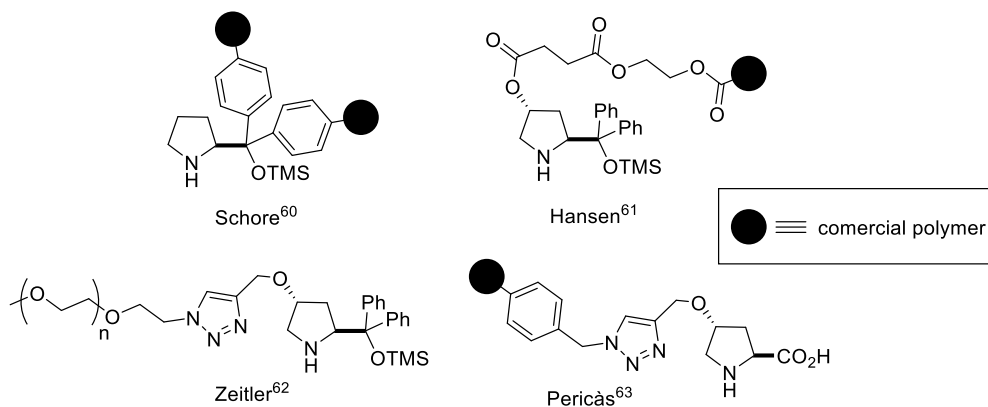
FIGURE 1.9 - Different supported pyrrolidine-type catalysts.

Gruttadauria and co-workers [64] supported the Singh´s catalyst onto Merrifield resin. The synthesis of this new polystyrene-supported prolinamide catalyst (**60**) was done step-wise where the starting materials are not ready available and are easy to prepare. To prepare the prolinamide catalyst prior to support, a peptide coupling process between **57** and **58** undergoes racemization, as previously discussed it is the negative implication for this synthetic methodology. The reported yield for **59** in this step does not exceed 62%; large amount of waste is produced and consequently low level of atom economy. Moreover, a mechanism of the free-radical thiol–ene coupling reaction needs the initiator Azobisisobutyronitrile (AIBN) in stoichiometric quantities (SCHEME 1.24).
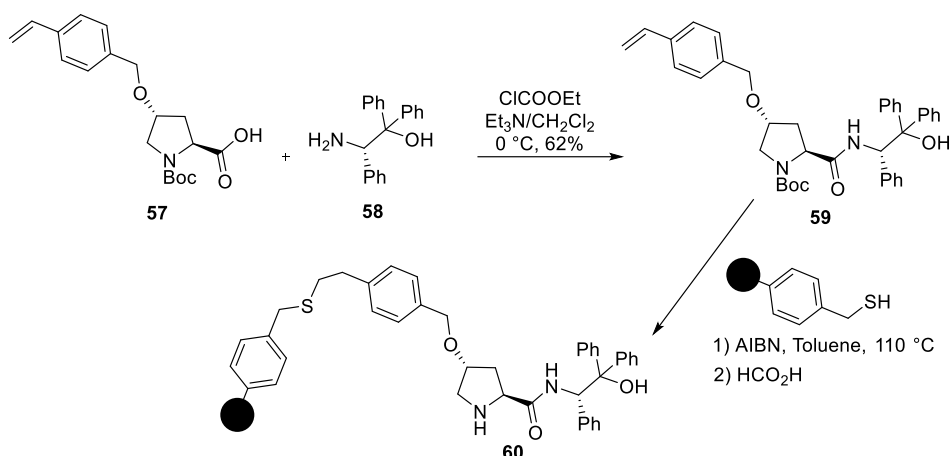
SCHEME 1.24 - Synthesis of polystyrene-supported prolinamide catalyst **60**.

The article `organocatalysts in textiles´ by List and co-workers is very interestingly. [65] In this paper, the author supports catalysts onto inexpensive abundant polymeric solid materials (nylon clothes) (FIGURE 1.10).
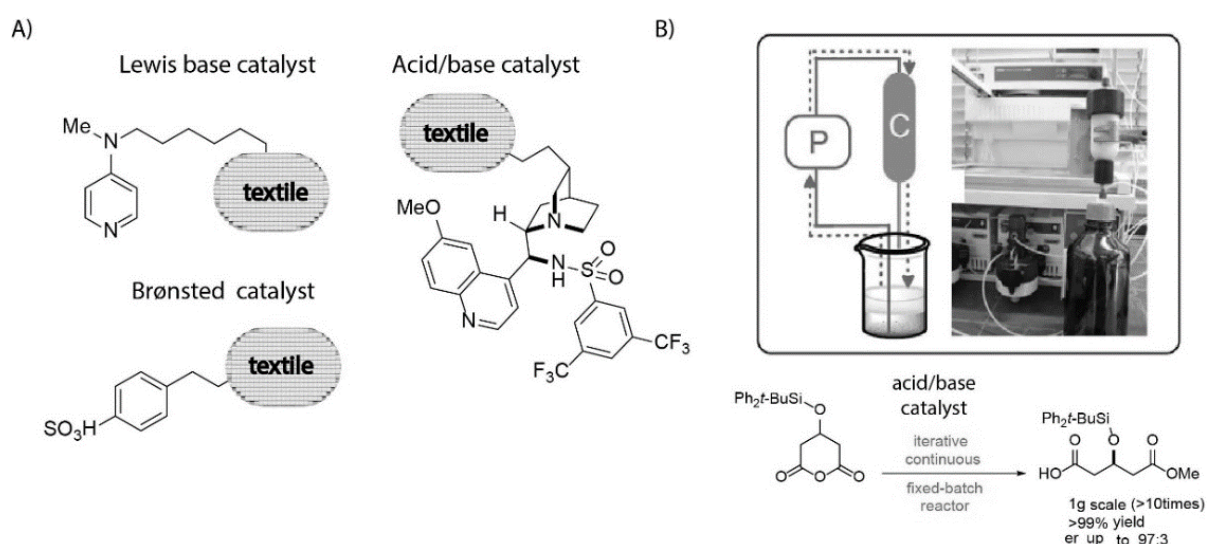
FIGURE 1.10 - A) Immobilized textiles organocatalysts: DMAP (as Lewis base catalyst), a sulfonic acid (Brønsted catalyst), and a bifunctional chiral organocatalyst (acid/base catalyst). B) Schematic illustration of the continuous reactor and desymmetrization of silylated glutamic anhydride with the immobilized acid/base catalyst.

Radical polymerization using ultraviolet light (UV) as alternative source of energy was the employed technique to immobilize the organocatalysis onto textile nylon. Three representative organocatalysts (See A, FIGURE 1.10), a dimethylaminopyridine (DMAP) derivative (as Lewis base catalyst), a sulfonic acid (Brønsted catalyst), and a bifunctional chiral organocatalyst (acid/base catalyst), were supported with catalyst loadings of up to 0.025 mmolg^{-1}. Very good efficiency and enantioselectivity (99%, >97:3 er) were obtained in the organocatalytic

desymmetrization of anhydrides. More interesting these cheap, green, and abundant functionalized textile was used in continuous-flow system (See B, FIGURE 1.10), maintaining its efficiency for more than 250 cycles.

As seen, the majority of immobilized organocatalysts employs commercial polymeric supports, mostly derived from petrochemical feedstock. As we know, petroleum is a non-renewable resource, the earth's supply of this substance will eventually be consumed, and when the world's supply be exhausted, alternative sources of these compounds will be required. With respect to Green Chemistry, the development of new bio-based process instead of petrochemical has great advantages, such as renewability, low environmental impact, and produce cost-competitive chemical products.

Objectives: Chapter 1

The application of Ugi-4CR in the field of organocatalysis can be a wonderful tool to generate versatility in combinatorial approaches to rapidly, efficiently and eco-friendly generate peptide derivatives with catalytic potential in the area of asymmetric catalysis. The main target in Chapter 1 was to develop an I-MCRs-based synthetic program for the combinatorial discovery of novel prolyl *pseudo*-peptides organocatalysts with applications in asymmetric reactions. The specific objective is to design novel organocatalytic motifs based on prolyl *pseudo*-peptides and mimetic scaffolds accessible, based on solution protocols to produce a diversity-oriented library of prolyl *pseudo*-peptides by Isocyanide Multicomponent Reactions (I-MCRs). Also to evaluate the organocatalytic activity, via parallel screening, on known asymmetric addition reactions (e.g., Aldol, Michael, Mannich reactions, etc…).

In accord to Green Chemistry principles, the development of new bio-based immobilized organocatalyst instead of petrochemical derived supported organocatalysts has great advantages, including renewability, low environmental impact and produce cost-competitive chemical products. Then, the next objective is to develop an I-MCRs polymerization based Ugi-4CR and cationic co-polymerization for the combinatorial discovery of new prolyl *pseudo*-peptide derived polymers organocatalysts with applications in asymmetric reactions. Besides, it is the evaluation of the organocatalytic activity of prolyl *pseudo*-peptide polymers as heterogeneous catalyst either in batch or in continuous-flow chemistry.

2 Results and discussion: Chapter 1

2.1 Combinatorial multicomponent synthesis of prolyl *pseudo*-peptide catalysts

I-MCR approach based on the Ugi-4CR reaction was implemented for the development of new prolyl *pseudo*-peptide catalysts. Three different elements of diversity were varied during the strategy adopted for the preparation of these catalysts library i.e. the amine, the oxo and the isocyano components while Pro remained as a fixed substrate aiming to enable enamine catalysis (FIGURE 1.2). The multicomponent nature of this process enabled the straightforward generation of a series of prolyl *pseudo*-peptides having the generic sequences Pro-*N*-R^1-Xaa-NHR^3, being Xaa either Gly (R^2 = H) or Aib (R^2 = *gem*-Me), and R^1 and R^3 either alkyl or amino acid substituents (FIGURE 2.1).
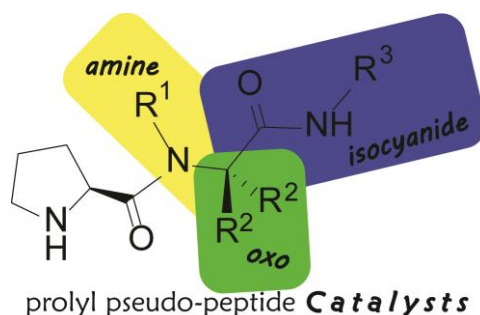
FIGURE 2.1-Combinatorial multicomponent strategy adopted for the preparation of the prolyl *pseudo*-peptide catalysts library.

Fourteen prolyl *pseudo*-peptides of the type Pro-*N*-R^1-Xaa-NHR^3 were synthesized in moderate to good yields (TABLE 2.1) by a two-step procedure comprising the one-pot assembly of the peptidic skeleton by the Ugi-4CR protocol,[66] followed by *N*-terminus deprotection (TABLE 2.1). The corresponding catalysts **61-74** were directly used after flash chromatographic purification.

Among the three distinct elements of diversity, initial attention was focused on the variation of the amine component (FIGURE 2.1; TABLE 2.1), while paraformaldehyde and cyclohexyl isocyanide were kept unchanged. A solution-phase Ugi-4CR procedure [66] was employed for all catalysts in a first instance, which proved to be suitable for reactive amines (TABLE 2.1, compounds **67-74**) but gave poor results when salts of α-amino acid methyl esters hydrochloride were used (TABLE 2.1, compounds **61-66**).

TABLE 2.1 - Multicomponent combinatorial synthesis of prolyl *pseudo*-peptides catalysts using the Ugi-4CR.
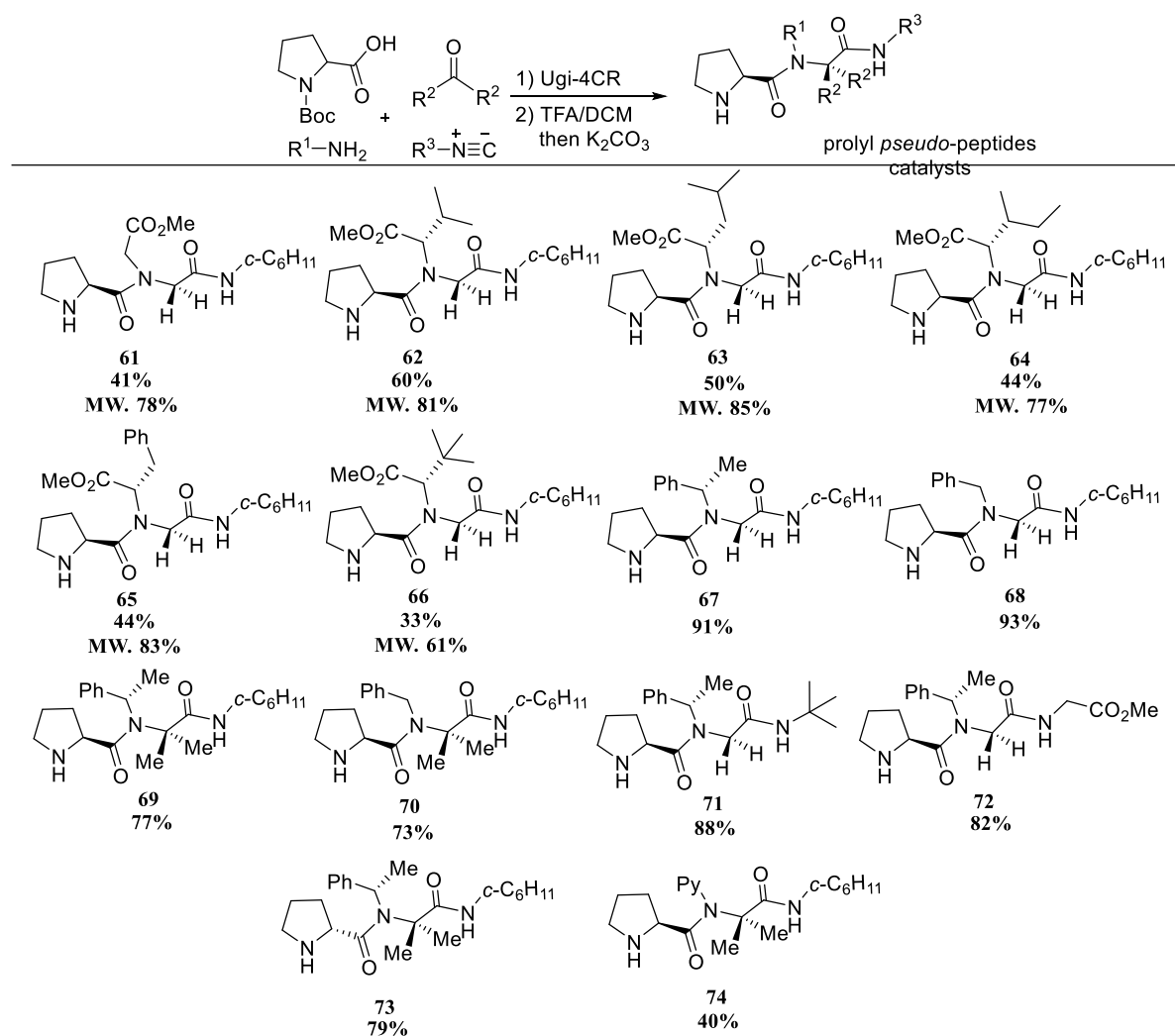
a) Reaction conducted at room temperature in MeOH for 24h. b) Yield of isolated pure product over two steps.

To solve this problem, microwave irradiation (MW) was used, which provided good efficiency in the multicomponent preparation of the catalysts **61-66**, (CHART 2.1). CHART 2.1 shows a considerable increment in the yield when MW irradiation was employed, the result was almost twice in comparison with the classic Ugi-4CR procedure. However, when, unreactive L-*tert*-butylglycine methyl ester (**66**) was used, up to three cycles (30 min, 150 W, 70 °C) of irradiation were required for the reaction in order to obtain a moderate yield (61%).
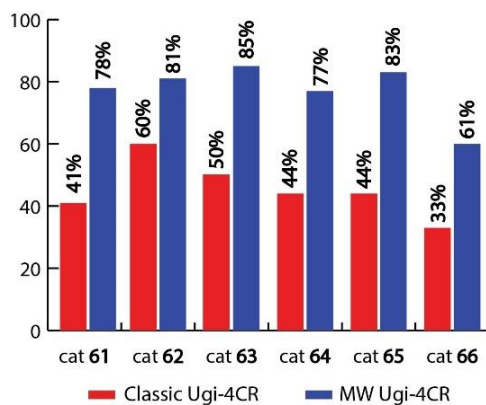
CHART 2.1 - Yields of compounds **61**-**66** obtained by classic or MW Ugi-4CR.

In an initial approach, the idea was to evaluate the efficacy of catalysts **61**-**66** in two possible approaches. Firstly, with a free carboxylic acid following to acts as Model A previously discussed (FIGURE 1.3), and, secondly, with methyl-ester group acting as steric directing group like Model B of catalysts. Then, boc-protected (**62a**) of compound **62** was selected for the ester deprotection, employing a basic hydrolysis with LiOH in methanolic solution. Unfortunately, an intramolecular cyclization was observed with the easy formation of diketopiperazine (DKP) **75** in high yield (91%) (SCHEME 2.1). Diketopiperazines have been used frequently in medicinal chemistry. These skeletons can be found in natural products such as the antibiotics cefoperazone and bycyclomycin. [67] There are some reports on the development of DKP as catalysts in the addition of cianidrine to benzaldehyde [68] but for our interest, this class of compound is not useful.
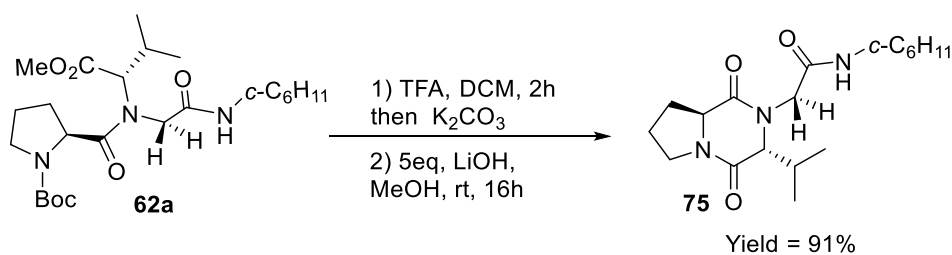
SCHEME 2.1 - Ester hydrolysis of compound **62a**, *in situ* formation of compound **75**.

By using this methodology the ester protected groups of the catalysts **61**-**66** were accomplished in the initial screening as a proline catalyst.

Other modifications in the structural skeleton were the oxo and isocyano components R^2 and R^3 (see FIGURE 2.1). Again relying on the use of readily available starting materials to produce accessible catalysts. Thus, acetone was utilized as oxo component in combination with both (*S*)-α-methylbenzyl and benzyl amines, leading to compounds **69** and **70** having the

33

secuence Pro-*N*-alkyl-Aib-OMe (Aib is α-aminoisobutyric acid). The variation of *N*-alkyl-Gly by *N*-alkyl-Aib derived from the change of formaldehyde by acetone, respectively aims to address the influence of the peptide conformational flexibility in the catalytic performance. Alternatively, *tert*-butylisocyanide and methyl isocyanoacetate were combined with (*S*)-α-methylbenzylamine and paraformaldehyde to produce the compounds **71** and **72**. With the change of isocyano components, we aimed to address the influence on the catalytic profile of the bulky character of substituents at the internal and *C*-terminal amides. Sequently, (*S*)-α-methylbenzyl amine, acetone and cyclohexylisocyanide were combined with *R*-Proline to produce compounds **73**, an analog of **69** having the opposite stereochemistry at proline. With this, we might be able to assess the actual role of the pyrrolidine-ring stereochemistry on the stereocontrol performed by such catalysts. In a last instance, 1-aminopyrene was used as steric hindrance aromatic amine to synthesize compound **74**, but only 40% yield was obtained.
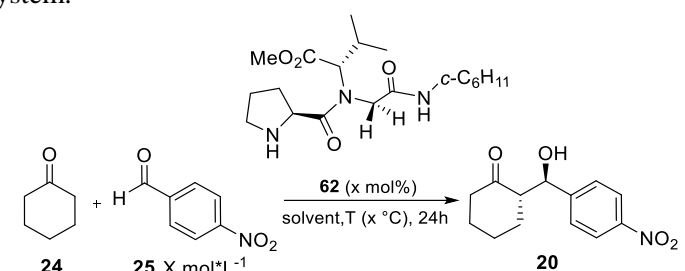
2.2 Prolyl *pseudo*-peptide catalysts: Application in the enamine catalysis

To evaluate the catalytic properties of the new class of prolyl *pseudo*-peptides, catalyst **62** was chosen, keeping in mind the possibility of mimicking the aldolase type I. The catalysts were tested in model reactions such as Aldol and Michael reaction.

2.2.1 Evaluation of prolyl *pseudo*-peptide catalysts in the asymmetric Aldol reaction

By MW Ugi-4CR procedure, catalyst **62** was synthesized and deprotected with TFA in DCM at 50% (v/v). Initially, 10 mol% of catalyst **62** was used for the reaction of 3 equivalents of cyclohexanone and 1 equivalent of 4-nitrobenzaldehyde. The concentration with respect to nitrobenzaldehyde was 0.25 M, compared to the solvent of choice. After approximately 24 h, only 20-89 % yield of aldol product was isolated. The diastereoisomeric ratio (*dr.*) *anti:syn* of the resulting product **20** was determined both by ^{1}H NMR and HPLC analysis and the best result with respect to *dr.* and enantioselectivity (ee) was observed using a mixture of DMSO/H$_2$O (7:3) as solvent (*dr.* 73:27 (*anti*:*syn*), 77 %ee, entry 6, TABLE 2.2).

TABLE 2.2 - Aldol reaction of cyclohexanone (**24)** and *p*-nitrobenzaldehyde (**25**) catalyzed by **62.** Optimization of the system.

Entry [a]	Catalyst (mol%)	Conc (M)	Solvent	Temp (°C)	Yield (%) [b]	*dr* anti:syn [c]	ee (%) [d]
1	10	0.25	H_2O	30	30	75:25	60
2	10	0.25	EtOH	30	25	68:32	43
3	10	0.25	H_2O:EtOH(1:1)	30	43	77:23	55
4	10	0.25	Brine	30	89	67:33	35
5	10	0.25	DMSO	30	20	88:12	47
6	10	0.25	DMSO-H_2O (7:3)	30	76	73:27	77
7	5	0.25	DMSO-H_2O (7:3)	30	65	61:39	75
8	20	0.25	DMSO-H_2O (7:3)	30	85	66:34	73
9	10	0.15	DMSO-H_2O (7:3)	30	30	83:17	51
10	10	0.50	DMSO-H_2O (7:3)	30	78	67:33	64
11	10	0.25	DMSO-H_2O (7:3)	0 °C	59	76:24	73
12	10	0.25	DMSO-H_2O (7:3)	-10 °C	50	57:43	72

a) Reactions using 3 equivalents of cyclohexanone and 0.25 mmol of *p*-nitrobenzaldehyde in 1 mL of solvent. b) Isolated yield. c) Determined by ¹H NMR analysis. d) Determined by chiral phase HPLC analysis.

After determining the best solvent system (entry 6), we systematically varied different reaction parameters of the reaction. First, we changed the catalyst loading and performed the standard reaction under otherwise identical conditions (entries 7 and 8, TABLE 2.2). Even with 5 mol% and 20 mol%, the ee and *dr.* were not affected, (entries 7 and 8, TABLE 2.2). As the best catalyst loading was 10 mol%, then, the next step was to change the concentration of the aldehyde (entries 9 and 10, TABLE 2.2) keeping the catalyst loading 10 mol% (entry 6, TABLE 2.2). The results obtained at higher concentrations of aldehyde (entry 10) were similar to those of the standard reaction and, as expected, the more diluted reaction was slower (entry 9). The enantioselectivity was not influenced by changes in the temperature (see entries 11 and 12, TABLE 2.2).
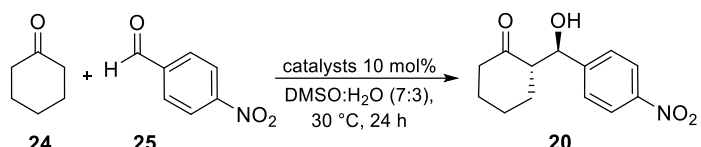
Taking account of these robust results, we next tested various catalysts with similar structure of catalyst **62**.

Initially we screened the amine group by using various natural and non-natural amino acid hydrochloride esters like *tert*-butylglycine (entry 6, TABLE 2.3) and glycine (Gly), leucine

(Leu), isoleucine (Ile), valine (Val), etc…These prolyl *pseudo*-peptides were then tested as catalysts for the same reaction discussed above between *p*-nitrobenzaldehyde and cyclohexanone under the standard conditions (TABLE 2.3).

A catalyst loading of 10 mol% of catalysts **62** was necessary to obtain the desired product **20** in 73% yield after 24 h and with a selectivity of *dr.* 7:3 and 77% ee (entry 2, TABLE 2.3). At the beginning, we hypothesized that the incorporation of a chiral and bulky R^1 group might increase the ee in the system, but, due to the lack of chiral and bulky group the enantioselectivity was not so high (i.e. 68% ee) in **61** compared to **62** (entry 1 and 2, TABLE 2.3).

TABLE 2.3 - Asymmetric Aldol reaction of cyclohexanone (**24)** and *p*-nitrobenzaldehyde (**25)**. Screening of different prolyl *pseudo*-peptide catalysts.

Entry [a]	Catalyst	Yield (%) [b]	dr (*syn/anti*) [c]	ee (%) [d]
1	**61**	47	60:40	68
2	**62**	73	73:27	77
3	**63**	60	70:30	51
4	**64**	43	70:30	51
5	**65**	39	74:26	58
6	**66**	40	79:21	40

a) Reactions using 3 equivalents of cyclohexanone and 0.25mmol of *p*-nitrobenzaldehyde in 1mL of a mixture of DMSO:H_2O (7:3) b) Yield of the isolated product. c) Determined by ^{1}H-NMR analysis. d) Determined by chiral-stationary phase HPLC analysis.

Analyzing these results of catalyst with chiral and bulky *N*-substituents that show only moderate enantioselectivity (entries 3-6, TABLE 2.3) as compared to **61**. We supposed that the enamine formation is not influenced by the *N*-substituent in the *pseudo*-peptide structure and maybe by the other substituent present in the structure, but did not found further evidence that allows to conclude this hypothesis. Further study is require in order to get the full explanation of the system behavior.

As this class of organocatalysts was not able to produce the aldol reaction in good manner, it was perhaps a logical effort to employ the prolyl *pseudo*-peptide catalyst in other asymmetric transformation to assess the catalytic properties. Then, we decide to continue the evaluation of prolyl *pseudo*-peptide in asymmetric Michael reaction.

2.2.2 Evaluation of prolyl *pseudo*-peptide catalysts in the asymmetric Michael reaction

To evaluate the catalytic properties of the prolyl *pseudo*-peptides in the conjugate addition reactions of aldehydes and nitroolefins, we used the reaction between *n*-butanal and *β*-nitrostyrene as a model reaction. First, catalyst **62** was tested in order to optimize the reaction conditions.

As shown in TABLE 2.4, a comprehensive screening of solvents were evaluated (entries 1-6, TABLE 2.4) in order to assess the effect of reaction conditions in the catalytic efficiency and stereocontrol of this type of catalysts. Similar to topic 2.2.1, catalyst **62** was chosen to accomplish this study, considering that its performance in the model system was high (entry 1, TABLE 2.4).

As shown in TABLE 2.4, the solvent has a significant effect upon the reaction yield. In general, the reaction proceeded more rapidly in polar solvents (entries 3, 4) but decreased the stereocontrol of the catalyst (entry 4, TABLE 2.4). For example, in isopropyl alcohol (*i*-PrOH), (entry 4, TABLE 2.4), high yield of compound **78** (98%) was obtained, whereas reactions in less polar solvent like Toluene and DCM were slightly sluggish (entries 1-2, TABLE 2.4). Interestingly, polar solvents marked a drop in the enantio- and diastereoselection (*dr.* 85:15 (*syn*:*anti*); 34% ee, entry 4, TABLE 2.4). Equally, mixtures containing a small amount of *i*-PrOH (entries 5 and 6, TABLE 2.4) were less successful. Whereas this proves that aprotic, hydrophobic solvents are required for a good stereocontrol, the results are quite intriguing since the mixture CHCl$_3$/*i*-PrOH is the solvent of choice for Michael additions with Wennemers' peptide catalysts.[69,70,71,72,73,74]

Solvent evaluation revealed that toluene was the best solvent for the reaction (*dr.* 92:8 (*syn*:*anti*); 91% ee, entry 1, TABLE 2.4), and no better results were obtained using other solvents. In order to check the variation of different parameters, further optimization of the Michael reaction was continued with the catalysts **62.** (TABLE 2.4).

TABLE 2.4 - Asymmetric Michael reaction of *n*-butanal and *β*-nitrostyrene catalyzed by **62**. Optimization of the system.
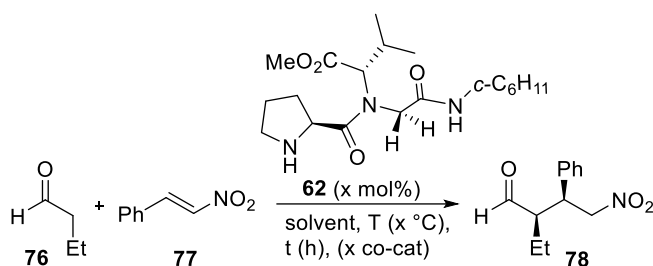
Entry [a]	Catalyst (mol%)	Solvent	Co-Cat (10 mol%)	T (°C)	Yield (%) [d]	*dr.* (*syn:anti*) [e]	ee (%) [f]
1	10	Toluene	-	30	90	92:8	91
2	10	DCM	-	30	54	94:6	79
3	10	THF	-	30	98	88:12	73
4	10	Iso	-	30	98	85:15	34
5	10	CHCl$_3$:Iso (9:1)	-	30	63	93:7	62
6	10	Tol:Iso (9:1)	-	30	90	95:5	80
7	2.5	Toluene	-	30	45	96:4	91
8 [b]	2.5	Toluene	-	30	74	96:4	89
9	5	Toluene	-	30	76	94:6	89
10 [c]	10	Toluene	-	30	56	94:6	90
11	10	Toluene	-	5 °C	89	95:5	90
12	10	Toluene	PhCO$_2$H	30	88	94:6	87
13	10	Toluene	4-NO$_2$Fenol	30	92	93:7	90

a) Reactions using 3 equivalents of *n*-butanal and 0.25 mmol of *β*-nitrostyrene in 1 mL of solvent. b) Reaction performed in 48h. c) Reaction performed at 0.125 M. d) Isolated yield. e) *dr. syn* (major):*anti*; determined by ^{1}H NMR. f) Determined by chiral-stationary phase HPLC analysis of the *syn* product.

Firstly, we turned our attention to study the amount of catalyst in the reaction. Lowering the loading of catalyst to 5 mol%, the desired product **78** was obtained in moderate yield but with excellent diastereoisomeric ratio and enantioselectivity (entry 9, TABLE 2.4). In terms of operational convenience, the use of 2.5 mol% of catalyst **62** ensures economy in the process while maintaining expedient reaction times (entry 7, TABLE 2.4), but led to erosion in terms of yield (45%), although without substantial changes in the *dr* and *ee* (entries 7 and 8, TABLE 2.4). Better yield was obtained with 2.5 mol% increasing the time to 48h (entry 8, TABLE 2.4). The results obtained at diluted concentrations were similar to those of the standard reaction, as expected; the more diluted reaction was slower (entry 10, TABLE 2.4). On the order hand, neither decreasing the temperature to 5 °C (entry 11) nor adding 10 mol% of either benzoic acid (entry 12, TABLE 2.4) or *p*-nitrophenol (entry 13, TABLE 2.4) provoked a significant change in the reaction yield and stereoselection. In the case of *p*-nitrophenol as additive, a qualitative study revealed an initial acceleration of the reaction, although the yield was not increased after 24 h.

Until now, the better conditions for the system in question for the synthesis of **78** is 10 mol% of catalyst **62** in toluene as solvent at room temperature with the concentration of 0.25 M for β-nitrostyrene.

During the initial screening, standard reaction conditions consisted in the use of 10 mol% of catalyst in toluene as solvent at room temperature. Thus, we next turned our attention to the evaluation of a library of prolyl *pseudo*-peptide hybrid catalysts in the Michael addition. These prolyl *pseudo*-peptides **61-74** were then tested as organocatalysts for the reaction of *n*-butanal and β-nitrostyrene under the standard conditions discussed above. A range of 77-94% yield after 24 h with good to excellent selectivity of *dr.* and ee were obtained with prolyl *pseudo*-peptides (see TABLE 2.5). Significantly better results were obtained with catalyst **69** (entry 9, TABLE 2.5). As shown in TABLE 2.5, compounds **61** and **68** with the presence of achiral *N*-substituents Gly-OMe of **61** and benzylamine of **68** respectively, provided similar results (i.e., *ca.* 90% ee, entries 1 and 8, TABLE 2.5) compared to chiral ones, **62**, **64** and **67**. On the other hand, catalyst **62** and catalyst **64** showed much better enantioselectivity than **63** and **65** (i.e., *ca.* 90 > 79% ee, entries 2 and 7, TABLE 2.5). We hypothesized that the incorporation of a bulky R^1 group might increase enantioselectivity in the system, but intriguingly **66** gave only moderate results (*dr.* 90:10 (*syn*:*anti*); 82% ee, entry 6, TABLE 2.5) despite of having the bulkiest side chain among all aminoacid methyl esters incorporated as *N*-substituents.

Therefore, little changes in *N*-substituents of pseudo-peptides did not bring great modification in the asymmetric Michael catalysis between *n*-butanal and β-nitrostyrene. As same as in the previous Aldol reaction, no effect of the *N*-substituents residue R^1 in the asymmetric induction was detected. The complexity of the structure in space may lead to a conformation not well understood, and this needs to be studied.

Due to the fact that changes in the side chain of *N*-substituents residue R^1 has not great influence in the stereoselectivity, we attempted to modify other substituents in the skeleton of prolyl *pseudo*-peptides.

TABLE 2.5 - Asymmetric Michael reaction of *n*-butanal and *β*-nitrostyrene. Screening of different prolyl *pseudo*-peptide catalysts.
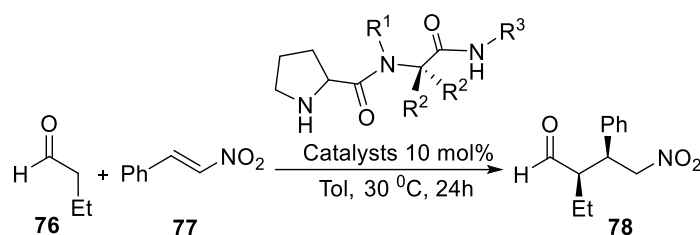
Entry	R^1	R^2	R^3	Catalyst	Yield (%) [b]	dr (*syn/anti*) [c]	ee (%) [d]
1	Gly-OMe	H	Cy	**61**	87	96:4	90
2	Val-OMe	H	Cy	**62**	92	92:8	91
3	Leu-OMe	H	Cy	**63**	83	97:3	79
4	Ile-OMe	H	Cy	**64**	89	97:3	90
5	Phe-OMe	H	Cy	**65**	84	93:7	64
6	^{t}BuGly-OMe	H	Cy	**66**	94	90:10	82
7	(*S*)-α-MeBn	H	Cy	**67**	74	96:4	89
8	Bn	H	Cy	**68**	91	93:7	92
9	(*S*)-α-MeBn	Me	Cy	**69**	85	94:6	98
10	Bn	Me	Cy	**70**	84	94:6	87
11	(*S*)-α-MeBn	H	*t*-Bu	**71**	93	94:6	91
12	(*S*)-α-MeBn	H	Gly-OMe	**72**	77	89:11	85
13 [f]	(*S*)-α-MeBn	Me	Cy	**73**	93	84:16	-86
14	pyrene	Me	Cy	**74**	90	84:16	83

a) All reactions were conducted using 3 equivalents of the aldehyde and 0.25 mmol of *β*-nitrostyrene in 1 mL of toluene. b) Yield of isolated product. c) Determined by ^{1}H NMR spectroscopy analysis. d) Determined by chiral-stationary phase HPLC analysis. f) Using D-Pro amino acid.

We next varied the oxo component. The incorporation of the aminoacid residue Aib derived from the use of acetone instead of formaldehyde as oxo component shed additional light into the catalytic-activity relationship. Thus, the combination of Aib (R^2 = Me) and the chiral (*S*)-α-methylbenzyl group as *N*-substituent led to the most effective catalyst **69** (98% ee). Notwithstanding these advances, we noted that **70** bearing benzyl as *N*-substitution exhibited only moderate enantioselectivity (87% ee) (entry 10, TABLE 2.5), despite of also having the aminoacid residue Aib (R^2 = Me) derived from the use of acetone in the Ugi-4CR. As well as compound **68** in spite of also enduring benzyl as *N*-substitution but aminoacid residue Gly (Xaa = H) instead of acetone have similar enantioselectivity (92% ee) like **70** but only a moderate results as **69**.

Up to here, two structural changes were accomplished and so far good results were determined. Based on these results, we decided to fix the chiral (*S*)-α-methylbenzyl group as *N*-substituent and formaldehyde instead of acetone as oxo compound in the next variation (i.e.; R^1 = (*S*)-α-MeBn and R^2 = H).

Then, we turned to vary the isocyanide component. The commercial isocyanides, *tert*-butylisocyanide ($R^3 = {}^t$Bu) and isocyanoacetate (R^3 = Gly-OMe) from Aldrich, were employed as isocyanide component. Thus, **71** ($R^3 = {}^t$Bu) showed slightly higher enantioselectivity (91% ee, entry 11, TABLE 2.5) than its analogue **67** (R^3 = Cy) (89% ee, entry 7, TABLE 2.5), probably due to bulkier character of the *tert*-butyl amide substituent compared to the cyclohexyl one. In contrast, the incorporation of the less bulky methyl isocyanoacetate in **72** (R^3 = Gly-OMe) led to a drop in both the enantio- and diastereoselectivity (*dr.* 89:11 (*syn*:*anti*); 85% ee, entry 12, TABLE 2.5) with respect to catalyst **67** (*dr.* 96:4 (*syn*:*anti*); 89% ee). Considering these results, we assumed that a steric effect of the R^3 of an isocyanide component is important, even though there are no great differences between catalysts having the terminal *tert*-butyl and cyclohexyl carboxamides. Thus, the use of cyclohexylisocyanide becomes more feasible than the *tert*-butyl one owing to the lower price and simpler synthesis of the former. Catalyst **74** only provided 82% ee and *dr.* 84:16 (*syn*:*anti*) (entry 14, TABLE 2.5) in despite of 1-aminopyrene was used as big aromatic amine in the peptoid structure. Finally, we synthesized catalyst **73** using D-Pro instead of L-Pro, to provide the reverse configuration at the asymmetric centers in the Michael reaction. Catalyst **73** provided good diastereo- and enantioselectivity (*dr.* 84:16 (*syn*:*anti*); -86% ee). This result proved that the stereocontrol is mainly based on the pyrrolidine-ring. Notwithstanding, comparing with its isomer **69**, catalyst **73** is less effective than **69**, assuming that the other substituents in the skeleton also plays a pivotal role in the catalysis.

Encouraged by these results, we next probed the scope of the reaction with a variety of aldehydes and nitroolefins (TABLE 2.6). All reactions were conducted in toluene at room temperature for 24 h in the presence of 10 mol% of **69**. In each case, smooth reactions occurred to generate Michael adducts in high yields (70–91%). These results eventually led to the successful development of catalyst **69** and higher stereoselectivities were achieved when reactions were performed with small amount of catalyst (10 mol%) and longer reaction time provided diastereoselectivities up to more than 94:6 (*syn:anti*) and enantioselectivities variables from 67 to 98%. As depicted, *β*-nitrostyrenes bearing *β*-aryl substituents with either electron withdrawing (e.g. F, Cl, Br) or electron-donating groups (e.g. MeO) are almost equally tolerated (entries 4-9, TABLE 2.6).

TABLE 2.6 - Scope of catalyst **69** in the asymmetric Michael reaction between different aldehydes and β-nitrostyrenes.
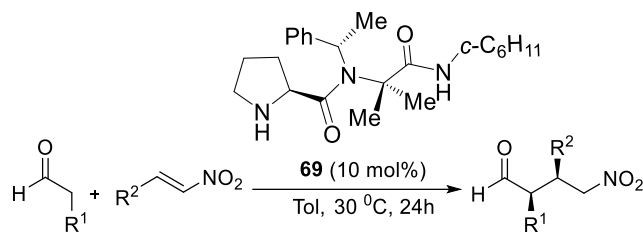
Entry [a]	R[1]	R[2]	Compound	Yield (%) [b]	dr. (syn/anti) [c]	ee (%) [d]
1	Et	Ph	**78**	85	94:6	98
2	Me	Ph	**23**	90	93:7	91
3	i-Pr	Ph	**79**	80	94:6	67
4	Et	4-MeOC$_6$H$_4$	**80**	83	82:18	93
5	Et	4-FC$_6$H$_4$	**81**	89	92:8	96
6	Et	4-ClC$_6$H$_4$	**82**	86	94:6	88
7	Et	4-BrC$_6$H$_4$	**83**	77	85:15	85
8	Et	2-BrC$_6$H$_4$	**84**	91	88:12	89
9	Et	3-NO$_2$C$_6$H$_4$	**85**	70	80:20	78
10	Et	2-Furyl	**86**	83	94:6	82

a) All reactions were conducted using 3 equivalents of the aldehyde and 0.25 mmol of β-nitrostyrene in 1 mL of toluene. b) Yield of isolated product. c) Determined by ^{1}H NMR spectroscopic analysis. d) Determined by chiral-stationary phase HPLC analysis.

The best result was obtained using a nitroolefin with an electron-poor aromatic substituent *trans*-4-fluoro-β-nitrostyrene: 89% yield (*dr.* 92:8 (*syn*:*anti*); 96% ee, entry 5, TABLE 2.6). Moreover, similar results were provided with an electron-rich aromatic substituent such as *trans*-4-methoxy-β-nitrostyrene: giving **80** in 83% yield (*dr.* 82:18(*syn*:*anti*); 93% ee, entry 4, TABLE 2.6).

Aldehydes bearing bulky substituents in the β-position (i.e. isovaleraldehyde) were also studied in the presence of 10 mol% of catalyst, the reaction provided **79** in 81% yield having *dr.* 91:9 (*syn*:*anti*), but a poor enantioselectivity was observed (67% ee) (entry 3, TABLE 2.6).

Utilization of *trans*-2-furyl-β-nitrostyrene as acceptor (entry 10, TABLE 2.6) provided Michael adduct with high diastereoselectivity but with only moderate enantioselectivity. When we employed *trans*-3-nitro-β-nitrostyrene, somehow not clearly, the ee was poor (78%, entry 9, compound **85**) as well as the yield (70%). We assume the possibility of a steric interaction between the 3-nitroaryl substituent and the chain of aldehyde when a *Si* face approximation of β-nitrostyrene is produced.

These results demonstrate that **69** is a good catalyst for conjugate addition reactions between a broad range of different substituted aromatic nitroolefins and aldehydes.

In terms of chemical efficiency and diastereoselection, it does not seem to be great differences between all catalysts, whereas the enantioselection resulted more dependent on some of the variable structural elements. The discussed results provide important insights into the structural requirements for this kind of catalysts. A conformational study of Pro-*N*-R^1-Xaa-NHR^3 catalysts was done to understand the possible mechanism of action of the catalyzed 1,4-addition reaction.

2.3 Conformational study of Pro-*N*-R^1-Xaa-NHR^3 catalysts

As known, the C–N bond in peptides has partial double bond character; the resonance delocalization is showed in A) FIGURE 2.2. Due to that, the free rotation around the C–N amide bond is drastically restricted with a rotational barrier of 105 kJ mol^{-1}. Consequently, two rotamers (see B) in FIGURE 2.2) of the peptide bond exist: 1) the *trans* isomer ($\omega = 180°$) and the *cis* isomer ($\omega = 0°$). [75,76,77]

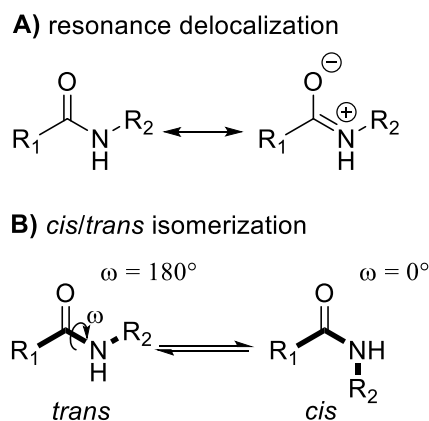**A)** resonance delocalization

B) *cis/trans* isomerization

FIGURE 2.2 - A) Resonance delocalization: partial double bond character B) cis/trans isomerization of the peptide bond.

The NMR analysis of almost all synthesized prolyl *pseudo*-peptides shows *cis/trans* isomers except for compounds **69**, **70**, **73** and **74** having a generic sequence of Pro-*N*-R^1-Xaa-NHR^3 where Xaa = Aib (R^2 = *gem*-Me). To explore the representative structures and possible mechanism of action in catalysis we chose the best catalyst until now (**69**) with Xaa = Aib (R^2 = *gem*-Me) and its analogue (**67**) with Xaa = Gly (R^2 = H) to analyze their conformations employing different methods such as nuclear magnetic resonance (NMR) and molecular modelling (MM).

Initially compound **69** was fully characterized (please see TABLE 2.7 and FIGURE 3.2). The NMR techniques were recorded in a 400 MHz spectrometer in CDCl$_3$.

43

In the ^{13}C NMR spectra is two peaks at 173.50 ppm and 170.95 ppm are observed, which correspond to C=O group of *C*-11 and *C*-5, respectively. The aromatic zone shows the Ph group shifts where 140.7 ppm resulting a quaternary carbon in the DEPT 135° experiment was assigned to *C*-18 (TABLE 2.6). In addition, at 64.6 ppm a deshielded signal was observed correspondent to a quaternary carbon by DEPT 135°. We attributed to *C*-8 as. In the DEPT 135° experiment, three *C*H deshielded aliphatic carbon peaks at: 59.7 ppm, 50.7 ppm and 48.9 ppm were observed. These are carbons directly attached to a heteroatom and the possible carbons are *C*-1, *C*-6 and *C*-12.

TABLE 2.7 - ^{13}C, DEPT 135°, HSQC and HMBC shifts assigment of compound **69**.

Atom No	[13]C (δ_C = ppm)	DEPT 135° (δ_C = ppm)	HSQC (δ_H = ppm)	HMBC (δ_H = ppm)
C-1	59.7	59.7 (*C*H)	4.30	3.32, 1.27
C-2	45.3	45.3 (*C*H$_2$)	3.32	4.30, 1.27
C-3	32.7	32.7 (*C*H$_2$)	1.27	4.30, 3.32
C-4	46.3	46.2 (*C*H$_2$)	3.20, 3.18	3.32, 1.27
C-5	170.6	(*C*=O)	-	5.12, 2.07
C-6	50.7	50.7 (*C*H)	5.12	1.88
C-7	19.0	19.0 (*C*H$_3$)	1.88	5.12, 2.07, 1.7
C-8	64.6	(*C*)	-	5.12, 1.64
C-9	24.8	24.8 (*C*H$_3$)	1.64	-
C-10	24.6	24.6 (*C*H$_3$)	1.53	-
C-11	173.7	(*C*=O)	-	5.70, 1.64, 1.53
C-12	48.9	48.9 (*C*H)	3.64	1.40, 1.15, 1.20, 1.11
C 13-17	32.7, 30.8, 28.9, 25.4	32.7, 30.8, 28.9, 25.4 (*C*H$_2$)	1.40, 1.15, 1.20, 1.11	3.64, 1.40, 1.15, 1.20, 1.11
C-18	140.7	(*C*)	-	7.42, 5.12, 1.88
C 19-23	129.2, 128.2, 128.0, 127.2	129.2, 128.2, 128.0, 127.2, (*C*H)	7.56, 7.42, 7.34	-

The heteronuclear single-quantum correlation (HSQC) shows a correlation between 50.7 ppm and 5.12 ppm. A relationship between 5.12 ppm and a doublet 1.88 ppm with coupling [3]*J*

= 7.0 Hz which is likewise derived from coupling with Me group for the *N*-substituent (*S*)-α-MeBn. Then, the COSY diagram confirms the location of *H*-6 at 5.12 ppm and the *C*H of C-6 at 50.7 ppm. Consequently the doublet at 1.88 ppm with coupling $^3J = 7.0$ Hz is assigned as *C*-7. The shift at 48.9 ppm is directly correlated by HSQC to the proton with shift 3.64 ppm. By the same way, was analyzed the COSY diagram. There is a correlation between shift 3.64 ppm and a doublet at 5.72 ppm with coupling $^3J \approx 8.0$ Hz. This doublet is attributed to the NH amide formed in the synthesis of *pseudo*-peptides by Ugi-4CR derived from the R3 isocyanide component. This correlation proved that *C*-12 is a *C*H attributed to the shift 48.9 ppm.

Unequivocally, the last *C*H at 59.7 ppm belongs to *C*-1, which has a COSY correlation with 4.30 ppm. This signal is a multiplet attributed to the *H*-1 of α-carbon in pyrrolidine ring. Moreover, the aliphatic zone shows eight-methylene groups for the five- and six-membered cyclic rings (see TABLE 2.6).

The ^{1}H NMR of **69** shows 5 protons in the aromatic zone corresponding to the phenyl group of the N-substituent (R^1=N-substituent) (see above spectrum in FIGURE 2.3). The signal of the MeBn of N-substituent (*H*-6) is a quartet at 5.12 ppm with coupling $^3J \approx 8.0$ Hz. Two singlets at 1.69 ppm and 1.53 ppm, each integrating to 3H correspond to Aib residue (R^2 = Me) (*H*-9 and *H*-10). Interestingly, the ^{1}H NMR spectra of compound **69** measured in CHCl$_3$ shows only one isomer in solution (see FIGURE 2.3) in comparison with compound **67** that has almost all signals are duplicated (see FIGURE 2.3). It is clearly seen in the ^{1}H-NMR spectra of catalyst **67** the shifts 4.74 ppm and 5.12 ppm, which were attributed to the *H*-6 proton of (*S*)-α-methylbenzyl amine corresponding to the *cis*/*trans* isomers. Moreover, when catalyst **69** shows only one signal at 5.12 ppm, compound **67** has two signals at 6.26 ppm and 5.87 ppm, again possibly due to the presence of *cis*/*trans* isomers. The CH$_3$ group also has duplicated signals with coupling $^3J \approx 8.0$ Hz at 1.69 ppm and 1.49 ppm.

The ^{1}H NMR behavior of both catalysts confirms the ocurrence of a single isomer of **69** and two isomers of **67**.

It is evident that the possibly of conformational rigidity for catalyst **69** is higher than that of **67** and could explain a single configurational isomer of **69** but gave no idea about stereo-conformation. A further conformation analysis as well as a Nuclear Overhouse Effect (NOE) study is needed, keeping in mind that NMR analysis of **69** showed almost a single configurational isomer while that of **67** showed a mixture of *cis* and *trans* isomers in solution.
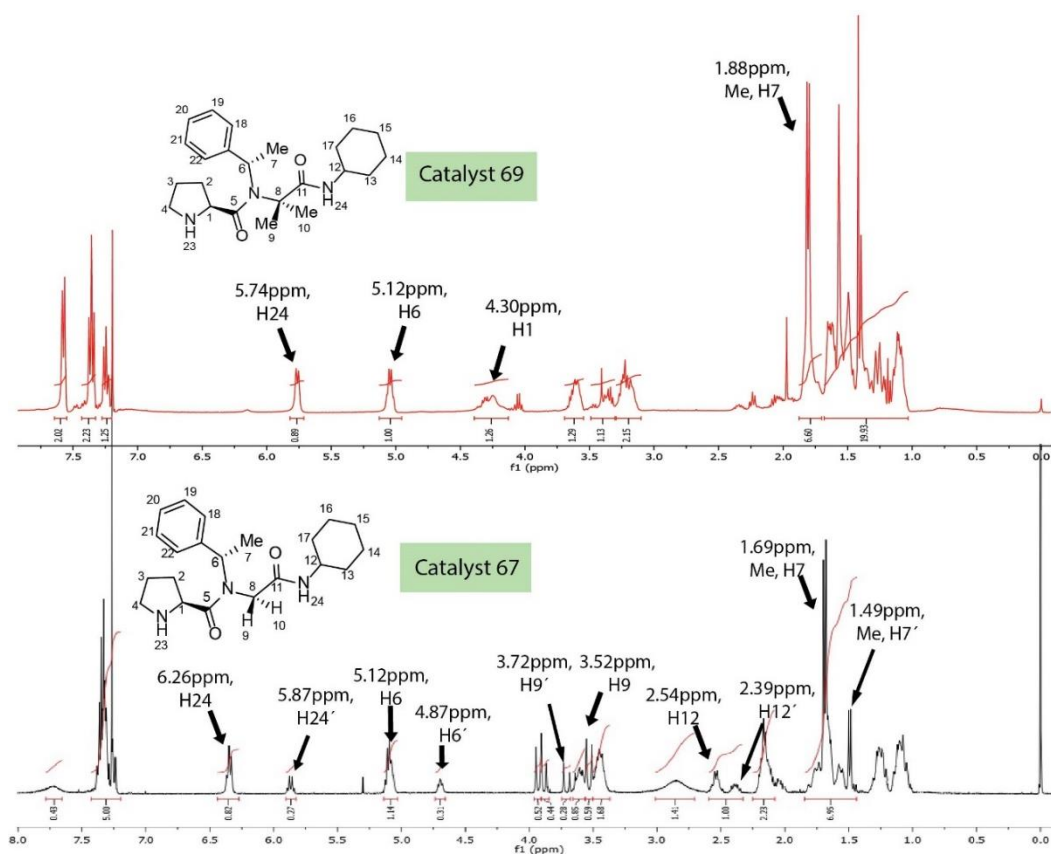
FIGURE 2.3 - 400 MHz ¹H NMR spectra in CDCl₃ of compound **67** (below) and compound **69** (above).

In order to determine the disposition of the peptidic chain with respect to the pyrrolidine faces, two NOE spectra were recorded for **69** in CDCl₃.

Initially, a NOE spectrum irradiation at 5.12 ppm (FIGURE 2.4) of *H*-6 showed NOE effects with one of the methylene *β*-hydrogen of Pro at 1.66 ppm (*H*-2), with the α-hydrogen (*H*-1) of proline at 4.30 ppm and *H*-7 the Me of Ph ring at $\delta_H = 1.89$ ppm.

Alternatively, a second NOE experiment was accomplished with irradiation of the N*H* signal of the cyclohexyl amide (R³) at 5.74 ppm (FIGURE 34 in selected figures and spectra). A NOE effects with hydrogens of the cyclohexyl ring at 1.90 ppm and 1.18 ppm, with the Me (*H*-7) of Ph ring at 1.89 ppm, and with *H*-10 of the gem-dimethyl (Xaa = *gem*-Me) groups of the Aib residue at 1.55 ppm were observed. Nevertheless, the lack of an NOE with the *α*-hydrogen of Pro at 4.30 ppm, which is positioned at the non-substituted pyrrolidine face, is a clear indication that the peptidic skeleton is directed toward the substituted pyrrolidine face.

Wherein by NOE analysis we can assume that the terminal cyclohexyl moiety is positioned at the opposite face of the Pro α-hydrogen.
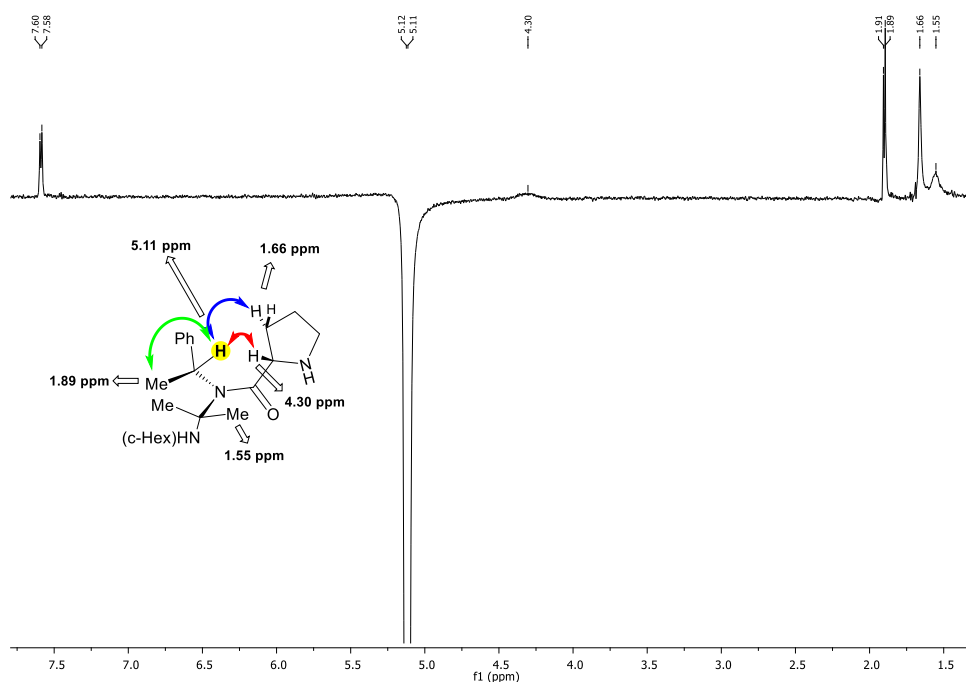
FIGURE 2.4 - 600 MHz NOE spectra in CDCl$_3$ of compound **69**. Signals of protons with NOE effect upon irradiation of the *α-H* of (S)-Me-BnNH$_2$ at 5.11 ppm.

To explore the representative structures of isomers, we chose compound **69** with Xaa = Aib (R^2 = *gem*-Me) and its analogue **67** with Xaa = Gly (R^2 = H) to analyze their conformations by MM.

In a collaboration with Prof. Marco Antonio Ferreira Barbosa from Federal University of São Carlos and Prof. Claudio Tormena from State University of Campinas we have done the conformational study of compound **67** and **69**. Monte Carlo Molecular Mechanics (MCMM) as implemented in Macromodel 9.9 was employed for this study.

Representative structures of low-energy clustered conformers were selected and reoptimized at M06-2X/6-31G(d) without the presence of any solvent (FIGURE 2.5). The conformers determined present almost the same shape. No further conclusion were observed, maybe because the behavior in solvents was not determined. Thus, for a better approximation to reality chloroform was included in the optimization of **67** and **69**.
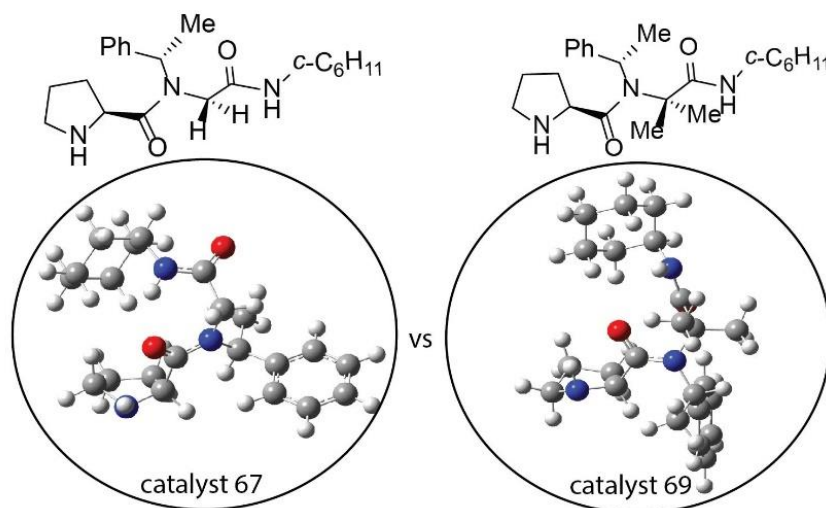
FIGURE 2.5- Low-energy optimized for compound **67** and **69** calculated at M06-2X/6-31+G(d,p) //M06-2X/6-31G(d) [SDM, in vacuum] level.

The electronic energies were refined by a single point using the 6-31+G(d,p) basis set. The relative Gibbs energies and Boltzmann population at 25 ºC in CDCl₃ where determined by MM analysis of reoptimized structures. Then, representative structures of low-energy clustered conformers were selected and reoptimized at the M06-2X/6-31G(d) level. The electronic energies were refined by single-point calculations using the 6-31+G(d,p) basis set. The relative Gibbs energies and Boltzmann populations at 25°C in CDCl₃ for all of the reoptimized low-energy conformers are shown in the Annex. It was found 673 different conformers of **67** with energies within 5 kcal mol^{-1} and subdivided in 43 groups after the clustering analysis (please for cluster structures of **67** see FIGURE 98 in the part of selected figures and spectra). The same conformational search analysis was performed with compound **69** resulting in 182 different conformers and subdivided in 26 groups after clustered-superimposed analysis (please for cluster structures of **69** see FIGURE 99 in the part of selected figures and spectra). Interestingly, a superposition of all geometries of these reoptimized low-energy conformers shows more randomly structure on **67** than **69** (FIGURE 2.6). Furthermore, the insight of methyl group in the skeleton of prolyl *pseudo*-peptides (Xaa=Me) increases the rigidity in the structure in comparisson to its congener **67** having Xaa=H.
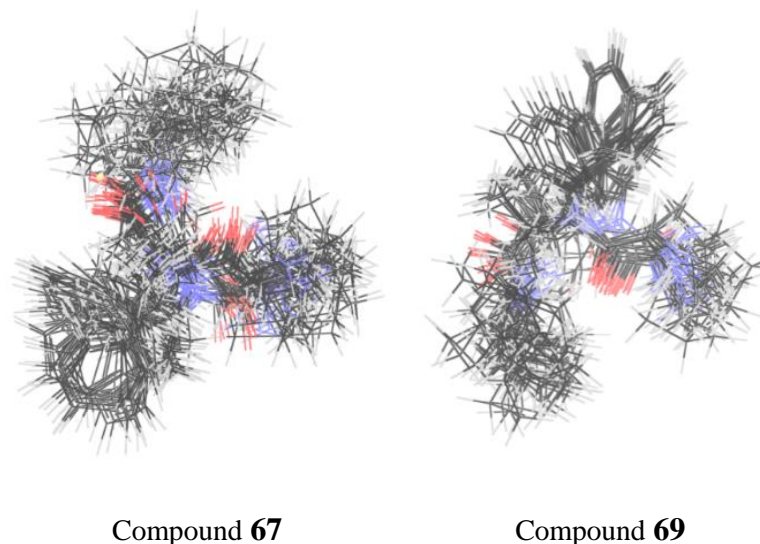
Compound **67**   Compound **69**

FIGURE 2.6 - Low-energy clustered-superimposed conformers of compound **67** and **69** calculated at M06-2X/6-31+G(d,p) // M06-2X/6-31G(d) [SDM, chloroform] level.

    The *cis*/*trans* distribution of the dihedral groups for **67** and **69** was determined and represented in TABLE 2.8; where the Ph- and (*c*-Hex)HN- substituents were selected to define the positive (+) or negative (-) orientation of the dihedrals Ψ_1 and Ψ_2. The dihedral orientation of **67** shows a 42:58 (*cis*:*trans*) ratio of isomers. Curiously **69** shows an inversion in the conformational equilibrium with a population of 98:2 (*cis*:*trans*) (TABLE 2.8). Based on these results, we assumed that this behavior is strictly related to the steric interaction between N-alkyl groups (Xaa = *gem*-Me and R^3) and the pyrrolidine ring. In this case, the *cis* isomers are lower in energy than in the catalyst **67** (Xaa= H) since the more substituted N-alkyl group, containing a quaternary carbon, is oriented toward the C=O of the pyrrolidine ring.

TABLE 2.8 - Graphical representation and excerpt of dihedral distribution for compound **67** and **69**.

		$\Psi1(+)/\Psi2(-)$	$\Psi1(-)/\Psi2(+)$	$\Psi1(+)/\Psi2(+)$	$\Psi1(-)/\Psi2(-)$
Compound **67** (R = H)	*cis*	0.1	39.2	2.6	0.0
	trans	42.0	0.0	0.7	15.2
Compound **69** (R = Me)	*cis*	17.3	9.9	17.3	53.6
	trans	0.0	0.0	0.0	1.9

The geometries of clusters **36**-*trans*, **11**-*trans*, and **20**-*cis* (FIGURE 2.7), Boltzmann population, and Gibbs energies of isomers involving the main *cis*:*trans* isomerization process of **67** were represented in FIGURE 2.7. We found that the more populated *trans*-isomers were the Ψ_1 dihedral-isomers **11**-*trans* (31%) and **36**-*trans* (15%) (FIGURE 2.7). A persistent HB between the oxygen lone pairs $LP_{O\,(1\,and\,2)}$ of tertiary amide carbonyl group and the pyrrolidine $\sigma^*_{N–H}$ group (NH--O=C) in a wide sort of conformers was noticed. Also, the transition states (**TS**) **TS-1** that represents the *cis*:*trans* equilibration of more populated **11**-*trans* (31%) to **20**-*cis* (26%) isomers were studied, giving an activation energy of 21 kcal/mol, and explaining the isomerization of catalyst **67** in the NMR time-scale (please see FIGURE 2.3).
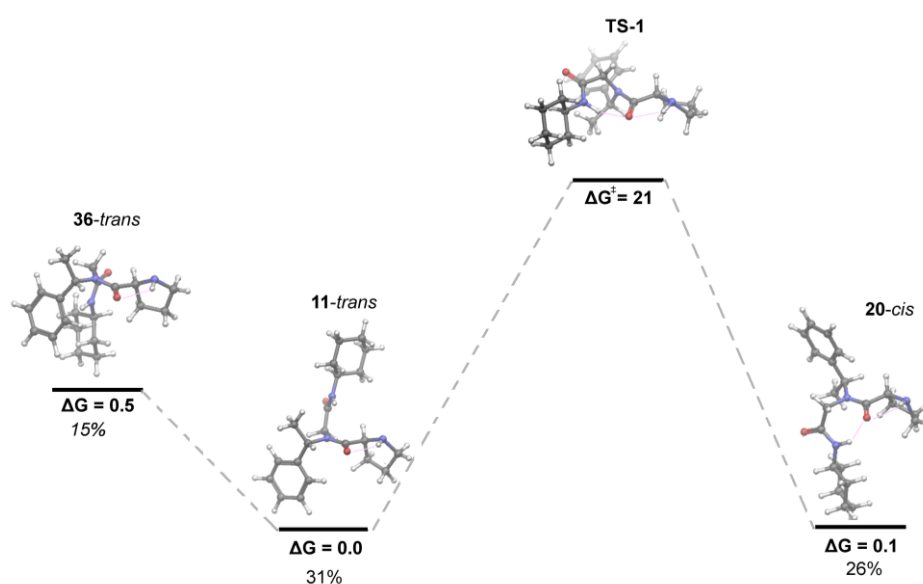
FIGURE 2.7 - Relevant low-Gibbs energy *cis*:*trans* amide conformers and transition state of compound **67** at M06-2X/6-31+G(d,p) // M06-2X/6-31G(d) [SDM, chloroform] level.

The study of **69** was done by the same way. FIGURE 2.8 represents the geometries of clusters **1**-*trans*, **17**-*cis*, and **26**-*cis*, Boltzmann population, and Gibbs energies. The **1**-*trans* (1.9%) and the lowest-energy **26**-*cis* (33%) isomers adopted a $\Psi1(-)/\Psi2(-)$ orientation, directing axially (according to imaginary plane of carbonyl of tertiary amide) the Me- group of PhC(Me)(H)- substituent. This orientation is directed by steric clashes involving the equatorial N-alkyl H $\Leftrightarrow$ Me interaction presented in **1**-*trans*, while a Me $\Leftrightarrow$ Me interaction increases **17**-*cis* (6.1%), a Ψ_1 dihedral-rotamer of **26**-*cis* (FIGURE 2.8) in 1 kcalmol⁻¹ in energy. In the same way of **67**, it was observed for **69** (FIGURE 2.8), a persistent hydrogen bond involving the pyrrolidine $\sigma^*_{N–H}$ group (NH--O=C). Curiously, the transition state **TS-2**, representing the main *cis*:*trans* isomerization, leads to an activation energy of 16 kcal.mol⁻¹, 5 kcal.mol⁻¹ lower in

energy than that observed for **67**. Nevertheless, **69** presented in NMR (please see FIGURE 2.3) time-scale solely one isomer due to the high energetic preference for the *cis*-isomer.
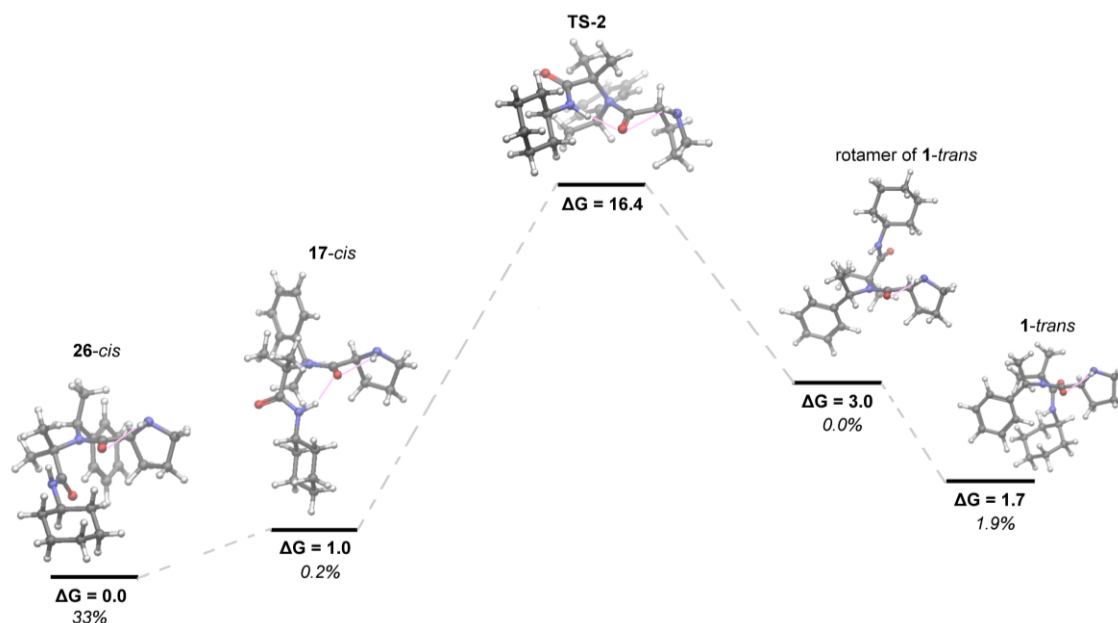

FIGURE 2.8 - Relevant low-Gibbs energy *cis*:*trans* amide conformers and transition state of compound **69** at M06-2X/6-31+G(d,p) // M06-2X/6-31G(d) [SDM, chloroform] level.

This conformational study by MM of compound **69** fully agrees with the *cis* isomer structure of **69** discussed before (FIGURE 2.4), wherein the terminal cyclohexyl moiety is positioned at the opposed face of the Pro α-hydrogen.

The knowledge of the conformational behavior of this class of catalyst is extremely important. Understanding the influence of substituents in the selective blocking of enamine faces will help us to understand the obtained results.

In most amine-catalyzed Michael addition, high *syn*-selectivity is noticed and can be explained by the acyclic synclinal transition state model. We know that the catalyst controls the geometry of the enamine. However, the mode of nitroalkenes approach depends upon the side chain pendant to the catalyst in some way, either by electronic orientation or by steric effects as previously discussed.

Catalyst **69** gave the major enantiomer (*2R,3S*)-2-ethyl-4-nitro-3-(3-nitrophenyl)butanal (*dr.* 94:6 (*syn*:*anti*); 98% ee, entry 9, TABLE 2.5). According to the above results we hypothesized that the *cis* conformer of **69** is the major conformer and the peptidic skeleton is overlapping the pyrrolidine face. In the same way, the peptidic skeleton might be blocking one face during the enamine formation and consequently leads to a high enantioselectivity.

To assess whether one of the pyrrolidine face is being blocked, a conformational search was performed for the *s-trans*-enamine derived from catalyst **69** and the aliphatic aldehyde.

We have determined the optimized lowest-energy structure of the enamine with *E* configuration, in toluene as a best solvent for Michael addition. Cluster **13** (please see FIGURE 100 in selected figures and spectra) was the lowest-energy determined structure. FIGURE 2.9 shows a significant overlap of the peptidic skeleton to the ***Re***-face, which according to Seebach's topological model explains the high enantioselection of **69**.
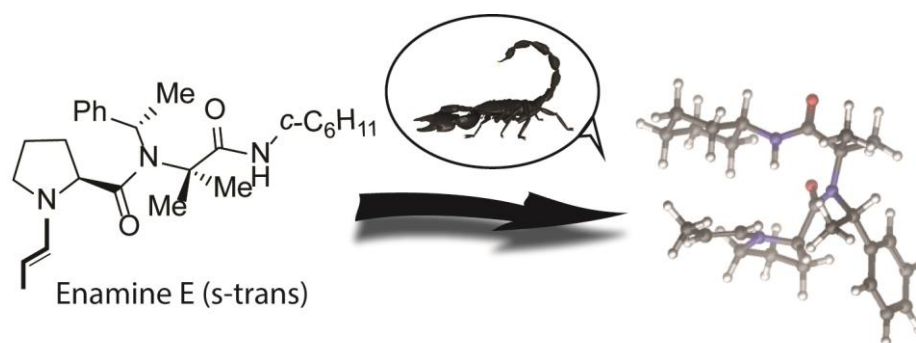
FIGURE 2.9 - Lowest-energy structure of the enamine *E* (*s-trans*) derived from catalyst **69**.

FIGURE 2.9 clearly shows that the face (***Re***-face) of the enamine is totally blocked by the peptidic skeleton (literally as a scorpion) and affirms the configuration obtained for *2R,3S* of compound **78**. Thus, now we can clearly justify how this catalyst works in the configuration of enamine *E* (*s-trans*) and its influence in the enantioselectivity for Michael adducts.

2.4 Polymeric chiral prolyl *pseudo*-peptide catalysts: Application in the Michael reaction as heterogeneous catalysts

Based on the source of biomass, biofuels are classified broadly into two major categories: a) woody (lignocellulose) and b) non-woody (sugar, starch, oils/fats). However, substantial amounts of potentially valuable by-products are produced.

Furfural is an aldehyde that can be obtained from hydrolysis of agricultural residues of sugar cane, corn and wheat. Most of the furfural produced worldwide is converted into furfuryl alcohol (**FA**) by a cheap process. [78] This latter furanic monomer can be easily polymerized through cationic condensation reactions. This polymer has a number of applications, such as utilization as precursor to synthesize nanostructured carbons and polymer nanocomposites for catalysis. [79] It is well known that the polymerization of **FA** by acid catalysis is very complex, and the resulting polymer is black, amorphous, and crosslinked.[80,81] Some authors refers that

polyfurfuryl alcohol (**PFA**) contributes to the formation of brown color in heated foods, in addition to the Maillard and caramelization reactions (*i.e*, brown color of roasted coffee).[82] SCHEME 2.2 shows the general accepted mechanism of **PFA** formation promoted by acid catalysis.

According to the results obtained with catalyst **69**, we have been attracted to insert a polymerizable (furan ring) group in the prolyl *pseudo* peptide skeleton using the Ugi-4CR and further polymerization of this monomer in presence of monomer **FA** and a Brönsted acid. The resulting polymer can be used in heterogeneous catalysis as well as in continuous-flow chemistry.
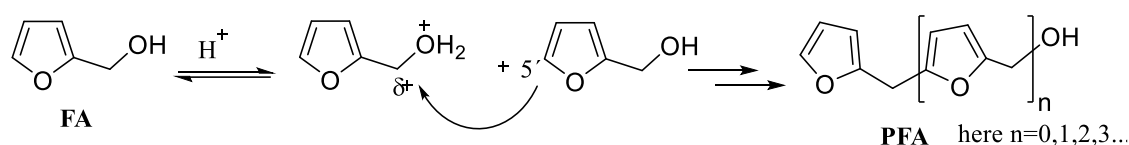
SCHEME 2.2 - General mechanism of polymerization of **FA**.

Keeping in mind that the polymerization of **FA** follows an addition of 5´-furan ring to the CH_2 of another molecule (SCHEME 2.2), we prepared new prolyl *pseudo*-peptides **87** and **88** with a furan ring pendant that will act as nucleophile during the copolymerization process (SCHEME 2.3).

An initial approach to the synthesis of the new prolyl *pseudo*-peptide catalysts, were focused on the variation of the *N*-substituent group (R^2 of amine) with the employment of methylfurfuryl amine, while acetone and cyclohexylisocyanide were kept as fixed components to guarantee the conformation type Aib as previously discussed in this thesis. Afterwards, we changed the isocyanide component (R^3) with methylfuryl isocyanide and kept the amine S-(α)-MeBn and acetone as oxo component. A solution-phase Ugi-4CR procedure was employed for all catalysts with little changes; both catalyst were kept in salt form after boc-deprotection procedure, giving the new catalysts **87** and **88**.

SCHEME 2.3 represents the adopted methodology for the synthesis of prolyl *pseudo*-peptides polymers from copolymerization of catalysts with **FA**.

The copolymerization of **FA** with TFA salts of **87** or **88** in $CHCl_3$ follows the adapted procedure reported by Martínez and co-workers.[83] The proceedures starts from green color solution that, with the passage of time, turns brown, then dark and in some cases even a black color is observed. The formation of brown color of the aliphatic **FA** arises from the formation of conjugated sequence, due to the successive proton and hydride ion losses. Base-neutralized

polymers **89** and **90** were isolated by precipitation in petroleum ether. The resulting dark solid was ground until 45μm diameter of particles size, obtaining the new prolyl-*pseudo* peptide polymers derivatives **89** and **90** (SCHEME 2.3).
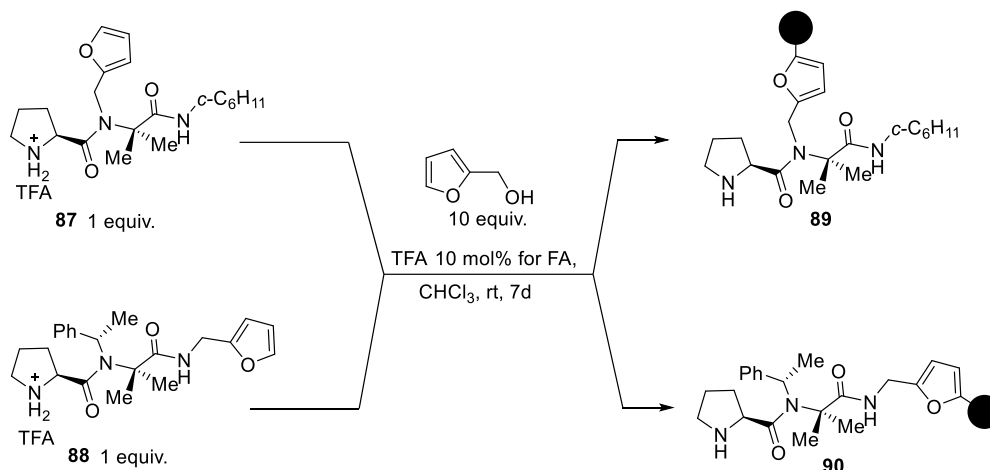
SCHEME 2.3 - Synthesis of polymeric chiral prolyl *pseudo*-peptide catalysts **89** and **90**.

The microanalysis of polymers **89** and **90** shows a functionalization of 0.64 mmolg^{-1} and 0.33 mmolg^{-1} of the catalysts **87** and **88**, respectively (calculation based on the content of nitrogen by CNHS analysis).

The FT-IR spectra of polymers **89**, **90** and **PFA** are shown in FIGURE 2.10. The main characteristic bands for **89**, **90** and **PFA** are similar. The band at 3500 cm^{-1} arises from OH residue groups of **FA**. The band at 2930 cm^{-1} is attributed to the sp^3 carbons. The band at 1720 cm^{-1} is assigned to the carbonylic structure that was formed due to the opening of some furan rings and for **89** and **90** for the carbonyl present in **89** and **90**. The band at 1420 cm^{-1} is attributed to aliphatic segments. The band at 1320 cm^{-1} arises from the ring stretching modes of the 2-substituted furan rings. The band at 1100 cm^{-1} is attributed to C-O stretching. The band at 1038 cm^{-1} is attributed to aliphatic segments. The band at 767 cm^{-1} is attributed to 2,5-disubstituted furan rings. In addition, there are no noticeable differences between the FT-IR spectra of **PFA**, **89** and **90** (FIGURE 2.10).
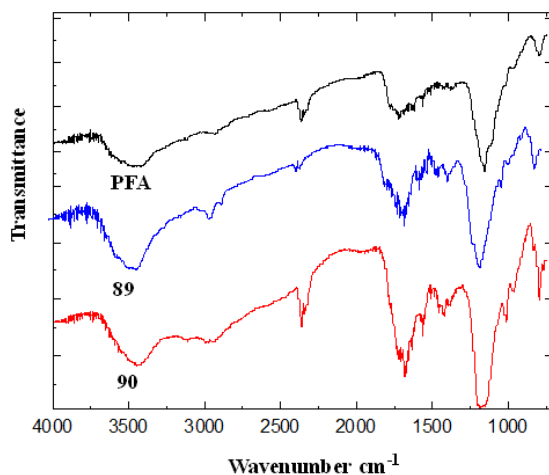
FIGURE 2.10 - FT-IR spectra of polymers **PFA** (black), **89** (blue) and **90** (red) in the range of 4000–600 cm^{-1}.

Furthermore, the thermo-oxidative degradation (TGA) pathway of **PFA**, **89** and **90** has been examined. FIGURE 2.11 represents the weight loss during the heating of samples. As we expected, **89** and **90** polymers are less stable than neat **PFA**. Co-polymers **89** and **90** being decomposed clearly in a range of 250-350 ℃ temperature than **PFA**. The first degradation step starts only above 250 ℃, corresponding to the pseudo-peptides used previously in the formation of **89** and **90**. At T>400 ℃ is stable and the polymers began depolymerization as well as **PFA**. Such behavior proved the incorporation of catalysts in the matrix of **PFA** occurs but it is less thermo stable than its **PFA** matrix, as total weight lost is seen at a range of 250-350 ℃. Thus, the TGA shows that they have thermo-stability.
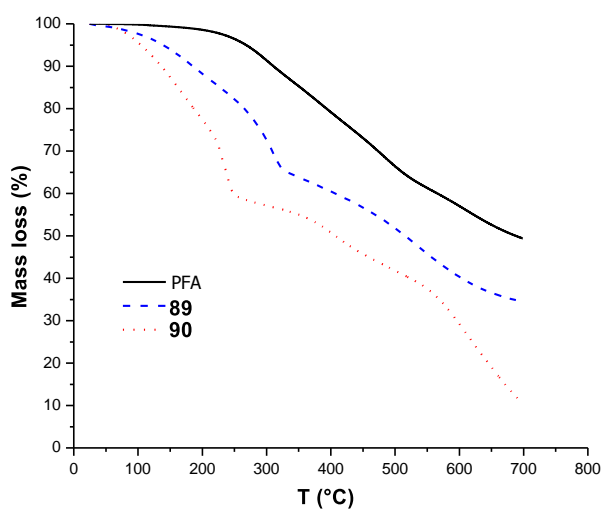
FIGURE 2.11 - Variation of mass vs. temperature measured by TGA for the **PFA**, **89** and **90** conducted under oxidative atmosphere at 10 ℃ min^{-1}.

After polymer characterization, we next evaluated their catalytic properties in the conjugate addition between *n*-butanal and *β*-nitrostyrene.

As mentioned above, toluene is the best solvent for our previous system using 10 mol% of catalysts. Then, we carried out the reaction under the same reaction conditions with **PFA**, polymers **89**, **90**, and catalyst **91**. As expected, the **PFA** did not produce Michael product (entry 1, TABLE 2.9) as the lack of pyrrolidine ring does not allow the formation of compound **78**. On the other hand, **89** and **90**, which contain catalyst immobilized into the polymer, only gave moderate yield (58%) in comparison with the non-immobilized catalyst **91**, which gave excellent yield (90%, entry 4, TABLE 2.9). Changes in the side chain of *N*-substituents residue R^1 were improbable to give good stereoselectivity.

Interestingly, the lack of Me- group in furfuryl amine in the residue R^1 (**89**) is probably the cause of a decrease of ee and *dr.* (entry 4, TABLE 2.9). In comparison, catalyst **69** having (S)-α-MeBn group in the residue R^1 has the best enantioselection (*dr.* 94:6 (*syn:anti*); 98% ee, entry 9, TABLE 2.5). Then, both residues R^1 and R^3 affects the enantioselectivity in the Michael reaction.

TABLE 2.9 - Asymmetric Michael reaction of *n*-butanal and *β*-nitrostyrene. Screening of different polymer catalysts in batch conditions.
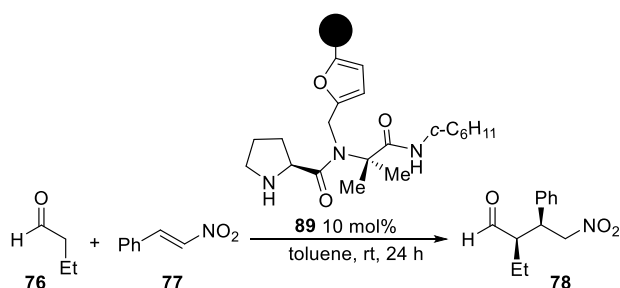
Entry[a]	Catalyst	Yield (%)[b]	dr. (syn/anti)[c]	ee (%)[d]
1	**PFA**	-	-	-
2	**89**	58	95:5	84
3	**90**	52	94:6	29
4	**91**	90	82:18	84

a) All reactions were conducted using 3 equivalents of *n*-butanal and 0.25 mmol of *β*-nitrostyrene in 1 mL of toluene. b) Yield of isolated product. c) Determined by ^{1}H NMR spectroscopy analysis. d) Determined by chiral-stationary phase HPLC analysis.

As noted, this results are in agreement with the previously discussed for the 3D conformation of prolyl *pseudo*-peptide structure determined by MM of enamine formation; where the residue R^3 blocks the Si face of the enamine. Catalyst **90** is pendant for the R^3 component, thus no 3D conformation like a scorpion is formed; consequently the stereoselectivity drops considerably (entry 3, *dr.* 94:6 (*syn:anti*); 29% ee, TABLE 2.9).

The screening of solvents with catalyst **89** was evaluated (TABLE 2.10) in order to determine the effect of reaction conditions in the catalytic efficiency and stereocontrol of this type of polymers. As shown in TABLE 2.10, the reaction yields and enantioselection varied significantly when polar solvents were tested (entries 6 and 7). The results are similar to the previously reported by **62** (entry 4, TABLE 2.4). In general, the reaction proceeds more rapidly in polar solvents.

TABLE 2.10 - Solvent screening for asymmetric Michael reaction of *n*-butanal and *β*-nitrostyrene catalyzed by **89** in batch conditions.

Entry [a]	Solvent	Yield(%) [c]	*dr.* (*syn:anti*) [d]	ee (%) [e]
1	Toluene	58	95:5	84
2	THF	83	93:7	77
3	Acetonitrila	72	94:6	54
4	Hexane	54	95:5	56
5	Hex:iso(9:1)	70	96:4	68
6	Isopropanol	90	97:3	61
7	Ethanol	69	96:4	53
8	H₂O	76	96:4	66
9 [b]	---	72	96:4	63

a) Reactions using 3 equivalents of *n*-butanal and 0.25 mmol of *β*-nitrostyrene in 1 mL of solvent. b) Reaction using 6 equivalents of *n*-butanal. c) Isolated yield. d) Determined by ^{1}H NMR spectroscopic analysis. e) Determined by chiral-stationary phase HPLC analysis.

Higher yield was obtained using isopropyl alcohol (iPrOH), (90%, entry 6, TABLE 2.10), in comparison with ethanol, where a decrease in terms of yield was observed (69%). In fact, non-polar solvents are required for a good stereocontrol. However when hexane was used instead of toluene, the enantioslection was poor (56% ee, entry 4, TABLE 2.10). This is attributed to the insolubility of *β*-nitrostyrene in hexane. The mixture *n*-hexane/*i*-PrOH (9:1)

increases the stereoselectivity and efficiency (*dr.* 96:4 (*syn*:*anti*); 68% ee, entry 5, TABLE 2.10).

When the reaction was performed in the absence of solvent or in water, the behavior is almost the same and no difference was found in terms of stereoselectivity and efficiency (entries 8 and 9, TABLE 2.10). The corresponding reaction in THF showed moderate to good stereoselecitivy (*dr.* 93:7 (*syn*:*anti*); 77% ee). Finally, toluene was chosen to be the best solvent for this system (entry 1, TABLE 2.10).

One disadvantage to mention for these chiral prolyl *pseudo*-peptide polymers is their impossibility to recover from the reaction system. The powder organic material results to be less dense in almost all solvents employed and this results an inconvenient for catalysts recovery by decantation. In addition, gravity filtration was employed but the powder material remains in the filter paper. To overcome this problem, we then charged an HPLC column for a continuous-flow approach.

For the implementation of a continuous-flow version of the Michael reactions, compound **89** was packed into a stainless-steel column ($\varnothing = 0.21$ cm (diameter), $l = 15$ cm (length), particle size $= 45\mu$m). The main features of the resulting packed microreactor **R1** was determined by pycnometry methodology (TABLE 2.11).[84] This method consists in filling the microreactor **R1** successively with two distinct solvents (here noted as 1. ethanol and 2. *n*-hexane) and then weight the filled microreactors accurately. The difference between the masses of a filled reactor and divided by the differences of densities of solvents permits to calculate the microreactor void volume (V_0) (dead volume).[85] This feature is important to know because it gives an idea of the volume unutilized into **R1**. The catalysts loading was kept as determined by microanalysis previously described for compound **89**. Packing amount (w_{tot}) was also determined by pycnometry. A porosity (ε_{tot}) of 0.67 is an optimum value for this material, which is according with the accepted values. One of the most important feature of microreactor for continuous-flow chemistry is the residence time (τ). Residence time is known as the time in which a substrate passes through the microreactor **R1** without interacting. In some case, this residence time is measured by the time needed to pass a determined dye through **R1**. In this work, it was calculated by dividing V_0 by the arbitrary used flow rate (ϕ) at 2.5 μL min^{-1}. (TABLE 2.11)

TABLE 2.11- Main Features of the microreactor **R1**.

Catalysts loading (mmol g^{-1}) [a]	Packing amount w_{tot} (mg) [b]	V_0 (µL) [c]	V_G (µL) [d]	V_{bed} (µL) [e]	τ (min) [f]	ε_{tot} [g]
0,639	264	349	519	170	140	0,67

a) Determined by elemental analysis. b) $w_{tot} = V_0\ \delta_0 + w_{ads} + w_{hw}$ c) $V_0 = w_1 - w_2 / \delta_1 - \delta_2$ d) Geometric Volume $V_G = \pi hr^2 * 10^3$ (h=15cm, r=0.105cm). e) $V_{bed} = V_G - V_0$ f) residence time calculated at flow rate $\phi = 2.5$ µL min^{-1}, $\tau = V_0/\phi$ g) Total porosity $\varepsilon_{tot} = V_0/V_G$

The study of the Michael reaction on continuous-flow model by using reactor **R1** started with the optimization of flow rate (TABLE 2.12). Initially a solution of β-nitrostyrene (1 equivalent, 0.25 M), n-butanal (3 equivalents, 0.75 M) at 2,5 µL min^{-1} (τ = 140 min) was pumped with a syringe-pump (FIGURE 2.12). After 22 h, only moderate conversion of the *β*-nitrostyrene in toluene was observed, the efficiency of the process was poor giving a productivity of 0.28 mmolproduct h^{-1} mmolcatalyst^{-1}.
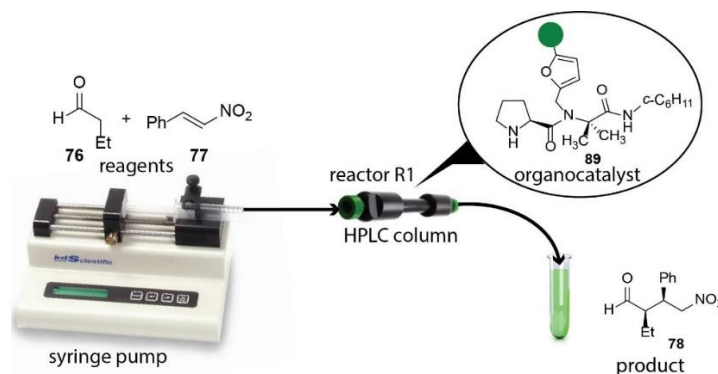
FIGURE 2.12 - Continuous-flow model of Michael reaction adopted in this study.

The concentration was chosen by considering the retention behavior of *n*-butanal and *β*-nitrostyrene in **R1**. It has clearly shown that the conversion of starting material is increasing until 24 h, after that, the reactor productivity decreases considerably. We hypothesized that the higher residence time of *β*-nitrostyrene in the reactor **R1** may lead to a lower yield or the catalyst may acquire inactivation. In this case, all the substrates were injected into the reactor **R1** coupled to HPLC system where the retention time of each substrate in reactor **R1** was measured by UV detector at a wavelength of 210 nm. A retention time of 70 min for *β*-nitrostyrene for a flow 0.1 mlmin into the reactor **R1** was observed (FIGURE 2.13).

TABLE 2.12 - Continuous flow optimization of Michael reaction between *n*-butanal and *β*-nitrostyrene using the microreactor **R1**.

Entry [a]	Flow rate $\phi(\mu L\ min^{-1})$	Running time (h)	Residence time $\tau(min)$[b]	Conversion [c]	*dr.* (*syn:anti*) [e]	ee% [f]
1	2.5	0-10	-	-	94:6	72
2	2.5	10-12	140	25	95:5	74
3	2.5	12-14	140	27	95:5	75
4	2.5	14-16	140	30	95:5	74
5	2.5	16-18	140	31	95:5	73
6	2.5	18-20	140	38	95:5	74
7[d]	2.5	20-22	140	42	95:5	72
8	1	24-36	349	43	94:6	72
9	1	36-48	349	21	94:6	72
10	1	48-72	349	24	94:6	72

a) Reactions conditions: HPLC column (0.21cm i.d. x 15cm, containing 0.639 mmol of catalyst); *β*-nitrostyrene (2.5 mmol, 1 equi, 0.25M), *n*-butanal (3 equi, 0.75M) in *n*-hexane/Iso (90:10) mixture. b) Residence time calculated as void volume/rate flow ($\tau=V_0/\phi$). c) Conversion determined by ^{1}H NMR spectroscopic analysis. d) Productivities are measured in mmolproduct h -1 mmolcatalyst -1. e) *dr.* determined by ^{1}H NMR spectroscopic analysis. f) Determined by chiral-stationary phase HPLC analysis.

Then, this preferential occupancy of the packing material by *β*-nitrostyrene (50 times as residence time calculated) limits the formation of the Michael product and, consequently, lowers the chemical efficiency. However, the enantioselection was constant with the time, having no change with the possible erosion by the excess accumulated substrate into **R1** (TABLE 2.12).
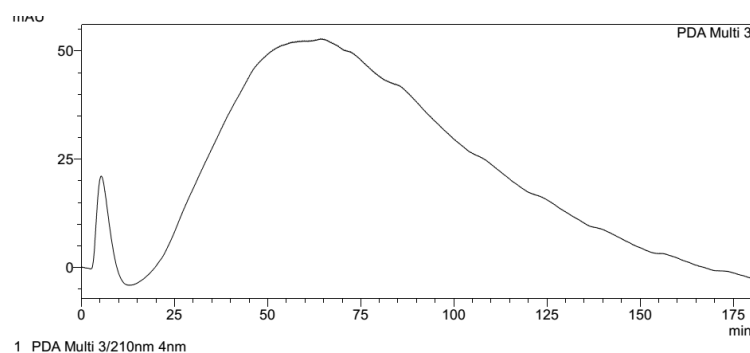
FIGURE 2.13- HPLC chromatogram of *β*-nitrostyrene directly injected to the microreactor **R1**.

Finally, the global yield isolated of compound **78** was 42% determined after flash column chromatography. This value is in accord to the conversion determined during the continuous-flow study.

Conclusions: Chapter 1

The results presented in this chapter showed that solution-phase combinatorial approaches based on I-MCRs are convenient tools for the discovery of organocatalysts for asymmetric organic transformations. This was illustrated by the Ugi-4CR-based generation of a small combinatorial collection of new prolyl *pseudo*-peptides and the screening of their catalytic efficacy in the asymmetric conjugate addition of aldehydes to nitroolefins. Thus, variation of three elements of diversity at the Ugi-derived *N*-substituted peptide led to fourteen prolyl *pseudo*-peptides catalysts of the type Pro-*N*-R^1-Xaa-NHR^3 in moderate to good yields (40-93%). Besides, it led to the discovery of catalysts providing good to excellent stereocontrol and catalytic efficacy, while provided new insights into their structure catalytic-activity relationship where catalyst **69** showed to be the best in Michael addition (85% Yield, *dr.* 96:4 (*syn*:*anti*); 98% ee). A conformational study explained the greater conformational rigidity and stereoselection provided by catalyst **69**, bearing the *N*-substituted amino acid Aib as *C*-terminal residue, compared to **67** that have Gly at the same position.

Considering the diversity-oriented character of I-MCRs, we introduced a multicomponent strategy for the one-pot assembly of chemical architectures having special functionalities that are suitable for further polymerization to obtain two novel prolyl *pseudo*-peptide polymers derivatives organocatalysts. Two different prolyl *pseudo*-peptide catalysts were produced by the Ugi-4CR and then polymerized using furfuryl alcohol as a renewable feedstock. Catalyst **89** and **90** were examined as heterogeneous organocatalysts in the direct Michael addition of enamines to nitroolefins to produce compound **78** in 84 and 29 %ee, respectively. Furthermore, a continuous-flow system using a syringe pump and HPLC column previously charged with catalyst **89** was setup. The high retention time of *β*-nitrostyrene into the reactor **R1** led to low conversion of starting materials (42%) with a productivity of 0.28 for 22 h of reaction. Michael adduct was produced in good *dr.* 95:5 (*syn*:*anti*) and moderate enantioselectivity 72% ee.

Perspectives: Chapter 1

→ Due to the results presented for the prolyl *pseudo*-peptide catalyst **69** in Michael reaction we consider that new asymmetric reactions should be tested in order to extend the scope of the catalyst.

→ Considering that the prolyl *pseudo*-peptide polymer derivatives are easily obtained from renewable feedstock, they could be employed as scavenger in order to give new application to the materials obtained.

Chapter 2

3 Introduction: Chapter 2

Isocyanide-based multicomponent reactions (I-MCRs) traditionally stand among the most versatile methods to produce medium-size cyclic compounds. These processes do not only comprise great chemical efficiency and atom economy, but also enable the easy implementation of the diversity-oriented synthesis concept to cover the wider chemical space. However, I-MCRs are known to be poorly stereoselective, and as result the majority of compounds obtained by this class of reactions are formed either as racemic or diastereomeric mixtures. So far, the development of a stereoselective version of such reactions has been a great challenge for organic chemists.

Three main strategies have been employed to accomplish stereoselective I-MCRs: 1) the development of new asymmetric catalytic versions leading to enantiomerically enriched products, 2) the use of enantiopure starting materials capable to perform diastereoselective transformations, and 3) the employment of chiral auxiliaries.[86,87]

Several inputs have been reported for the first strategy. For example, the first catalytic enantioselective version of P-3CR reaction was described by Dömling and co-workers.[88] The authors performed a massive parallel screening of a large number of Lewis acid-chiral ligands combinations with stoichiometric amount of Ti(i-OPr)$_4$ combined with Taddol to promote α-hydroxyamides in moderate enantioselectivity (36 % ee).

Another example is the use of chiral aluminum-organophosphate-catalyst **92**, which catalyzes the P-3CR to obtain 2-(1-hydroxyalkyl)-5-aminooxazoles **93** in good yield (84%) but only in moderate ee (7-62%) (SCHEME 3.1).[89]
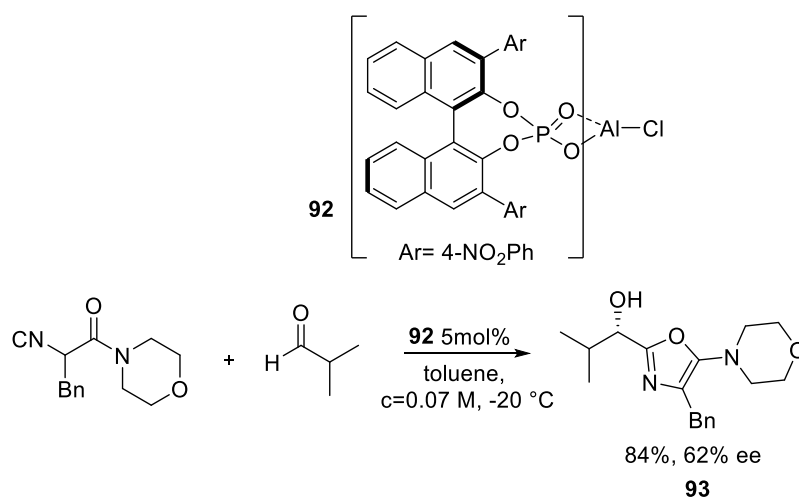
SCHEME 3.1- Enantioselective Paserinni-type reaction using catalyst **92**.

Due to the inefficiency in terms of ee, other groups have studied the use organocatalytic synthesis for this class of chiral compounds. Alternatively, an Ugi-type 3CR was employed in the synthesis of oxazoles **95** in the presence of chiral Brønsted acid **94**. High values of ee (87%) were obtained by this methodology (SCHEME 3.2). [90] Interestingly, the authors discovered a new methodology to obtain natural-like polycyclic compounds in a stereoselective manner by using an Ugi-type 4CR procedure. Compound **96** was obtained as a single diastereomer with high yield (94%) and ee (89%) (SCHEME 3.2).
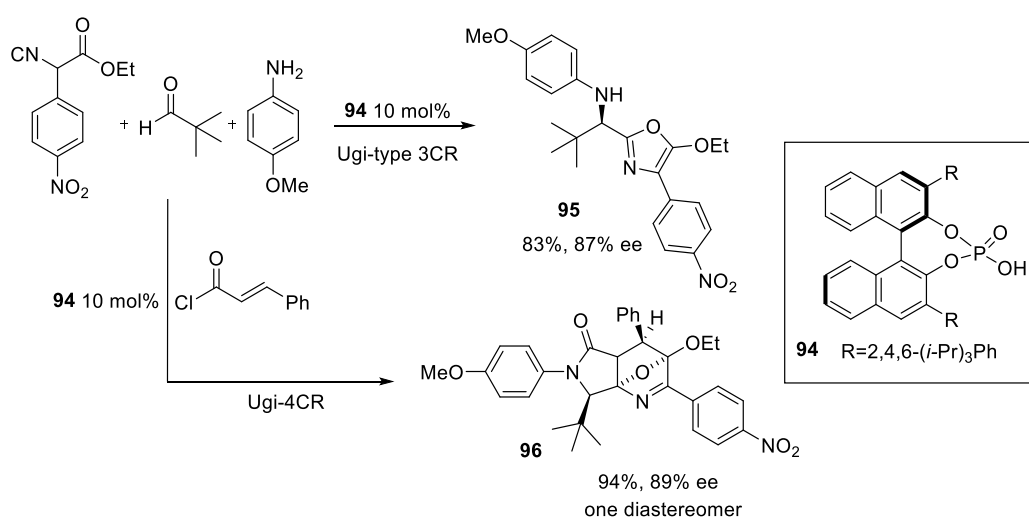
SCHEME 3.2 - Enantioselective version of Ugi-type 3CR and Ugi-type 4CR using the catalyst **94**.

3.1 Multicomponent combination to the synthesis of cyclic compounds

Most important results of the implementation of the second strategy (i.e., the use of enantiopure compounds as starting material of MCRs) rely on the utilization of chiral bifunctional scaffolds capable to perform intramolecular multicomponent transformations. It is well-accepted that intramolecular I-MCRs are more diastereoselective than their intermolecular version. A known example is the Ugi 5-center 3-component reaction (Ugi-5C-3CR) with amino acids as bifunctional scaffolds (see **A** in SCHEME 3.3), which is more diastereoselective than the classic Ugi-4CR based on the separate use of *N*- and *C*-protected amino acids as individual components. As mentioned above, the first variant of Ugi-5C-4CR to perform an intramolecular multicomponent transformation was described in 1998. [91] The *α*-homoserine, an aldehyde and isocynide component were reacted to obtain the five-member ring *N*-carbamoylmethyl-*α*-aminobutyrolactones **98** (see **A**, in SCHEME 3.3). This reaction occurs via an intramolecular acylation where the OH functional group of α-homoserine attacks the C=O of the intermediate

97 (α-adduct) to produce a lactone. Interestingly, this variant of the Ugi reaction is similar to the known classic Ugi 5-center 4-component reaction (Ugi-5C-4CR) (see **B**, in SCHEME 3.3). In this case, the solvent MeOH is the fourth component of the reaction. Linear peptoids are obtained (**100**) considering that MeOH attacks the α-adduct intermediate **99** as shown in **B**) (SCHEME 3.3). This explains why the author uses the solvent trifluroethanol (TFE) instead of MeOH in the Ugi-5C-3CR variant (see **A**, in SCHEME 3.3), in order to avoid the Ugi-5C-4CR product. However, the classic Ugi-5C-4CR has a diastereoselective version using titanium catalysts but it only works with aromatic aldehydes. [92]
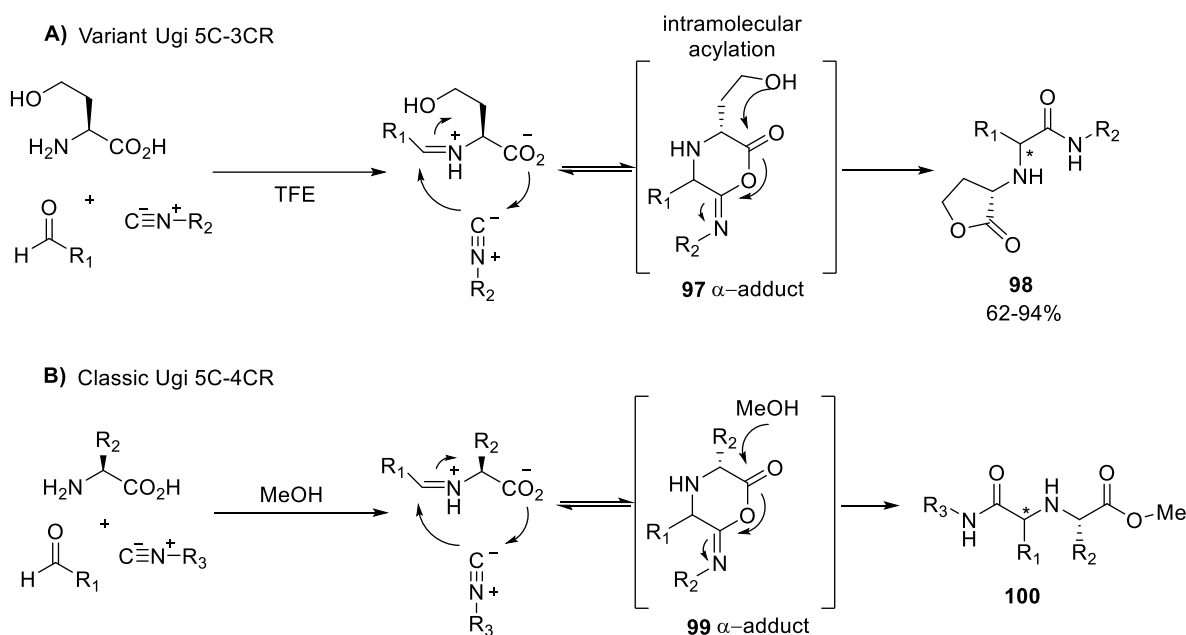
SCHEME 3.3 - A) Mechanism of Ugi-5C-3CR reaction in the synthesis of lactone **98**. B) Classic mechanism of Ugi 5C-4CR in the formation of lineal peptides **100**.

Employing the same methodology of Ugi-5C-3CR, novel 3-substituted morpholin-2-one-5-carboxamide derivatives **102** were obtained in moderate yield (30-81%) by the same group (SCHEME 3.4). [93] In this case, glycoaldehyde (**101**) was employed instead of α-homoserine. The mechanism involves the same attack of the OH group to the α-adduct intermediate. The only difference is in the intramolecular nature of the OH group attack.
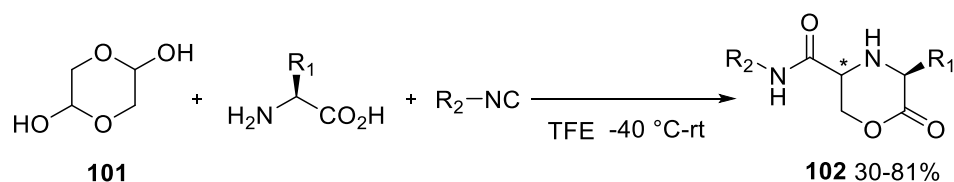
SCHEME 3.4 - Synthesis of compound **102** by an Ugi-5C-3CR.

Recently, Yudin and co-workers [94] employed chiral bifunctional aziridine aldehydes to react in MCRs/cyclization approaches. L-Phe, *tert*-butyl isocyanide, and amphoteric aziridine aldehyde were reacted by an Ugi-5C-3CR to obtain cyclic piperazinone **104** as a single diastereoisomer in excellent yield (92%) (SCHEME 3.5). The nucleophilic attack to the α-adduct is done by the NH group of the aziridine, so the diastereoselection of compound **104** is governed by the chirality of the aziridine ring.
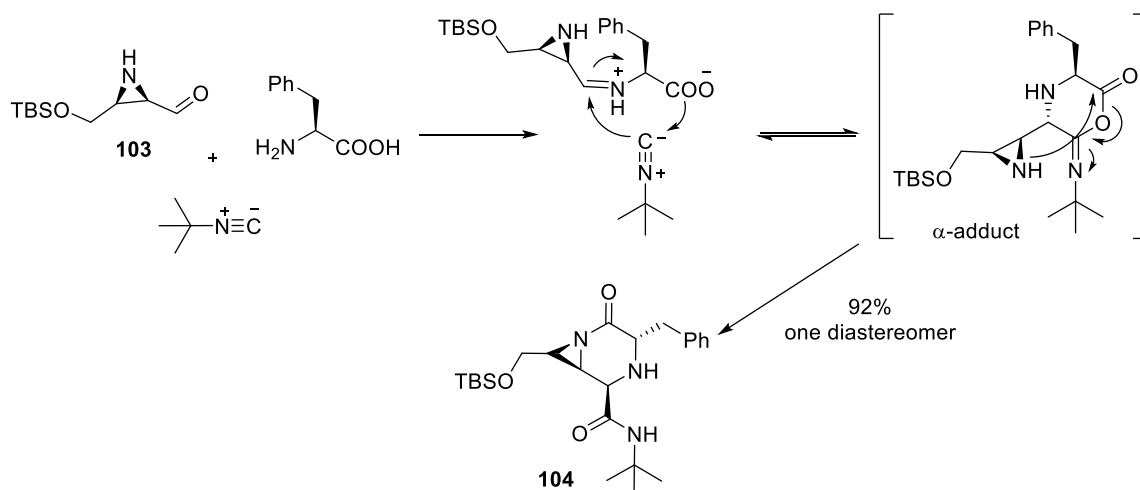
SCHEME 3.5 - Mechanism of synthesis of piperazinone **104** by an Ugi-5C-3CR.

3.2 Organocatalytic/multicomponent sequential reactions

Nowadays, there is an emerging topic of research dealing with the combination of organocalysis with IMCRs to develop new stereoselective transformations. Looking at the repertoire of IMCRs, one realizes the ubiquity of the carbonyl component, i.e. ketones or aldehydes, in these reactions. Only recently, early efforts have been directed towards implementation of an aminocatalytic asymmetric functionalization of such carbonyl functionalities followed by a subsequent IMCR.[95] Aminocatalysis has been applied with great success in the α-, β-, γ- and even ε-asymmetric functionalization of carbonyls. Hence, combination of aminocatalysis with the available repertoire of IMCRs provides endless possibilities for scaffold generation. Some works referring to this combination are in development by our group and some articles have been published.

An example developed by our group is the tandem nucleophilic epoxidation of *α,β*-unsaturated aldehydes followed by the P-3CR to access a green process of a new library of epoxy-depsipetides **106** (SCHEME 3.6).[96] Excellent enantioselectivity of epoxides **105** (>90% ee) were obtained employing catalyst **18** in a greener mixture of solvents. The *dr.* determined

was low (52:48) because of the poor stereoselectivity of the Passerini reaction carried out as second step.
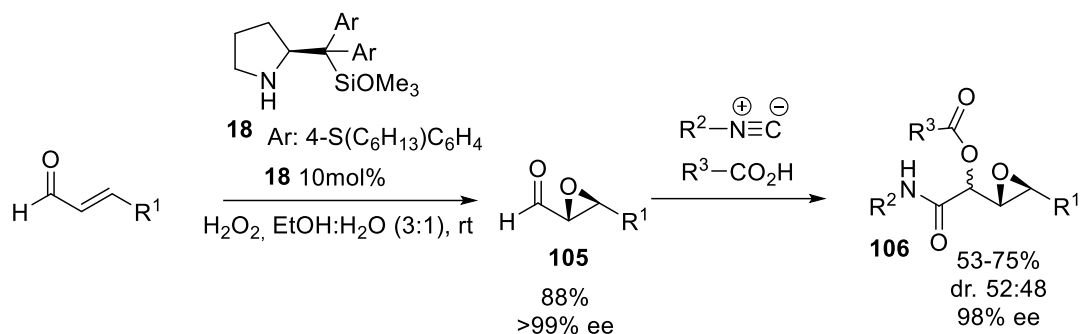
SCHEME 3.6 - Tandem organocatalytic-P-3CR reaction for the synthesis of epoxy-depsipetides **106**.

An interesting combination of organocatalysis with MCRs is the one-pot reaction of Friedel-Crafts indole alkylation followed by an Ugi 4-center 3-component reaction (Ugi-4C-3CR) as shown in SCHEME 3.7. In this case, chiral lactams (**110**) were obtained.[97] The 5-hydroxyfuran-2(5H)-one (**107**) was used as α,β-unsaturated aldehyde for iminium activation organocatalysis in the Friedel-Crafts indole alkylation. Then, by a simple intramolecular Ugi-4C-3CR, lactam (**110**) was obtained in high yield (77%) and enantiomeric relation *er.* (94:6). However, the *dr.* obtained (1:4:1) was poor, which is attributed to the new stereogenic center formed in a racemic manner in the Ugi reaction.
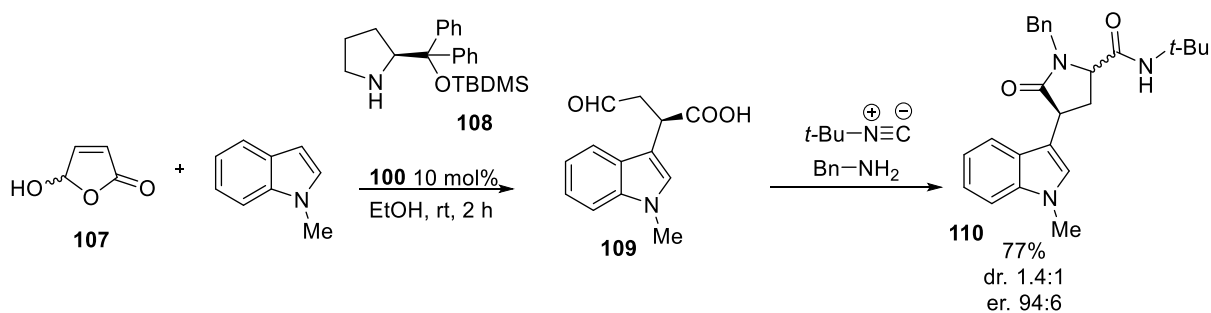
SCHEME 3.7 - One-pot organocatalytic Friedel-Crafts/Ugi-4C-3CR intramolecular cyclization.

Recently, a new methodology involving one pot sequential procedure Organocatalytic-MCRs/cyclization was described.[98] The *N*-Boc-indole-2-boronic acid was reacted with **107** in the presence of Hayashi´s catalyst to produce the bifunctional intermediate **112** (SCHEME 3.8). Then, a P-3CR was done using an isocyanide component to give α-indole-γ-substituted lactones **113** in 73% yield and good stereoselectivity (*dr.* 72:28, *er.* 90:10).
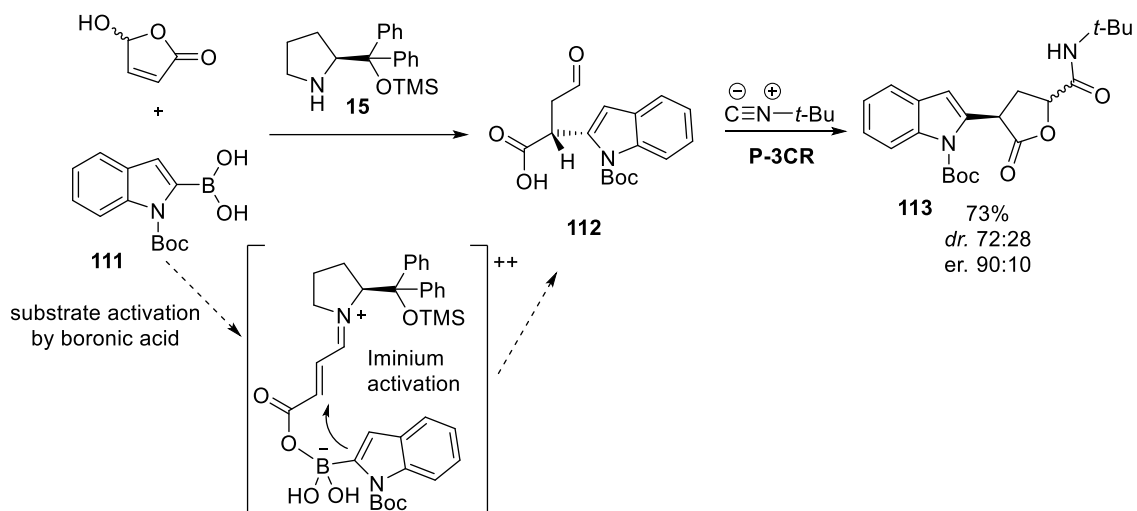
SCHEME 3.8 - One pot organocatalytic Michael reaction/P-3CR intramolecular cyclization.

As will be seen, the synthetic design of this Chapter 2 focuses on the utilization of chiral bifunctional scaffolds (obtained by organocatalysis) for the development of new, eventually stereoselective, I-MCRs.

Objectives: Chapter 2

In an endeavor to further demonstrate the potential of this concept, this chapter focuses on the development of sequential organocatalytic multicomponent sequences leading to structurally varied cyclic compounds. Considering the need of chiral starting materials to pursuit stereoselective intramolecular I-MCRs, we focused on methodologies where the organocatalytic processes provide the enantiomerically enriched compounds having two functionalities capable to react in a subsequent MCR. In especial, we will focus on developing variations of the Ugi reaction, as this class of I-MCR is considered a wonderful tool to generate cyclic compounds.

For this aim, we envisioned to employ hemiacetal, previously prepared by organocatalysis, as chiral bifunctional scaffolds aiming at perfoming subsequent multicomponent steps capable to generate cyclic compounds. Such organocatalytic/multicomponent sequences will rely on initial Michael conjugate additions followed by Ugi-type reactions.
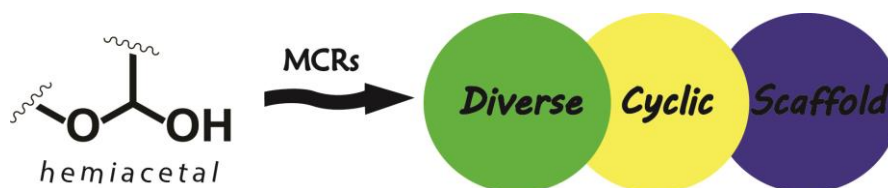
4 Results and discussion: Chapter 2

4.1 Organocatalytic multicomponent approach to obtain medium-sized cyclic peptidomimetics

As shown in FIGURE 4.1, the initial objective is the organocatalytic synthesis of enantio-rich 1-hydroxy-*trans*-3,4-disubstituted tetrahydropyrans and its subsequent utilization in Ugi-5C-3CR-based cyclization approach. As result of this synthetic design, medium-sized cyclic peptidomimetics (i.e., 9 members) will derive from natural amino acids, isocyanides, and substituted tetrahydropyrans.
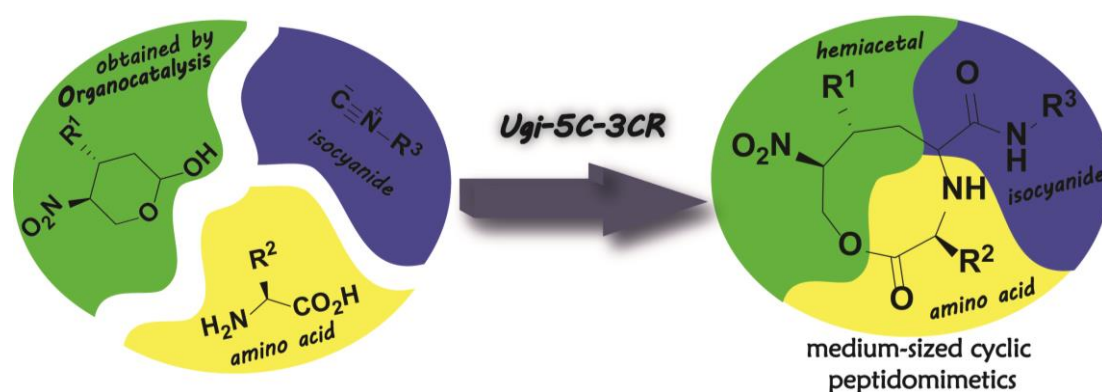
FIGURE 4.1- Ugi-5C-3CR-based cyclization approach to obtain medium-sized cyclic peptidomimetics.

A previously described, Michael reaction between α,β-unsaturated aldehydes and nitroethanol catalyzed by diphenylprolinol silyl ether (**15**) leading to 1-hydroxy-trans-3,4-disubstituted tetrahydropyrans was used as initial study of this Chapter.[99] This reaction occurs via iminium ion activation mode where catalyst **15** lowers the energy of the LUMO orbital of the α,β-unsaturated aldehyde to permit the attack of the nucleophile (nitroethanol). Steric shielding produced by catalyst **15** blocks the *Si* face of the α,β-unsaturated aldehyde, resulting in the *syn*-isomer **114** as the major product, as shown in SCHEME 4.1. An inconvenient for this reaction is the low *dr.* reported for the *syn*-isomer obtained. To solve this, a base such as NaHCO$_3$(s) is needed to convert the *syn*-isomer into the more thermodynamically stable *anti*-isomer.
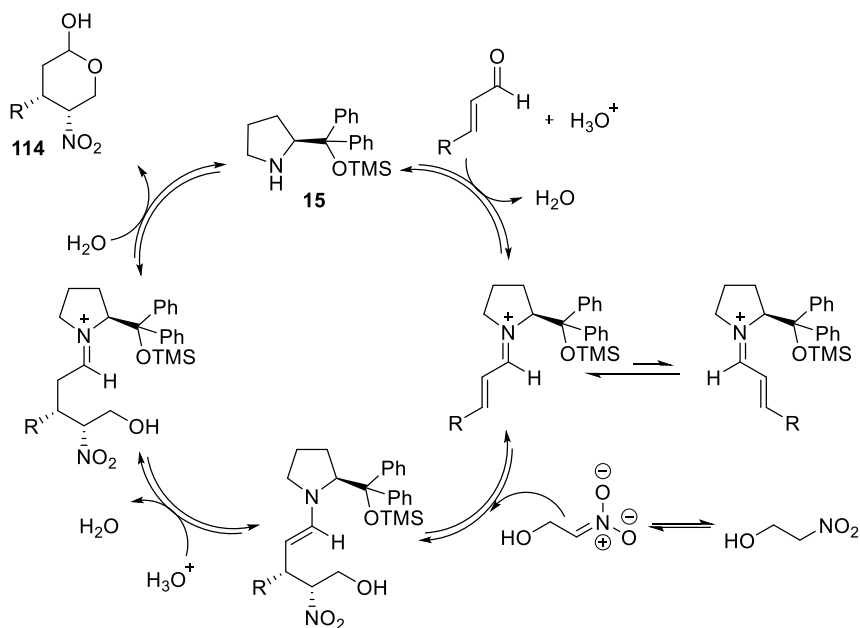
SCHEME 4.1 - Catalytic cycle mechanism of Michael reaction of nitroethanol and α,β-unsaturated aldehydes.

We tried to reproduce the conditions reported at room temperature (25 °C), using MeOH as solvent and 10 mol% of Hayashi´s catalyst, with 20 mol% of benzoic acid as co-catalyst and 3 equivalents of nitroethanol during 20 h of reaction. For this condition, the reported values are: yield = 86%, *dr.* 89:11 (*anti*:*syn*) and 95% ee. However, in our hands it was not possible to reproduce the stereoselection already reported by the authors (entry 1, TABLE 4.1), although little increase in efficiency was obtained (yield = 96%). Therefore, different catalysts were evaluated, in order to improve the ee. Unfortunately, all the catalysts examined showed lower results as compared to **15** (entries 2-4, TABLE 4.1). Then, catalyst **15** was chosen to optimize the reaction system. In the next step, we tried to enhance the preliminary results by changing the temperature. An increase in terms of ee (95%) was observed at 10 °C or even at lower temperature (-10 °C) (entries 5 and 6, TABLE 4.1). Then, 10 mol% of **15** and 20 mol% of benzoic acid at 10 °C was the initial condition selected to continue this study. As known, TFE is the preferred non-nucleophilic solvent to be used in a one pot process in the access to medium-sized rings. Unfortunately, using TFE as solvent, long time of reaction is required (72 h) and only poor yields (40%) and moderate ee (92%) were obtained. We then tried to change the solvent to EtOH, but unfortunately, the results were unsatisfactory since lower yield and ee were obtained (entry 8, TABLE 4.1). Using DCM, the ee was excellent (96%), and accordingly this solvent seems to be the best selection of choice for a tandem procedure. Nevertheless, the isolated yield was only 60%. Other optimization screening was done to evaluate the catalyst loading and the behavior with the concentration of the reaction system. Using 5 mol% of

catalyst **15** produces compound **114** in 50% yield, *dr.* 73:27 (*anti*:*syn*) and 83% ee. Moreover, 20 mol% of catalyst produces 96% of **114** with moderate selectivity (entry 11, TABLE 4.1). A more diluted reaction was also tested, but as expected, the kinetics of the reaction was slow and only 50% of isolated product could be obtained after 20 h of reaction.

TABLE 4.1- Asymmetric Michael reaction of nitroethanol and cynammaldehyde. Optimization of the system.

Entry [a]	Catalyst	solvent	Cat mol%	Temp (°C)	Yield[c] (%) [c]	*dr.* [d]	ee (%) [e]
1	**15**	MeOH	10	25	96	88:12	83
2	**12**	MeOH	10	25	34	74:26	58
3	**69**	MeOH	10	25	43	80:20	21
4	**18**	MeOH	10	25	71	83:17	75
5	**15**	MeOH	10	10	95	82:18	95
6	**15**	MeOH	10	-10	95	84:10	94
7 [b]	**15**	TFE	10	10	40	84:16	92
8	**15**	EtOH	10	10	73	88:12	91
9	**15**	DCM	10	10	60	82:18	96
10	**15**	MeOH	5	10	50	73:27	83
11	**15**	MeOH	20	10	96	86:14	84
12 [f]	**15**	MeOH	10	10	53	75:25	52
13 [g]	**15**	MeOH	10	10	-	-	-
14 [h]	**15**	MeOH	10	10	90	86:14	92

a) Reactions using 1.5 equivalents of nitroethanol and 0.6 mmol of cynammaldehyde in 1 mL of solvent. b) Reaction finished after 72 h. c) Isolated yield. d) *dr.* determined by ^{1}H NMR spectroscopic analysis. e) Determined by chiral-stationary phase HPLC analysis. f) Reaction accomplished at 0.3 M g) Using 3 equivalents of Cs_2CO_3 as base. h) Reaction using 1.5 equivalents of nitroethanol and 6 mmol of cynammaldehyde.

The ee was also affected considerably under these conditions (entry 12, TABLE 4.1). When Cs_2CO_3 (s) was used instead of $NaHCO_3$ (s), no product was obtained. Finally, a scale-up of the reaction was accomplished using six millimoles of cinnamaldehyde. A little erosion of the ee (92%) was observed after 20 h of reaction (entry 14, TABLE 4.1).

When the best reaction conditions were determined (entry 5, TABLE 4.1), we next synthesized 1-hydroxy-*trans*-3,4-disubstituted tetrahydropyrans varying *α,β*-unsaturated aldehydes (TABLE 4.2). All reactions were conducted in the presence of three equivalents of

nitroethanol, MeOH as solvent, 10 mol% of catalyst **15,** 20 mol% of benzoic acid, at 10 °C for

20 h, followed by the addition of 3 equivalents of $NaHCO_3$ (s) and stirring at room temperature

for 48 h. Michael adducts were obtained in moderate to high yields (59-92%). The best

stereoselectivity was obtained using an *α,β*-unsaturated aldehyde with an electron-withdrawing

aromatic *p*-nitro substituent: 92% ee and *dr.* 93:7 (*anti*:*syn*) (entry 3, TABLE 4.2). Moreover,

the best results in terms of yield were provided with *p*-bromo aromatic substituent, giving **116**

in 92% isolated yield (*dr.* 84:16 (*anti*:*syn*); 92% ee, entry 1, TABLE 4.2). Unfortunately, the

presence of an electron-donating aromatic substituents in the *α,β*-unsaturated aldehydes, like

the *p*-methoxy, rendered poor enantioselectivity in compound **117** (59% ee, entry 3, TABLE

4.2).

TABLE 4.2 - Synthesis of different 3,4-disubstituted tetrahydropyrans by the asymmetric reaction of nitroethanol with different *α,β*-unsaturated aldehydes.

Entry [a]	R^1	Compound	Yield[c] (%) [b]	*dr.* (anti: syn) [c]	ee (%) [d]
1	*p*-BrC₆H₄	**116**	92	84:16	92
2	*p*-MeOC₆H₄	**117**	82	84:16	59
3	*p*-NO₂C₆H₄	**118**	59	93:7	92
4	C₂H₅	**119**	87	75:25	92

a) Reactions using 3 equivalents of nitroethanol and 0.6 mmol of *α,β*-unsaturated aldehyde in 1 mL of MeOH. b) Isolated yield. c) *dr.* determined by ¹H NMR spectroscopic analysis of the crude mixture. d) Determined by chiral-stationary phase HPLC analysis.

On the other hand, alkyl-substituted *α,β*-unsaturated aldehydes were employed

successfully. Compound **119** was obtained in excellent yield and enantioselectivity

(87%, 92% ee) but with low *dr.* (entry 4, TABLE 4.2). In general, catalyst **15** proved to

be a good catalyst for conjugate addition reactions between different *α,β*-unsaturated

aldehydes and nitroethanol.

With the optimized conditions for the organocatalytic transformation in hands, we turned

to the synthesis of medium-sized ring compounds through a subsequent multicomponent

cyclization relying on the Ugi-5C-3CR.

We proposed a mechanism (SCHEME 4.2) similar to the previous mentioned in SCHEME 3.3 and SCHEME 3.5. The correspondent tetrahydropyrans in presence of amino acid is going to condense to the corresponding imine. After that, a nucleophilic attack is produced from isocyanide component to the protonated imine and simultaneously the carboxylic acid will add to the isocyanide component to form the α-aduct intermediate. An intramolecular acylation may occur to produce the desirable medium-sized cyclic peptidomimetic. The new stereocenter was formed in a non selective manner, due to the lack of chiral induction as observed in the mechanism. Maybe the lack of a substituent in the α-position of the carbonyl group in the tetrahydropyrans is an inconvenient in the stereoselective formation of the new stereocenter generated in the intramolecular cyclization.
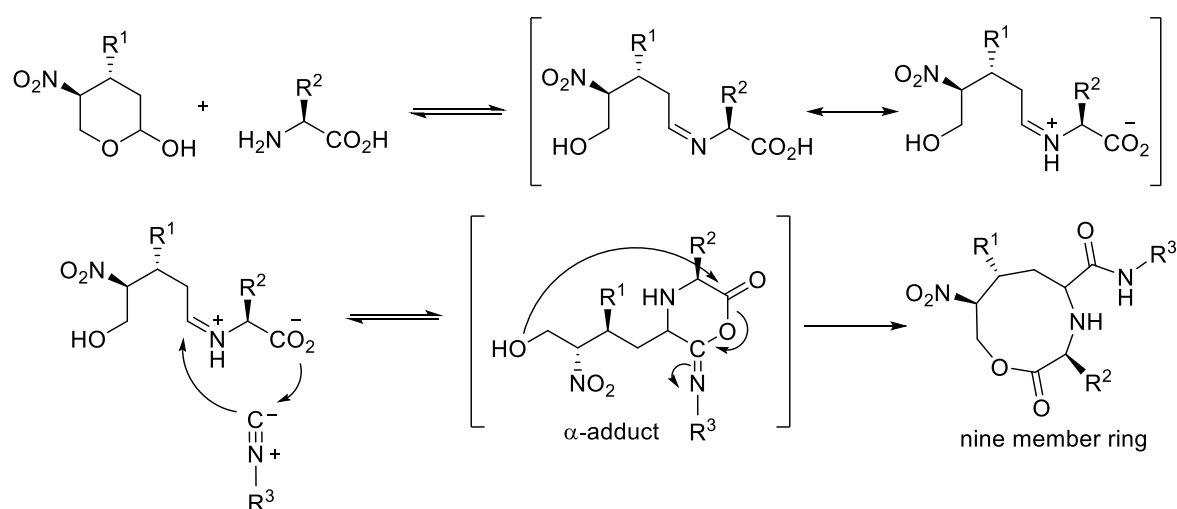
SCHEME 4.2 - Proposed mechanism for Ugi-5C-3CR to form medium-sized cyclic peptidomimetics.

Initially, compound **114** and the amino acid alanine (R^2=Me) were kept as fixed components in the Ugi-5C-3CR. Different R^3-substituents of the isocyanide component were varied (compounds **120-123**, TABLE 4.3). The reactions were conducted in TFE as non-nucleophilic solvent to avoid addition of the solvent to the α-adduct intermediate. The concentration was fixed at 0.25 M and temperature of 30 °C. Insolubility of starting material in TFE is observed at the beginning of the reaction, this heterogeneous mixture gradually disappears with time (24 h). When the R^3-substituent is changed to a bulky substituent in the isocyanide component (e.g., *tert*-butyl group), a decrease in the yield of reaction was detected (compound **120**, TABLE 4.3). Aliphatic long chain isocyanide substituents ($R^3 = n$-C_8H_{17}) also gave low yield (51%) of compound **122**. When methylisocyanoacetate was employed, not more than 67% yield was obtained (compound **123**, TABLE 4.3).

TABLE 4.3 - Multicomponent combinatorial synthesis of medium-sized cyclic peptidomimetics using Ugi-5C-4CR.
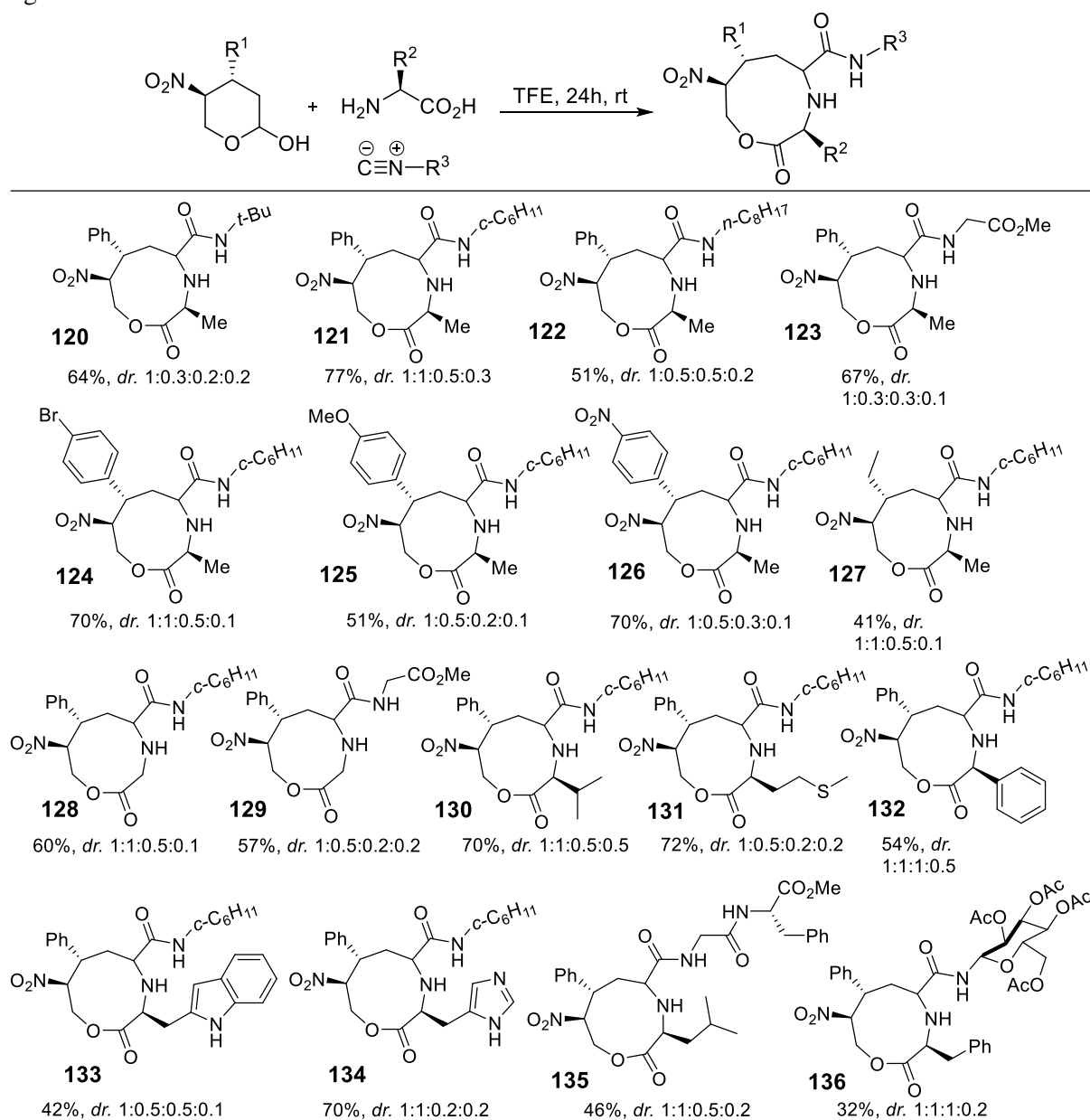
a) Yield of isolated product as mixture of diastereomers. b) *dr.* determined by ^{1}H NMR spectroscopy analysis of the crude mixture.

The best isocyanide component tested was cyclohexylisocyanide ($R^3 = c\text{-}C_6H_{11}$), where a yield of 77% was obtained (compound **121**, TABLE 4.3). As seen in TABLE 4.3, the *dr.* of all compounds is low, giving a mixture of up to four diastereomers in the overall process. To improve this we replicated entry 2 using catalytic amount (5 mol%) of $Ti(OCH(CH_3)_2)_4$. Unfortunately, neither variation in the yield nor in the *dr.* was detected in the reaction. This result is in agreement with the already reported by Ciufolini [92] where aliphatic aldehydes do not render high diastereoselection in this Ugi reaction in the presence of titanium catalyst.

Then, we chose cyclohexyl isocyanide to continue the synthesis of medium-sized rings. We next fixed R^3-substituent as cyclohexyl and alanine ($R^2 = $ Me) continues as fixed component, then R^1-substituent was varied in the tetrahydrofuran structures (TABLE 4.3). As noted, electron-withdrawing groups in R^1-substituent, like the *p*-bromophenyl and *p*-nitrophenyl, proved higher efficiency in the intramolecular cyclization with 70% yield for both compounds (compound **124** and **126**, TABLE 4.3).

Compound **125**, with electro-donating group (OMe) in R^1-substituent, gave moderate results with no more than 51% of isolated product. On the other hand, $R^1 = C_2H_5$ gave only low yield of 41% after 72 h of reaction (compound **126**). We can explain this yield by the probable low rigidity that the ethyl group confers, in comparison to the phenyl group as R^1-substituent.

In the same way, R^2-substituent was varied employing accessible natural α-amino acids in the synthesis of medium-sized cyclic peptidomimetics. In this case, Ph as R^1-substituent and Cy as R^3-substituent were kept as fixed substituents. Seven compounds were obtained in moderate to good yields (i.e., 42-72%, compounds **128**-**134**, TABLE 4.3). When amino acids with hydrophobic side chains were employed, like Val and methionine (Met), higher yields were observed (compounds **130** and **131**, TABLE 4.3). Intriguingly, phenylglycine and tryptophan (Trp) gave moderate yield (54% and 42%), respectively (entries 11 and 12, TABLE 4.3). Otherwise, Gly produces compound **128** in moderate yield (60%). In addition, amino acids with basic side chain were used (Histidine) producing compound **134** in excellent yield (70%).

Compound **135** was obtained employing a non-commercial isocyanopeptide having a sequence of CN-Gly-Phe-OMe and L-leu as amino acid (TABLE 4.3). This reaction also needed more time as expected (72 h), and yield no higher than 46% was obtained, a result comparable with lineal aliphatic isocyanide substituents ($R^3 = n$-C_8H_{17}) (see compound **122**, TABLE 4.3). The non-commercial isocyanopeptide was synthesized following a reported procedure.[100] A simple coupling of the methyl esters of L-Phe with the salt of potassium isocyanoacetate (**137**), in presence of the coupling reagent 2-(1*H*-Benzotriazole-1-yl)-1,1,3,3-tetramethyluronium tetrafluoroborate (TBTU) produced the isocyanide derived product in 60% yield (SCHEME 4.3).
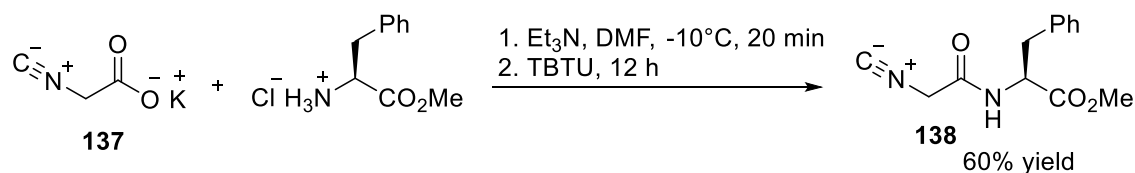
SCHEME 4.3 - Synthesis of *N*-isocyanopeptide **138**.

On the other hand, compound **136** (TABLE 4.3) was synthesized with β-glucosyl isocyanide as R^3-component and L-Phe as amino acid. Perhaps this bulky substituent (R^3-substituent) is the principal feature to diminish the yield considerable (32%). The synthesis of β-glucosyl isocyanide ((AcO)$_4$-β-Glc-NC) **142**[101] was accomplished by previously reported method (SCHEME 4.4). [102] The synthetic sequence used was: 1) formation of the (AcO)$_4$-β-Glc-N$_3$ **139** using SnCl$_4$ and trimethylsilyl azide (TMSN$_3$); 2) followed by catalytic hydrogenation (5% Pd-C, MeOH) of **139** to obtain pure **140** in 85% yield; 3) synthesis of formamide (AcO)$_4$-β-Glc-NH-CHO **141** reacting acetic formic anhydride with **140** and *in situ* dehydration of **141** under mild conditions (PPh$_3$, CBr$_4$, Et$_3$N) to give **142** in 83% yield as a light yellow solid after flash column chromatographic purification.
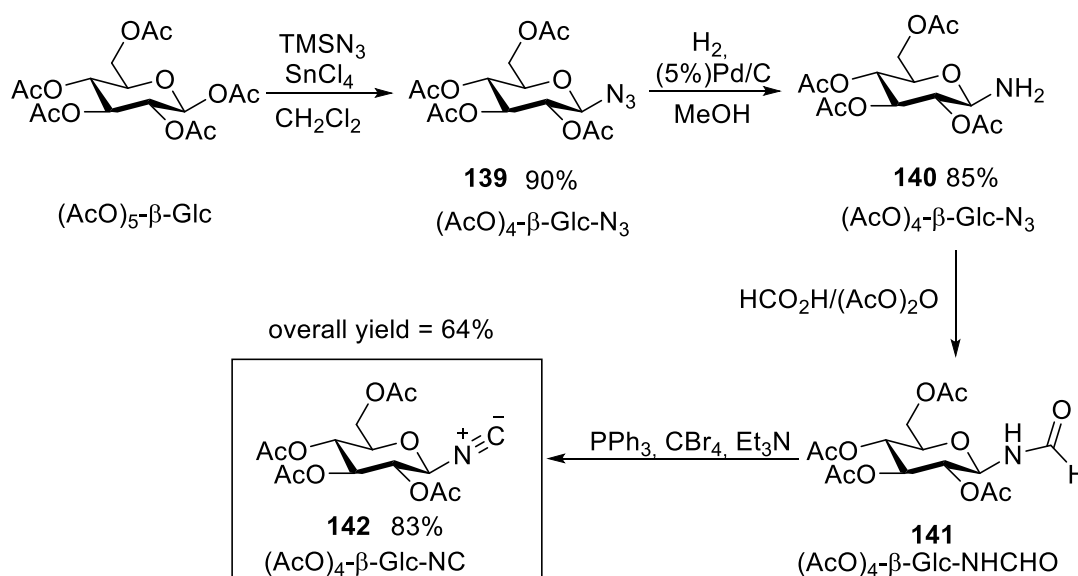
SCHEME 4.4 - Synthesis of β-glucosyl isocyanide **142**.

The NMR characterization of this medium sized cyclic peptidomimetics is not an easy task due to the presence in all spectra of several sets of signals that can be assigned to the same protons. It must be noticed that a mixture of diastereoisomers was observed in both the ^{1}H and ^{13}C-NMR spectra of all compounds. To this end, compound **121** was selected to carry out an NMR study and general characterization of medium-sized cyclic peptidomimetic compounds has been done.

TABLE 4.4 - ^{13}C, DEPT 135°, HSQC and HMBC shifts assignments of compound **121**.

Atom No	^{13}C (δ_C = ppm)	DEPT 135° (δ_C = ppm)	HSQC (δ_H = ppm)	HMBC (δ_H = ppm)
C-2	173.58, 173.19, 173.09	C=O	-	1.23, 1.14, 0.92
C-3	55.32, 55.19	55.32, 55.20 (CH)	3.20, 3.18	3.01, 2.85, 1.23, 1.14
C-5	59.79, 59.28, 59.18, 58.67	59.80, 59.28, 59.18, 58.67 (CH)	3.01, 2.85, 2.81, 2.65	3.20, 2.18, 2.00
C-6	37.66, 36.47, 35.36	37.66, 36.46, 35.36 (CH₂)	2.38, 2.18, 2.03	2.86, 1.38
C-7	43.05, 42.82, 42.44	43.34, 43.05, 42.82, 42.44 (CH)	3.63, 3.50, 3.45.	3.01, 2.85, 2.18, 1.94
C-8	94.14, 94.02, 93.54	94.14, 94.02, 93.54, 93.37 (CH)	4.78, 4.73	4.11, 3.50, 2.18
C-9	62.52, 61.85, 60.85, 60.71	62.52, 61.85, 60.85, 60.71 (CH₂)	4.49, 4.20, 4.14	3.20, 2.18, 2.00
C-10	19.47, 19.30, 18.40, 18.18	19.47, 19.30, 18.39, 18.18 (CH₃)	1.23, 1.14, 1.07, 0.92	3.20
C-11	172.47, 172.29, 171.83	C=O	-	3.02, 2.86, 2.18, 2.00
C-13	48.30, 48.14, 47.74	48.30, 48.14, 47.74 (CH)	3.73, 3.70, 3.65	1.14
C₁₄₋₁₈	33.57, 33.01, 32.79, 25.56, 24.83	33.57, 33.06, 33.01, 32.79 25.56, 24.87, 24.83, 24.77 (CH₂)	2.17, 1.85, 1.61, 1.24, 1.14	3.73, 3.70, 3.65, 2.17, 1.85, 1.61, 1.24, 1.14
C-19	138.37, 137.68, 137.00	C	-	7.37, 7.34, 2.18
C₂₀₋₂₄	129.68, 129.39, 129.27, 129.01, 128.58, 128.52, 128.42, 128.17	129.68, 129.39, 129.27, 129.01, 128.59, 128.52, 128.42, 128.37, 128.17 (CH)	7.23-7.42	7.36, 7.24, 4.50, 3.52

The ^{13}C NMR shows either triplicate or quadruplicate set of signals that makes difficult the analysis. Six signals appear for the C=O group and eight for the aromatic ring carbons. Since only two carbonyl groups are in compound **121**, by heteronuclear multiple-bond correlation (HMBC) we determined that the signals at 173.5, 173.1, 173.0 ppm (*C*=O, *C*-2), correlates with three shifts 1.22, 1.14, 0.92 ppm (TABLE 4.4). A correlation with shifts 19.47, 19.30, 18.40, 18.18 ppm was identified by HSQC and correspond to the CH_3 group that is in accordance with the experiment DEPT 135° that have positive signals at same shifts and assigned to *C*-10. Unequivocally, 172.47, 172.2 and 171.8 ppm correspond to carbonyl *C*-11 (TABLE 4.4). Larger shifts 94.1, 94.0 and 93.5 ppm are assigned to *C*H directly attached to electro-withdrawing NO_2 group (*C*-8) which have positive signals in the experiment DEPT 135°. By HSQC the *H*-8 at 4.78 ppm was determined. In DEPT 135° experiment four more positives signal are clearly seen and correspond to *C*H of *C*-3, *C*-5, *C*-7 and *C*-13. As seen in HMBC the Me (*C*-10) correlates with 3.20 and 3.19 ppm corresponding to a multiplet that by HSQC full correlate with 55.32, 55.19 ppm then assigned to *C*-3. The COSY diagram shows two correlations of *H*-8 at 4.78 ppm with 4.49, 4.20, 4.14 ppm and 3.63, 3.50, 3.45 ppm. This *H*-8 has two vicinal groups: the *C*H for *H*-7 and CH_2 for *H*-9. It was easy to distinguish which is *C*H or CH_2. The *C-9* is the most deshielded CH_2 present in the backbone due to be attached to an heteroatom oxygen, then by DEPT 135° experiment 62.5, 61.8, 60.8, 60.7 ppm belongs to *C-9*. The HSQC correlates the 4.49, 4.20, 4.14 (H-9) ppm for a CH_2-9 and consequently 3.63, 3.50, 3.45 ppm correspond to *C*H of *H*-7, which correlates with 43.0, 42.8, 42.4 ppm. The *C*-3 correlates with 3.01, 2.85, 1.23, 1.14 ppm by HMBC. The two more shielded shifts correspond to the Me at *C-10*. Then the deshielded shift 3.01 and 2.85 ppm correspond with the *C*H at *C-5* (59.79, 59.28, 59.18, 58.67 ppm). Undoubtedly, the last *C*H identified with shifts 48.3, 48.1, 47.7 ppm corresponds with *C*-13 and the proton shifts result 3.73, 3.70, 3.65 ppm by HSQC (TABLE 4.4).

In FIGURE 4.2, the range 7.46-7.20 ppm in ^{1}H aromatic signals corresponds to the Ph group of R^1-substituent. Three *^{1}H* signals with a typical aromatic shifts of 7.02, 6.84 and 6.72 ppm splits in three doublets with coupling $^3J_{H12-H13}$ = 8.3 Hz unequivocally belong to *N*H-12 signal of the cyclohexyl amide. Since *N*H-12 can be identified by common coupling constant, the *H-H* relationship which is likewise derived from the COSY diagram confirms the location of *H*-13 at 3.73-3.65 ppm. Also, the fourth shift of *N*H-12 was determined underneath the aromatic zone (7.23 ppm) that clearly correlates with the *C*H of cyclohexyl moiety.
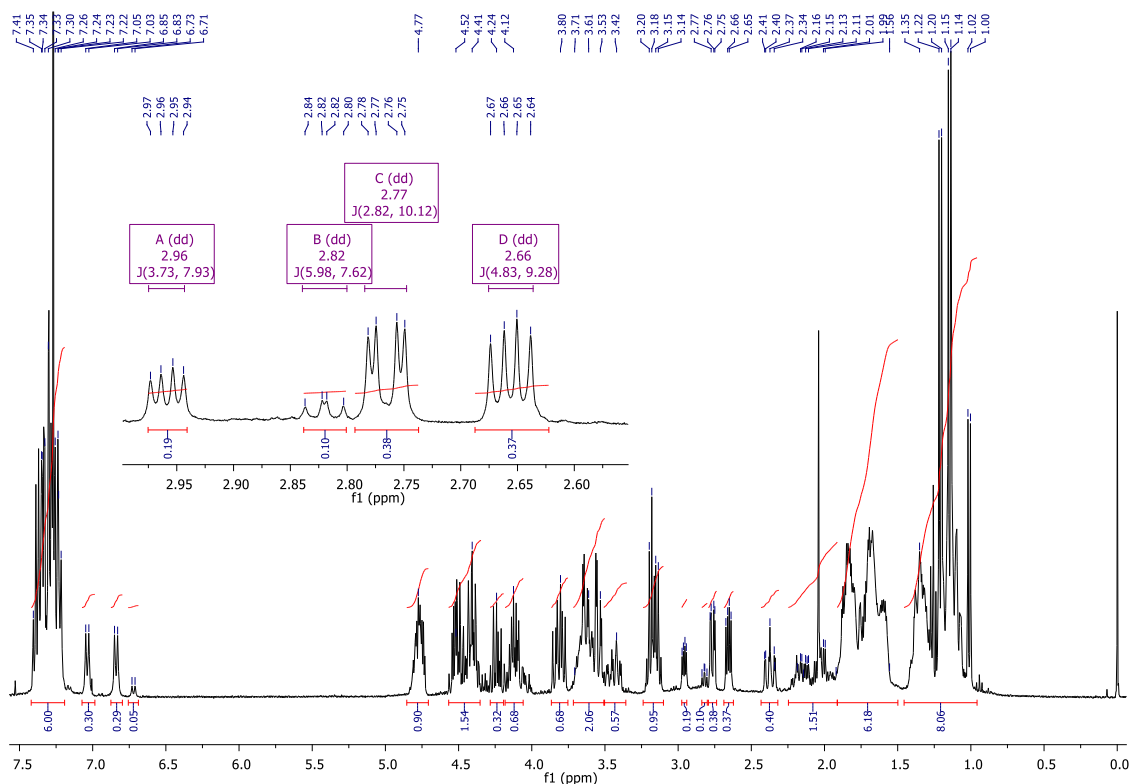
FIGURE 4.2 - 400 MHz ^{1}H NMR spectra in CDCl$_3$ of compound **121**. Zoom range (2.60-3.00 ppm).

We cannot determine the *dr.* of compound **121** by simple ^{1}H NMR analysis of *N*H-12 signal because all of these shifts are not very visible. Other signals should be analyzed to determinate the dr. At 4.78 ppm there is a multiplet that corresponds to *H*-8 previously discussed. The multiplet with shift 3.50 ppm corresponds to *H*-7. Other important signals to mention are the three doublets at 1.22, 1.14, 0.99 ppm of Me *H*-10 having a coupling $^3J_{\text{H10-H3}} = 7.1$ Hz.

The most important proton signal to discuss is the generated *C*-5 in Ugi-5C-3CR that will give the *dr.* of medium-sized cyclic peptidomimetics. FIGURE 4.2 shows a zoom of the range between 2.60-3.00 ppm where four doublets of doublets integrated for one proton are clearly seen. These doublets of doublets correspond to stereogenic *H*-5 which couples with *H*-6 in a two-spin system of type *AX*. Considering the new formed stereogenic center *C*-5 remains as a mixture and was started with a *dr.* 8:2 (*anti*:*syn*) of **114** we should observe four diastereoisomers as expected. TABLE 4.5 shows the shifts of *H*-5 with its respective integration values and coupling constants ($^3J_{\text{H5-H6}}$). As seen, a poor dr. 1:1:0.5:0.3 is obtained. The doublets at $\delta_H =$ 2.77 and 2.66 ppm have $^3J_{\text{H5-H6}} = 10.1$ and 9.2 Hz respectively, resulting the most populated *dr.* a pseudo-axial proton *H*-5 of the cyclic compound **121**. It seems that the amide R^3-substituent should remain in the pseudo-equatorial position of conformation of this class of nine-member ring.

81

TABLE 4.5 - Shifts, integration values and coupling constants of *H*-5 of compound **121**.
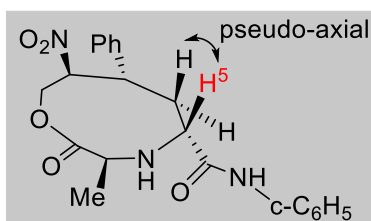
δ_{H-5} (ppm)	Integration values	dd $^3J_{H5-H6}$ (Hz)	% of *H*-5	position of *H*-5
2.96	0.19	3.7/7.9	18	pseudo-equatorial
2.82	0.10	5.9/7.6	10	pseudo-equatorial
2.77	0.38	2.8/10.1	36	pseudo-axial
2.66	0.37	4.8/9.2	36	pseudo-axial

a) 400 MHz ^{1}H NMR data in CDCl$_3$ of compound **121**.

FIGURE 4.3 shows the zoom range between 2.60-3.00 ppm of rotating frame nuclear overhauser effect spectroscopy (ROESY) of compound **121**. Here we observed a ROESY effect between the *H*-5 and *H*-8 where the *pseudo*-equatorial proton of H-5 is close to the *H*-8.
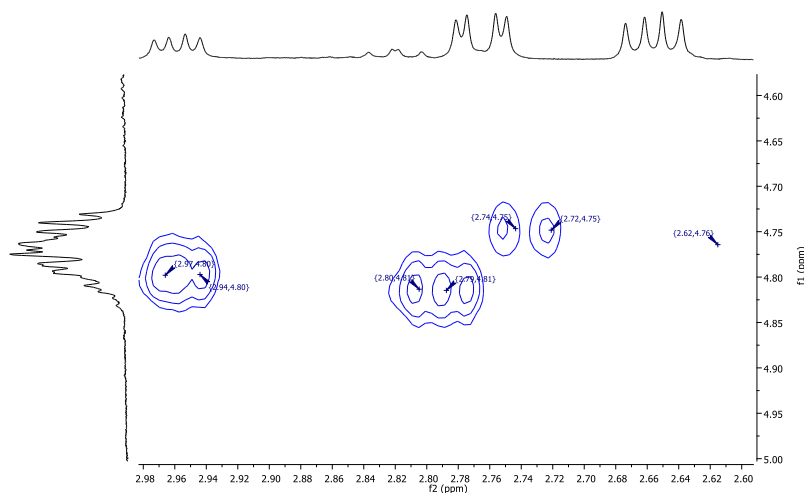
FIGURE 4.3 - 600 MHz ROESY spectra in CDCl$_3$ of compound **121**. Zoom range (2.60-3.00 ppm).

4.2 Stereoselective organocatalytic multicomponent reaction sequence to hydroquinolinone scaffolds
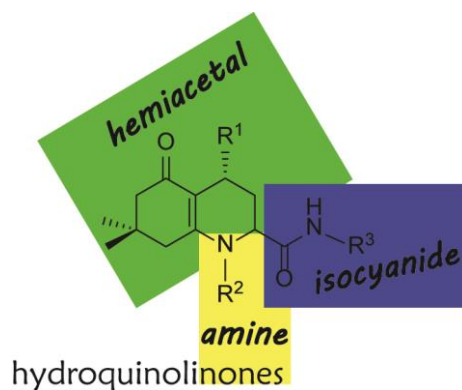
The second part of this chapter describes a highly stereoselective approach for the one-pot synthesis of a natural product-like based on the hydroquinoline platform. The approach involves an asymmetric organocatalytic conjugate addition of dicarbonyl compounds to α,β-unsaturated aldehydes, followed by a new intramolecular 4-center 3-component reaction including amine and isocyanide components.

We formulated two main selection criteria for the organocatalytic and multicomponent approaches. First, the organocatalytic process should provide enantiomerically enriched hemiacetal suitable for a subsequent I-MCR. Second, we aimed at utilizing intramolecular I-MCRs, as these typically provide better stereocontrol as compared to their intermolecular versions. As shown in TABLE 4.6, the first procedure is an organocatalytic cascade developed independently by Rueping [103] and Jørgensen.[104]

The cascade process comprises the asymmetric conjugate addition of 1,3-cycloalkanediones to α,β-unsaturated aldehydes followed by acetalization, thus enabling the installation of two reactive functionalities onto a single skeleton. Dimedone (**143**) and *trans*-2-pentenal (**144**) were initially selected for the organocatalytic conjugate addition as first step in the multicomponent sequence. Conditions originally described by Rueping.[103] employing 10 mol% of catalyst diarylprolinol silyl ether **12**, successfully produced chromenone **145** (TABLE 4.6). This intermediate fulfills the requisite of being a biologically relevant core for scaffold diversification as well as having two functionalities suitable for I-MCRs, (i.e., an aldehyde and a conjugated enol). Both racemic and enantiomerically enriched **145** were prepared and subsequently subjected to the I-MCR by treatment with a primary amine and an isocyanide. Such a multicomponent process resembles the Ugi-Smiles reaction, [105] which has been previously implemented with heterocyclic and conjugated enols [106] as surrogate of the classic

phenol component. However, neither intramolecular variants of this type of I-MCR nor combinations with a pre-MCR organocatalytic process have been reported so far.

Initial experiments using methanol, toluene, or dichloromethane in the second reaction step were unsatisfactory as the first solvent gave a mixture of products and the two latter ones did not lead to any product formation (entries 1-4, TABLE 4.6). Products **146, 147** and **148, 149** were formed in a ratio of about 1.5:1 when methanol was used, as a result of the competition between the rearrangement of the α-adduct (i.e., migration of the amine component) and the addition of methanol to the conjugated position.

As shown in (TABLE 4.6), the intermediate α-adduct is a rigid, fused bicyclic system, in which the low conformational flexibility may disfavor the amine migration, thus enabling the attack of a nucleophilic solvent like methanol. To circumvent this problem, TFE was used, which led to 2-amido-hydroquinolin-6-one **146** as the sole product in good yield (entry 5, TABLE 4.6). Importantly, the use of microwave irradiation enabled the reaction to proceed in similar chemical efficiency and significantly shorter reaction times, i.e. 15 min at 70 °C (entry 6, TABLE 4.6). Since the second step did not proceed in CH_2Cl_2, we evaluated the possibility of implementing a one-pot sequence by addition of TFE after formation of organocatalytic product **145**, thus carrying out the second step in the solvent mixture CH_2Cl_2/TFE (1:1, *v/v*). To our delight, both yield and stereoselectivity remained high in this one-pot process comprising the organocatalytic step and the I-MCR (entries 7 and 8, TABLE 4.6). Importantly, the presence of secondary amine catalyst **12** did not interfere in the IMCR, as no product including this fragment was detected.

A key feature of this approach is the different stereochemical outcome derived from variation of primary amine. As illustrated in TABLE 4.6, the use of benzyl amine led to almost no diastereoselectivity in the I-MCR, producing **146** as a mixture of diastereoisomers (entries 1 and 5). Conversely, the utilization of the chiral (*S*)-α-methylbenzyl amine provided enantiomerically pure product **147** with an excellent diastereoselectivity (>99:1). Interestingly, the diastereomeric ratio of product **147** correlates with the enantiomeric ratio of intermediate **145**, confirming the great stereocontrol of the multicomponent step with the use of a chiral amine.

TABLE 4.6 - Screening of the one-pot organocatalytic conjugate addition/Ugi-4C-3CR sequence to 2-amido-hydroquinolin-6-ones and concise reaction mechanism.
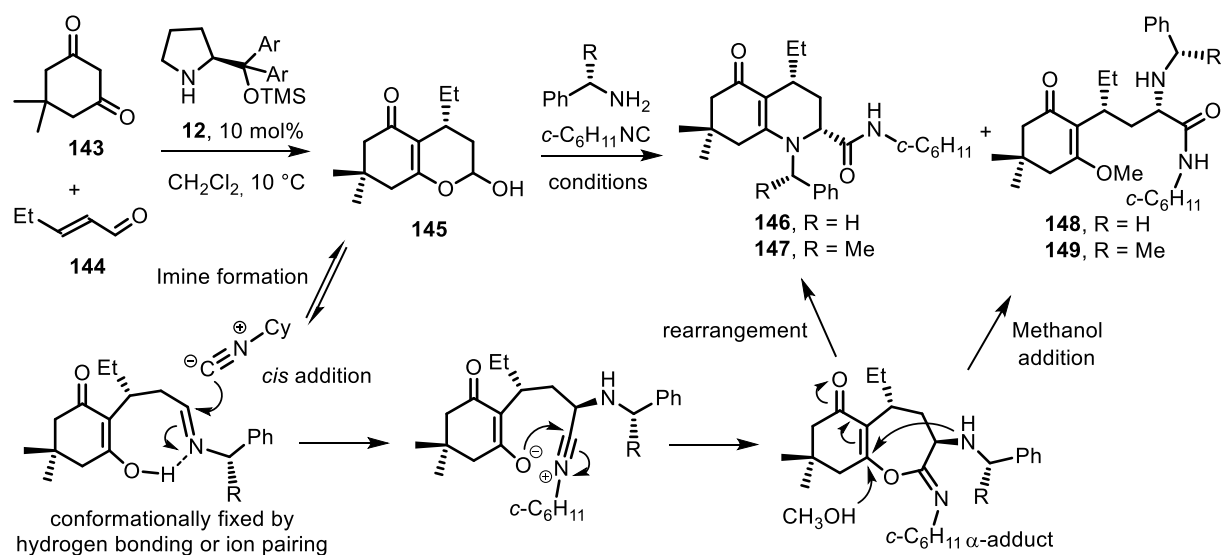
Entry [a]	R	Conditions [b]	Yield (%) [c] 146-147/148-149	dr. (syn/anti) [d] 146-147	ee (%) [e] 146-147
1 [f]	H	MeOH, RT	39/25	54:46	92
2 [g]	Me	MeOH, MW	42/28	>99:1	>99
3 [g]	H	Toluene, MW	n.r.	-	-
4 [f]	Me	CH₂Cl₂, RT	n.r.	-	-
5 [f]	H	TFE, RT	77/0	58:42	93
6 [g]	Me	TFE, MW	75/0	>99:1	>99
7 [f,h]	Me	CH₂Cl₂/TFE, RT	64/0	>99:1	>99
8 [g,h]	Me	CH₂Cl₂/TFE, MW	71/0	>99:1	>99

a) First step performed with dimedone **143** (1 equivalents) and aldehyde **144** (1.3 equivalents). b) Second step performed either with benzyl or (S)-α-methylbenzyl amine (1.3 equivalents) and cyclohexylisocyanide (1.3 equivalents). c) Yield of isolated product over two steps. d) Determined by ^{1}H NMR spectroscopic analysis. e) Determined by chiral-stationary phase HPLC analysis. f) Conducted at room temperature for 36 h. g) Conducted under MW for 15 min at 70° C. h) Addition of TFE to the reaction mixture containing CH₂Cl₂ to make a 1:1 (v/v) mixture. TFE: Trifluoroethanol. Ar: 3,5-(CF₃)-C₆H₃

The relative configuration of hydroquinolin-6-ones **146** and **147** was determined by NMR analysis on the basis of the absolute configuration at C-4 of intermediate **145**, as previously assessed by X-ray analysis.[103] The solid-state structures showed the axial orientation (directing toward the α face) of the substituent at position 4 in product **145**. In a first instance, the two diastereoisomers of compound **146** derived from benzyl amine were isolated and analyzed by NMR. In the major stereoisomer of **146** (and also in the only one of **147**), various NOE couplings between hydrogens of the ethyl chain at position 4 and the substituent at position 2 were found. Similarly, strong NOE couplings were observed between the amide substituent at position 2 and one of the geminal methyl groups of the fused bicyclic skeleton.

These results unambiguously prove the *cis* configuration in which both substituents at positions 2 and 4 have a *pseudo*-axial orientation directing toward the α-face of the hydroquinolin-6-one skeleton. As highlighted in SCHEME 4.7, these NOE couplings are only possible due to the 1,3 and 1,5-diaxial interactions of the amide substituent at C-2 and the substituent at position 4 and the geminal axial methyl group, respectively. In contrast, the minor stereoisomer of compound **146** showed a strong NOE coupling between the hydrogen at C-2 and the ethyl group at C-4, indicating the *trans* configuration of substituents at positions 2 and 4. As shown in TABLE 4.6, the diastereoselection of this process derives from the preferential addition of the isocyanide to the conformational fixed imine (or iminium ion) by the same face of ethyl group (*cis* addition). Further enolate addition leads to the α-adduct featuring the *trans* disposition between the ethyl group and the exocyclic amine moiety. Finally, migration of the amine (rearrangement) generates the piperidine ring with the *cis* configuration of the amide substituent at C-2 with respect to the ethyl group at C-4. A further evidence that the stereocontrol lies at the isocyanide addition step is that the acyclic side-product **149**, derived from methanol addition, was obtained with the same diastereoselectivity of **147**, whilst formation of side-product **148** proceeded with poor stereoselection, as resulted for **146**. To get deeper insight into stereoselectivity, we turned to implement the reaction sequence with variation of the four different components.

As shown in TABLE 4.7, several hydroquinolin-6-ones were produced by variation of three structural elements, i.e. the aldehyde incorporated in the organocatalytic step, as well as the amine and isocyanide in the I-MCR. As before, the one-pot processes were performed without isolation of intermediate hemiacetal **145**, but simply carrying out the subsequent I-MCR through addition of TFE, the amine and isocyanide components immediately after completion of the organocatalytic step.

TABLE 4.7 - One-pot synthesis of hydroquinolin-6-one.
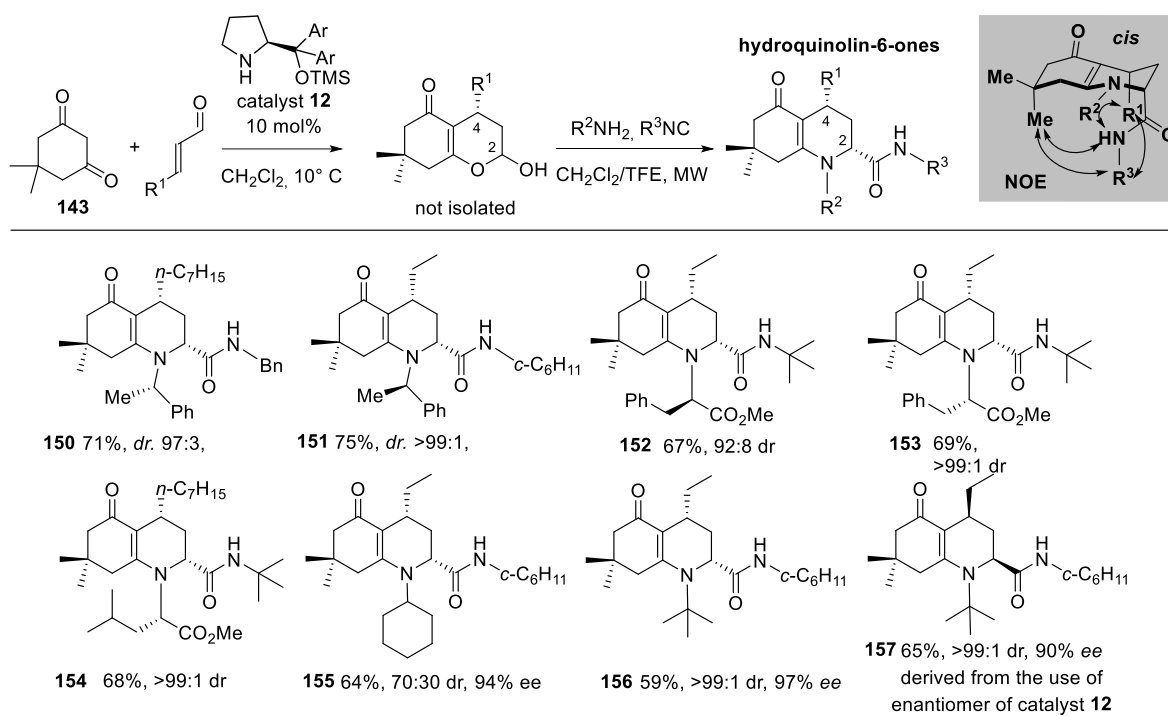
a) First step performed with dimedone **143** (1 equivalents) and different aldehydes (1.3 equivalents). b) Second step performed with either aliphatic amines or amino acid (1.3 equivalents) and isocyanides (1.3 equivalents). c) Yield of isolated pure product over two steps. d) *dr.* determined by ^{1}H NMR spectroscopic analysis. e) ee determined by chiral-stationary phase HPLC analysis. f) Ar: 3,5-(CF$_3$)-C$_6$H$_3$.

The stereoselectivity of the multicomponent sequence leading to hydroquinolin-6-ones **150** proved once more to be excellent when the amine is chiral (α-MeBn and amino acids). As before, NMR evidences proved the *cis* configuration for major isomers. The use of either *S* or *R*-α-methylbenzyl amine as well as either D- or L-amino acid methyl esters provided the same stereo-differentiation to the *cis* isomers of compound **150-154**. An interesting result was obtained when the bulky character of the achiral amine was increased from cyclohexyl to *tert*-butyl amine. Thus, cyclohexylamine gave compound **155** with moderate diastereoselectivity (*dr.* 70:30, 94% ee), while the highly crowed *t*-butyl amine rendered **156** with excellent diastereoselectivity (*dr.* 99>1, 97% ee). This confirms that not only chiral amines, but also achiral ones with great steric congestion at the α-position can induce stereoselection in this I-MCR. A further experiment proceeding *via* the enantiomer of intermediate **145** (prepared using the enantiomer of catalyst **12**) resulted in the highly stereoselective formation of compound **157** (*dr.* 99>1, 90% ee), which is the enantiomer of **156** (*dr.* 99>1, 97% ee) as revealed by chiral-stationary phase HPLC and optical rotation analysis. This result confirms the great stereofacial selectivity (*cis* addition) when a bulky, eventually chiral amine is used.

4.3 Diastereoselective organocatalytic multicomponent reaction sequence to pentasubstituted cyclopentenes

pentasubstituted cyclopentenes
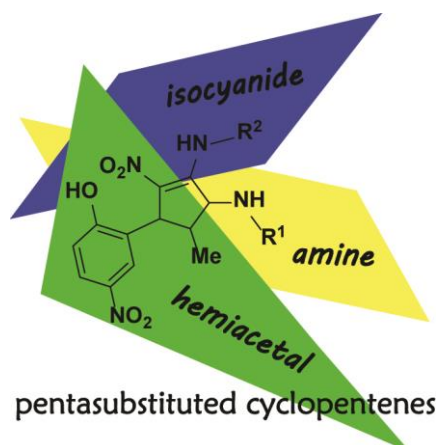
Based on the success of the above-described stereoselective three-component four-center reaction, we focused implementing a similar organocatalytic approach rendering an hemiacetal capable to react in an Ugi-Smiles type reaction. As shown in SCHEME 4.5, we devised the utilization of such I-MCR to produce tetrahydroquinolines, an important class of nitrogenated scaffold commonly found in bioactive natural products.

Following the same above criteria of combining organocatalysis and multicomponent approaches, we focus on the implementation of an organocatalytic process providing enantio-enriched nitro-functionalized chromans capable to react in an intramolecular Ugi-Smiles type reaction. The Ugi-Smiles reaction is a modification of the classic Ugi-4CR using phenols as acidic component instead of carboxylic acids (SCHEME 4.5). In this case, the last step of the Ugi procedure is a Smiles rearrangement. El Kaïm and Grimaud [105] proposed that electron withdrawing groups, such as -NO$_2$, should be present at *-para* and/or *-ortho* position with respect to the -OH group to give the Smiles rearrangement. In addition, they mentioned MeOH as the best solvent for this specific reaction.
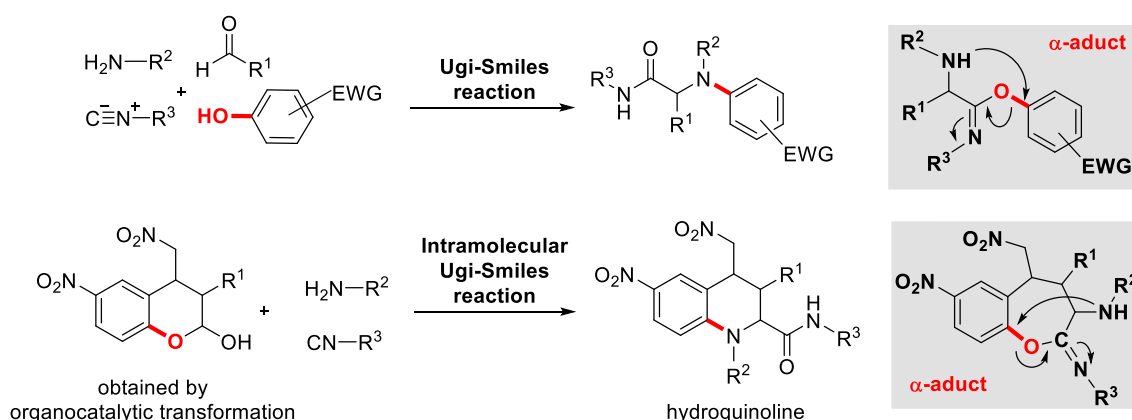
SCHEME 4.5 - The Ugi-Smiles reaction and its possible utilization to access hydroquinolines.

To this end, we selected an organocatalytic approach leading to 3-alkyl-4-nitromethylchromans reported independently by Gong [107] and Ramachary.[108] Such a process comprises an organocatalytic tandem Michael addition-hemiacetalization producing the desired 3-alkyl-4-nitromethylchromans. They reported excellent efficiency and good enantio- and diastereoselectivity for this class of chromans (please see **A** in SCHEME 4.6), although in none case a nitro group was included as substituent of the phenol ring.
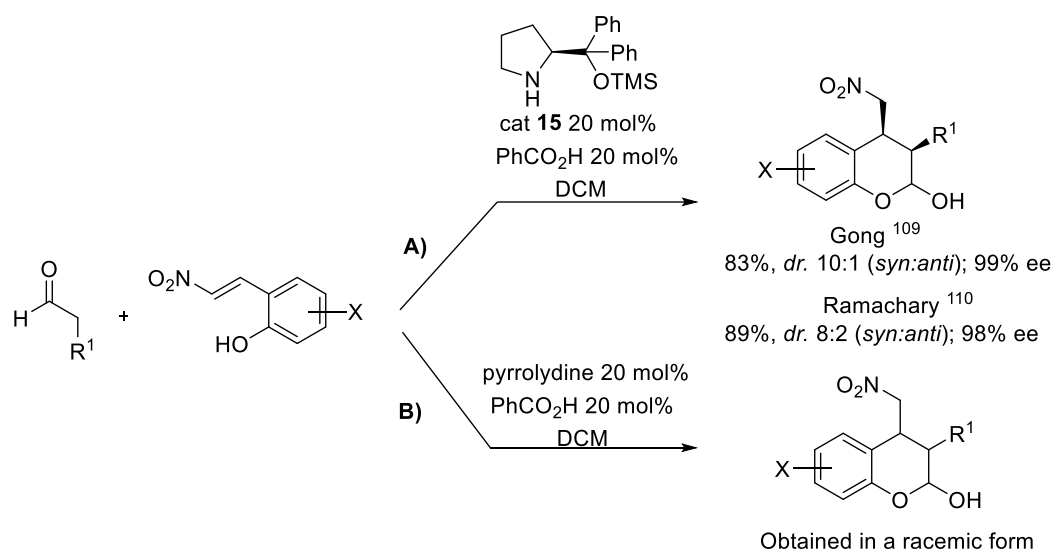
SCHEME 4.6 - A) Direct organocatalytic access to a 3-alkyl-4-nitromethylchromans. Gong´s and Ramachary´s results. B) Synthesis of racemic 3-alkyl-4-nitromethylchromans.

Initially, with the use of this methodology [107], we planned to obtain the racemic 6-nitro-3-methyl-4-nitromethylchroman-2-ol (**158**) (please see **B** in SCHEME 4.6), by the reaction of *trans*-2-hydroxy-*β*-nitrostyrene with *n*-propanal in the presence of 20 mol% of pyrrolidine and 20 mol% of PhCO2H in DCM. After chromatographic purification 93% yield of **158** was obtained in a *dr.* 8:2 (*syn:anti*). Compound **158** was further reacted in the presence of benzyl amine and *tert*-butyl isocyanide in an Ugi-Smiles type reaction. As depicted in SCHEME 4.7, the reaction of hemiacetal **158** with benzyl amine and and *tert*-butyl isocyanide led to the formation of the pentasubstituted cyclopentene **160**, while only traces of the real Ugi-Smiles product **159** were detected. The explanation for this can be found on the mechanism of the reaction. Initially, the hemiacetal group of compound **158** forms the imine by reaction with the primary amine. After that, a nitrilium ion is formed by addition of the isocyanide to the imine (or the activated inimium ion). This ion can be trapped by the phenolate anion to give the classic imidate intermediate, which would yield via the Smiles rearrangement (see SCHEME 4.7) the expected tetrahydroquinoline **159**. However, that compound was only found in traces, and the

main reaction product was the unexpected pentasubstituted cyclopentene **160**. Such experimental evidences show that the actual reaction pathway involves the nucleophilic attack of the α-carbon of the nitro group to the nitrilium ion. This process leads to an exocyclic imine intermediate that tautomerizes to the corresponding nitro-conjugated enamine at the cyclopentene ring.
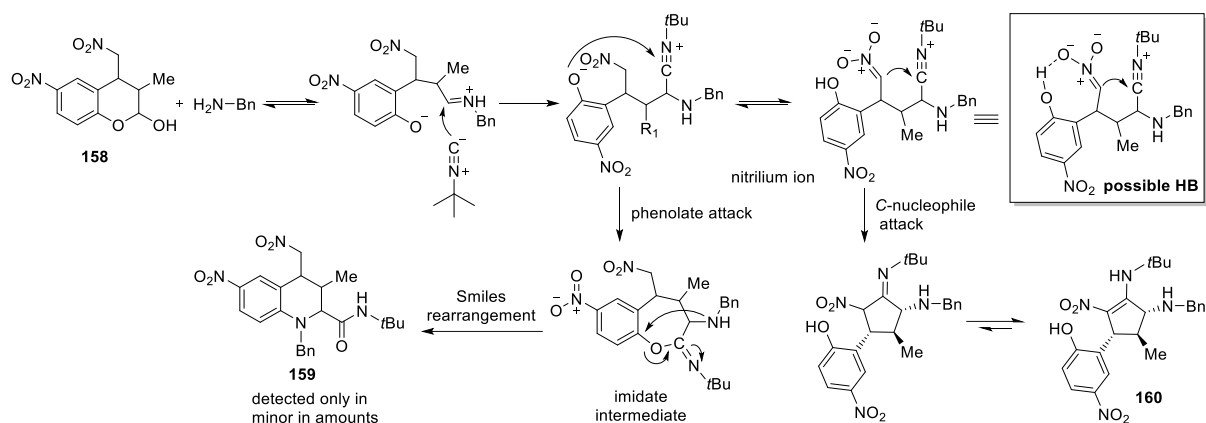
SCHEME 4.7 - Mechanism explaining the favored formation of the cyclopentene **160** over the formation of the tetrahydroquinoline **159**.

The best results were obtained using benzylamine and *tert*-butyl isocyanide in MeOH as solvent and with MW irradiation at 300 W and 80 °C for twenty minutes. After 20 min the solution gets a brown color, and the TLC analysis shows that starting material (**158**) is consumed with the appearance of new spots. Without any work up, the crude was directly purified by flash column chromatography obtaining compound **160** as a brown solid in 40% yield.

To determine the effect of the different substituents on the reaction outcome, several experiments were carried out with starting material having or not the phenol and nitro groups. Interestingly, no reaction took place when the starting material lack either the phenol or the nitro group at *para* position, indicating the importance of an acidic phenol for the reaction to proceed. Intriguingly, no product was formed either using the *ortho*-nitro-chroman, which is unexpected considering the similar acidity of the phenol group compared to the *para*-nitro substituted. In our opinion, the preferential addition of the *C*-nucleophile over the addition of the phenolate may be explained by the possible participation of the OH in intramolecular HB with the aliphatic nitro group, which disfavors its attack to the nitrilium ion (See SCHEME 4.7). Such HB interaction also explains the enhanced acidity of the α-carbon to the aliphatic nitro group and therefore its good carbanion behavior. It is also possible that the presence of a nitro group at *ortho* position of the phenol avoids the formation of such HB with the aliphatic -

NO$_2$, substituting it with the HB between the OH and the aromatic NO$_2$. Nevertheless, as this is a new intramolecular I-MCR, much remains to be studied by means of computational modeling in order to elucidate the mechanistic insights explaining such a pathway. Further studies are being conduced in our laboratory to explain this mechanism, but this is beyond the objective of the present work. In addition, the temperature of reaction and the way of heating were varied to determine if the unexpected cyclopentene could be formed. Unfortunately, at room temperature the cyclopentene product is only formed in very little amounts. With conventional heating, 20% yield was the maximum value obtained after 48 h of reaction.

We next varied the isocyanide and amine components in this reaction (TABLE 4.8) in order to determine its scope. Only a few examples were described here because this work will be further developed by our group in a near future.

TABLE 4.8 - Multicomponent combinatorial synthesis of different pentasubstituted cyclopentenes.
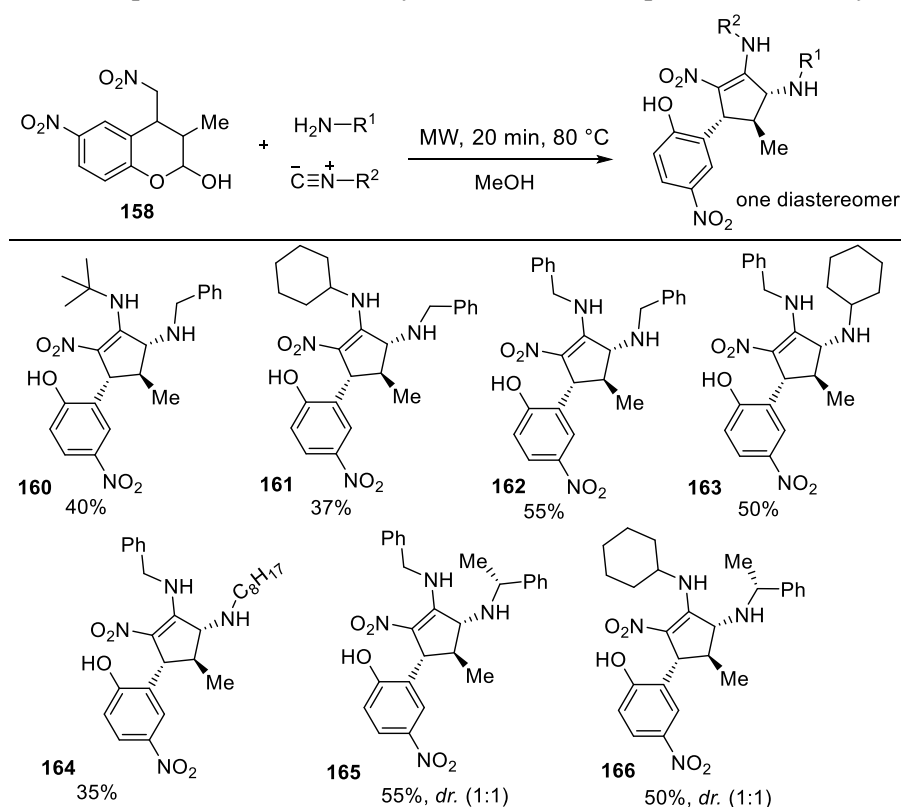
a) Reaction performed with 0.25 mmol of **158** (1 equivalent), aliphatic amines (1 equivalent) and isocyanides (1 equivalent) in 1 mL of MeOH. b) Yield of isolated product. c) *dr.* determined by ^{1}H NMR spectroscopic analysis.

The R^2-component of isocyanide was varied to *Cy* and *Ph* producing compounds **161** and **162** in 37% and 55% yield, respectively. Benzylisocyanide, as affixed component, was reacted with different aliphatic amines (i.e., cyclohexylamine and octylamine) in the presence of chroman **158**. Non-drastic changes in yield were observed (see compounds **163** and **164**,

TABLE 4.8). With chiral amines, such as α-MeBnNH$_2$, two diastereoisomers were detected in proportion (1:1) for compounds **165** and **166**.

Compound **160** was selected to carry an NMR study and general characterization of penta-substituted cyclopentene. The ^{1}H and ^{13}C-NMR spectra of compound **160** shows a single diastereomer.

TABLE 4.9 - ^{13}C, DEPT 135°, HSQC and HMBC shifts assignments of compound **160**.

Atom No	^{13}C (δ_C = ppm)	DEPT 135° (δ_C = ppm)	HSQC (δ_H = ppm)	HMBC (δ_H = ppm)
C-1	158.07	*C*	-	3.95, 3.84, 2.44
C-2	121.31	*C*	-	9.51, 3.95, 3.84, 2.44
C-3	52.47	52.47 (*C*H)	3.95	8.21, 2.44, 1.29
C-4	39.14	39.14 (*C*H)	2.44	3.95, 1.29
C-5	66.67	66.67 (*C*H)	3.84	9.51, 4.02, 3.95, 3.65, 3.84, 2.44, 1.29
C-6	21.40	21.40 (*C*H$_3$)	1.29	3.95, 3.84, 2.44
C-8	51.55	51.55 (*C*H$_2$)		7.24, 3.84
C-9	136.17	*C*	-	7.36, 4.02, 3.65
C-16	55.26	*C*	-	1.40
C-17	31.13 (3x*C*H$_3$)	31.13 (*C*H$_3$)	1.40	9.51
C-10´	161.41	*C*	-	8.21, 8.02, 6.85
C-11´	119.28	119.28 (*C*H)	6.85	8.21
C-12´	124.93	124.93 (*C*H)	8.02	8.21
C-13´	140.39	*C*	-	8.21, 8.02, 6.85
C-14´	128.5	128.5 (*C*H)	8.22	8.02

The ^{13}C NMR shows two deshield shifts at 161.4 ppm and 158.0 ppm where by DEPT 135° and HSQC were proved as quaternary carbons (see TABLE 4.9). Ten signals in the unsaturated zone (100-150 ppm) proved there are two aromatic rings present. In the most shielded zone of the spectra seven peaks that correspond to aliphatic carbons were observed. Since a peak having 21.5 ppm correlates directly with 1.29 ppm by HSQC, which is a duplet (J = 7.3 Hz) in the ^{1}H

NMR (FIGURE 4.4) that integrates for 3H, we can attribute it to the methyl group *C*-6. By HMBC it was determined that *C*-6 correlates with three peaks at 3.95 ppm, 3.84 ppm and 2.44 ppm. By HSQC and DEPT 135° (TABLE 4.9) we could identify each proton as *C*H groups. As previously mentioned, only one *C*H$_2$ with 51.5 ppm was observed in DEPT 135° spectra and can be arbitrarily attributed to *C*-8. In the HMBC spectra the *C*-8 correlates only with the shifts 7.23 ppm and 3.84 ppm. Then, by HSQC carbon correlation with 3.84 ppm, we determined *C*-5 as another *C*H.
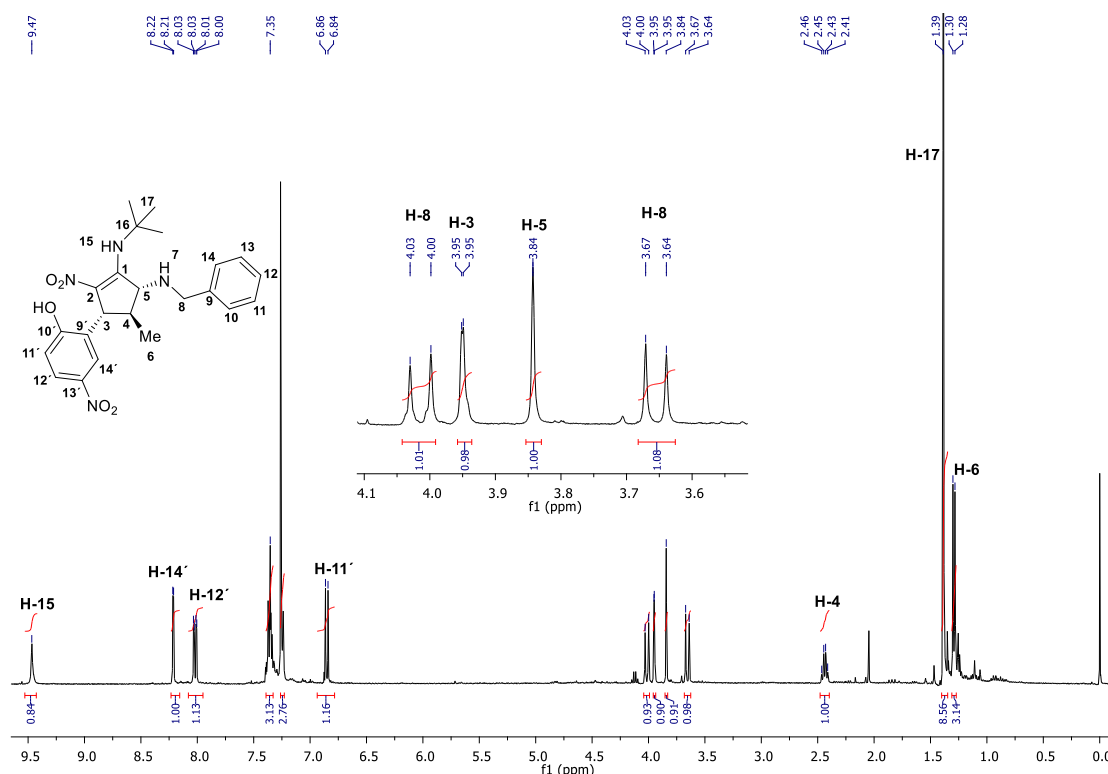
FIGURE 4.4- 400 MHz ^{1}H NMR spectra in CDCl$_3$ of compound **160**. Zoom range between 3.50-4.10 ppm.

To continue the attributions we proceed to analyze the ^{1}H NMR spectra (FIGURE 4.4). In the aromatic zone of ^{1}H NMR two multiplets at 7.23 ppm and 7.35ppm attributed to the benzyl aromatic ring. In the same aromatic zone of the spectra some signals appear that confirm the substituted aromatic ring with nitro and phenol groups. A duplet at 8.21 ppm with coupling constant *J* = 2.8 Hz is attributed to *H*-14´, a duplet of duplet with *J* = 8.9, 2.8 Hz at 8.01 ppm is assigned to *H*-12´ and a duplet at 6.86 ppm (*J* = 8.9 Hz) for H-11´. In the aliphatic zone, there is a singlet at 1.39 ppm which integrates to 9H. This was assigned to the three methyl of *tert*-butyl group with carbon shift 31.1 ppm (*C*-17). At 2.44 ppm a quartet of duplet (*J$_q$* = 7.5 Hz, *J$_d$* = 2.5 Hz) was identified as *H*-4 due to the COSY correlation with the methyl *C*-6. Analyzing the HSQC experiment, *H*-4 correlates with the carbon at shift 39.1 ppm, which is a *C*H

93

determined by DEPT 135°. A singlet at 9.50 ppm can be attributed to an heteroatom due to the lack of carbon coupling in the HSQC experiment.

The attribution of the range of 3.60-4.10 ppm results to be complex. In FIGURE 4.4 two identical duplet at 4.01 ppm and 3.65 ppm with $J = 12.7$ Hz are observed. By HSQC was observed that both shifts correlates directly with the same shift at 51.5 ppm, which correspond to the only methylene group in the molecule (C-8). Then these two duplet are attributed to H-8. At 3.95 ppm a duplet was observed with low coupling constant ($J = 1.0$ Hz). This signal correlates by COSY with H-4 at 2.44 ppm and by HSQC with 52.47 ppm which is a CH carbon. The HMBC correlation of this carbon shows a correlation with 8.21 ppm this shift 3.95 ppm as H-3 was attributed. The lower value of J was important to us to identify the relative configuration of the five-member ring. Generally this lower values are due to the angle adopted and is known that dihedral angles of 90° produce $J \approx 1.0$ Hz or less. Then, H-3 and H-4 are in different planes. Finally, the last signal to attribute is a singlet with shift 3.84 ppm and corresponds to H-5, which also is in different plane to H-4.

Conclusions: Chapter 2

A conjugate addition of nitroethanol to α,β-unsaturated aldehydes mediated by diphenylprolinol silyl ether organocatalyst was performed to obtain 1-hydroxy-*trans*-3,4-disubstituted tetrahydropyrans in excellent ee and moderate *dr.* (up to 90% ee, *dr.* 8:2). Some modifications of the reported procedure have been done to improve the ee as well as the efficiency of the reaction, giving the best results for α,β-unsaturated aldehydes with an electron withdrawing group attached to the *para* position of Ph group. Furthermore, a new class of medium-sized cyclic peptidomimetics were obtained by a MCR approach based on the Ugi-5C-3CR. Seventeen compounds in a yield range of 32-77% were described and fully characterized by NMR techniques. A complex mixture of diastereoisomers was detected by NMR analysis showing low diastereoisomeric ratio for all medium sized cyclic peptidomimetics. In addition, two non-commercial isocyanides have been synthesized; (e.g., isocyanopeptides and sugar derived isocyanide) which were obtained in a global yield of 60% and 64%, respectively.

A highly stereoselective and one-pot sequence leading to complex natural product-like was developed. Hydroquinolin-6-ones were obtained in a yield range of 59-75% and high stereoselectivity (*dr.* >99:1, >99% ee). From a synthetic point of view, the present approach can be regarded as an asymmetric multicomponent ligation process that integrates up to four different molecular fragments into a single skeleton. This report confirms that the asymmetric aminocatalytic functionalization of carbonyl compounds is an effective pre-MCR process capable of providing enantiomerically enriched building blocks for subsequent multicomponent diversification. The versatility of this diversity-oriented strategy relies on the vast number of 1,3-dicarbonyls and α,β-unsaturated aldehydes that could be combined with amines and isocyanides of biomolecular nature. Such a facile variation of reaction components combines with the great levels of molecular complexity available with low synthetic cost. Finally, we envision that other iminium, enamine, and NHC-organocatalytic processes may be combined with varied MCRs, hence expanding the repertoire of stereoselective multicomponent cascade reactions.

A tandem Michael addition-hemiacetalization, mediated by pyrrolidine, to obtain 3-alkyl-4-nitromethylchromans was developed. The new variant of the Ugi-Smile reaction to produce new tetrahydroquinolines natural products-like was employed. Unfortunately, the desirable compounds were not obtained by this methodology. However, a new pentasubstituted cyclopentene obtained as a single diastereomer and moderate yield. Compound **160** was fully characterized by NMR techniques.

Perspectives: Chapter 2

→ After synthesizing the small library of medium-sized cyclic peptidomimetics we might develop some derivatization of compounds to extend the methodology to other classes of compounds and then conclude this results to submit an article.

→ A computational calculus for the proposed mechanism of pentasubstituted cyclopentenes will be done to confirm the results obtained until now. The asymmetric version also is planned to be develop in our group soon.

Experimental Section

5 Experimental Section

5.1 General Aspects

Materials and reagents were of the highest commercially available grade purchased from Aldrich and used without further purification. Compounds were visualized by UV, $KMnO_4$, I_2 and Vanillin solutions. Flash chromatography was performed using silica gel 60, particle size 40-63 μm and analytical thin layer chromatography (TLC) was performed using silica gel aluminum sheets. Solvents for extractions and for column chromatography were previously distilled. Chemical yields were given after chromatographical purification. ^{1}H NMR and ^{13}C NMR spectra were recorded at 400 MHz for ^{1}H and 100 MHz for ^{13}C, respectively. Chemical shifts (δ) are reported in parts per million relative to the residual solvent signals, and coupling constants (J) are reported in hertz. NMR peak assignments were accomplished by analysis of the COSY, HSQC, HMBC and NOE data. High resolution ESI mass spectra were obtained from a Fourier transform ion cyclotron resonance (FT-ICR) mass spectrometer, an RF-only hexapole ion guide and an external electrospray ion source. Normal Phase HPLC analysis were carried out on an analytical HPLC with a diode array detector SPD-M20A from Shimadzu using Chiralpak columns (AD-H, OD-H) (250 mm x 4.6 mm) from Daicel Chemical Ind. LTD. Optical rotations were measured on a Perkin Elmer Polarimeter 341. Thermogravimetric analysis (TGA) was conducted using a thermogravimetric analyzer (TGA, Perkin Elmer) operated in the temperature range of 10–700 ^{o}C under nitrogen gas and a heating rate of 10 ^{o}C min^{-1}. For compounds arising from the Ugi-4CR, the assigned signals belong to a mixture of conformers.

5.2 Experimental section of Chapter 1

5.2.1 General procedures

General Procedures: Synthesis of prolyl *pseudo*-peptides by Ugi-4CR
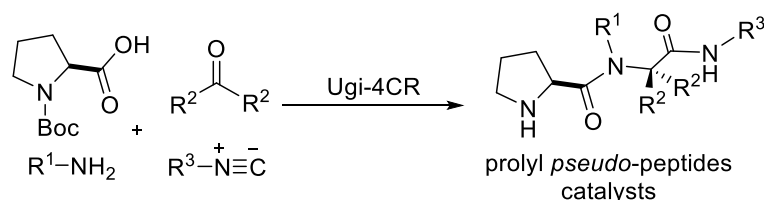
General Procedure 1: α-Amino acid methyl ester hydrochloride (1.0 mmol), aldehyde (1.0 mmol) and NEt$_3$ (1.0 mmol) were dissolved in MeOH (5 mL). The carboxylic acid (1.0 mmol) and the isocyanide (1.0 mmol) were then added and the reaction mixture was stirred at

room temperature for 24 h and then concentrated under reduced pressure to dryness. The resulting crude product was dissolved in CH$_2$Cl$_2$ (100 mL) and the organic phase was washed sequentially with aqueous saturated solution of citric acid (50 mL), aqueous 10% NaHCO$_3$ (50 mL), and brine (50 mL), and then dried over anhydrous Na$_2$SO$_4$ and concentrated under reduced pressure. The resulting amorphous solid was used in the Boc deprotection step without further purification.

General Procedure 2: Aliphatic amine (1.0 mmol) and the aldehyde (or ketone) (1.0 mmol) in MeOH (5 mL) was stirred for 1 h at room temperature. The carboxylic acid (1.0 mmol) and the isocyanide (1.0 mmol) were then added and the reaction mixture was stirred at room temperature for 24 h and then concentrated under reduced pressure to dryness. The resulting crude product was dissolved in CH$_2$Cl$_2$ (100 mL) and the organic phase was washed sequentially with aqueous saturated solution of citric acid (50 mL), aqueous 10% NaHCO$_3$ (50 mL), and brine (50 mL), and then dried over anhydrous Na$_2$SO$_4$ and concentrated under reduced pressure. The resulting amorphous solid was used in the Boc deprotection step without further purification.

General Procedure 3: The α-amino acid methyl ester hydrochloride (1.0 mmol), aldehyde (1.0 mmol) and NEt$_3$ (1.0 mmol) were dissolved in MeOH (5 mL) and added to a 10 mL glass tube. The suspension was treated with the carboxylic acid (1.0 mmol) and the isocyanide (1.0 mmol) and the glass tube was sealed and introduced in the microwave reactor (CEM Co., Discover). The flask was irradiated for 30 min (150 W) under high speed magnetic stirring, while the temperature was raised up to 70 °C. The reaction course was monitored by TLC, and additional 30 min cycles were applied in cases of poor consumption of the starting material. The resulting crude product was dissolved in CH$_2$Cl$_2$ (100 mL) and the organic phase was washed sequentially with aqueous saturated solution of citric acid (50 mL), aqueous 10% NaHCO$_3$ (2×50 mL), and brine (50 mL), and then dried over anhydrous Na$_2$SO$_4$ and concentrated under reduced pressure. The resulting amorphous solid was used in the Boc deprotection step without further purification.

General Procedure 4: Boc deprotection of prolyl *pseudo*-peptides using TFA

The crude product resulting form the Ugi-4CR was dissolved in 3 mL of CH₂Cl₂ and treated with 1 mL of trifluoroacetic acid at 0 °C. The reaction mixture was allowed to reach room temperature, stirred for 4 h and then concentrated to dryness (TFA was removed completely by repetitive addition and evaporation of further CH₂Cl₂). The crude product was dissolved in 10 mL of CH₂Cl₂, treated with solid K₂CO₃ until basic pH and the solution was filtered and evaporated under reduced pressure.

General Procedure 5: Polymerization of prolyl *pseudo*-peptides
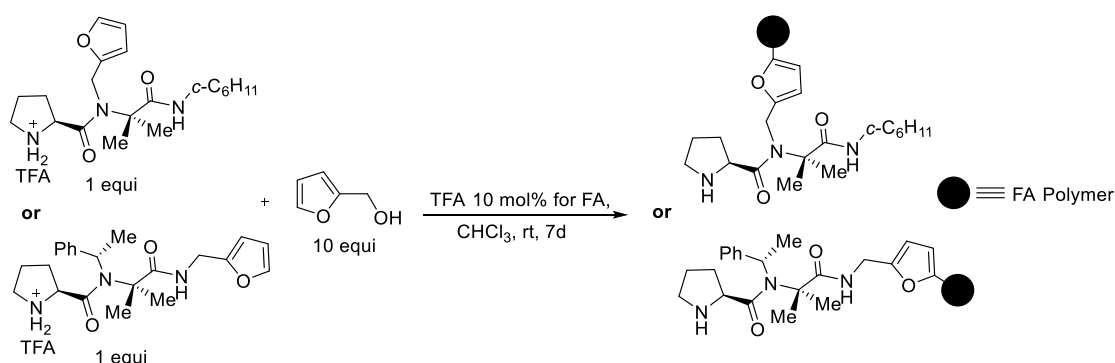
To a suspension of the pseudo-peptide catalysts (1.0 mmol) and furfuryl alcohol (10 mmol) in CHCl₃ (5 mL) was added TFA (0.5 mmol) drop by drop for 10 min, and then, the yellow mixture was stirred for 7 d at room temperature. The mixture changed the color during the time of reaction from yellow- green to brown or dark color. The neutralization of the polymerizing solution was carried out with a concentrated basic solution. The use of a 1 M NaOH (5 mL) solution requires two washes of 10 min each but at the end of the reaction an emulsion may appear. In order to avoid this problem an excess of 0.1 M NaOH solution was used. Polymers were isolated by precipitation in petroleum ether and dried by using a high vacuum line. The resulting dark solid was ground until 45 μm of diameter of particles using a molecular tamizes.

General Procedure 6: Hydrolysis of methyl ester to carboxylic acid

The ester obtained in the above step was stirred with 10% LiOH solution in methanol water mixture for 8-12 hours. Methanol was removed under vacuum and cold water was added to this mixture and acidified with dilute hydrochloric acid to precipitate the acid. The acid was filtered and dried.

5.2.2 General procedures for asymmetric reactions

General procedure 7: Asymmetric Aldol reaction
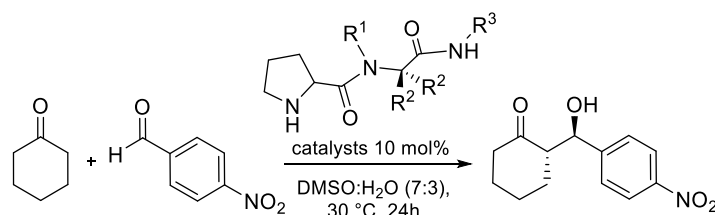
The aldehyde (0.25 mmol, 1.0 equiv) and the ketone (0.75 mmol, 3.0 equiv) were added to a solution of the prolyl *pseudo*-peptide (0.025 mmol, 0.01 equiv.) in the solvent of choice (1 mL). The reaction mixture was stirred for 24 h. Then, the reaction was treated with saturated ammonium chloride solution and the layers were extracted with ethyl acetate (3×2 mL). The combined organic layers were dried (MgSO₄) and concentrated under reduced pressure. The resulting crude product was purified by flash column chromatography on silica gel using *n*-hexane/EtOAc (9:1) as eluent. Enantiomeric excess (ee) was determined by chiral HPLC analysis through comparison with the authentic racemic material. Assignment of the stereoisomers was performed by comparison with literature data.[111]

General procedure 8: Asymmetric 1,4-addition of aldehydes to nitro-olefins
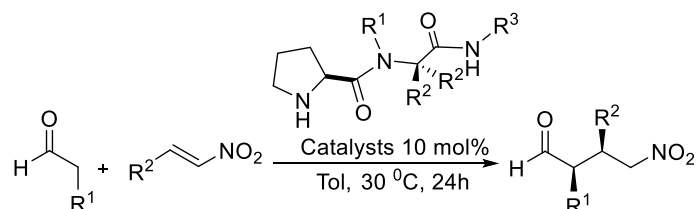
The nitroolefin (0.25 mmol, 1.0 equiv) and the aldehyde (0.75 mmol, 3.0 equiv) were added to a solution of the prolyl *pseudo*-peptide (0.025 mmol, 0.01 equiv.) in the solvent of choice (1 mL). The reaction mixture was stirred for 24 h and then concentrated under reduced pressure. The resulting crude product was purified by flash column chromatography on silica gel using *n*-hexane/EtOAc as eluent. Enantiomeric excess (ee) was determined by chiral HPLC analysis through comparison with the authentic racemic material. Assignment of the stereoisomers was performed by comparison with literature data. 114[110,111,112,113]

5.2.3 Synthesis and spectroscopy data of prolyl *pseudo*-peptides

Compound 61:
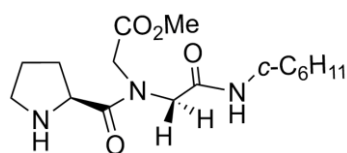
HCl·Gly-OMe (125 mg, 1 mmol), triethylamine (140 μL, 1 mmol) paraformaldehyde (30 mg, 1 mmol), Boc-L-Pro-OH (215 mg, 1 mmol) and cyclohexylisocyanide (125 μL, 1 mmol) were reacted in MeOH (5 mL) according to the general Ugi-4CR-based procedure 3. The resulting Boc protected compound was subjected to the general deprotection procedure 4. Flash column chromatography purification (MeOH/EtOAc 4:1) afforded peptide-peptoid hybrid **61** (254 mg, 78%) as a colorless oil. A mixture of conformers in a 6:4 ratio was observed by NMR.

R_f = 0.25 (EtOAc / MeOH 8:2).

$[\alpha]_D^{25}$ = -15.1 (*c* 0.62, MeOH, 25 °C).

^{1}H NMR (400 MHz, CDCl$_3$) δ = 6.95, 7.48 (2×d, 1H, *J* = 8.0 Hz); 4.96 (m, 1H); 4.15 (m, 1H); 4.31 (d, 1H, *J* = 17.2 Hz); 4.10 (d, 1H, *J* = 17.2 Hz); 3.76, 3.80 (2×s, 3H); 3.67-3.80 (m, 1H); 3.37-3.50 (m, 2H); 2.41 (m, 1H); 1.99-2.17 (m, 3H); 1.55-1.95 (m, 6H); 1.09-1.40 (m, 6H).

^{13}C NMR (100 MHz, CDCl$_3$) δ = 170.1, 169.6, 165.9, 57.9, 53.4, 52.7, 51.7, 49.4, 46.4, 32.5, 29.0, 25.3, 24.9, 24.8.

HRMS (ESI-FT-ICR) [MH]$^+$ calcd. for $C_{16}H_{28}N_3O_4$: 326.2069, found 326.2072

Compound 62:
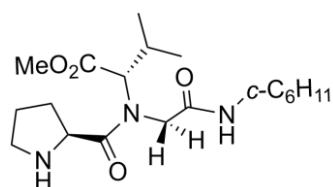
HCl·Val-OMe (168 mg, 1 mmol), triethylamine (140 μL, 1 mmol) paraformaldehyde (30 mg, 1 mmol), Boc-L-Pro-OH (215 mg, 1 mmol) and cyclohexylisocyanide (125 μL, 1 mmol) were reacted in MeOH (5 mL) according to the microwave-assisted Ugi-4CR-based procedure 3, using two cycles of 30 min. The resulting Boc protected compound was subjected to the general deprotection procedure 4. Flash column chromatography purification (MeOH/EtOAc 4:1) afforded peptide-peptoid hybrid **62** (297.7 mg, 81%) as a colorless oil. A mixture of conformers in a 7:3 ratio was observed by NMR.

R_f = 0.45 (EtOAc/MeOH 8:2).

$[\alpha]_D^{25}$ = -56.1 (*c* 0.56, MeOH, 25 °C).

^{1}H NMR (400 MHz, CDCl$_3$) δ = 6.59, 7.11 (2×d, 1H, *J* = 7.8 Hz); 4.78, 4.85(2×m, 1H); 3.81, 4.46 (2×d, 1H, *J* = 10.4/9.7 Hz); 4.13, 4.25 (2×d, 1H, *J* = 18 Hz); 3.95, 4.15 (2×d, 1H, *J* = 16 Hz); 3.62-3.76 (m, 1H); 3.72, 3.74 (2×s, 3H); 3.38-3.53 (m, 2H); 3.16-3.34 (m, 1H); 1.94-2.54

(m, 5H); 1.54-1.91 (m, 5H); 1.06-1.39 (m, 5H); 0.98 (d, 3H, J = 6.6 Hz); 0.87 (d, 3H, J = 6.6 Hz).

^{13}C NMR (100 MHz, CDCl$_3$) δ = 168.2, 167.5, 163.1, 67.6, 58.8, 51.1, 48.2, 44.5, 32.9, 32.8, 30.9, 29.5, 25.5, 24.6, 21.7, 20.0, 15.8.

HRMS (ESI-FT-ICR) [MH]$^+$ calcd. for C$_{19}$H$_{34}$N$_3$O$_4$: 368.2538, found 368.2543

Compound 63:
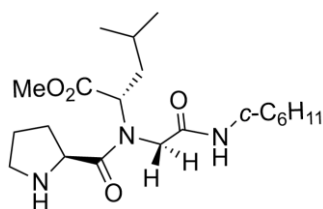
HCl·Leu-OMe (182 mg, 1 mmol), triethylamine (140 μL, 1 mmol) paraformaldehyde (30 mg, 1 mmol), Boc-L-Pro-OH (215 mg, 1 mmol) and cyclohexylisocyanide (125 μL, 1 mmol) were reacted in MeOH (5 mL) according to the microwave-assisted Ugi-4CR-based procedure 3, using two cycles of 30 min. The resulting Boc protected compound was subjected to the general deprotection procedure 4. Flash column chromatography purification (MeOH/EtOAc 4:1) afforded peptide-peptoid hybrid **63** (324 mg, 85%) as a colorless oil. A mixture of conformers in a 7:3 ratio was observed by NMR.

R_f = 0.50 (EtOAc/MeOH 8:2).

[α]$_D^{25}$ = -42.7 (*c* 0.66, MeOH, 25 °C).

^{1}H NMR (400 MHz, CDCl$_3$) δ = 6.59, 7.56 (2×d, 1H, J = 7.7 Hz); 4.79 (t, 1H, J = 7.1 Hz); 4.66 (t, 1H, J = 7.1 Hz); 4.32 (2×d, 1H, J = 8.8/5.1 Hz); 4.19 (d, 1H, J = 18.2 Hz); 4.04 (d, 1H, J = 18.2 Hz); 3.74 (s, 3H); 3.64-3.71 (m, 2H); 3.40-3.50 (m, 2H); 3.05 (br. s, 1H); 2.44 (m, 1H); 1.98-2.23 (m, 2H); 1.54-1.91(m, 7H); 1.07-1.39 (m, 5H); 0.84-1.00 (m, 6H).

^{13}C NMR (100 MHz, CDCl$_3$) δ = 172.2, 170.4, 166.5, 58.3, 58.1, 52.7, 49.4, 49.2, 46.2, 38.4, 37.6, 32.3, 29.1, 25.3, 25.0, 24.9, 24.6, 22.4, 22.1.

HRMS (ESI-FT-ICR) [MH]$^+$ calcd. for C$_{20}$H$_{36}$N$_3$O$_4$: 382.2698, found 382.2700

Compound 64:
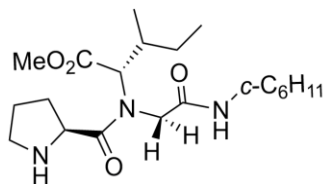
HCl·Ile-OMe (182 mg, 1 mmol), triethylamine (140 μL, 1 mmol) paraformaldehyde (30 mg, 1 mmol), Boc-L-Pro-OH (215 mg, 1 mmol) and cyclohexylisocyanide (125 μL, 1 mmol) were reacted in MeOH (5 mL) according to the microwave-assisted Ugi-4CR-based procedure 3, using two cycles of 30 min. The resulting Boc protected compound was subjected to the general deprotection procedure 4. Flash column chromatography purification

(MeOH/EtOAc 4:1) afforded peptide-peptoid hybrid **64** (294 mg, 77%) as a colorless oil. A mixture of conformers in a 1:1 ratio was observed by NMR.

R_f = 0.50 (EtOAc / MeOH 8:2).

$[\alpha]_D^{25}$ = -59.1 (*c* 0.65, MeOH, 25 °C).

^{1}H NMR (400 MHz, CDCl$_3$) δ = 6.46, 6.85 (2×d, 1H, *J* = 8.0 Hz); 4.81, 4.90 (2×t, 1H, *J* = 8.0 Hz); 3.88, 4.66 (2×d, 1H, *J* = 10.0 Hz); 4.14, 4.26 (2×d, 1H, *J* = 18.2 Hz); 4.02, 4.16 (2×d, 1H, *J* = 16.0 Hz); 3.73 (s, 3H); 3.63-3.71 (m, 1H); 3.46 (m, 2H); 2.40, 2.49 (2×m, 1H); 1.49-2.26 (m, 10H); 1.01-1.44 (m, 6H); 0.94 (d, 3H, *J* = 6.5 Hz); 0.86 (t, 3H, *J* = 7.35 Hz).

^{13}C NMR (100 MHz, CDCl$_3$) δ = 170.9, 169.4, 166.6, 63.1, 58.4, 52.6, 48.9, 47.8, 47.00, 46.6, 46.3, 34.1, 32.4, 29.5, 25.6, 25.3, 25.2, 24.8, 15.7, 11.4.

HRMS (ESI-FT-ICR) [MH]$^+$ calcd. for C$_{20}$H$_{36}$N$_3$O$_4$: 382.2695, found 382.2700

Compound 65:
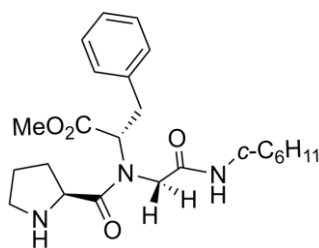
HCl·Phe-OMe (216 mg, 1 mmol), triethylamine (140 μL, 1 mmol) paraformaldehyde (30 mg, 1 mmol), Boc-L-Pro-OH (215 mg, 1 mmol) and cyclohexylisocyanide (125 μL, 1 mmol) were reacted in MeOH (5 mL) according to the microwave-assisted Ugi-4CR-based procedure 3, using two cycles of 30 min. The resulting Boc protected *pseudo*-peptide was subjected to the general deprotection procedure 4. Flash column chromatography purification (MeOH/EtOAc 4:1) afforded peptide-peptoid hybrid **65** (345 mg, 83%) as a light yellow oil. A mixture of conformers in a 7:3 ratio was observed by NMR.

R_f = 0.40 (EtOAc/MeOH 8:2).

$[\alpha]_D^{25}$ = -87.6 (*c* 0.47, MeOH, 25 °C).

^{1}H NMR (400 MHz, CDCl$_3$) δ = 7.71 (d, 1H, *J* = 7.8 Hz); 7.18-7.38 (m, 4H); 7.12-7.14 (m, 1H); 4.55 (dd, 1H, *J* = 7.2 Hz); 4.25 (dd, 1H, *J* = 10.0/5.9 Hz); 4.20 (m, 1H); 3.77 (s, 3H); 3.66 (m, 1H); 3.22-3.54 (m, 4H); 2.30 (m, 1H); 2.08 (m, 2H); 1.52-1.99 (m, 5H); 1.06-1.43 (m, 5H).

^{13}C NMR (100 MHz, CDCl$_3$) δ = 170.4, 169.5, 165.4, 136.2, 129.9, 129.2, 129.0, 128.4, 127.5, 63.8, 57.9, 53.0, 52.6, 49.2, 46.1, 34.4, 32.4, 29.1, 25.3, 25.0, 24.9, 24.7.

HRMS (ESI-FT-ICR) [M+H]$^+$ calcd. for C$_{23}$H$_{34}$N$_3$O$_4$: 416.2535, found 416.2541

Compound 66:
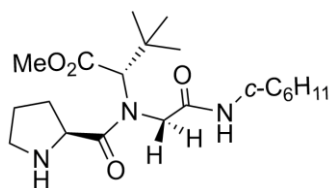
HCl·*t*BuGly-OMe (182 mg, 1 mmol), triethylamine (140 µL, 1 mmol) paraformaldehyde (30 mg, 1 mmol), Boc-L-Pro-OH (215 mg, 1 mmol) and cyclohexylisocyanide (125 µL, 1 mmol) were reacted in MeOH (5 mL) according to the microwave-assisted Ugi-4CR-based procedure 3, using three cycles of 30 min. The resulting Boc protected compound was subjected to the general deprotection procedure 4. Flash column chromatography purification (MeOH/EtOAc 4:1) afforded peptide-peptoid hybrid **66** (233 mg, 61%) as a colorless oil. A mixture of conformers in a 1:1 ratio was observed by NMR.

R_f = 0.55 (EtOAc/MeOH 8:2).

$[\alpha]_D^{25}$= -5.9 (*c* 0.43, MeOH, 25 °C).

^{1}H NMR (400 MHz, CDCl₃) δ = 5.12 (s, 1H); 4.18, 4.29 (2×d, 1H, *J* = 18.4 Hz); 4.12 (dd, 1H, *J* = 7.7/3.1 Hz); 3.67-3.77 (m, 1H); 3.73, 3.80 (2×s, 3H); 3.55-3.65 (m, 1H); 3.13 (m, 1H); 2.81 (m, 1H); 2.50 (m, 1H); 2.19 (m, 1H); 1.55-2.02 (m, 13H); 1.00-1.43 (m, 3H); 1.05, 1.09 (2×s, 9H).

^{13}C NMR (100 MHz, CDCl₃) δ = 170.0, 169.6, 164.3, 62.0, 59.2, 51.8, 50.7, 47.8, 45.6, 36.4, 32.8, 30.8, 28.6, 28.1, 27.8, 25.6, 25.4, 25.1, 23.2.

HRMS (ESI-FT-ICR) [MH]$^+$ calcd. for $C_{20}H_{36}N_3O_4$: 382.2695, found 382.2700

Compound 67:
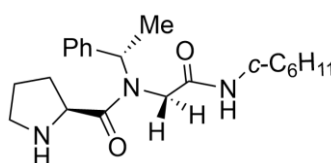
(*S*)-α-Methylbenzylamine (128 µL, 1 mmol), paraformaldehyde (30 mg, 1 mmol), Boc-L-Pro-OH (215 mg, 1 mmol) and cyclohexylisocyanide (125 µL, 1 mmol) were reacted in MeOH (5 mL) according to the general Ugi-4CR-based procedure 2. The resulting Boc protected compound was subjected to the general deprotection procedure 4. Flash column chromatography purification (MeOH/EtOAc 4:1) afforded peptide-peptoid hybrid **67** (325 mg, 91%) as a colorless oil. A mixture of conformers in a 6:4 ratio was observed by NMR.

R_f = 0.55 (EtOAc / MeOH 8:2).

$[\alpha]_D^{25}$ = -62.8 (*c* 0.64, MeOH, 25 °C).

^{1}H NMR (400 MHz, CDCl₃) δ = 7.72 (br. s, 1H); 7.22-7.40 (m, 5H); 5.87, 6.35 (2×q, 1H, *J* = 7.25 Hz); 4.70, 5.10 (2×m, 1H); 3.51, 3.93 (2×d, 1H, *J* = 16.0 Hz); 3.71, 3.89 (2×d, 1H, *J* = 18.0 Hz); 3.61 (m, 1H); 3.45 (m, 2H); 2.85 (br. m, 1H); 3.40, 2.54 (2×m, 1H); 2.17 (m, 2H); 1.47-1.84 (m, 4H); 1.49, 169 (2×d, 3H, *J* = 7.2 Hz); 1.01-1.36 (m, 5H).

13C NMR (100 MHz, CDCl₃) δ = 166.5, 162.7, 137.7, 129.1, 128.8, 128.6, 127.4, 127.1, 60.4, 58.2, 55.6, 49.2, 48.7, 46.6, 46.1, 32.5, 32.2, 29.8, 25.3, 24.9, 17.4.

HRMS (ESI-FT-ICR) [MH]⁺ calcd. for $C_{21}H_{32}N_3O_2$: 358.2483, found 358.2483

Compound 68:
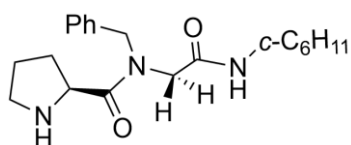
Benzylamine (110 µL, 1 mmol), paraformaldehyde (30 mg, 1 mmol), Boc-L-Pro-OH (215 mg, 1 mmol) and cyclohexylisocyanide (125 µL, 1 mmol) were reacted in MeOH (5 mL) according to the general Ugi-4CR-based procedure 2. The resulting Boc protected compound was subjected to the general deprotection procedure 4. Flash column chromatography purification (MeOH/EtOAc 4:1) afforded peptide-peptoid hybrid **68** (639 mg, 93%) as a pale green oil. A mixture of conformers in a 7:3 ratio was observed by NMR.

R_f = 0.45 (EtOAc/MeOH 8:2).

$[\alpha]_D^{25}$ = -21.1 (c 0.41, MeOH, 25 °C).

1H NMR (400 MHz, CDCl₃) δ = 7.18-7.40 (m, 5H); 6.76 (d, 1H, J = 8.0 Hz); 4.79, 4.90 (2×m, 1H); 4.66 (m, 2H); 3.97 (m, 2H); 3.69 (m, 1H); 3.39-3.55 (m, 2H); 2.83 (br. s, 1H); 2.23, 2.38 (2×m, 1H); 1.96-2.10 (m, 3H); 1.52-1.85 (m, 4H); 1.05-1.37 (m, 5H).

13C NMR (100 MHz, CDCl₃) δ = 170.0, 166.4, 134.2, 129.3, 128.9, 128.5, 128.3, 127.3, 58.3, 52.2, 50.8, 49.3, 48.8, 45.9, 32.5, 29.5, 25.4, 25.0, 24.8.

HRMS (ESI-FT-ICR) [MH]⁺ calcd. for $C_{20}H_{30}N_3O_2$: 344.2328, found 344.2328

Compound 69:
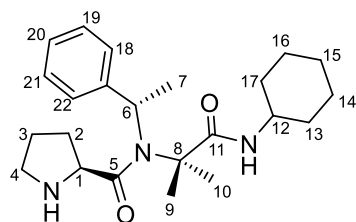
(S)-α-Methylbenzylamine (128 µL, 1 mmol), acetone (74 µL, 1 mmol), Boc-L-Pro-OH (215 mg, 1 mmol) and cyclohexylisocyanide (125 µL, 1 mmol) were reacted in MeOH (5 mL) according to the general Ugi-4CR-based procedure 2. The resulting Boc protected compound was subjected to the general deprotection procedure 4. Flash column chromatography purification (MeOH/EtOAc 4:1) afforded peptide-peptoid hybrid **69** (309 mg, 77%) as a colorless oil.

R_f = 0.55 (EtOAc / MeOH 8:2).

$[\alpha]_D^{25}$ = -1.9 (c 0.38, MeOH, 25 °C).

1H NMR (600 MHz, CDCl₃) δ = 7.56 (d, 2H, J = 7.7 Hz, Ph); 7.42 (m, 2H, Ph); 7.28-7.34 (m, 1H, Ph); 5.70 (d, 1H, J = 7.6 Hz, NH); 5.10 (q, J = 8.0 Hz, 1H, H-6); 4.30 (m, 1H, H-1); 3.64

(m, 1H, H-12); 3.22 (m, 1H); 3.05 (m, 1H); 1.92-2.05 (m, 3H); 1.88 (d, 3H, J = 7.0 Hz, H-7); 1.77-1.82 (m 2H); 1.66-1.73 (m, 3H); 1.64 (s, 3H, H-9); 1.53 (s, 3H, H-10); 1.27-1.42 (m, 6H); 1.15-1.19 (m, 4H).

¹³C NMR (100 MHz, CDCl₃) δ = 173.7 (*C*=O, *C*-11), 170.6 (*C*=O, *C*-5), 140.7 (*C*, *C*-18); 129.2, 128.2, 128.0, 127.2, (*C*H, Ph); 64.6 (*C*, *C*-8); 59.7 (*C*H, *C*-1), 50.7 (*C*H, *C*-6), 48.9, (*C*H ,*C*-12) (*C*H); 46.3, 25.4, 28.9, 30.8, 32.7 (*C*H₂); 24.8 (*C*H₃, *C*-9), 24.6 (*C*H₃, *C*-10); 24.3 (*C*H₂); 19.0 (*C*H₃, *C*-7).

DEPT 135 (100 MHz, CDCl₃) δ =129.2, 128.2, 128.0, 127.2, (*C*H, Ph); 59.7 (*C*H, *C*-1), 50.7 (*C*H, *C*-6), 48.9, (*C*H ,*C*-12) (*C*H); 46.3, 25.4, 28.9, 30.8, 32.7 (*C*H₂); 24.8 (*C*H₃, *C*-9), 24.6 (*C*H₃, *C*-10); 24.3 (*C*H₂); 19.0 (*C*H₃, *C*-7).

HRMS (ESI-FT-ICR) [MH]⁺ calcd. for $C_{23}H_{36}N_3O_2$: 386.2802, found 386.2800

Compound 70:
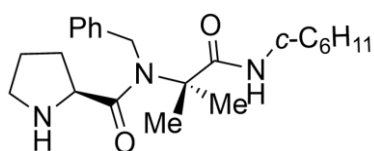
Benzylamine (110 μL, 1 mmol), acetone (74 μL, 1 mmol), Boc-L-Pro-OH (215 mg, 1 mmol) and cyclohexylisocyanide (125 μL, 1 mmol) were reacted in MeOH (5 mL) according to the general Ugi-4CR-based procedure 2. The resulting Boc protected compound was subjected to the general deprotection procedure 4. Flash column chromatography purification (MeOH/EtOAc 4:1) afforded peptide-peptoid hybrid **70** (229 mg, 73%) as a colorless oil.

R_f = 0.50 (EtOAc/MeOH 8:2).

[α] $_D^{20}$ = -20.6 (*c* 0.41, MeOH, 25 °C).

¹H NMR (400 MHz, CDCl₃) δ = 7.22-7.44 (m, 5H); 5.98 (d, 1H, J = 8.0 Hz); 4.76 (d, 2H, J = 6.91 Hz); 4.69 (m, 1H); 3.68 (m, 1H); 3.40 (m, 2H); 3.03 (br. m, 1H); 1.78-2.06 (m, 6H); 1.55-1.75 (m, 3H); 1.50 (s, 3H); 1.46 (s, 3H); 1.06-1.39 (m, 5H).

¹³C NMR (100 MHz, CDCl₃) δ = 173.0, 169.9, 136.9, 129.2, 128.0, 126.4, 64.1, 58.9, 48.8, 47.9, 46.0, 32.7, 32.6, 29.7, 25.4, 24.9, 24.5, 24.1.

HRMS (ESI-FT-ICR) [MH]⁺ calcd. for $C_{22}H_{33}N_3O_2$: 372.2654, found 372.2651

Compound 71:
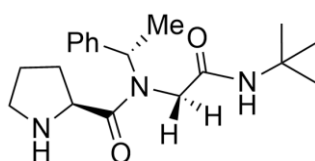
(*S*)-α-Methylbenzylamine (128 μL, 1 mmol), paraformaldehyde (30 mg, 1 mmol), Boc-L-Pro-OH (215 mg, 1 mmol) and *t*-butylisocyanide (125 μL, 1 mmol) were reacted in MeOH (5 mL) according to the general Ugi-4CR-based procedure 2. The resulting

Boc protected compound was subjected to the general deprotection procedure 4. Flash column chromatography purification (MeOH/EtOAc 4:1) afforded peptide-peptoid hybrid **71** (298 mg, 88%) as a light yellow oil. A mixture of conformers in a 8:2 ratio was observed by NMR.

R_f = 0.55 (EtOAc/MeOH 8:2).

$[\alpha]_D^{25}$ = -78.9 (*c* 0.65, MeOH, 25 °C).

^{1}H NMR (400 MHz, CDCl$_3$) δ = 7.80 (br. s, 1H); 7.24-7.39 (m, 5H); 5.78 (m, 1H); 4.98, 5.11 (2×m, 1H); 3.45, 3.95 (2×d, 1H, *J* = 16.0 Hz); 3.61, 3.88 (2×d, 1H, *J* = 18.0 Hz); 3.32-3.55 (m, 1H); 2.42, 2.58 (2×m, 1H); 1.87-2.25 (m, 3H); 1.46, 1.68 (2×d, 3H, *J* = 6.88 Hz); 1.49 (2×s, 3H); 1.23, (2×s, 6H).

^{13}C NMR (100 MHz, CDCl$_3$) δ = 170.2, 167.2, 137.9, 129.2, 128.8, 128.6, 127.0, 125.8, 58.2, 55.5, 53.6, 51.3, 47.0, 46.9, 29.9, 28.5, 28.4, 24.9, 17.4.

HRMS (ESI-FT-ICR) [MH]$^+$ calcd. for C$_{19}$H$_{30}$N$_3$O$_2$: 332.2293, found 332.2327

Compound 72:
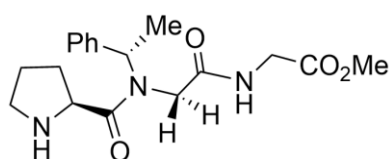
(*S*)-α-Methylbenzylamine (128 μL, 1 mmol), paraformaldehyde (30 mg, 1 mmol), Boc-L-Pro-OH (215 mg, 1 mmol) and methyl isocyanoacetate (91 μL, 1 mmol) were reacted in MeOH (5 mL) according to the general Ugi-4CR-based procedure 2. The resulting Boc protected compound was subjected to the general deprotection procedure 4. Flash column chromatography purification (MeOH/EtOAc 4:1) afforded peptide-peptoid hybrid **72** (590.6 mg, 82%) as a light yellow oil. A mixture of conformers in a 7:3 ratio was observed by NMR.

R_f = 0.45 (EtOAc / MeOH 8:2).

$[\alpha]_D^{25}$ = -18.9 (*c* 0.65, MeOH, 25 °C).

^{1}H NMR (400 MHz, CDCl$_3$) δ =8.35 (m, 1H); 7.22-7.36 (m, 5H); 5.08, 5.95 (2×m, 1H); 4.69, 4.98 (2×m, 1H); 3.55, 4.02 (2×d, 1H, *J* = 16.2 Hz); 3.62, 3.81 (2×d, 1H, *J* = 18.0 Hz); 3.65, 3.70 (2×s, 3H); 3.37-3.55 (m, 2H); 2.51 (m, 4H); 2.17 (m, 3H); 1.55, 1.71 (2×d, 3H, *J* = 6.8 Hz).

^{13}C NMR (100 MHz, CDCl$_3$) δ = 171.1, 168.8, 137.6, 129.0, 128.9, 128.6, 127.1, 127.0, 58.8, 55.6, 52.3, 52.2, 46.3, 45.6, 40.8, 29.1, 24.6, 17.4.

HRMS (ESI-FT-ICR) [MH]$^+$ calcd. for C$_{18}$H$_{25}$N$_3$O$_4$: 348.1917, found 348.1915

Compound 73:
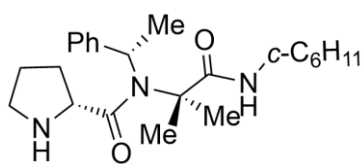
(*S*)-α-Methylbenzylamine (128 µL, 1 mmol), acetone (74 µL, 1 mmol), Boc-D-Pro-OH (215 mg, 1 mmol) and cyclohexylisocyanide (125 µL, 1 mmol) were reacted in MeOH (5 mL) according to the general Ugi-4CR-based procedure 2. The resulting Boc protected compound was subjected to the general deprotection procedure 4. Flash column chromatography purification (MeOH/EtOAc 4:1) afforded peptide-peptoid hybrid **73** (317 mg, 77%) as a colorless oil.

R_f = 0.55 (EtOAc/MeOH 8:2).

$[\alpha]_D^{25}$ = +15.6 (*c* 0.44, MeOH, 25 °C).

^{1}H NMR (400 MHz, CDCl$_3$) δ = 7.49 (d, 2H, *J* = 8.0 Hz); 7.28-7.41 (m, 3H); 5.58 (d, 1H, *J* = 6.3 Hz); 5.17 (m, 1H); 3.70 (m, 2H); 3.09 (m, 2H); 2.71 (m, 1H); 1.89-2.00 (m, 3H); 1.87 (d, 3H, *J* = 7.2 Hz); 1.67-1.83 (m 2H); 1.61 (m, 2H); 1.57 (s, 3H); 1.54 (s, 3H); 1.07-1.41 (m, 8H).

^{13}C NMR (100 MHz, CDCl$_3$) δ = 173.9. 170.4, 142.2, 128.8, 127.2, 126.0, 64.4, 60.0, 48.4, 47.5, 32.9, 31.4, 28.5, 26.5, 25.6, 24.9, 25.2, 20.8.

Compound 74
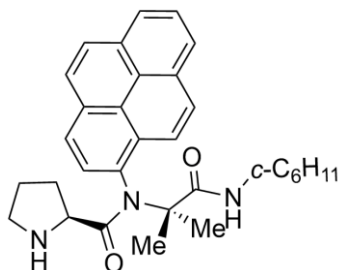
1-amino pyrene (217, 1 mmol), acetone (74 µL, 1 mmol), Boc-D-Pro-OH (215 mg, 1 mmol) and cyclohexylisocyanide (125 µL, 1 mmol) were reacted in MeOH (5 mL) according to the general Ugi-4CR-based procedure 2. The resulting Boc protected compound was subjected to the general deprotection procedure 4. Flash column chromatography purification (MeOH/EtOAc 4:1) afforded peptide-peptoid hybrid **74** (317 mg, 77%) as a colorless oil.

R_f = 0.65 (EtOAc/MeOH 8:2).

$[\alpha]_D^{25}$ = -15.6 (*c* 0.44, MeOH, 25 °C).

^{1}H NMR (400 MHz, CDCl$_3$) δ = 8.65 (d, *J* = 9.21 Hz ,1H); 8.04-8.26 (m, 8H); 5.87 (d, 1H, *J* = 7.6 Hz, N*H*); 3.91 (m, 1H); 3.05 (m, 2H); 2.45 (m, 3H); 2.08 (m, 2H); 1.78 (m, 2H); 1.55-1.68 (m, 3H); 1.59 (s, 3H); 1.36-1.49 (m, 3H); 1.31 (s, 3H); 1.25 (m, 4H).

^{13}C NMR (100 MHz, CDCl$_3$) δ = 175.4, 174.0, 132.3, 131.6, 131.1, 131.0, 130.8, 129.9, 128.7, 127.1, 126.7, 126.1, 124.4, 122.8, 63.8, 60.3, 48.9, 47.9, 33.3, 33.2, 31.7, 26.7, 25.8, 25.7, 25.1.

Compound 75:
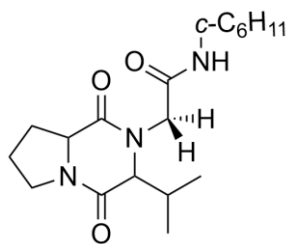
Compound **62** (168 mg, 1 mmol), and 10% LiOH were stirred in MeOH (2 mL) according to the general procedure 6. Methanol was removed under vacuum and added cold water to this mixture; acidify with dilute hydrochloric acid to obtain a solid. Flash column chromatography purification (MeOH/EtOAc 4:1) afforded compound **75** (91%) as a white solid.

Mp = 60 ºC.

R_f = 0.61 (EtOAc/MeOH 8:2).

[α]$_D^{25}$ = -56.1 (*c* 0.56, MeOH, 25 °C).

¹H NMR (400 MHz, CDCl₃) δ = 6.58 (d, 1H, *J* = 7.44 Hz, N*H*), 4.12 (d, 1H, *J* = 15.2 Hz); 3.99-4.08 (m, 2H); 3.88 (d, 1H, *J* = 15.2 Hz); 3.80-3.85 (m, 1H); 3.67-3.79 (m, 1H); 3.34-3.45 (m, 1H); 2.39-48 (m, 1H); 2.28-2.38 (m, 1H); 1.97-2.17 (m, 2H); 1.79-1.96 (m, 4H); 1.53-1.77 (m, 3H); 1.31-1.44 (m, 2H); 1.25 (d, 3H, *J* = 7.0 Hz); 0.87 (d, 3H, *J* = 7.0 Hz).

¹³C NMR (100 MHz, CDCl₃) δ = 168.2, 167.4, 163.2, 67.4, 53.4, 48.2, 44.4, 32.9, 32.8, 30.8, 29.8, 25.4, 24.5, 20.0, 58.8, 21.7, 15.8.

Compound 87:
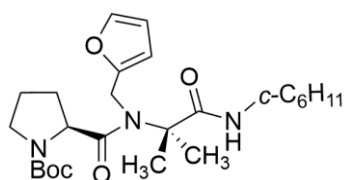
Furfuylamine (177 μL, 2 mmol), acetone (116 mg, 2 mmol), Boc-(L)-Pro-OH (431 mg, 2 mmol) and cyclohexylisocyanide (249 μL, 2 mmol) were reacted in MeOH (5 mL) according to the general procedure 2 for the Ugi-4CR. Flash column chromatography purification (*n*-hexane/EtOAc 1:1) afforded the Boc-Proline-based peptoid **87** (81%) as a white solid. A mixture of conformers was observed by NMR (ratio 3:1). Assigned signals belong to the mixture of conformers.

R_f = 0.34 (*n*-hexane/EtOAc 1:1)

[α]$_D^{20}$ = -19.9 (*c* 0.85, MeOH, 20 °C)

¹H NMR (400 MHz, CDCl₃) δ = 0,99-1.19 (m, 3H); 1,29-1.39 (m, 2H); 1.43 (s, 3H); 1.45 (s, 9H); 1.48 (s, 3H); 1,58-2.01 (m, 9H); 2.10 (m, 1H); 3.39 (m, 1H); 3.53 (m, 1H); 3.65 (m, 1H); 4.50, 4.52 (2×d, 1H, *J* = 16.0 Hz); 4.60 (m, 1H); 4.77, 5.09 (2×d, 1H, *J* = 18.2 Hz); 5.70, 5.94 (2×d, 1H, *J* = 7.2 Hz, N*H*) 6.39 (m, 1H); 7.40 (d, 1H, *J* = 7.8 Hz).

¹³C NMR (100 MHz, CDCl₃) δ = 23.1, 24.2, 24.4, 24.9, 25.1, 25.5, 28.6, 30.2, 32.7, 32.8, 41.5, 47.2, 48.4, 56.9, 63.3, 79.5, 107.3, 110.8, 141.9, 152.2, 154.7, 173.7, 174.1.

Compound 88:
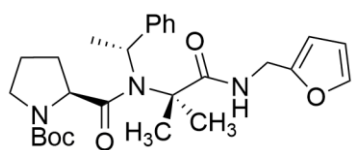
(S)-(-)-alpha-Methylbenzylamine (257 µL, 2 mmol), acetone (147 µL, 2 mmol), Boc-(L)-Pro-OH (431 mg, 2 mmol) and furfurylisocyanide (216 µL, 2 mmol) were reacted in MeOH (5 mL) according to the general procedure 2 for the Ugi-4CR. Flash column chromatography purification (*n*-hexane/EtOAc 1:1) afforded the Proline-based peptoid **88** (78%) as oil.

R_f = 0.30 (*n*-hexane/EtOAc 1:1).

$[\alpha]_D^{23}$ = -6.26 (*c* 0.47, MeOH, 23 °C).

¹H NMR (400 MHz, CDCl₃) δ = 1.40 (s, 9H); 1.41-1.75 (m, 9H); 1.94 (m, 3H); 3.26-3.37 (m, 2H); 4.08-4.11 (m, 2H); 4.59-4.65 (m, 1H); 6.23-6.29 (m, 2H); 7.26-7.40 (m, 4H); 7.53 (m, 2H).

¹³C NMR (100 MHz, CDCl₃) δ = 19.2, 24.2, 24.4, 26.7, 28.9, 37.2, 47.7, 51.9, 59.3, 64.8, 79.5, 106.4, 110.4, 127.4, 128.9, 141.3, 142.8, 152.9, 154.8, 175.4, 175.5.

Compound 91:
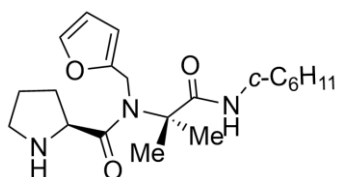
The compound **87** was subjected to the general deprotection procedure 4. Flash column chromatography purification (MeOH/EtOAc 4:1) afforded peptide-peptoid hybrid **91** (91%) as a colorless oil.

R_f = 0.34 (*n*-hexane/EtOAc 1:1).

$[\alpha]_D^{23}$ = -39.4 (*c* 0.54, MeOH, 23 °C).

¹H NMR (400 MHz, CDCl₃) δ = 0,99-1.17 (m, 3H); 1,19-1.31 (m, 2H); 1.36 (s, 3H); 1.39 (s, 3H); 1,48-1.98 (m, 9H); 2.77 (m, 1H); 3.11 (m, 3H); 3.61 (m, 1H); 4.04 (m, 1H); 4.56, 4.63 (2xd, 2H, *J* = 17.8 Hz); 5.72 (d, 1H, *J* = 8.19 Hz, *N*H); 6.25 (dd, 1H, *J* = 0.74, 3.26 Hz); 6.32 (dd, 1H, *J* = 1.86, 3.26 Hz).

¹³C NMR (100 MHz, CDCl₃): δ = 24.3, 24.8 (*C*H₃), 24.9 (*C*H₂); 25.7 (*C*H); 26.6 (*C*H₂); 30.7, 32.7, 33.0, (*C*H₂); 40.7 (*C*H); 47.6, 48.2 (*C*H₂); 58.9 (*C*H); 63.1 (*C*); 107.8 (⁴*C*H), 111.1 (³*C*H), 142.3 (⁵*C*H), 151.2 (¹*C*) (fu); 173.6, 174.4 (*C*=O).

PFA:
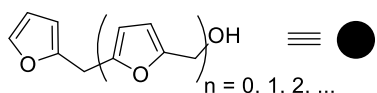
Furfuryl alcohol (860 µL, 10mmol) and TFA (38 µL, 0.5 mmol) were reacted in CHCl₃ (5 mL) according to the general

polymerization procedure 5. After precipitation in petroleum ether, afford the **PFA** as brown solid.

IR (KBr): 3500, 2930, 1720, 1420, 1320, 1100, 1038, 767 cm^{-1}

Elemental analysis (%): N: 0.0, C: 56.14, H: 4.10

Compound 89:
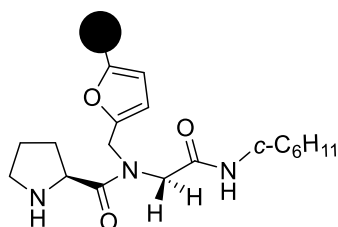
Compound **87** (476mg, 1 mmol), furfuryl alcohol (860 μL, 10mmol) and TFA (38 μL, 0.5 mmol) were reacted in CHCl$_3$ (5 mL) according to the general polymerization procedure 5. After precipitation in petroleum ether, afford the compound **89** as black solid

IR (KBr): 3500, 2930, 1720, 1420, 1320, 1100, 1038, 767 cm^{-1}

Elemental analysis (%): N: 2.68, C: 58.29, H: 5.12

f = 0.64 mmol·g^{-1}

Compound 90:
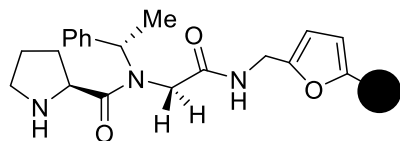
Compound **88** (545 mg, 1 mmol), furfuryl alcohol (860 μL, 10mmol) and TFA (38 μL, 0.5 mmol) were reacted in CHCl$_3$ (5 mL) according to the general polymerization procedure 5.

After precipitation in petroleum ether, afford the compound **90** as black solid.

IR (KBr): 3500, 2930, 1720, 1420, 1320, 1100, 1038, 767 cm^{-1}

Elemental analysis (%): N: 1.36, C: 50.52, H: 3.77

f = 0.33 mmol·g^{-1}

5.2.4 Synthesis and spectroscopy data of asymmetric Aldol and Michael products

Compound 20: (S)-2-[(R)-Hydroxy(4-nitrophenyl)methyl]cyclohexanone
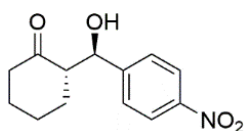
Prepared by reaction of 4-nitrobenzaldehyde with cyclohexanone according to the general procedure 7. The compound was purified by flash column chromatography n-hexane/EtOAc 9:1 v/v). The spectroscopic data are in agreement with the published data. [109] The enantiomeric excess was determined by chiral-stationary phase HPLC (Chiralpak AD-H, n-hexane/i-PrOH 90:10, 25°C) at 1 ml/min, UV detection at 254 nm: t_R: (anti, major) = 30.4 min, (anti, minor) = 22.8 min.

R_f = 0.30 (*n*-hexane/EtOAc 9:1).

[α]$_D^{25}$ = +15.21 (*c* 0.0050 g. mL^{-1}, MeOH, 25 °C).

^{1}H-NMR (400 MHz, CDCl$_3$) δ = 8.21 (2H, d, *J*=8.8 Hz), 7.51 (2H, d, *J*=8.8 Hz), 4.90 (1H, dd, *J*=8.4, 2.8 Hz), 4.08 (1H, m), 2.67-2.33 (3H, m), 2.12 (1H, m), 1.85 (1H, m), 1.73-1.34 (4H, m).

^{13}C-NMR (100 MHz, CDCl$_3$) δ= 214.8, 148.4, 147.7, 128.0, 123.4, 74.1, 57.3, 42.8, 30.9, 27.7, 24.9.

Compound 78: (2*R*,3*S*)-2-Ethyl-4-nitro-3-phenylbutanal
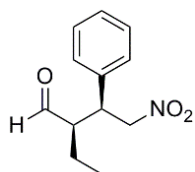
Prepared by reaction of *n*-butanal with *trans*-β-nitrostyrene according to the general procedure 8. The compound was purified by flash column chromatography *n*-hexane/EtOAc 9:1 *v/v*). The spectroscopic data are in agreement with the published data.[110] The enantiomeric excess was determined by chiral-stationary phase HPLC (Chiralpak AD-H, *n*-hexane/*i*-PrOH 99:1, 25°C) at 0.75 ml/min, UV detection at 210 nm: t_R: (*syn*, major) = 24.6 min, (*syn*, minor) = 29.3 min.

R_f = 0.26 (*n*-hexane/EtOAc 8:2).

[α]$_D^{23}$ = +25.21 (*c* 0.0046 g. mL^{-1}, MeOH, 23 °C).

^{1}H NMR (400 MHz, CDCl$_3$) δ = 9.72, 9.49 (2xd, *J* = 2.6 Hz, 1H; CHO), 7.36- 7.29 (m, 3H; Ph), 7.19- 7.17 (m, 2H; Ph), 4.72 (dd, *J* = 5.0 Hz, 12.7 Hz, 1H; CH$_2$NO$_2$), 4.63 (dd, *J* = 9.6 Hz, 12.7 Hz, 1H, CH$_2$NO$_2$), 3.79 (td, *J* = 5.0 Hz, 9.8 Hz, 1H; CHPh), 2.71- 2.65 (m, 1H; CHCHO), 1.54- 1.47 (m, 2H; CH$_2$CH$_3$), 0.83 (t, *J* = 0.83 Hz, 3H, CH$_3$).

^{13}C NMR (100 MHz, CDCl$_3$) δ = 203.2, 136.8, 129.1, 128.1, 128.0, 78.5, 55.0, 42.7, 20.4, 10.7.

Compound 23: (2*R*,3*S*)-2-Methyl-4-nitro-3-phenylbutanal
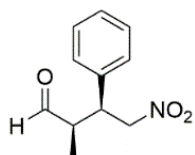
Prepared by reaction of *n*-propanal with *trans*-β-nitrostyrene according to the general procedure 8. The compound was purified by flash column chromatography *n*-hexane/EtOAc 9:1 *v/v*). The spectroscopic data are in agreement with the published data.[110] The enantiomeric excess was determined by chiral-stationary phase HPLC (Chiralpak OD-H, *n*-hexane/*i*-PrOH 95:5, 25°C) at 1 ml/min, UV detection at 210 nm: t_R: (syn, major) = 57.87 min, (syn, minor) = 35.61 min.

R_f = 0.35 (*n*-hexane/EtOAc 8:2).

[α] $_D^{25}$ = +25.21 (*c* 0.0046 g. mL^{-1}, MeOH, 25 °C).

¹H NMR (400 MHz, CDCl₃) δ = 9.71, 9.53 (2xd, J = 2.6 Hz, 1H; CHO), 7.36- 7.29 (m, 3H; Ph), 7.19- 7.17 (m, 2H; Ph), 4.72 (dd, J = 5.0 Hz, 12.7 Hz, 1H; CH₂NO₂), 4.63 (dd, J = 9.6 Hz, 12.7 Hz, 1H, CH₂NO₂), 3.82 (m, 1H; CHPh), 2.77 (m, 1H; CHCHO), 1.21, 0.99 (2xd, J = 7.28 Hz, 3H, CH₃).

¹³C NMR (100 MHz, CDCl₃) δ = 202.4, 136.7, 129.0, 128.2, 78.2, 48.6, 44.2, 12.3.

Compound 79: (*2R,3S*)-2-Isopropyl-4-nitro-3-phenylbutanal
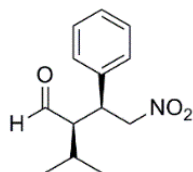
Prepared from isovaleraldehyde and *trans*-β-nitrostyrene according to the general procedure 8. The compound was purified by flash column chromatography *n*-hexane/EtOAc 9:1 *v/v*). The spectroscopic data are in agreement with the published data.[110] The enantiomeric excess was determined by HPLC (Chiralpak AD-H, *n*-hexane/*i*-PrOH 97:3, 25°C) at 0.4ml/min, UV detection at 210 nm: t_R: (*syn*, major) = 24.5 min, (*syn*, minor) = 28.9 min.

R_f = 0.40 (*n*-hexane/EtOAc 8:2).

$[\alpha]_D^{23}$ = +24.25 (*c* 0.0044 g. mL⁻¹, MeOH, 23 °C).

¹H-NMR (400 MHz, CDCl₃) δ = 9.93 (d, J=2.4 Hz, 1H, CHO); 7.36- 7.27 (m, 3H; Ph), 7.19-7.17 (m, 2H; Ph), 4.67 (dd, J = 5.0 Hz, 12.9 Hz, 1H; CH₂NO₂), 4.58 (dd, J = 9.9 Hz, 12.5 Hz, 1H, CH₂NO₂), 3.90 (m, 1H; CHPh), 2.71- 2.65 (m, 1H; CHCHO), 1.72 (m, 1H; CH(CH₃)₂), 1.10 (d, J = 7.0 Hz, 3H, CH₃); 0.89(d, J = 7.0 Hz, 3H, CH₃).

¹³C-NMR (100 MHz, CDCl₃) δ = 204.5, 137.2, 129.3, 128.3, 128.1, 79.1, 58.9, 42.1, 28.1, 21.8, 17.1.

Compound 80: (*2R,3S*)-2-Ethyl-4-nitro-3-(4-methoxyphenyl)butanal
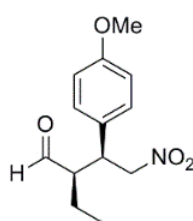
Prepared from *n*-butanal and *trans*-4-methoxy-β-nitrostyrene according to the general procedure 8. The spectroscopic data are in agreement with the published data.[111] The enantiomeric excess was determined by chiral-stationary phase HPLC (Chiralpak AD-H, *n*-hexane/*i*-PrOH 95:5, 25°C) at 0.8ml/min, UV detection at 210 nm: t_R: (*syn*, major) = 16.9 min, (*syn*, minor) = 20.8 min.

R_f = 0.43 (*n*-hexane/EtOAc 8:2).

$[\alpha]_D^{23}$ = +19.90 (*c* 0.0041 g. mL⁻¹, MeOH, 23 °C).

¹H NMR (400 MHz, CDCl₃) δ = 9.70, 9.47 (2xd, J = 2.6 Hz, 1H, CHO), 7.09 (d, J = 8.6 Hz, 2H, Ph), 6.88- 6.83 (m, 2H, Ph), 4.69 (dd, J = 4.9 Hz, 12.5 Hz, 1H, CH₂NO₂), 4.61- 4.55 (m,

1H, CH$_2$NO$_2$), 3.78 (s, 3H, OMe), 3.75- 3.71 (m, 1H, CHPh), 2.63 (m, 1H, CHCHO), 1.50 (m, 2H, CH$_2$CH$_3$), 0.82 (t, J = 7.5 Hz, 3H, CH$_3$).

^{13}C NMR (100 MHz, CDCl$_3$) δ = 203.5, 159.4, 129.4, 129.2, 114.6, 78.9, 55.4, 55.3, 42.2, 20.5, 10.8.

Compound 81: (*2R,3S*)-3-(4-Fluorophenyl)-2-ethyl-4-nitrobutanal
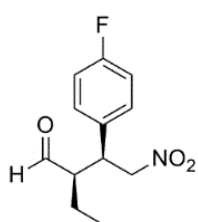
Prepared from *n*-butanal and *trans*-4-fluoro-β-nitrostyrene according to the general procedure 8. The compound was purified by flash column chromatography *n*-hexane/EtOAc 9:1 *v/v*). The spectroscopic data are in agreement with the published data.[112] The enantiomeric excess was determined by HPLC (Chiralpak AD-H, *n*-hexane/*i*-PrOH 95:5, 25°C) at 0.8ml/min, UV detection at 210 nm: t_R: (*syn*, major) = 15.4 min, (*syn*, minor) = 19.3 min.

R_f = 0.45 (*n*-hexane/EtOAc 8:2).

[α] $_D^{23}$ = +11.03 (*c* 0.0058 g. mL^{-1}, MeOH, 23 °C).

^{1}H NMR (400 MHz, CDCl$_3$) δ = 9.74-9.51 (2xd, J = 2.4 Hz, 1H; CHO), 7.20- 7.17 (m, 2H; Ph), 7.08- 7.02 (m, 2H; Ph), 4.74 (dd, J = 4.8 Hz, 12.7 Hz, 1H; CH$_2$NO$_2$), 4.61 (dd, J = 9.9 Hz, 12.7 Hz, 1H; CH$_2$NO$_2$), 3.84- 3.78 (m, 1H; CHPh), 2.71- 2.65 (m, 1H; CHCHO), 1.58–1.44 (m, 2H; CH$_2$CH$_3$), 0.86 (t, J = 7.5 Hz, 3H; CH$_3$).

^{13}C NMR (100 MHz, CDCl$_3$) δ = 203.0, 163.7, 132.7, 129.8, 129.7, 116.4, 116.2, 78.7, 55.0, 42.7, 20.4, 10.7.

Compound 82: (*2R,3S*)-3-(4-Chlorophenyl)-2-ethyl-4-nitrobutanal
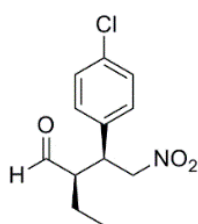
Prepared from *n*-butanal and *trans*-4-chloro-β-nitrostyrene according to the general procedure 8. The compound was purified by flash column chromatography *n*-hexane/EtOAc 9:1 *v/v*). The spectroscopic data are in agreement with the published data.[112] The enantiomeric excess was determined by HPLC (Chiralpak AD-H, *n*-hexane/*i*-PrOH 95:5, 25°C) at 0.8ml/min, UV detection at 210 nm: t_R: (*syn*, major) = 15.4 min, (*syn*, minor) = 19.3 min.

R_f = 0.43 (*n*-hexane/EtOAc 8:2).

[α] $_D^{23}$ = +17.76 (*c* 0.0051 g. mL^{-1}, MeOH, 23 °C).

^{1} H NMR (400 MHz, CDCl$_3$) δ = 9.71, 9.49 (2xd, J = 2.8 Hz, 1H; CHO), 7.34-7.30 (m, 2H; Ph), 7.15-7.12 (m, 2H; Ph), 4.73 (dd, J = 4.8 Hz, 12.8 Hz, 1H; CH$_2$NO$_2$), 4.62 (dd, J = 9.9 Hz, 12.8 Hz, 1H; CH$_2$NO$_2$), 3.80 (dt, J = 4.8 Hz, 10.0 Hz, 1H; CHPh), 2.67 (m, 1H; CHCHO), 1.57-1.47 (m, 2H; CH$_2$CH$_3$), 0.86 (t, J = 7.5 Hz, 3H; CH$_3$).

^{13}C NMR (100 MHz, CDCl$_3$) δ = 202.8, 135.5, 134.2, 129.8, 129.5, 54.8, 42.2, 20.5, 10.7.

Compound 83: (*2R,3S*)-3-(4-Bromophenyl)-2-ethyl-4-nitrobutanal
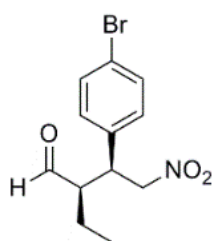
Prepared from *n*-butanal and *trans*-4-bromo-β-nitrostyrene according to the general procedure 8. The compound was purified by flash column chromatography *n*-hexane/EtOAc 9:1 *v/v*). The spectroscopic data are in agreement with the published data.[112] The enantiomeric excess was determined by HPLC (Chiralpak AD-H, *n*-hexane/*i*-PrOH 95:5, 25°C) at 0.8ml/min, UV detection at 210 nm: t_R: (*syn*, major) = 15.4 min, (*syn*, minor) = 19.3 min.

R_f = 0.40 (*n*-hexane/EtOAc 8:2).

[α] $_D^{23}$ = +2.54 (*c* 0.0036 g. mL^{-1}, MeOH, 23 °C)

^{1}H NMR (400 MHz, CDCl$_3$) δ = 9.72, 9.49 (2xd, *J* = 2.3 Hz, 1H, CHO), 7.49- 7.43 (m, 2H, Ph), 7.07 (d, *J* = 8.3 Hz, 2H, Ph), 4.81-4.70 (m, 1H, CH$_2$NO$_2$), 4.62- 4.57 (m, 1H, CH$_2$NO$_2$), 3.80- 3.74 (m, 1H, CHPh), 2.67 (m, 1H, CHCHO), 1.81- 1.18 (m, 2H, CH$_2$CH$_3$), 0.84 (t, *J* = 7.5 Hz, 3H, CH$_3$).

^{13}C NMR (100 MHz, CDCl$_3$) δ = 202.8, 135.9, 132.5, 129.8, 122.2, 78.4, 54.8, 42.2, 20.5, 10.7.

Compound 84: (*2R,3S*)-3-(2-Bromophenyl)-2-ethyl-4-nitrobutanal
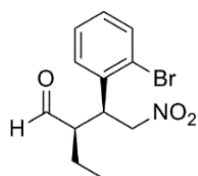
Prepared from *n*-butanal and *trans*-2-bromo-β-nitrostyrene according to the general procedure 8. The compound was purified by flash column chromatography *n*-hexane/EtOAc 9:1 *v/v*). The spectroscopic data are in agreement with the published data.[111] The enantiomeric excess was determined by HPLC (Chiralpak AD-H, *n*-hexane/*i*-PrOH 97:3, 25°C) at 0.5ml/min, UV detection at 210 nm: t_R: (*syn*, major) = 20.8 min, (*syn*, minor) = 23.1 min.

R_f = 0.33 (*n*-hexane/EtOAc 8:2).

[α] $_D^{23}$ = +2.98 (*c* 0.0057 g. mL^{-1}, MeOH, 23 °C).

^{1}H NMR (400 MHz, CDCl$_3$) δ = 9.74, 9.59 (2xd, *J* = 2.4 Hz, 1H, CHO), 7.61 (dd, *J* = 1.1 Hz, 8 Hz, 1H, Ph), 7.34- 7.30 (m, 1H, Ph), 7.21-7.15 (m, 2H, Ph), 4.89- 4.83 (m, 1H,CH$_2$NO$_2$), 4.67 (dd, *J* = 4.6 Hz, 13 Hz, 1H, CH$_2$NO$_2$), 4.37 (m, 1H, CHPh), 2.95 (m, 1H, CHCHO), 1.67- 1.48 (m, 2H, CH$_2$CH$_3$), 0.88 (t, *J* = 0.9 Hz, 3H, CH$_3$).

^{13}C NMR (100 MHz, CDCl$_3$) δ = 202.9, 136.2, 134.1, 129.8, 129.6, 128.1, 76.3, 54.4, 41.4, 20.6, 11.1.

Compound 85: (*2R,3S*)-2-Ethyl-4-nitro-3-(3-nitrophenyl)butanal
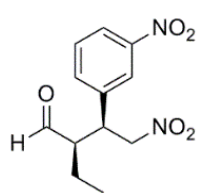
Prepared from *n*-butanal and *trans*-3-nitro-β-nitrostyrene according to the general procedure 8. The compound was purified by flash column chromatography *n*-hexane/EtOAc 9:1 *v/v*). The spectroscopic data are in agreement with the published data.[113] The enantiomeric excess was determined by HPLC (Chiralpak AD-H, *n*-hexane/*i*-PrOH 95:5, 25°C) at 0.8ml/min, UV detection at 210 nm: t_R: (*syn*, major) = 36.0 min, (*syn*, minor) = 39.1 min.

R_f = 0.26 (*n*-hexane/EtOAc 8:2).

$[α]_D^{23}$ = -8.09 (*c* 0.0042 g. mL^{-1}, MeOH, 23 °C).

¹H NMR (400 MHz, CDCl₃) δ = 9.74, 9.55 (2xd, *J* = 2.8 Hz, 1H; CHO), 8.19-8.08 (m, 2H; Ph), 7.55-7.47 (m, 2H; Ph), 4.74 (dd, *J* = 4.8 Hz, 12.8 Hz, 1H; CH₂NO₂), 4.63 (dd, *J* = 9.9 Hz, 12.8 Hz, 1H; CH₂NO₂), 3.69 (dt, *J* = 4.8 Hz, 10.0 Hz, 1H; CHPh), 2.79 (m, 1H; CHCHO), 1.57-1.38 (m, 2H; CH₂CH₃), 0.80 (t, *J* = 7.5 Hz, 3H; CH₃).

¹³C NMR (100 MHz, CDCl₃) δ = 202.2, 148.8, 139.5, 134.6, 130.3, 123.4, 123.0, 78.0, 54.4, 42.2, 20.5, 10.5.

Compound 86: (*2R,3S*)-2-Ethyl-4-nitro-3-(2-furyl)butanal
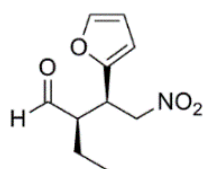
Prepared from *n*-butanal and *trans*-2-furyl-β-nitrostyrene according to the general procedure 8. The compound was purified by flash column chromatography *n*-hexane/EtOAc 9:1 *v/v*). The spectroscopic data are in agreement with the published data.[113] The enantiomeric excess was determined by HPLC (Chiralpak AD-H, *n*-hexane/*i*-PrOH 97:3, 25°C) at 0.5ml/min, UV detection at 210 nm: t_R: (*syn*, major) = 22.1 min, (*syn*, minor) = 23.9 min.

R_f = 0.35 (*n*-hexane/EtOAc 8:2).

$[α]_D^{23}$ = +26.75 (*c* 0.0042 g. mL^{-1}, MeOH, 23 °C).

¹H NMR (400 MHz, CDCl₃) δ = 9.65, 9.54 (2xd, *J* = 2.6 Hz, 1H; CHO), 7.29 (dd, *J* = 0.75, 1.85 Hz, 1H; fu), 6.24 (dd, *J* = 0.75, 1.85 Hz, 1H; fu), 4.68 (m, 2 H; CH₂NO₂), 4.02 (m, 1H), 2.77 (m, 1H; CHfu), 1.56 (m, 3H; CHCHO, CH₂CH₃), 0.90 (t, *J* = 0.83 Hz, 3H, CH₃).

¹³C NMR (100 MHz, CDCl₃) δ = 202.5, 150.3, 142.8, 110.6, 108.9, 76.3, 53.6, 36.7, 20.8, 11.0.

5.2.5 Conformational studies

The conformational searches were done in gas phase using the Monte Carlo (MCMM) method, the energy minimization were carried out using the Polak-Ribiere Conjugate Gradient (PRCG),[114] and the MMFF force field,[115] using dielectric constant-dependent electrostatics (e=1) and normal cut-off points to model the nonbonded interactions, as implemented in MacroModel (Version 9.9).[116]All heavy atoms and hydrogens on heteroatoms were included in the test for redundant conformers, using the default cutoff (maximum atom deviation) of 0.5 Å. We included all rotatable single bonds in the conformational search, even N-C=O amide single bond. The energy window for saving new structures was 5 kcal/mol relative to the current global minimum, using a maximum number of steps of 30000 and 1000 steps per rotable bond. Each search was continued until the global energy minima were found at least 10-20 times, thus giving confidence that all the relevant conformers had been found.

The cluster analyses were performed using a python script "Clustering of Conformers" interfaced to the Maestro (Version 9.3) program, [117] and available in schrödinger script-center website.[118] Several works have been shown the cluster analysis in the precise description of organic molecules in solution. [119] To generate the RMS matrix, all heavy atoms and hydrogens on heteroatoms were included. The *average* method was used to calculate the best number of cluster in all cases. The low-energy structures of each cluster were selected and submitted to a full geometry optimization using Quantum Mechanics. All conformer were clustered and graphically represented in the supporting information (SI).

The representative structures (low energy) of each cluster were fully optimized using the Truhlar M06-2X [120] density functional in conjunction with the 6-31G(d) basis set through Gaussian09 program.[121] The SMD model[122] was used for inclusion of the solvent effect for all optimizations. All the Cartesian coordinates are supplied in the SI. Frequency calculations at 295.15 K (1 atm) ensured that the stationary points represent either minima (no imaginary frequency) or transition states (single imaginary frequency) on the potential-energy surface, furnished also the zero-point vibrational energies, the thermal and entropic correction from which the Gibbs free energies were determined. The corresponding eigenvectors were inspected to confirm the expected isomerization transition state. The electronic energies were further refined using 6-31+g(d,p) basis set. The natural bond orbital (NBO) analysis was calculated at M06-2X/6-31+G(d,p) level using NBO 5.0 program as implemented in Gaussian 09.

5.2.6 Determination of main features of microreactor R1.

HPLC column preparation and characterization.

Compound **89** (500 mg, excess, suspended in 25 mL of ethanol) was packed into a stainless-steel column (Ø = 2.1 mm, l = 150 mm, particle size = 10 mm). The packing was performed under constant pressure (2500 psi) using ethanol (250 mL) as the solvent by using an air-driven liquid pump.

Void-volume

The void volume (V_0) was determined by pycnometry. [123, 124]

The microreactor was filled with two different solvents successively; first ethanol and then hexane, R1 with the different solvents were weighted and V_0 was calculated by a simple equation math (1):

$$V_0 = w_1 - w_2 / \delta_E - \delta_H \qquad (1)$$

w_1 and w_2 are, the weights of **R1** filled with solvents ethanol and hexane

δ_E and δ_H are the densities of the solvents ethanol and hexane.

Packing amount

The determination of the amount of material contained in the microreactor is based on the consideration that the microreactor weight, w_{tot}, can be expressed as:

$$w_{tot} = w_0 + w_{ads} + w_{hw} \qquad (2)$$

where w_0 and w_{ads} are the weights of the liquid and that of the adsorbent inside the reactor (packing), respectively. w_{hw} is the weight of the stainless steel hardware (i.e., the weight of the empty microreactor). Eq. 2 can be rewritten as:

$$w_{tot} = V_0 \, \delta_0 + w_{ads} + w_{hw} \qquad (3)$$

where δ_0 is the density of the solvent with which the microreactor was filled. Since V_0 is known from Eq. 1, w_{tot} is readily available and w_{hw} can be measured before packing, Eq. 3 permits the estimation of w_{ads} for R1.

5.3 Experimental section of Chapter 2

5.3.1 General procedure for asymmetric reaction

General procedure 9: conjugate addition of 2-nitroethanol to α,β-unsaturated aldehyde
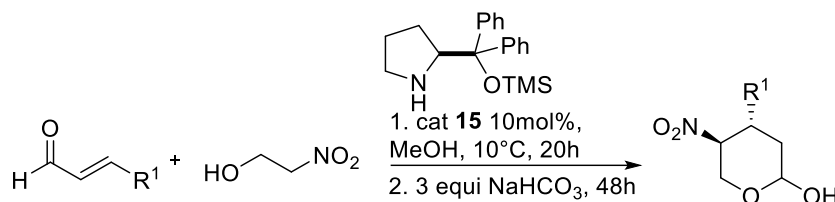
To a solution of catalyst **15** (0.06 mmol, 10 mol%) and α,β-unsaturated aldehyde (0.6 mmol, 1.0 equivalent) in MeOH (1.2 mL), PhCOOH (0.12 mmol, 20 mol%) and 2-nitroethanol (0.9 mmol, 1.5 equivalent) were added. The reaction mixture was stirred for 24 h at 10 °C and then NaHCO$_3$ (3.0 mmol, 5.0 equivalents) was added and stirred for 48 h. The resulting mixture was quenched with phosphate buffer (pH 7.0) and the organic material was extracted with AcOEt (3x30 mL), dried over anhydrous Na$_2$SO$_4$ and then concentrated under reduced pressure. The resulting crude product was purified by flash column chromatography on silica gel using *n*-hexane/EtOAc as eluent. The enantiomeric excess was determined by chiral-stationary phase HPLC analysis through comparison with the authentic racemic material. Assignment of the stereoisomers was performed by comparison with literature data where (*) correspond to the minor isomer.[99]

5.3.2 General procedure for I-MCR

General procedure 10: Ugi-5C-3CR based
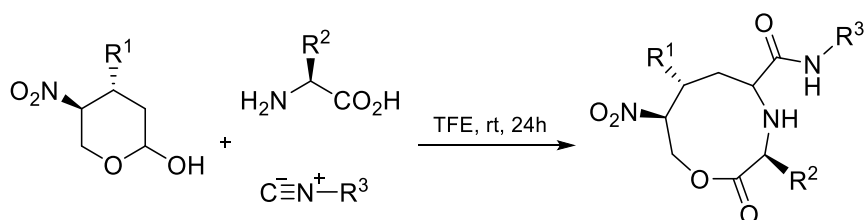
To a suspension of the correspondent tetrahydropyrane (0.25 mmol) and aminoacid (0.25 mmol) in TFE (1 mL) the isocyanide (0.25 mmol) was added slowly. The resulting mixture was stirred for 24 h at 25 °C. The volatiles were removed under pressure and then the crude product was purified by flash column chromatography on silica gel using *n*-hexane/EtOAc as eluent.

5.3.3 Synthesis and spectroscopy data of the asymmetric conjugated addition products

Compound 114: 5-nitro-4-phenyl tetrahydro-2*H*-pyran-2-ol
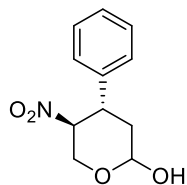
Prepared by reaction of cinnamaldehyde with 2-nitroethanol according to the general procedure 9. The compound was purified by flash column chromatography *n*-hexane/EtOAc 7:3 *v/v*). The spectroscopic data are in agreement with the published data.[99] The enantiomeric excess was determined by chiral-stationary phase HPLC (Chiralpak AD-H, *n*-hexane/*i*-PrOH 90:10, 25 °C) at 1.0 ml/min, UV detection at 210 nm: t_R: (*anti*, minor)= 11.6 min, (*anti*, major) = 17.8 min.

Mp = 140-141 °C.

R_f = 0.25 (*n*-hexane/EtOAc 7:3).

$[\alpha]_D^{23}$ = -39.1 (*c* 0.56, MeOH, 23 °C).

¹H NMR (400 MHz, CDCl₃) δ= 7.28-7.20 (m, 5H), 5.41 (d, *J* = 2.7 Hz, 1H), 5.05* (dd, *J* = 9.3, 2.3 Hz, 0.5H), 4.90 (dt, J_t = 11.1, J_d = 4.7 Hz, 1H), 4.82* (dt, J_d= 4.8Hz, J_t =10.8 Hz, 0.5H), 4.45-4.40 (t, *J* = 8.0, 1H), 4.12-4.03* (m, 1H), 4.08 (dd, *J* = 10.6, 4.7 Hz, 1H), 3.95* (dd, *J*= 9.6, 1.4 Hz, 1H), 3.93-3.83 (m, 1H), 3.53* (ddd, *J* = 13.2, 11.1, 4.3 Hz, 1H), 2.26* (ddd, *J* = 13.6, 4.2, 2.4 Hz, 1H), 2.13 (dd, *J* = 1.2 Hz, 1H), 1.99 (dt, J_d= 3.6Hz, J_t = 13.2 Hz), 1.84* (dt, J_d= 9.4 Hz, J_t = 13.4 Hz, 1H).

¹³C NMR (100 MHz, CDCl₃) δ= 138.90, 138.29*, 129.28*, 129.16, 128.29, 128.04, 127.37, 127.28*, 95.89*, 90.95, 86.67, 86.37*, 66.51*, 60.71, 44.42*, 39.42, 38.26*, 36.52.

Compound 116: 4-(4-bromophenyl)-5-nitrotetrahydro-2*H*-pyran-2-ol
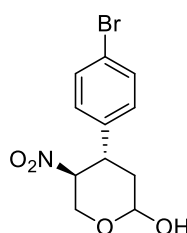
Prepared by reaction of 4-bromocinnamaldehyde with 2-nitroethanol according to the general procedure 9. The compound was purified by flash column chromatography *n*-hexane/EtOAc 7:3 *v/v*). The spectroscopic data are in agreement with the published data.[99] The enantiomeric excess was determined by chiral-stationary phase HPLC (Chiralpak AD-H, *n*-hexane/*i*-PrOH 90:10, 25 °C) at 1.0 ml/min, UV detection at 210 nm: t_R: (*anti*, minor)= 13.3 min, (*anti*, major) = 16.1 min.

Mp = 153-154 °C.

R_f = 0.35 (*n*-hexane/EtOAc 7:3).

$[\alpha]_D^{23}$ = -33.2 (*c* 0.58, MeOH, 23 °C).

¹H NMR (400 MHz, CDCl₃) δ= 7.47-7.45 (m, 2H), 7.13-7.09 (m, 2H), 5.40 (d, J = 2.6 Hz, 1H), 5.04* (d, J = 7.0 Hz, 1H), 4.83 (dt, J = 3.6Hz, J = 7.1 Hz, 1H), 4.77* (ddd, J= 4.8, 10.0, 10.4 Hz, 1H), 4.43* (t, J= 5.2 Hz, 1H), 4.41 (t, J= 8.0 Hz, 1H), 4.08 (dd, J = 10.6, 4.8 Hz, 1H), 3.93* (dd, J= 9.9, 11.2 Hz, 1H), 3.86 (dt, J= 4.4Hz, J = 12.4 Hz, 1H), 2.79 (bs, 1H), 2.14-2.02 (dt, J_d= 4.4 Hz, J_t = 14.0 Hz, 1H), 3.50* (ddd, J = 4.0, 11.2, 15.2 Hz, 1H), 2.23* (ddd, J= 2.4, 4.4, 13.6 Hz, 1H), 1.94 (dt, J = 1.9 Hz, J = 13.5 Hz, 1H), 1.80* (dt, J_d= 9.2 Hz, J= 13.3 Hz, 2H).

¹³C NMR (100 MHz, CDCl₃) δ= 137.94, 137.31*, 132.46*, 132.33, 129.10, 129.00*, 122.27*, 121.98, 95.70*, 90.76, 86.41, 86.10*, 66.36*, 60.59, 43.85*, 38.95, 37.99*, 36.37.

Compound 117: 4-(4-methoxyphenyl)-5-nitrotetrahydro-2*H*-pyran-2-ol
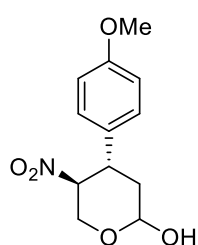
Prepared by reaction of 4-bromocinnamaldehyde with 2-nitroethanol according to the general procedure 9. The compound was purified by flash column chromatography *n*-hexane/EtOAc 7:3 *v/v*). The spectroscopic data are in agreement with the published data.[99] The enantiomeric excess was determined by chiral-stationary phase HPLC (Chiralpak AD-H, *n*-hexane/*i*-PrOH 90:10, 25 °C) at 1.0 ml/min, UV detection at 210 nm: t_R: (*anti*, minor)= 15.2 min, (*anti*, major) = 17.6 min.

Mp = 158 °C.

R_f = 0.37 (*n*-hexane/EtOAc 7:3).

[α]$_D^{23}$ = -46.5 (*c* 0.47, MeOH, 23 °C).

¹H NMR (400 MHz, CDCl₃) δ= 7.31 (m, 2H), 7.01 (m, 2H), 5.56 (d, J = 2.2 Hz, 1H), 5.18 (dd, J = 9.3, 2.4 Hz, 1H), 4.98 (td, J = 11.1, 4.7 Hz, 1H), 4.87* (td, J = 11.1, 4.7 Hz, 1H), 4.57 (t, J = 10.8 Hz, 1H), 4.21* (dd, J = 10.6, 4.7 Hz, 1H), 4.08 (dd, J = 11.3, 10.0 Hz, 1H), 3.99 (dt, J = 4.4 Hz, J = 12.8 Hz, 1H), 3.94* (s, 3H), 3.93 (s, 3H), 2.82 (bs, 1H), 3.62* (ddd, J = 13.2, 11.2, 4.2 Hz, 1H), 2.39* (ddd, J = 13.7, 4.2, 2.4 Hz, 1H), 2.12 (ddd, J = 1.2, 4.4, 14 Hz, 1H), 1.97 (dt, J = 9.4 Hz, J = 13.2 Hz, 1H).

¹³C NMR (100 MHz, CDCl₃) δ= 159.45*, 159.28, 129.80, 129.75*, 128.42, 128.31*, 127.43, 127.02*, 114.63*, 114.53, 95.95*, 91.04, 87.11, 86.77*, 60.75, 55.40, 45.80, 43.77, 38.73.

Compound 118: 4-(4-nitrophenyl)-5-nitrotetrahydro-2*H*-pyran-2-ol
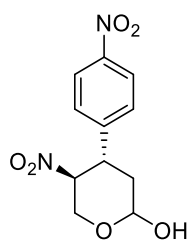
Prepared by reaction of 4-nitrocinnamaldehyde with 2-nitroethanol according to the general procedure 9. The compound was purified by flash column chromatography *n*-hexane/EtOAc 7:3 *v/v*). The spectroscopic data are in agreement with the published data.[99] The enantiomeric excess was determined by chiral-stationary phase HPLC (Chiralpak AD-H, *n*-hexane/*i*-PrOH 90:10, 25 °C) at 1.0 ml/min, UV detection at 210 nm: t_R: (*anti*, minor)= 33.3 min, (*anti*, major) = 37.9 min.

Mp = 139 °C.

R_f = 0.15 (*n*-hexane/EtOAc 7:2).

$[\alpha]_D^{23}$ = -30.3 (*c* 0.68, MeOH, 23 °C)

^{1}H NMR (400 MHz, MeOD) δ= 8.29-8.14 (m, 2H), 7.68-7.51 (m, 2H), 5.31 (t, *J* = 12.9 Hz, 1H), 5.20-5.05 (td, *J* = 11.0, 4.8 Hz, 1H), 5.01* (ddd, *J* = 4.8, 10.0, 14.8 Hz, 1H), 4.59-4.53 (m, 1H), 4.46* (dd, J = 4.8, 11.6 Hz, 1H), 4.40 (t, *J* = 11.0 Hz, 1H), 4.13-3.93* (m, 1H), 3.77 (ddd, *J* = 13.0, 11.3, 4.1 Hz, 1H), 2.20-2.09 (m, 1H), 2.10-1.95 (m, 1H), 1.83 (td, *J* = 13.2, 9.3 Hz, 1H).

^{13}C NMR (100 MHz, MeOD) δ= 148.82, 148.34*, 129.83, 124.94, 96.59*, 91.25, 86.93, 86.51*, 67.29, 61.17, 59.41*, 45.70*, 41.06, 37.93, 39.47*.

Compound 119: 4-(4-ethyl)-5-nitrotetrahydro-2*H*-pyran-2-ol
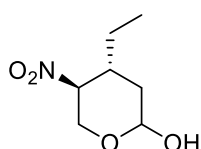
Prepared by reaction of *trans*-pentenal with 2-nitroethanol according to the general procedure 9. The compound was purified by flash column chromatography *n*-hexane/EtOAc 7:3 *v/v*). The spectroscopic data are in agreement with the published data.[99] The enantiomeric excess was determined by chiral-stationary phase HPLC (Chiralpak AD-H, *n*-hexane/*i*-PrOH 90:10, 25 °C) at 1.0 ml/min, UV detection at 210 nm: t_R: (*anti*, minor)= 7.0 min, (*anti*, major) = 7.8 min.

Mp = 55 °C.

R_f = 0.45 (*n*-hexane/EtOAc 7:3).

$[\alpha]_D^{23}$ = -15.1 (*c* 0.62, MeOH, 23 °C).

^{1}H NMR (400 MHz, CDCl₃) δ= 5.31 (m, 1H), 5.17* (d, *J* = 9.0 Hz, 1H), 4.93 (dd, *J* = 8.9, 2.6 Hz, 1H), 4.86-4.78* (m, 1H), 4.40 (m, 2H), 4.29 (m, 2H), 3.92 (dd, *J* = 10.5, 4.4 Hz, 2H), 3.84* (dd, *J* = 11.3, 9.4 Hz, 2H), 3.42-3.17* (m, 1H), 2.81 (b.s, 1H), 2.60 (m, 1H), 2.29* (b.s, 1H), 2.17* (ddd, *J* = 13.5, 4.4, 2.6 Hz, 2H), 2.04 (ddd, *J* = 13.9, 4.3, 1.7 Hz, 2H), 1.65-1.39 (m, 2H), 1.27* (m, 4H), 0.92 (q, *J* = 7.5 Hz, 3H).

¹³C NMR (100 MHz, CDCl₃) δ= 95.67*, 91.08, 86.64, 85.83*, 65.54*, 60.48, 38.79*, 34.79*, 34.23, 33.21, 25.16*, 24.99, 9.94, 10.08*.

5.3.4 Synthesis and spectroscopy data of medium-sized cyclic compounds

Compound 120:
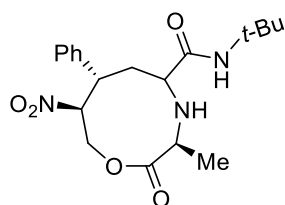
5-nitro-4-phenyl tetrahydro-2H-pyran-2-ol **114** (55.8 mg, 0.25 mmol), L-alanine (22.3 mg, 0.25 mmol), and *tert*-Butylisocyanide (28 µL, 0.25 mmol) were reacted in TFE (1 mL) according to the general procedure 10. Flash column chromatography purification (Hex/EtOAc 1:1) afforded **120** (60 mg, 64%) as a colorless oil. A mixture of four diastereoisomers was detected.

R_f = 0.57 (*n*-hexane/EtOAc 1:1).

¹H NMR (400 MHz, CDCl₃) δ = 7.44-7.18 (m, 5H), 7.04, 6.82, 6.65 (s, 1H, *N*H$_{(amide)}$), 4.79-4.74 (m, 1H), 4.40, 4.29 (2×m, 2H), 3.83 (m, 1H), 3.52 (m, 1H), 3.19-3.12 (m, 1H), 2.87, 2.76, 2.67, 2.56 (4×dd, *J* = 8.2, 3.5 Hz, *J* = 7.3, 6.3 Hz, *J* = 10.3, 2.7, *J* = 9.4, 4.8 Hz, 1H), 2.37, 2.18, 1.98, 1.82 (4×dd, *J* = 14.5, 12.0, 2.7 Hz, 2H), 1.33, 1.28 (2×s, 9H, CH₃), 1.22, 1.17, 1.03 (3×d, *J* = 7.1 Hz, 3H, CH₃).

¹³C NMR (100 MHz, CDCl₃) δ= 173.58, 172.59, 172.06, 137.74, 136.96, 129.71, 129.29, 129.05, 128.52, 128.41, 128.15, 94.08, 93.94, 93.46, 62.48, 61.79, 60.83, 60.70, 60.46, 60.34, 59.72, 59.26, 58.77, 55.28, 50.92, 50.76, 43.01, 42.85, 42.44, 37.91, 35.47, 29.82, 28.75, 28.63, 28.41, 19.58, 18.48.

HRMS (ESI-FT-ICR) [MH]⁻ calcd. for C₁₉H₂₆N₃O₅: 376,1951, found 376,1870

Compound 121:
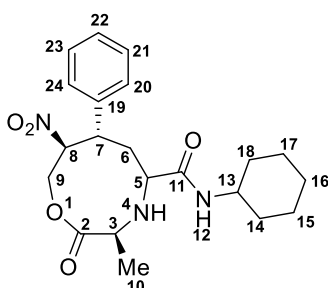
5-nitro-4-phenyl tetrahydro-2H-pyran-2-ol (55.8 mg, 0.25 mmol), L-Alanine (22.3 mg, 0.25 mmol), and cyclohexylisocyanide (31 µL, 0.25 mmol) were reacted in TFE (1 mL) according to the general procedure 10. Flash column chromatography purification (Hex/EtOAc 1:1) afforded **121** (78mg, 77%) as a colorless oil. A mixture of four diastereoisomers was detected.

R_f = 0.50 (*n*-hexane/EtOAc 1:1).

¹H NMR (400 MHz, CDCl₃) δ= 7.46-7.20 (m, 5H, Ph), 7.25, 7.02, 6.84, 6.72 (4×d, *J* = 8.3 Hz, 1H, *N*H-12), 4.77 (m, 1H, H-8), 4.21-4.12 (m, 2H, H-9), 3.82 (m, 1H, H-7), 3.69-3.62 (m, 1H,

H-13), 3.21-3.19 (m, 1H, H-3), 2.96, 2.82, 2.78, 2.65 (4×dd, J = 7.9, 3.7 Hz, J = 7.6, 5.9 Hz, J= 10.2, 2.8 Hz, J = 9.2, 4.8 Hz, 1H, H-5), 2.38, 2.18, 2.03 (3×m, 2H, H-6), 1.94-1.56 (m, 6H), 1.36-1.00(m, 5H), 1.22, 1.14, 0.99 (3×d, J = 7.1 Hz, 3H, H-10).

^{13}C NMR (100 MHz, CDCl$_3$) δ= 173.58, 173.19, 173.09 (*C*=O, *C*-2), 172.47, 172.29, 171.83 (*C*=O, *C*-11), 138.37, 137.68, 137.00 (*C*, *C*-19), 129.68, 129.39, 129.27, 129.01, 128.58, 128.52, 128.42, 128.17 (*C*H, *C*-20-24), 94.14, 94.02, 93.54 (*C*H, *C*-8), 62.52, 62.45, 61.85, 60.85, 60.71, 60.48, 60.34 (*C*H$_2$, *C*-9), 59.79, 59.28, 59.18, 58.67 (*C*H, *C*-5), 55.32, 55.19 (*C*H, *C*-3), 48.30, 48.14, 47.74 (*C*H, *C*-13), 43.05, 42.82, 42.44 (*C*H, *C*-7), 37.66, 36.47, 35.36 (*C*H$_2$, *C*-6), 33.57, 33.01, 32.79 (*C*H$_2$), 25.56, 24.83 (*C*H$_2$), 19.47, 19.30, 18.40, 18.18 (*C*H$_3$, *C*-10).

DEPT 135° δ= 129.68, 129.39, 129.27, 129.01, 128.59, 128.52, 128.42, 128.37, 128.17 (*C*H, *C*-20-24), 94.14, 94.02, 93.54, 93.37 (*C*H, *C*-8), 62.52, 62.45, 61.85, 60.85, 60.71, 60.49, 60.34 (*C*H$_2$, *C*-9), 59.80, 59.28, 59.18, 58.67 (*C*H, *C*-5), 55.32, 55.20 (*C*H, *C*-3), 48.30, 48.14, 47.74 (*C*H, *C*-13), 43.34, 43.05, 42.82, 42.44 (*C*H, *C*-7), 37.66, 36.46, 35.36 (*C*H$_2$, *C*-6), 33.57, 33.06, 33.01, 32.79 (*C*H$_2$), 25.56, 24.87, 24.83, 24.77 (*C*H$_2$), 19.47, 19.30, 18.39, 18.18 (*C*H$_3$, *C*-10).

HRMS (ESI-FT-ICR) [M-H]$^-$ calcd. for C$_{21}$H$_{28}$N$_3$O$_5$: 402,2107, found 402,2034.

Compound 122:
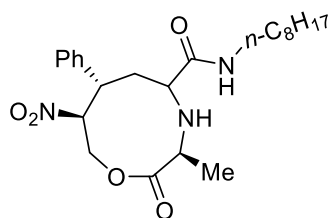
5-nitro-4-phenyl tetrahydro-2H-pyran-2-ol **114** (55.8 mg, 0.25 mmol), L-Alanine (22.3 mg, 0.25 mmol), and octylisocyanide (44 μL, 0.25 mmol) were reacted in TFE (1 mL) according to the general procedure 10. Flash column chromatography purification (Hex/EtOAc 1:1) afforded **122** (55 mg, 51%) as a colorless oil. A mixture of four diastereoisomers was detected.

R_f = 0.50 (*n*-hexane/EtOAc 1:1).

^{1}H NMR (400 MHz, CDCl$_3$) δ= 7.42-7.19 (m, 5H), 7.12, 6.96, 6.86 (3×t, J = 5.6 Hz, 1H, *N*H$_{(amide)}$), 4.77 (m, 1H), 4.51, 4.40 (2×m, 2H), 4.28 (m, 1H), 3.82 (m, 1H), 3.53 (m, 1H), 3.23 (m, 1H), 2.98, 2.87, 2.78, 2.69 (4×dd, J = 7.6, 3.8 Hz, J = 11.2, 5.1 Hz, J = 10.1, 2.7 Hz, J = 9.0, 4.9 Hz, 1H), 2.38, 2.18, 1.86, 1.78 (4×m, 2H), 1.45 (m, 2H), 1.27 (b.s, 8H), 1.21, 1.15, 1.00 (3×d, J = 7.0 Hz, 3H, CH$_3$), 0.88 (t, J = 7.1, 3.4 Hz, 3H, CH$_3$).

^{13}C NMR (100 MHz, CDCl$_3$) δ= 173.64, 173.38, 173.22, 173.16, 172.69, 138.40, 137.70, 137.01, 129.69, 129.41, 129.25, 129.12, 128.99, 128.60, 128.54, 128.41, 128.18, 127.36, 94.14, 94.02, 93.54, 62.51, 62.42, 61.85, 60.89, 60.72, 60.53, 60.36, 59.30, 59.15, 58.68, 55.42, 55.24, 55.17, 43.26, 43.02, 42.81, 42.44, 39.60, 39.48, 39.14, 37.47, 35.36, 33.45, 31.88, 29.59, 29.52, 29.30, 27.00, 22.74, 19.44, 18.40, 18.19, 14.18.

Compound 123:
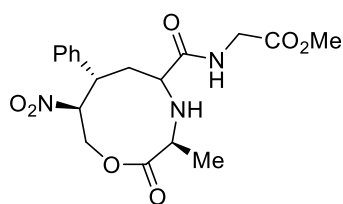
5-nitro-4-phenyl tetrahydro-2H-pyran-2-ol **114** (55.8 mg, 0.25 mmol), L-alanine (22.3 mg, 0.25 mmol), and methylisocyanoacetate (22.7 μL, 0.25 mmol) were reacted in TFE (1 mL) according to the general procedure 10. Flash column chromatography purification (Hex/EtOAc 1:1) afforded **123** (65.9 mg, 67%) as a light yellow oil. A mixture of four diastereoisomers was detected.

R_f = 0.20 (*n*-hexane/EtOAc 1:1).

^{1}H NMR (400 MHz, CDCl$_3$) δ = 7.68, 7.51 (2×t, J = 6.0 Hz, 1H, $NH_{(amide)}$), 7.42-7.23 (m, 5H), 4.77 (m, 1H), 4.54, 4.41 (2×m, 2H), 4.29-4.22 (m, 1H), 3.95 (t, J = 5.8 Hz, 1H), 3.75, 3.72, 3.71 (4×s, 1H), 3.65-3.43 (m, 2H), 3.27 (m, 1H), 3.04, 2.94, 2.87, 2.79 (4×dd, J = 8.3, 3.6 Hz, J = 7.7, 5.5 Hz, J = 10.1, 2.8 Hz, J = 8.9, 4.8 Hz, 1H), 2.42, 2.27, 1.95, 1.83 (m, 2H), 1.47, 1.42, 1.17, 1.05 (4×d, J = 7.0 Hz, 3H, CH$_3$).

^{13}C NMR (100 MHz, CDCl$_3$) δ = 174.27, 174.05, 174.05, 173.77, 173.24, 173.20, 171.38, 170.26, 170.26, 137.53, 136.96, 136.96, 129.70, 129.70, 129.39, 129.24, 129.24, 128.62, 128.62, 128.54, 128.40, 128.40, 128.22, 128.22, 94.10, 93.99, 93.99, 93.66, 93.53, 62.52, 62.52, 62.39, 61.80, 61.72, 60.96, 60.71, 60.55, 60.34, 59.02, 59.02, 58.45, 56.33, 55.40, 55.09, 55.09, 54.80, 52.67, 52.52, 52.42, 52.42, 42.82, 42.70, 42.70, 42.40, 42.08, 41.07, 40.99, 40.99, 40.75, 40.31, 37.06, 35.26, 35.26, 33.74, 32.29, 21.15, 19.45, 18.37, 18.37, 18.19, 16.93, 14.29.

Compound 124:
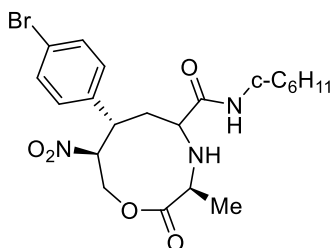
4-(4-bromophenyl)-5-nitrotetrahydro-2H-pyran-2-ol **116** (32.3 mg, 0.125 mmol), L-alanine (22.3 mg, 0.125 mmol), and cyclohexylisocyanide (14 μL, 0.125 mmol) were reacted in TFE (1 mL) according to the general procedure 10. Flash column chromatography purification (Hex/EtOAc 1:1) afforded **124** (84mg, 70%) as a colorless oil. A mixture of four diastereoisomers was detected.

R_f = 0.30 (*n*-hexane/EtOAc 1:1).

^{1}H NMR (400 MHz, CDCl$_3$) δ = 7.53, 7.49, 7.48 (3×d, J = 8.4 Hz, 2H), 7.20, 7.15, 7.11 (3×d, J = 8.4 Hz, 2H), 6.94, 6.89, 6.77 (3×d, J = 8.1 Hz, 1H), 4.71 (m, 1H), 4.49-4.42 (m, 2H), 4.25 (m, 1H), 4.12 (m, 1H), 3.77 (m, 1H), 3.60 (m, 1H), 3.52 (m, 1H), 3.19 (m 1H), 2.95, 2.75, 2.61

(3×dd, J = 7.7, 4.4 Hz, J = 10.1, 2.9 Hz, J = 9.9, 4.5 Hz, 1H), 2.33, 2.12, 2.03 (3×m, 2H), 1.79 (m, 2H), 1.35 (m, 4H), 1.24, 1.19, 1.11 (3×d, J = 7.2 Hz, 3H, CH$_3$), 1.28-1.07 (m, 3H).

^{13}C NMR (100 MHz, CDCl$_3$) δ = 173.76, 172.07, 171.59, 137.37, 136.65, 136.16, 132.83, 132.55, 132.40, 130.34, 130.16, 93.65, 93.46, 92.97, 62.29, 61.73, 60.94, 60.57, 58.97, 58.61, 55.46, 55.15, 48.22, 47.77, 42.24, 42.15, 41.87, 37.55, 35.45, 33.06, 32.85, 25.57, 24.87, 19.63, 18.53, 18.34.

Compound 125:
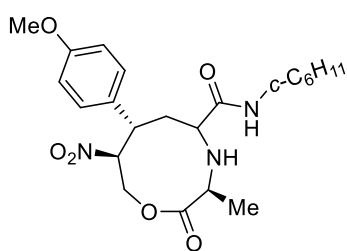
4-(4-methoxyphenyl)-5-nitrotetrahydro-2H-pyran-2-ol **117** (63.3 mg, 0.25 mmol), L-alanine (22.3 mg, 0.25 mmol), and cyclohexylisocyanide (31 μL, 0.25 mmol) were reacted in TFE (1 mL) according to the general procedure 10. Flash column chromatography purification (Hex/EtOAc 1:1) afforded **125** (57mg, 51%) as a colorless oil. A mixture of four diastereoisomers was detected.

R_f = 0.50 (*n*-hexane/EtOAc 1:1).

^{1}H NMR (400 MHz, CDCl$_3$) δ = 7.20, 7.16, 7.13 (3×d, J = 8.8 Hz, 2H), 6.91, 6.88, 6.87 (3×d, J = 8.7 Hz, 2H), 7.07, 6.83 (d, J = 8.2 Hz, 1H, NH$_{(amide)}$), 4.71 (m, 1H), 4.52 (m, 1H), 4.39 (m, 1H), 4.31-4.20 (m, 1H), 4.16-4.10 (m, 1H), 3.81, 3.79, 3.78 (3×s, 3H, OCH$_3$), 3.58 (m, 1H), 3.35 (m, 1H), 3.24-3.12 (m, 1H), 2.95, 2.85, 2.78, 2.68 (4×dd, J = 8.1, 3.6 Hz, J = 11.5, 6.2 Hz, J = 10.1, 2.5 Hz, J = 9.1, 4.8 Hz, 1H), 2.38, 2.20, 2.05 (3×m, 2H), 1.91-1.56 (m, 6H), 1.43 – 1.03 (m, 5H), 1.22, 1.17, 1.06 (3×d, J = 7.1 Hz, 3H).

^{13}C NMR (100 MHz, CDCl$_3$) δ= 173.65, 173.21, 173.21, 172.41, 172.41, 171.88, 159.66, 159.66, 159.38, 129.55, 129.47, 129.47, 128.55, 128.55, 115.05, 115.05, 114.77, 114.63, 114.63, 94.24, 94.14, 94.14, 93.68, 62.52, 62.52, 62.44, 61.80, 60.86, 60.50, 59.29, 59.29, 58.78, 58.70, 58.55, 55.45, 55.37, 55.37, 55.26, 48.14, 48.14, 47.75, 42.31, 42.08, 42.08, 41.74, 37.60, 37.60, 35.49, 35.49, 33.79, 33.03, 33.03, 32.80, 29.82, 25.58, 25.58, 24.85, 24.85, 19.53, 19.53, 18.47, 18.47, 18.29.

Compound 126:
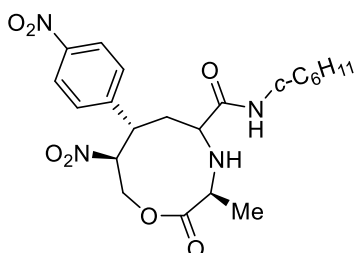
4-(4-nitrophenyl)-5-nitrotetrahydro-2H-pyran-2-ol **118** (67 mg, 0.25 mmol), L-alanine (22.3 mg, 0.25 mmol), and cyclohexylisocyanide (31 μL, 0.25 mmol) were reacted in TFE (1 mL) according to the general procedure 10. Flash column

chromatography purification (Hex/EtOAc 1:1) afforded **126** (45mg, 71%) as a colorless oil. A mixture of four diastereoisomers was detected.

R_f = 0.30 (*n*-hexane/EtOAc 1:1).

^{1}H NMR (400 MHz, CDCl$_3$) δ = 8.19, 8.17, 8.14 (3×d, *J* = 8.7 Hz, 2H), 7.47, 7.43, 7.36 (3×d, *J* = 8.8 Hz, 2H), 6.92, 6.89, 6.82 (3×d, *J* = 8.7 Hz, 1H, *N*H), 4.70 (m, 1H), 4.43, 4.19 (m, 2H), 3.64 (m, 1H), 3.54 (m, 1H), 3.19 (q, *J* = 7.2 Hz, 1H), 3.10, 2.85, 2.66, 2.49 (4×dd, *J* = 14.7, 6.6 Hz, *J* = 8.2, 4.8 Hz, *J* = 9.8, 3.2 Hz, *J* = 10.2, 4.3 Hz, 1H), 2.31, 2.11, 1.90 (3×m, 2H), 1.90-1.50 (m, 6H), 1.19, 1.15, 1.10 (3×d, *J* = 7.1 Hz, 3H, CH$_3$), 1.36-0.99 (m, 5H).

^{13}C NMR (100 MHz, CDCl$_3$) δ = 173.65, 173.09, 171.77, 171.25, 147.80, 147.62, 145.11, 144.84, 129.67, 129.55, 129.41, 124.52, 124.26, 124.15, 93.08, 92.85, 92.42, 61.94, 58.64, 58.35, 55.30, 54.92, 48.19, 47.68, 42.18, 37.33, 35.63, 33.04, 32.90, 32.70, 25.40, 24.71, 19.55, 18.32, 18.22.

Compound 127
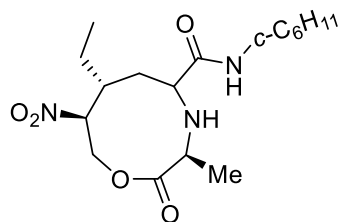
4-(4-ethylphenyl)-5-nitrotetrahydro-2H-pyran-2-ol **119** (15 mg, 0.07 mmol), L-alanine (5 mg, 0.07 mmol), and cyclohexylisocyanide (7 µL, 0.07 mmol) were reacted in TFE (1 mL) according to the general procedure 10. Flash column chromatography purification (Hex/EtOAc 1:1) afforded **127** (10.2 mg, 41%) as a colorless oil. A mixture of four diastereoisomers was detected.

R_f = 0.50 (*n*-hexane/EtOAc 1:1).

^{1}H NMR (400 MHz, CDCl$_3$) δ = 7.11, 7.06, 6.92, 6.73 (d, *J* = 8.8 Hz, 1H, *N*H$_{(amide)}$), 4.84-4.36 (m, 2H), 4.25-4.00 (m, 1H), 3.89 (m, 1H), 3.73 (m, 1H), 3.50, 3.35 (2×m, 1H), 3.27, 3.16, 3.07, 2.98 (4×dd, *J* = 8.0, 6.1 Hz, *J* = 13.3, 6.9 Hz, *J* = 8.2, 5.6 Hz, 1H), 2.22 (m, 1H), 1.97-1.09 (m, 13H), 1.40, 1.36 (2×d, *J* = 7.0 Hz, 3H), 0.97 (dt, *J* = 14.4, 4.7 Hz, 3H).

^{13}C NMR (100 MHz, CDCl$_3$) δ = 174.02, 173.92(*C*=O), 172.86, 172.86 (*C*=O), 90.97, 90.55, 90.25, 90.25 (*C*H), 61.20, 61.20, 61.09, 60.84 (*C*H$_2$), 59.87, 59.87, 58.74 (*C*H), 55.45, 55.45, 55.28 (*C*H), 48.02, 47.88, 47.88, 47.25 (*C*H), 37.42, 37.42, 37.27, 36.83 (*C*H), 34.91, 34.91, 34.61 (*C*H$_2$), 33.15, 33.15, 32.89 (*C*H$_2$), 25.58, 25.58, 24.92, 24.84 (*C*H$_2$), 24.31, 23.73, 23.37, 23.10 (*C*H$_2$), 19.75, 19.75, 18.01, 18.01 (*C*H$_3$), 11.15, 11.02, 10.89, 10.89 (*C*H$_3$).

DEPT 135° δ = 90.89, 90.82, 90.41, 90.10 (*C*H), 61.05, 60.94, 60.82, 60.70 (*C*H$_2$), 59.74, 59.72, 59.25, 58.59 (*C*H), 55.31, 55.26, 55.14 (*C*H), 47.88, 47.74, 47.63 (*C*H), 37.28, 37.13 (*C*H), 34.76, 34.46, 34.39, 34.30 (*C*H$_2$), 33.04, 33.00, 32.95, 32.75 (*C*H$_2$), 25.44, 24.78, 24.69,

24.64 (CH_2), 24.16, 23.59, 23.23, 22.96 (CH_2), 19.61, 19.58, 17.87 (CH_3), 11.01, 10.88, 10.78, 10.75 (CH_3).

Compound 128:
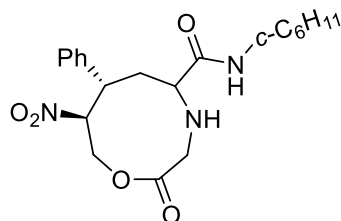
5-nitro-4-phenyl tetrahydro-2H-pyran-2-ol **114** (55.8 mg, 0.25 mmol), glycine (18.7 mg, 0.25 mmol), and cyclohe×ylisocyanide (31 μL, 0.25 mmol) were reacted in TFE (1 mL) according to the general procedure 10. Flash column chromatography purification (Hex/EtOAc 1:1) afforded **128** (57mg, 60%) as a colorless oil. A mixture of four diastereoisomers was detected.

R_f = 0.25 (n-hexane/EtOAc 1:1)

^{1}H NMR (400 MHz, CDCl$_3$) δ = 7.39-7.23 (m, 5H), 7.04, 6.96, 6.76 (3×d, J = 8.4 Hz, 1H, NH$_{(amide)}$), 4.76 (m, 1H), 4.49 (m, 1H), 4.44-4.37 (m, 1H), 3.88-3.74 (m, 1H), 3.69-3.48 (m, 1H), 3.38, 3.30, 3.24, 3.18 (4×d, J = 18.0 Hz, 2H), 2.85, 2.75, 2.68 (3×dd, J = 8.8, 3.6 Hz, J = 8.8, 5.1 Hz, J = 10.4, 2.6 Hz, 1H), 2.33, 2.18, 1.97 (3×m, 2H), 1.88-1.55 (m, 6H), 1.34 (m, 2H), 1.21-1.03 (m, 3H).

^{13}C NMR (100 MHz, CDCl$_3$) δ = 171.96, 171.53, 170.91, 170.38, 137.73, 137.07, 129.54, 129.40, 129.22, 129.15, 128.47, 128.44, 128.39, 128.29, 94.07, 93.34, 62.71, 62.40, 61.66, 61.25, 60.88, 60.79, 60.52, 60.43, 60.24, 60.03, 60.03, 48.71, 48.63, 48.16, 47.99, 43.29, 42.93, 42.93, 37.10, 36.09, 36.09, 34.46, 33.01, 33.01, 25.55, 25.55, 24.83, 24.83.

Compound 129:
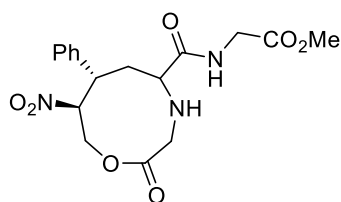
5-nitro-4-phenyl tetrahydro-2H-pyran-2-ol **114** (55.8 mg, 0.25 mmol), glycine (18.7 mg, 0.25 mmol), and methylisocyanoacetate (22.7 μL, 0.25 mmol) were reacted in TFE (1 mL) according to the general procedure 10. Flash column chromatography purification (Hex/EtOAc 1:1) afforded **129** (54 mg, 57%) as a colorless oil. A mixture of four diastereoisomers was detected.

R_f = 0.23 (n-hexane/EtOAc 1:1).

^{1}H NMR (400 MHz, CDCl$_3$) δ = 7.56, 7.47 (2×t, J = 5.8 Hz, 1H, NH$_{(amide)}$), 7.40-7.23 (m, 5H), 4.83-4.74 (m, 1H), 4.53-4.47 (m, 1H), 4.41 (q, J = 8.4 Hz, 1H), 4.06, 4.02, 3.99, 3.93 (4×d, J = 6.4 Hz, 2H), 3.82, 3.54 (m, 1H), 3.75, 3.74, 3.73 (3×s, 3H, OCH$_3$), 3.63-3.48, 3.44, 3.36, 3.27 (4×d, J = 18.1 Hz, 2H), 3.00, 2.95, 2.88, 2.80 (4×dd, J = 7.7, 5.7 Hz, J = 9.0, 3.6 Hz, J = 8.6, 4.9 Hz, J = 10.4, 2.6 Hz, 1H), 2.34, 2.16, 2.00, 1.78 (4×m, 2H), 1.43, 1.34, 1.26 (3×s, 1H).

¹³C NMR (100 MHz, CDCl₃) δ = 173.69, 173.13, 173.13, 170.95, 170.49, 170.49, 170.30, 170.30, 137.56, 137.56, 136.98, 129.59, 129.59, 129.43, 129.43, 129.26, 129.26, 129.12, 128.47, 128.47, 128.40, 128.40, 94.00, 94.00, 62.71, 62.38, 62.38, 61.60, 60.93, 60.83, 60.56, 60.46, 59.97, 59.97, 59.78, 52.52, 52.52, 48.63, 48.63, 43.06, 43.06, 42.78, 40.90, 40.79, 40.79, 36.58, 36.58, 35.94.

Compound 130:
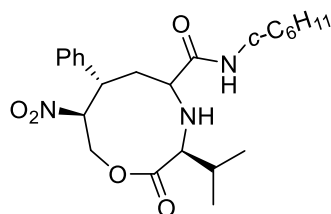
5-nitro-4-phenyl tetrahydro-2H-pyran-2-ol **114** (55.8 mg, 0.25 mmol), L-valine (29.3 mg, 0.25 mmol), and cyclohexylisocyanide (31 µL, 0.25 mmol) were reacted in TFE (1 mL) according to the general procedure 10. Flash column chromatography purification (Hex/EtOAc 1:1) afforded **130** (75mg, 70%) as a colorless oil. A mixture of four diastereoisomers was detected.

R_f = 0.45 (*n*-hexane/EtOAc 1:1).

¹H NMR (400 MHz, CDCl₃) δ = 7.42-7.19 (m, 5H), 7.05, 6.91, 6.58 (d, *J* = 8.8 Hz, 1H), 4.79-4.70 (m, 1H), 4.51, 4.35 (2×dd, *J* = 12.7, 8.5 Hz, 1H), 4.21-4.06 (m, 1H), 3.89-3.75 (m, 1H), 3.73-3.50 (m, 1H), 2.97, 2.89, 2.70, 2.59 (4×dd, *J* = 9.9, 2.7 Hz, *J* = 9.6, 4.8 Hz, 1H), 2.32, 2.18, 2.08 (3×ddd, *J* = 14.5, 11.8, 2.9 Hz, 3H), 1.93-1.60 (m, 6H), 1.45-0.76 (m, 5H), 1.04 (d, *J* = 6.8 Hz, 1H), 0.97, 0.90, 0.80 (3×d, *J* = 6.9 Hz, 6H), 0.92, 0.77 (2×d, *J* = 7.0 Hz, 3H).

¹³C NMR (100 MHz, CDCl₃) δ = 172.93, 172.69, 172.41, 171.64, 137.44, 129.69, 129.25, 128.64, 128.55, 128.42, 128.15, 94.17, 93.93, 66.48, 65.68, 62.50, 60.57, 60.13, 59.28, 48.23, 47.83, 43.05, 42.84, 38.01, 36.35, 33.12, 32.81, 31.88, 31.38, 25.60, 24.88, 19.86, 18.77, 18.48, 17.41.

HRMS (ESI-FT-ICR) [MH]⁻ calcd. for C₂₃H₃₂N₃O₅: 430,2420, found 430,2344

Compound 131:
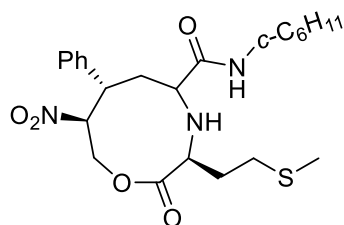
5-nitro-4-phenyl tetrahydro-2H-pyran-2-ol **114** (55.8 mg, 0.25 mmol), L-methionine (37.3 mg, 0.25 mmol), and cyclohexylisocyanide (31 µL, 0.25 mmol) were reacted in TFE (1 mL) according to the general procedure 10. Flash column chromatography purification (Hex/EtOAc 1:1) afforded **131** (75mg, 72%) as a colorless oil. A mixture of four diastereoisomers was detected.

R_f = 0.45 (*n*-hexane/EtOAc 1:1)

¹H NMR (400 MHz, CDCl₃) δ = 7.46-7.19 (m, 5H), 6.86, 6.82, 6.48 (3×d, *J* = 8.3 Hz, 1H, *N*H(amide)), 4.74 (m, 1H), 4.51 (dd, *J* = 12.7, 8.4 Hz, 1H), 4.40 (dd, *J* = 12.7, 8.4 Hz, 1H), 4.22, 4.12 (2×dd, *J* = 16.7, 8.4 Hz, 1H), 3.78 (m, 1H), 3.69-3.50 (m, 2H), 3.31 (m, 1H), 2.74, 2.65, 2.54, 2.50 (4×dd, *J* = 12.8, 8.1 Hz, *J* = 11.9, 5.9 Hz, *J* = 8.3, 5.1 Hz, *J* = 8.3, 5.1 Hz, 1H), 2.31, 2.09 (2×m, 1H), 2.07, 2.05, 2.04, 2.03 (4×s, 3H), 1.67 (m, 8H), 1.23 (m, 6H).

¹³C NMR (100 MHz, CDCl₃) δ = 172.61, 172.12, 137.30, 129.77, 129.77, 129.27, 128.61, 128.61, 128.43, 93.91, 62.58, 59.28, 58.99, 48.30, 42.73, 36.31, 33.11, 32.90, 32.10, 30.00, 25.59, 24.90, 15.39.

Compound 132:
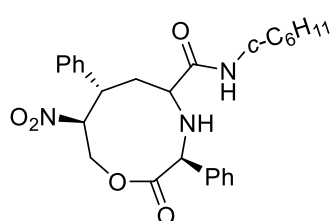
5-nitro-4-phenyl tetrahydro-2H-pyran-2-ol (55.8 mg, 0.25 mmol), L-phenylglycine (37.8 mg, 0.25 mmol), and cyclohexylisocyanide (31 µL, 0.25 mmol) were reacted in TFE (1 mL) according to the general procedure 10. Flash column chromatography purification (Hex/EtOAc 1:1) afforded **132** (63mg, 54%) as a colorless oil. A mixture of four diastereoisomers was detected.

*R*f = 0.40 (*n*-hexane/EtOAc 1:1).

¹H NMR (400 MHz, CDCl₃) δ= 7.49-6.88 (m, 10H), 4.95-4.61 (m, 1H), 4.58-4.21 (m, 1H), 4.21-3.91 (m, 1H), 3.84 (m, 1H), 3.73-3.41 (m, 1H), 3.37-2.69 (m, 3H), 2.68-2.22 (m, 1H), 2.00-1.45 (m, 7H), 1.44-0.91 (m, 8H).

¹³C NMR (100 MHz, CDCl₃) δ= 172.32, 171.67, 137.95, 129.82, 129.28, 129.03, 128.91, 128.30, 128.11, 127.52, 93.48, 62.35, 61.75, 51.17, 48.97, 48.29, 47.23, 43.30, 42.37, 39.25, 34.75, 33.14, 32.67, 25.53, 24.83.

Compound 133:
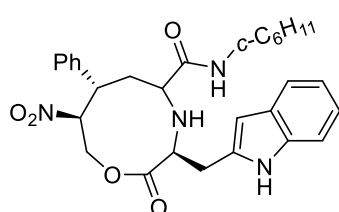
5-nitro-4-phenyl tetrahydro-2H-pyran-2-ol **114** (55.8 mg, 0.25 mmol), L-tryptophan (51.1 mg, 0.25 mmol), and cyclohexylisocyanide (31 µL, 0.25 mmol) were reacted in TFE (1 mL) according to the general procedure 10. Flash column chromatography purification (Hex/EtOAc 1:1) afforded **133** (54mg, 42%) as a yellow solid. A mixture of four diastereoisomers was detected.

*R*f = 0.10 (*n*-hexane/EtOAc 1:1).

¹H NMR (400 MHz, CDCl₃) δ = 8.77, 8.26, 8.07 (3×s, 1H), 7.70-7.64 (m, 1H), 7.51-7.41 (m, 1H), 7.39-7.05 (m, 7H), 7.01, 6.59 (d, *J* = 6.6 Hz, 1H, *N*H(amide)), 6.35, 6.33, 6.32 (3×s, 1H),

4.77-4.69 (m, 1H), 4.53, 4.32 (2×m, 2H), 4.54-4.38 (m, 1H), 2.88, 2.81, 2.74, 2.64 (4×dd, J = 14.5, 10.4 Hz, J = 10.6, 3.9 Hz, J = 14.6, 9.6 Hz, J = 9.3, 4.7 Hz, 1H), 2.40, 2.20 (2×m, 2H), 1.86-1.41 (m, 8H), 1.38-1.05 (m, 6H).

13C NMR (100 MHz, CDCl3) δ = 173.21, 173.02, 172.65, 171.80, 138.22, 137.28, 136.76, 136.46, 129.10, 129.10, 128.93, 128.61, 128.61, 128.20, 128.20, 127.23, 123.64, 123.29, 123.29, 122.86, 122.58, 122.58, 120.14, 120.14, 118.71, 118.71, 118.52, 112.10, 111.62, 111.06, 110.27, 93.68, 93.56, 93.50, 61.94, 61.78, 61.39, 61.30, 60.33, 60.33, 59.70, 59.70, 48.37, 48.37, 47.57, 47.57, 47.28, 47.28, 43.20, 43.20, 42.42, 42.42, 36.48, 36.48, 34.79, 33.16, 33.16, 32.60, 32.60, 32.00, 29.76, 29.32, 25.54, 25.54, 24.84, 24.84.

Compound 134:
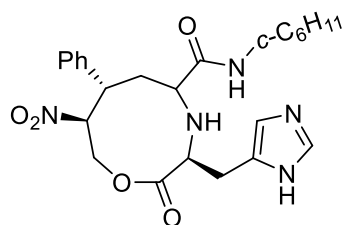
5-nitro-4-phenyl tetrahydro-2H-pyran-2-ol **114** (55.8 mg, 0.25 mmol), L-histidine (38.8 mg, 0.25 mmol), and cyclohexylisocyanide (31 μL, 0.25 mmol) were reacted in TFE (1 mL) according to the general procedure 10. Flash column chromatography purification (Hex/EtOAc 1:1) afforded **134** (82mg, 70%) as an orange solid. A mixture of four diastereoisomers was detected.

R_f = 0.45 (*n*-hexane/EtOAc 1:1).

1H NMR (400 MHz, CDCl3) δ = 7.70, 7.68, 6.94, 6.91 (4×s, 1H), 7.54, 7.51, 6.77, 6.72 (4×d, J = 2.98 Hz, 1H), 7.45-7.25 (m, 5H), 7.09, 7.00 (2×d, J = 6.9 Hz, 1H, NH$_{(amide)}$), 4.73 (m, 1H), 4.54-4.40 (m, 1H), 4.36-4.24 (m, 1H), 4.01 (m, 1H), 3.81, 3.71 (2×d, J = 8.6 Hz, 2H), 3.64-3.36 (m, 2H), 3.25-2.95 (m, 1H), 2.91, 2.81, 2.71, 2.65 (4×dd, J = 14.5, 8.7 Hz, J = 7.9 Hz, 10.5 Hz, 1H), 2.36, 2.25 (2×m, 2H), 1.94-1.56 (m, 6H), 1.36-1.00 (m, 5H).

13C NMR (100 MHz, CDCl3) δ = 173.07, 172.93, 172.93, 172.60, 137.90, 137.19, 137.19, 136.15, 135.34, 129.55, 129.55, 129.15, 128.90, 128.36, 128.13, 128.06, 124.22, 121.47, 116.14, 112.76, 94.57, 94.53, 94.44, 62.35, 61.60, 61.36, 60.76, 60.40, 60.40, 60.03, 60.03, 59.63, 59.63, 48.35, 43.04, 42.66, 37.27, 37.27, 36.04, 32.96, 32.82, 32.61, 30.58, 25.57, 25.49, 24.93, 24.89.

Compound 135:
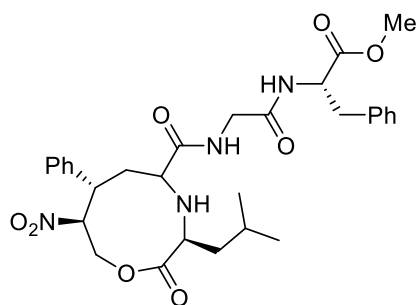
5-nitro-4-phenyl tetrahydro-2H-pyran-2-ol **114** (27.9 mg, 0.1 mmol), L-leucine (16.4 mg, 0.1mmol), and CN-Gly-Phe-OMe (30.8 mg, 0.1 mmol) were reacted in TFE (1 mL) according to the general procedure 10. Flash column chromatography purification (Hex/EtOAc 1:1) afforded **135** (26.8 mg, 46%) as a yellow solid. A mixture of four diastereoisomers was detected.

R_f = 0.15 (*n*-hexane/EtOAc 1:1).

^{1}H NMR (400 MHz, CDCl$_3$) δ = 7.55 (dt, *J* = 10.5, 5.3 Hz, 1H), 7.44-6.98 (m, 10H), 6.65, 6.54, 6.43, 6.36 (4×d, *J* = 6.8 Hz, 1H, *N*H$_{(amide)}$), 4.93-4.66 (m, 1H), 4.48-4.20 (m, 1H), 4.16-3.93 (m, 1H), 3.73, 3.70, 3.69 (3×s, 3H), 3.87-3.44 (m, 1H), 3.26-2.96 (m, 1H), 3.08, 2.84, 2.73, 2.70 (4×dd, *J* = 14.0, 5.9 Hz, 1H), (d, *J* = 4.9 Hz, 1H), (dd, *J* = 8.9, 3.5 Hz, 1H), (dd, *J* = 10.4, 2.9 Hz, 1H), 2.41, 2.18, 2.00 (3×m, 2H), 1.81-1.15 (m, 5H), 0.93, 0.90 (2×d, *J* = 6.4 Hz, 3H), 0.87, 0.80 (2×d, *J* = 6.6 Hz, 3H).

^{13}C NMR (100 MHz, CDCl$_3$) δ = 174.12, 173.36, 171.86, 171.69, 170.55, 168.66, 137.06, 135.88, 135.85, 129.81, 129.81, 129.54, 129.37, 129.25, 128.78, 128.78, 128.64, 128.57, 127.40, 127.33, 127.19, 93.96, 93.91, 93.81, 93.81, 62.57, 62.31, 59.59, 59.35, 59.10, 53.54, 53.47, 53.16, 52.60, 52.55, 52.40, 43.13, 42.83, 42.62, 37.90, 37.86, 37.10, 36.44, 24.85, 24.79, 22.85, 22.66, 22.59.

HRMS (ESI-FT-ICR) [MH]$^-$ calcd. for C$_{30}$H$_{37}$N$_4$O$_8$: 581,2690, found 581,2603

Compound 136:
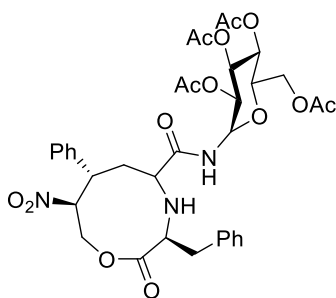
5-nitro-4-phenyl tetrahydro-2H-pyran-2-ol (55.8 mg, 0.25 mmol), L-Phenylalanine (41.3 mg, 0.25 mmol), and (AcO)$_4$-β-Glc-NC **142** (89.3 mg, 0.25 mmol) were reacted in TFE (1 mL) according to the general procedure 10. Flash column chromatography purification (Hex/EtOAc 1:1) afforded **136** (58.2 mg, 32%) as a light yellow solid. A mixture of four diastereoisomers was detected.

R_f = 0.5 (*n*-hexane/EtOAc 1:1).

^{1}H NMR (400 MHz, CDCl$_3$) δ = 7.45-7.22 (m, 10H), 7.00, 6.83 (2×d, *J* = 9.2 Hz, 1H, *N*H), 5.28 (dd, *J* = 15.2, 5.7 Hz, 1H), 5.12 (dd, *J* = 9.3 Hz, 1H), 5.07 (m, 1H), 4.87 (dd, *J* = 9.5 Hz, 1H), 4.61 (m, 1H), 4.50 (dd, *J* = 12.7, 8.5 Hz, 1H), 4.32-4.21 (m, 2H), 4.05 (dd, *J* = 12.4, 2.0

Hz, 1H), 3.78 (m, 1H), 3.68 (dd, J = 12.4, 8.3 Hz, 1H), 3.45 (dd, J = 12.4, 2.0 Hz, 1H), 3.17-3.10 (m, 1H), 2.99, 2.78, 2.59 (3×dd, J = 13.8, 4.7 Hz, J = 13.7, 9.0 Hz, J = 10.9, 4.1 Hz, 1H), 2.06 (s, 3H), 2.03 (s, 3H), 2.02 (s, 3H), 2.01 (s, 3H), 1.65 (d, J = 7.4 Hz, 3H), 1.53-1.10 (m, 3H).

^{13}C NMR (100 MHz, CDCl$_3$) δ= 174.26, 171.94, 171.13, 170.75, 170.03, 169.69, 137.08, 136.77, 129.79, 129.71, 128.95, 128.56, 128.13, 127.37, 93.85, 78.32, 73.75, 72.88, 70.73, 68.12, 62.56, 61.69, 60.68, 58.85, 42.24, 39.29, 36.82, 20.71.

5.3.5 Synthesis and spectroscopy data of non-conversional isocyanides

Synthesis of potassium isocyanoacetate [125]
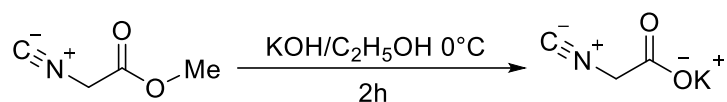
To a solution of 600 mg (11mmol) of powdered potassium hydroxide in 10 ml absolute ethanol; then, 908 μL (10 mmol) of methyl isocyanoacetate dissolved in 1,2 ml of absolute ethanol was added dropwise at 0°C under nitrogen. The resulting solution was stirred at room temperature for 2 h after precipitates appears. Then was cooled the mixture at 0°C, quickly filtered and washed with ice-cold ethanol and ether. The volatiles were removed under vacuum, resulting in 1.1 g (yield = 93 %) as light yellow solid with Mp = 205°C.

Compound 138:
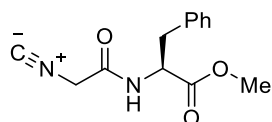
A mixture of potassium isocyanoacetate (160 mg, 1.3 mmol, 1.3 equiv.) and Phenylalanine (1.0 mmol, 1.0 equiv.) were stirred in DMF at room temperature for 5min. Then, triethylamine (0.29 mL, 2.1 mmol, 2.1 equiv.) was slowly added and stirred for another 20 min and cooled to -10 ºC. TBTU (481 mg, 1.5 mmol, 1.5 equiv.) was added and the final mixture was stirred for 12 h until completion of the reaction (monitored by TLC). The mixture was diluted with 100 mL of EtOAc, transferred to a separatory funnel and washed with saturated solution of NaHCO$_3$ (2x 50 mL) and sequentially with Brine (2x 30 mL). The organic phase was dried over anhydrous Na$_2$SO$_4$ and concentrated under reduced pressure. The crude product was purified by flash column chromatography on silica gel using *n*-hexane/EtOAc as eluent to give 60% of compound CN-Gly-Phe-OMe **138** as white solid.

Mp = 105 °C.

R$_f$ = 0.55 (*n*-hexane/EtOAc 7:2).

$[\alpha] \mathrm{D}^{23}$ = +15.2 (*c* 0.54, MeOH, 23°C).

^{1}H NMR (400 MHz, CDCl$_3$) δ= 7.34-7.26 (m, 3H), 7.17-7.09 (m, 2H), 6.76 (d, *J* = 7.2 Hz, 1H, *N*H), 4.87 (t, *J* = 3.9 Hz, 1H), 4.85 (t, *J* = 3.9 Hz, 1H), 4.12 (s, 2H), 3.76 (s, 3H), 3.20 (dd, *J* = 13.9, 5.7 Hz, 1H), 3.13 (dd, *J* = 13.9, 6.3 Hz, 1H).

^{13}C NMR (100 MHz, CDCl$_3$) δ= 171.12, 162.93, 162.12, 135.18, 129.26, 129.01, 127.66, 53.51, 52.77, 45.22, 37.78.

Synthesis of 2,3,4,6-tetra-o-acetyl- β-d-glucopyranosyl isocyanide 142 [126]

Compound 139:
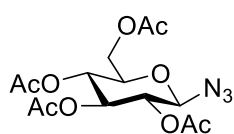
To a solution of SnCl$_4$ (234 μL, 2 mmol) in toluene (6.0 mL) a suspension of AgClO$_4$ (415 mg, 2 mmol) in CH$_2$Cl$_2$ (60 mL) was added at room temperature. The mixture was stirred at room temperature for 1h in the absence of light. Then, the mixture was added to a solution of comercial (AcO)$_5$-β-Glc (7.8 g, 20 mmol) and trimethylsilyl azide (TMSN$_3$; 5.26 mL, 40 mmol) in CH$_2$Cl$_2$. The mixture was stirred at room temperature. After stirring for 3h at room temperature the residue was washed with saturated aqueous NaHCO$_3$ and extracted with CH$_2$Cl$_2$, and the organic layer was dried over Na$_2$SO$_4$ and filtered. After solvent evaporation, the residue was purified by flash column chromatography (Hex/AcOEt 7:3), affording the title compound (AcO)$_4$-β-Glc-N$_3$ **139** as white amorphous solid (6.72 g, 90%). [127]

Mp = 126 °C.

R_f = 0.55 (*n*-hexane/EtOAc 7:2).

$[\alpha] \mathrm{D}^{23}$ = -30° (c =2.40 CHCl$_3$, 23 °C).

^{1}H NMR (400 MHz, CDCl$_3$) δ= 5.23 (t, *J* = 9.5 Hz, 1H), 5.11 (t, *J* = 9.7 Hz, 1H), 4.99 – 4.93 (m, 1H), 4.66 (d, *J* = 8.9 Hz, 1H), 4.28 (dd, *J* = 12.5, 4.8 Hz, 1H), 4.18 (dd, *J* = 12.5, 2.3 Hz, 1H), 3.81 (ddd, *J* = 10.0, 4.8, 2.3 Hz, 1H), 2.11 (s, 3H), 2.08 (s, 3H), 2.04 (s, 3H), 2.01 (s, 3H).

^{13}C NMR (100 MHz, CDCl$_3$) δ= 170.69, 170.21, 169.40, 169.30, 88.00, 74.12, 72.70, 70.74, 67.99, 61.76, 20.79, 20.63.

Compound 140:
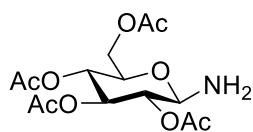
To a solution of (AcO)$_4$-β-Glc-N$_3$ **139** (932 mg, 2.5 mmol) in anhydrous CH$_2$Cl$_2$ was added Pd/C (5%) (0.1 g). The mixture was stirred under H$_2$ at atmospheric pressure for 2 h. The Pd/C (5%) was removed by filtration through Celite, and the filtrate was concentrated in vacuo to remove the CH$_2$Cl$_2$. Purification

of the residue by flash column chromatography (Hex/AcOEt 1:1) afforded $(AcO)_4$-β-Glc-NH_2 **140** as a white amorphous solid (738 mg, 85%).

Mp = 121 °C

$\boldsymbol{R_f}$ = 0.55 (*n*-hexane/EtOAc 7:2).

[α] $_D^{23}$ = +11.1° (c = 0.54 in $CHCl_3$, 23°C).

^{1}H NMR (400 MHz, MeOD) δ= 5.26 (t, *J* = 9.5 Hz, 1H), 5.01 (t, *J* = 9.7 Hz, 1H), 4.82 (dd, *J* = 9.6, 9.1 Hz, 1H), 4.29 (d, *J* = 9.0 Hz, 1H), 4.25 (dd, *J* = 12.2, 4.9 Hz, 1H), 4.11 (dd, *J* = 12.3, 2.4 Hz, 1H), 3.83 (ddd, *J* = 10.1, 4.8, 2.4 Hz, 1H), 2.05 (s, 3H), 2.04 (s, 3H), 2.02 (s, 3H), 1.98 (s, 3H).

^{13}C NMR (100 MHz, MeOD) δ= 172.29, 171.52, 171.18, 170.94, 88.81, 75.01, 74.07, 72.14, 69.41, 62.93, 20.57, 20.49, 20.45.

Compound 142:
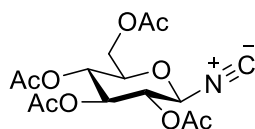
A solution of acetic anhydride (1 mL, 1mmol) and formic acid (0.6 mL, 1.5 mmol) was heated at 60 °C for 3 h. The resulting solution was cooled to room temperature, then added to the amine $(AcO)_4$-β-Glc-NH_2 **139** (347 mg, 1 mmol) solution and left under vigorous stirring overnight. The mixture was filtered through Celite and the solid obtained after concentration afford the crude formamide $(AcO)_4$-β-Glc-NH-CHO **141**. Without purification, the crude of reaction was dissolved in dry DCM (6 mL) under nitrogen, together with carbon tetrabromide (497 mg, 1.5 mmol) and TEA (280 μL, 2.0 mmol); the resulting solution was cooled to 20 °C. Triphenylphosphane (393 mg, 1.5 mmol) in dry DCM (5 mL) was added. After stirring at 20 °C for 30 min, the mixture was diluted with DCM, washed with a saturated solution of ammonium chloride and water, dried with anhydrous sodium sulfate and concentrated. Purification the residue by flash column chromatography (hexane/EtOAc 8:2) afforded $(AcO)_4$-β-Glc-NC **142** (296 mg, 83%).

Mp = 91 °C.

$\boldsymbol{R_f}$ = 0.55 (*n*-hexane/EtOAc 7:2).

[α] $_D^{23}$ = +15.2 (*c* 0.54, MeOH, 23°C).

^{1}H NMR (400 MHz, CDCl$_3$) δ= 5.19 (dt, *J* = 5.1, 1.5 Hz, 2H), 5.16-5.09 (m, 1H), 4.85-4.81 (m, 1H), 4.26 (dd, *J* = 12.6, 4.8 Hz, 1H), 4.16 (dd, *J* = 12.6, 2.3 Hz, 1H), 3.75 (ddd, *J* = 9.7, 4.8, 2.3 Hz, 1H), 2.12 (s, 3H), 2.12 (s, 3H), 2.03 (s, 3H), 2.02 (s, 3H).

^{13}C NMR (100 MHz, CDCl$_3$) δ= 170.62, 170.11, 169.26, 168.98, 164.88, 79.52, 74.76, 72.20, 71.17, 67.43, 61.42, 20.79, 20.60, 20.55.

5.3.6 Synthesis and spectroscopy data of hydroquinolinones

General procedures for one-pot organocatalytic multicomponent reaction sequence to hydroquinolinone
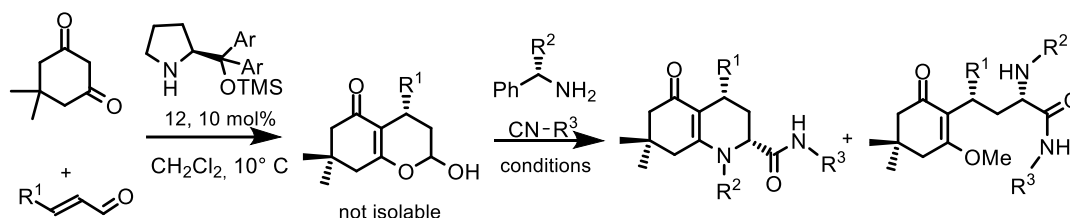
General procedure 11:

The 1,3-dicarbonyl compound (0.25 mmol, 1 equiv.) was added to a stirring solution of catalyst 1**2** (0.025 mmol, 0.1 equiv.) and α,β-unsaturated aldehyde **144** (0.33 mmol, 1.3 equiv) in CH_2Cl_2 (0.5 mL) at 10 °C in a 10 mL glass tube. The reaction mixture was stirred at that temperature for 48 h and then allowed to reach room temperature. Trifluoroethanol (0.5 mL), the amine (0.33 mmol, 1.3 equiv.) and the isocyanide (0.33 mmol, 1.3 equiv.) were added and the glass tube was sealed and introduced in the microwave reactor. Et_3N (0.33 mmol) was added when α-amino acid and peptide methyl ester hydrochlorides were employed as amino components. The flask was irradiated for 15 min (300 W) under high-speed magnetic stirring, while the temperature was raised up to 70 °C. The reaction course was monitored by TLC, and additional cycles of 15 min were applied in cases of poor consumption of the starting material. The volatiles were concentrated under reduced pressure and the resulting crude product was purified by flash column chromatography.

Compound 146 (*cis*):
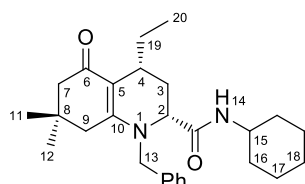
Dimedone **143** (35 mg, 0.25 mmol), *trans*-2-pentenal (32 μL, 0.33 mmol), benzylamine (36 μL, 0.33 mmol) and cyclohexylisocyanide (41 μL, 0.33 mmol) were reacted according to the general procedure 11. Flash column chromatography purification (*n*-hexane/EtOAc 1:1) afforded the diastereomers *cis* (47.5 mg, 45%) and *trans* (34 mg, 32%) of compound **146** as pale yellow oils.

Cis: R_f = 0.33 (*n*-hexane/EtOAc 1:1).

$[α]_D^{20}$ = -62.1 (*c* 6.0, acetone, 20°C).

¹H NMR (400 MHz, CDCl₃) δ = 7.38-7.27 (m, 3H, Ph); 7.10 (d, J = 7.2 Hz, 2H, Ph); 5.83 (d, J=8.1 Hz, 1H, H-14); 4.86 (d, J= 17.0 Hz, 1H, H-13a); 4.17 (d, J = 17.0 Hz, 1H, H-13b); 3.79 (d, J= 6.5Hz, 1H, H-2); 3.73 (m, 1H, H-15); 2.76 (m, 1H, H-4); 2.56 (d, J = 14.1 Hz, 1H, H-3a); 2.50(d, J = 16.1 Hz, 1H, H-9a); 2.34 (d, J = 16.2 Hz, 1H, H-9b); 2.27 (d, J = 16.1 Hz, 1H, H-7a); 2.18 (d, J = 16.2 Hz, 1H, H-7b); 2.04 (m, 1H); 1.93-1.85 (m, 2H, H-16a); 1.74-1.65 (m, 4H, H-19a, H-3b, H-17a); 142-1.32 (m, 4H, H-16b, H-17b); 1.20-1.11 (m, 2H, H-18); 1.05 (s, 3H, H-12); 1.02 (s, 3H, H-11); 0.98 (m, 1H, H-19b); 0.89 (m, 3H, H-20). The *cis* configuration was assigned based analysis of the NOESY spectrum. Important NOE contacts are: between H-14 (NH) and H-12 (axial methyl) as well as between H-14 and H-19 (methylene of the axial ethyl group). There are also NOE contacts between H-4 and H-2.

¹³C NMR (100 MHz, CDCl₃) δ= 194.4, 170.0 (C=O), 155.0, 136.6 (C), 129.2, 128.0, 126.0 (CH), 112.4 (C), 60.6 (CH), 53.9, 50.0 (CH₂), 48.4 (CH), 40.8 (CH₂), 33.1 (C), 33.0, 32.4 (CH₂), 30.3 (CH), 28.7, 28.4 (CH₃), 25.8, 25.6, 24.9, 24.7, 24.3(CH₂), 12.1 (CH₃).

HRMS (ESI-FT-QQTOF) *m/z*: 423.30011 [M+H]⁺; calcd. for $C_{27}H_{39}N_2O_2$: 423.30060.

Compound 146 (*trans*):
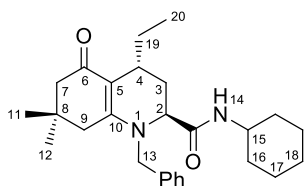
***Trans*:** R_f = 0.16 (*n*-hexane/EtOAc 1:1).

[α]$_D^{23}$ = -33.3 (*c* 5.4, acetone, 20°C).

¹H NMR (400 MHz, CDCl₃) δ = 7.37-7.29 (m, 3H, Ph); 7.12 (d, J = 7.1 Hz, 2H, Ph); 5.54 (d, J = 8.6 Hz, 1H, H-14); 4.85 (d, J = 16.9 Hz, 1H, H-13a); 4.12 (d, J = 16.9 Hz, 1H, H-13b); 3.78 (m, 1H, H-15); 3.71 (dd, J = 10.3/5.0 Hz, 1H, H-2); 2.79 (m, 1H, H-4); 2.45 (d, J = 16.4 Hz, 1H, H-9a); 2.39 (d, J = 16.5 Hz, 1H, H-9b); 2.23 (d, J = 16.3 Hz, 1H, H-7a), 2.18 (d, J = 16.0 Hz, 1H, H-7b); 2.02 (m, 1H); 1.98 (m, 1H, H-3a); 1.92 (m, 1H, H-3b); 1.88 (m, 2H, H-16a); 1.71-1.54 (m, 5H, H-19a, H-17); 1.43-1.25 (m, 4H, H-16b, H-18); 1.17 (m, 1H, H-19b); 1.05 (s, 3H, H-12); 1.01 (s, 3H, H-11); 0.87 (t, J = 7.4 Hz, 3H, H-20). The *trans* configuration was assigned based analysis of the NOESY spectrum. Important NOE contacts are: between axial H-2 and H-12 (axial methyl) as well as between axial H-2 and H-19 (methylene of the axial ethyl group).

^{13}C NMR (100 MHz, CDCl$_3$) δ = 194.4, 170.7 (C=O), 156.9, 136.4 (C), 131.0, 129.1, 129.0, 128.0, 126.7 (CH), 112.7 (C), 59.5 (CH), 52.0, 49.3 (CH$_2$), 48.4 (CH), 40.9, 33.1 (CH$_2$), 32.1 (C), 30.5 (CH$_2$), 30.3 (CH), 29.1, 28.3 (CH$_3$), 27.6, 26.9, 25.5, 24.8, 23.8 (CH$_2$), 11.6 (CH$_3$).

HRMS (ESI-FT-QQTOF) *m/z*: 423.30012 [M+H]$^+$; calcd. for C$_{27}$H$_{39}$N$_2$O$_2$: 423.30060.

Compound 147:
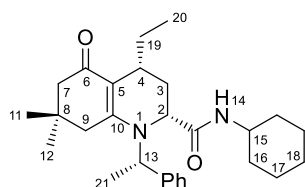
Dimedone **143** (35 mg, 0.25 mmol), *trans*-2-pentenal (32 μL, 0.33 mmol), (*S*)-α-methylbenzylamine (43μL, 0.33 mmol)and cyclohexylisocyanide (41 μL, 0.33 mmol) were reacted according to the general procedure 11. Flash column chromatography purification (*n*-hexane/EtOAc 1:1) afforded compound **147** (82 mg, 75%, isomer *cis*) as a pale yellow oil.

***R*$_f$** = 0.36 (*n*-hexane/EtOAc 1:1).

[α]$_D^{23}$ = -42.3 (*c* 3.5, acetone, 20°C).

^{1}H NMR (400 MHz, CDCl$_3$) δ = 7.28-7.21 (m, 3H, Ph); 7.07 (m, 2H, Ph); 6.00 (d, *J* = 8.3Hz, 1H, H-14); 5.15 (q, *J* = 7.0 Hz, 1H, H-13); 3.65 (m, 1H, H-15); 3.52 (dd, *J* = 6.0/1.8 Hz, 1H, H-2); 2.72 (m, 1H, *J* = 15.4 Hz, H-9a); 2.42 (m, 1H, H-4); 2.33 (d, *J* = 15.5 Hz, 1H, H-9b); 2.25 (m, 1H, H-9a); 2.22 (m, 1H, H-3a); 2.21(m, 2H, H-7); 1.86 (m, 2H, H-16a); 1.74 (m, 1H, H-17a); 1.64-1.56 (m, 4H, H-16b, 17b); 1.54 (d, *J* = 7.0 Hz, 3H, H-21); 1.37-1.23 (m, 2H, H-18); 1.12 (s, 3H); 1.07 (s, 3H); 0.92 (m, 1H, H-3b); 0.81-0.69 (m, 5H, H-19, H-20).

^{13}C NMR (100 MHz, CDCl$_3$) δ = 194.9, 170.9 (C=O), 154.4, 139.1 (C), 128.8, 128.2, 126.9 (CH), 115.4 (C), 56.3, 54.9 (CH), 50.1, 48.2, 43.2(CH$_2$), 33.3 (C), 32.7(CH), 32.55, 31.1(CH$_2$), 30.5, 26.2(CH$_3$), 25.6(CH), 25.4, 24.8, 24.7, 23.3(CH$_2$), 17.7, 11.9 (CH$_3$).

HRMS (ESI-FT-QQTOF) *m/z*: 437.31629 [M+H]$^+$; calcd. for C$_{28}$H$_{41}$N$_2$O$_2$: 437.31684.

Compound 148:
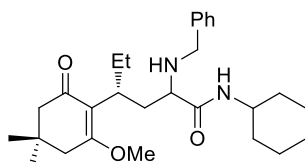
Dimedone **143** (35 mg, 0.25 mmol), *trans*-2-pentenal (32 μL, 0.33 mmol), benzylamine (36μL, 0.33 mmol) and cyclohexylisocyanide (41 μL, 0.33 mmol) were reacted according to the general procedure 11 using MeOH as solvent of the second multicomponent step. Flash column chromatography purification (*n*-hexane/EtOAc 9:1) afforded diastereomeric mixtures of **146** (41 mg, 42%) and **148** (28 mg, 25%) as colorless oils. *dr.* 74:26.

Compound 148: *R*$_f$ = 0.47 (*n*-hexane/EtOAc 9:1).

¹H NMR (400 MHz, CDCl₃) δ = 9.73, 9.49 (2×d, J = 9.4 Hz, 1H); 7.27-7.18 (m, 5H, Ph); 3.91-3.79 (m, 2H); 3.66-3.61 (m, 1H); 3.55 (s, 3H, OCH₃); 2.80, 2.60 (2×m, 1H); 2.48-2.37 (m, 3H); 2.19 (t, J = 13.8 Hz, 1H); 1.92-1.87 (m, 2H); 1.81-1.74 (m, 1H); 1.69-1.60 (m, 3H); 1.56-1.45 (m, 4H); 1.26-1.05 (m, 6H); 1.05, 1.04 (2×s, 3H); 1.03, 1.02 (2×s, 3H); 0.89, 0.77 (t, J = 7.4 Hz, 3H).

¹³C NMR (100 MHz, CDCl₃) δ = 195.6 (C=O), 173.2 (C=O), 164.8 (C), 140.2 (C), 128.7 (2×CH), 128.5 (2×CH), 127.6 (CH), 110.6 (C), 59.9 (CH₃), 52.5 (CH₂), 51.9 (CH₂), 50.9 (CH), 48.8 (CH), 45.9(CH₂), 41.3 (C), 36.2 (CH), 35.6 (CH₂), 34.6 (CH₂), 33.8 (CH₂), 32.0 (CH₂), 29.8 (CH₃), 28.1 (CH₃), 25.6 (CH₂), 25.2 (CH₂), 13.0 (CH₂), 11.9 (CH₃).

HRMS (ESI-FT-QQTOF) m/z: 455.3279 [M+H]⁺; calcd. for C₂₈H₄₃N₂O₃: 455.3274.

Compound 149:
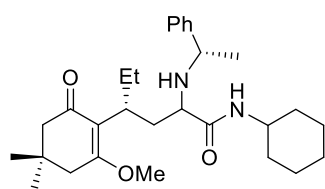
Dimedone **143** (35 mg, 0.25 mmol), *trans*-2-pentenal (32 μL, 0.33 mmol), (*S*)-α-methylbenzylamine (43μL, 0.33 mmol)and cyclohexylisocyanide (41 μL, 0.33 mmol) were reacted according to the general procedure 11 using MeOH as solvent of the second multicomponent step. Flash column chromatography purification (*n*-hexane/EtOAc 9:1) afforded **147** (46 mg, 42%) and **149** (33 mg, 28%) as colorless oils.

Compound 149: R_f = 0.47 (*n*-hexane/EtOAc 9:1).

¹H NMR (400 MHz, CDCl₃) δ = 9.69 (d, J = 9.8 Hz); 7.31-7.19 (m, 5H, Ph); 3.79 (q, J = 6.6 Hz, 1H); 3.78 (m, 1H); 3.57 (s, 3H, OCH₃); 3.46 (t, J = 6.7 Hz, 1H); 2.78 (br. m, 1H); 2.49-2.39 (m, 3H); 2.16 (d, J = 14.7 Hz, 1H); 2.00 (m, 1H); 1.83 (ddd, J = 13.0/7.2/3.0 Hz, 1H); 1.76-1.69 (m, 2H); 1.57-1.45 (m, 6H); 1.38 (d, J = 6.5 Hz, 1H); 1.34-1.31 (m, 1H); 1.27 (d, J = 6.5 Hz, 3H); 1.24-1.15 (m, 2H); 1.06 (s, 3H); 1.04 (s, 3H); 1.07-0.96 (m, 5H); 0.71 (t, J = 7.4 Hz, 3H).

¹³C NMR (100 MHz, CDCl₃) δ = 195.4 (C=O), 173.2 (C=O), 165.6 (C), 144.6 (C), 128.6 (2×CH), 127.5 (2×CH), 126.7 (CH), 109.7 (C), 58.1 (CH), 55.6 (CH₃), 51.9 (CH₂), 51.2 (CH₂), 48.9 (CH), 45.9 (CH), 41.0 (C), 36.3 (CH), 35.4 (CH₂), 34.4 (CH₂), 33.8 (CH₂), 29.8 (CH₂), 28.2 (CH₃), 28.1 (CH₃), 25.6 (CH₂), 25.4 (CH₂), 25.2 (CH₂), 25.1 (CH₃), 11.5 (CH₃).

HRMS (ESI-FT-QQTOF) m/z: 469.3436 [M+H]⁺; calcd. for C₂₉H₄₅N₂O₃: 469.3430.

Compound 150:
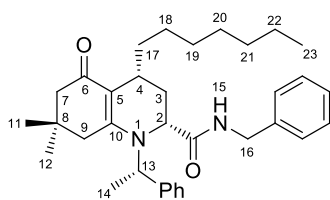
Dimedone **143** (35 mg, 0.25 mmol), *trans*-2-decenal (61μL, 0.33 mmol), (*S*)-α-methylbenzylamine (43μL, 0.33 mmol)and benzylisocyanide (32.5 μL, 0.33 mmol) were reacted according to the general procedure 11. Flash column chromatography purification (*n*-hexane/EtOAc 1:1) afforded compound **150** (79 mg, 71%, isomer *cis*) as a pale yellow oil.

R_f = 0.50 (*n*-hexane/EtOAc 2:1).

$[\alpha]_D^{20}$ = -3.34 (*c* 5.5, acetone, 20°C).

^{1}H NMR (400 MHz, CDCl₃) δ = 7.34-7.28 (m, 6H, Ph); 7.23 (m, 2H, Ph); 7.13 (m, 2H, Ph); 6.26 (t, *J* = 5.2 Hz, 1H, H-15); 5.16 (q, *J*= 6.9 Hz, 1H, H-13); 4.42 (dd, *J* = 14.1/5.4 Hz, 1H, H-16a); 4.26 (dd, *J* = 14.1/5.2 Hz, 1H, H-16b); 3.66(d, *J* = 4.4 Hz, 1H, H-2); 2.69 (d, *J* = 15.5 Hz, 1H, H-9a); 2.60 (m, 1H, H-4); 2.29(d, *J* = 12.0 Hz, 1H, H-3a); 2.26 (d, *J* = 15.8 Hz, 1H, H-9b); 2.23(s, 2H, H-7); 1.56 (d, *J* = 7.0 Hz, 3H, H-14); 1.50 (m, H, H-17a); 1.36 (m, 1H, H-18a); 1.30-1.16 (m, 9H, H-19, H-18b, H-20, H-21, H-22); 1.09 (s, 3H, H-11); 0.87 (m, 1H, H-3b); 0.85 (m, 3H, H-23); 0.83 (s, 3H, H-12); 0.82 (m, 1H, H-17b).

^{13}C NMR (100 MHz, CDCl₃) δ = 194.9 , 171.8 (C=O), 154.4, 139.3, 137.2 (C), 131.0, 129.0, 128.8, 128.3, 128.2, 128.0, 126.8 (CH), 115.3 (C), 56.2, 54.8 (CH), 50.0, 44.5, 42.9 (CH₂), 32.7 (C), 32.4, 32.0 (CH₂), 30.7 (CH₃), 29.7, 29.4 (CH₂), 28.5 (CH), 27.2 (CH₂), 26.0 (CH₃), 24.2, 22.7 (CH₂), 17.6, 14.2 (CH₃).

HRMS (ESI-FT-QQTOF) *m/z*: 515.36321 [M+H]⁺; calcd. for $C_{34}H_{47}N_2O_2$: 515.36279.

Compound 151:
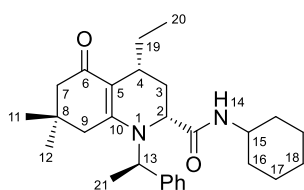
Dimedone **143** (35 mg, 0.25 mmol), *trans*-2-pentenal (32 μL, 0.33 mmol), (*R*)-α-methylbenzylamine (43μL, 0.33 mmol) and cyclohexylisocyanide (41 μL, 0.33 mmol) were reacted according to the general procedure 11. Flash column chromatography purification (*n*-hexane/EtOAc 1:1) afforded compound **151** (82 mg, 75%) as a pale yellow oil.

R_f = 0.36 (*n*-hexane/EtOAc 1:1).

$[\alpha]_D^{23}$ = -10.36 (*c* 4.0, acetone, 20°C).

^{1}H NMR (400 MHz, CDCl₃) δ = 7.28-7.21 (m, 5H, Ph); 5.78 (d, *J* = 8.1Hz, 1H, H-14); 5.19 (q, *J*= 6.9 Hz, 1H, H-13); 3.83 (dd, *J*= 5.8/1.4 Hz, 1H, H-2); 3.39-3.36 (m, 1H, H-15); 2.73-2.62 (m, 2H, H-9a); 2.59 (dd, *J* = 11.8/5.9 Hz, 1H, H-4); 2.53 (d, *J* = 15.5 Hz, 1H, H-9b); 2.28

(s, 2H, H-7); 1.44 (d, J = 7.0 Hz, 3H, H-21); 1.41-1.32 (m, 2H); 1.24 (dd, J = 11.5/6.7 Hz, 2H); 1.19 (s, 1H, H-11); 1.16 (d, J = 8.2 Hz, 2H); 1.12 (s, 3H, H-12); 0.88 (t, J = 7.0 Hz, 3H, H-20); 0.84-0.75 (m, 2H).

^{13}C NMR (100 MHz, CDCl$_3$) δ = 195.5, 170.0 (C=O), 154.3, 139.1 (C), 129.4, 129.2, 128.8, 128.4, 127.2 (CH), 118.1 (C), 57.3, 54.8 (CH), 50.4, 48.2, 44.1, 32.9 (CH$_2$), 32.8 (C), 31.4 (CH), 31.1(CH$_2$), 29.4, 26.6 (CH$_3$), 25.9, 25.7, 25.0, 24.7 (CH$_2$), 16.5, 12.3 (CH$_3$).

HRMS (ESI-FT-QQTOF) *m/z*: 437.31580 [M+H]$^+$; calcd. for C$_{28}$H$_{41}$N$_2$O$_2$: 437.31626.

Compound 152:
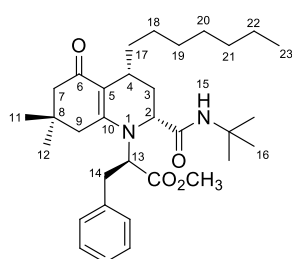
Dimedone **143** (35 mg, 0.25 mmol), *trans*-2-decenal (61 µL, 0.33 mmol), D-phenylalanine methyl ester hydrochloride (97mg, 0.33 mmol), Et$_3$N (46 µL, 0.33 mmol) and *t*-butylisocyanide (37 µL, 0.33 mmol) were reacted according to the general procedure 11. Flash column chromatography purification (*n*-hexane/EtOAc 1:1) afforded compound **152** (72 mg, 67%, isomer *cis*) as a pale yellow oil.

R_f = 0.55 (*n*-hexane/EtOAc 2:1).

[α]$_D^{20}$ = 25.3 (*c* 1.10, acetone, 20°C).

^{1}H NMR (400 MHz, CDCl$_3$) δ = 7.29-7.23 (m, 3H, Ph); 7.13 (m, 2H, Ph); 6.19 (s, 1H, H-15); 4.69 (t, *J*= 7.2 Hz, 1H, H-13); 4.01 (d, *J* = 4.3 Hz, 1H, H-2); 3.75(s, 3H, CH$_3$O); 3.26 (dd, *J* = 14.0/7.5 Hz, 1H, H-14a); 2.84 (dd, *J* = 14.0/6.9 Hz, 1H, H-14b); 2.66 (d, *J* = 14.6 Hz, 1H, H-3a); 2.60 (m, 1H, H-4); 2.27 (d, *J* = 15.3 Hz, 1H, H-9a); 2.18 (d, *J* = 16.8 MHz 1H, H-7a); 2.13 (d, *J* = 15.3 Hz, 1H, H-9b); 2.05(d, H, *J* = 16.7 Hz, H-7b); 1.47 (m, 1H, H-17a); 1.46 (m, 1H, H-18a); 1.40 (m, 1H, H-3b); 1.28 (s, 9H, H-16); 1.31-1.17 (m, 9H, H-18b, H-19, H-20, H-21, H-22); 1.05 (s, 6H, H-11, H-12); 0.98 (m, 1H, H-17b); 0.85 (t, *J* = 6.9 Hz, H-23).

^{13}C NMR (100 MHz, CDCl$_3$) δ = 195.3, 170.4, 169.6 (C=O), 153.4, 136.2 (C), 129.3, 129.2, 128.1, 127.4 (CH), 117.1(C), 62.8, 56.1 (CH), 52.9 (CH$_3$), 51.9 (C), 49.9, 42.6, 35.8, 32.6 (CH$_2$), 32.5 (C), 32.1 (CH$_2$), 30.8 (CH$_3$), 29.6, 29.5, 27.5 (CH$_2$), 26.2 (CH$_3$), 24.5 (CH$_2$), 22.8 (CH$_3$), 22.8 (CH$_2$), 14.3 (CH$_3$).

HRMS (ESI-FT-QQTOF) *m/z*: 539.38367 [M+H]$^+$; calcd. for C$_{33}$H$_{51}$N$_2$O$_4$: 539.38433.

Compound 153:
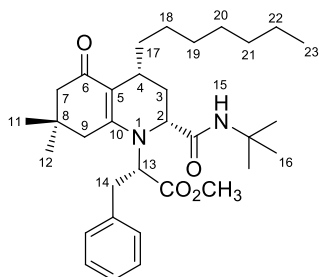
Dimedone **143** (35 mg, 0.25 mmol), *trans*-2-decenal (61 µL, 0.33 mmol), L-phenylalanine methyl ester hydrochloride (97 mg, 0.33 mmol), Et$_3$N (46 µL, 0.33 mmol) and *t*-butylisocyanide (37 µL, 0.33 mmol) were reacted according to the general procedure 11. Flash column chromatography purification (*n*-hexane/EtOAc 1:1) afforded compound **153** (74 mg, 69%, isomer *cis*) as a pale yellow oil.

R_f = 0.50 (*n*-hexane/EtOAc 2:1).

[α] $_D^{20}$ = -12.5 (*c* 1.10, acetone, 20°C).

^{1}H NMR (400 MHz, CDCl$_3$) δ = 7.33-7.24 (m, 3H, Ph); 7.15 (m, 2H, Ph); 6.17 (s, 1H, H-15); 4.68(t, *J* = 7.2 Hz, 1H, H-13); 4.05(d, *J* = 4.5 Hz, 1H, H-2); 3.73 (s, 3H, CH$_3$O); 3.24 (dd, *J* = 14.0/7.5 Hz, 1H, H-14a); 2.83 (dd, *J* = 14.0/7.0 Hz, 1H, H-14b); 2.68-2.55 (m, 2H); 2.29 (d, *J* = 14.4 Hz, 1H, H-9a); 2.22 (d, *J* = 7.5 MHz 1H); 2.18-2.24 (m, 1H); 2.08 (d, H, *J* = 16.6 Hz, H-7b); 1.46 (m, 1H, H-17a); 1.44 (m, 1H, H-18a); 1.36 (m, 1H, H-3b); 1.29 (s, 11H); 1.26-1.21 (m, 9H); 1.04 (s, 6H, H-11, H-12); 0.97 (m, 1H, H-17b); 0.85 (t, *J* = 7.0 Hz, H-23).

^{13}C NMR (100 MHz, CDCl$_3$) δ = 195.2, 170.3, 169.5 (C=O), 153.3, 136.2 (C), 130.9, 129.2, 128.7, 127.2 (CH), 62.7, 55.9 (CH), 52.7 (CH$_3$), 50.9 (C), 49.8, 42.5, 32.6, 32.5 (CH$_2$), 32.3 (C), 31.9 (CH$_2$), 30.7 (CH$_3$), 29.5, 29.4, 28.3 (CH$_2$), 27.3 (CH$_3$), 26.0 (CH$_2$), 24.4 (CH$_3$), 22.7 (CH$_2$), 14.1 (CH$_3$).

HRMS (ESI-FT-QQTOF) *m/z*: 539.38330 [M+H]$^+$; calcd. for C$_{33}$H$_{51}$N$_2$O$_4$: 580.38433.

Compound 154:
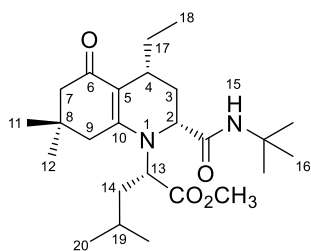
Dimedone **143** (35 mg, 0.25 mmol), *trans*-2-pentenal (32 µL, 0.33 mmol), L-leucine methyl ester hydrochloride (60 mg, 0.33 mmol), Et$_3$N (46 µL, 0.33 mmol) and *t*-butylisocyanide (37 µL, 0.33 mmol) were reacted according to the general procedure 11. Flash column chromatography purification (*n*-hexane/EtOAc 1:1) afforded compound **154** (74 mg, 68%) as a pale yellow oil.

R_f = 0.33 (*n*-hexane/EtOAc 1:1).

[α] $_D^{20}$ = -12.3 (*c* 1.10, acetone, 20°C).

^{1}H NMR (400 MHz, CDCl$_3$) δ = 4.23 (br s, 1H, H-13); 3.80 (br s, 1H, H-2); 3.74 (s, 3H); 2.62 (d, *J* = 13.8 Hz, 1H, H-3); 2.26 (d, *J* = 16.9 Hz, 1H, H-7); 2.20 (d, *J* = 16.8 Hz, 1H, H-7); 2.10

(d, *J* = 15.3 Hz, 1H, H-9); 1.90 (br s, 2H); 1.73-1.55 (m, 4H); 1.49-1.39 (m, 2H); 1.31 (s, 9H); 1.08 (d, *J* = 16.8 Hz, 3H); 0.99 (dd, J=6.3/2.9 Hz, 6H); 0.91 (t, J=7.1 Hz, 3H).

13C NMR (100 MHz, CDCl₃) δ = 195.1, 171.6, 170.2 (C=O), 153.9, 116.7 (C), 62.2, 52.6 (CH), 51.2 (CH₃), 50.1 (CH), 45.2 (C), 42.5 (CH₂), 32.6 (C), 30.2 (CH), 29.7, 28.5 (CH₂), 28.3 (CH₃), 26.7 (CH₂), 25.4 (CH₃), 25.1, 23.2 (CH₂), 22.9, 22.3, 11.7 (CH₃).

HRMS (ESI-FT-QQTOF) *m/z*: 435.32068 [M+H]⁺; calcd. for $C_{25}H_{43}N_2O_4$: 435.32173.

Compound 155:
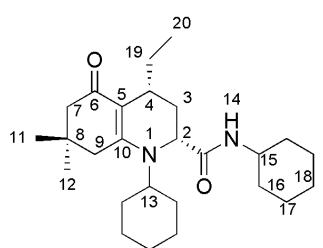
Dimedone **143** (35 mg, 0.25 mmol), trans-2-pentenal (32 μL, 0.33 mmol), cyclohexylamine (38μL, 0.33 mmol) and cyclohexylisocyanide (41 μL, 0.33 mmol) were reacted according to the general procedure 11. Flash column chromatography purification (n-hexane/EtOAc 1:1) afforded compound **155** (66 mg, 64%) as a pale yellow oil.

***R*f** = 0.26 (n-hexane/EtOAc 1:1).

[α] D²⁰ = -4.9 (*c* 0.6, methanol, 20°C).

1H NMR (400 MHz, CDCl₃) δ = 6.06 (d, *J* = 8.1Hz, 1H, H-14); 3.93 (d, *J*= 6.0/1.6 Hz, 1H, H-2); 3.71 (m, 1H, H-13); 3.66-3.62 (m, 1H, H-15); 2.67 (d, *J* = 13.7 Hz, 1H, H-9a); 2.59-2.52 (m, 1H); 2.48 (d, *J*= 8.4 Hz, 1H, H-3a); 2.43 (m, 1H); 2.17(m, 2H, H-7); 1.85 (m, 1H, H-3b); 1.78 (m, 6H); 1.64 (m, 4H); 1.55 (m, 4H); 1.35 (s, 2H, H-9); 1.39 (m, 4H); 1.12 (s, 3H, H-12); 1.08 (d, 4H); 1.06 (s, 3H, H-11); 0.89 (t, 3H, H-20).

13C NMR (100 MHz, CDCl₃) δ = 194.6, 170.9 (C=O), 154.3, 115.7, 58.6, (C), 55.9, 54.5, 50.4, 49.8 (CH₂), 47.9 (CH), 42.5, 30.0, 32.8 (CH₂), 32.4(C), 32.3, 32.2 (CH), 31.0, 30.9, 30.8, 30.4, 30.2 (CH₂), 29.2 (CH), 26.1, 25.9, 25.6, 25.4, 25.3, 25.1 (CH₂), 24.6 (CH₃), 24.5, 24.2 (CH₂), 11.8, 10.6 (CH₃).

HRMS (ESI-FT-QQTOF) *m/z*: 415.63175 [M+H]⁺; calcd. for $C_{26}H_{43}N_2O_2$: 415.63188.

Compound 156:
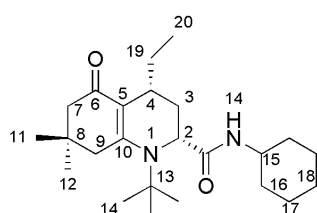
Dimedone **143** (35 mg, 0.25 mmol), trans-2-pentenal (32 μL, 0.33 mmol), *tert*-butilamine (35μL, 0.33 mmol) and cyclohexylisocyanide (41 μL, 0.33 mmol) were reacted according to the general procedure 11. Flash column chromatography purification (n-hexane/EtOAc 1:1) afforded compound **156** (57 mg, 59%) as a pale yellow oil.

$\boldsymbol{R_f}$ = 0.31 (n-hexane/EtOAc 1:1).

$[\alpha]_D^{20}$ = -1.85 (*c* 5.4, methanol, 20°C).

^{1}H NMR (400 MHz, CDCl$_3$) δ = 6.07 (d, *J* = 8.1Hz, 1H, H-14); 4.27 (dd, *J*= 5.8/2.4 Hz, 1H, H-2); 3.73-3.63 (m, 1H, H-15); 2.67 (d, *J* = 15.6 Hz, 1H, H-9a); 2.65 (dd, *J* = 13.9/2.3 Hz, 1H, H-3a); 2.56-2.52 (m, 1H, H-4); 2.49 (dd, *J* = 15.1/1.5 Hz, 1H, H-7a); 2.18 (d, *J* = 16.0 Hz, 1H, H-9b); 1.86 (m, 1H, H-3b); 1.79 (m, 2H, H-16); 1.66 (m, 2H); 1.60 (m, 2H); 1.45 (s, 9H, H-14); 1.32 (m, 4H); 1.14 (m, 1H); 1.08 (s, 3H, H-11); 1.05 (s, 3H, H-12); 1.06 (m, 1H); 0.88 (t, *J* = 16.0 Hz, 3H, H-20).

^{13}C NMR (100 MHz, CDCl$_3$) δ = 195.5, 171.3 (C=O), 155.8, 118.7, 60.9, (C), 57.2, 50.5, 48.3, 46.3 (CH$_2$), 33.1 (CH), 32.9 (C), 30.6, 29.8 (CH), 26.8, 25.4, 25.3, 24.9, (CH$_2$), 24.8, 24.7, 23.9, 11.7 (CH$_3$).

HRMS (ESI-FT-QQTOF) *m/z*: 389.58342 [M+H]$^+$; calcd. for C$_{24}$H$_{41}$N$_2$O$_2$: 389.58357.

Compound 157:
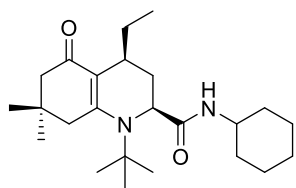
Dimedone **143** (35 mg, 0.25 mmol), trans-2-pentenal (32 μL, 0.33 mmol), *tert*-butilamine (35μL, 0.33 mmol) and cyclohexylisocyanide (41 μL, 0.33 mmol) were reacted according to the general procedure 11. Flash column chromatography purification (n-hexane/EtOAc 1:1) afforded compound **143** (63 mg, 65%) as a pale yellow oil.

$\boldsymbol{R_f}$ = 0.31 (n-hexane/EtOAc 1:1).

$[\alpha]_D^{20}$ = +2.5 (*c* 6.4, methanol, 20°C).

^{1}H NMR (400 MHz, CDCl$_3$) δ = 6.07 (d, *J* = 8.1Hz, 1H, H-14); 4.27 (dd, *J*= 5.8/2.4 Hz, 1H, H-2); 3.73-3.63 (m, 1H, H-15); 2.67 (d, *J* = 15.6 Hz, 1H, H-9a); 2.65 (dd, *J* = 13.9/2.3 Hz, 1H, H-3a); 2.56-2.52 (m, 1H, H-4); 2.49 (dd, *J* = 15.1/1.5 Hz, 1H, H-7a); 2.18 (d, *J* = 16.0 Hz, 1H, H-9b); 1.86 (m, 1H, H-3b); 1.79 (m, 2H, H-16); 1.66 (m, 2H); 1.60 (m, 2H); 1.45 (s, 9H, H-14); 1.32 (m, 4H); 1.14 (m, 1H); 1.08 (s, 3H, H-11); 1.05 (s, 3H, H-12); 1.06 (m, 1H); 0.88 (t, *J* = 16.0 Hz, 3H, H-20).

^{13}C NMR (100 MHz, CDCl$_3$) δ = 195.5, 171.3 (C=O), 155.8, 118.7, 60.9, (C), 57.2, 50.5, 48.3, 46.3 (CH$_2$), 33.1 (CH), 32.9 (C), 30.6, 29.8 (CH), 26.8, 25.4, 25.3, 24.9, (CH$_2$), 24.8, 24.7, 23.9, 11.7 (CH$_3$).

HRMS (ESI-FT-QQTOF) *m/z*: 389.58342 [M+H]$^+$; calcd. for C$_{24}$H$_{41}$N$_2$O$_2$: 389.58357.

5.3.7 Synthesis and spectroscopy data of pentasubstituted cylopentenes

General procedure 12: MW Ugi-Smiles type reaction
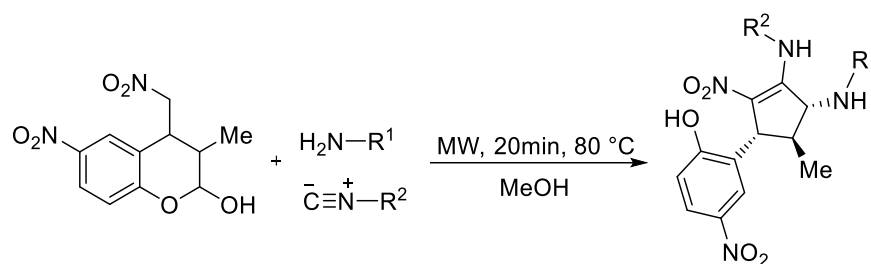
To a mixture of **158** (0.25 mmol, 1 equiv) and amine (0.25 mmol, 1 equiv) in MeOH (1 mL), isocyanide (0.25 mmol, 1 equiv) was added slowly. The resulting mixture was submitted to a microwave irradiation for 20 min at 80 °C. The volatiles were concentrated under reduced pressure. The crude was submitted to flash column chromatography on silica gel using *n*-hexane/EtOAc as eluent.

Compound 158:
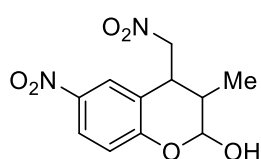
Trans-2-hydroxy-β-nitrostyrene (0.5 mmol), pyrrolidine (0.1 mmol), PhCO$_2$H (0.1 mmol) and aldehyde (1.5 mmol) were reacted in DCM (1 mL) according to the general procedure for Michael-hemiacetilation described in the literature. [107] Flash column chromatography purification (Hex/EtOAc 7:3) afforded 6-nitro-3-methyl-4-nitromethylchroman-2-ol **158** (47 mg, 93%) as a yellow oil. *d*r. (8:2).

R$_f$ = 0.35 (n-hexane/EtOAc 7:3)

^{1}H NMR (400 MHz, CDCl$_3$) δ= 8.11 (m, 2H), 7.00-6.94 (m, 1H), 5.53 (s, 1H), 5.14 (dd, *J* = 13.5, 9.0 Hz, 1H), 4.73 (dd, *J* = 13.5, 5.9 Hz, 1H), 3.52 (dd, *J* = 8.6, 6.3 Hz, 1H), 2.44 (m, 1H), 1.22-1.11 (m, 2H), 1.06 (d, *J* = 7.3 Hz, 3H), 0.98 (m, 3H).

^{13}C NMR (100 MHz, CDCl$_3$) δ= 156.06, 142.14, 126.44, 125.23, 118.69, 96.20, 79.78, 37.82, 32.20, 16.81.

Compound 160:
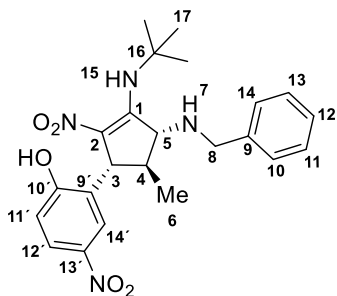
6-nitro-3-methyl-4-nitromethylchroman-2-ol **158** (67 mg, 0.25 mmol), benzylamine (27.3 μL, 0.25 mmol), and *tert*-Butylisocyanide (28 μL, 0.25 mmol) were reacted in MeOH (1 mL) according to the general procedure 12. Flash column chromatography purification (Hex/EtOAc 7:3) afforded **160** (47 mg, 40%) as a brown solid.

Mp = 89.9 °C.

R_f = 0.25 (n-hexane/EtOAc 7:3).

$[\alpha]_D^{23}$ = +139.9 (*c* 4.5, CHCl$_3$, 23°C).

^{1}H NMR (400 MHz, CDCl$_3$) δ= 9.50 (s, 1H, N*H*-15), 8.21 (d, *J* = 2.8 Hz, 1H, H-14´), 8.01 (dd, *J* = 8.9, 2.8 Hz, 1H, H-12´), 7.35 (m, 3H, H-12, H-11, H-13), 7.26 (m, 2H, H-14, H-10), 6.86 (d, *J* = 8.9 Hz, 1H, H-11´), 4.01, 3.65 (2xd, *J* = 12.7 Hz, 2H, H-8), 3.95 (d, *J* = 1.0 Hz, 1H, H-3), 3.84 (s, 1H, H-5), 2.44 (qd, J_q = 7.5 Hz, J_d = 2.5 Hz, H-4), 1.39 (s, 9H, 3xC*H*$_3$), 1.29 (d, *J* = 7.3 Hz, 3H, H-6).

^{13}C NMR (100 MHz, CDCl$_3$) δ= 161.41 (*C*-10´), 158.07 (*C*-1), 140.39 (*C*-13´), 136.17 (*C*-9), 129.21 (*C*-11), 129.06 (*C*H-13), 128.83 (*C*H-12), 128.63 (*C*H-14´), 127.15 (*C*-14´), 124.93 (*C*H-12´), 121.31 (*C*-2), 119.28 (*C*H-11´), 66.67 (*C*H-5), 55.26 (*C*-16), 52.47 (*C*H-3), 51.55 (*C*H$_2$-8), 39.14 (*C*H-4), 31.13 (3x*C*H$_3$), 21.55 (*C*H$_3$-6)ppm. DEPT 135° (100 MHz, CDCl$_3$) δ= 129.06 (*C*H-13), 128.83 (*C*H-12), 128.63 (*C*H-14´), 124.93 (*C*H-12´), 119.28 (*C*H-11´), 66.67 (*C*H-5), 52.47 (*C*H-3), 51.55 (*C*H$_2$-8), 39.14 (*C*H-4), 30.98 (3x*C*H$_3$), 21.40 (*C*H$_3$-6).

HRMS (ESI-FT-ICR) *m/z*: 439,1975 [M-H]$^+$; calcd. for C$_{23}$H$_{28}$N$_4$O$_5$: 440,2060.

Compound 161:
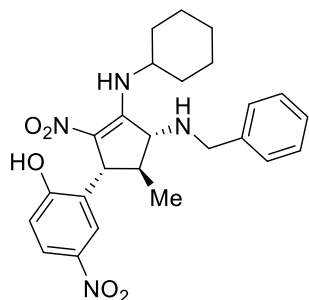
6-nitro-3-methyl-4-nitromethylchroman-2-ol **158** (67 mg, 0.25 mmol), benzylamine (27.3 μL, 0.25 mmol), and ciclohexylisocyanide (31 μL, 0.25 mmol) were reacted in MeOH (1 mL) according to the general procedure 12. Flash column chromatography purification (Hex/EtOAc 7:3) afforded **161** (43 mg, 37%) as a brown solid.

Mp = 89.9 °C.

R_f = 0.25 (n-hexane/EtOAc 7:3).

[α]$_D^{23}$ = +28.8 (*c* 6.6, CHCl$_3$, 23°C).

^{1}H NMR (400 MHz, CDCl$_3$) δ = 8.92 (d, *J* = 10.4 Hz, 1H, *N*H), 8.23 (d, *J* = 2.7 Hz, 1H), 8.04 (dd, *J* = 8.9, 2.8 Hz, 1H), 7.47-7.27 (m, 5H), 6.85 (d, *J* = 8.9 Hz, 1H), 4.10, 3.65 (2xd, *J* = 13.5 Hz, 1H), 3.98 (d, *J* = 1.3 Hz, 1H), 3.49 (s, 1H), 2.91 (m, 1H), 2.40 (qd, *J$_q$* = 7.5 Hz, *J$_d$* = 2.5 Hz, 1H), 1.77 (m, 6H), 1.26 (d, *J* = 7.3 Hz, 3H), 1.45-0.82 (m, 7H).

^{13}C NMR (100 MHz, CDCl$_3$) δ = 161.16, 157.72, 140.62, 137.08, 129.40, 129.03, 128.60, 128.12, 127.76, 124.87, 118.90, 63.86, 54.19, 52.40, 50.47, 39.80, 35.62, 33.50, 24.83, 24.64, 24.53, 21.89.

Compound 162:
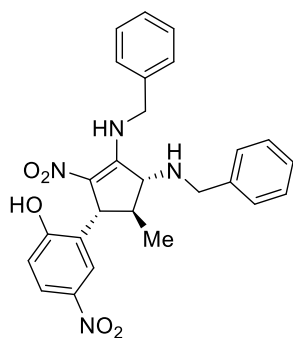
6-nitro-3-methyl-4-nitromethylchroman-2-ol **158** (67 mg, 0.25 mmol), benzylamine (27.3 μL, 0.25 mmol), and benzylisocyanide (30 μL, 0.25 mmol) were reacted in MeOH (1 mL) according to the general procedure 12. Flash column chromatography purification (Hex/EtOAc 7:3) afforded **162** (65 mg, 55%) as orange solid.

Mp = 88 °C.

R_f = 0.23 (n-hexane/EtOAc 7:3).

[α]$_D^{23}$ = -4.2 (*c* 3.5, CHCl$_3$, 23°C).

^{1}H NMR (400 MHz, CDCl$_3$) δ = 9.34 (t, *J* = 7.1 Hz, 1H, *N*H), 8.20 (d, *J* = 2.9 Hz, 1H), 7.98 (dd, *J* = 8.9, 2.8 Hz, 1H), 7.40-7.25 (m, 6H), 7.19 (d, *J* = 7.6 Hz, 2H), 6.96 (dd, *J* = 7.6, 1.5 Hz, 2H), 6.76 (d, *J* = 8.9 Hz, 1H), 4.27 (dd, *J* = 15.9, 6.2 Hz, 1H), 4.15 (dd, *J* = 15.7, 7.1 Hz, 2H), 4.05 (d, *J* = 13.6 Hz, 1H), 3.95 (d, *J* = 1.3 Hz, 1H), 3.56 (d, *J* = 13.6 Hz, 1H), 3.47 (s, 1H), 2.34 (qd, *J$_q$* = 7.5 Hz, *J$_d$* = 2.5 Hz, 1H), 1.15 (d, *J* = 7.3 Hz, 3H), 1.06 (t, *J* = 7.8 Hz, 1H).

^{13}C NMR (100 MHz, CDCl$_3$) δ= 161.21, 158.28, 140.65, 136.64, 136.48, 129.33, 129.30, 128.95, 128.55, 128.43, 128.33, 127.86, 126.42, 124.92, 119.83, 119.36, 64.00, 53.14, 50.41, 47.97, 39.95, 21.56.

HRMS (ESI-FT-ICR) *m/z*: 473,1817 [M-H]⁺; calcd. for $C_{26}H_{26}N_4O_5$: 474,1903.

Compound 163:
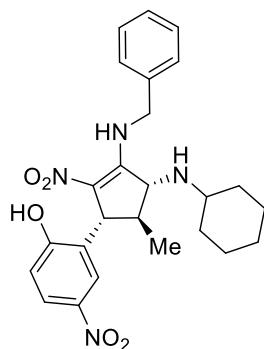
6-nitro-3-methyl-4-nitromethylchroman-2-ol **158** (67 mg, 0.25 mmol), cyclohexylamine (29 μL, 0.25 mmol), and benzylisocyanide (30 μL, 0.25 mmol) were reacted in MeOH (1 mL) according to the general procedure 12. Flash column chromatography purification (Hex/EtOAc 7:3) afforded **163** (58 mg, 50%) as light yellow solid.

Mp = 96 °C.

R_f = 0.30 (n-hexane/EtOAc 7:3).

$[\alpha]_D^{23}$ = -22.3 (*c* 4.4, CHCl₃, 23°C).

¹H NMR (400 MHz, CDCl₃) δ= 9.40 (t, *J* = 6.6 Hz, 1H, *N*H), 8.20 (d, *J* = 2.8 Hz, 1H), 7.96 (dd, *J* = 8.9, 2.8 Hz, 1H), 7.44-7.36 (m, 3H), 7.25-7.21 (m, 2H), 6.72 (d, *J* = 8.9 Hz, 1H), 4.55 (dd, *J* = 16.0, 7.5 Hz, 1H), 4.48 (dd, *J* = 15.8, 6.0 Hz, 1H), 4.17-4.09 (m, 1H), 3.92 (d, *J* = 0.9 Hz, 1H), 3.74 (s, 1H), 2.50 (m, 1H), 2.21 (m, 1H), 1.79-1.56 (m, 5H), 1.27-0.91 (m, 6H), 1.18 (d, *J* = 7.3 Hz, 3H).

¹³C NMR (100 MHz, CDCl₃) δ= 161.78(*C*), 158.26(*C*), 140.23(*C*), 136.63(*C*), 129.52(*C*H), 129.46(*C*H), 128.79(*C*H), 128.61(*C*H), 128.50(*C*H), 127.63(*C*), 126.42(*C*H), 124.92(*C*H), 119.77(*C*H), 62.92(*C*H), 54.12(*C*H), 53.69(*C*H), 48.10(*C*H₂), 40.61(*C*H), 38.16(*C*H), 33.66(*C*H₂), 31.71(*C*H₂), 25.60(*C*H₂), 25.01(*C*H₂), 24.84(*C*H₂), 21.74(*C*H₃)ppm. DEPT 135º (100 MHz, CDCl₃) δ= 129.39(*C*H), 129.33(*C*H), 128.66(*C*H), 128.48(*C*H), 128.37(*C*H), 126.29(*C*H), 124.79(*C*H), 119.64(*C*H), 62.79(*C*H), 53.98(*C*H), 53.56(*C*H), 47.97 (*C*H₂), 40.47(*C*H), 38.03(*C*H), 33.53(*C*H₂), 31.58(*C*H₂), 25.47(*C*H₂), 25.23(*C*H₂), 24.88(*C*H₂), 24.71(*C*H₂), 21.61 (*C*H₃).

Compound 164:
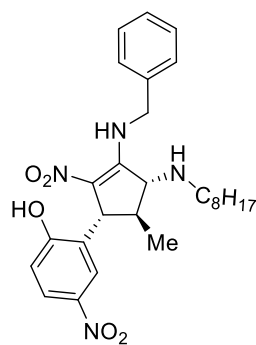
6-nitro-3-methyl-4-nitromethylchroman-2-ol **158** (67 mg, 0.25 mmol), octylamine (42 μL, 0.25 mmol), and benzylisocyanide (30 μL, 0.25 mmol) were reacted in MeOH (1 mL) according to the general procedure 12. Flash column chromatography purification (Hex/EtOAc 7:3) afforded **164** (43 mg, 35%) as light orange solid.

Mp = 96°C.

R_f = 0.40 (n-hexane/EtOAc 7:3).

¹H NMR (400 MHz, CDCl₃) δ = 7.97 (dd, J = 9.2, 2.7 Hz, 1H), 7.77 (d, J = 2.6 Hz, 1H), 7.41-7.22 (m, 3H), 6.66 (d, J = 9.4 Hz, 1H), 6.49 (t, J = 5.7 Hz, 1H), 4.64-4.53 (m, 1H), 4.54-4.42 (m, 1H), 3.98 (d, J = 5.8 Hz, 1H), 3.71 (dd, J = 11.6, 6.5 Hz, 1H), 3.64-3.54 (m, 1H), 3.10-2.99 (m, 1H), 2.58 (dd, J = 11.9, 5.7 Hz, 1H), 1.56 (m, 2H), 1.21 (m, 12H), 1.21 (d, J = 7.2 Hz, 3H), 0.90-0.86 (m, 3H).

¹³C NMR (101 MHz, CDCl₃) δ = 169.40, 158.26, 137.91, 128.95, 128.17, 128.02, 125.45, 124.47, 121.48, 111.59, 65.67, 51.42, 43.94, 39.73, 32.65, 31.71, 29.24, 29.16, 26.87, 25.83, 22.60, 14.07, 13.42.

Compound 165:
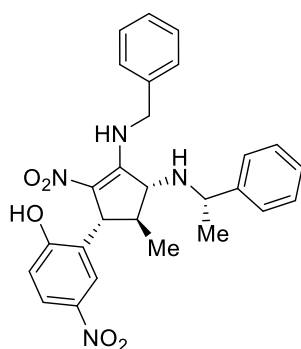
6-nitro-3-methyl-4-nitromethylchroman-2-ol **158** (67 mg, 0.25 mmol), (S)-α-Methylbenzylamine (32 µL, 0.25 mmol), and benzylisocyanide (30 µL, 0.25 mmol) were reacted in MeOH (1 mL) according to the general procedure 12. Flash column chromatography purification (n-hexane/EtOAc 7:3) afforded **165** (67 mg, 55%) as light orange solid. A mixture of diastereosiomers were detected *dr.* 1:1.

Mp = 96.5 °C.

R_f = 0.21 (n-hexane/EtOAc 7:3).

¹H NMR (400 MHz, CDCl₃) δ = 9.53 (t, J = 6.7 Hz, 0.5H), 9.28 (t, J = 7.0 Hz, 0.5H), 8.23 (d, J = 2.8 Hz, 0.5H), 8.17 (d, J = 2.7 Hz, 0.5H), 8.01 (dd, J = 8.9, 2.8 Hz, 0.5H), 7.91 (dd, J = 8.9, 2.8 Hz, 0.5H), 7.47-7.11 (m, 10H), 6.95-6.88 (m, 1H), 6.80 (d, J = 8.9 Hz, 0.5H), 6.68 (d, J = 8.9 Hz, 0.5H), 4.51 (dd, J = 14.3, 8.0 Hz, 2H), 4.20 (dd, J = 16.0, 6.6 Hz, 0.5H), 4.04 (dd, J = 16.0, 7.3 Hz, 0.5H), 3.93 (s, 0.5H), 3.84 (s, 0.5H), 3.83-3.74 (m, 1H), 3.60 (s, 0.5H), 3.23 (s, 0.5H), 2.85-2.73 (m, 0.5H), 2.37 (qd, J_q = 7.5 Hz, J_d = 2.5 Hz, 0.5H), 1.76 (qd, J_q = 7.5 Hz, J_d = 2.5 Hz, 0.5H), 1.54 (d, J = 6.5 Hz, 0.5H), 1.43 (d, J = 6.7 Hz, 2H), 1.38 (d, J = 6.6 Hz, 1H), 1.11 (d, J = 7.4 Hz, 0.5H), 1.05 (d, J = 7.3 Hz, 2H), 0.90 (d, J = 7.3 Hz, 1H).

¹³C NMR (100 MHz, CDCl₃) δ = 161.39, 160.88, 159.73, 158.44, 142.71, 141.57, 136.64, 136.50, 129.49, 129.41, 129.29, 129.08, 128.93, 128.74, 128.49, 128.39, 128.28, 127.76, 127.46, 127.05, 126.95, 126.53, 126.31, 124.93, 124.64, 119.89, 119.49, 118.98, 66.00, 63.16, 58.52, 56.96, 55.39, 53.23, 52.15, 48.36, 47.89, 41.53, 39.67, 22.44, 22.35, 21.46, 21.30.

Compound 166:
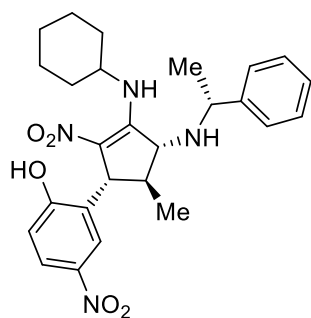
6-nitro-3-methyl-4-nitromethylchroman-2-ol **158** (67 mg, 0.25 mmol), (S)-α-Methylbenzylamine (32 μL, 0.25 mmol), and cyclohexylisocyanide (31 μL, 0.25 mmol) were reacted in MeOH (1 mL) according to the general procedure 12. Flash column chromatography purification (n-hexane/EtOAc 7:3) afforded **166** (60 mg, 50%) as brown solid. *dr.* 3:2

Mp = 105 °C.

*R*f = 0.40 (n-hexane/EtOAc 7:3).

¹H NMR (400 MHz, CDCl₃) δ= 8.94 (d, *J* = 10.3 Hz, 1H, *N*H), 8.24 (d, *J* = 2.8 Hz, 1H), 8.01 (dd, *J* = 8.9, 2.8 Hz, 1H), 7.50-7.10 (m, 5H), 6.86 (d, *J* = 9.0 Hz, 1H), 3.95 (d, *J* = 1.1 Hz, 1H), 3.85-3.78 (m, 1H), 3.22 (s, 1H), 2.45-2.36 (m, 1H), 1.91 (m, 1H), 1.49 (d, *J* = 6.7 Hz, 3H), 1.73-1.09 (m, 12H), 1.17 (d, *J* = 7.3 Hz, 3H).

¹³C NMR (100 MHz, CDCl₃) δ= 161.30, 158.11, 141.98, 140.52, 129.43, 128.95, 127.95, 127.07, 126.67, 125.75, 124.83, 118.93, 63.50, 55.53, 52.33, 50.02, 42.21, 39.69, 35.64, 33.44, 25.26, 24.79, 24.43, 23.88, 22.68, 21.80.

References

References

[1] HARV, T. ``Secrets of the Millionaire Mind´´ 2ª Edição – SEXTANTE, 2005.

[2] IUPAC, Compendium of Chemical Terminology (Gold book), Version 2.3.3. 2014.

[3] HAJOS, Z. G.; PARRISH, D. R. ``Stereocontrolled synthesis of trans-hydrindan steroidal intermediates´´. *J. Org. Chem.* **38**: 3239, 1973.

[4] HAJOS, Z. G.; PARRISH, D. R. ``Asymmetric synthesis of bicyclic intermediates of natural product chemistry´´. *J. Org. Chem.,* **39**: 1615, 1974.

[5] EDER, U.; SAUER, G.; WIECHERT, R. ``New Type of Asymmetric Cyclization to Optically Active Steroid CD Partial Structures´´. Angew. Chem. Int. Ed. Engl., **10**: 496, 1971.

[6] Ahrendt, K. A.; Borths, C. J.; MacMillan, D. W. C., ``New Strategies for Organic Catalysis: The First Highly Enantioselective Organocatalytic Diels-Alder Reaction´´. *J. Am. Chem. Soc.,* **122**: 4243, 2000.

[7] *BUI, T.; BARBAS III, C. F. ``A proline-catalyzed asymmetric Robinson annulation reaction´´.* Tetrahedron Lett., **41**: 6951, 2000.

[8] LIST, B.; LERNER, R. A.; BARBAS III, C. F. ``Proline-Catalyzed Direct Asymmetric Aldol Reactions´´. *J. Am. Chem. Soc.,* **122**: 2395, 2000.

[9] MACMILLAN, D. W. C. ``The advent and development of organocatalysis´´. *Nature.,* **18**: 304, 2008.

[10] BETANCORT, J. M.; BARBAS III, C. F. ``Catalytic Direct Asymmetric Michael Reactions: Taming Naked Aldehyde Donors´´. *Org. Lett.* 3(23): 3737, 2001.

[11] BETANCORT, J. M.; SAKTHIVEL, K.; THAYUMANAVAN, R.; BARBAS III, C. F. ``Catalytic enantioselective direct Michael additions of ketones to alkylidene malonates´´. *Tetrahedron Lett.,* **42**: 4441, 2001.

[12] NAKADAI, M.; SAITO, S.; YAMAMOTO, H.; ``Diversity-based strategy for discovery of environmentally benign organocatalyst: diamine–protonic acid catalysts for asymmetric direct aldol reaction´´. *Tetrahedron.,* 58(41): 8167, 2002.

[13] ALEXAKIS, A.; ANDREY, O. ``Diamine-Catalyzed Asymmetric Michael Additions of Aldehydes and Ketones to Nitrostyrene´´. Org. Lett., 4(21): 3611, 2002.

[14] HALLAND, N.; ABUREL, P. S.; Jørgensen, K. A. ``Highly Enantioselective Organocatalytic Conjugate Addition of Malonates toAcyclic α,β-Unsaturated Enones´´. *Angew. Chem. Int.* Ed., **42**: 661, 2003.

[15] MELCHIORRE, P.; JØRGENSEN, K. A. ``Direct Enantioselective Michael Addition of Aldehydes to Vinyl Ketones Catalyzed by Chiral Amines´´. *J. Org. Chem.,* **68**: 4151, 2003.

[16] WENNEMERS, H. ``Peptides as Asymmetric Catalysis for Aldol Reactions´´. *Chimia.,* **61**: 276, 2007.

[17] COBB, A. J. A.; SHAW, D. M.; LEY, S. V. ``5-Pyrrolidin-2-yltetrazole: A New Catalytic More Soluble Alternative to Proline in an Organocatalytic Asymmetric Mannich-type Reaction´´. *Synlett.,* **3**: 558, 2004.

[18] HAYASHI, Y.; GOTOH, H.; HAYASHI, T.; SHOJI, M. ``Diphenylprolinol Silyl Ethers as Efficient Organocatalysts for the Asymmetric Michael Reaction of Aldehydes and Nitroalkenes´´. *Angew. Chem. Int. Ed.,* **44**: 4412, 2005.

[19] VISHNUMAYA, R. M.; GINOTRA, S. K.; SINGH, V. K. ``Highly Enantioselective Direct Aldol Reaction Catalyzed by Organic Molecules´´. *Org. Lett.,* **8**(18): 4097, 2006.

[20] ZNABET, A.; RUIJTER, E.; DE KANTER, F.J. J.; KOHLER, V.; HELLIWELL, M.; TURNER, N. J.; ORRU, R. V. A. ``Highly Stereoselective Synthesis of Substituted Prolyl Peptides Using a Combination of Biocatalytic Desymmetrization and Multicomponent Reactions´´. *Angew. Chem. Int. Ed.,* **49**: 5289, 2010.

[21] DEOBALD, A. M.; CORRÊA, A. G.; RIVERA, D. G.; PAIXÃO, M. W. ``Organocatalytic asymmetric epoxidation and tandem epoxidation/Passerini reaction under eco-friendly reaction conditions´´. *Org. Biomol. Chem.,* **10**: 7681, 2012.

[22] MUKHERJEE, S.; YANG, J. W.; HOFFMANN, S.; LIST, B. ``Asymmetric Enamine Catalysis´´. *Chem. Rev.,* **107**: 5471, 2007.

[23] CLEMENTE, F. R.; HOUK, K. N. `` Computational Evidence for the Enamine Mechanism of Intramolecular Aldol Reactions Catalyzed by Proline´´. *Angew. Chem. Int. Ed.,* **43**: 5766, 2004.

[24] LIST, B. ``Direct Catalytic Asymmetric α-Amination of Aldehydes´´. *J. Am. Chem. Soc.*, **124** (20): 5656, 2002.

[25] MASE, N.; NAKAI, Y.; OHARA, N.; YODA, H.; TAKABE, K.; TANAKA, F.; BARBAS III, C. F. ``Organocatalytic Direct Asymmetric Aldol Reactions in Water´´. *J. AM. CHEM. SOC.* **128**: 734, 2006.

[26] MARIGO, M.; WABNITZ, T. C.; FIELENBACH, D.; JØRGENSEN, K. A. ``Enantioselective Organocatalyzed a Sulfenylation of Aldehydes´´. Angew. Chem. Int. Ed., **44**: 794, 2005.

[27] BAHMANYAR, S.; HOUK, K. N. ``Transition States of Amine-Catalyzed Aldol Reactions Involving Enamine Intermediates: Theoretical Studies of Mechanism, Reactivity, and Stereoselectivity´´. *J. Am. Chem. Soc.*, **123**(45): 11273, 2001.

[28] BAHMANYAR, S.; HOUK, K. N.; MARTIN, H. J.; LIST, B. ``Quantum Mechanical Predictions of the Stereoselectivities of Proline-Catalyzed Asymmetric Intermolecular Aldol Reactions´´. *J. Am. Chem. Soc.*, **125**(9): 2475, 2003.

[29] WIESNER, M.; REVELL, J. D.; WENNEMERS, H. ``Tripeptides as Efficient Asymmetric Catalysts for 1,4-Addition Reactions of Aldehydes to Nitroolefins–A Rational Approach´´. *Angew. Chem. Int. Ed*., **47**: 1871, 2008.

[30] BUR, J.; ARMSTRONG, A.; BLACKMOND, D. G. `` Mechanistic Rationalization of Organocatalyzed Conjugate Addition of Linear Aldehydes to Nitro-olefins ´´. J. Am. Chem. Soc., **133**: 8822, 2011.

[31] COLBY, E. A.; MENNEN, S. M.; XU, Y.; MILLER, S. J. ``Asymmetric Catalysis Mediated by Synthetic Peptides´´. *Chem. Rev.,* **107**: 5759, 2007.

[32] VENKATRAMAN, J.; SHANKARAMMA, S.C.; BALARAM, P. ``Design of Folded Peptides´´. Chem. Rev., **101**: 3131, 2001.

[33] KOFOED, J.; NIELSEN, J.; REYMOND, J. L. ``Discovery of new peptide-based catalysts for the direct asymmetric aldol reaction´´. Bioorg. Med. Chem. Lett., **13**: 2445, 2003.

[34] Sewald, N.; Jakubke, H-D. ``Peptides: Chemistry and Biology´´. Copyright © 2002 Wiley-VCH Verlag GmbH & Co. KGaA ISBNs: 3-527-30405-3 (Hardback); 3-527-60068-X (Electronic), pp 36.

[35] TANG, Z.; YANG, Z.H.; CUN, L.F.; GONG, L.Z.; MI, A.Q.; JIANG, Y.Z. `` Small Peptides Catalyze Highly Enantioselective Direct Aldol Reactions of Aldehydes with Hydroxyacetone: Unprecedented Regiocontrol in Aqueous Media´´ *Org Lett.* **6**: 2285, 2004.

[36] COLONNA, S.; MOLINARI, H.; BANFI, S.; JULIÁ, S.; MASANA, J.; ALVAREZ, A. `` Synthetic enzymes: Highly enantioselective epoxidation by means of polyaminoacids in a triphase system: influence of structural variations within the catalysts´´. Tetrahedron., **39**: 1635,1983.

[37] NAGANO, M.; DOI, M.; KURIHARA, M.; SUEMUNE, H.; TANAKA, M. ``Stabilized α-Helix-Catalyzed Enantioselective Epoxidation of αβ-Unsaturated Ketones´´. *Org. Lett*., **12**(15): 3564, 2010.

[38] MILLER, S. J. ``In Search of Peptide-Based Catalysts for Asymmetric Organic Synthesis´´. Acc. Chem. Res., **37**: 601, 2004.

[39] LINTON, B. R.; REUTERSHAN, M. H.; ADERMAN, C. M.; RICHARDSON, E. A.; BROWNELL, K. R.; ASHLEY, C. W.; EVANS, C. A.; MILLER, S. J. ``Asymmetric Michael addition of a-nitro-ketones using catalytic peptides´´. *Tetrahedron Letters*., **48**: 1993, 2007.

[40] KRATTIGER, P.; KOVASY, R.; REVELL, J. D.; IVAN, S.; WENNEMERS, H. ``Increased Structural Complexity Leads to Higher Activity: Peptides as Efficient and Versatile Catalysts for Asymmetric Aldol Reactions´´. *Org. Lett.* **7** (6): 1101, 2005.

[41] Zhu, J.; Bienyamé. H. ``*Multicomponent Reactions´´. 2da* Eds, Wiley-VCH, Weinheim, 2005.

[42] UGI, I.; FETZER, U.; EHOLZER, U.; KNUPFER, H.; OFFERMANN, K. `` Isonitrile Synthesis´´. Angew. Chem. Int. Ed., **4**: 472, 1965.

[43] GU, Y. ``Multicomponent reactions in unconventional solvents: state of the art´´. *Green Chem.*, **14**: 2091, 2012.

[44] BANFI, L.; RIVA, R.; ``The Passerini Reaction´´. Org. React., **65**: 1, 2005.

[45] DÖMLING, A.; UGI, I. ``Multicomponent Reactions with Isocyanides´´. *Angew. Chem. Int. Ed.,* **39**: 3168, 2000.

[46] DÖMLING, A. ``Recent Developments in Isocyanide Based Multicomponent Reactions in Applied Chemistry´´. Chem. Rev., **106**: 17, 2006.

[47] DÖMLING, A.; WANG, W.; WANG, K. ``Chemistry and Biology of Multicomponent Reactions´´. *Chem. Rev.,* **112** (6): 3083, 2012.

[48] XIA, Q.; GANEM, B. ``Metal-Promoted Variants of the Passerini Reaction Leading to Functionalized Heterocycles´´. Org. Lett., **4**: 1631, 2002.

[49] BON, R. S.; HONG, C. G.; BOUMA, M. J.; SCHMITZ, R. F.; DE KANTER, F. J. J.; LUTZ, M.; SPEK, A. L.; ORRU, R. V. A. ``Novel Multicomponent Reaction for the Combinatorial Synthesis of 2-Imidazolines´´. *Org. Lett.*, **5**: 3759, 2003.

[50] HENKEL, B.; BECK, B.; WESTNER, B.; MEJAT, B.; DÖMLING, A. ``Convergent multicomponent assembly of 2-acyloxymethyl thiazoles´´. Tetrahedron Letters., **44**(50): 8947, 2003.

[51] Ugi, I.; Werner, B.; Dömling, A. ``The Chemistry of Isocyanides, their MultiComponent Reactions and their Libraries´´. Molecules., **8**: 53, 2003.

[52] UGI, I. ``The Ugi reaction´´. Angew. Chem., **74**: 9, 1962

[53] DÖMLING, A.; UGI, I. ``Multicomponents reactions with isocyanides´´. *Angew. Chem. Int. Ed.,* **39**: 3168, 2000.

[54] RON, N. C.; RAMOZZI, R.; KAÏM, L. E.; GRIMAUD, L.; FLEURAT-LESSARD, P. ``Challenging 50 Years of Established Views on Ugi Reaction:A Theoretical Approach´´. *J. Org. Chem.,* **77**: 1361, 2012.

[55] SHMATOVAA, O. I.; NENAJDENKO, V. G. ``Synthesis of Tetrazole-Derived Organocatalysts via Azido-Ugi Reaction with Cyclic Ketimines´´. *J. Org. Chem.*, **78** (18): 9214, 2013.

[56] KREYE, O.; TÓTH, T.; MEIER, M. A. R. ``Introducing Multicomponent Reactions to Polymer Science: Passerini Reactions of Renewable Monomers´´. *J. Am. Chem. Soc.*, **133**: 1790, 2011.

[57] KREYE, O.; TÜRÜNÇ, O.; SEHLINGER, A.; RACKWITZ, J.; MEIER, M. A. R. ``Structurally Diverse Polyamides Obtained from Monomers Derived via the Ugi Multicomponent Reaction´´. Chemistry - A European Journal., **18**: 5767, 2012.

[58] LIN, W.; SUN, T.; ZHENG, M.; XIE, Z.; HUANG, Y.; JING, X. ``Synthesis of cross-linked polymers via multicomponent Passerini reaction and their application as efficient photocatalysts´´. RSC Adv., **4**: 25114, 2014.

[59] KONDO, K.; YAMANO, T.; TAKEMOTO, K. ``Functional monomers and polymers, 129. Asymmetric Robinson cyclization reaction catalyzed by polymer-bound L-proline´´. *Makromol. Chem.*, **186**: 1781, 1985.

[60] VARELA, M. C.; DIXON, S. M.; LAM, K. S.; SCHORE, N. E. ``Asymmetric epoxidation, Michael addition, and triple cascade reaction using polymer-supported prolinol-based auxiliaries´´. *Tetrahedron.*, **64**: 10087, 2008.

[61] KRISTENSEN, T. E.; VESTLI, K.; JAKOBSEN, M. G.; HANSEN, F. K.; HANSEN, T. ``A General Approach for Preparation of Polymer-Supported Chiral Organocatalysts via Acrylic Copolymerization´´. *J. Org. Chem.,* **75**: 1620, 2010.

[62] MAGER, K.; ZEITLER, A. ``Efficient, Enantioselective Iminium Catalysis with an Immobilized, Recyclable Diarylprolinol Silyl Ether Catalyst´´. *Org. Lett.,* **12**: 1480, 2010.

[63] FONT, D.; JIMENO, C.; PERICÀS, M. A.; `` Polystyrene-Supported Hydroxyproline: An Insoluble, Recyclable Organocatalyst for the Asymmetric Aldol Reaction in Water´´. *Org. Lett.,* **8**: 4653, 2006.

[64] GRUTTADAURIA, M.; GIACALONE, F.; MARCULESCU, A. M.; NOTO, R. ``Novel Prolinamide-Supported Polystyrene as Highly Stereoselective and Recyclable Organocatalyst for the Aldol Reaction´´. *Adv. Synth. Catal.,* **350**: 1397, 2008.

[65] LEE, J-W.; MAYER-GALL, T.; OPWIS, K.; SONG, C. E.; GUTMANN, J. S.; LIST, B. ``Organotextile Catalysis´´. *Science.,* **341**: 1225, 2013.

[66] UGI, I.; MEYR, R.; FETZER, U.; Steinbrücker, C. *Angew. Chem.*, **71**: 386, 1959.

[67] DINSMORE, C. J.; BESHORE, D.C. ``Recent advances in the synthesis of diketopiperazines´´. Tetrahedron., **58**: 3297, 2002.

[68] OKU, J. I.; ITO, N.; INOUE, S. ``Asymmetric cyanohydrin synthesis catalyzed by synthetic dipeptides, 1´´. Makromol. Chem., **180**: 1089, 1979.

[69] WIESNER, M.; REVELL, J. D.; WENNEMERS, H. ``Tripeptides as Efficient Asymmetric Catalysts for 1,4-Addition Reactions of Aldehydes to Nitroolefins–A Rational Approach´´. *Angew. Chem. Int. Ed.,* **47**: 1871, 2008.

[70] WIESNER, M.; REVELL, J. D.; TONAZZI, S.; WENNEMERS, H. ``Peptide Catalyzed Asymmetric Conjugate Addition Reactions of Aldehydes to Nitroethylene—A Convenient Entry into γ_2-Amino Acids´´. *J. Am. Chem. Soc.,* **130**: 5610, 2008.

[71] WIESNER, M.; NEUBURGER, M.; WENNEMERS, H. ``Tripeptides of the Type H-D-Pro-Pro-Xaa-NH$_2$ as Catalysts for Asymmetric 1,4-Addition Reactions: Structural Requirements for High Catalytic Efficiency´´. *Chem. Eur. J.,* **15**: 10103, 2009.

[72] WIESNER, M.; UPERT, G.; ANGELICI, G.; WENNEMERS, H. ``Enamine Catalysis with Low Catalyst Loadings - High Efficiency via Kinetic Studies´´. *J. Am. Chem. Soc.,* **132**: 6, 2010.

[73] DUSCHMALÉ, J.; WENNEMERS, H. ``Adapting to Substrate Challenges: Peptides as Catalysts for Conjugate Addition Reactions of Aldehydes to α,β-Disubstituted Nitroolefins´´. *Chem. Eur. J.,* **18**: 1111, 2012.

[74] DUSCHMALÉ, J.; WIEST, J.; WIESNER, M.; WENNEMERS, H. ``Effects of internal and external carboxylic acids on the reaction pathway of organocatalytic 1,4-addition reactions between aldehydes and nitroolefins´´. *Chem. Sci.,* **4**: 1312, 2013.

[75] LAURSEN, J. S.; ENGEL-ANDREASEN, J.; FRISTRUP, P.; HARRIS, P.; OLSEN. C. A. ``*Cis–Trans* Amide Bond Rotamers in β-Peptoids and Peptoids: Evaluation of Stereoelectronic Effects in Backbone and Side Chains´´. *J. Am. Chem. Soc.*, **135** (7): 2835, 2013.

[76] BISCEGLIA, J. Á.; MOLLO, M. C.; ORELLI, L. R. ``E/Z equilibrium in tertiary amides – Part 3: N-acyl-N′-arylhexahydro-1,3-diazepine´´. *J. Mol. Struct.,* **65**: *1026*, 2012.

[77] HOSOYA, M.; OTANI, Y.; KAWAHATA, M.; YAMAGUCHI, K.; OHWADA, T. ``Water-STABLE Helical Structure of Tertiary Amides of Bicyclic β-Amino Acid Bearing 7-Azabicyclo[2.2.1]heptane. Full Control of Amide Cis−Trans Equilibrium by Bridgehead Substitution´´. *J. Am. Chem. Soc.,* **132**: 14780, 2010.

[78] WANG, H. T.; YAO, J. F. ``Use of Poly(furfuryl alcohol) in the Fabrication of Nanostructured Carbons and Nanocomposites´´. Ind Eng Chem Res., **45**: 6393, 2006.

[79] STHEL, M.; RIEUMONT, J.; MARTINEZ, R. ``Testing a furfuryl alcohol resin as a negative photoresist´´. Polym Test., **18**, 47, 1999.

[80] CHOURA, M.; BELGACEM, N. M.; GANDINI, A. ``Acid-Catalyzed Polycondensation of Furfuryl Alcohol: Mechanisms of Chromophore Formation and Cross-Linking´´. Macromolecules., **29**: 3839, 1996.

[81] GANDINI, A.; BELGACEM, M. N. ``Furans in polymer chemistry´´. Prog Polym Sci., **22**: 1203, 1997.

[82] SWASTI, Y. R.; MURKOVIC, M. ``Characterization of the polymerization of furfuryl alcohol during roasting of coffee´´. Food Funct., **3**: 965, 2012.

[83] PRINCIPE, M.; MARTÍNEZ, R.; ORTIZ, P.; RIEUMONT, J. ``The Polymerization of Furfuryl Alcohol with p-toluenesulfonic Acid: PhotocrossLinkeable Feature of the Polymer´´. Polímeros: Ciência e Tecnologia., **10**: 8, 2000.

[84] BORTOLINI, O.; CAVAZZINI, A.; GIOVANNINI, P. P.; GRECO, R.; MARCHETTI, N.; MASSI, A.; PASTI, L.; ``A Combined Kinetic and Thermodynamic Approach for the Interpretation of Continuous-Flow Heterogeneous Catalytic Processes´´. *Chem Eur J*., **19** (24): 7802, 2013.

[85] MCCORMICK, R.M.; KARGER, B.L. ``Distribution phenomena of mobile-phase components and determination of dead volume in reversed-phase liquid chromatography´´. Anal. Chem., **52**: 2249, 1980.

[86] HERAVI, M.M.; MOGHIMI, S. ``Catalytic Multicomponent Reactions Based on Isocyanides´´. J. Iran. Chem. Soc., **8**: 306, 2011.

[87] VAN BERKEL, S.S.; BÖGELS, B. G. M.; WIJDEVEN, M. A.; WESTERMANN, B.; RUTJES, F.P.J.T. ``Recent Advances in Asymmetric Isocyanide-Based Multicomponent Reactions´´. *Eur. J. Org. Chem.,* **2***:* 3543, 2012.

[88] KUSEBAUCH, U.; BECK, B.; MESSER, K.; HERDTWECK, E.; DOMLING, A. ``Massive Parallel Catalyst Screening: Toward Asymmetric MCRs´´. Org. Lett., **5**: 4021, 2003.

[89] YUE, T.; WANG, M.X.; WANG, D. X.; MASSON, G.; ZHU, J. ``Catalytic Asymmetric Passerini-Type Reaction: Chiral Aluminum-Organophosphate-Catalyzed Enantioselective R-Addition of Isocyanides to Aldehydes´´. J. Org. Chem., **74**: 8396, 2009.

[90] SU, Y.; BOUMA, M. J.; ALCARAZ, L.; STOCKS, M.; FURBER, M.; MASSON, G.; ZHU, J. ``Organocatalytic Enantioselective One-Pot Four-Component Ugi-Type Multicomponent Reaction for the Synthesis of Epoxy-tetrahydropyrrolo[3,4-*b*]pyridin-5-ones´´. Chemistry-A European Journal., **18**: 12624, 2012.

[91] PARK, S. J.; KEUM, G.; KANG, S. B.; KOH, H. Y.; KIM, Y.; LEE, D. H. ``A facile synthesis of *N*-carbamoylmethyl- α -aminobutyrolactones by the Ugi multicomponent condensation reaction´´. Tetrahedron Letters., **39**: 7109, 1998.

[92] GODET, T.; BONVIN, Y.; VINCENT**,** G.; MERLE**,** D.; THOZET**,** A.; CIUFOLINI, M. A. ``Titanium Catalysis in the Ugi Reaction of α-Amino Acids with Aromatic Aldehydes´´. *Org. Lett.*, *6* (19), 3281, 2004.

[93] KIM, Y. B.; CHOI, E. H.; KEUM, G.; KANG, S. B.; LEE, D. H.; KOH, H. Y.; KIM, Y. ``An Efficient Synthesis of Morpholin-2-one Derivatives Using Glycolaldehyde Dimer by the Ugi Multicomponent Reaction´´. Org. Lett., **3**: 4149, 2001.

[94] HILI, R.; RAI, V.; YUDIN, A. K. ``Macrocyclization of Linear Peptides Enabled by Amphoteric Molecules´´ J. AM. CHEM. SOC. **132**, 2889–2891, 2010.

[95] BANFI, L.; BASSO, A.; MONI, L.; RIVA, R. ``The Alternative Route to Enantiopure Multicomponent Reaction Products: Biocatalytic or Organocatalytic Enantioselective Production of Inputs for Multicomponent Reactions´´. *Eur. J. Org. Chem. **2014***, 2005-2015, 2014.

[96] DEOBALD, A. M.; CORRÊA, A. G.; RIVERA, D. G.; PAIXÃO, M. W. ``Organocatalytic asymmetric epoxidation and tandem epoxidation/Passerini reaction under eco-friendly reaction conditions´´. Org. Biomol. Chem., **10**: 7681, 2012.

[97] RIGUET, E.; ``Enantioselective Organocatalytic Friedel-Crafts Alkylation Reaction of Indoles with 5-Hydroxyfuran-2(5H)-one: Access to Chiral γ-Lactones and γ-Lactams via a Ugi 4-Center 3-Component Reaction´´. J. Org. Chem., **76**: 8143, 2011.

[98] BOS, M.; RIGUET, E. ``Synthesis of Chiral γ- Lactones by One-Pot Sequential Enantioselective Organocatalytic Michael Addition of Boronic Acids and Diastereoselective Intramolecular Passerini Reaction´´. *J. Org. Chem.*, **79**(22): 10881, 2014.

[99] GOTOH, H.; OKAMURA, D.; ISHIKAWA, H.; HAYASHI, Y. ``Diphenylprolinol Silyl Ether as a Catalyst in an Asymmetric, Catalytic, and Direct Michael Reaction of Nitroethanol with α, β-UnsaturatedAldehydes´´. *Org. Lett.,* **11**: 4056, 2009.

[100] LANG, M. A.; BECK, W. ``Metal Complexes of Biologically Important Ligands, CLVII [1] Halfsandwich Complexes of Isocyanoacetylamino acid esters and of Isocyanoacetyldi- and tripeptide esters („Isocyanopeptides")´´. *Z. Anorg. Allg. Chem.,* **631**: 2333, 2005.

[101] ICHIKAWA, Y.; NISHIYAMA, T.; ISOBE, M. ``A New Synthetic Method for a- and b-Glycosyl Ureas and its Application to the Synthesis of Glycopeptide Mimics with Urea-glycosyl Bonds´´. *Synlett.,* **9**: 1253, 2000.

[102] BADÍA, C.; SOUARD, F.; VICENT, C. ``Sugar-Oligoamides: Synthesis of DNA Minor Groove Binders´´. J. Org. Chem., **77**: 10870, 2012.

[103] RUEPING, M.; SUGIONO, E.; MERINO, E. `` Enantioselective Organocatalytic Reactions of 4-Hydroxycoumarin and 4-Hydroxypyrone with α,β-Unsaturated Aldehydes – An Efficient Michael Addition-Acetalization Cascade to Chromenones, Quinolinones and Pyranones´´ *Adv. Synth. Catal. 350*, 2127, 2008.

[104] FRANKE, P. T.; RICHTER, B.; JØRGENSEN, K. A. `` Organocatalytic Asymmetric Synthesis of Functionalized 3,4-Dihydropyran Derivatives´´. *Chem. Eur. J.* **14**, 6317, 2008.

[105] EL KAÏM, L.; GRIMAUD, L.; OBLE, J. ``Phenol Ugi −Smiles Systems: Strategies for the Multicomponent N-Arylation of Primary Amines with Isocyanides, Aldehydes, and Phenols´´. *Angew. Chem., Int. Ed.* **44**, 7961, 2005.

[106] CASTELLANO, T. G.; NEO, A. G.; MARCACCINI, S.; MARCOS, C. F. ``Enols as Feasible Acid Components in the Ugi Condensation´´. *Org. Lett.*, *14* (24), 6218–6221, 2012.

[107] LU, D.; LI, Y.; GONG, Y. ``Organocatalytic Asymmetric Tandem Michael Addition-Hemiacetalization: A Route to Chiral Dihydrocoumarins, Chromanes, and 4H-Chromenes´´ *J. Org. Chem.* **75**, 6900, 2010.

[108] RAMACHARY, D. B.; PRASAD, M. S.; MADHAVACHARY, R. ``A general approach to high-yielding asymmetric synthesis of chiral 3-alkyl-4-nitromethyl chromans *via* cascade Barbas–Michael and acetalization reactions´´. Org. Biomol. Chem., **9**, 2715, 2011.

[109] MASE, N.; NAKAI, Y.; N. OHARA, YODA, H.; TAKABE, K.; F.; TANAKA, C. F. BARBAS III. ``Organocatalytic Direct Asymmetric Aldol Reactions in Water´´. J. Am. Chem. Soc., **128**: 734, 2006.

[110] BETANCORT, J. M.; BARBAS, C. F. ``Catalytic Direct Asymmetric Michael Reactions: Taming Naked Aldehyde Donors´´. Org. Lett., **3**: 3737, 2001.

[111] BARROS, M. T.; PHILLIPS, A. M. F. ``Chiral Piperazines as Efficient Catalysts for the Asymmetric Michael Addition of Aldehydes to Nitroalkenes´´. Eur. J. Org. Chem., **1**: 178, 2007.

[112] WIESNER, M.; REVELL, J. D.; WENNEMERS, H. ``Tripeptides as Efficient Asymmetric Catalysts for 1,4-Addition Reactions of Aldehydes to Nitroolefins–A Rational Approach´´. Angew. Chem. Int. Ed., **47**: 1871, 2008.

[113] CHENG, Y.-Q.; BIAN, Z.; HE, Y.-B.; HAN, F.-S.; KANG, C.-Q.; NING, Z.-L.; GAO, L.-X. ``Asymmetric Michael addition of aldehydes to nitroolefins catalyzed by L-prolinamide derivatives using phenols as co-catalysts´´. Tetrahedron Asymm., **20**(15): 1753, 2009.

[114] POLAK, E.; RIBIERE, G. ``Note sur la convergence de méthodes de directions conjuguées´´. Revenue Francaise Informat. Recherche Operationelle, Serie Rouge, **3**(16): 35, 1969.

[115] HALGREN, T. A. ``Merck molecular force field. I. Basis, form, scope, parameterization, and performance of MMFF94´´. J. Comput. Chem., **17**(5): 490, 1996.

[116] RICHARDS, N. G. J.; GUIDA, W. C.; LISKAMP, R.; LIPTON, M.; CAUFIELD, C.; CHANG, G.; HENDRICKSON, T.; STILL, W. C. ``Macromodel—an integrated software system for modeling organic and bioorganic molecules using molecular mechanics´´. J. Comput. Chem., **11**: 440, 1990.

[117] Maestro, version 9.3, Schrödinger, LLC, New York, NY, 2012.

[118] http://www.schrodinger.com/scriptcenter

[119] SHAO, J.; TANNER, S. W.; THOMPSON, N.; CHEATHAM III, T. E. `` Clustering Molecular Dynamics Trajectories: 1. Characterizing the Performance of Different Clustering Algorithms´´. J. Chem. Theory. Comput., **3**(6): 2312, 2007.

[120] ZHAO, Y.; TRUHLAR, D. G. ``The M06 suite of density functionals for main group thermochemistry, thermochemical kinetics, noncovalent interactions, excited states, and transition elements: two new functionals and systematic testing of four M06-class functionals and 12 other functionals´´. Theor. Chem. Acc., **120**: 215, 2008.

[121] GAUSSIAN 09, REVISION B.1, FRISCH, M. J.; TRUCKS, G. W.; SCHLEGEL, H. B.; SCUSERIA, G. E.; ROBB, M. A.; CHEESEMAN, J. R.; SCALMANI, G.; BARONE, V.; MENNUCCI, B.; PETERSSON, G. A.; NAKATSUJI, H.; CARICATO, M.; LI, X.; HRATCHIAN, H. P.; IZMAYLOV, A. F.; BLOINO, J.; ZHENG, G.; SONNENBERG, J. L.; HADA, M.; EHARA, M.; TOYOTA, K.; FUKUDA, R.; HASEGAWA, J.; ISHIDA, M.; NAKAJIMA, T.; HONDA, Y.; KITAO, O.; NAKAI, H.; VREVEN, T.; MONTGOMERY, JR., J. A.; PERALTA, J. E.; OGLIARO, F.; BEARPARK, M.; HEYD, J. J.; BROTHERS, E.; KUDIN, K. N.; STAROVEROV, V. N.; KOBAYASHI, R.; NORMAND, J.; RAGHAVACHARI, K.; RENDELL, A.; BURANT, J. C.; IYENGAR, S. S.; TOMASI, J.; COSSI, M.; REGA, N.; MILLAM, N. J.; KLENE, M.; KNOX, J. E.; CROSS, J. B.; BAKKEN, V.; ADAMO, C.; JARAMILLO, J.; GOMPERTS, R.; STRATMANN, R. E.; YAZYEV, O.; AUSTIN, A. J.; CAMMI, R.; POMELLI, C.; OCHTERSKI, J. W.; MARTIN, R. L.; MOROKUMA, K.; ZAKRZEWSKI, V. G.; VOTH, G. A.; SALVADOR, P.; DANNENBERG, J. J.; DAPPRICH, S.; DANIELS, A. D.; FARKAS, Ö.; FORESMAN, J. B.; ORTIZ, J. V.; CIOSLOWSKI, J.; FOX, D. J. Gaussian, Inc., Wallingford CT, 2009.

[122] MARENICH, A. V.; CRAMER, C. J.; TRUHLAR, D. G. ``Universal Solvation Model Based on Solute Electron Density and on a Continuum Model of the Solvent Defined by the Bulk Dielectric Constant and Atomic Surface Tensions´´. J. Phys. Chem. B., **113**: 6378, 2009.

[123] BORTOLINI, O.; CAVAZZINI, A.; GIOVANNINI, P. P.; GRECO, R.; MARCHETTI, N.; MASSI, A.; PASTI, L.; ``A Combined Kinetic and Thermodynamic Approach for the Interpretation of Continuous-Flow Heterogeneous Catalytic Processes´´. *Chem Eur J*., **19** (24): 7802, 2013.

[124] MCCORMICK, R.M.; KARGER, B.L. ``Distribution phenomena of mobile-phase components and determination of dead volume in reversed-phase liquid chromatography´´. Anal. Chem., **52**: 2249, 1980.

[125] HOPPE, I.; SCHIILLKOPF, U. ``Cycloaddition von Isocyanketen an Benzophenonanil und Thioimidsaureester zu β-Lactamen´´. Chem. Ber., *109*: 482, 1976.

[126] PROSPERI, D.; RONCHI, S.; LAY, L.; RENCUROSI, A.; RUSSO, G. ``Efficient Synthesis of Unsymmetrical Ureido-Linked Disaccharides´´. *Eur. J. Org. Chem., 2:*395, 2004.

[127] BADÍA, C.; SOUARD, F.; VICENT, C. ``Sugar-Oligoamides: Synthesis of DNA Minor Groove Binders´´. J. Org. Chem., **77**: 10870, 2012.

Selected figures and spectra
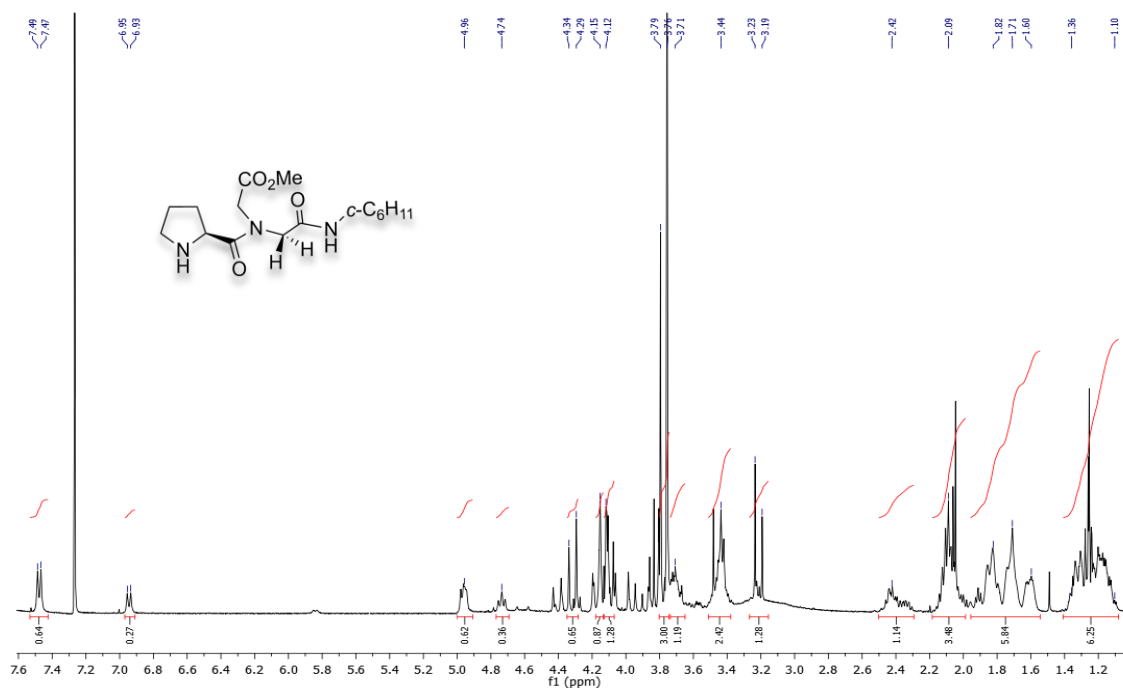
FIGURE 1: 400 MHz ^{1}H NMR spectra in CDCl$_3$ of compound **61**.
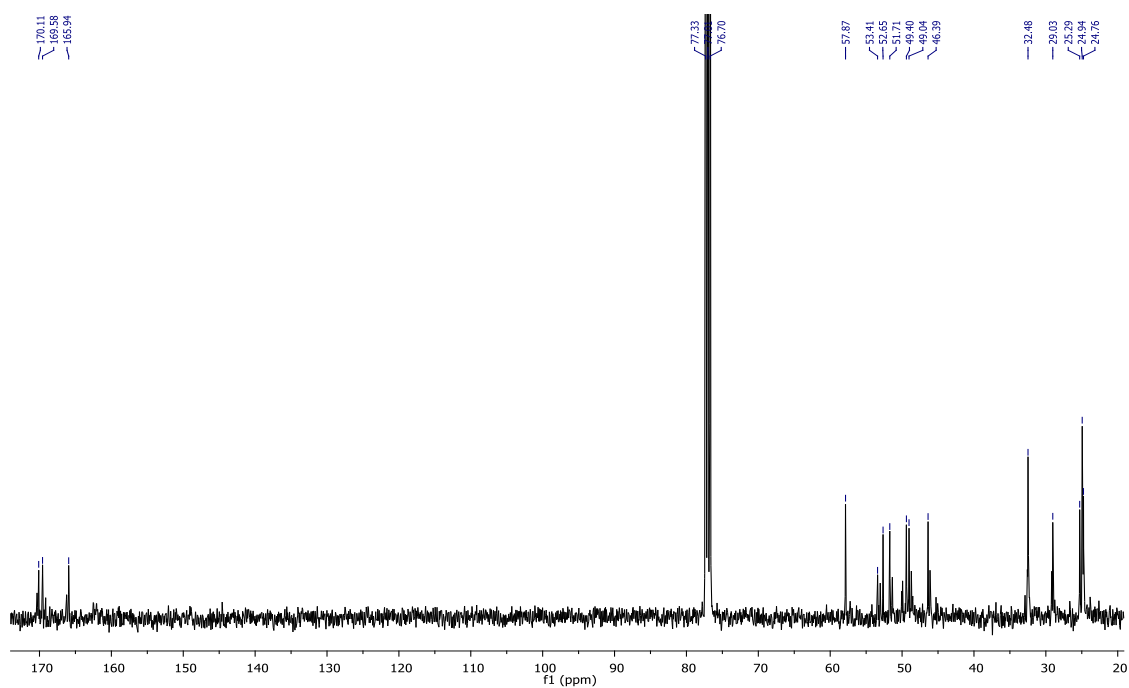
FIGURE 2: 100 MHz ^{13}C NMR spectra in CDCl$_3$ of compound **61**.
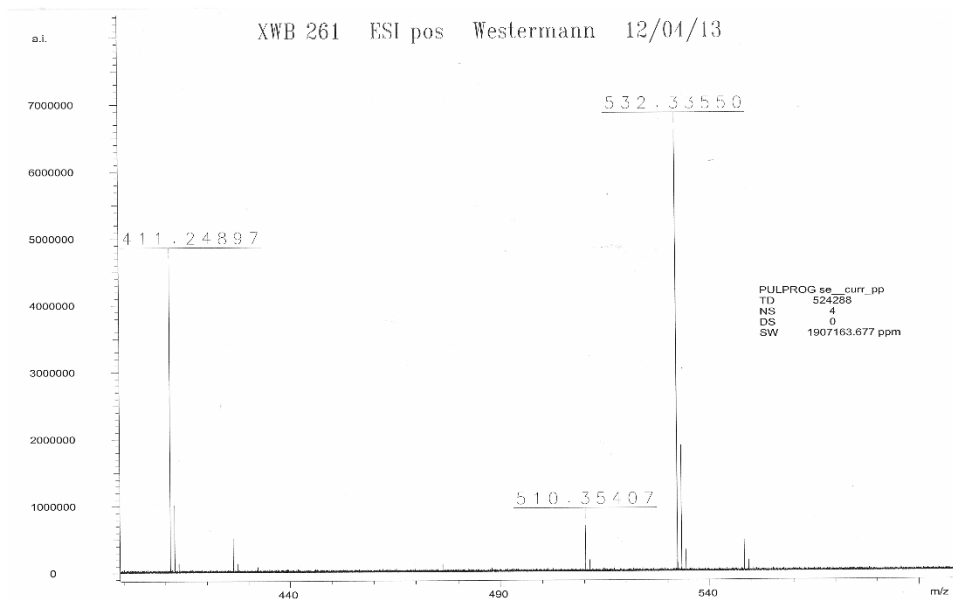
FIGURE 3: HRMS (ESI-FT-ICR) m/z: of compound **61**.
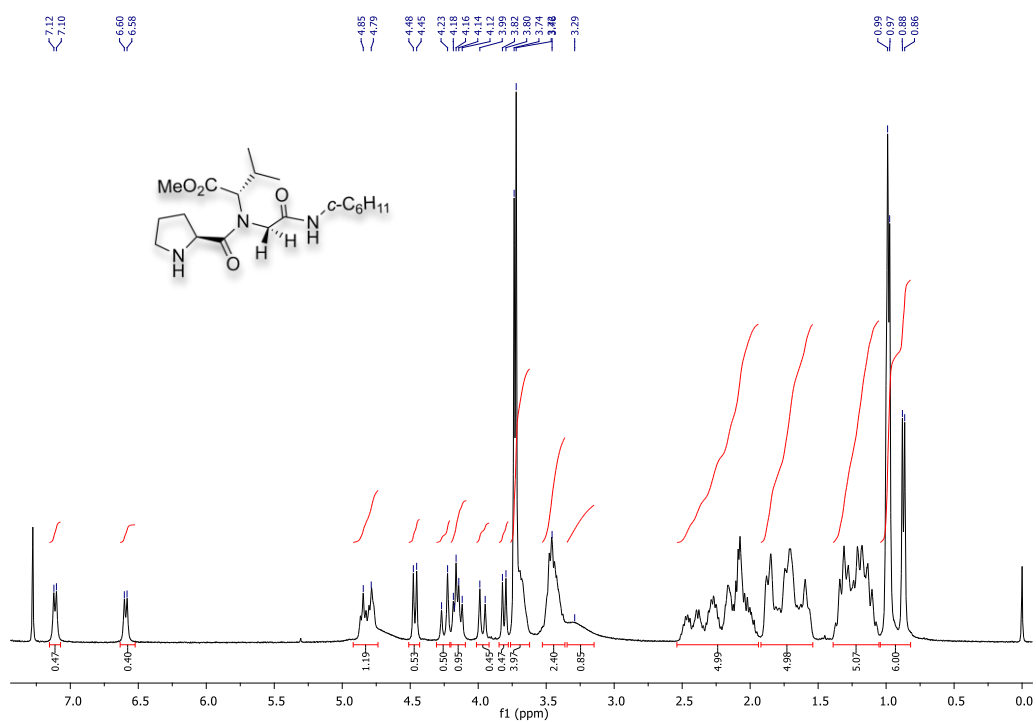
FIGURE 4: 400 MHz ^{1}H NMR spectra in CDCl$_3$ of compound **62**.
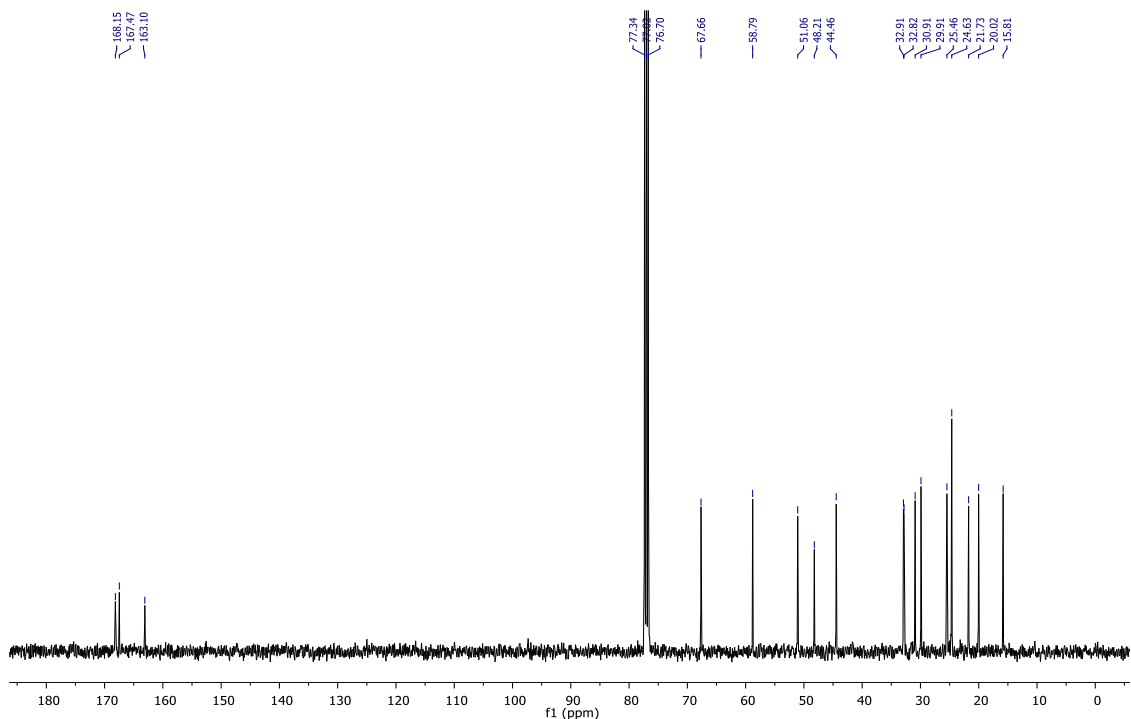
FIGURE 5: 100 MHz ^{13}C NMR spectra in CDCl$_3$ of compound **62**.
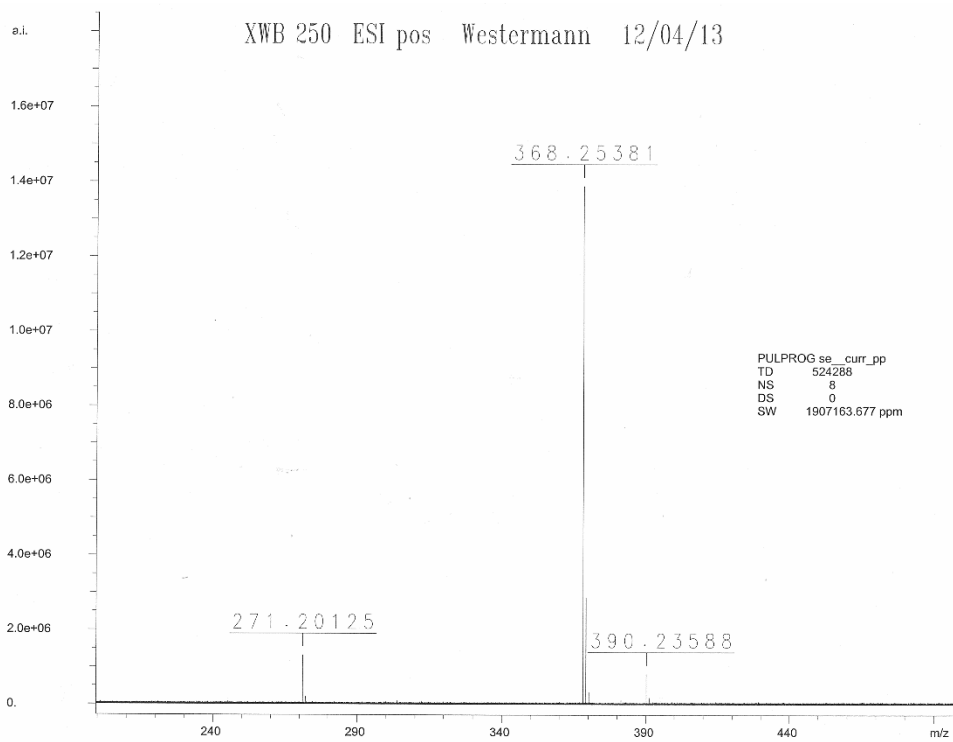
FIGURE 6: HRMS (ESI-FT-ICR) m/z: of compound **62**.
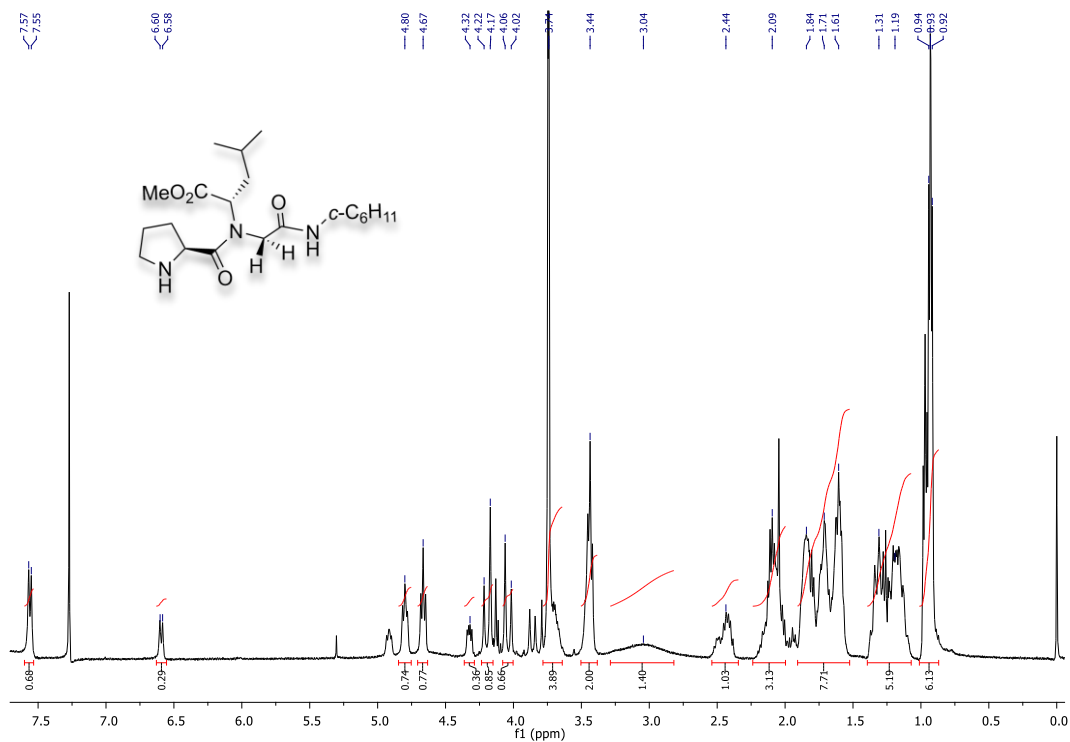
FIGURE 7: 400 MHz ^{1}H NMR spectra in CDCl$_3$ of compound **63**.
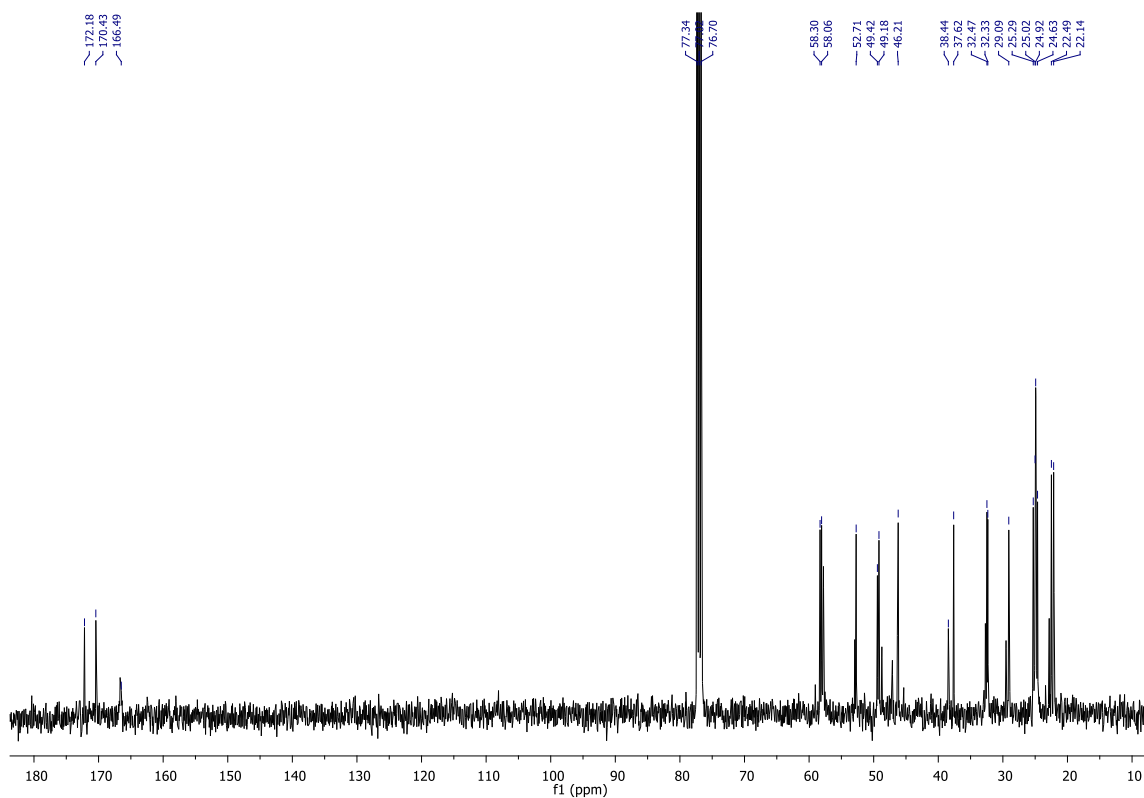
FIGURE 8: 100 MHz ^{13}C NMR spectra in CDCl$_3$ of compound **63**.
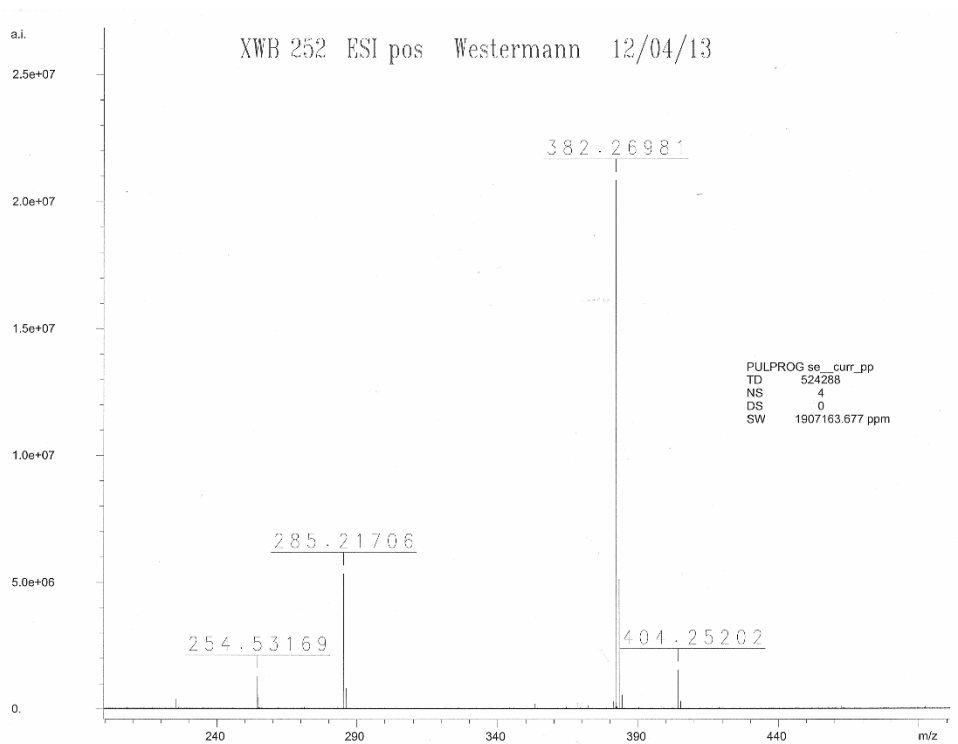
FIGURE 9: HRMS (ESI-FT-ICR) m/z: of compound **63**.
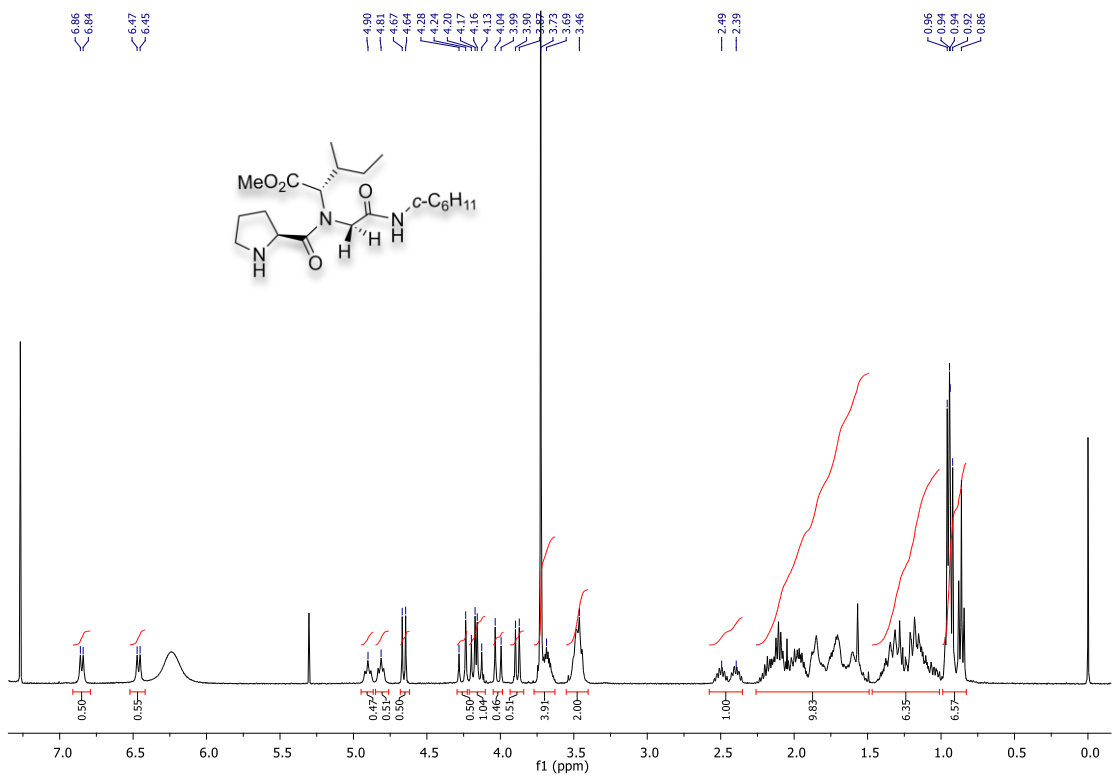
FIGURE 10: 400 MHz ^{1}H NMR spectra in CDCl$_3$ of compound **64**.
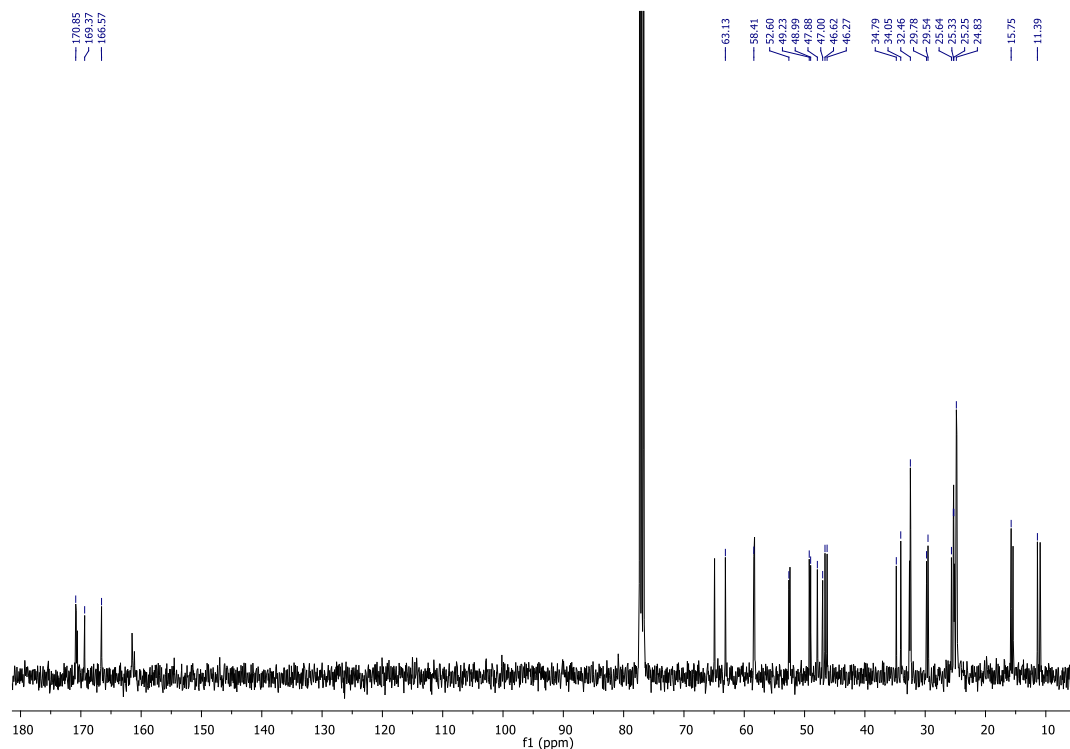
FIGURE 11: 100 MHz ^{13}C NMR spectra in CDCl$_3$ of compound **64**.
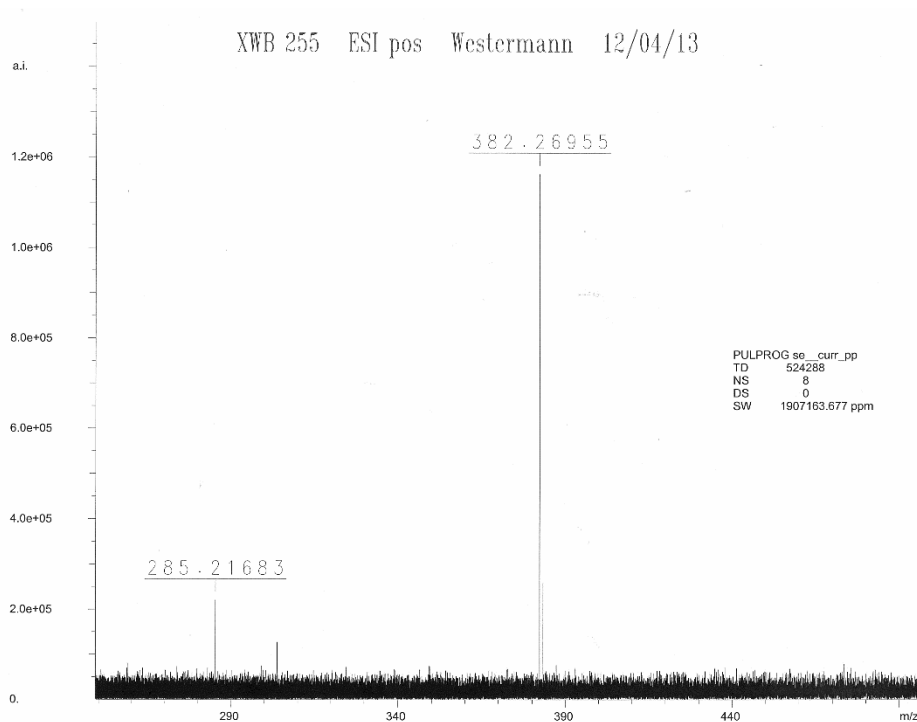
FIGURE 12: HRMS (ESI-FT-ICR) m/z: of compound **64**.
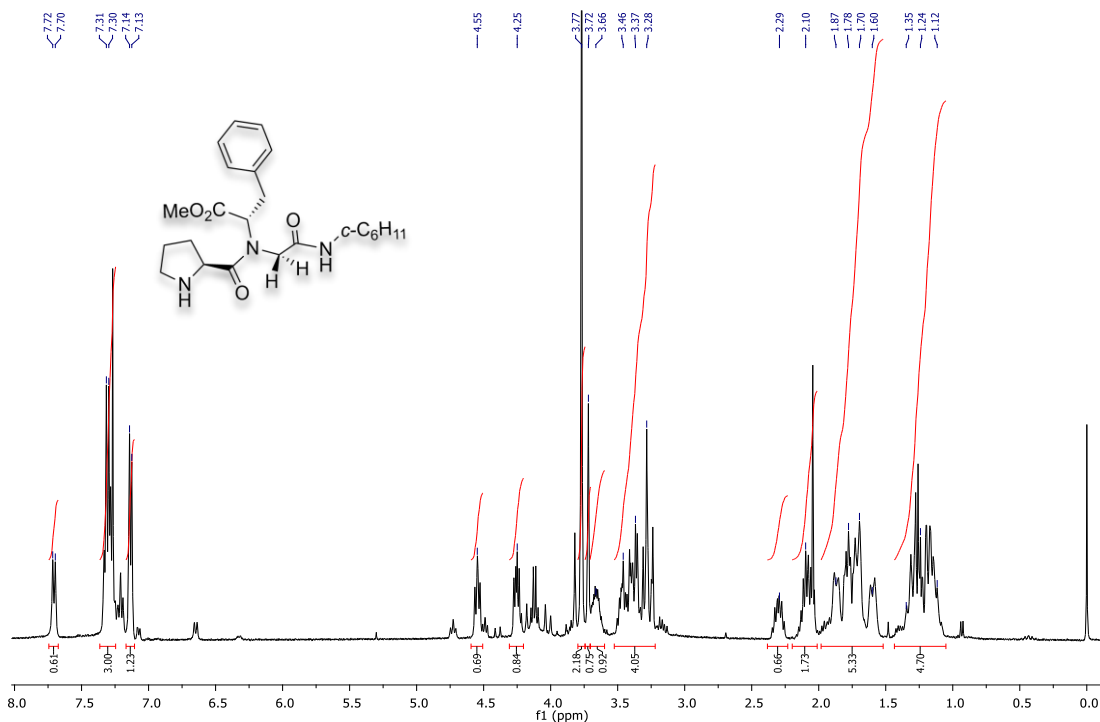
FIGURE 13: 400 MHz ^{1}H NMR spectra in CDCl$_3$ of compound **65**.
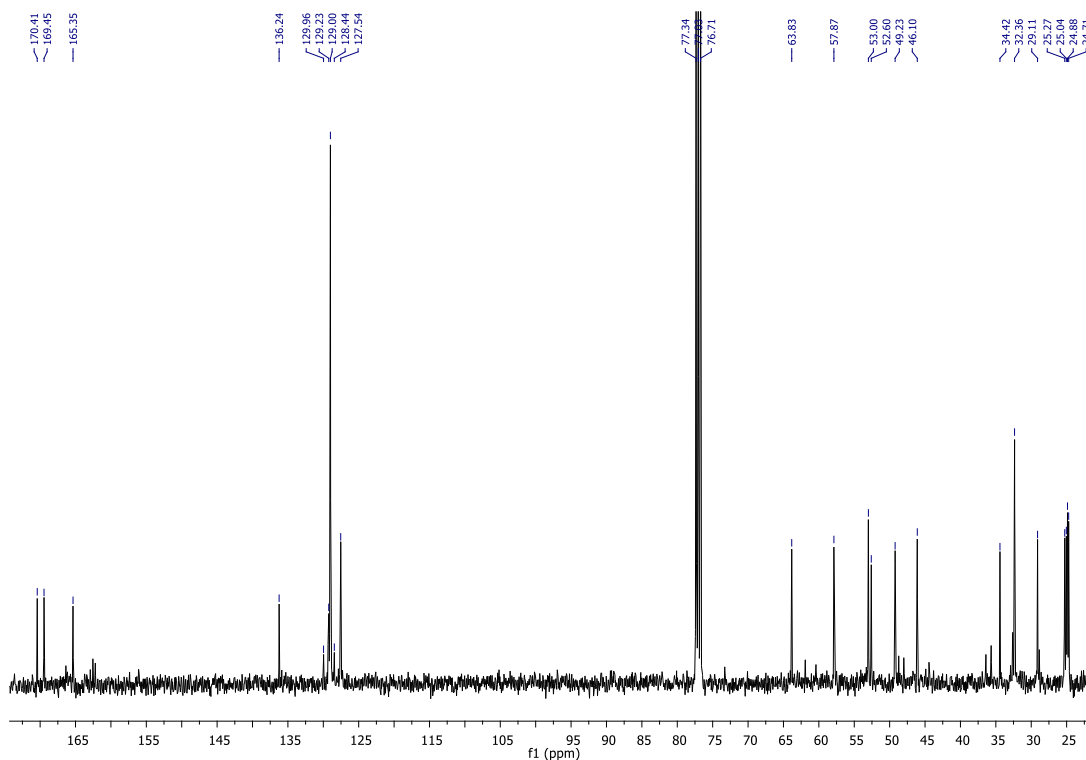
FIGURE 14: 100 MHz ^{13}C NMR spectra in CDCl$_3$ of compound **65**.
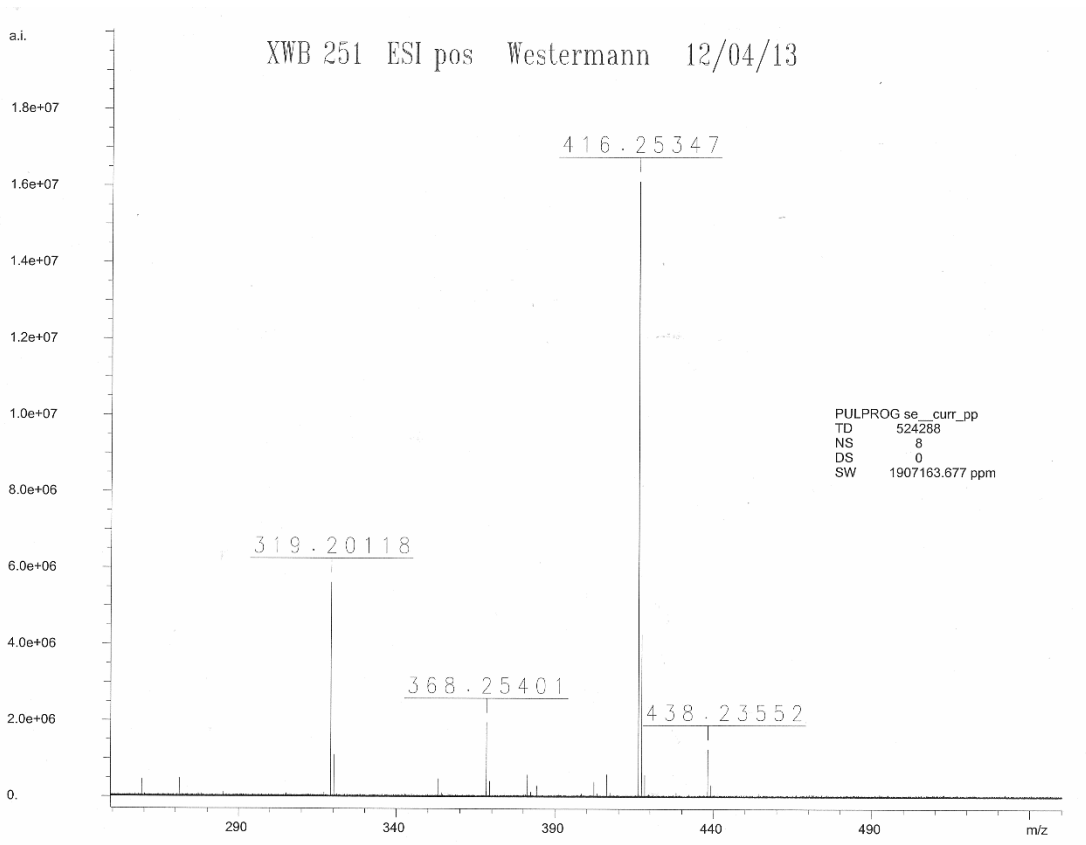
FIGURE 15: HRMS (ESI-FT-ICR) m/z: of compound **65**.
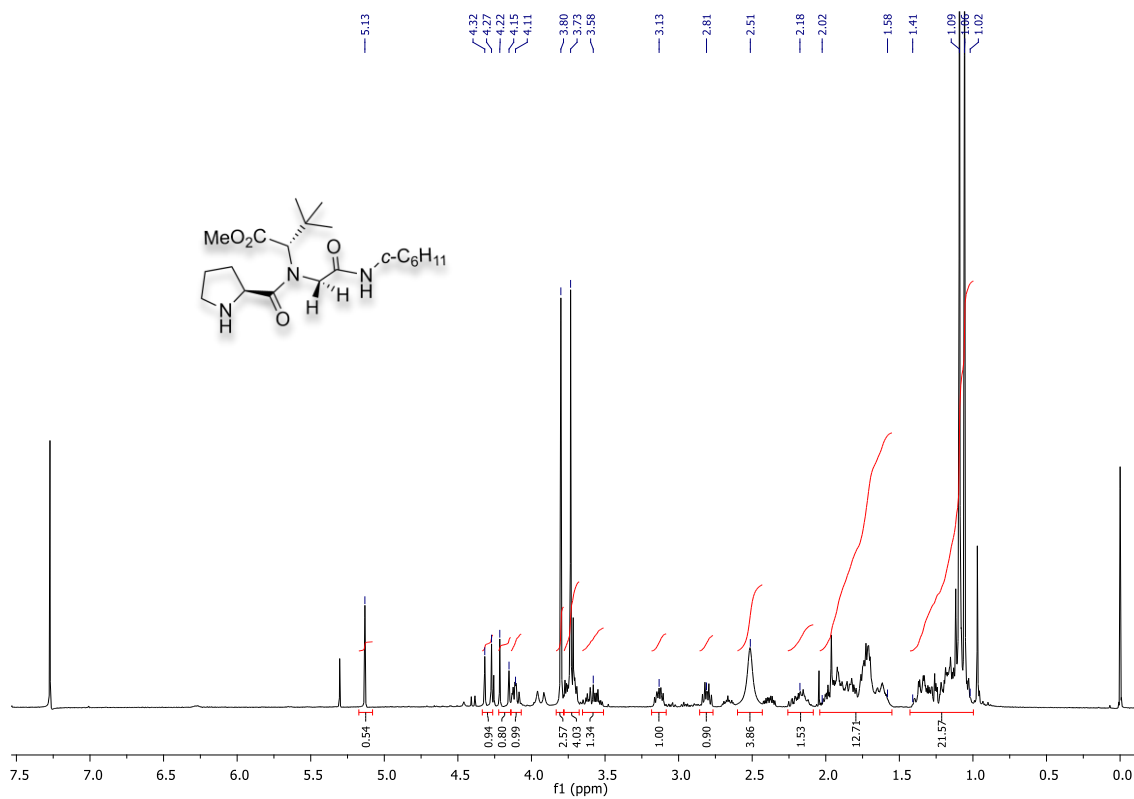
FIGURE 16: 400 MHz ^{1}H NMR spectra in CDCl$_3$ of compound **66**.
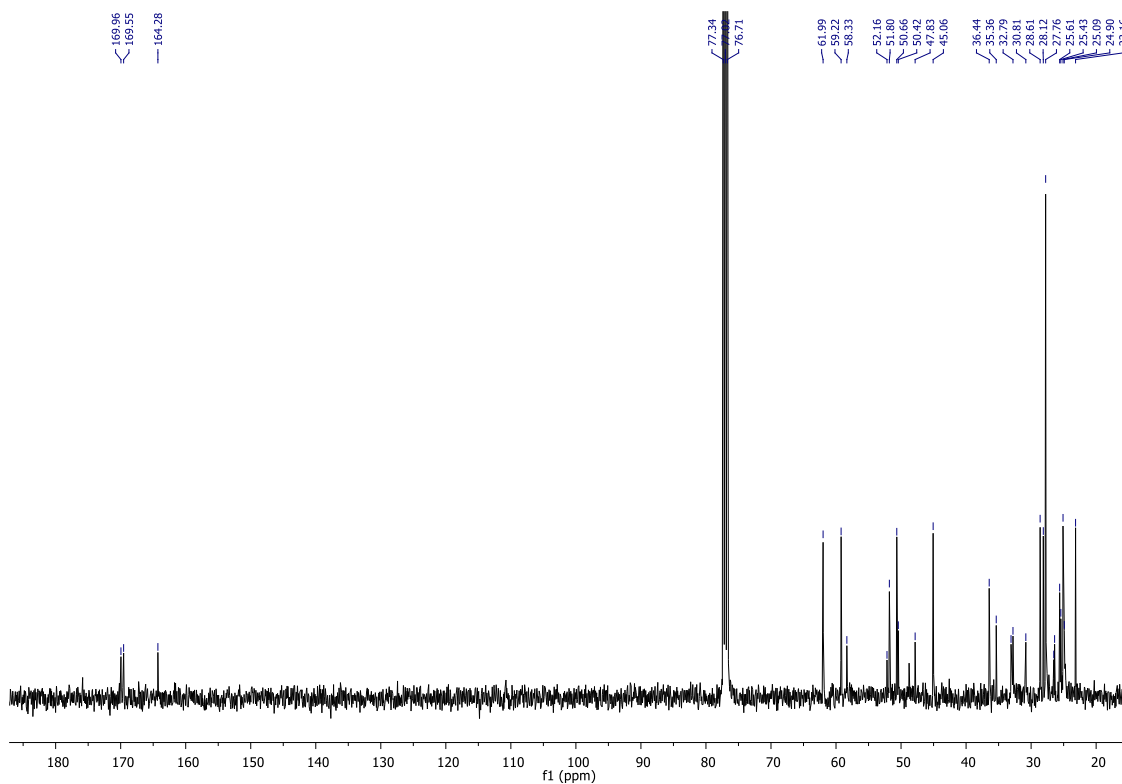
FIGURE 17: 100 MHz ^{13}C NMR spectra in CDCl$_3$ of compound **66**.
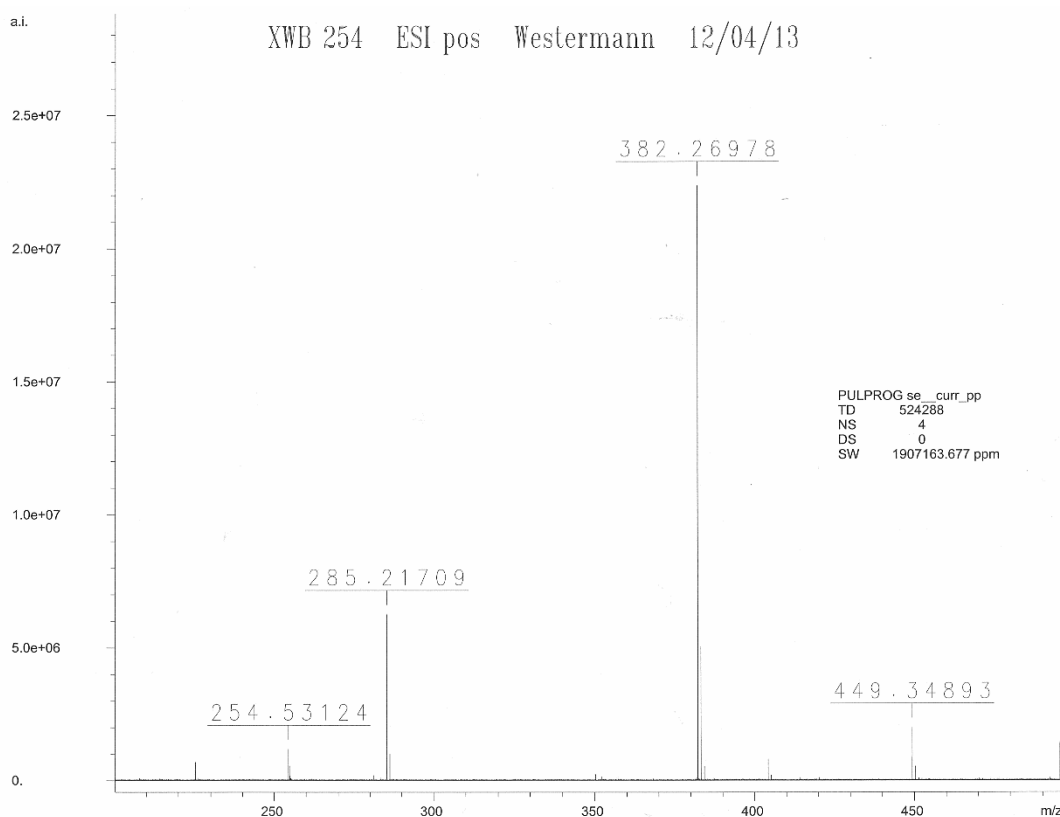
FIGURE 18: HRMS (ESI-FT-ICR) m/z: of compound **66**.
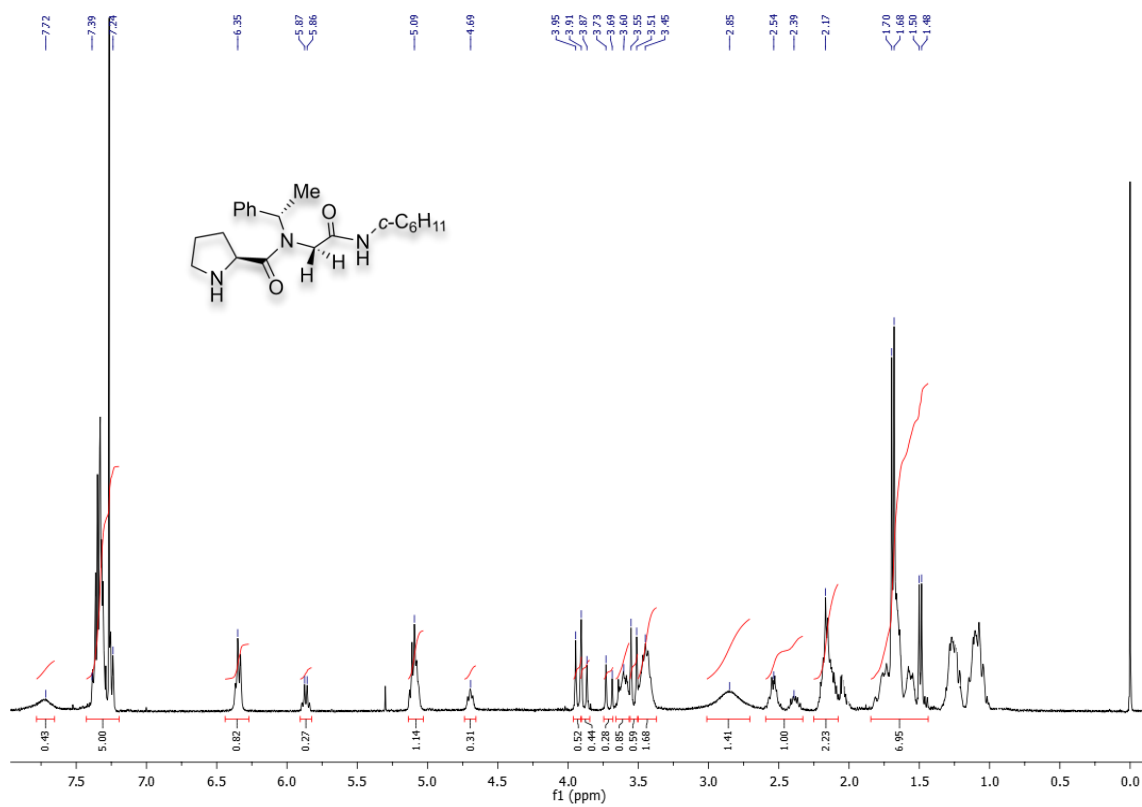
FIGURE 19: 400 MHz ^{1}H NMR spectra in CDCl$_3$ of compound **67**.
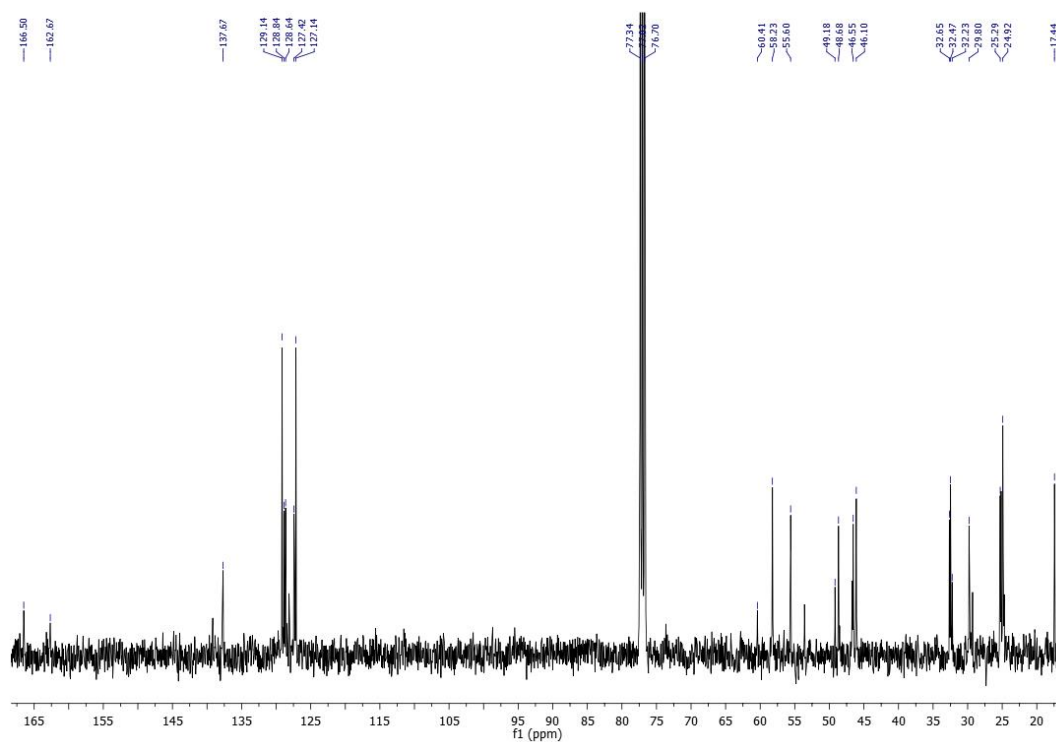
FIGURE 20: 100 MHz ^{13}C NMR spectra in CDCl$_3$ of compound **67**.
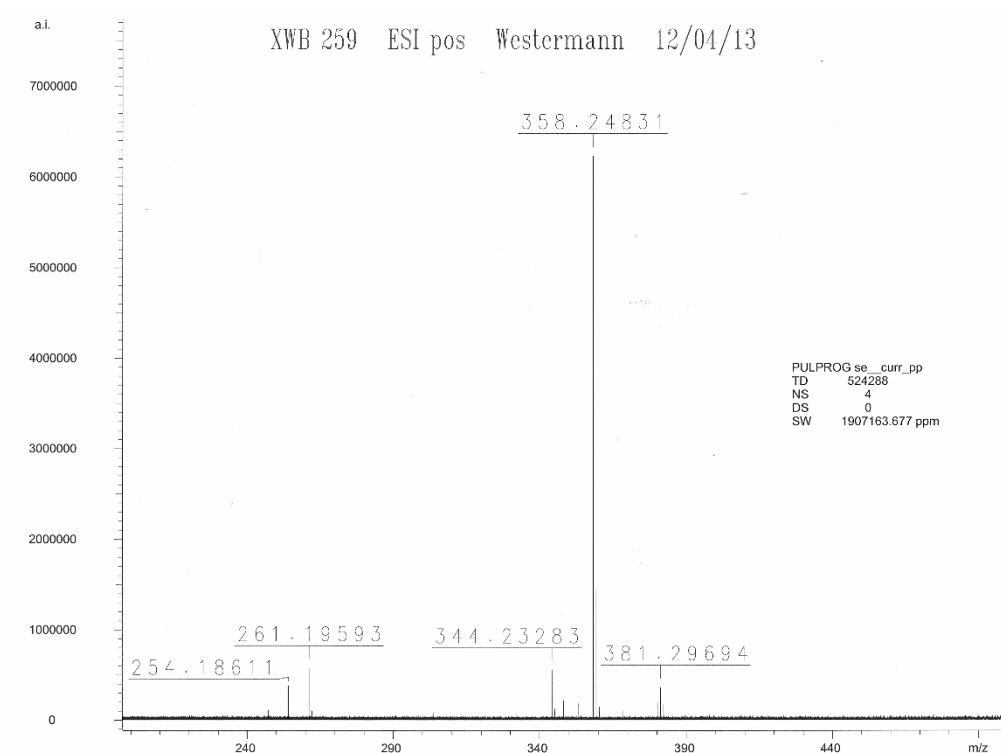
FIGURE 21: HRMS (ESI-FT-ICR) m/z: of compound **67**.
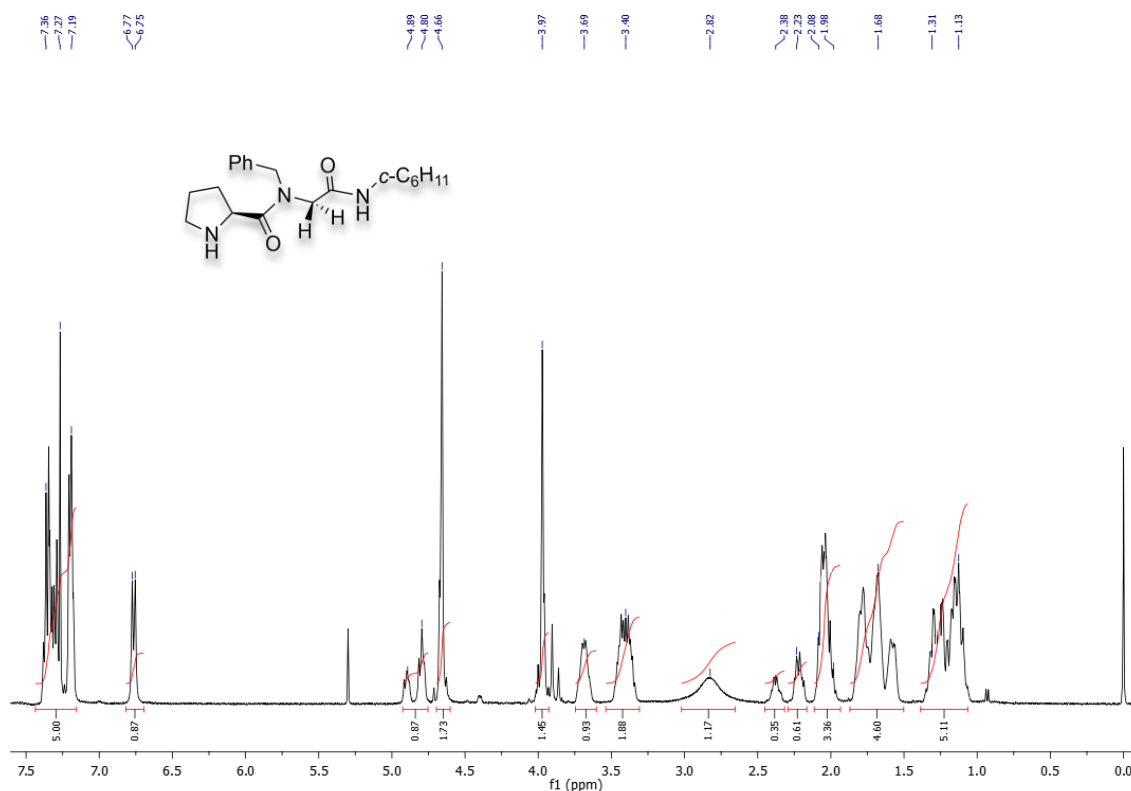
FIGURE 22: 400 MHz ^{1}H NMR spectra in in CDCl$_3$ of compound **68**.
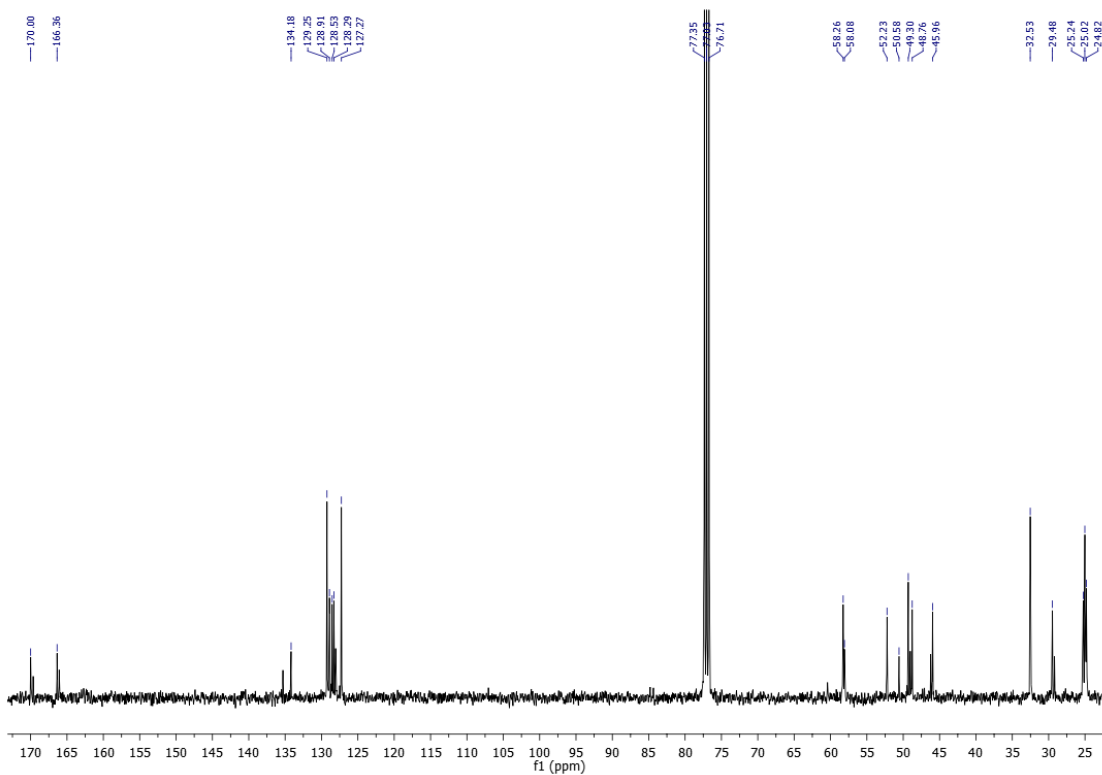
FIGURE 23: 100 MHz ^{13}C NMR spectra in in CDCl$_3$ of compound **68**.
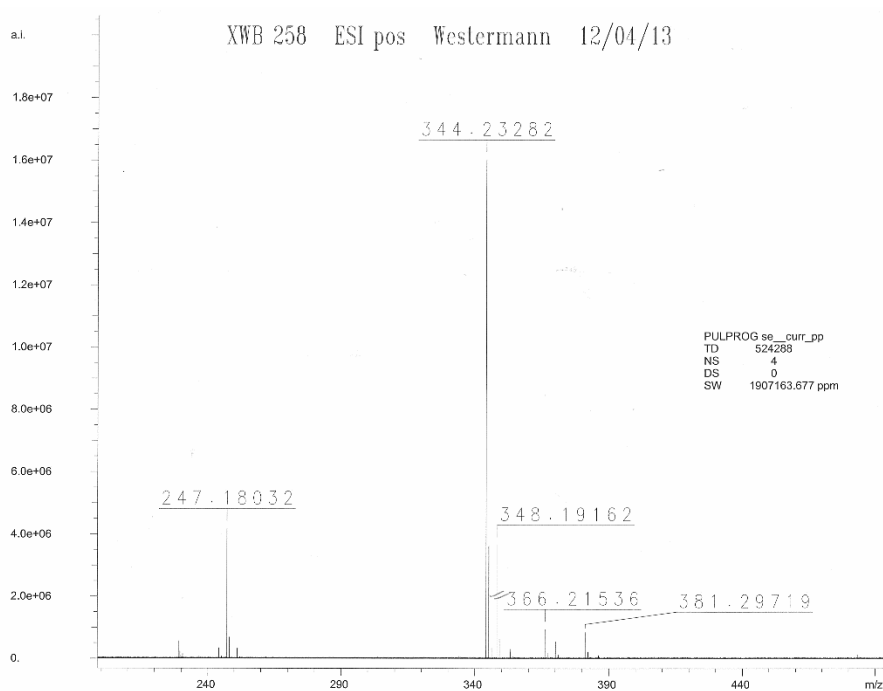
FIGURE 24: HRMS (ESI-FT-ICR) m/z: of compound **68**.
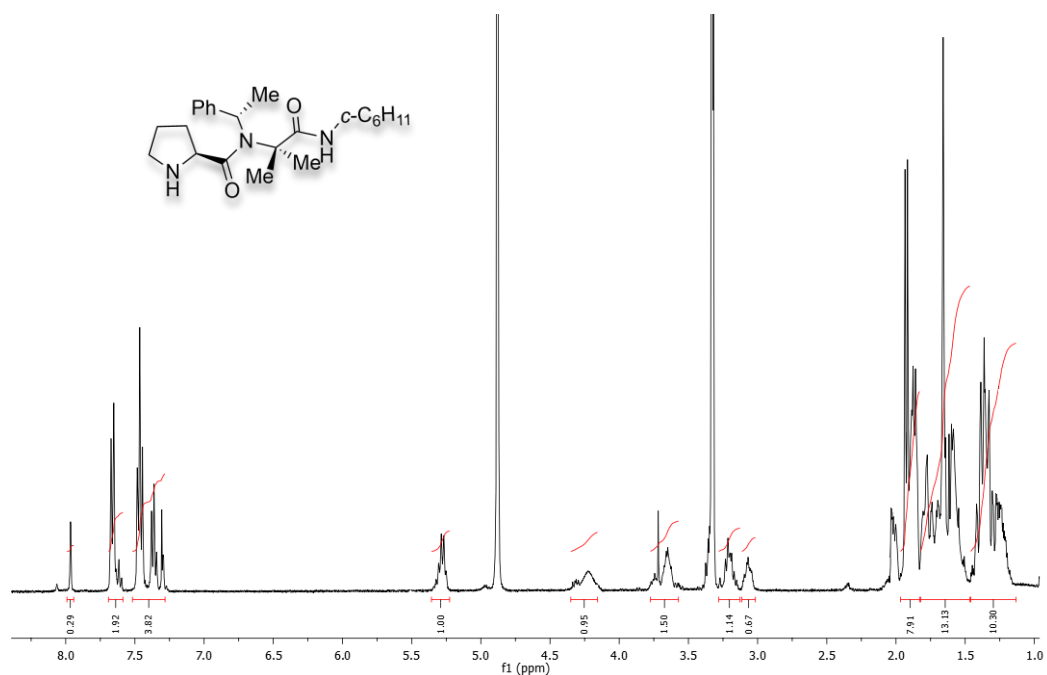
FIGURE 25: 400 MHz ^{1}H NMR spectra in CD$_3$OD of compound **69**.
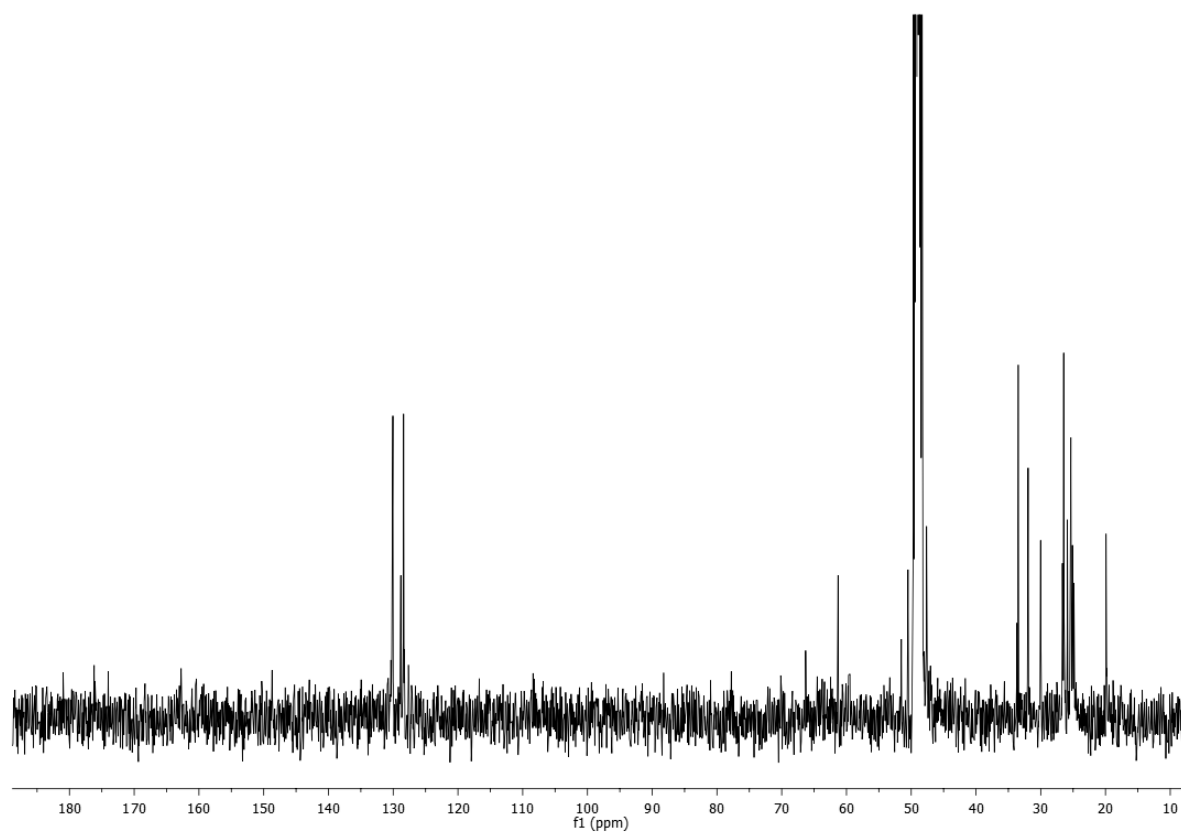
FIGURE 26: 100 MHz ^{13}C NMR spectra in CD$_3$OD of compound **69**.
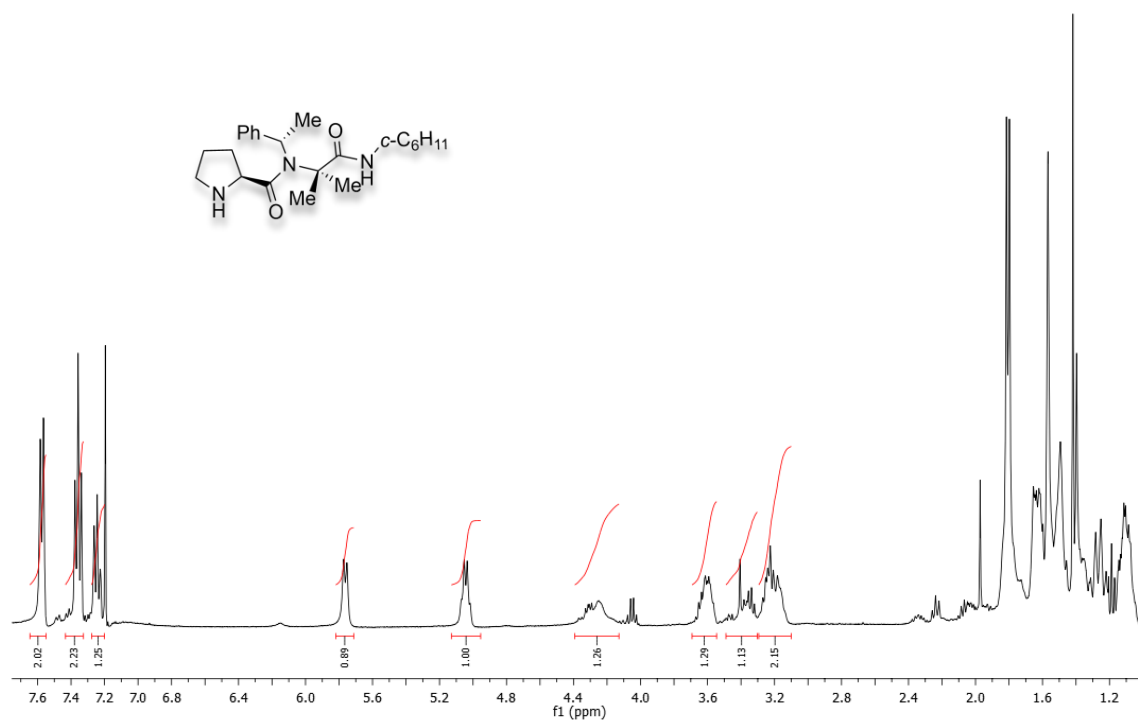
FIGURE 27: 600 MHz ^{1}H NMR spectra in CDCl$_3$ of compound **69**.
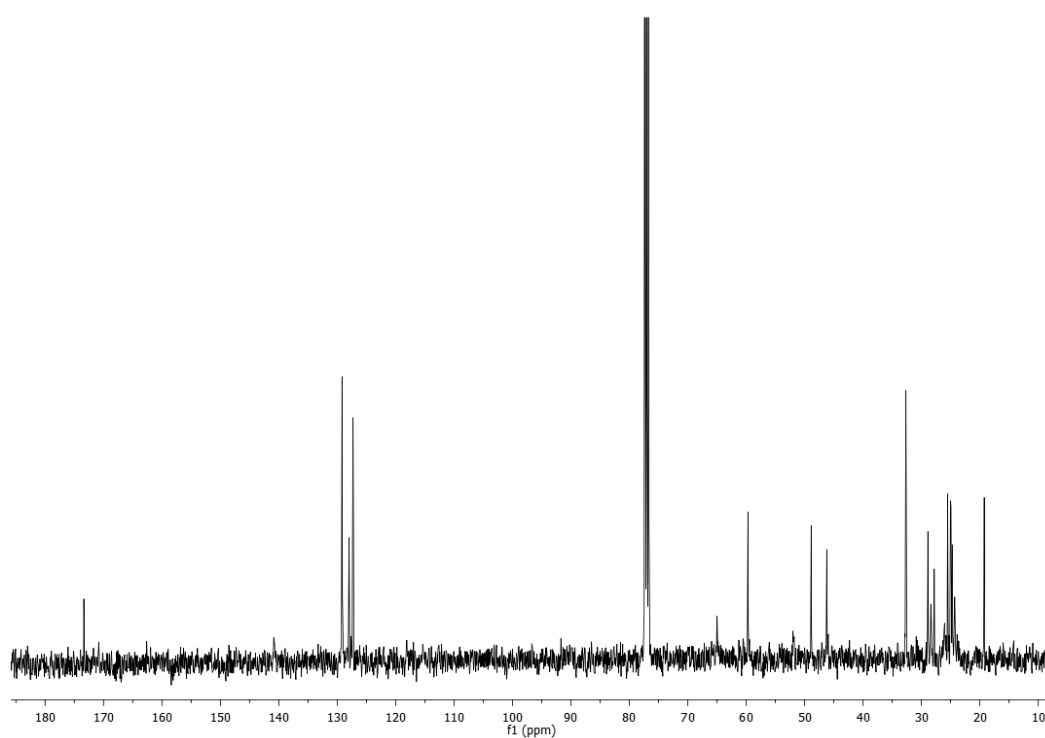
FIGURE 28: 100 MHz ^{13}C NMR spectra in CDCl$_3$ of compound **69**.
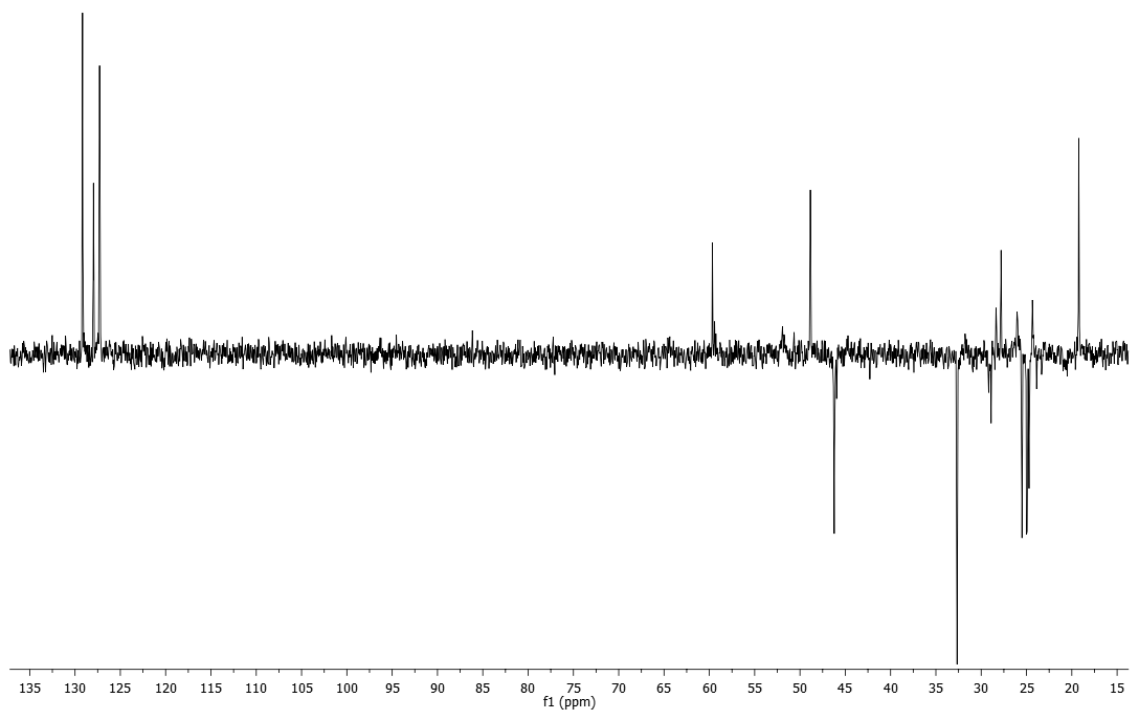
FIGURE 29: 100 MHz DEPT 135 spectra in CDCl$_3$ of compound **69**.
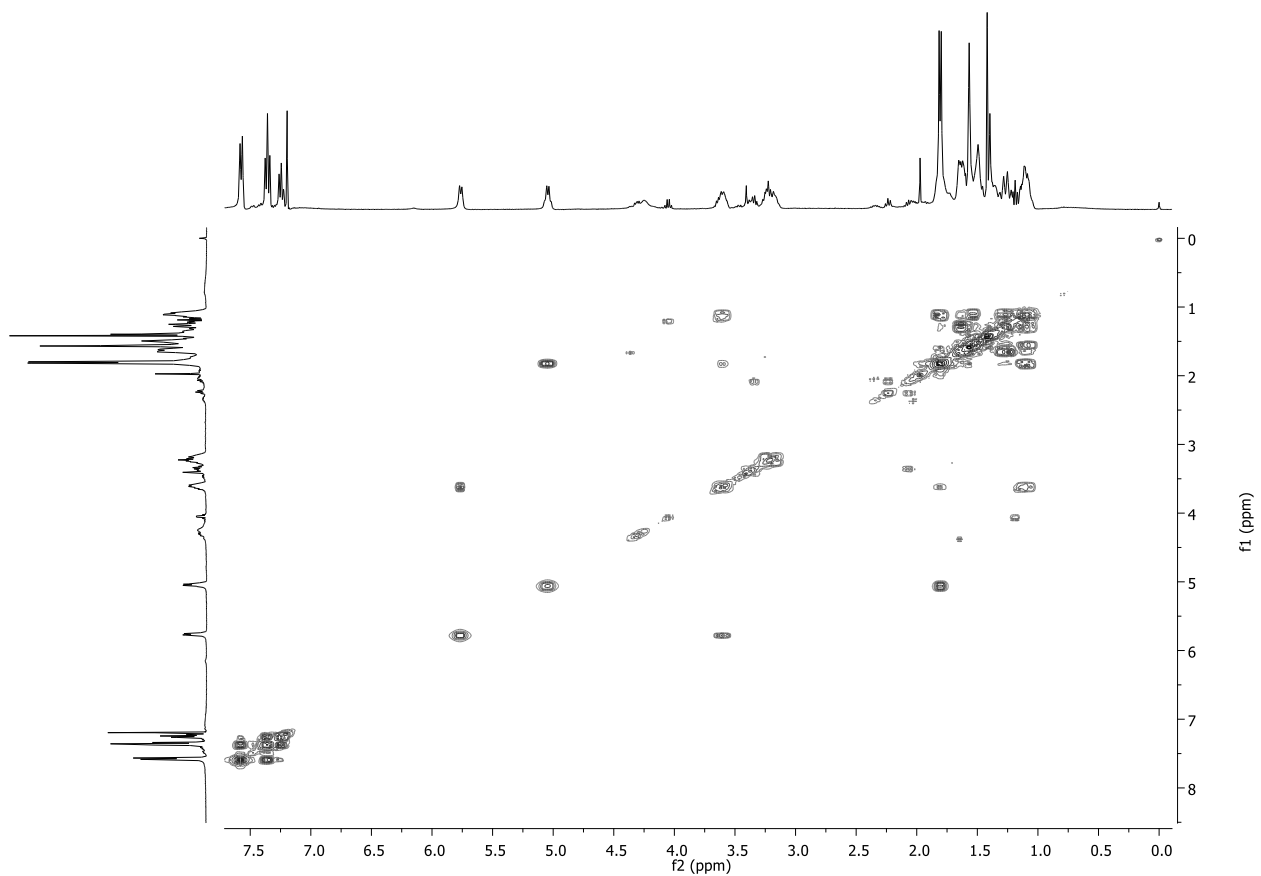
FIGURE 30: 600 MHz COSY spectra in CDCl$_3$ of compound **69**.
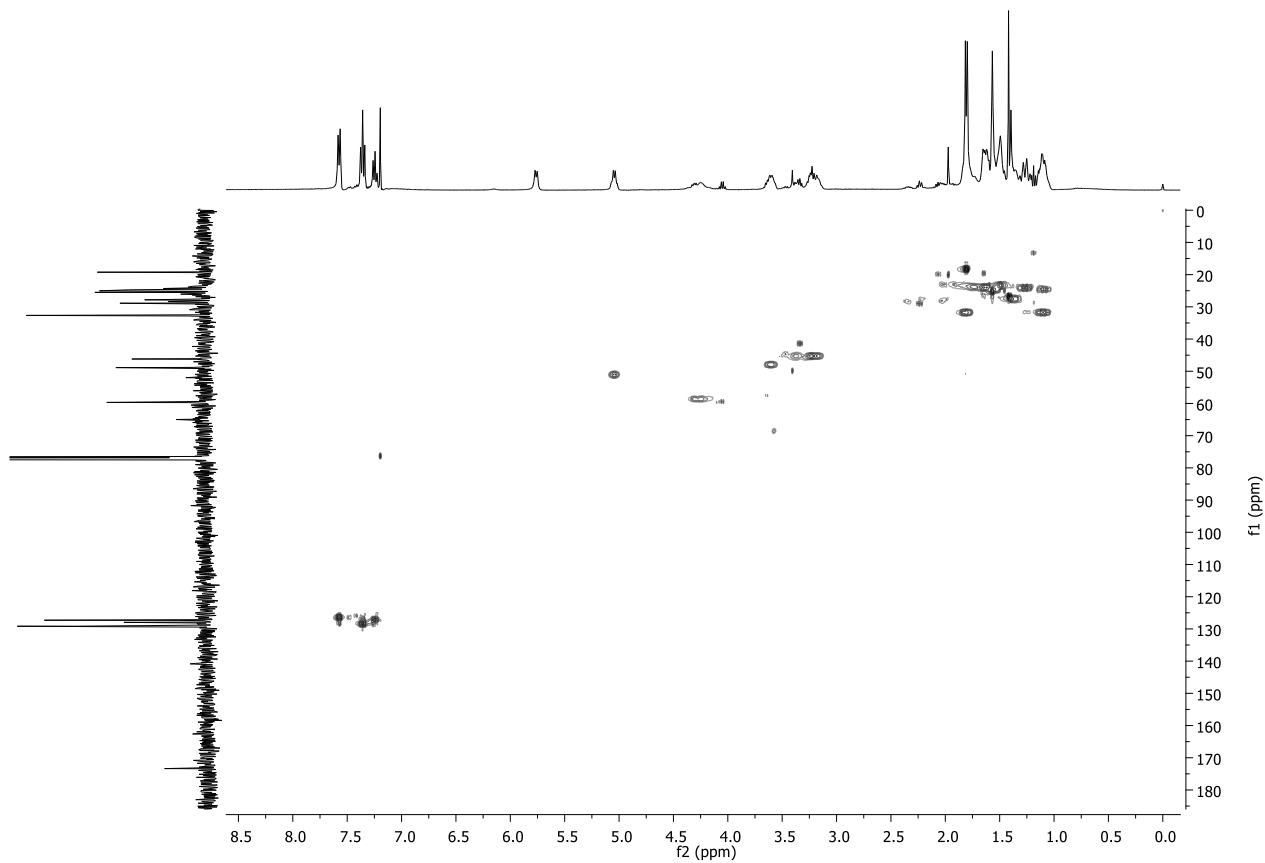
FIGURE 31: 600 MHz HSQC spectra in CDCl₃ of compound **69**.
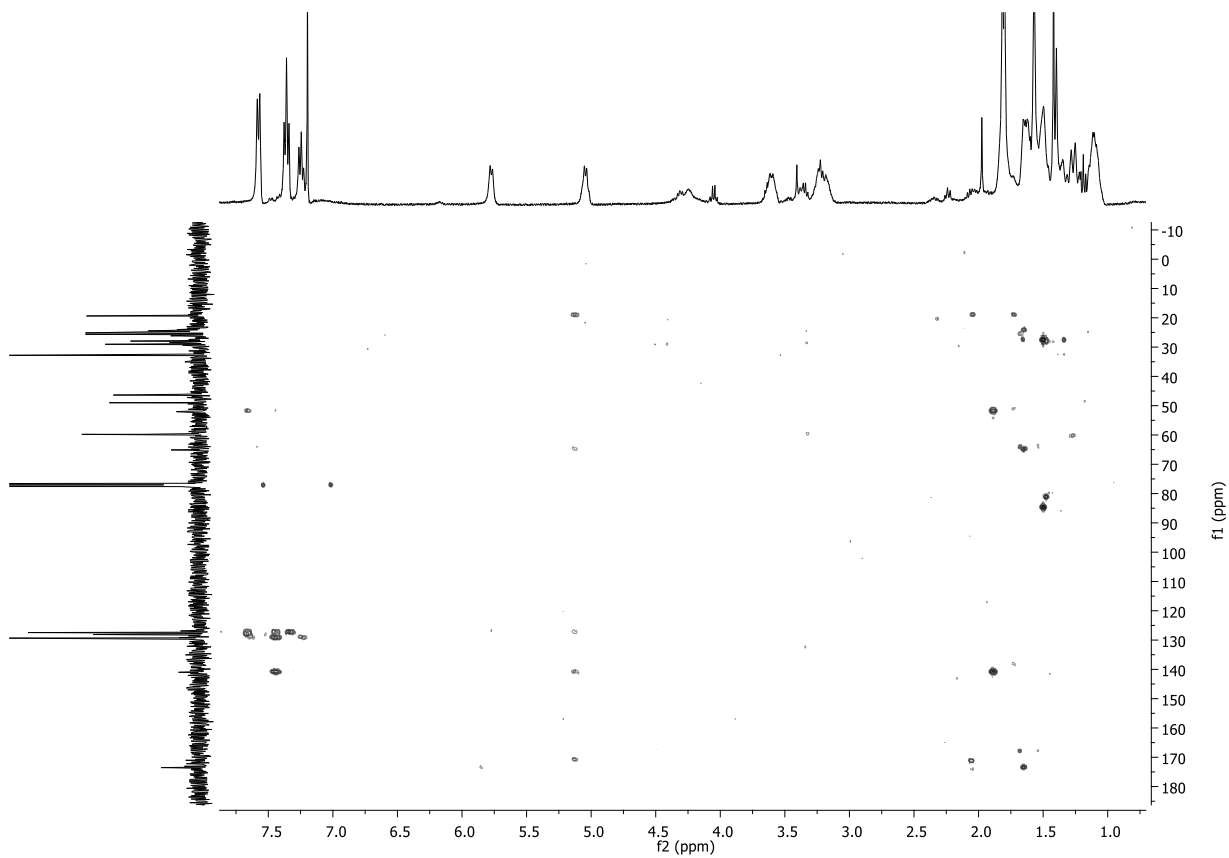
FIGURE 32: 400 MHz HMBC spectra in CDCl$_3$ of compound **69**.
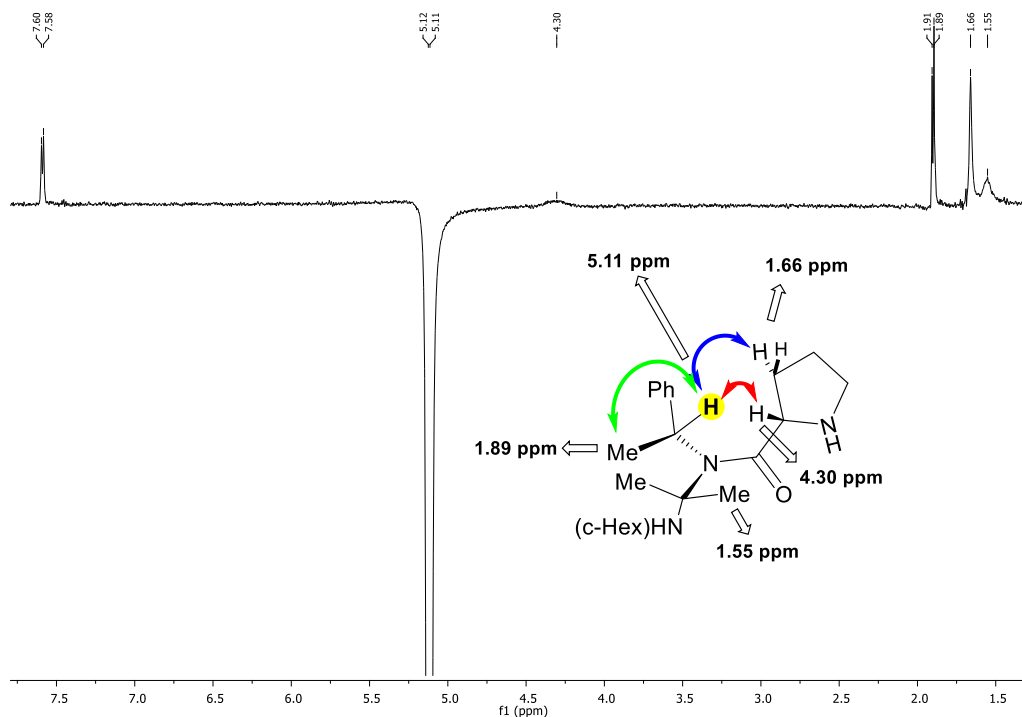
FIGURE 33: 600 MHz NOESY spectra in CDCl₃ of compound **69**. Signals of protons with NOE effect upon irradiation of the α-H of (S)-methyl-benzylamine at 5.10 ppm.
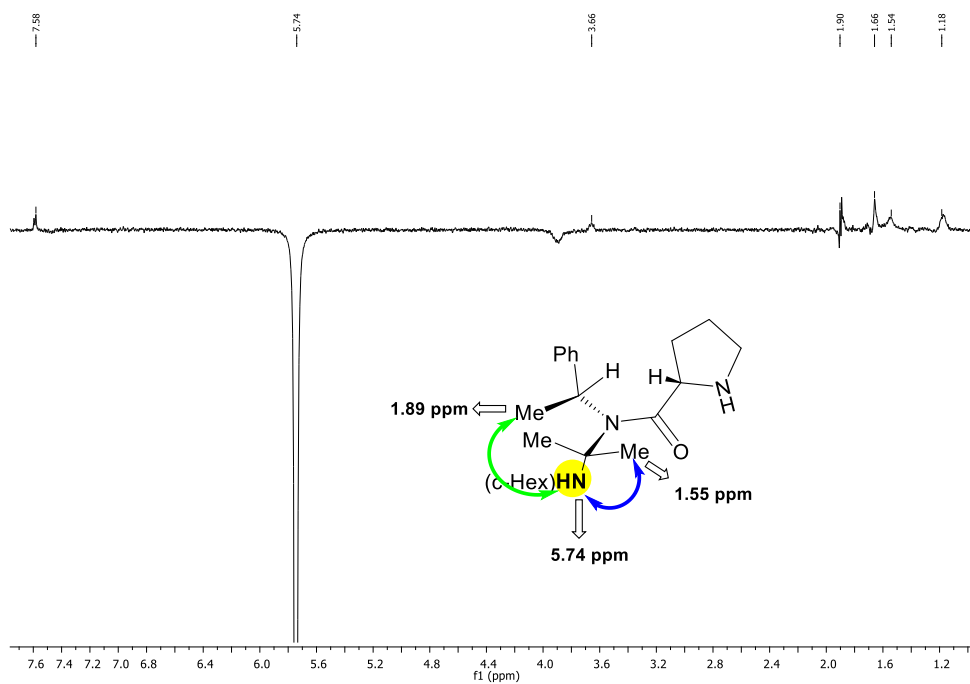
FIGURE 34: 600 MHz NOESY spectra in CDCl₃ of compound **69**. Signals of protons with NOE effect upon irradiation of the NH of c-Hex at 5.74 ppm.
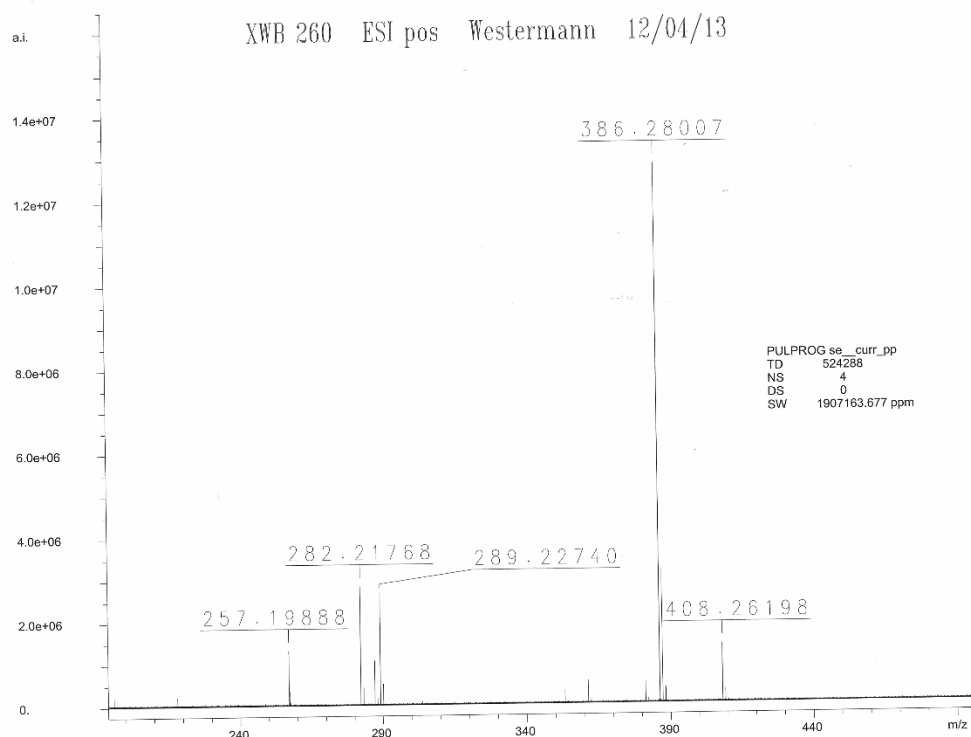
FIGURE 35: HRMS (ESI-FT-ICR) m/z: of compound **69**.
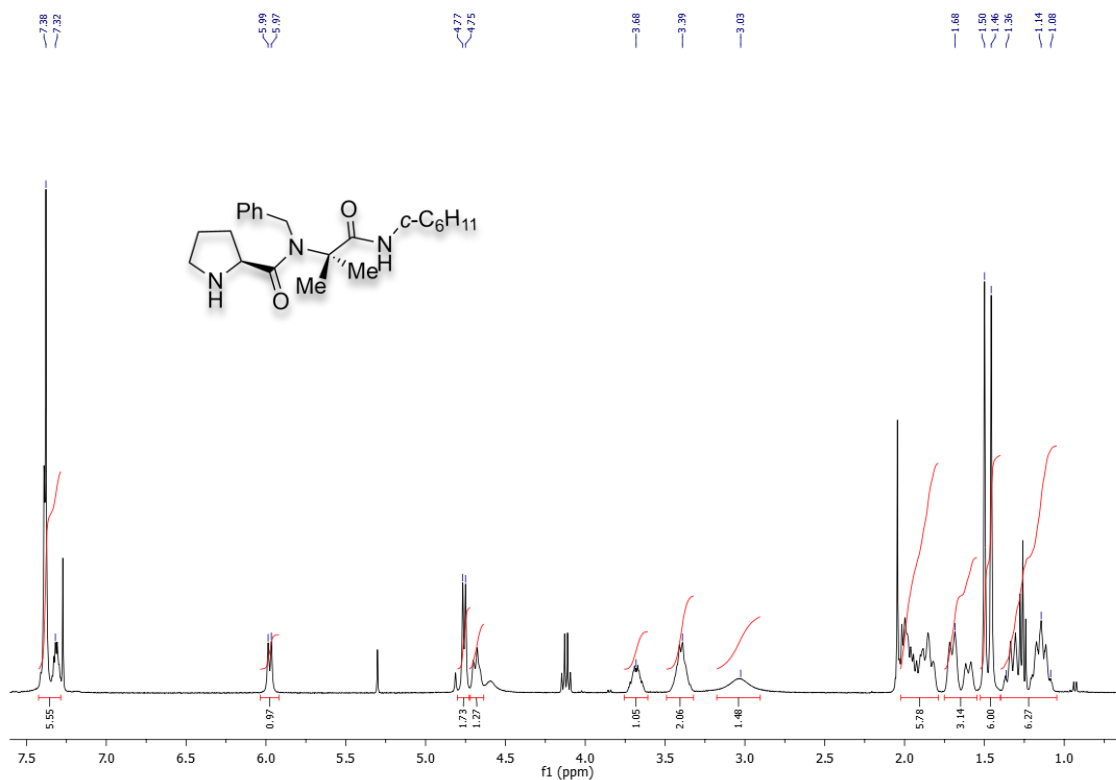
FIGURE 36: 400 MHz ^{1}H NMR spectra in CDCl$_3$ of compound **70**.
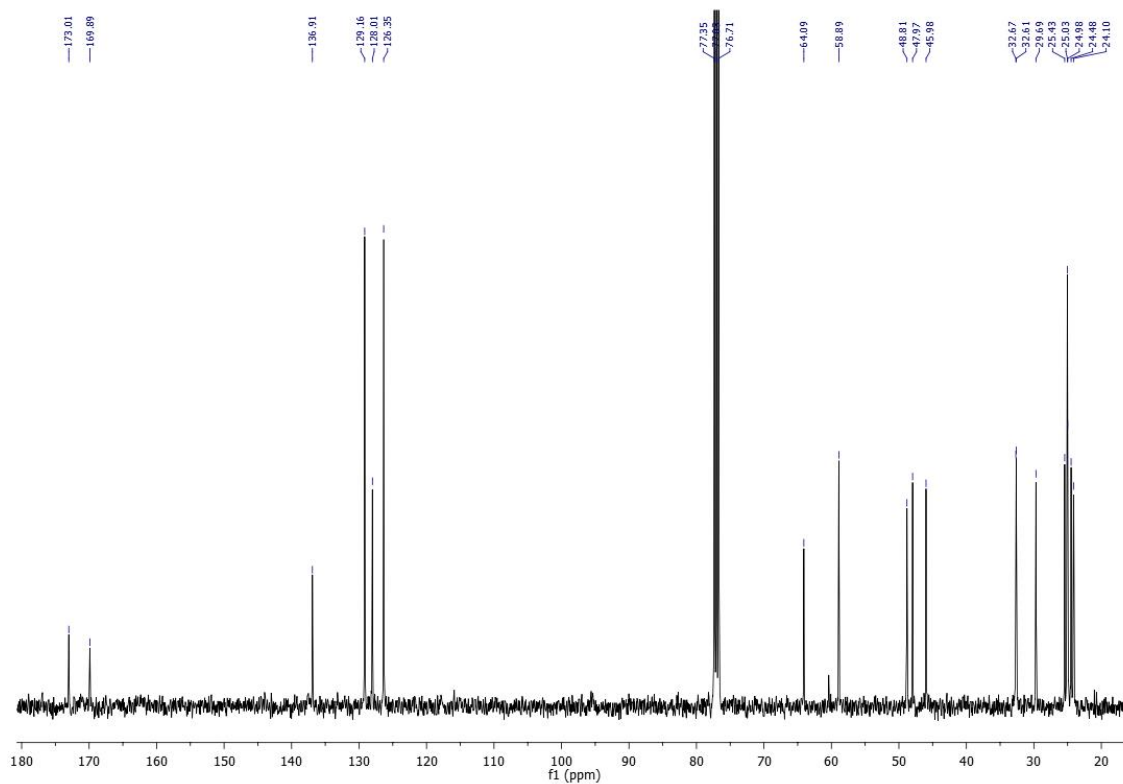
FIGURE 37: 100 MHz ^{13}C NMR spectra in CDCl$_3$ of compound **70**.
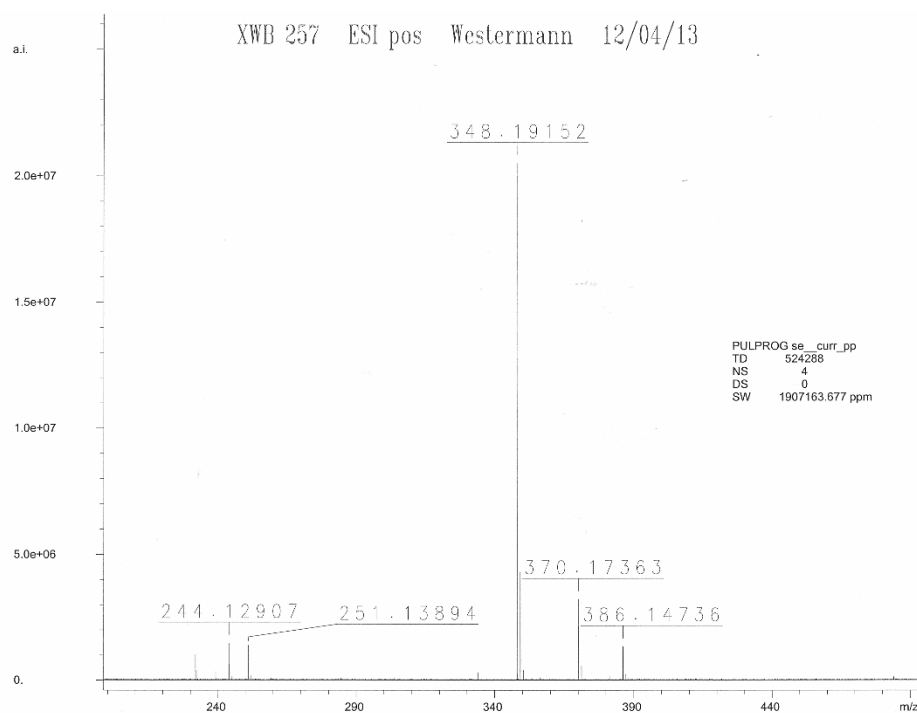
FIGURE 38: HRMS (ESI-FT-ICR) m/z: of compound **70**.
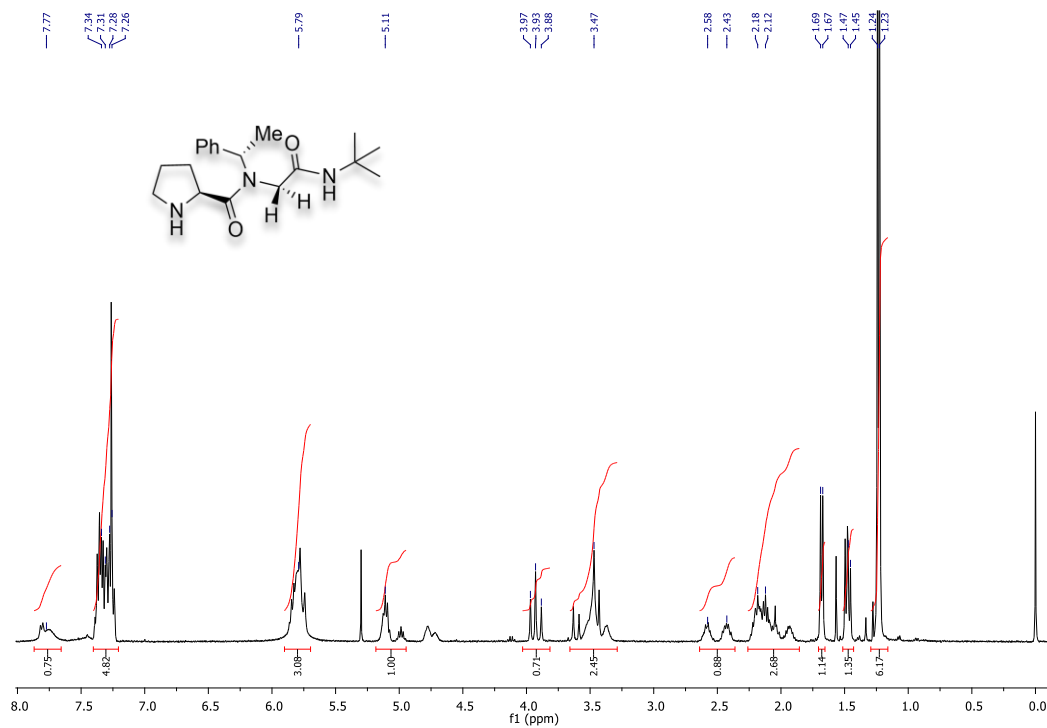
FIGURE 39: 400 MHz ^{1}H NMR spectra in CDCl$_3$ of compound **71**.
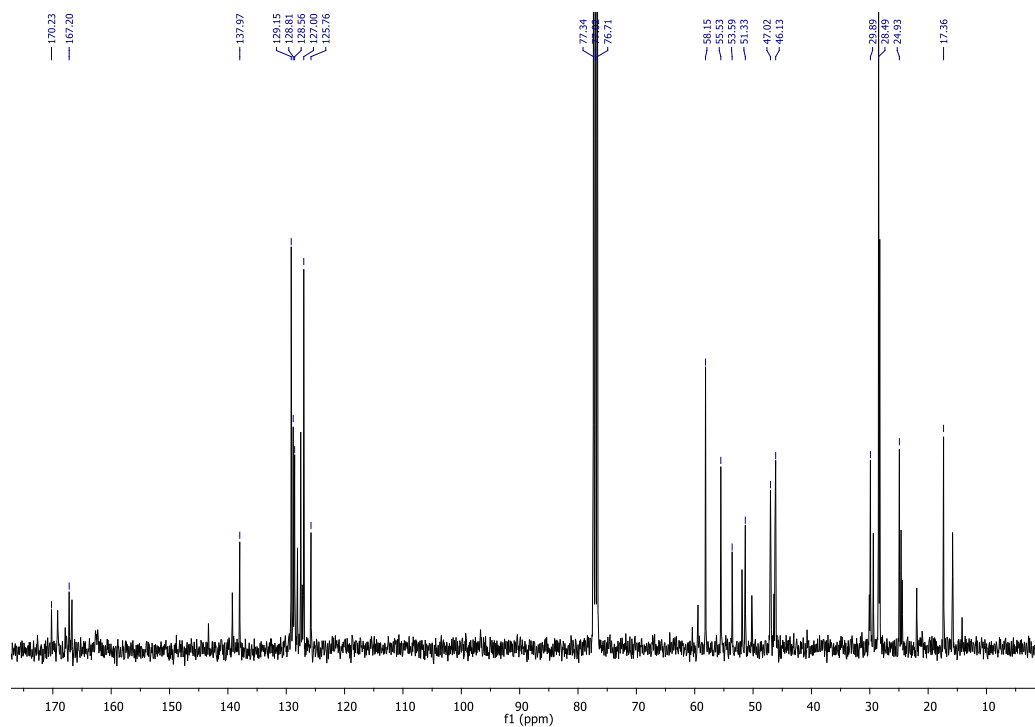
FIGURE 40: 100 MHz ^{13}C NMR spectra in CDCl$_3$ of compound **71**.
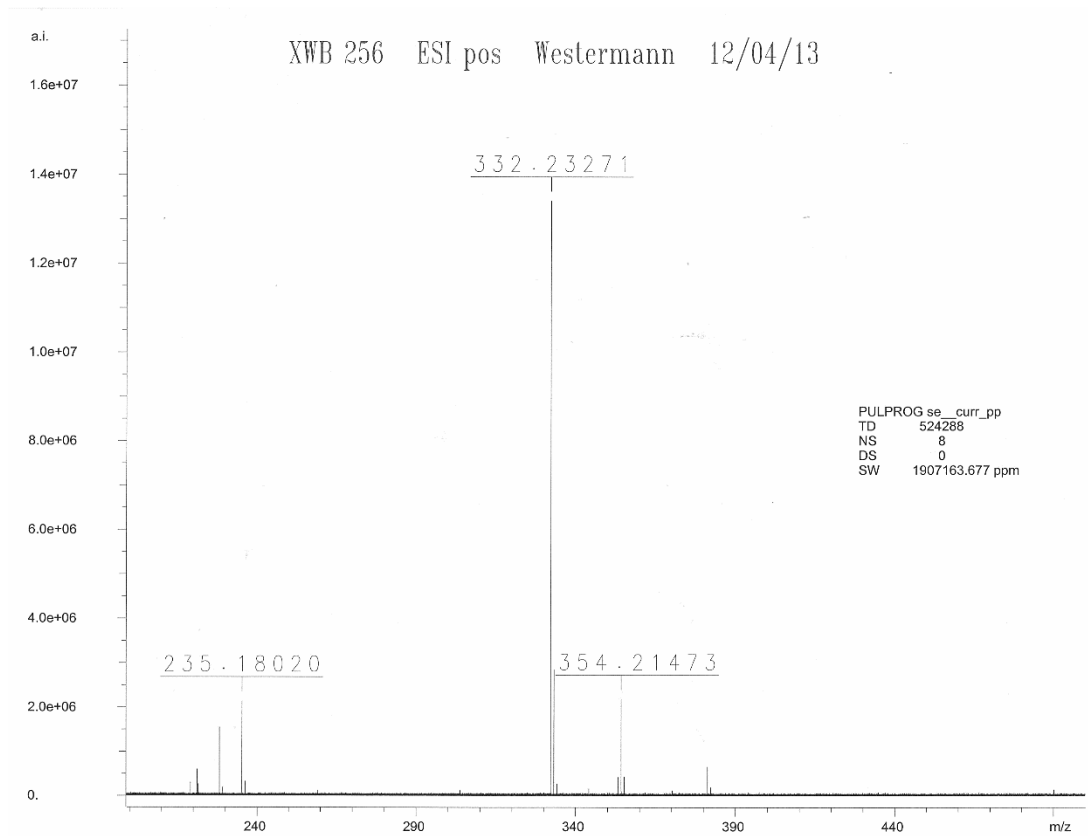
FIGURE 41:HRMS (ESI-FT-ICR) m/z: of compound **71**.
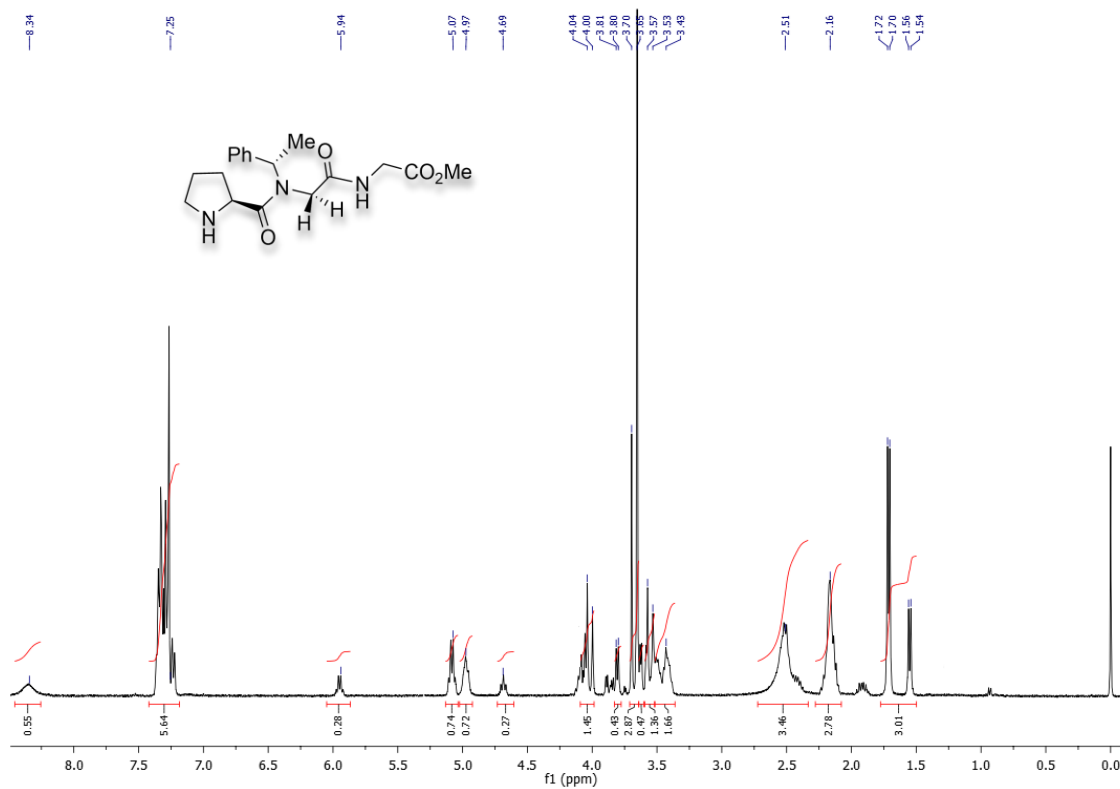
FIGURE 42: 400 MHz ^{1}H NMR spectra in CDCl$_3$ of compound **72**.
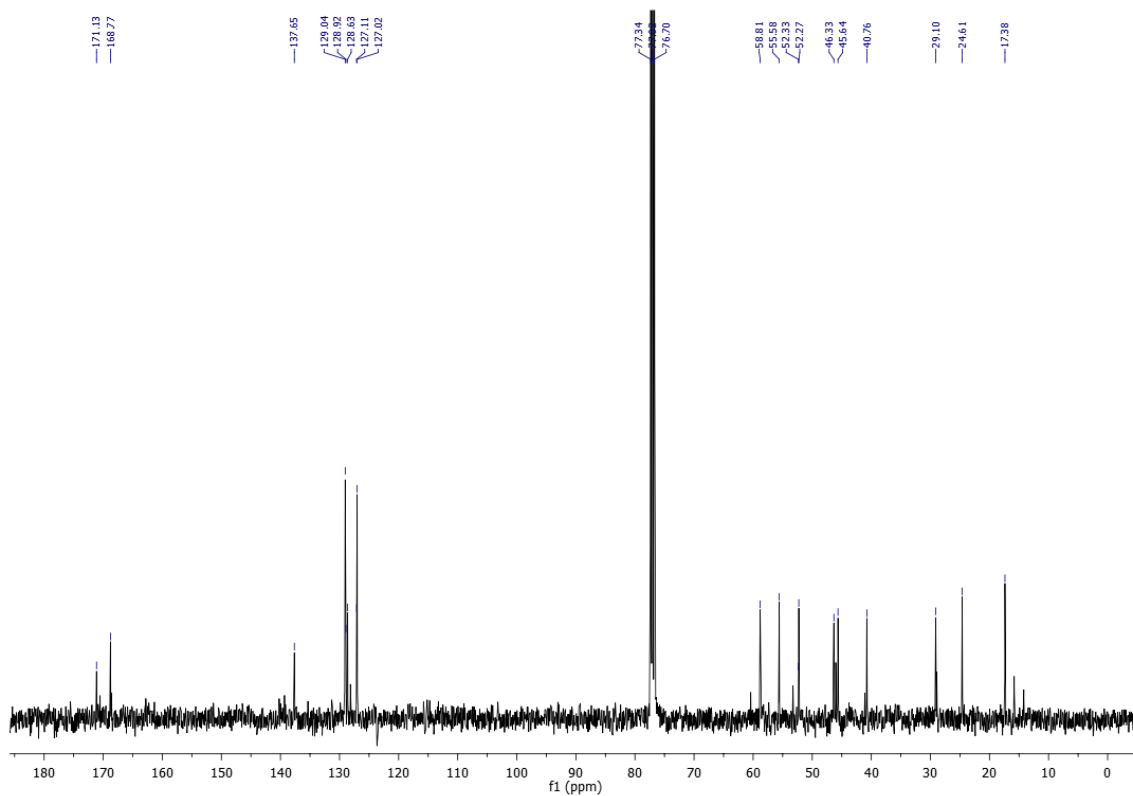
FIGURE 43: 100 MHz ^{13}C NMR spectra in CDCl$_3$ of compound **72**.
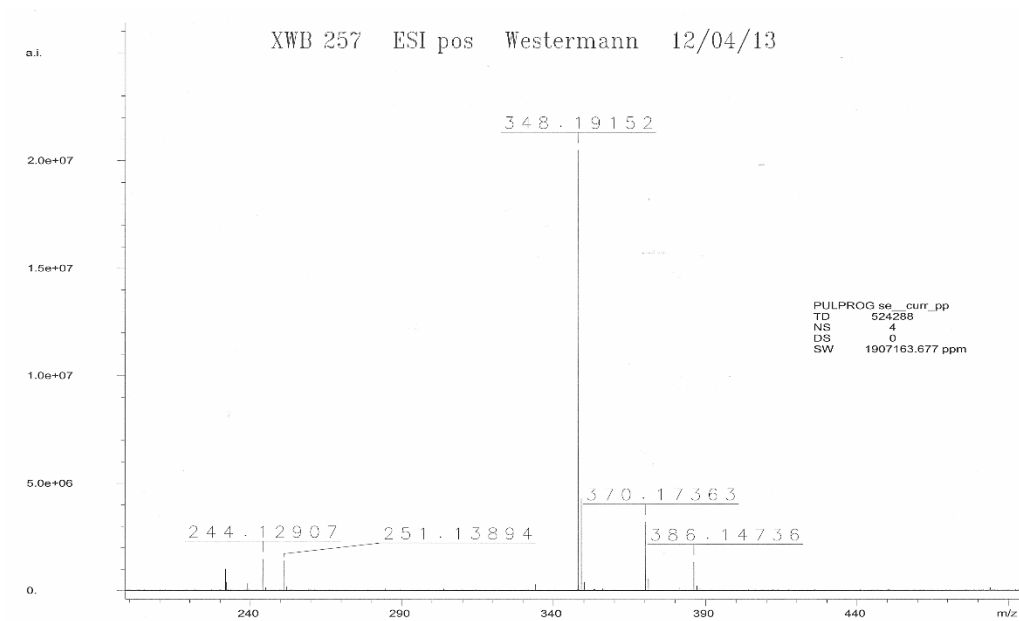
FIGURE 44: HRMS (ESI-FT-ICR) m/z: of compound **72**.
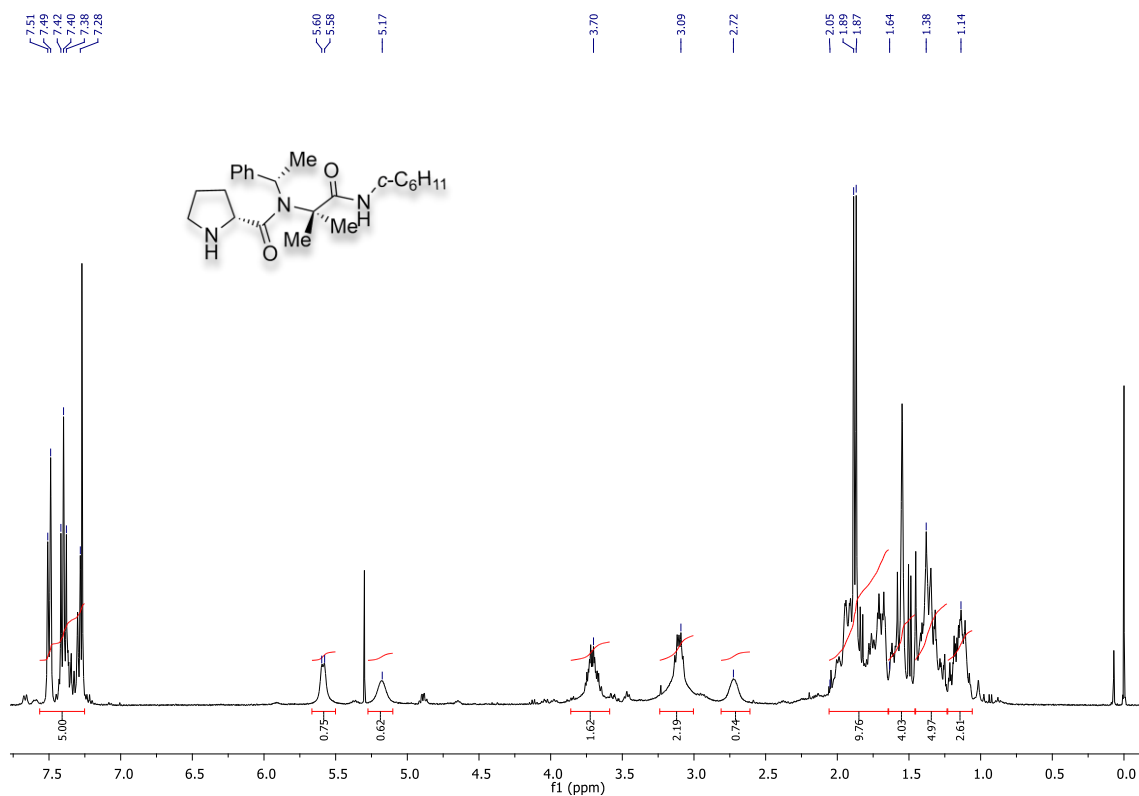
FIGURE 45: 400 MHz ^{1}H NMR spectra in CDCl$_3$ of compound **73**.
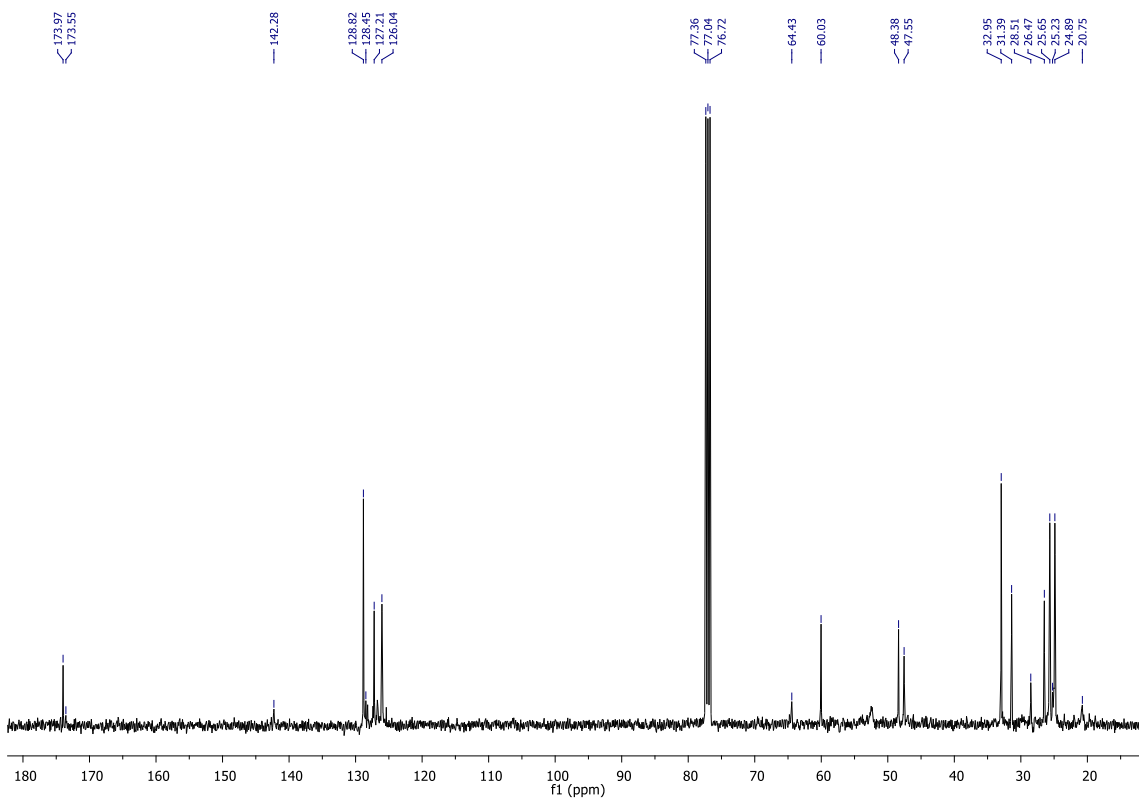
FIGURE 46: 100 MHz ^{13}C NMR spectra in CDCl$_3$ of compound **73**.
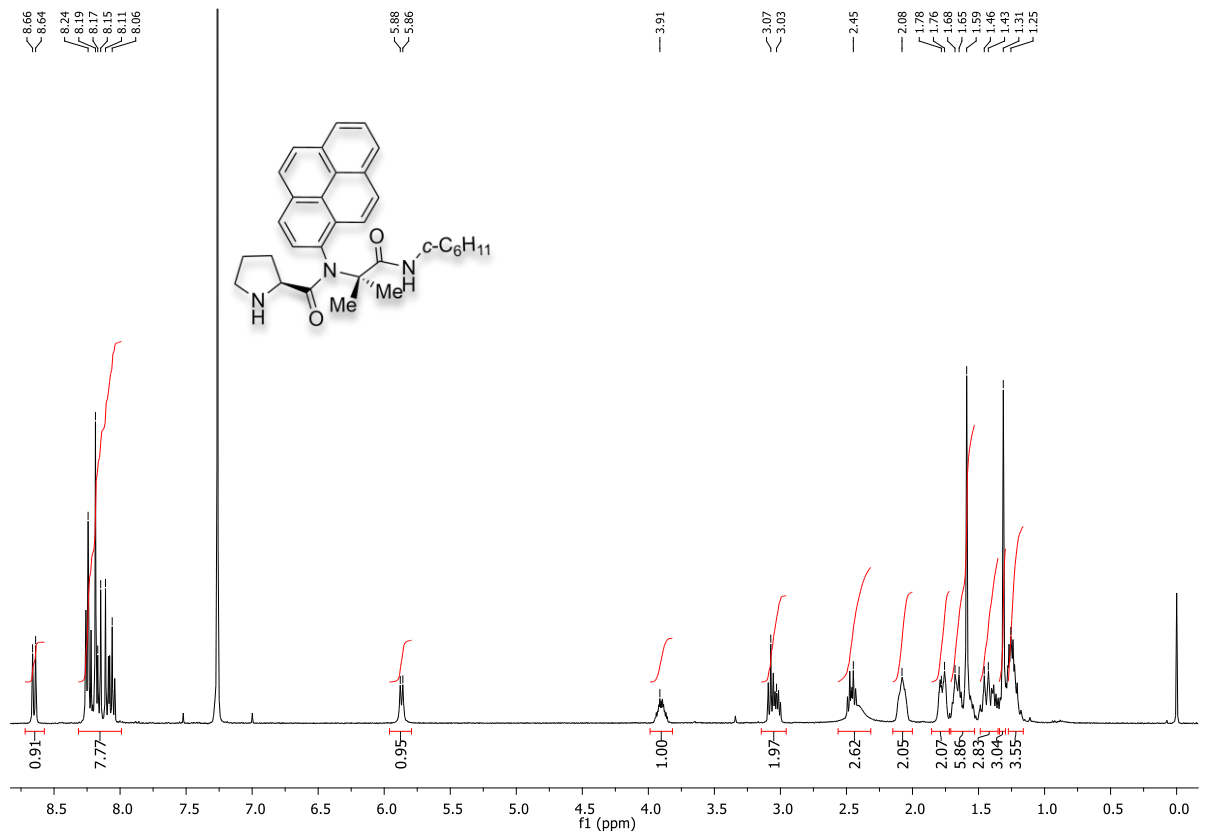
FIGURE 47: 400 MHz ^{1}H NMR spectra in CDCl$_3$ of compound **74**.
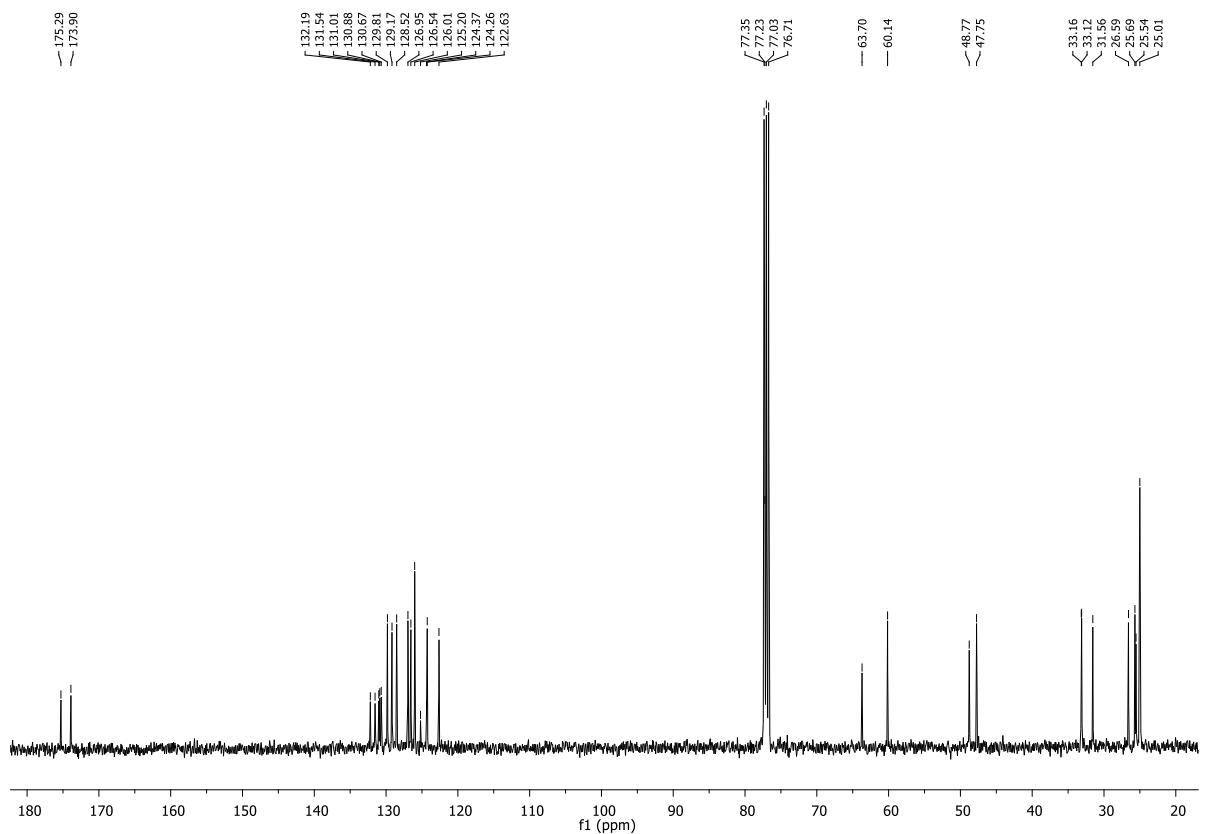
FIGURE 48: 100 MHz ^{13}C NMR spectra in CDCl$_3$ of compound **74**.

186
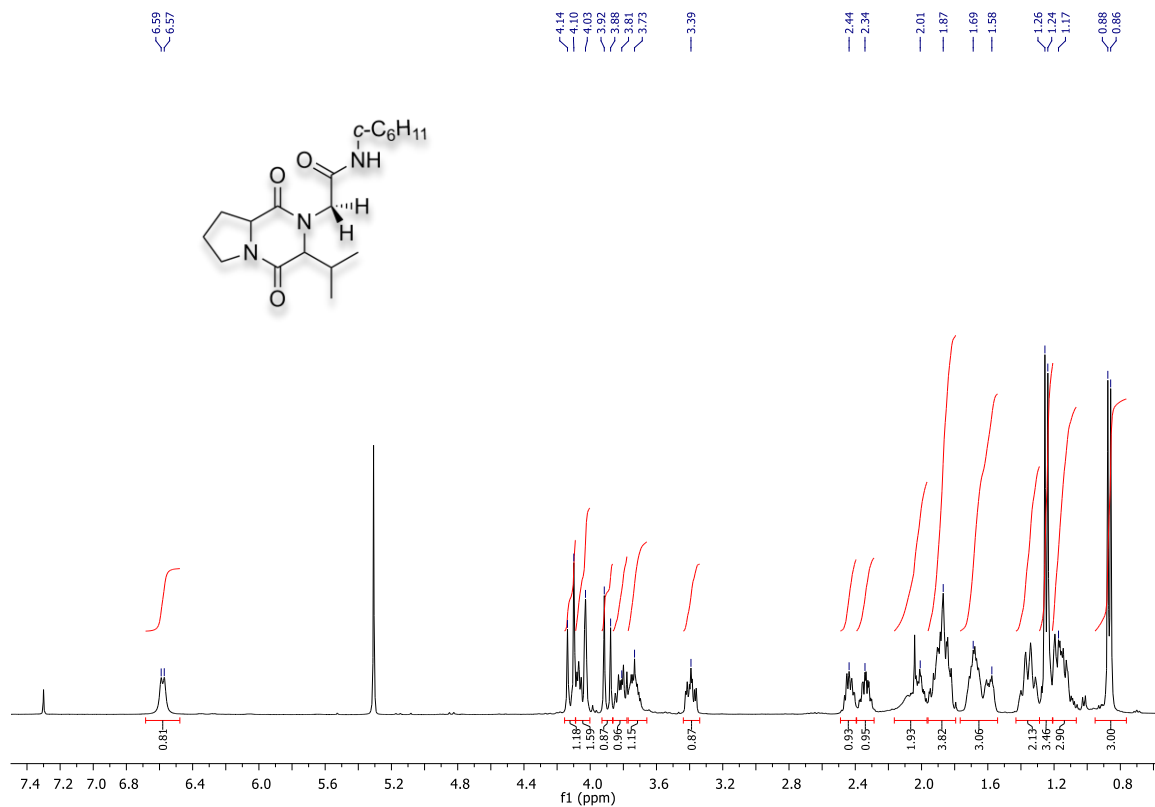
FIGURE 49: 400 MHz ^{1}H NMR spectra in CDCl$_3$ of compound **75**.
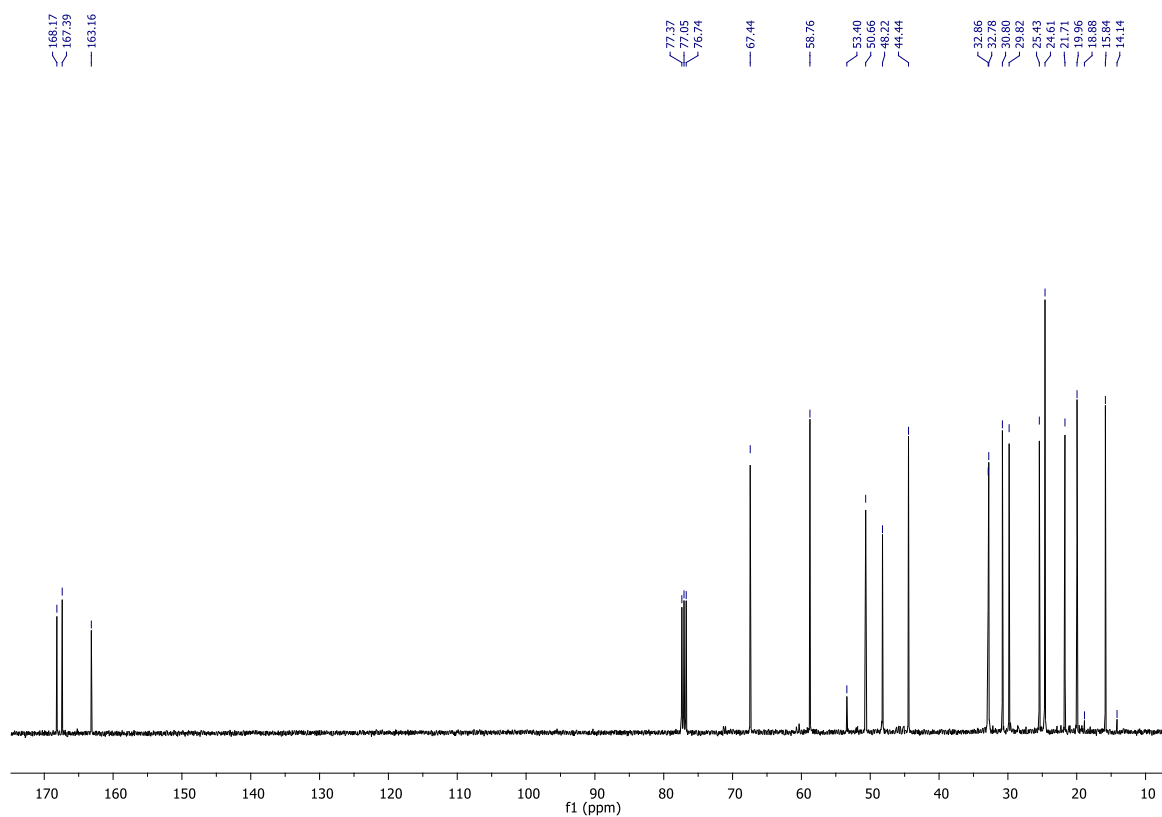
FIGURE 50: 100 MHz ^{13}C NMR spectra in CDCl$_3$ of compound **75**.
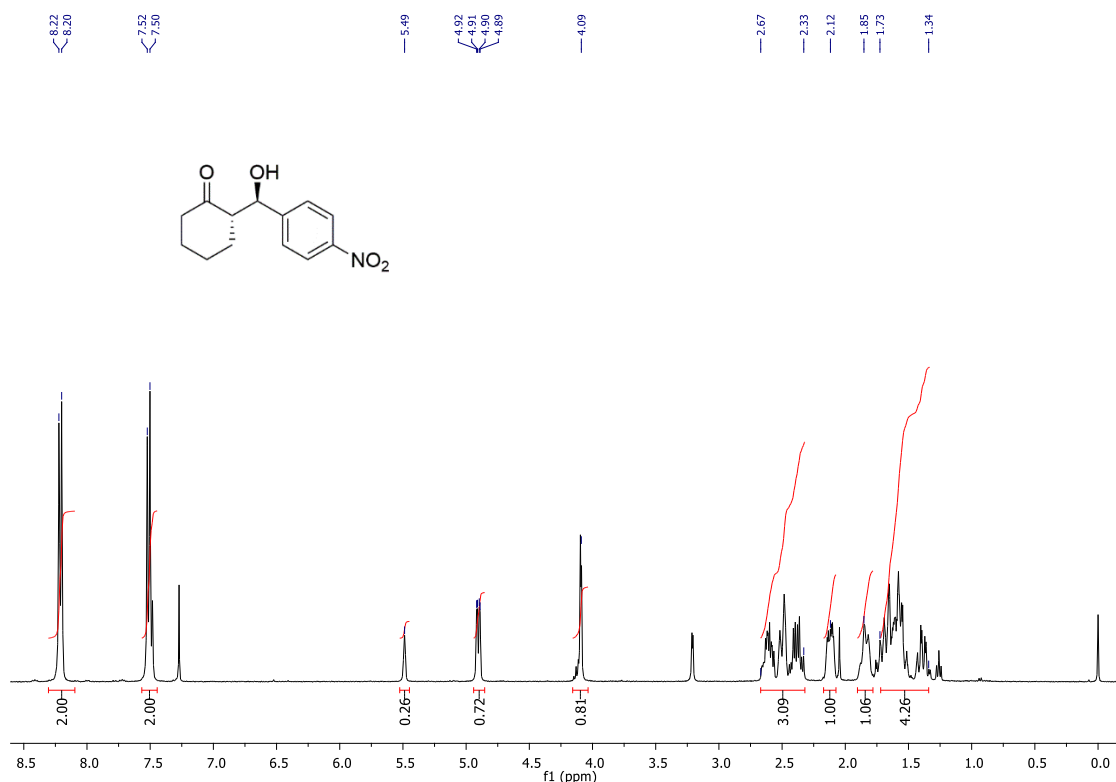
FIGURE 51: 400 MHz ^{1}H NMR spectra in CDCl$_3$ of (S)-2-[(R)-Hydroxy(4-nitrophenyl)methyl]cyclohexanone (**20**).
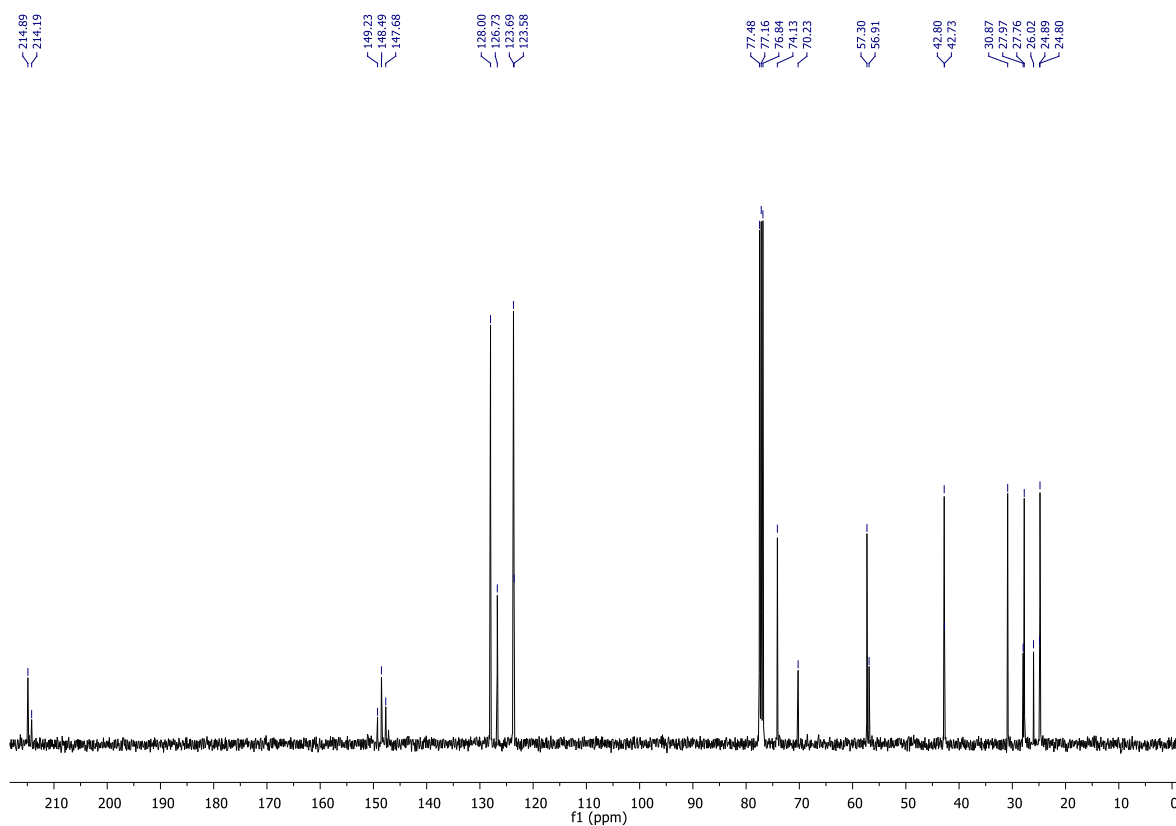
FIGURE 52: 100 MHz ^{13}C NMR spectra in CDCl$_3$ of (S)-2-[(R)-Hydroxy(4-nitrophenyl)methyl]cyclohexanone (**20**).
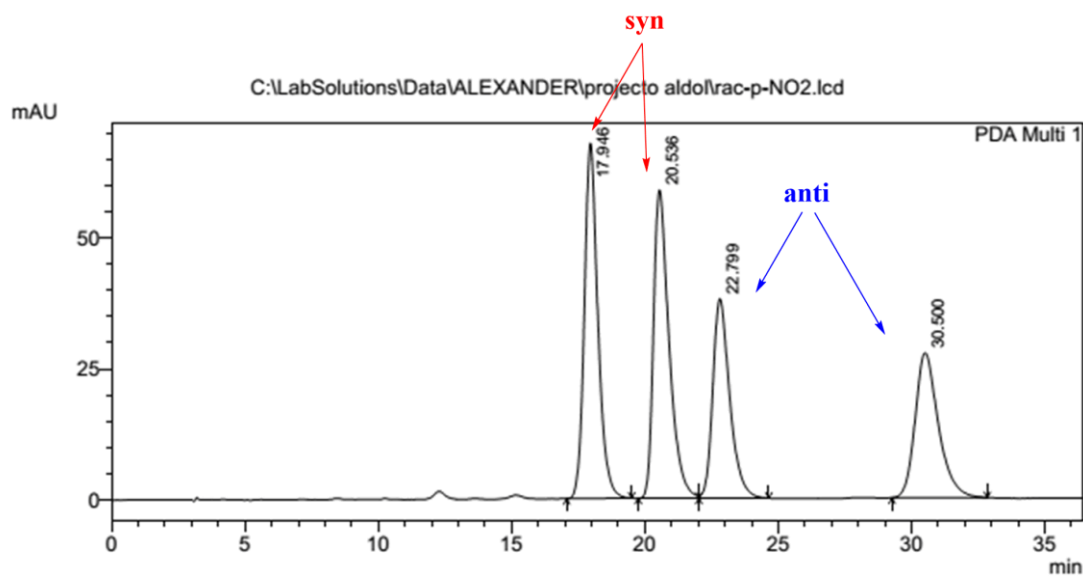
FIGURE 53: Chiral HPLC of racemic of compound **20**. Chiralpak AD-H, n-hexane/i-PrOH 90:10, 25°C at 1 ml/min, UV detection at 254 nm.
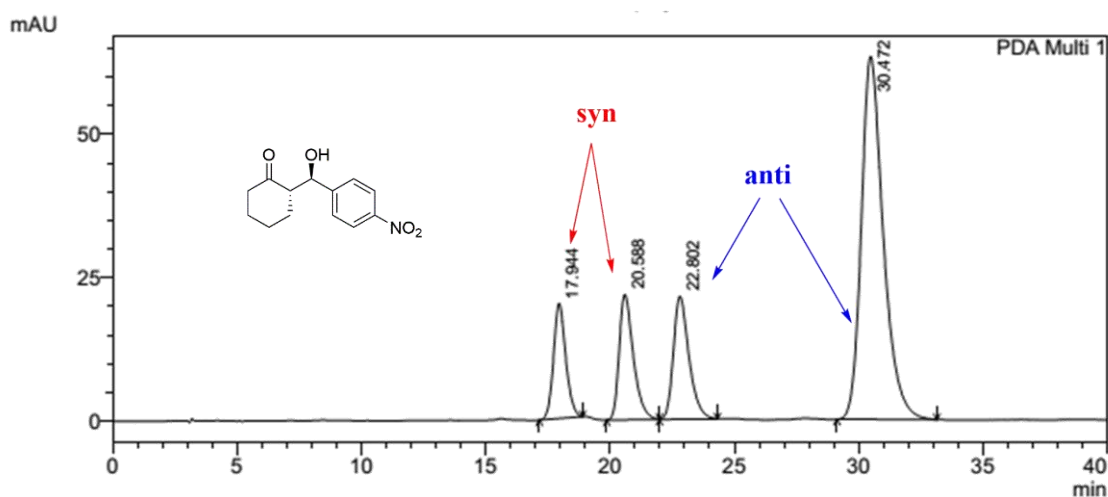
FIGURE 54: Chiral HPLC of (S)-2-[(R)-Hydroxy(4-nitrophenyl) methyl]cyclohexanone (**20**) obtained by Aldol reaction catalyzed by **64**.
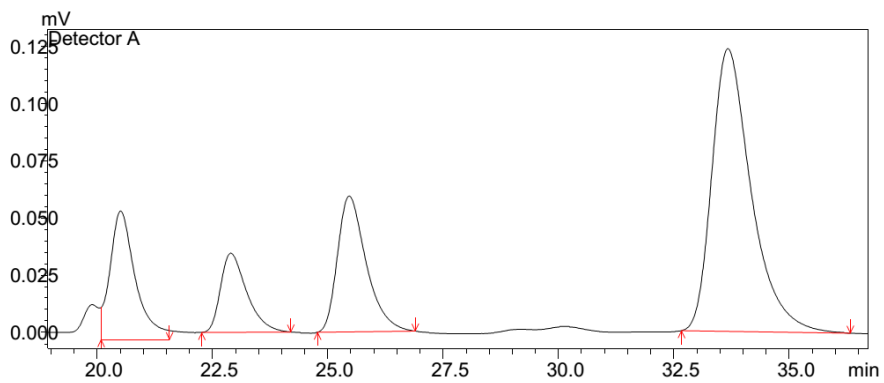
catalyzed by **61**.
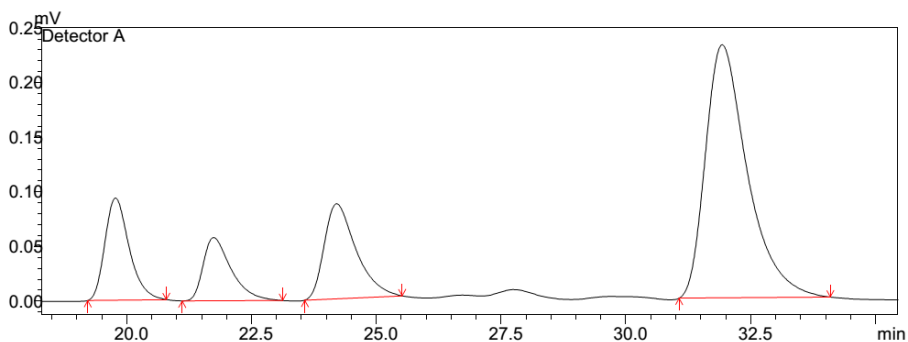
catalyzed by **63**.
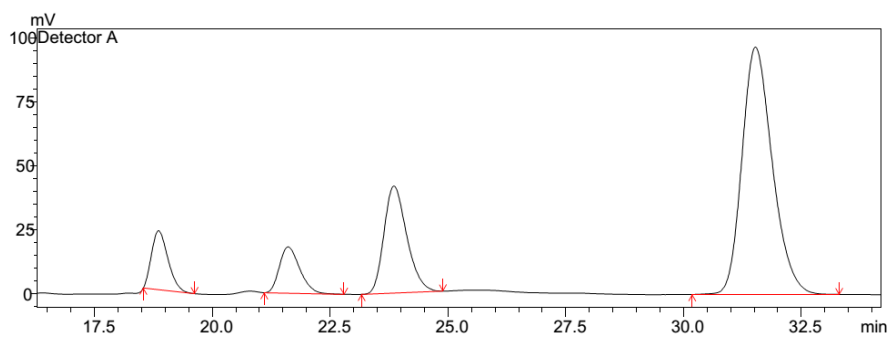
catalyzed by **64**.
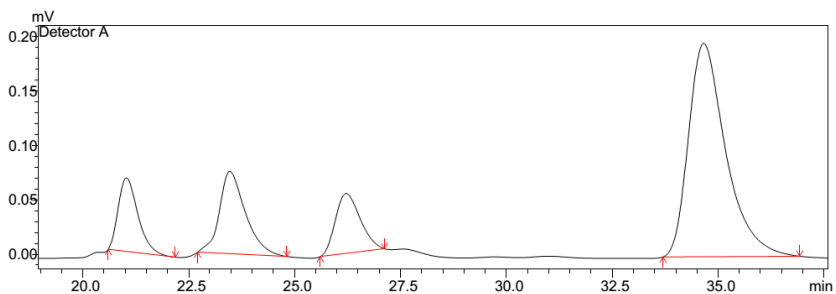
catalyzed by **65**.
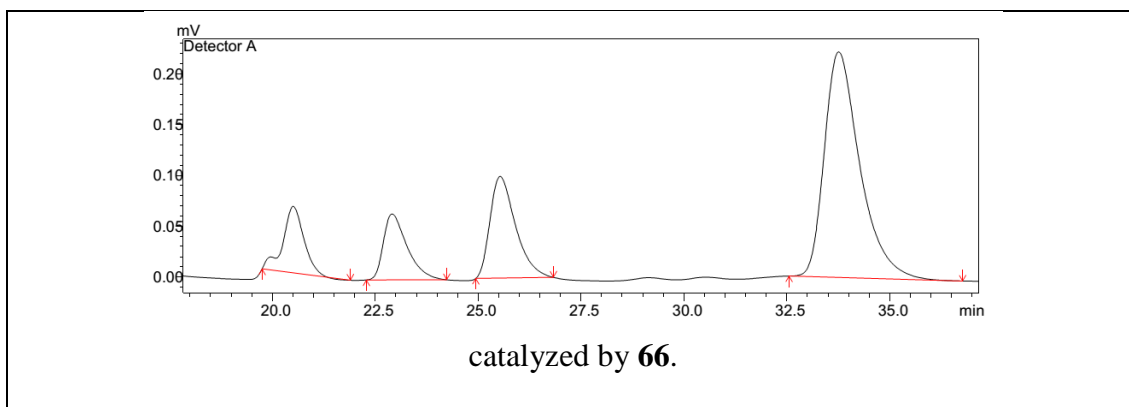
catalyzed by **66**.

FIGURE 55: Chiral HPLC of (S)-2-[(R)-Hydroxy(4-nitrophenyl) methyl]cyclohexanone (**20**) obtained by Aldol reaction catalyzed by **61**, **63**, **64**, **65**, and **66**.
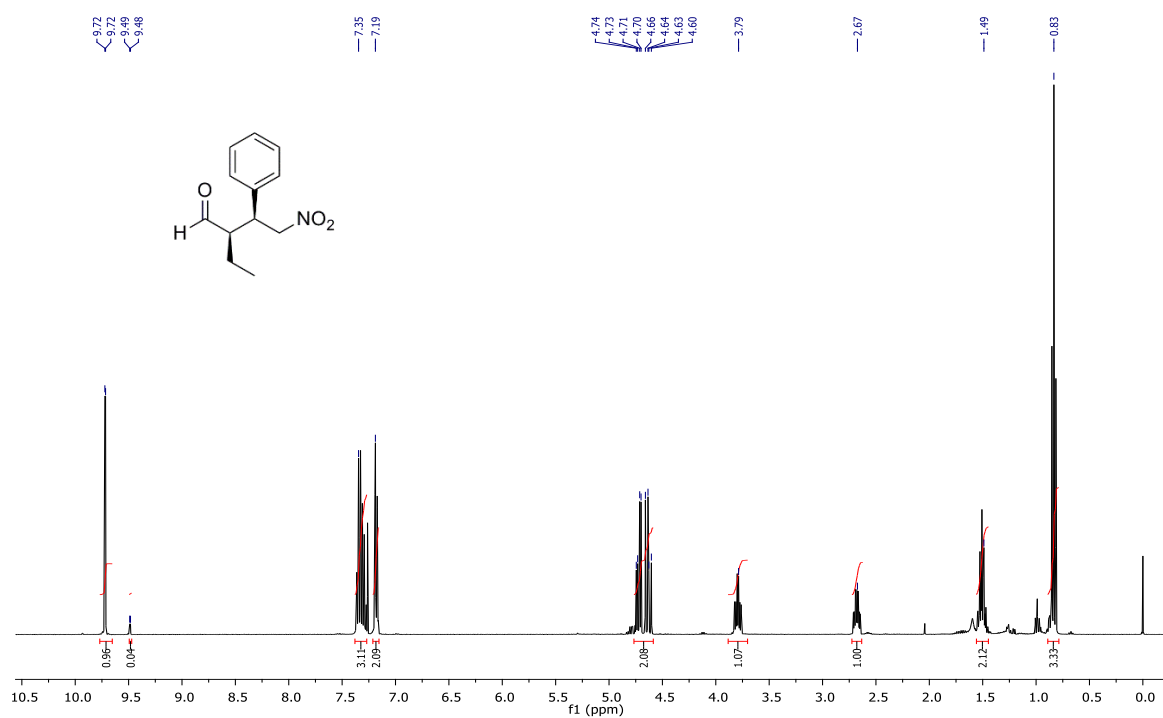
FIGURE 56: 400 MHz ^{1}H NMR spectra in CDCl$_3$ of (2R,3S)-2-Ethyl-4-nitro-3-phenylbutanal (**78**).
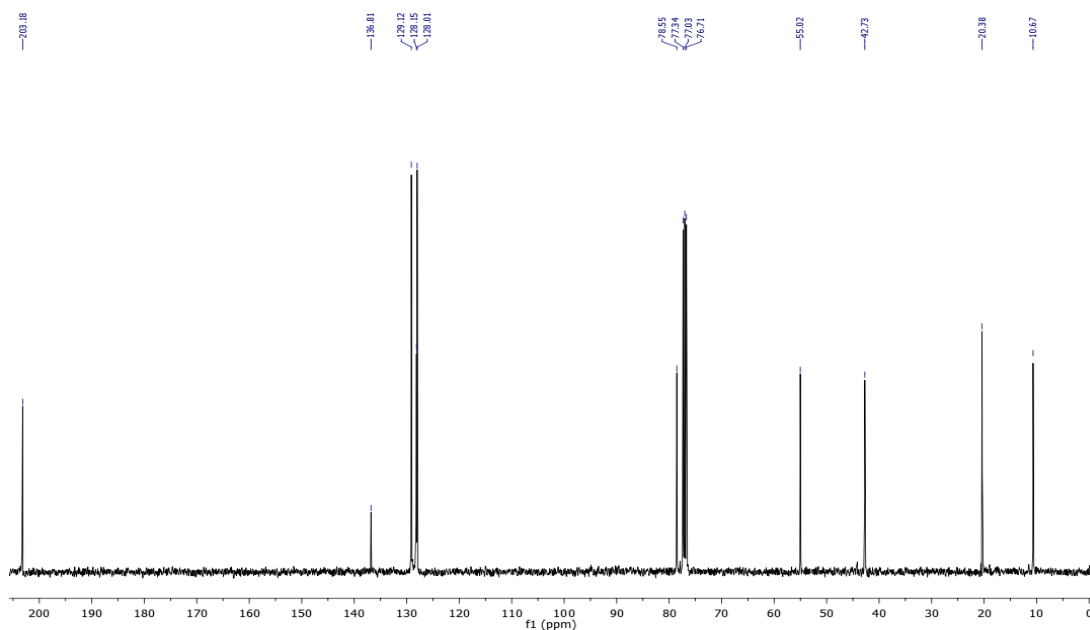
FIGURE 57: 100 MHz ^{13}C NMR spectra in CDCl$_3$ of (2R,3S)-2-Ethyl-4-nitro-3-phenylbutanal (**78**).

Peak#	Ret. Time	Area	Height	Area %	Height %
1	23.903	31729922	993615	39.711	42.944
2	25.177	7525316	246431	9.418	10.651
3	26.038	7885931	226631	9.869	9.795
4	27.877	32761417	847057	41.002	36.610
Total		79902586	2313734	100.000	100.000
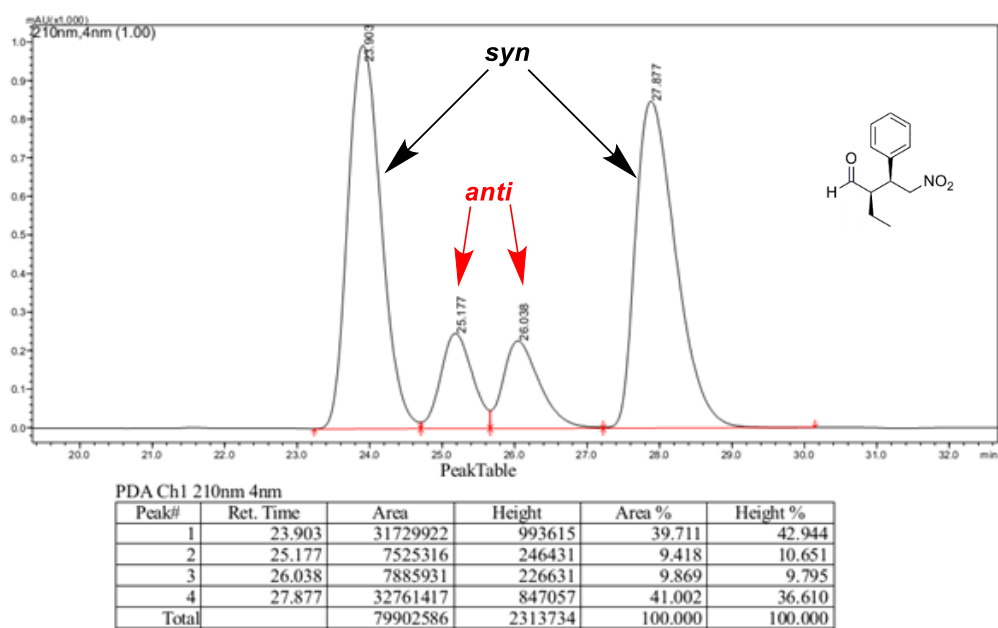
FIGURE 58: Chiral HPLC of racemic 2-ethyl-4-nitro-3-phenylbutanal (**78**). Chiralpak AD-H (*n*-hexane/i-PrOH 99:1), 25°C at 0.75 ml/min, UV detection at 210 nm.
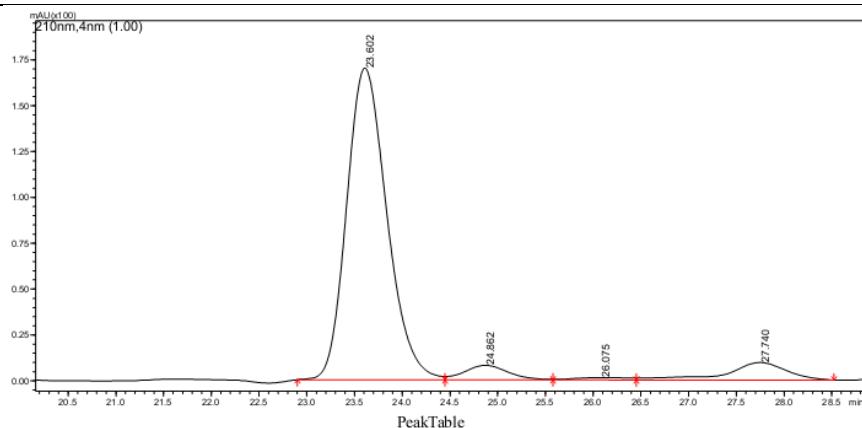
PDA Ch1 210nm 4nm

Peak#	Ret. Time	Area	Height	Area %	Height %
1	23.602	4975837	169890	87.373	90.083
2	24.862	250801	7918	4.404	4.198
3	26.075	49104	1242	0.862	0.659
4	27.740	419175	9542	7.361	5.060
Total		5694917	188592	100.000	100.000

catalyzed by **61**.
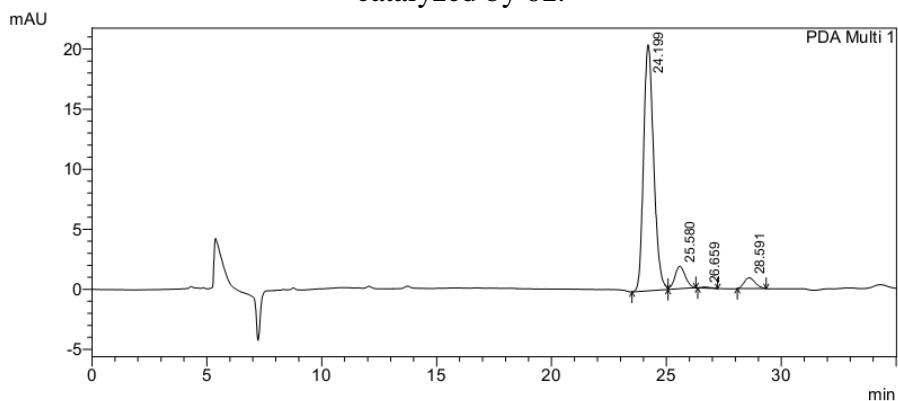
1 PDA Multi 1/254nm 4nm

PeakTable

PDA Ch1 254nm 4nm

Peak#	Ret. Time	Area	Height	Area %	Height %
1	24.199	627694	20498	87.329	87.767
2	25.580	59254	1881	8.244	8.055
3	26.659	1791	80	0.249	0.341
4	28.591	30027	896	4.178	3.837
Total		718766	23355	100.000	100.000

.

catalyzed by **62**
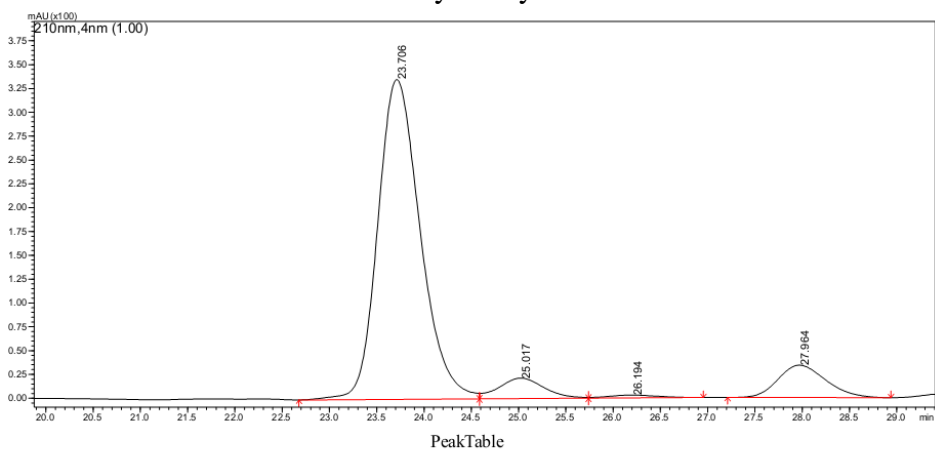
PDA Ch1 210nm 4nm

Peak#	Ret. Time	Area	Height	Area %	Height %
1	23.706	10467968	335721	83.853	85.197
2	25.017	714631	21526	5.725	5.463
3	26.194	107971	2893	0.865	0.734
4	27.964	1193157	33916	9.558	8.607
Total		12483728	394055	100.000	100.000

catalyzed by **63**.
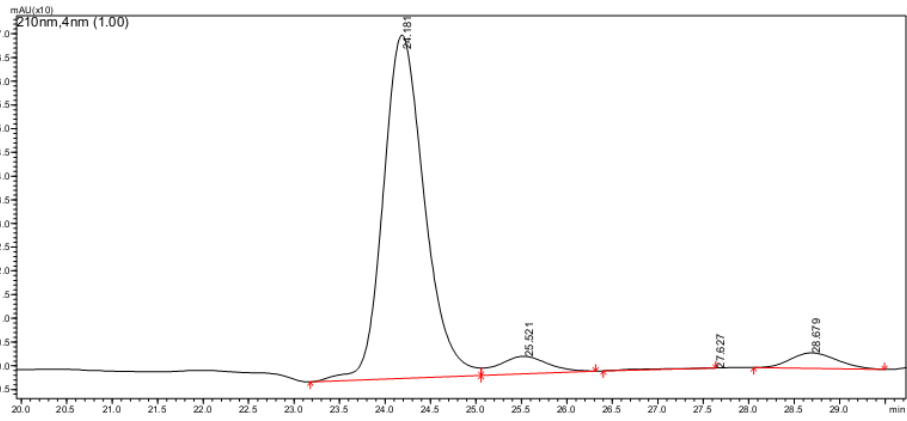
PDA Ch1 210nm 4nm

Peak#	Ret. Time	Area	Height	Area %	Height %
1	24.181	2281452	72408	89.684	91.208
2	25.521	138860	3698	5.459	4.658
3	27.627	5364	-2	0.211	-0.003
4	28.679	118211	3284	4.647	4.137
Total		2543887	79388	100.000	100.000

catalyzed by **64**.
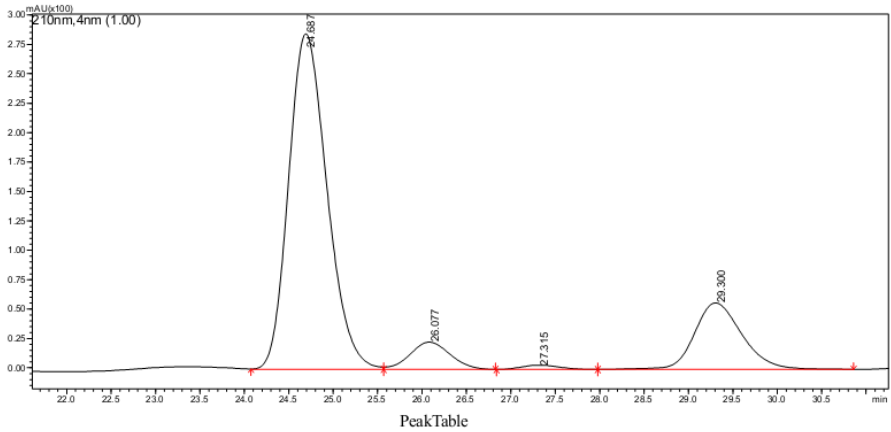
PDA Ch1 210nm 4nm

Peak#	Ret. Time	Area	Height	Area %	Height %
1	24.687	8569371	285137	74.436	77.366
2	26.077	727696	23209	6.321	6.297
3	27.315	107838	3693	0.937	1.002
4	29.300	2107442	56517	18.306	15.335
Total		11512346	368556	100.000	100.000

catalyzed by **65**.
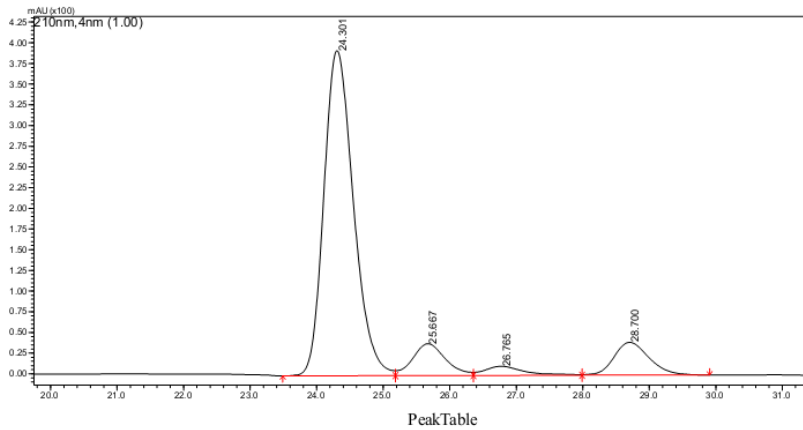
PDA Ch1 210nm 4nm

Peak#	Ret. Time	Area	Height	Area %	Height %
1	24.301	12155782	392787	79.021	81.498
2	25.667	1320551	38531	8.584	7.995
3	26.765	455923	11063	2.964	2.295
4	28.700	1450747	39581	9.431	8.212
Total		15383002	481962	100.000	100.000

catalyzed by **66**.

PDA Ch1 210nm 4nm
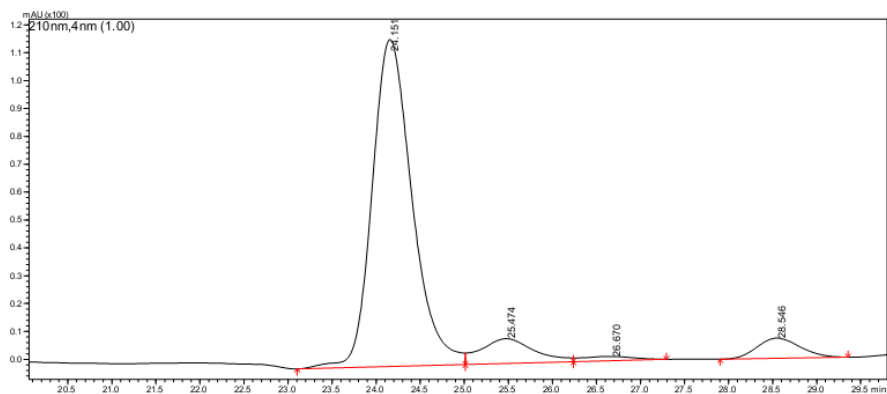
Peak#	Ret. Time	Area	Height	Area %	Height %
1	24.151	3699095	117335	84.408	86.867
2	25.474	372284	8930	8.495	6.611
3	26.670	64158	1573	1.464	1.165
4	28.546	246856	7236	5.633	5.357
Total		4382392	135074	100.000	100.000

catalyzed by **67**.

PDA Ch1 210nm 4nm
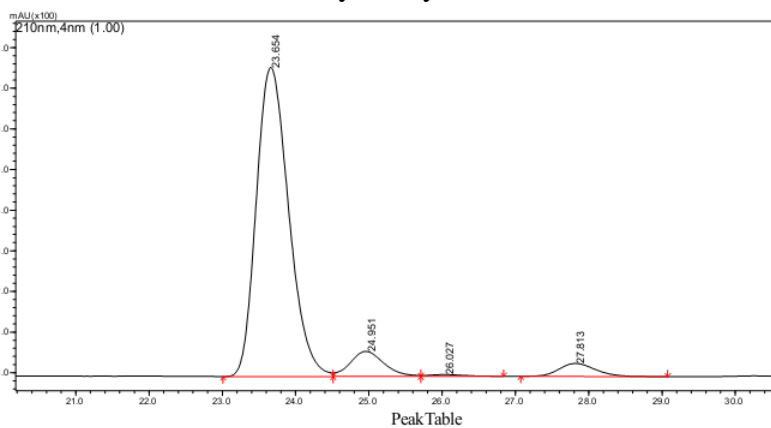
Peak#	Ret. Time	Area	Height	Area %	Height %
1	23.654	23374747	760950	87.896	88.590
2	24.951	1971992	61797	7.415	7.194
3	26.027	137931	4204	0.519	0.489
4	27.813	1109059	32001	4.170	3.726
Total		26593729	858953	100.000	100.000

catalyzed by **68**.
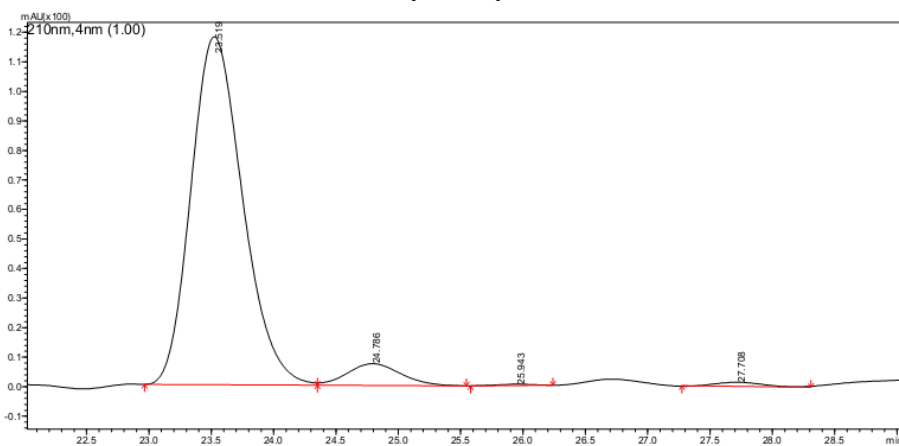
PDA Ch1 210nm 4nm

Peak#	Ret. Time	Area	Height	Area %	Height %
1	23.519	3396509	117779	92.755	92.756
2	24.786	220372	7378	6.018	5.810
3	25.943	8384	410	0.229	0.323
4	27.708	36556	1411	0.998	1.111
Total		3661821	126978	100.000	100.000

catalyzed by **69**.
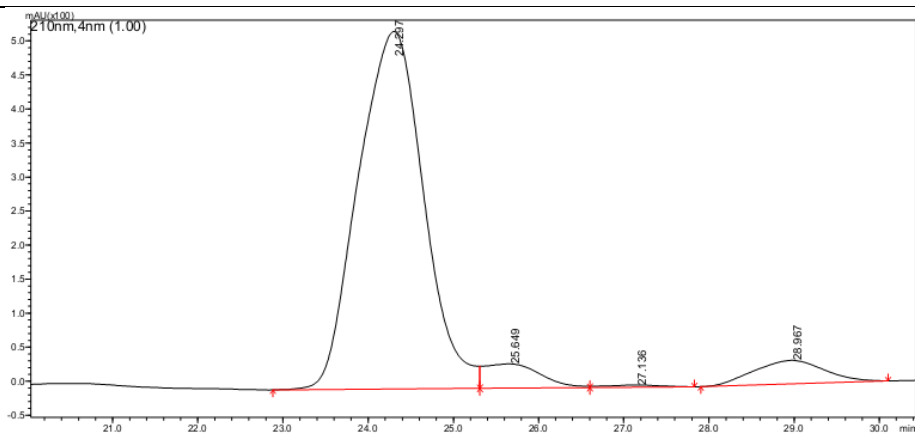
PDA Ch1 210nm 4nm

Peak#	Ret. Time	Area	Height	Area %	Height %
1	24.297	28027983	525330	88.204	87.773
2	25.649	1613206	35621	5.077	5.952
3	27.136	142504	3102	0.448	0.518
4	28.967	1992713	34455	6.271	5.757
Total		31776407	598508	100.000	100.000

catalyzed by **70**.
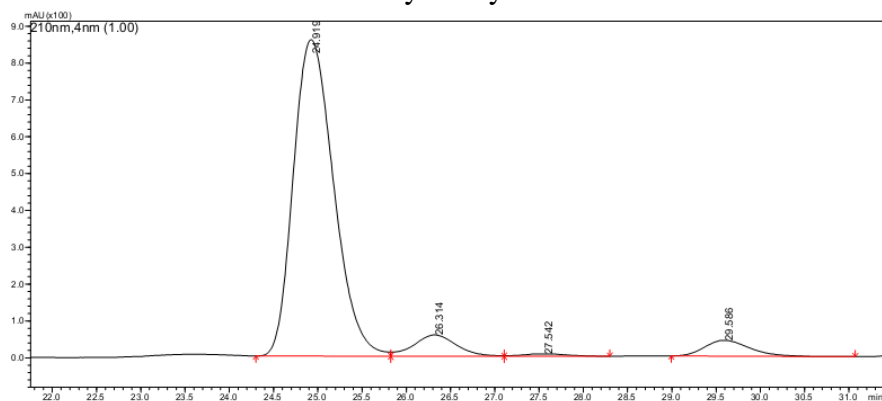
PDA Ch1 210nm 4nm

Peak#	Ret. Time	Area	Height	Area %	Height %
1	24.919	27238765	859558	88.195	88.922
2	26.314	1917226	57570	6.208	5.956
3	27.542	209353	6506	0.678	0.673
4	29.586	1519370	43014	4.919	4.450
Total		30884714	966648	100.000	100.000

catalyzed by **71**.
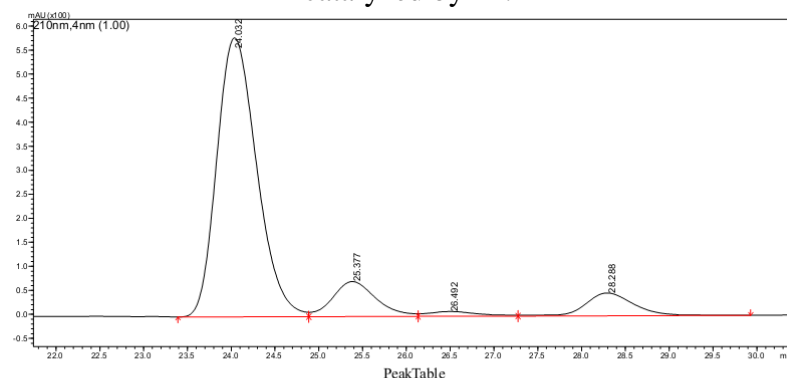
PDA Ch1 210nm 4nm

Peak#	Ret. Time	Area	Height	Area %	Height %
1	24.032	18360197	580493	79.613	81.697
2	25.377	2503139	72797	10.854	10.245
3	26.492	385554	9798	1.672	1.379
4	28.288	1812840	47453	7.861	6.678
Total		23061730	710542	100.000	100.000

catalyzed by **72**.

FIGURE 59: Chiral HPLC of 2-ethyl-4-nitro-3-phenylbutanal (**78**). For catalyst **61-72**. Chiralpak AD-H (*n*-hexane/i-PrOH 99:1), 25°C at 0.75 ml/min, UV detection at 210 nm.

196

PeakTable

PDA Ch1 210nm 4nm

Peak#	Ret. Time	Area	Height	Area %	Height %
1	28.689	743817	15506	37.584	45.497
2	32.532	212372	4013	10.731	11.774
3	38.713	822185	12768	41.544	37.465
4	71.812	200698	1794	10.141	5.264
Total		1979073	34081	100.000	100.000
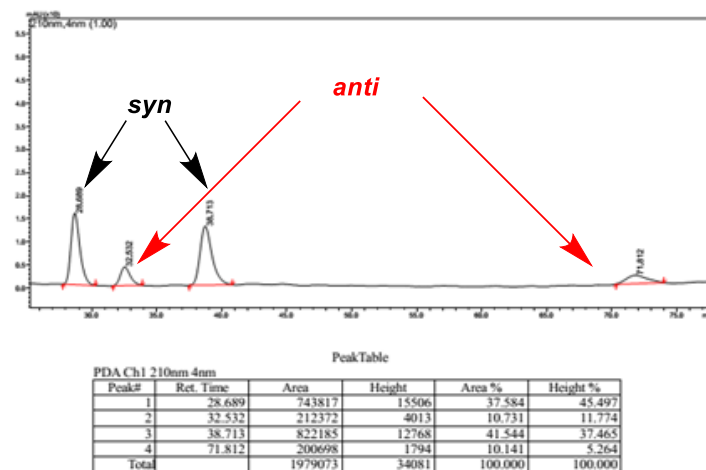
FIGURE 60: Chiral HPLC of racemic 2-ethyl-4-nitro-3-phenylbutanal (**78**). Chiralpak OD-H (n-hexane/i-PrOH 91:9), 25°C at 0.9 ml/min, UV detection at 210 nm.

PeakTable

PDA Ch1 210nm 4nm

Peak#	Ret. Time	Area	Height	Area %	Height %
1	28.566	15972256	319081	78.407	81.218
2	32.501	2843276	51761	13.958	13.175
3	38.810	1234871	19132	6.062	4.870
4	71.307	320538	2895	1.574	0.737
Total		20370941	392869	100.000	100.000

catalyzed by **73**.

PeakTable

PDA Ch1 210nm 4nm

Peak#	Ret. Time	Area	Height	Area %	Height %
1	26.711	536810	12108	7.249	10.648
2	29.960	112807	2187	1.523	1.924
3	35.842	5740647	90075	77.519	79.216
4	65.231	1015169	9338	13.708	8.213
Total		7405434	113708	100.000	100.000

catalyzed by **74**

FIGURE 61: Chiral HPLC of 2-ethyl-4-nitro-3-phenylbutanal (**78**) obtained by the 1,4-addition reaction catalyzed by catalyst **73** and **74**. Chiralpak OD-H (*n*-hexane/i-PrOH 91:9), 25 °C at 0.9 ml/min, UV detection at 210 nm.
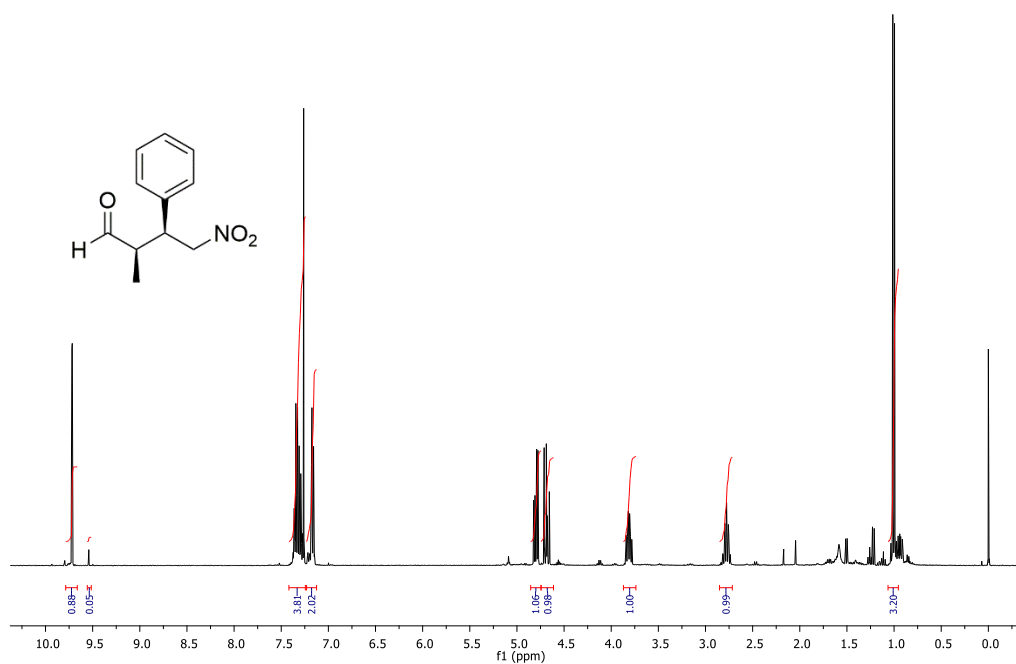
FIGURE 62: 400 MHz ^{1}H NMR spectra in CDCl$_3$ of (2R,3S)-2-Methyl-4-nitro-3-phenylbutanal (**23**).
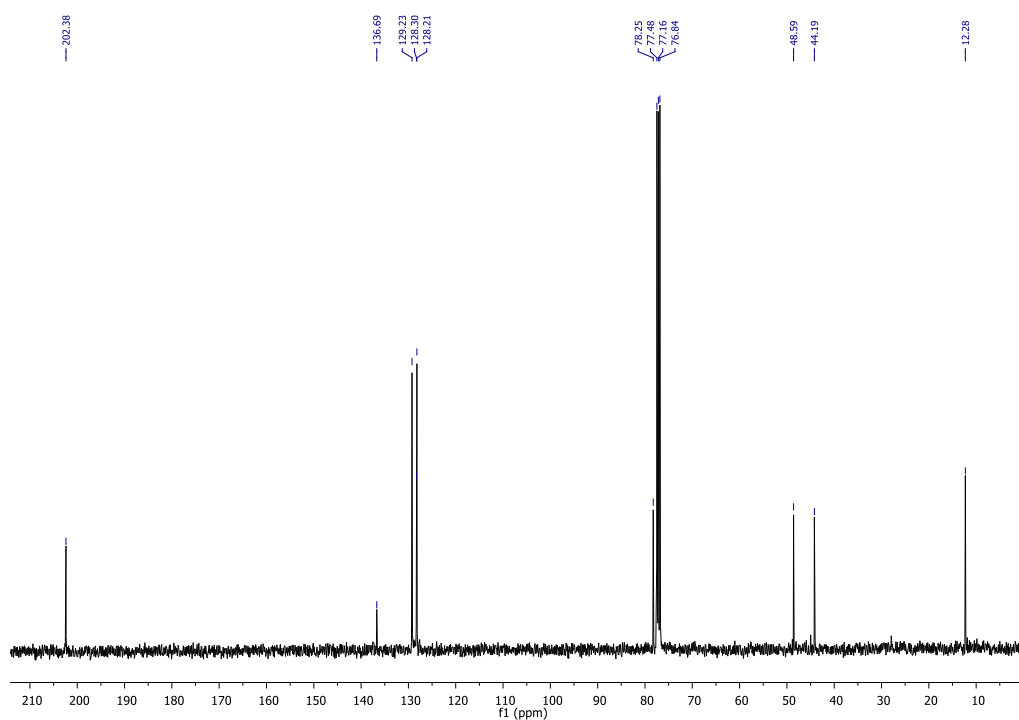
FIGURE 63: 100 MHz ^{13}C NMR spectra in CDCl$_3$ of (2R,3S)-2-Methyl-4-nitro-3-phenylbutanal (**23**).

PeakTable

PDA Ch1 210nm 4nm
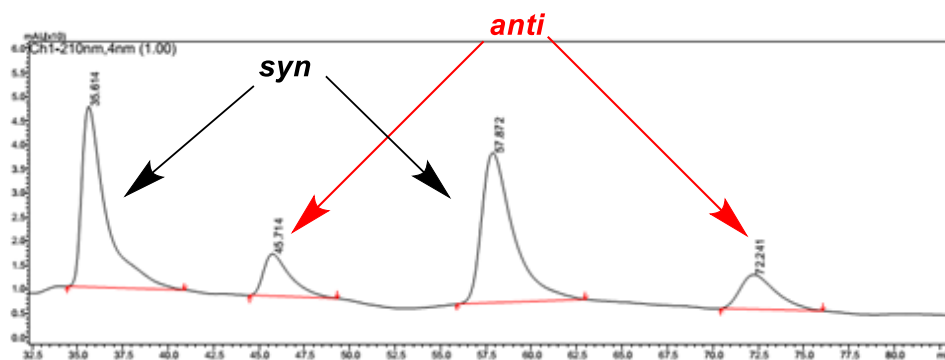
Peak#	Ret. Time	Area	Height	Area %	Height %
1	35.614	3513478	37480	38.136	44.314
2	45.714	903624	8770	9.808	10.369
3	57.872	3806053	31125	41.312	36.799
4	72.241	989820	7205	10.744	8.519
Total		9212975	84580	100.000	100.000

FIGURE 64: Chiral HPLC of racemic 2-Methyl-4-nitro-3-phenylbutanal (**23**). Chiralpak OD-H (*n*-hexane/i-PrOH 95:5), 25 °C at 1 ml/min, UV detection at 210 nm.

PeakTable

PDA Ch1 210nm 4nm
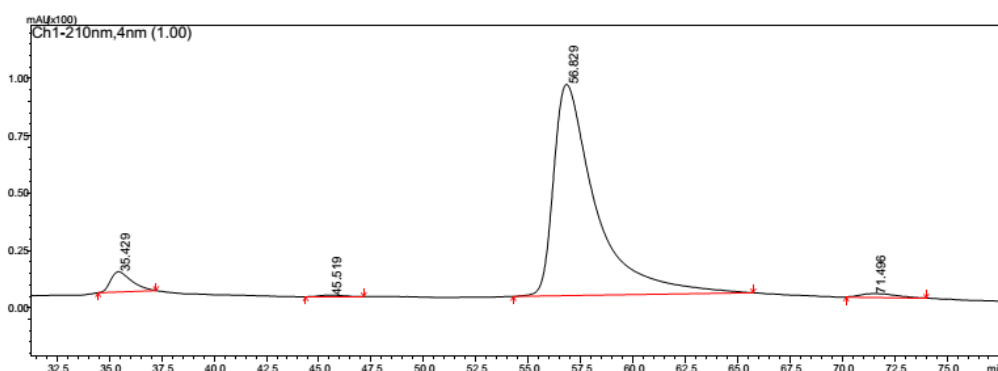
Peak#	Ret. Time	Area	Height	Area %	Height %
1	35.429	618916	8802	4.486	8.517
2	45.519	56556	680	0.410	0.658
3	56.829	12922303	92143	93.660	89.153
4	71.496	199231	1729	1.444	1.673
Total		13797006	103354	100.000	100.000

FIGURE 65: Chiral HPLC of (2R,3S)-2-Methyl-4-nitro-3-phenylbutanal (**23**) obtained by the 1,4-addition reaction catalyzed by catalyst **69**. Chiralpak OD-H (n-hexane/i-PrOH 95:5), 25 °C at 1 ml/min, UV detection at 210 nm.
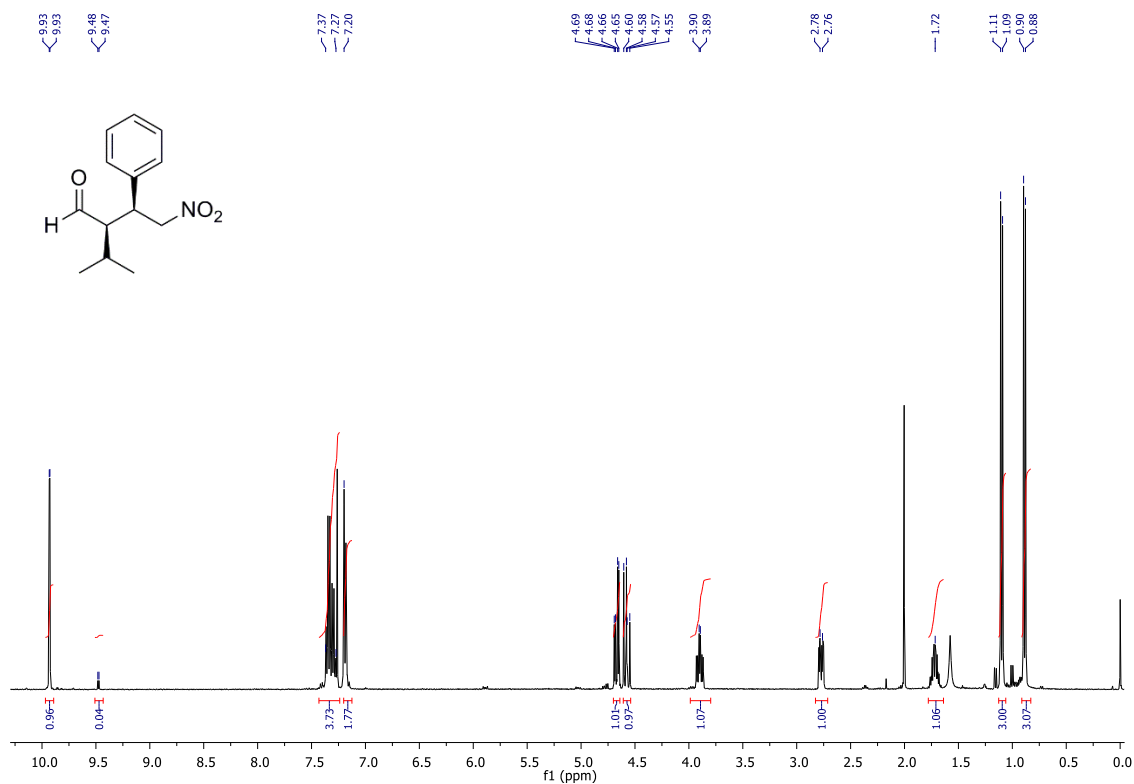
FIGURE 66: 400 MHz ^{1}H NMR spectra in CDCl$_3$ of (2R,3S)-2-Isopropyl-4-nitro-3-phenylbutanal (**79**).
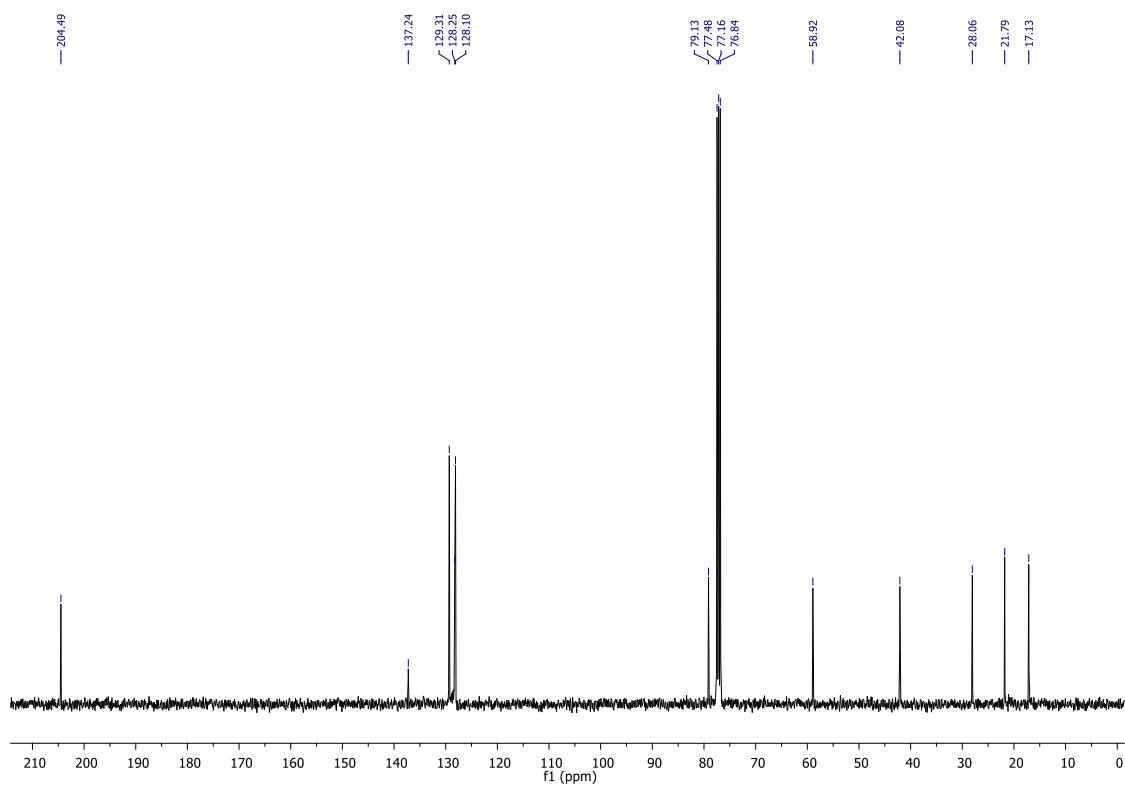
FIGURE 67: 100 MHz ^{1}C NMR spectra in CDCl$_3$ of (2R,3S)-2-Isopropyl-4-nitro-3-phenylbutanal (**79**).

PeakTable

PDA Ch1 210nm 4nm

Peak#	Ret. Time	Area	Height	Area %	Height %
1	24.452	47534031	1224610	46.974	47.029
2	25.673	9413867	270849	9.303	10.401
3	28.784	44245010	1108487	43.723	42.570
Total		101192908	2603945	100.000	100.000
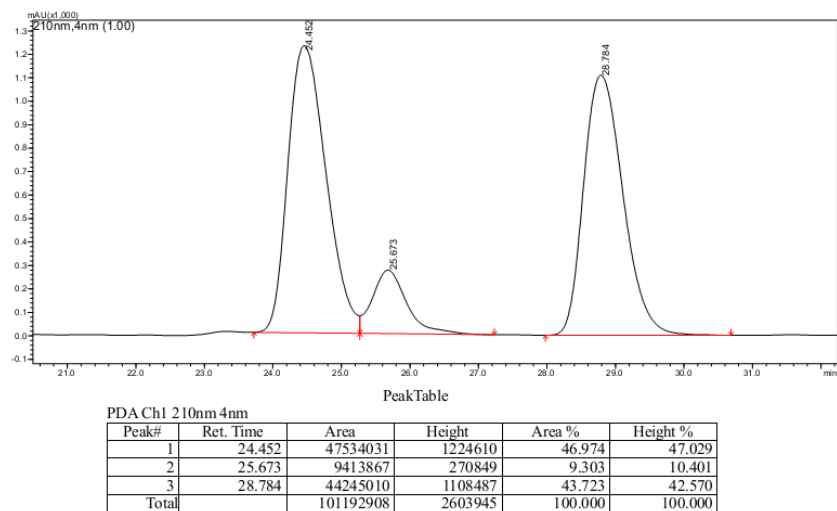
FIGURE 68: Chiral HPLC of racemic 2-isopropyl-4-nitro-3-phenylbutanal (**79**). Chiralpak AD-H (n-hexane/i-PrOH 97:3), 25 °C at 0.4ml/min, 210 nm.

PeakTable

PDA Ch1 210nm 4nm

Peak#	Ret. Time	Area	Height	Area %	Height %
1	24.461	14582609	474405	73.335	80.178
2	25.658	2440513	61173	12.273	10.339
3	28.996	2861808	56113	14.392	9.483
Total		19884930	591690	100.000	100.000
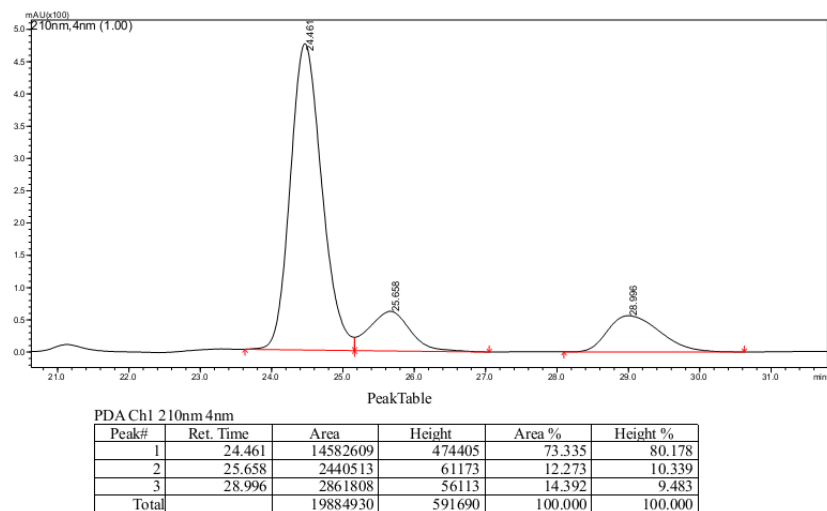
FIGURE 69: Chiral HPLC of 2-Isopropyl-4-nitro-3-phenylbutanal (**79**) obtained by the 1,4-addition reaction catalyzed by catalyst **69**. Chiralpak AD-H (n-hexane/i-PrOH 97:3), 25 °C at 0.4ml/min, 210 nm.
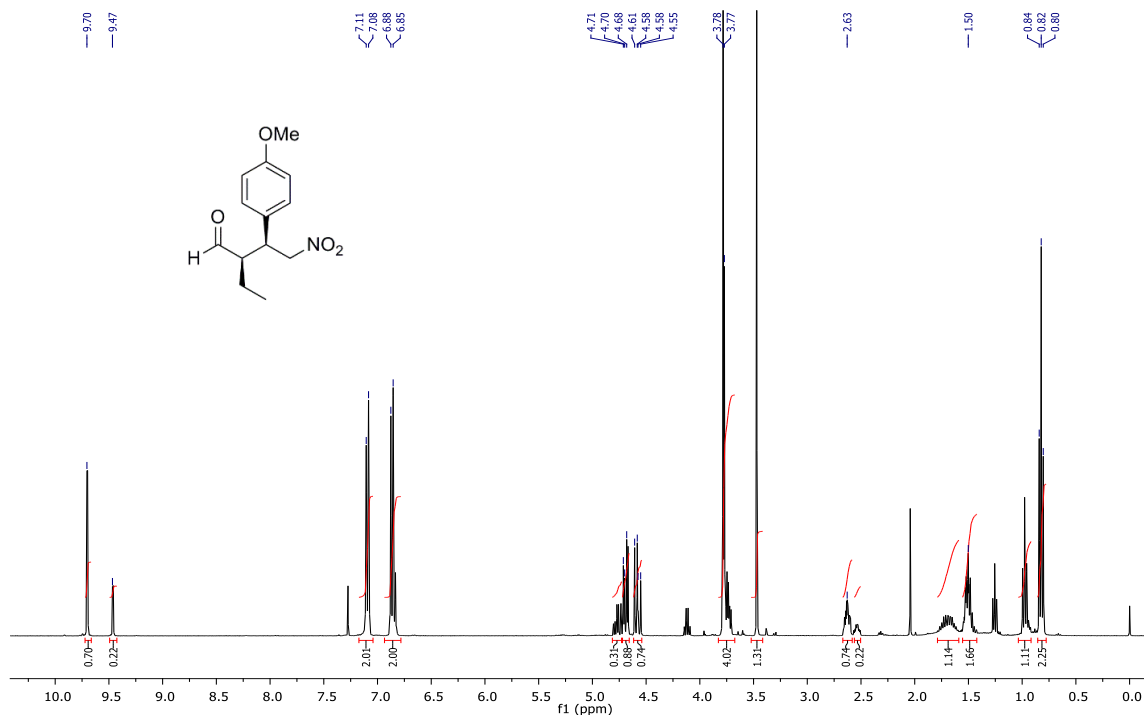
FIGURE 70: 400 MHz ^{1}H NMR spectra in CDCl$_3$ of (2R,3S)-2-Ethyl-4-nitro-3-(4-methoxyphenyl)butanal (**80**).
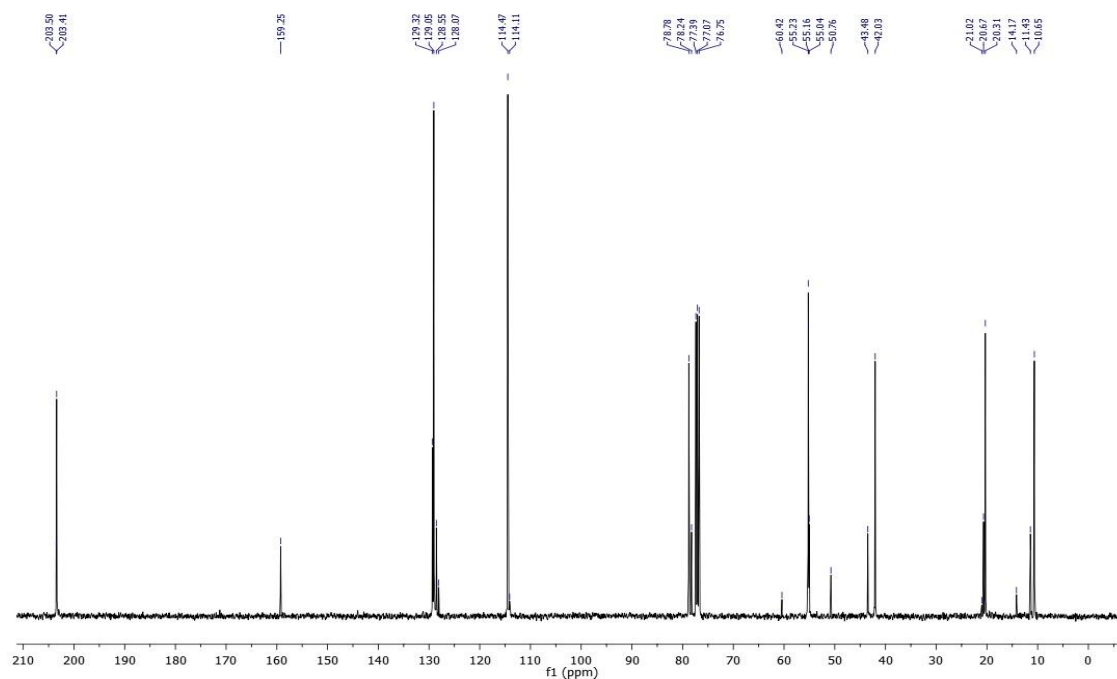
FIGURE 71: 100 MHz ^{13}C NMR spectra in CDCl$_3$ of (2R,3S)-2-Ethyl-4-nitro-3-(4-methoxyphenyl)butanal (**80**).
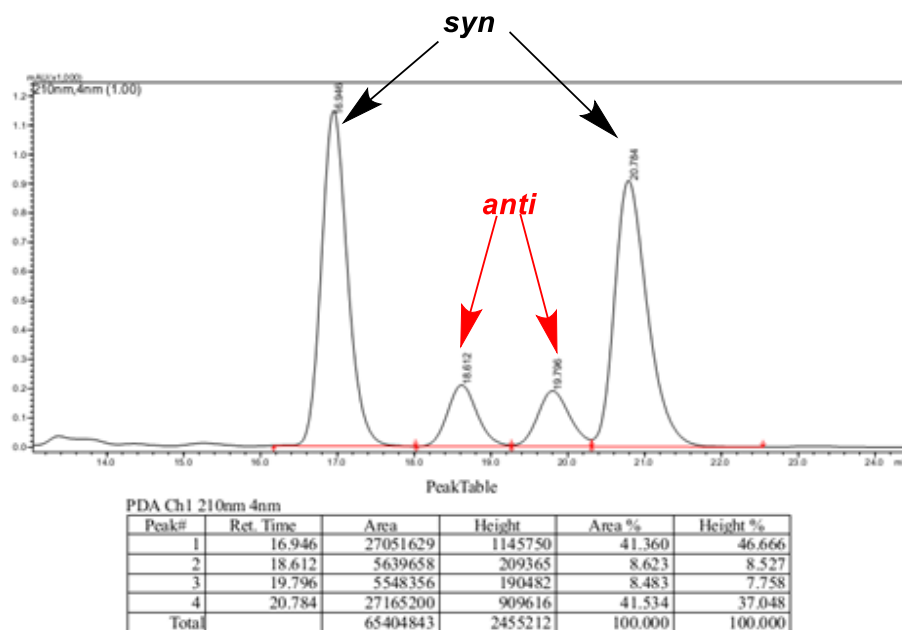
FIGURE 72: Chiral HPLC of racemic 2-Ethyl-4-nitro-3-(4-methoxyphenyl)butanal (**80**). Chiralpak AD-H (n-hexane/i-PrOH 95:5), 25 °C at 0.8ml/min, 210 nm.

PDA Ch1 210nm 4nm

Peak#	Ret. Time	Area	Height	Area %	Height %
1	16.946	27051629	1145750	41.360	46.666
2	18.612	5639658	209365	8.623	8.527
3	19.796	5548356	190482	8.483	7.758
4	20.784	27165200	909616	41.534	37.048
Total		65404843	2455212	100.000	100.000
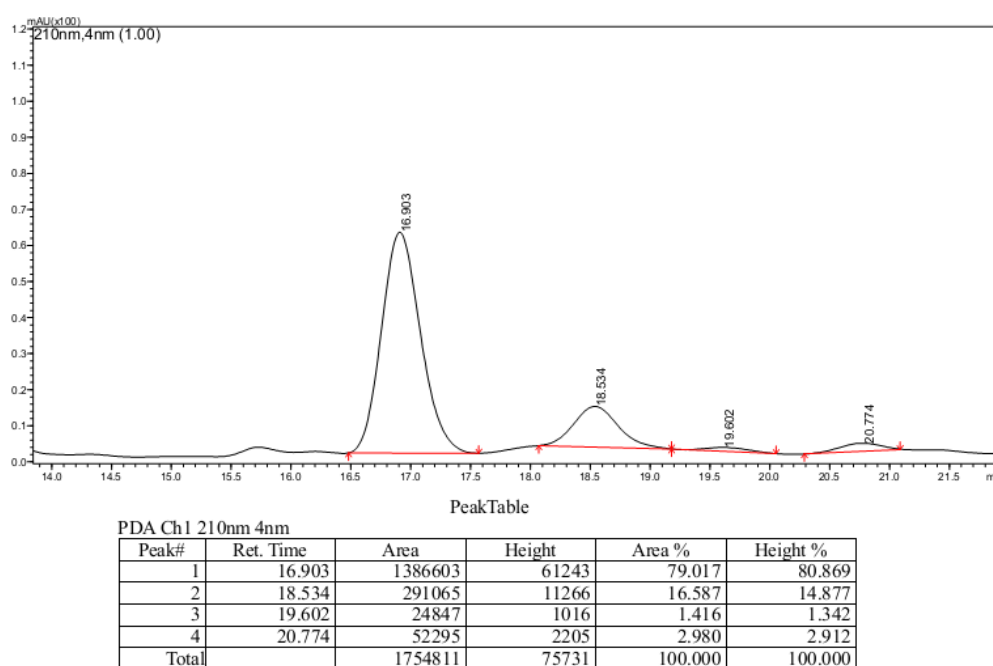
FIGURE 73: Chiral HPLC of 2-Ethyl-4-nitro-3-(4-methoxyphenyl)butanal (**80**) obtained by the 1,4-addition reaction catalyzed by catalyst **69**. Chiralpak AD-H (n-hexane/i-PrOH 95:5), 25 °C at 0.8ml/min, 210 nm.

PDA Ch1 210nm 4nm

Peak#	Ret. Time	Area	Height	Area %	Height %
1	16.903	1386603	61243	79.017	80.869
2	18.534	291065	11266	16.587	14.877
3	19.602	24847	1016	1.416	1.342
4	20.774	52295	2205	2.980	2.912
Total		1754811	75731	100.000	100.000
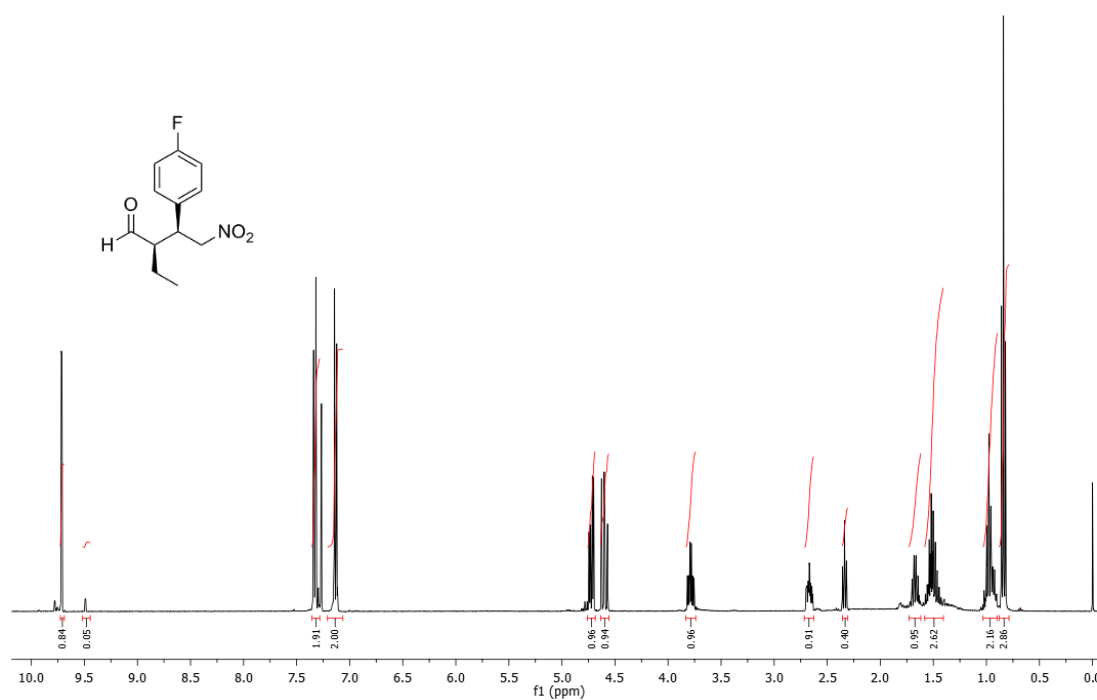
FIGURE 74: 400 MHz ^{1}H NMR spectra in CDCl$_3$ of (2R,3S)-3-(4-Fluorophenyl)-2-ethyl-4-nitrobutanal (**81**).
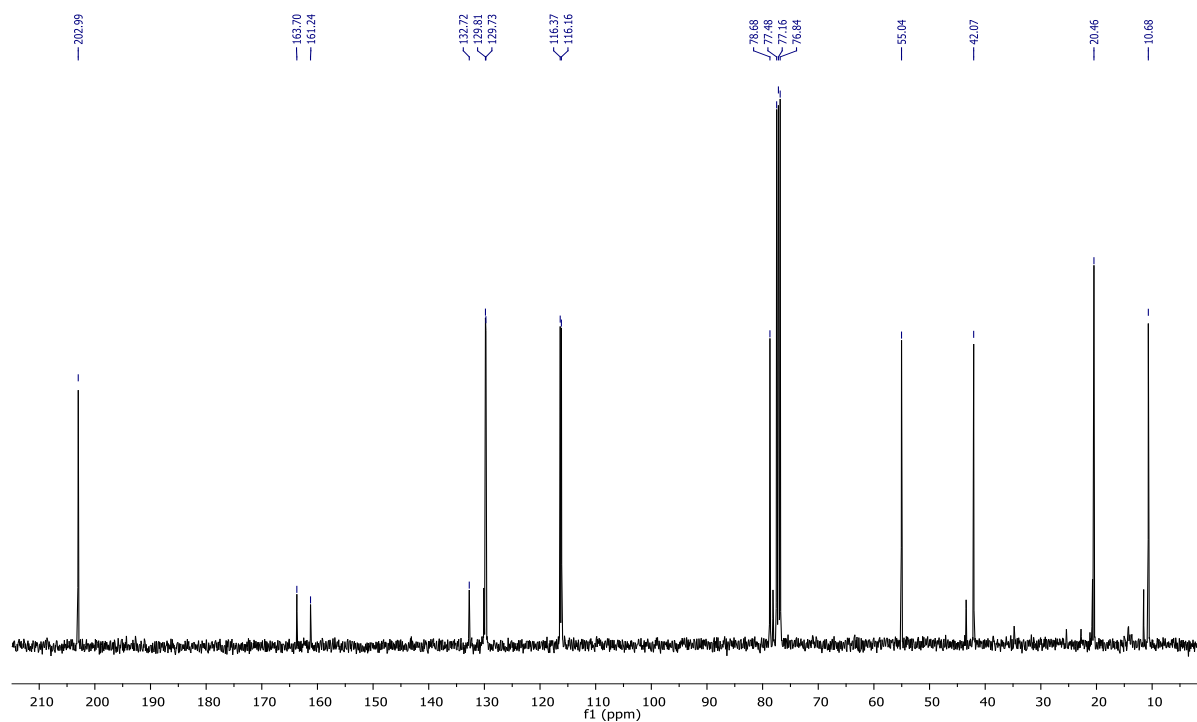
FIGURE 75: 100 MHz ^{13}C NMR spectra in CDCl$_3$ of (2R,3S)-3-(4-Fluorophenyl)-2-ethyl-4-nitrobutanal (**81**).
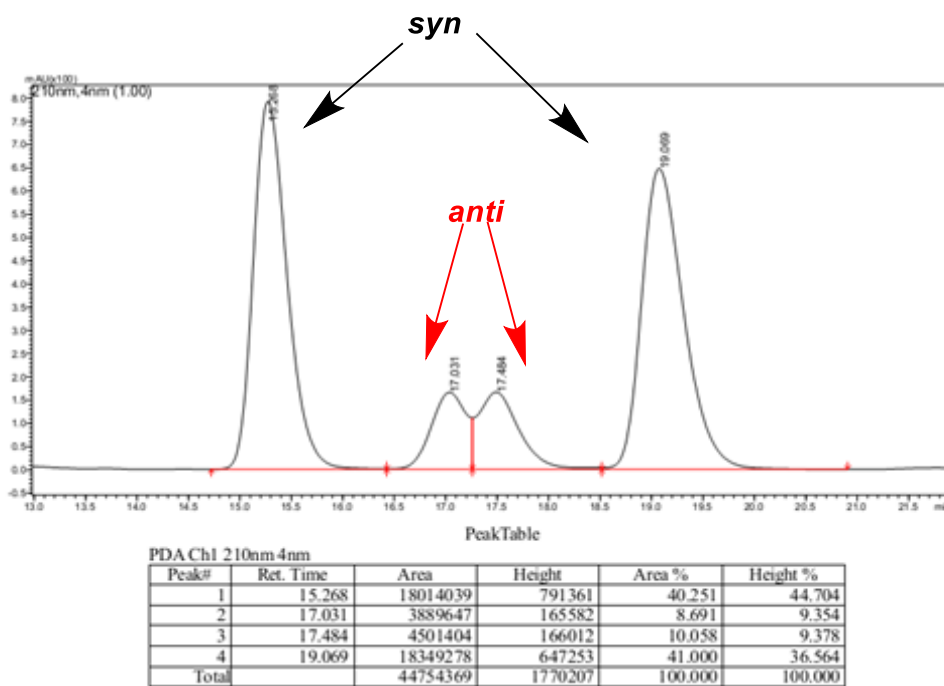
FIGURE 76: Chiral HPLC of racemic 3-(4-Fluorophenyl)-2-ethyl-4-nitrobutanal (**81**). Chiralpak AD-H (n-hexane/i-PrOH 95:5), 25 °C at 0.8ml/min, 210 nm.

PDA Ch1 210nm 4nm

Peak#	Ret. Time	Area	Height	Area %	Height %
1	15.268	18014039	791361	40.251	44.704
2	17.031	3889647	165582	8.691	9.354
3	17.484	4501404	166012	10.058	9.378
4	19.069	18349278	647253	41.000	36.564
Total		44754369	1770207	100.000	100.000
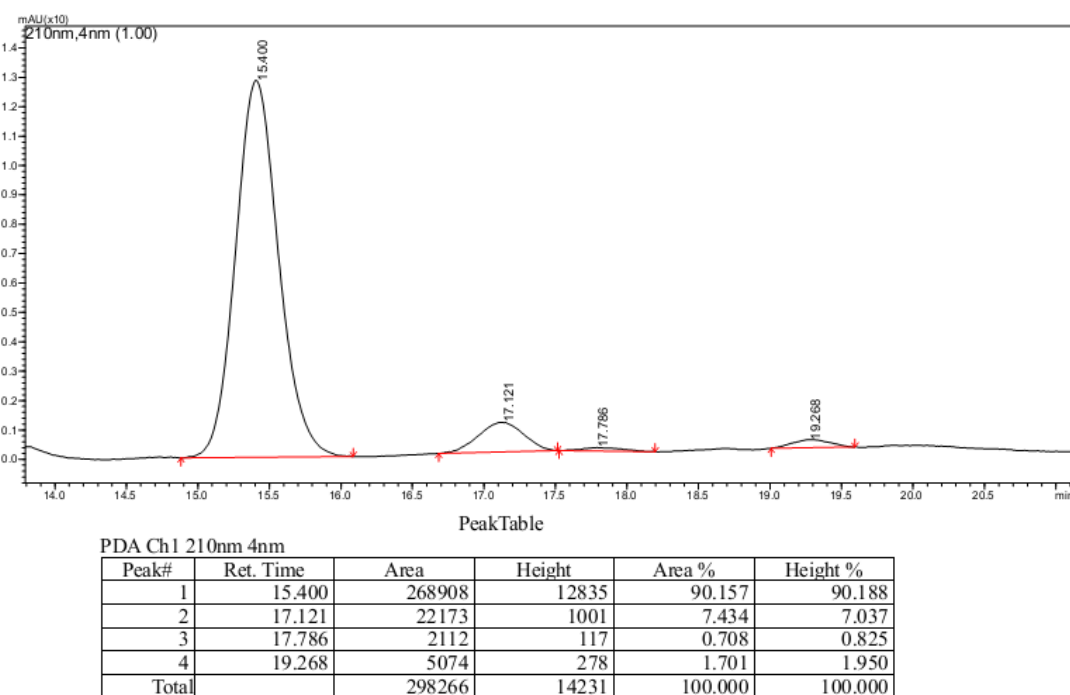
FIGURE 77: Chiral HPLC of 3-(4-Fluorophenyl)-2-ethyl-4-nitrobutanal (**81**) obtained by the 1,4-addition reaction catalyzed by catalyst **69**. Chiralpak AD-H (n-hexane/i-PrOH 95:5), 25 °C at 0.8ml/min, 210 nm.

PDA Ch1 210nm 4nm

Peak#	Ret. Time	Area	Height	Area %	Height %
1	15.400	268908	12835	90.157	90.188
2	17.121	22173	1001	7.434	7.037
3	17.786	2112	117	0.708	0.825
4	19.268	5074	278	1.701	1.950
Total		298266	14231	100.000	100.000
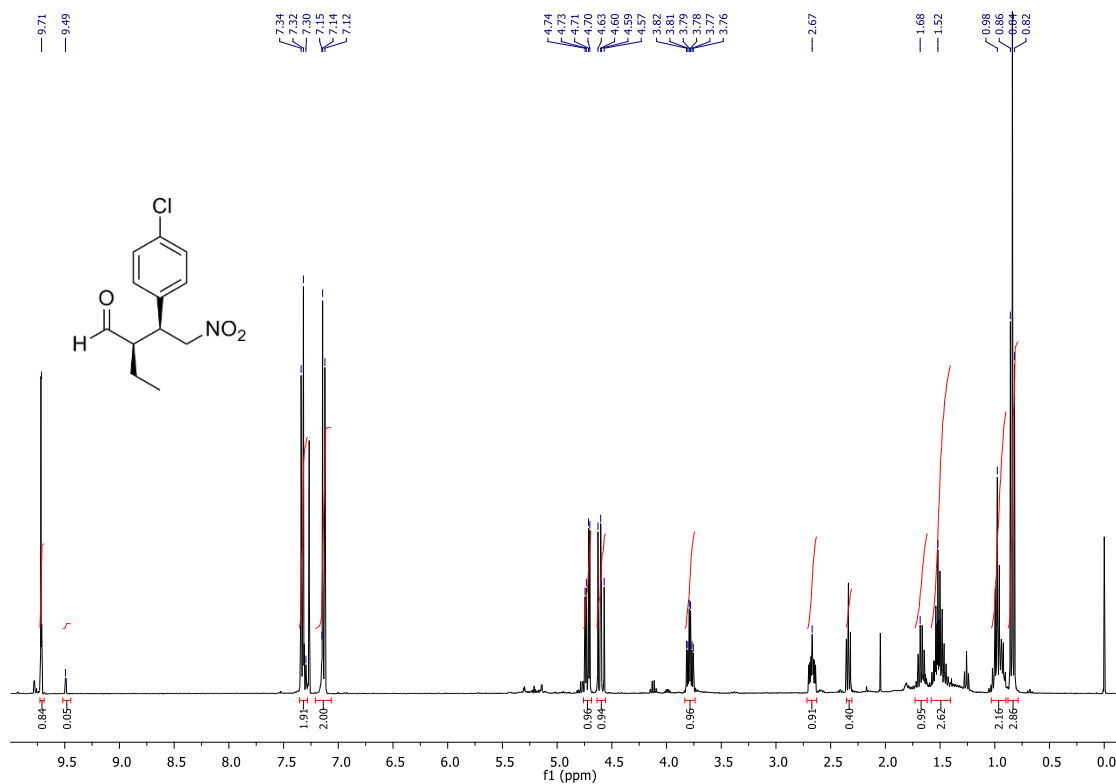
FIGURE 78: 400 MHz ^{1}H NMR spectra in CDCl$_3$ of (2R,3S)-3-(4-Chlorophenyl)-2-ethyl-4-nitrobutanal (**82**).
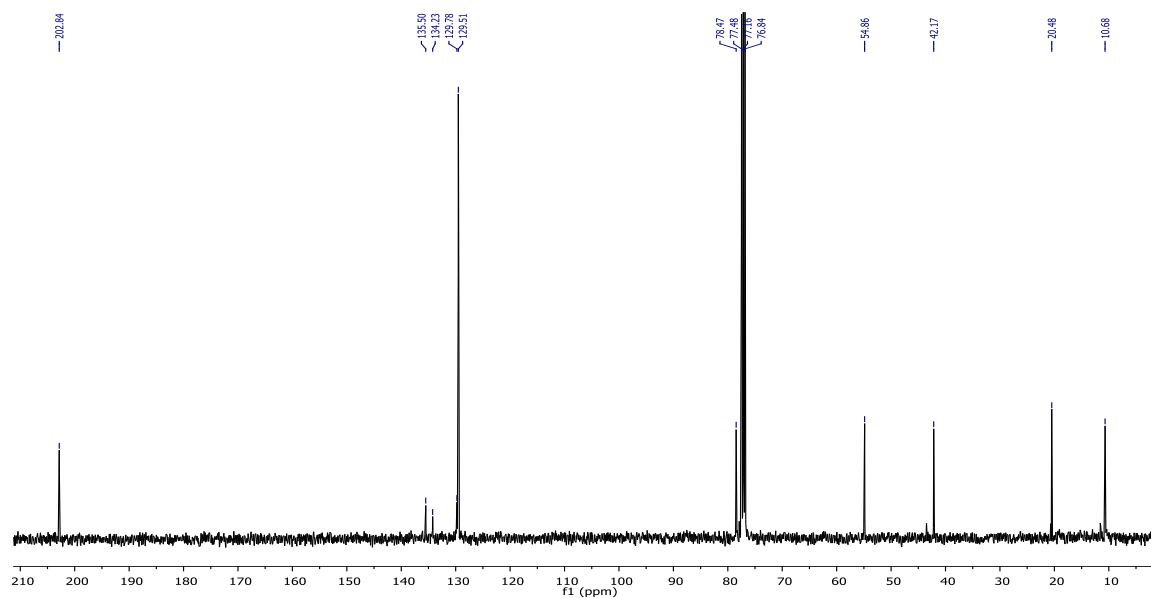
FIGURE 79: 100 MHz ^{13}C NMR spectra in CDCl$_3$ of (2R,3S)-3-(4-Chlorophenyl)-2-ethyl-4-nitrobutanal (**82**).
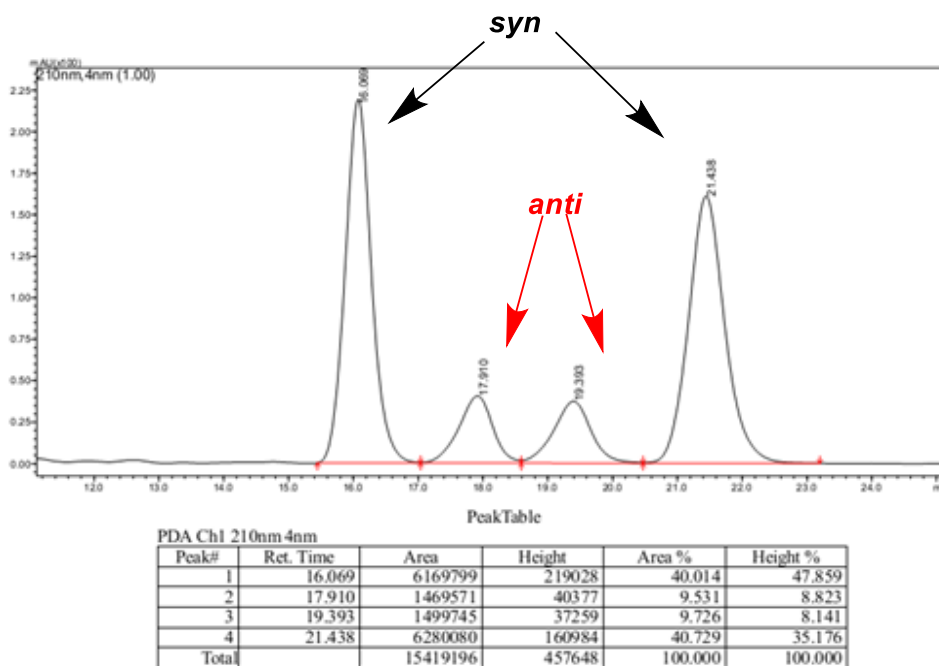
FIGURE 80: Chiral HPLC of racemic 3-(4-Chlorophenyl)-2-ethyl-4-nitrobutanal (**82**). Chiralpak AD-H (n-hexane/i-PrOH 95:5), 25 °C at 0.8ml/min, 210 nm.

PDA Ch1 210nm 4nm

Peak#	Ret. Time	Area	Height	Area %	Height %
1	16.069	6169799	219028	40.014	47.859
2	17.910	1469571	40377	9.531	8.823
3	19.393	1499745	37259	9.726	8.141
4	21.438	6280080	160984	40.729	35.176
Total		15419196	457648	100.000	100.000
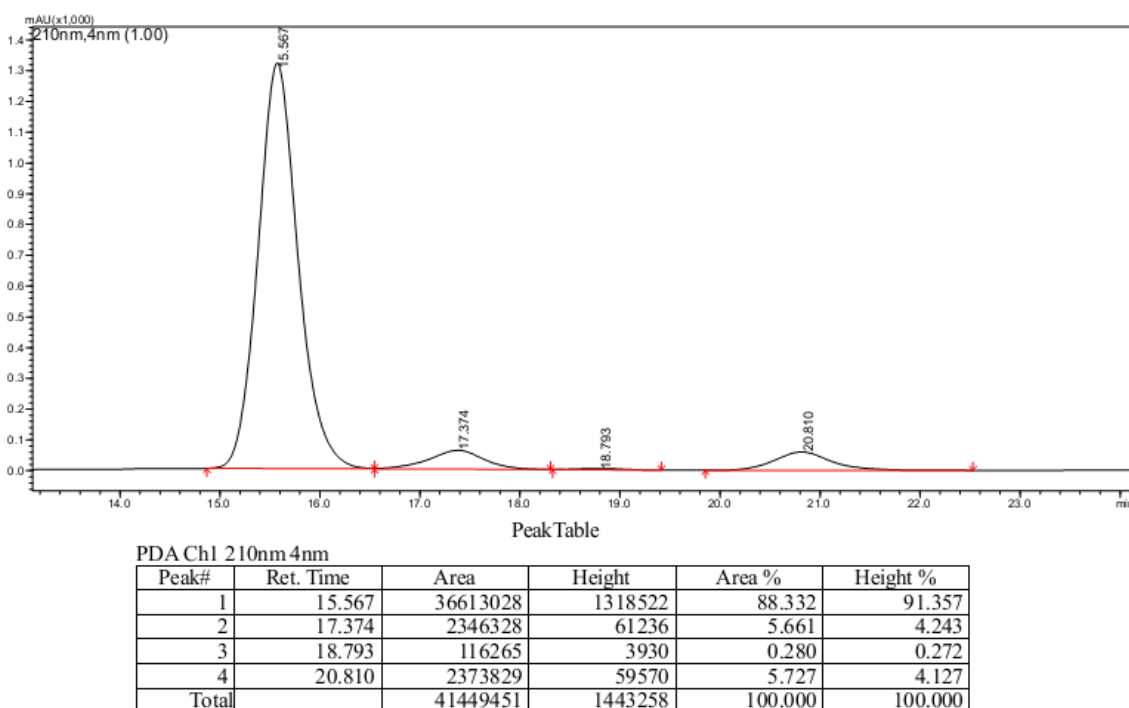
FIGURE 81: Chiral HPLC of 3-(4-Chlorophenyl)-2-ethyl-4-nitrobutanal (**82**) obtained by the 1,4-addition reaction catalyzed by catalyst **69**. Chiralpak AD-H (n-hexane/i-PrOH 95:5), 25 °C at 0.8ml/min, 210 nm.

PDA Ch1 210nm 4nm

Peak#	Ret. Time	Area	Height	Area %	Height %
1	15.567	36613028	1318522	88.332	91.357
2	17.374	2346328	61236	5.661	4.243
3	18.793	116265	3930	0.280	0.272
4	20.810	2373829	59570	5.727	4.127
Total		41449451	1443258	100.000	100.000
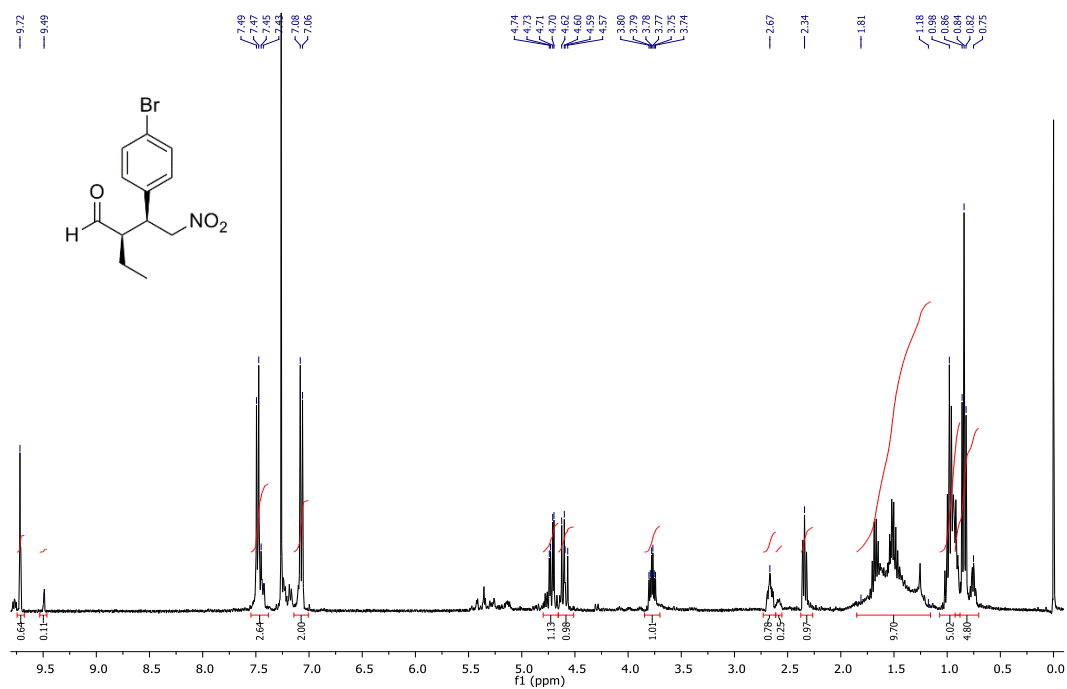
FIGURE 82: 400 MHz ^{1}H NMR spectra in CDCl$_3$ of (2R,3S)-3-(4-Bromophenyl)-2-ethyl-4-nitrobutanal (**83**).
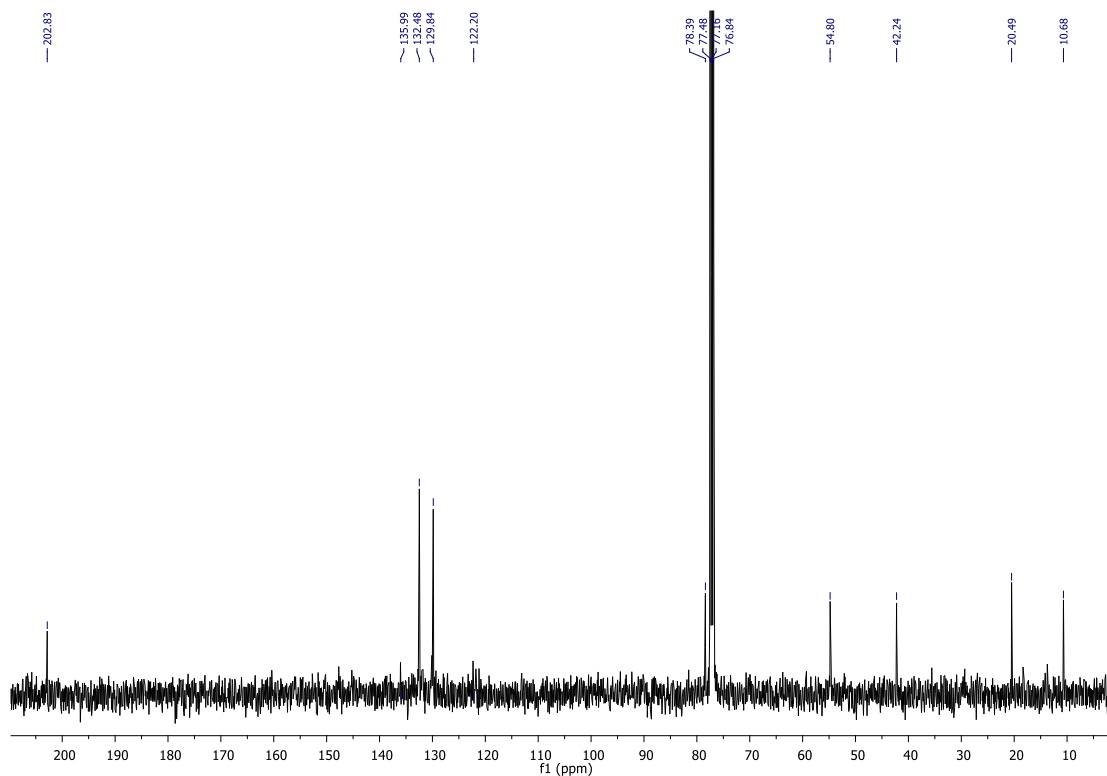
FIGURE 83: 100 MHz ^{13}C NMR spectra in CDCl$_3$ of (2R,3S)-3-(4-Bromophenyl)-2-ethyl-4-nitrobutanal (**83**).

PeakTable

PDA Ch1 210nm 4nm

Peak#	Ret. Time	Area	Height	Area %	Height %
1	16.273	10985951	522499	36.415	41.857
2	18.148	4338108	195344	14.380	15.649
3	20.521	4189422	164548	13.887	13.182
4	21.689	10654959	365913	35.318	29.313
Total		30168440	1248304	100.000	100.000
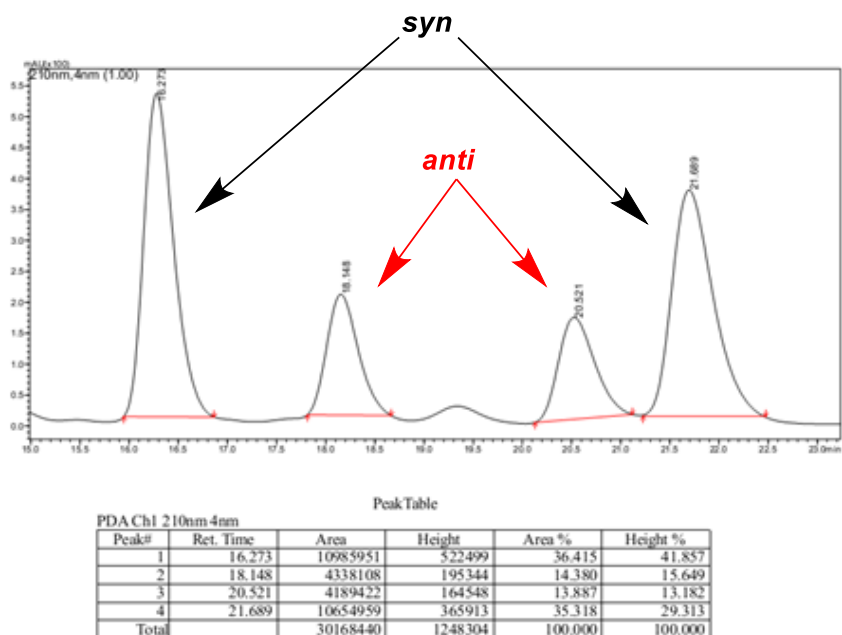
FIGURE 84: Chiral HPLC of racemic 3-(4-Bromophenyl)-2-ethyl-4-nitrobutanal (**83**). Chiralpak AD-H (n-hexane/i-PrOH 95:5), 25 °C at 0.8ml/min, 210 nm.

PeakTable

PDA Ch1 210nm 4nm

Peak#	Ret. Time	Area	Height	Area %	Height %
1	16.376	3373805	158330	78.443	79.591
2	18.248	437937	21318	10.182	10.717
3	21.621	212873	7240	4.949	3.640
4	21.830	276365	12041	6.426	6.053
Total		4300980	198930	100.000	100.000
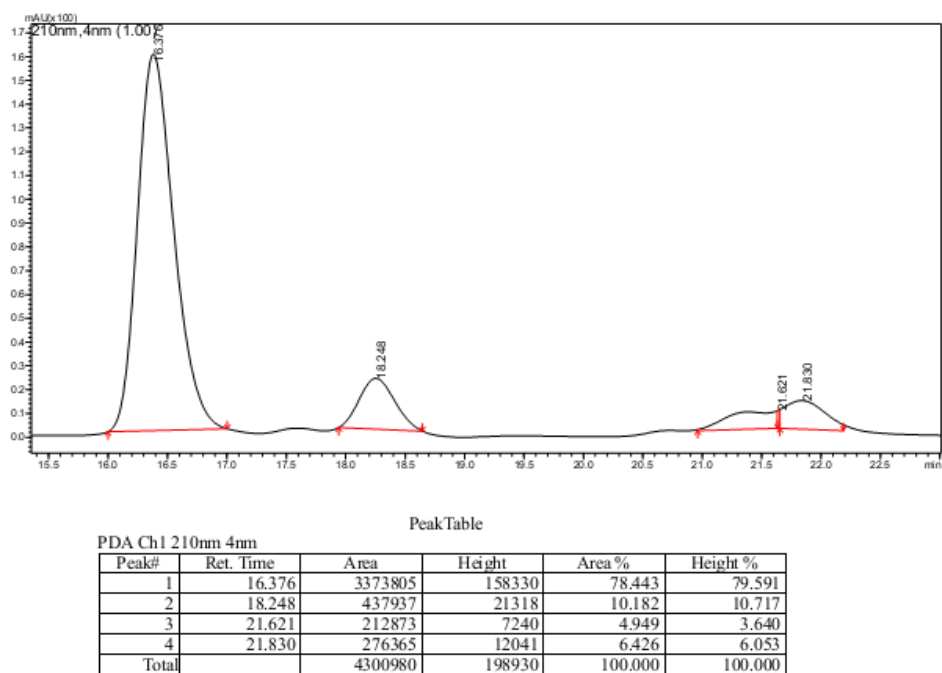
FIGURE 85: Chiral HPLC of 3-(4-Bromophenyl)-2-ethyl-4-nitrobutanal (**83**) obtained by the 1,4-addition reaction catalyzed by catalyst **69**. Chiralpak AD-H (n-hexane/i-PrOH 95:5), 25 °C at 0.8ml/min, 210 nm.

209
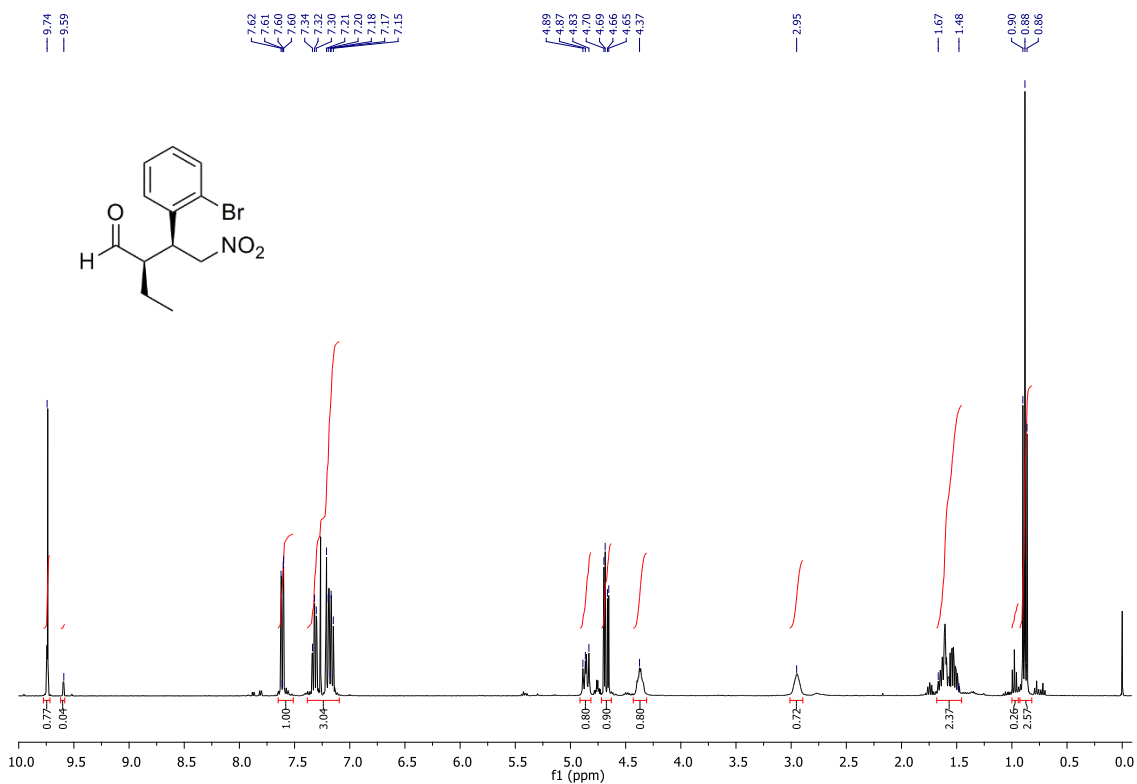
FIGURE 86: 400 MHz ^{1}H NMR spectra in CDCl$_3$ of (2R,3S)-3-(2-Bromophenyl)-2-ethyl-4-nitrobutanal (**84**).
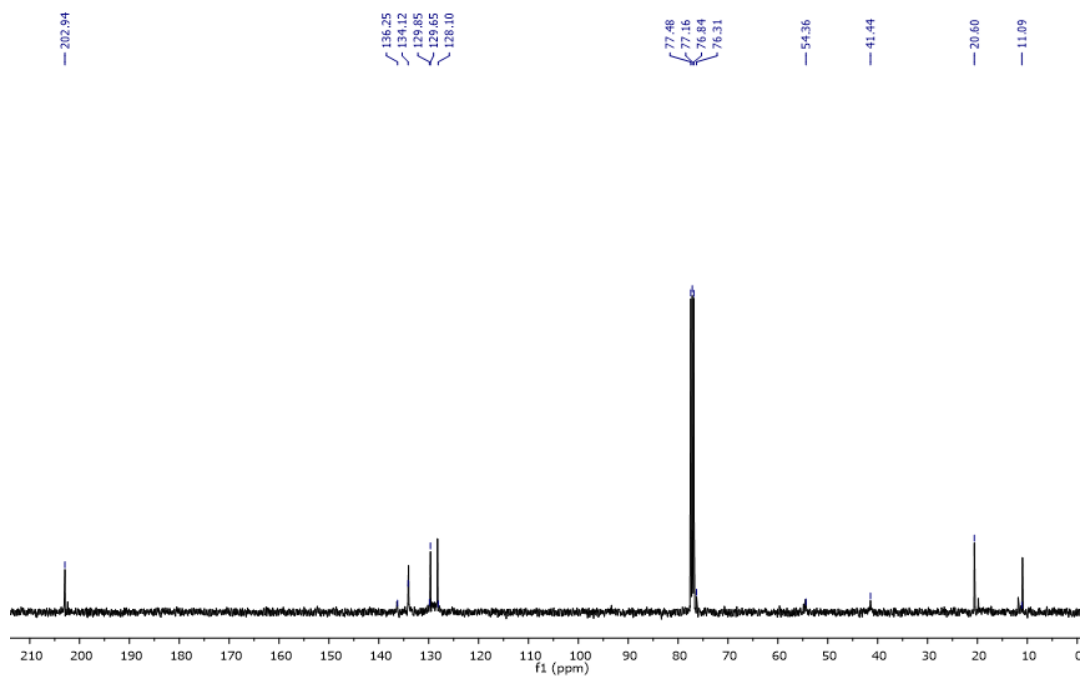
FIGURE 87: 100 MHz ^{13}C NMR spectra in CDCl$_3$ of (2R,3S)-3-(2-Bromophenyl)-2-ethyl-4-nitrobutanal (**84**).

PDA Ch1 210nm 4nm

Peak#	Ret. Time	Area	Height	Area %	Height %
1	20.722	40695835	1120654	38.969	45.341
2	23.008	39674527	991187	37.991	40.103
3	24.612	24061909	359776	23.041	14.556
Total		104432271	2471617	100.000	100.000
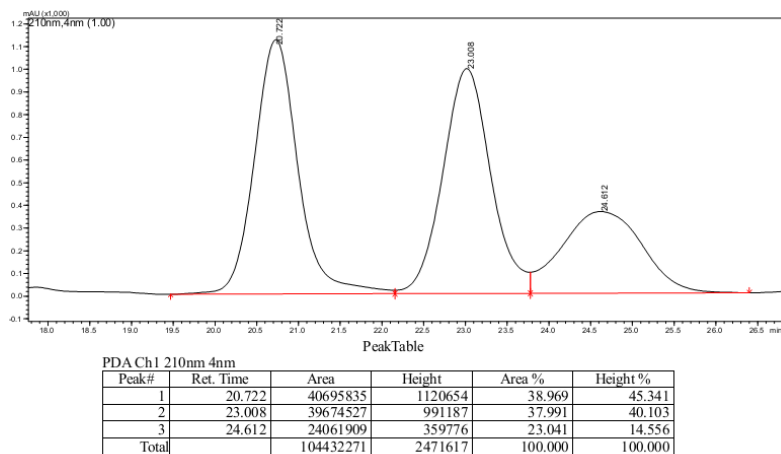
FIGURE 88: Chiral HPLC of racemic 3-(2-Bromophenyl)-2-ethyl-4-nitrobutanal (**84**). Chiralpak AD-H (n-hexane/i-PrOH 97:3), 25 °C at 0.5ml/min, 210 nm.

PDA Ch1 210nm 4nm

Peak#	Ret. Time	Area	Height	Area %	Height %
1	20.773	36021302	1048810	83.428	89.385
2	23.115	2116901	53650	4.903	4.572
3	24.607	5038347	70901	11.669	6.043
Total		43176550	1173361	100.000	100.000
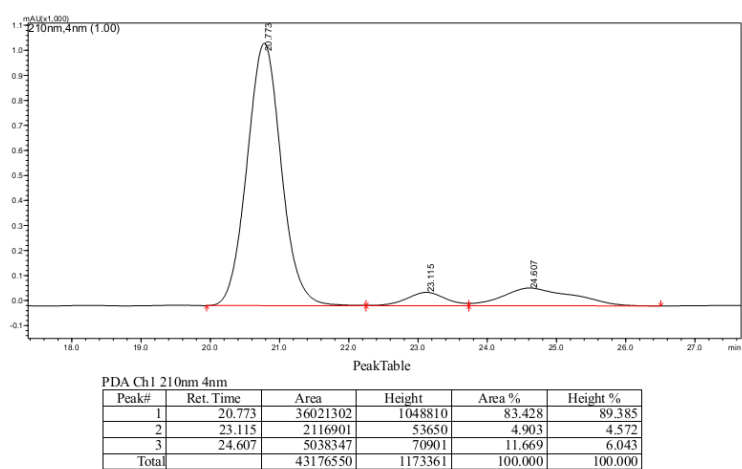
FIGURE 89: Chiral HPLC of 3-(4-Bromophenyl)-2-ethyl-2-nitrobutanal (**84**) obtained by the 1,4-addition reaction catalyzed by catalyst **69**. Chiralpak AD-H (n-hexane/i-PrOH 97:3), 25 °C at 0.5ml/min, 210 nm.
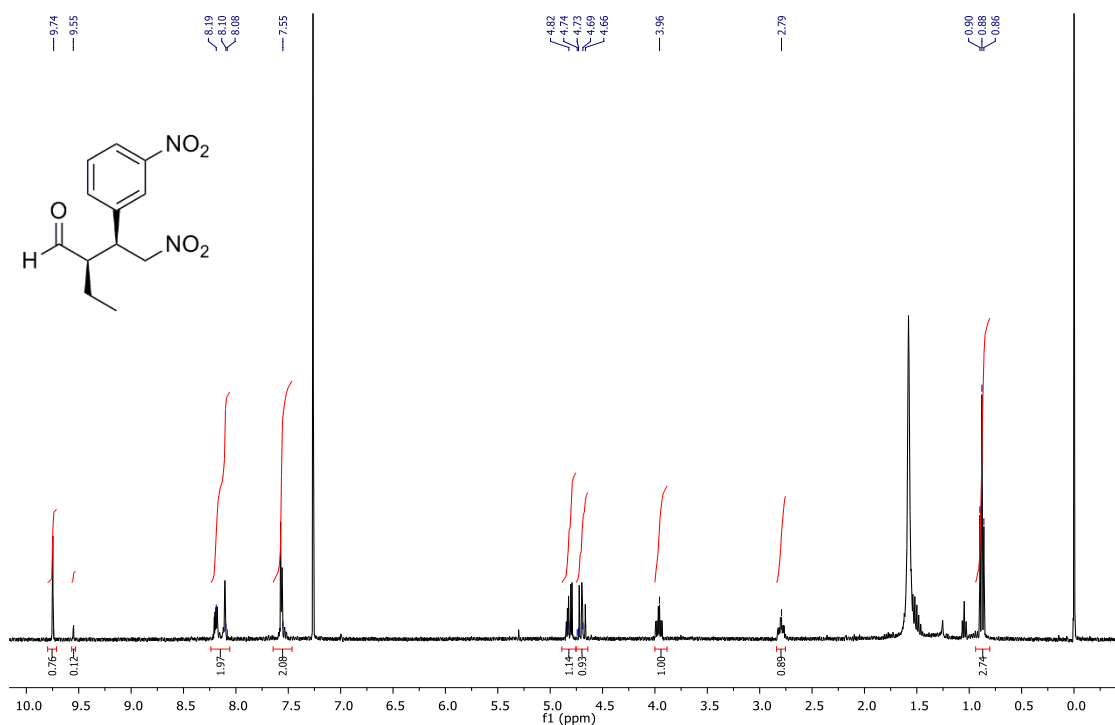
FIGURE 90: 400 MHz ^{1}H NMR spectra in CDCl$_3$ of (2R,3S)-2-Ethyl-4-nitro-3-(3-nitrophenyl)butanal (**85**).
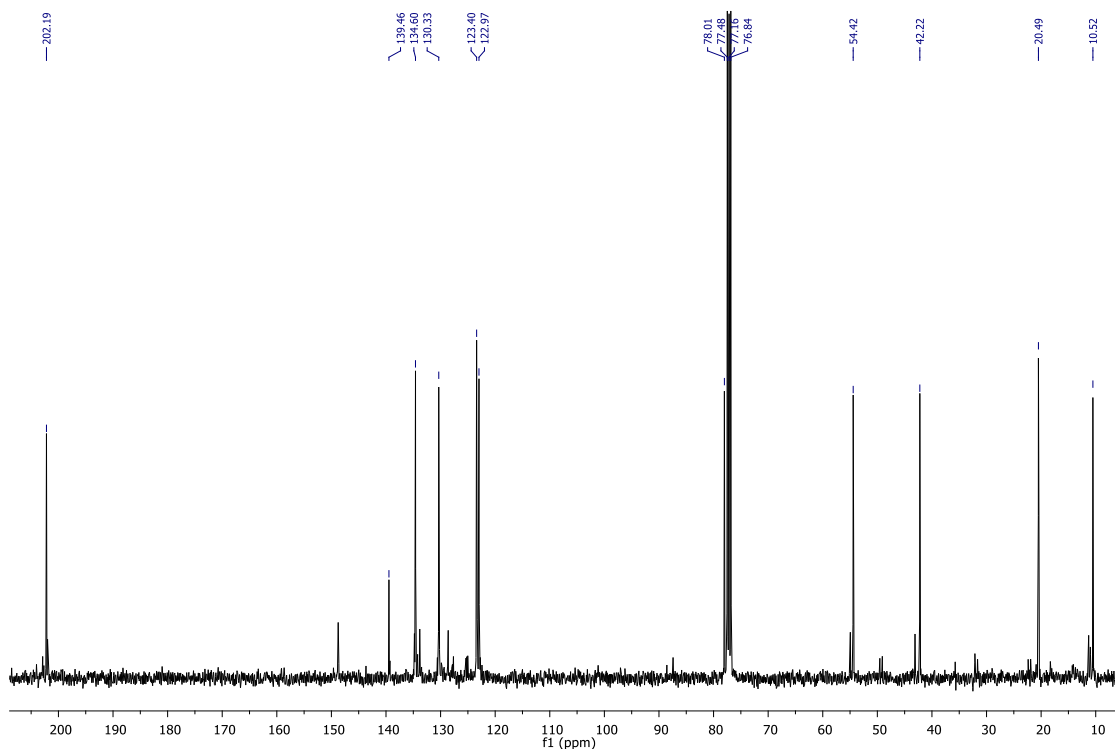
FIGURE 91: 100 MHz ^{13}C NMR spectra in CDCl$_3$ of (2R,3S)-2-Ethyl-4-nitro-3-(3-nitrophenyl)butanal (**85**).

PeakTable

PDA Ch1 210nm 4nm

Peak#	Ret. Time	Area	Height	Area %	Height %
1	36.228	3478627	58277	36.146	42.440
2	38.893	6145291	79039	63.854	57.560
Total		9623919	137315	100.000	100.000
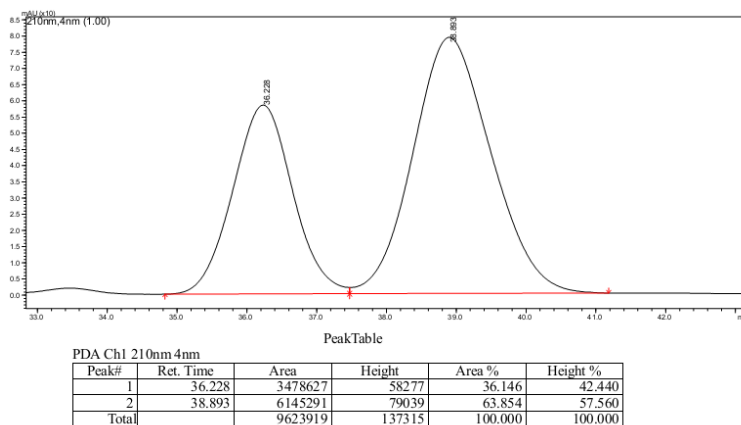
FIGURE 92: Chiral HPLC of racemic 2-Ethyl-4-nitro-3-(3-nitrophenyl)butanal (**85**). Chiralpak AD-H (*n*-hexane/i-PrOH 95:5), 25 °C at 0.8ml/min, 210 nm.

PeakTable

PDA Ch1 210nm 4nm

Peak#	Ret. Time	Area	Height	Area %	Height %
1	36.010	4773586	76581	87.659	89.827
2	39.153	672058	8672	12.341	10.173
Total		5445644	85254	100.000	100.000
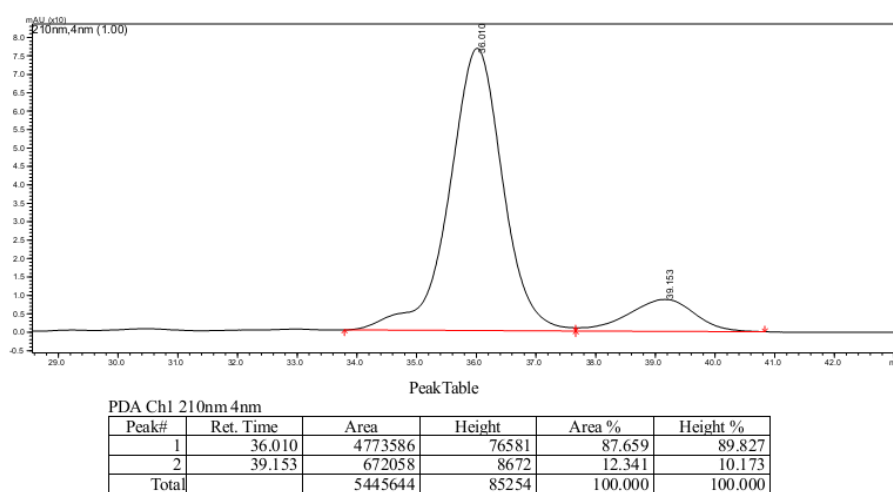
FIGURE 93: Chiral HPLC of 2-Ethyl-4-nitro-3-(3-nitrophenyl)butanal (**85**) obtained by the 1,4-addition reaction catalyzed by catalyst **69**. Chiralpak AD-H (*n*-hexane/i-PrOH 95:5), 25 °C at 0.8ml/min, 210 nm.
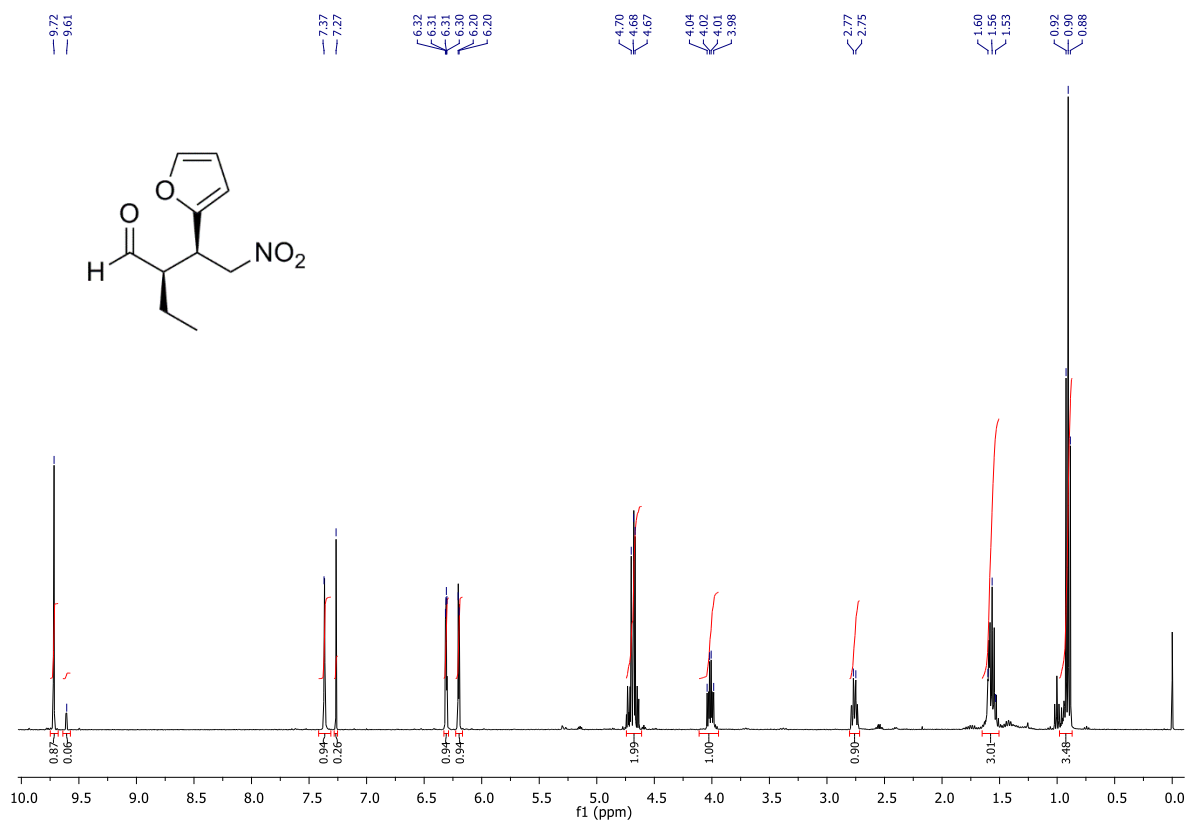
FIGURE 94: 400 MHz ^{1}H NMR spectra in CDCl$_3$ of (2R,3S)-2-Ethyl-4-nitro-3-(2-furyl)butanal (**86**).
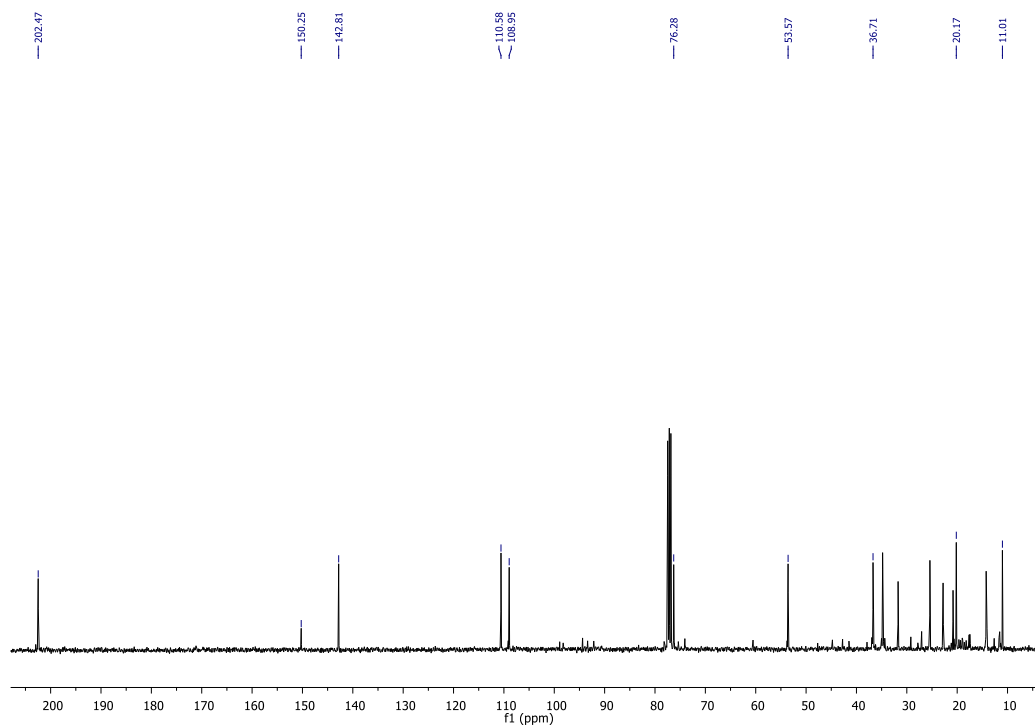
FIGURE 95: 100 MHz ^{13}C NMR spectra in CDCl$_3$ of (2R,3S)-2-Ethyl-4-nitro-3-(2-furyl)butanal (**86**).

PeakTable

PDA Ch1 210nm 4nm

Peak#	Ret. Time	Area	Height	Area %	Height %
1	21.125	724888	28638	8.601	13.958
2	21.756	3035476	83296	36.017	40.597
3	23.443	4667631	93243	55.382	45.445
Total		8427996	205177	100.000	100.000
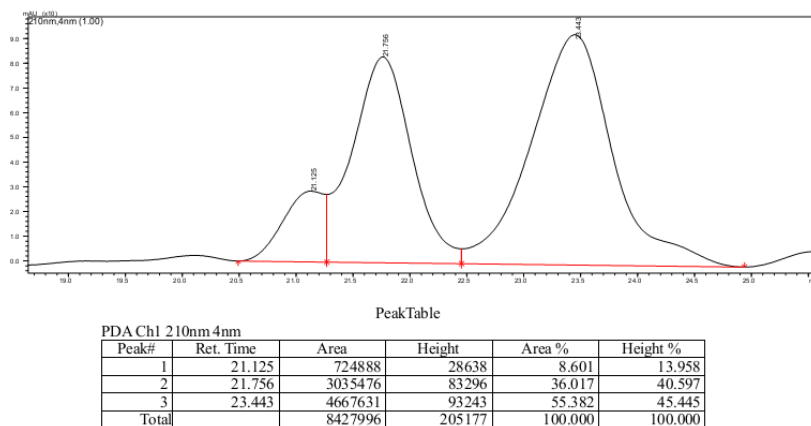
FIGURE 96: Chiral HPLC of racemic 2-Ethyl-4-nitro-3-(2-furyl)butanal (**86**). Chiralpak AD-H (n-hexane/i-PrOH 97:3), 25 °C at 0.5ml/min, 210 nm.

PeakTable

PDA Ch1 210nm 4nm

Peak#	Ret. Time	Area	Height	Area %	Height %
1	22.116	51964063	1306218	91.172	93.438
2	23.936	5031747	91729	8.828	6.562
Total		56995810	1397947	100.000	100.000
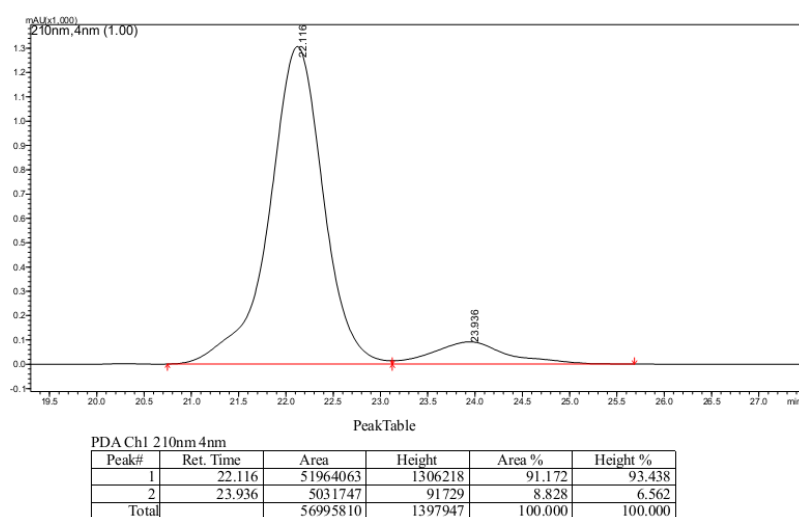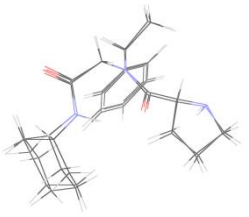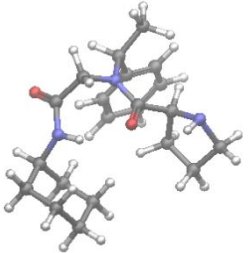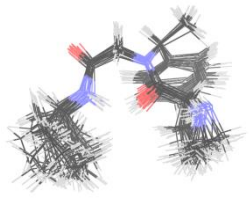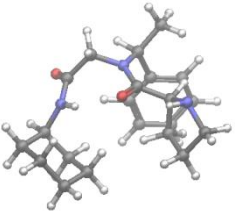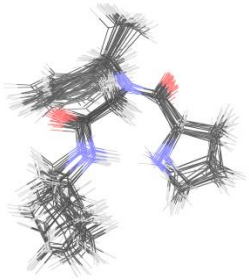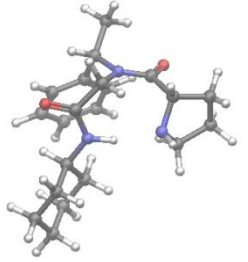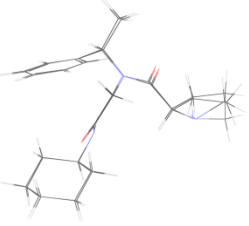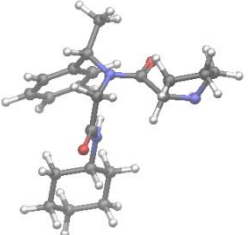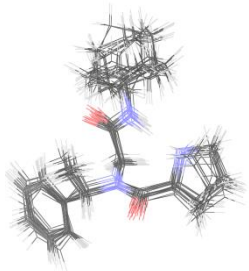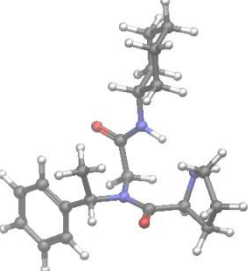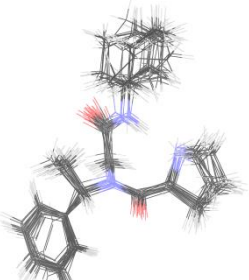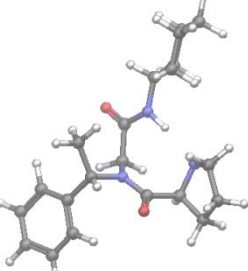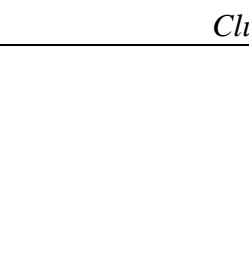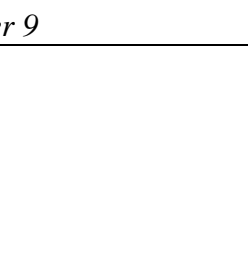
FIGURE 97: Chiral HPLC of 2-Ethyl-4-nitro-3-(2-furyl)butanal (**86**) obtained by the 1,4-addition reaction catalyzed by catalyst **69**. Chiralpak AD-H (n-hexane/i-PrOH 97:3), 25 °C at 0.5ml/min, 210 nm.

Clusters	Reoptimized low-energy conformer	Clusters	Reoptimized Low-energy conformer
Cluster 1		*Cluster 2*	
Cluster 3		*Cluster 4*	
Cluster 5		*Cluster 6*	
Cluster 7		*Cluster 8*	
Cluster 9		*Cluster 10*	

Cluster 11

Cluster 12

Cluster 13

Cluster 14

Cluster 15

Cluster 16

Cluster 17

Cluster 18

Cluster 19

Cluster 20

Cluster 21

Cluster 22

Cluster 23

Cluster 24

Cluster 25

Cluster 26

218

Cluster 27

Cluster 28

Cluster 29
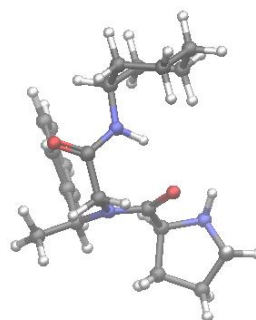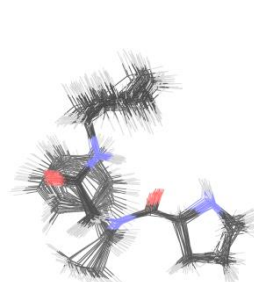
Cluster 30
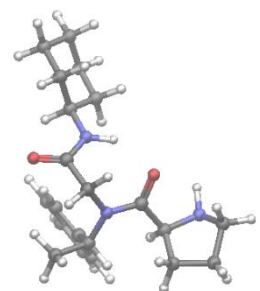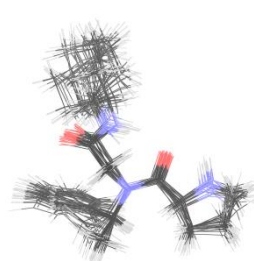
Cluster 31
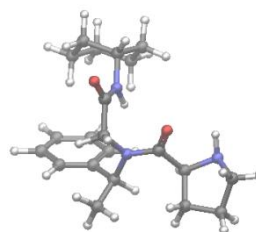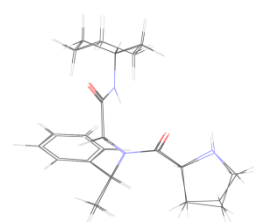
Cluster 32
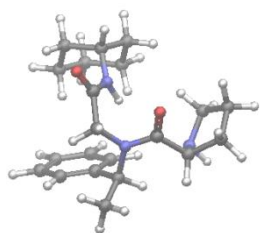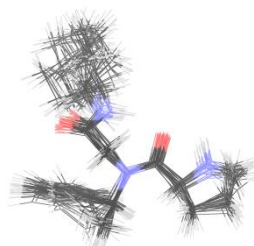
Cluster 33
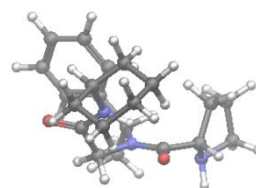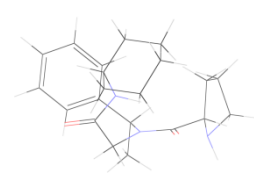
Cluster 34

Cluster 35

Cluster 36

219

	Cluster 37		Cluster 38

	Cluster 39		Cluster 40

	Cluster 41		Cluster 42
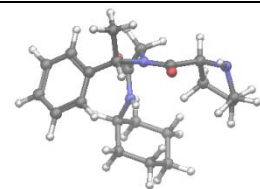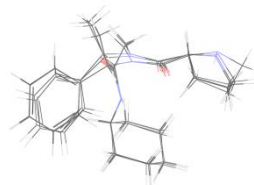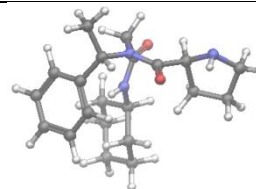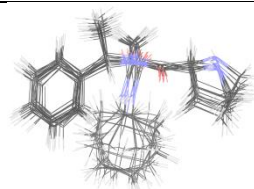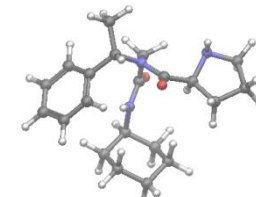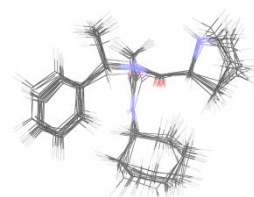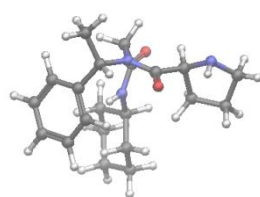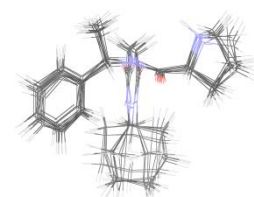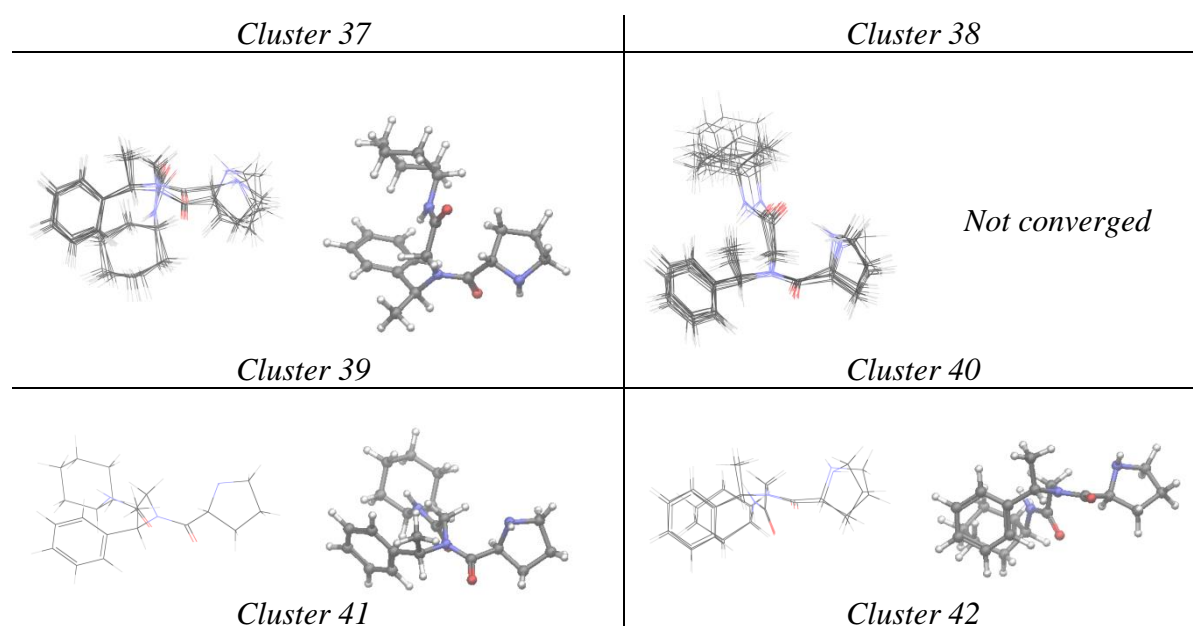
FIGURE 98: Geometries of clustered-superposed conformers and reoptimized low-energy conformers at M06-2X/6-31G(d) of catalyst **67**.

TABLE 1: Energies (in Hartree) and relative energies (in kcal.mol^{-1}) for catalyst **67**.

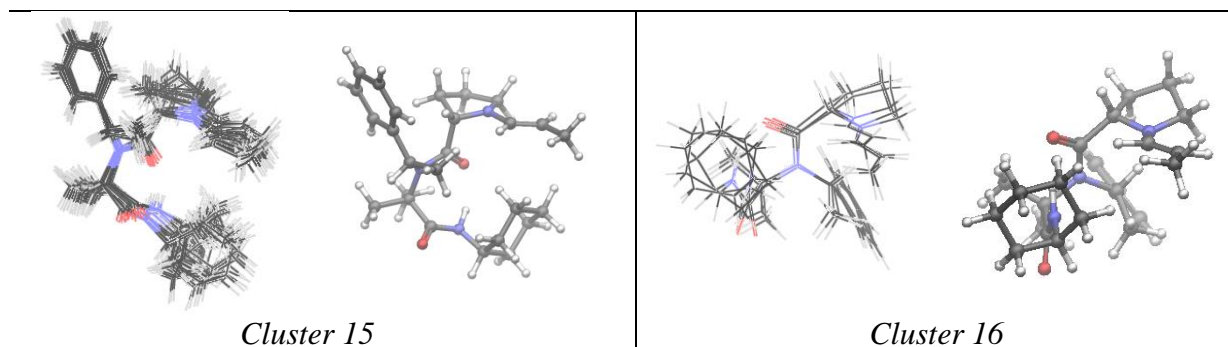| Cluster	M06-2X/6-31G(d) [SDM, chloroform]					M06-2X/6-31+G(d,p) // M06-2X/6-31G(d) [SDM, chloroform]		
	ΔG	ΔG_{rel}	ΔE_{elec}+ZPE	$[\Delta E_{elec}$+ZPE]$_{rel}$	Thermal correction to Gibbs Free Energy	ΔE_{elec}	ΔG^*	ΔG_{rel}
1	-1132.731995	3.2	-1132.678008	2.0	0.455716	-1133.256649	-1132.800933	3.9
2				converged to 1				
3				converged to 4				
4	-1132.734704	1.5	-1132.680966	0.2	0.455261	-1133.257539	-1132.802278	3.1
5	-1132.732840	2.7	-1132.676789	2.8	0.452627	-1133.255393	-1132.802766	2.8
6	-1132.733516	2.3	-1132.678038	2.0	0.452815	-1133.255607	-1132.802792	2.8
7	-1132.737050	0.1	-1132.680714	0.3	0.452378	-1133.257804	-1132.805426	1.1
8	-1132.734817	1.5	-1132.680232	0.6	0.454766	-1133.257392	-1132.802626	2.9
9	-1132.736024	0.7	-1132.680301	0.6	0.453276	-1133.257347	-1132.804071	2.0
10	-1132.735117	1.3	-1132.679292	1.2	0.453839	-1133.256675	-1132.802836	2.7
11	-1132.736310	0.5	-1132.680123	0.7	0.452985	-1133.260192	-1132.807207	0.0
12	-1132.735392	1.1	-1132.680166	0.7	0.454179	-1133.259594	-1132.805415	1.1

13	-1132.730301	4.3	-1132.674751	4.1	0.453847	-1133.252111	-1132.798264	5.6
14	-1132.729848	4.6	-1132.674208	4.4	0.454003	-1133.253084	-1132.799081	5.1
15	-1132.736107	0.7	-1132.677861	2.1	0.450260	-1133.255258	-1132.804998	1.4
16	-1132.727908	5.8	-1132.673326	5.0	0.455632	-1133.251895	-1132.796263	6.9
17	-1132.729195	5.0	-1132.675162	3.8	0.455937	-1133.253416	-1132.797479	6.1
18	-1132.727982	5.8	-1132.674250	4.4	0.456331	-1133.252551	-1132.796220	6.9
19	-1132.734865	1.4	-1132.681263	0.0	0.456473	-1133.260229	-1132.803756	2.2
20	-1132.737159	0.0	-1132.680075	0.7	0.452438	-1133.259478	-1132.807040	0.1
21				converged to 19				
22	-1132.734881	1.4	-1132.679586	1.1	0.454312	-1133.258875	-1132.804563	1.7
23	-1132.736587	0.4	-1132.680430	0.5	0.452818	-1133.258698	-1132.805880	0.8
24	-1132.731964	3.3	-1132.678633	1.7	0.456867	-1133.257360	-1132.800493	4.2
25	-1132.731319	3.7	-1132.676391	3.1	0.454661	-1133.256270	-1132.801609	3.5
26	-1132.729374	4.9	-1132.677244	2.5	0.458956	-1133.256276	-1132.797320	6.2
27	-1132.734706	1.5	-1132.680188	0.7	0.454211	-1133.257980	-1132.803769	2.2
28	-1132.734419	1.7	-1132.679840	0.9	0.454848	-1133.258183	-1132.803335	2.4
29	-1132.732553	2.9	-1132.677636	2.3	0.455137	-1133.256569	-1132.801432	3.6
30	-1132.730973	3.9	-1132.676376	3.1	0.455414	-1133.254905	-1132.799491	4.8
31	-1132.733584	2.2	-1132.676894	2.7	0.452988	-1133.255620	-1132.802632	2.9
32	-1132.733046	2.6	-1132.678077	2.0	0.453925	-1133.257748	-1132.803823	2.1
33	-1132.733276	2.4	-1132.679508	1.1	0.455681	-1133.257664	-1132.801983	3.3
34	-1132.730101	4.4	-1132.675534	3.6	0.454219	-1133.254137	-1132.799918	4.6
35	-1132.732461	2.9	-1132.677591	2.3	0.453669	-1133.255655	-1132.801986	3.3
36	-1132.735954	0.8	-1132.679943	0.8	0.452564	-1133.259052	-1132.806488	0.5
37				converged to 36				
38	-1132.733111	2.5	-1132.677250	2.5	0.453233	-1133.256467	-1132.803234	2.5
39	-1132.732227	3.1	-1132.676816	2.8	0.454345	-1133.256129	-1132.801784	3.4
40				not converged				
41	-1132.731973	3.3	-1132.677424	2.4	0.454912	-1133.255623	-1132.800711	4.1
42	-1132.731922	3.3	-1132.676654	2.9	0.453998	-1133.254869	-1132.800871	4.0

*Obtained from the sum of ΔE_{elec} at M06-2X/6-31+G(d,p) // M06-2X/6-31G(d) [SDM, chloroform] and **Thermal correction to Gibbs Free Energy** at M06-2X/6-31G(d) [SDM, chloroform].

TABLE 2: Boltzmann population, and orientation of the dihedrals Ψ_1 and Ψ_2 for catalyst **67**.

		M06-2X/6-31+G(d,p) // M06-2X/6-31G(d) [SDM, chloroform]					
Clust	%Boltz	dihedrals (Ψ_1/Ψ_2)	*isomer*	Clust	%Boltz	dihedrals (Ψ_1/Ψ_2)	*geometry*
1	*0.0*	-/-	***cis***	**22**	1.9	-/+	***cis***
2		*converged to 1*		**23**	7.6	-/+	***cis***
3		*converged to 4*		**24**	0.0	+/-	***cis***
4	0.2	+/+	***trans***	**25**	0.1	+/-	***cis***
5	0.3	+/+	***trans***	**26**	0.0	+/-	***cis***
6	0.3	+/+	***trans***	**27**	0.8	+/+	***cis***
7	4.7	+/-	***trans***	**28**	0.5	+/+	***cis***
8	0.2	+/-	***trans***	**29**	0.1	+/+	***cis***
9	1.1	+/-	***trans***	**30**	0.0	+/+	***cis***
10	0.3	+/-	***trans***	**31**	0.2	+/+	***cis***
11	31.0	+/-	***trans***	**32**	0.9	+/+	***cis***
12	4.6	+/-	***trans***	**33**	0.1	+/+	***cis***
13	0.0	-/+	***cis***	**34**	0.0	+/+	***cis***
14	0.0	-/+	***cis***	**35**	0.1	-/-	***trans***
15	3.0	-/+	***cis***	**36**	14.5	-/-	***trans***
16	0.0	-/+	***cis***	**37**		*converged to 36*	
17	0.0	-/+	***cis***	**38**	0.5	-/-	***trans***
18	0.0	-/+	***cis***	**39**	0.1	-/-	***trans***
19	0.8	-/+	***cis***	**41**	0.0	-/-	***trans***
20	26.0	-/+	***cis***	**42**	0.0	-/-	***trans***
21		*converged to 19*					
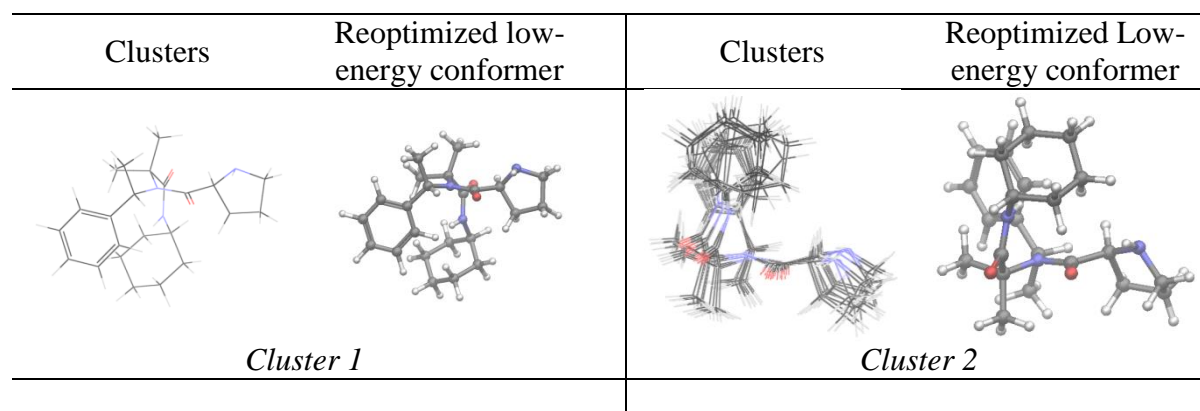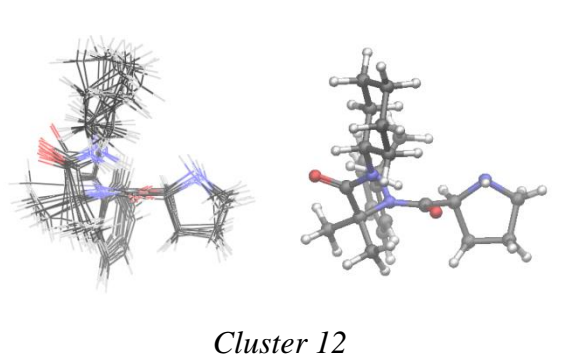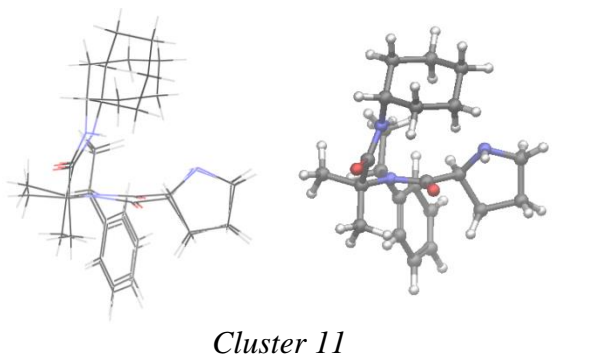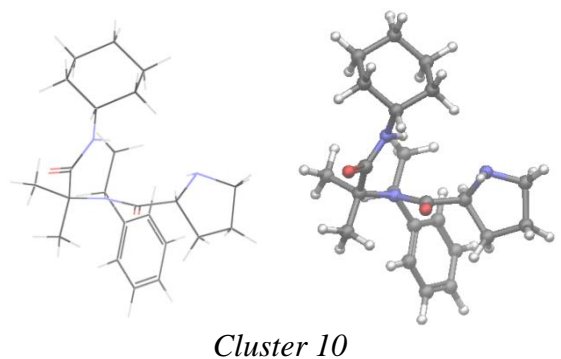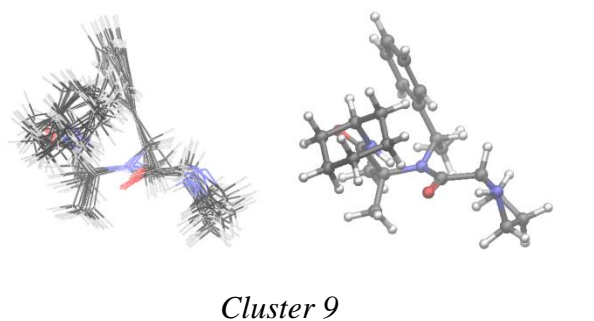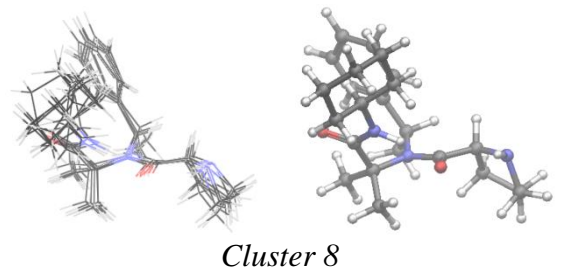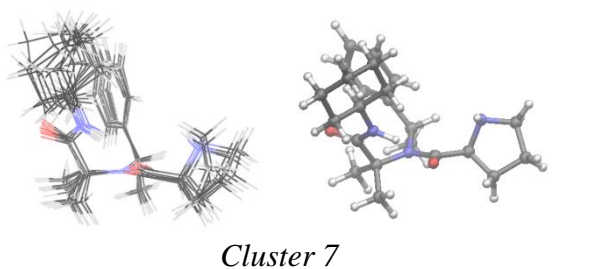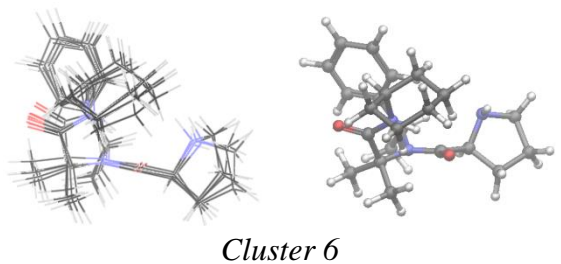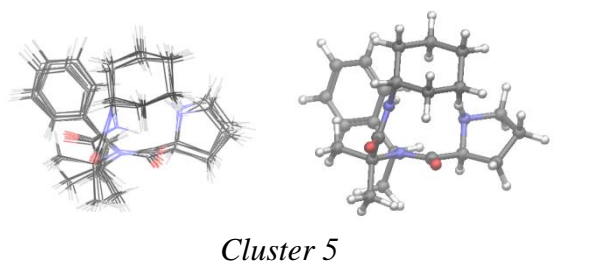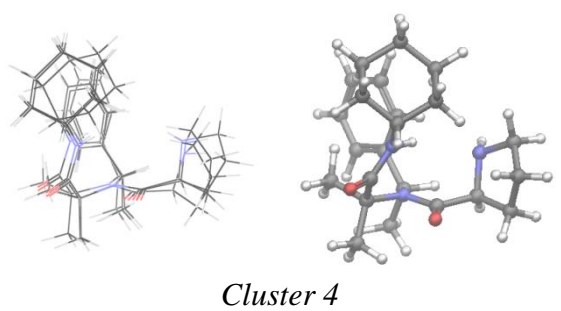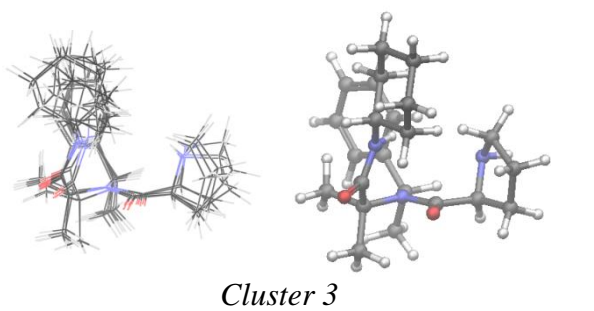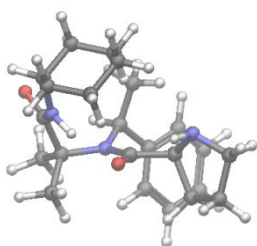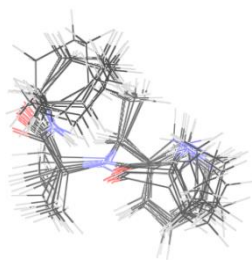
Clusters	Reoptimized low-energy conformer	Clusters	Reoptimized Low-energy conformer
Cluster 1		*Cluster 2*	
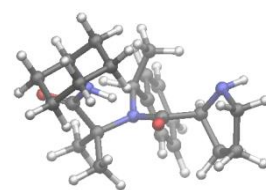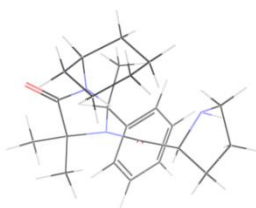
Cluster 3

Cluster 4

Cluster 5

Cluster 6

Cluster 7

Cluster 8

Cluster 9

Cluster 10

Cluster 11

Cluster 12

Cluster 13

Cluster 14

Cluster 15

Cluster 16

Cluster 17

Cluster 18

Cluster 19
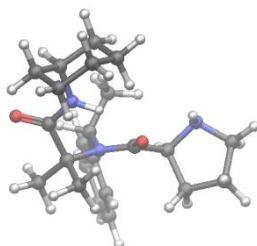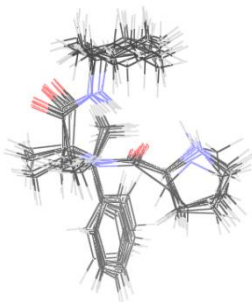
Cluster 20
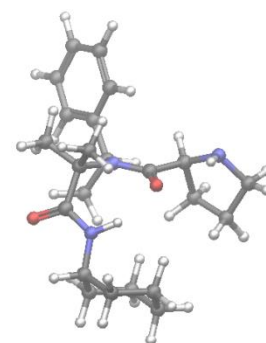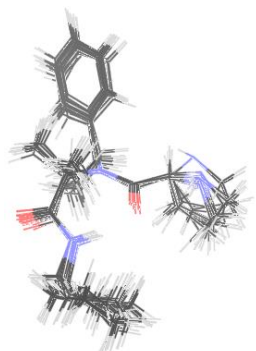
Cluster 21
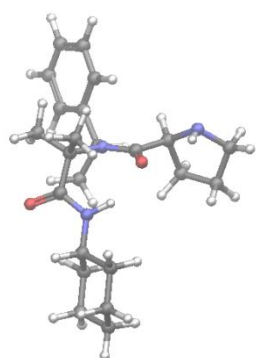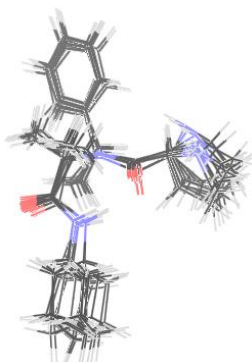
Cluster 22
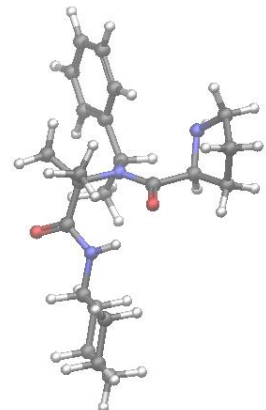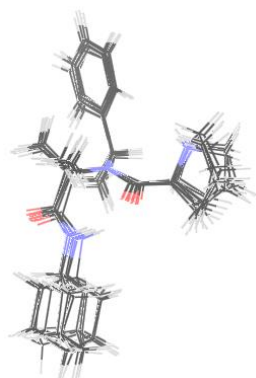
Cluster 23
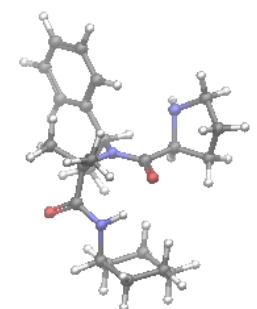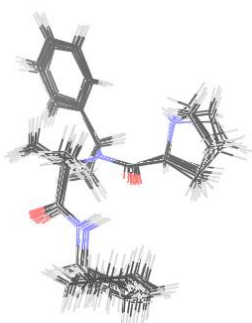
Cluster 24
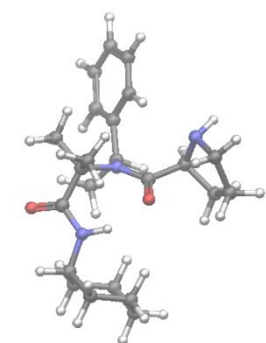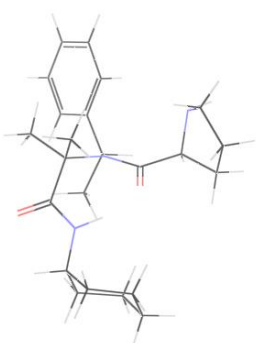
Cluster 25
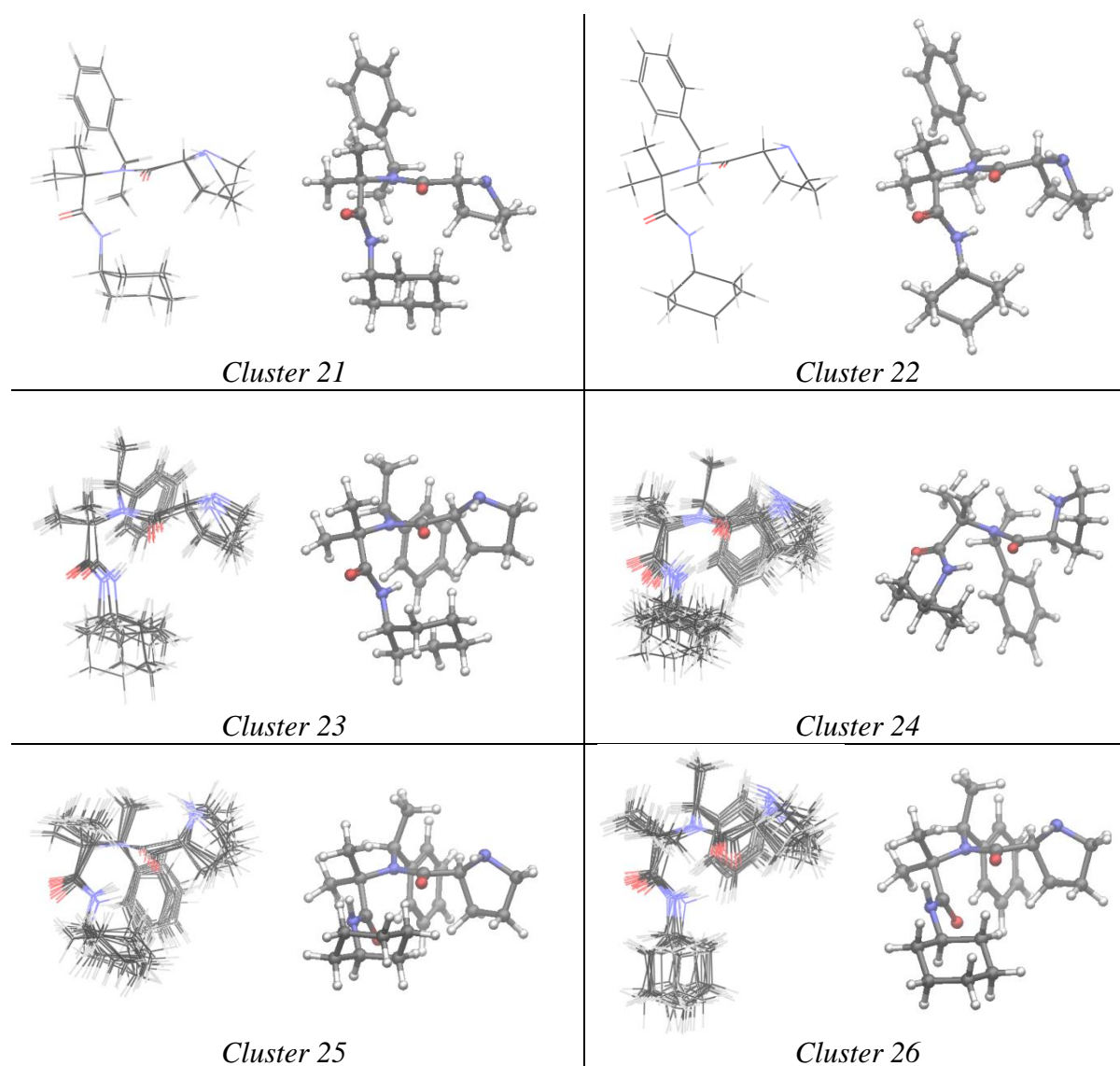
Cluster 26

FIGURE 99: Geometries of clustered-superposed conformers and reoptimized low-energy conformers at M06-2X/6-31G(d) of catalyst **69**.

TABLE 3: Energies (in Hartree) and relative energies (in kcal.mol^{-1}) for catalyst **69**.

Clust		M06-2X/6-31G(d) [SDM, chloroform]				M06-2X/6-31+G(d,p) // M06-2X/6-31G(d) [SDM, chloroform]		
	ΔG	ΔG_{rel}	ΔE_{elec}+ZPE	$[\Delta E_{elec}$+ZPE$]_{rel}$	Thermal correction to Gibbs Free Energy	ΔE_{elec}	ΔG^*	ΔG_{rel}
1	-1211.258480	2.2	-1211.202411	2.4	0.510145	-1211.842590	-1211.332445	1.7
2	-1211.260514	0.9	-1211.205150	0.7	0.510203	-1211.844232	-1211.334029	0.7
3	-1211.260457	1.0	-1211.204993	0.8	0.510056	-1211.843467	-1211.333411	1.1
4	-1211.259226	1.8	-1211.203803	1.5	0.509958	-1211.841909	-1211.331951	2.0

5	-1211.258890	2.0	-1211.203888	1.5	0.510472	-1211.841790	-1211.331318	2.4
6	-1211.255815	3.9	-1211.198657	4.7	0.508590	-1211.837486	-1211.328896	3.9
7	-1211.253069	5.6	-1211.198476	4.9	0.511345	-1211.837915	-1211.326570	5.4
8	-1211.254219	4.9	-1211.197666	5.4	0.509643	-1211.837843	-1211.328200	4.4
9	-1211.254461	4.7	-1211.198052	5.1	0.509257	-1211.837170	-1211.327913	4.5
10	-1211.259905	1.3	-1211.205300	0.6	0.510740	-1211.843948	-1211.333208	1.2
11	-1211.260930	0.7	-1211.205299	0.6	0.510905	-1211.844702	-1211.333797	0.8
12	-1211.258594	2.2	-1211.201612	2.9	0.508205	-1211.840716	-1211.332511	1.6
13	-1211.257104	3.1	-1211.201079	3.2	0.510925	-1211.840778	-1211.329853	3.3
14	-1211.254909	4.5	-1211.198017	5.1	0.508704	-1211.836847	-1211.328143	4.4
15	-1211.259436	1.6	-1211.201697	2.8	0.507454	-1211.840296	-1211.332842	1.4
16	-1211.256454	3.5	-1211.201291	3.1	0.511559	-1211.840972	-1211.329413	3.6
17	-1211.259413	1.6	-1211.201617	2.9	0.507521	-1211.841065	-1211.333544	1.0
18	-1211.254074	5.0	-1211.196188	6.3	0.507278	-1211.833926	-1211.326648	5.3
19	-1211.252756	5.8	-1211.196845	5.9	0.510156	-1211.834714	-1211.324558	6.6
20	-1211.254617	4.6	-1211.197999	5.2	0.509499	-1211.836150	-1211.326651	5.3
21	-1211.258194	2.4	-1211.202442	2.4	0.510370	-1211.842113	-1211.331743	2.1
22	-1211.258865	2.0	-1211.202058	2.6	0.509005	-1211.841837	-1211.332832	1.4
23	-1211.259780	1.4	-1211.205714	0.3	0.512782	-1211.845872	-1211.333090	1.3
24	-1211.253701	5.2	-1211.197378	5.5	0.509342	-1211.836006	-1211.326664	5.3
25	-1211.261837	0.1	-1211.205734	0.3	0.510275	-1211.844785	-1211.334510	0.4
26	-1211.262027	0.0	-1211.206207	0.0	0.510495	-1211.845627	-1211.335132	0.0
rotamer of 1	-1211.256311	3.6	-1211.199698	4.1	0.508950	-1211.839282	-1211.330332	3.0

*Obtained from the sum of **ΔE$_{elec}$** at M06-2X/6-31+G(d,p) // M06-2X/6-31G(d) [SDM, chloroform] and **Thermal correction to Gibbs Free Energy** at M06-2X/6-31G(d) [SDM, chloroform].

TABLE 4: Boltzmann population, and orientation of the dihedrals Ψ_1 and Ψ_2 for catalyst **69**.

	M06-2X/6-31+G(d,p) // M06-2X/6-31G(d) [SDM, chloroform]						
Clust	%Boltz	dihedrals (Ψ1/Ψ2)	*isomer*	Clust	%Boltz	dihedrals (Ψ1/Ψ2)	*isomer*
1	*1.9*	-/-	**trans**	**14**	*0.0*	+/-	**cis**
2	*10.2*	+/+	**cis**	**15**	*2.9*	+/-	**cis**

3	5.3	+/+	*cis*	16	0.1	-/+	*cis*
4	1.1	+/+	*cis*	17	6.1	-/+	*cis*
5	0.6	+/+	*cis*	18	0.0	-/+	*cis*
6	0.0	+/+	*cis*	19	0.0	-/+	*cis*
7	0.0	+/+	*cis*	20	0.0	-/+	*cis*
8	0.0	+/+	*cis*	21	0.9	-/+	*cis*
9	0.0	+/+	*cis*	22	2.9	-/+	*cis*
10	4.3	+/-	*cis*	23	3.8	-/-	*cis*
11	8.0	+/-	*cis*	24	0.0	-/-	*cis*
12	2.0	+/-	*cis*	25	17.0	-/-	*cis*
13	0.1	+/-	*cis*	26	32.8	-/-	*cis*

TABLE 5: Energies (in Hartree) and relative energies (in kcal.mol^{-1}) of transition structure **TS-1** and **TS-2**.

	M06-2X/6-31G(d) [SDM, chloroform]				M06-2X/6-31+G(d,p) // M06-2X/6-31G(d) [SDM, chloroform]		
TS	ΔG	ΔG_{rel}	Thermal correction to Gibbs Free Energy	Imaginary Frequency (cm^{-1})	ΔE_{elec}	ΔG^*	ΔG_{rel}
TS-1	-1132.703866	20.9	0.451358	-79.23	-1133.225341	-1132.773983	20.8
TS-2	-1211.235697	16.5	0.508228	-59.98	-1211.817241	-1211.309013	16.4

*Obtained from the sum of **ΔE_{elec}** at M06-2X/6-31+G(d,p) // M06-2X/6-31G(d) [SDM, chloroform] and **Thermal correction to Gibbs Free Energy** at M06-2X/6-31G(d) [SDM, chloroform].

Clusters	Reoptimized low-energy conformer	Clusters	Reoptimized Low-energy conformer
Cluster 1		*Cluster 2*	
Cluster 3		*Cluster 4*	

Cluster 5

Cluster 6

Cluster 7

Cluster 8

Cluster 9

Cluster 10

Not converged

Cluster 11

Not converged

Cluster 12

Cluster 13

Cluster 14

| | *Cluster 15* | | *Cluster 16* |
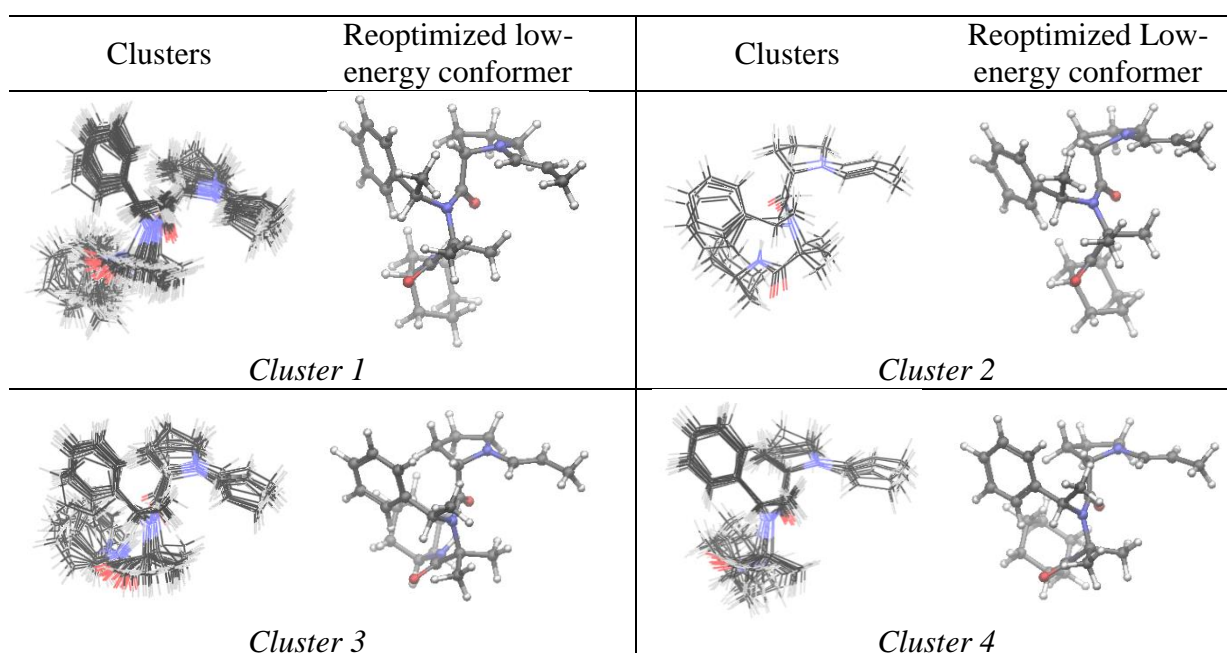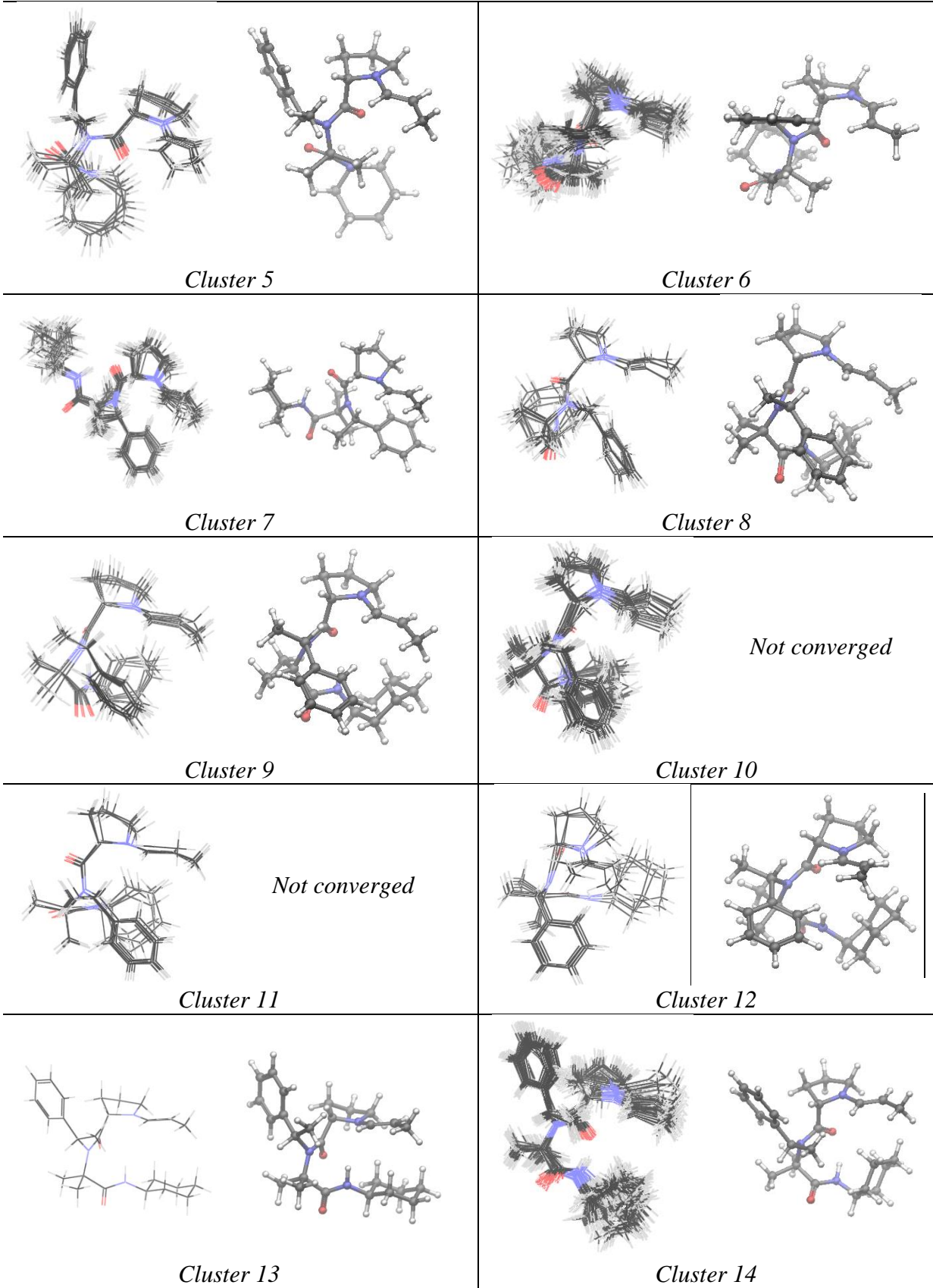
FIGURE 100: Geometries of clustered-superposed conformers and reoptimized low-energy conformers at M06-2X/6-31G(d) of enamine 2 for catalyst **69**.

TABLE 6: Energies (in Hartree) and relative energies (in kcal.mol^{-1}) for enamine **2-en**.

| | M06-2X/6-31G(d) [SDM, chloroform] | | | | M06-2X/6-31+G(d,p) // M06-2X/6-31G(d) [SDM, chloroform] | | | |
Clust	ΔG	ΔG_{rel}	ΔE_{elec}+ZPE	Thermal correction to Gibbs Free Energy	ΔE_{elec}	ΔG^*	ΔG_{rel}	Boltz(%)
1	-1327.860737	2.0	-1327.799359	0.565971	-1328.503939	-1327.937968	2.2	2.2
2	-1327.860734	2.0	-1327.799358	0.565973	-1328.503940	-1327.937967	2.2	2.2
3	-1327.859699	2.7	-1327.798553	0.566339	-1328.502782	-1327.936443	3.2	0.4
4	-1327.860028	2.5	-1327.798686	0.566002	-1328.502753	-1327.936751	3.0	0.6
5	-1327.860048	2.5	-1327.798283	0.565629	-1328.502842	-1327.937213	2.7	1.0
6	-1327.858215	3.6	-1327.797929	0.567188	-1328.502390	-1327.935202	3.9	0.1
7	-1327.853551	6.6	-1327.793413	0.567778	-1328.498353	-1327.930575	6.8	0.0
8	-1327.85288	7.0	-1327.794258	0.570180	-1328.500556	-1327.930376	7.0	0.0
9	-1327.852799	7.0	-1327.793952	0.569581	-1328.499779	-1327.930198	7.1	0.0
10				*not converged*				
11				*not converged*				
12	-1327.858168	3.7	-1327.798419	0.567970	-1328.503377	-1327.935407	3.8	0.1
13	-1327.863997	0.0	-1327.802916	0.565707	-1328.507195	-1327.941488	0.0	93.2
14	-1327.857252	4.2	-1327.797991	0.568694	-1328.502324	-1327.933630	4.9	0.0
15	-1327.857257	4.2	-1327.797992	0.568689	-1328.502324	-1327.933635	4.9	0.0
16	-1327.854425	6.0	-1327.792382	0.565595	-1328.496937	-1327.931342	6.4	0.0

*Obtained from the sum of **ΔE_{elec}** at M06-2X/6-31+G(d,p) // M06-2X/6-31G(d) [SDM, chloroform] and **Thermal correction to Gibbs Free Energy** at M06-2X/6-31G(d) [SDM, chloroform].
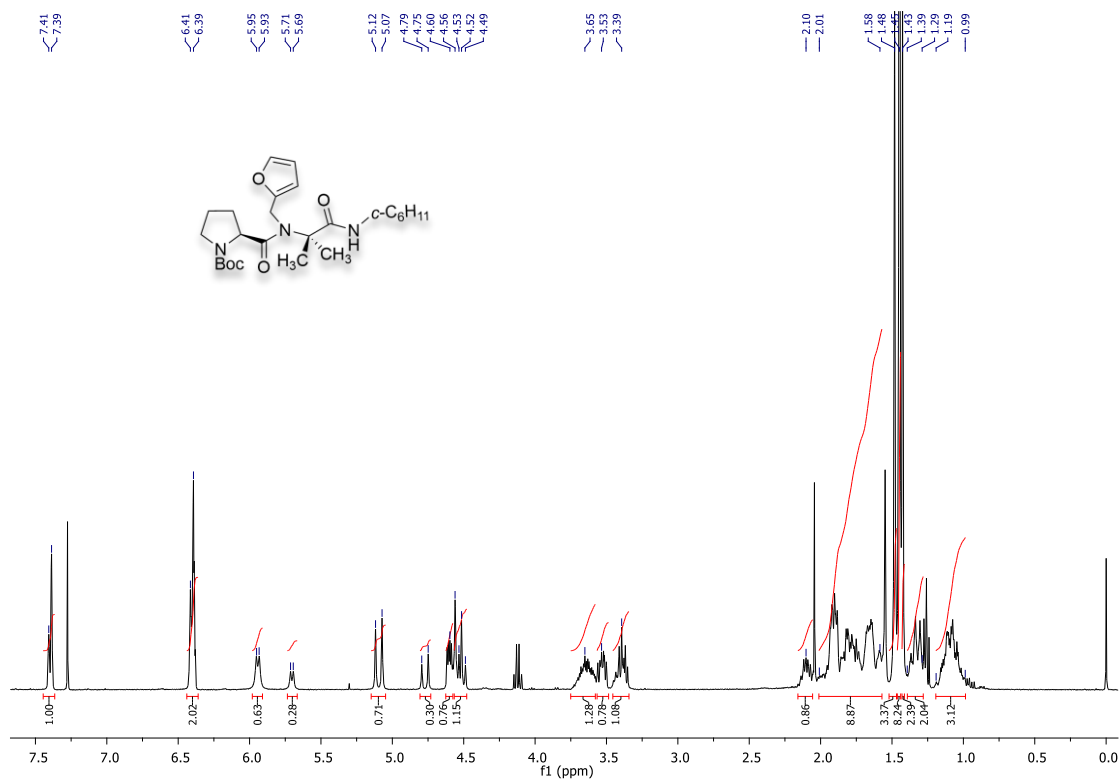
FIGURE 101: 400 MHz ^{1}H NMR spectra in CDCl$_3$ of **87**.

FIGURE 102: 100 MHz ^{13}C NMR spectra in CDCl$_3$ of **87**.

FIGURE 103: 400 MHz ^{1}H NMR spectra in CDCl$_3$ of **91**.

FIGURE 104: 100 MHz ^{13}C NMR spectra in CDCl$_3$ of **91**.

FIGURE 105: 400 MHz ^{1}H NMR spectra in CDCl$_3$ of **88**.

FIGURE 106: 100 MHz ^{13}C NMR spectra in CDCl$_3$ of **88**.

C:\...\Polimeros project\reacciones en fluxo\Reacciones en fluxo toluene F165\F220 0-2h entry 2.lcd — PDA Multi 1 / 210nm 4nm

PeakTable — PDA Ch1 210nm 4nm

Peak#	Ret. Time	Area	Height	Area %	Height %
1	20.220	1587854	45517	12.317	16.913
2	23.057	229856	6527	1.783	2.425
3	27.506	10678706	211414	82.837	78.558
4	49.536	394748	5660	3.062	2.103
Total		12891163	269118	100.000	100.000

C:\...\Polimeros project\reacciones en fluxo\Reacciones en fluxo toluene F165\F220 2-4h entry 3.lcd — PDA Multi 1 / 210nm 4nm

PeakTable — PDA Ch1 210nm 4nm

Peak#	Ret. Time	Area	Height	Area %	Height %
1	20.484	1557976	46209	11.639	16.702
2	23.407	260434	7046	1.946	2.547
3	27.937	11116474	217305	83.047	78.543
4	50.451	450875	6108	3.368	2.208
Total		13385758	276669	100.000	100.000

C:\...\Polimeros project\reacciones en fluxo\Reacciones en fluxo toluene F165\F220 4-6h entry 4.lcd — PDA Multi 1 / 210nm 4nm

PeakTable — PDA Ch1 210nm 4nm

Peak#	Ret. Time	Area	Height	Area %	Height %
1	20.643	1759063	50465	12.300	17.081
2	23.561	304022	7992	2.126	2.705
3	28.108	11808725	230951	82.570	78.168
4	50.939	429640	6046	3.004	2.046
Total		14301450	295454	100.000	100.000

C:\...\Polimeros project\reacciones en fluxo\Reacciones en fluxo toluene F165\F220 6-8h entry 5.lcd — PDA Multi 1 / 210nm 4nm

PeakTable — PDA Ch1 210nm 4nm

Peak#	Ret. Time	Area	Height	Area %	Height %
1	20.750	2558251	71344	12.801	17.688
2	23.713	430531	11138	2.154	2.761
3	28.268	16396233	312604	82.044	77.501
4	51.318	599641	8266	3.001	2.049
Total		19984657	403353	100.000	100.000

C:\...\Polimeros project\reacciones en fluxo\Reacciones en fluxo toluene F165\F220 8-10h entry 6.lcd — PDA Multi 1 / 210nm 4nm

PeakTable — PDA Ch1 210nm 4nm

Peak#	Ret. Time	Area	Height	Area %	Height %
1	20.814	2609783	72871	12.500	17.194
2	23.814	445781	11406	2.135	2.691
3	28.346	17230466	330988	82.526	78.095
4	51.577	592685	8561	2.839	2.020
Total		20878715	423826	100.000	100.000

C:\...\Polimeros project\reacciones en fluxo\Reacciones en fluxo toluene F165\F220 10-12h entry 7.lcd — PDA Multi 1 / 210nm 4nm

PeakTable — PDA Ch1 210nm 4nm

Peak#	Ret. Time	Area	Height	Area %	Height %
1	20.860	3875196	104361	13.278	17.997
2	23.873	674856	16601	2.312	2.863
3	28.403	23865884	447601	81.774	77.189
4	51.773	769271	11317	2.636	1.952
Total		29185207	579880	100.000	100.000

C:\...\Polimeros project\reacciones en fluxo\Reacciones en fluxo toluene F165\F220 12-24h entry 8.lcd — PDA Multi 1 / 210nm 4nm

PeakTable — PDA Ch1 210nm 4nm

Peak#	Ret. Time	Area	Height	Area %	Height %
1	21.149	34196	1054	10.236	16.098
2	24.245	4504	148	1.348	2.267
3	29.106	288448	5240	86.342	80.030
4	51.168	6929	105	2.074	1.606
Total		334078	6547	100.000	100.000

C:\...\Polimeros project\reacciones en fluxo\Reacciones en fluxo toluene F165\F220 24-36h entry9 1micro.lcd — PDA Multi 1 / 210nm 4nm

PeakTable — PDA Ch1 210nm 4nm

Peak#	Ret. Time	Area	Height	Area %	Height %
1	19.790	2045275	58935	13.030	17.215
2	22.489	308886	8179	1.968	2.389
3	26.707	12772745	267759	81.372	78.214
4	47.250	569814	7469	3.630	2.182
Total		15696720	342341	100.000	100.000

233

FIGURE 107: Chiral HPLC of **78** obtained by continuous flow chemistry reaction with polymer **89**. Chiralpak OD-H (*n*-hexane/i-PrOH 90:10), 25°C) at 1.0 ml/min, UV detection at 210 nm of the crude reaction.
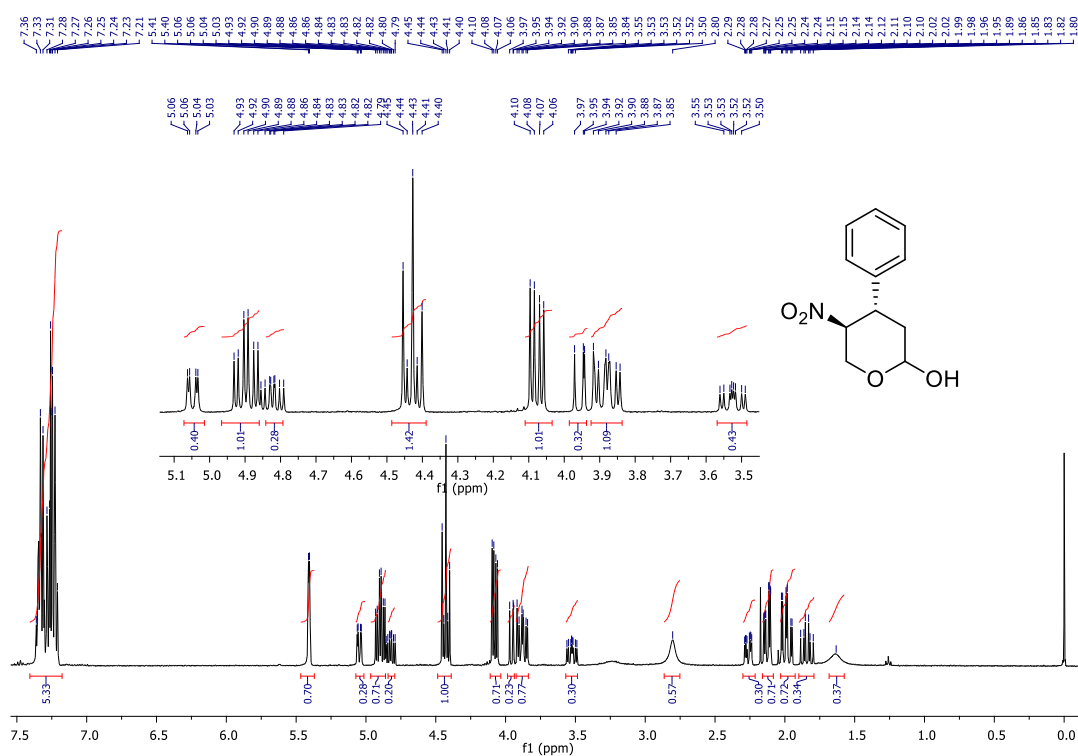
FIGURE 108: 400 MHz ^{1}H NMR spectra in CDCl$_3$ of 5-nitro-4-phenyl tetrahydro-2H-pyran-2-ol (**114**).
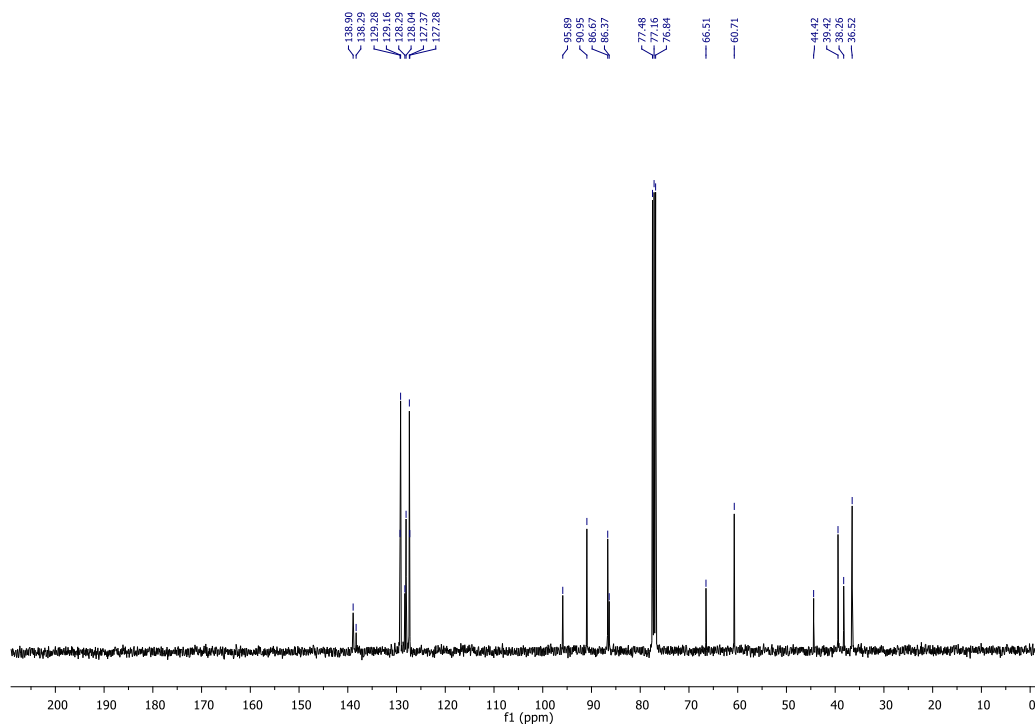
FIGURE 109: 100 MHz ^{13}C NMR spectra in CDCl$_3$ of 5-nitro-4-phenyl tetrahydro-2H-pyran-2-ol (**114**).

PeakTable

PDA Ch1 210nm 4nm
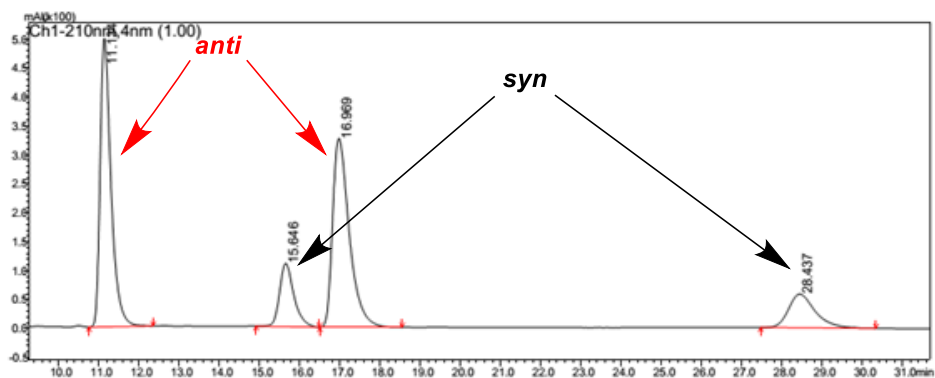
Peak#	Ret. Time	Area	Height	Area %	Height %
1	11.134	9360466	497988	38.711	50.209
2	15.646	2705159	109219	11.187	11.012
3	16.969	9425154	326562	38.978	32.925
4	28.437	2689792	58067	11.124	5.855
Total		24180570	991837	100.000	100.000

FIGURE 110: Chiral HPLC analysis of racemic 5-nitro-4-phenyl tetrahydro-2H-pyran-2-ol (**114**).

235

PeakTable

PDA Ch1 210nm 4nm
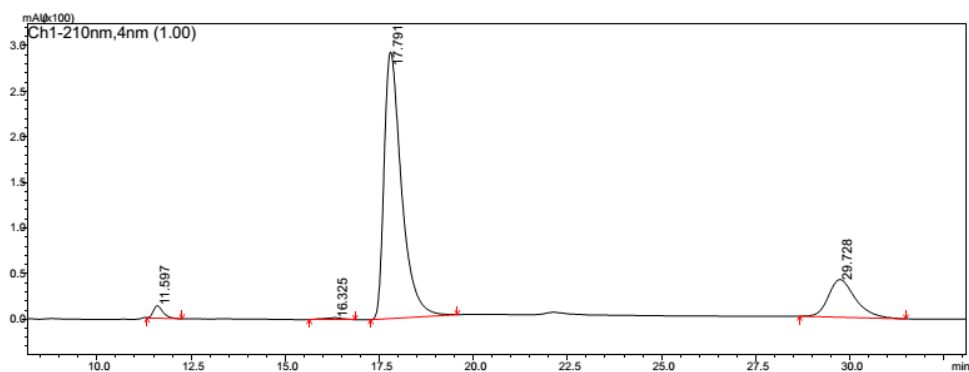
Peak#	Ret. Time	Area	Height	Area %	Height %
1	11.597	241952	13607	2.049	3.896
2	16.325	66392	1890	0.562	0.541
3	17.791	9427283	292431	79.848	83.732
4	29.728	2070962	41318	17.541	11.831
Total		11806590	349247	100.000	100.000

FIGURE 111: Chiral HPLC analysis of 5-nitro-4-phenyl tetrahydro-2H-pyran-2-ol (**114**) obtained by the 1,4-addition reaction catalyzed by **15**. Chiralpak AD-H (*n*-hexane/i-PrOH 90:10), 25°C at 1.0 ml/min, UV detection at 210 nm.
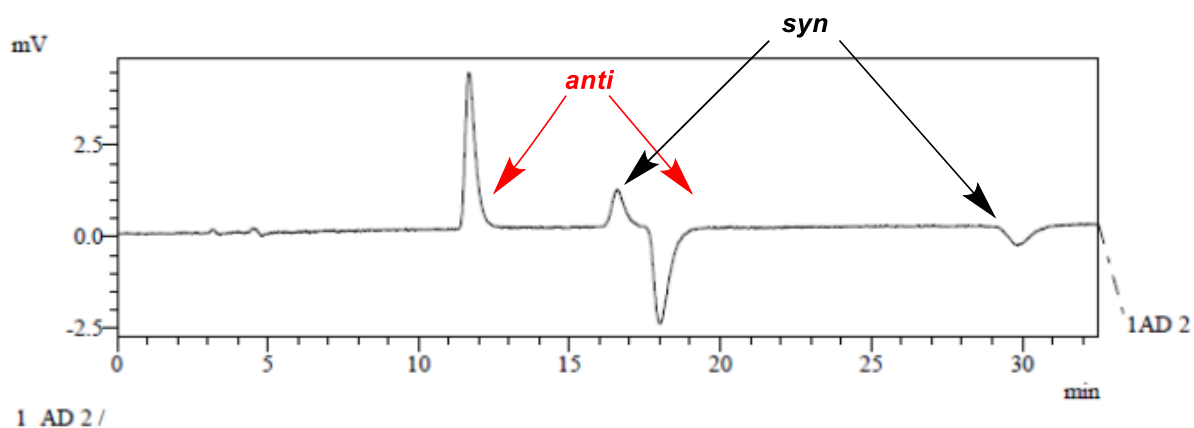
FIGURE 112: Dichroism circular of compound **114**.
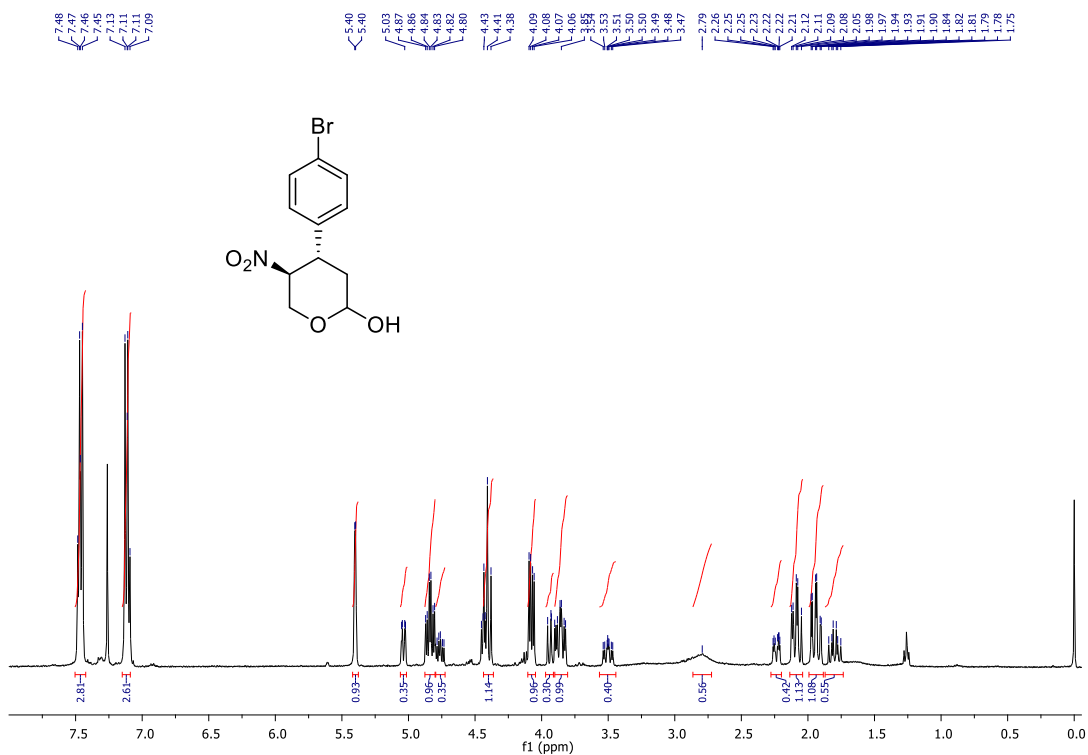
FIGURE 113: 400 MHz ^{1}H NMR spectra in CDCl$_3$ of 4-(4-bromophenyl)-5-nitrotetrahydro-2H-pyran-2-ol (**116**).
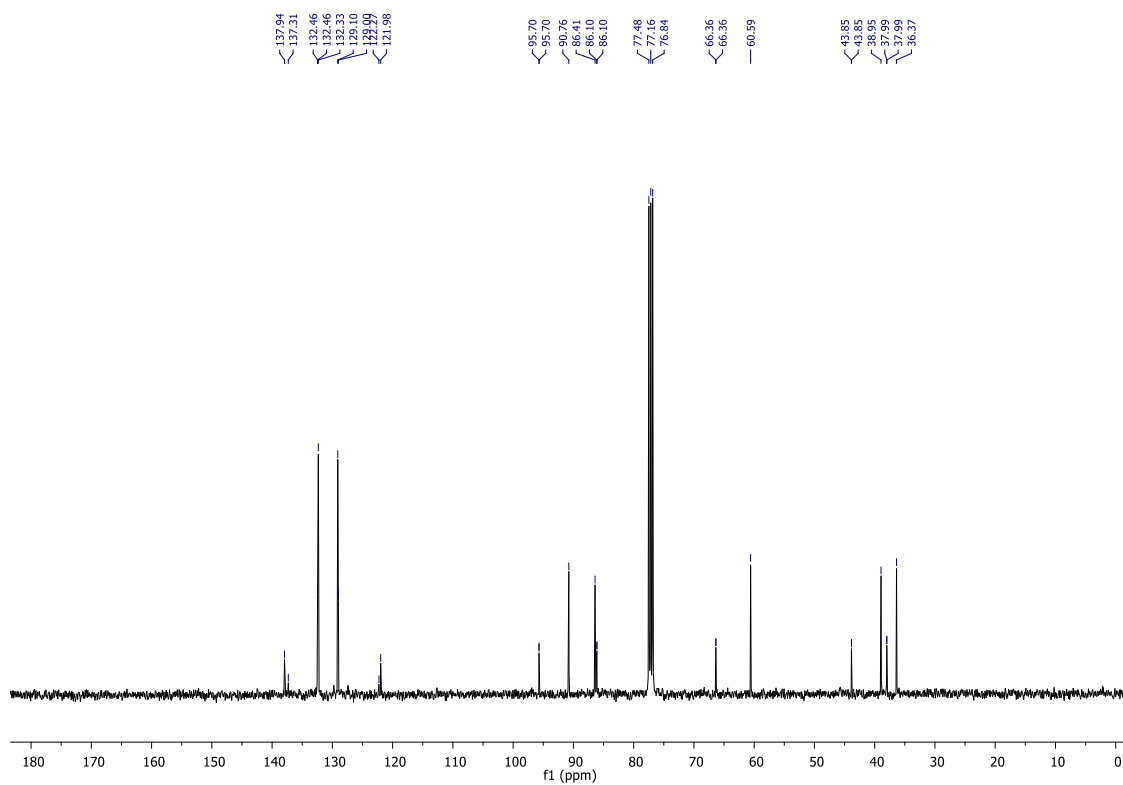
FIGURE 114: 100 MHz ^{13}C NMR spectra in CDCl$_3$ of 4-(4-bromophenyl)-5-nitrotetrahydro-2H-pyran-2-ol (**116**).
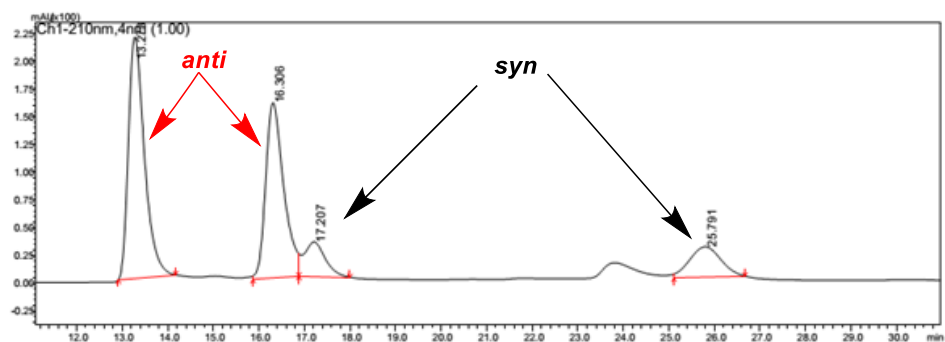
PeakTable

PDA Ch1 210nm 4nm

Peak#	Ret. Time	Area	Height	Area %	Height %
1	13.273	5333689	217496	44.338	50.128
2	16.306	4356893	157820	36.218	36.374
3	17.207	1034801	31310	8.602	7.216
4	25.791	1304093	27258	10.841	6.282
Total		12029476	433884	100.000	100.000

FIGURE 115: Chiral HPLC analysis of racemic 4-(4-bromophenyl)-5-nitrotetrahydro-2H-pyran-2-ol (**116**).
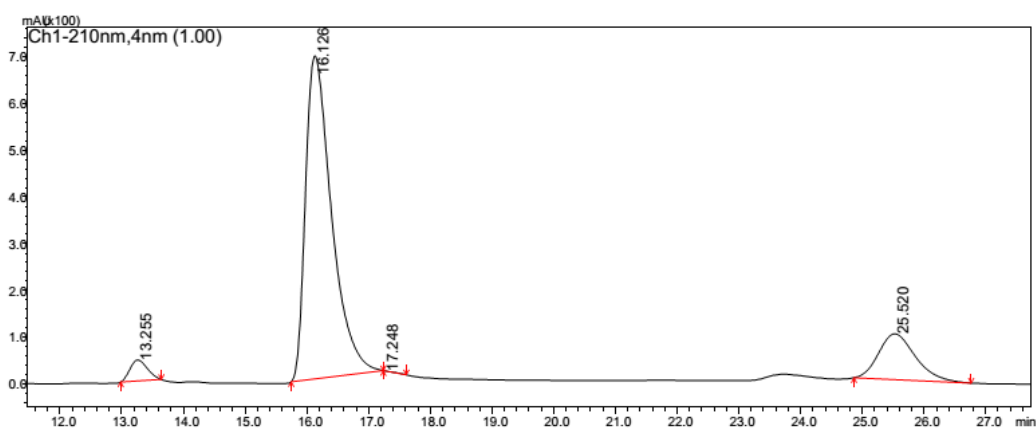
PeakTable

PDA Ch1 210nm 4nm

Peak#	Ret. Time	Area	Height	Area %	Height %
1	13.255	879551	44700	3.490	5.371
2	16.126	20260799	689739	80.384	82.883
3	17.248	4014	-42	0.016	-0.005
4	25.520	4060524	97790	16.110	11.751
Total		25204888	832187	100.000	100.000

FIGURE 116: Chiral HPLC analysis of 4-(4-bromophenyl)-5-nitrotetrahydro-2H-pyran-2-ol (**116**) obtained by the 1,4-addition reaction catalyzed by **15**. Chiralpak AD-H (n-hexane/i-PrOH 90:10), 25°C at 1.0 ml/min, UV detection at 210 nm.
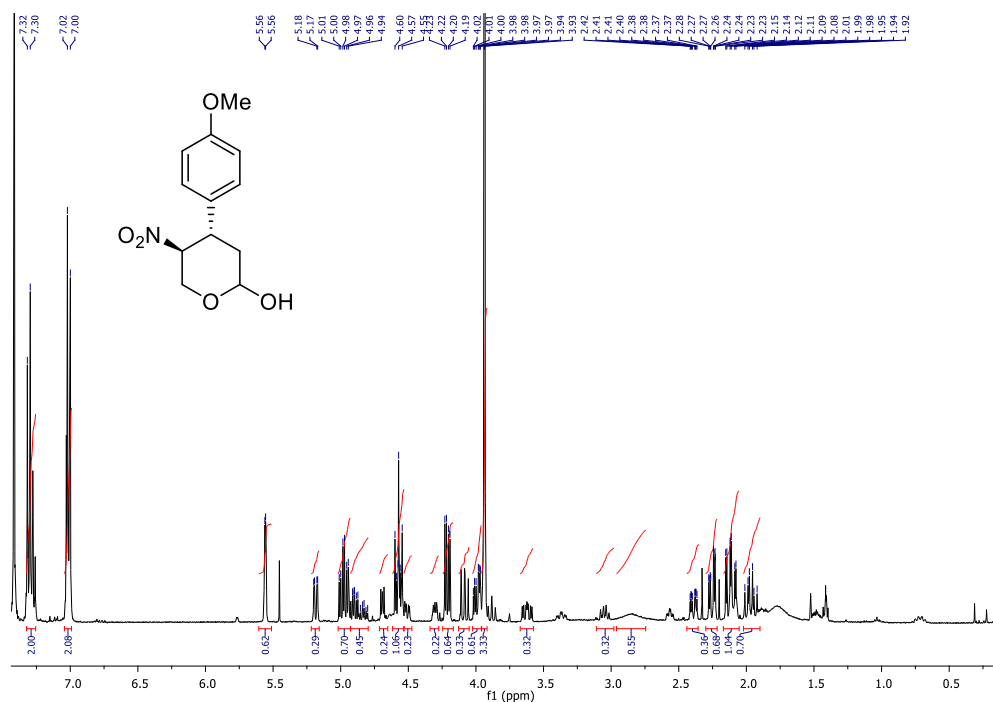
FIGURE 117: 400 MHz ^{1}H NMR spectra in CDCl$_3$ of 4-(4-methoxyphenyl)-5-nitrotetrahydro-2H-pyran-2-ol (**117**).
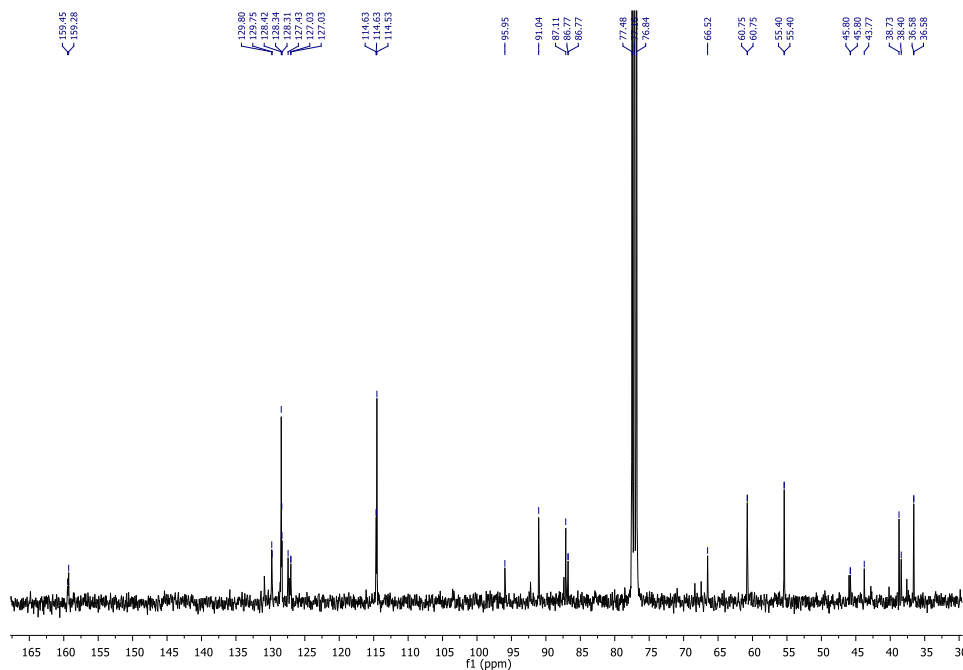
FIGURE 118: 100 MHz ^{13}C NMR spectra in CDCl$_3$ of 4-(4-methoxyphenyl)-5-nitrotetrahydro-2H-pyran-2-ol (**117**).
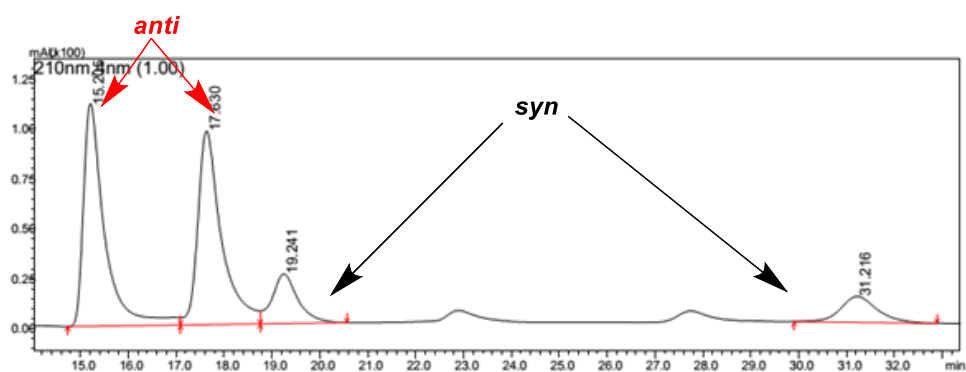
PeakTable

PDA Ch1 210nm 4nm

Peak#	Ret. Time	Area	Height	Area %	Height %
1	15.205	3413146	111454	40.808	45.287
2	17.630	3324202	96900	39.745	39.374
3	19.241	933899	24820	11.166	10.085
4	31.216	692582	12930	8.281	5.254
Total		8363829	246105	100.000	100.000

FIGURE 119: Chiral HPLC analysis of racemic 4-(4-methoxyphenyl)-5-nitrotetrahydro-2H-pyran-2-ol (**117**).
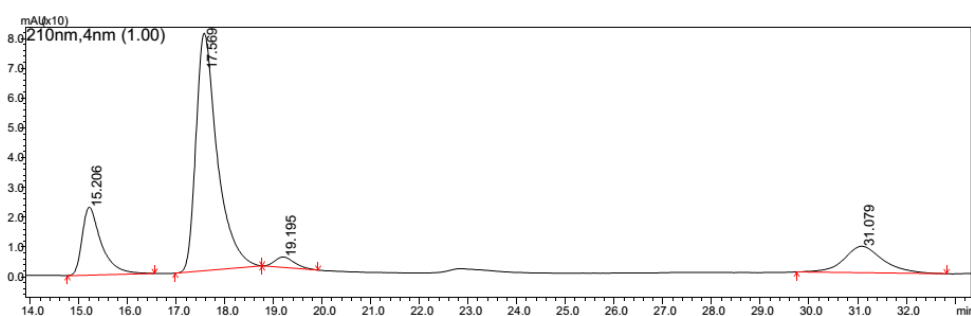
PeakTable

PDA Ch1 210nm 4nm

Peak#	Ret. Time	Area	Height	Area %	Height %
1	15.206	625100	22821	17.072	19.851
2	17.569	2437204	79717	66.563	69.341
3	19.195	99616	3519	2.721	3.061
4	31.079	499575	8906	13.644	7.747
Total		3661495	114964	100.000	100.000

FIGURE 120: Chiral HPLC analysis of 4-(4-methoxyphenyl)-5-nitrotetrahydro-2H-pyran-2-ol (**117**) obtained by the 1,4-addition reaction catalyzed by **15**. Chiralpak AD-H (n-hexane/i-PrOH 90:10), 25°C at 1.0 ml/min, UV detection at 210 nm.
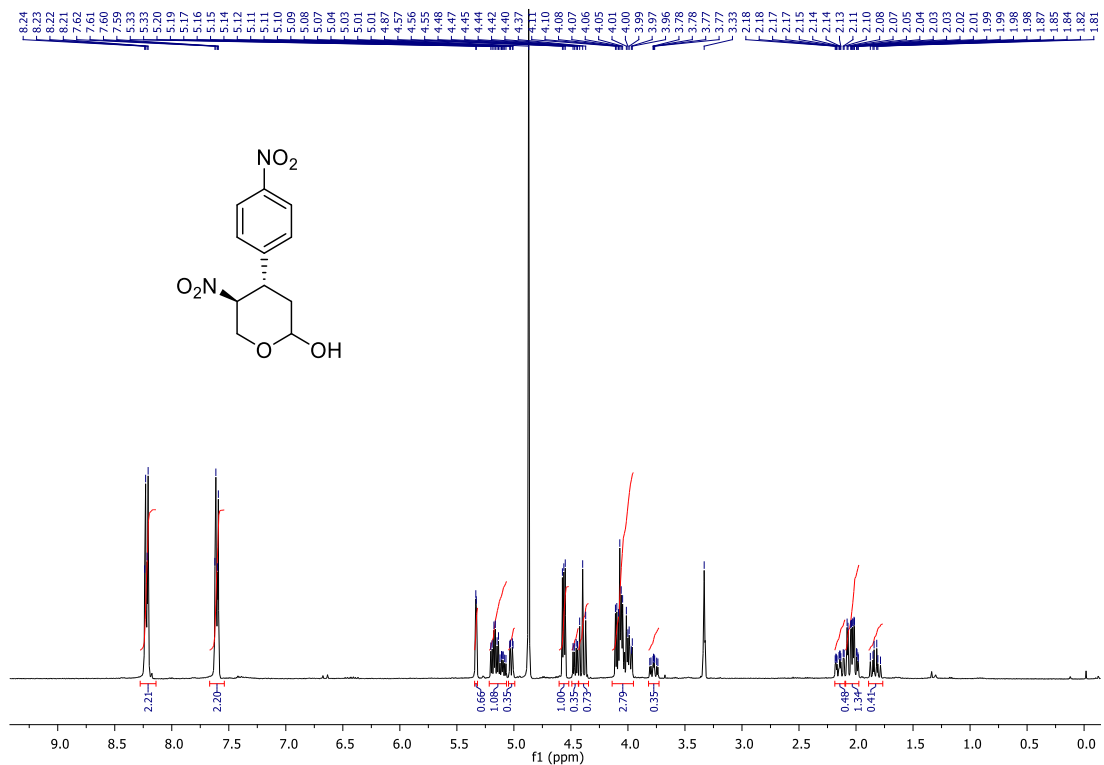
FIGURE 121: 400 MHz ^{1}H NMR spectra in MeOD of 4-(4-nitrophenyl)-5-nitrotetrahydro-2H-pyran-2-ol (**118**).
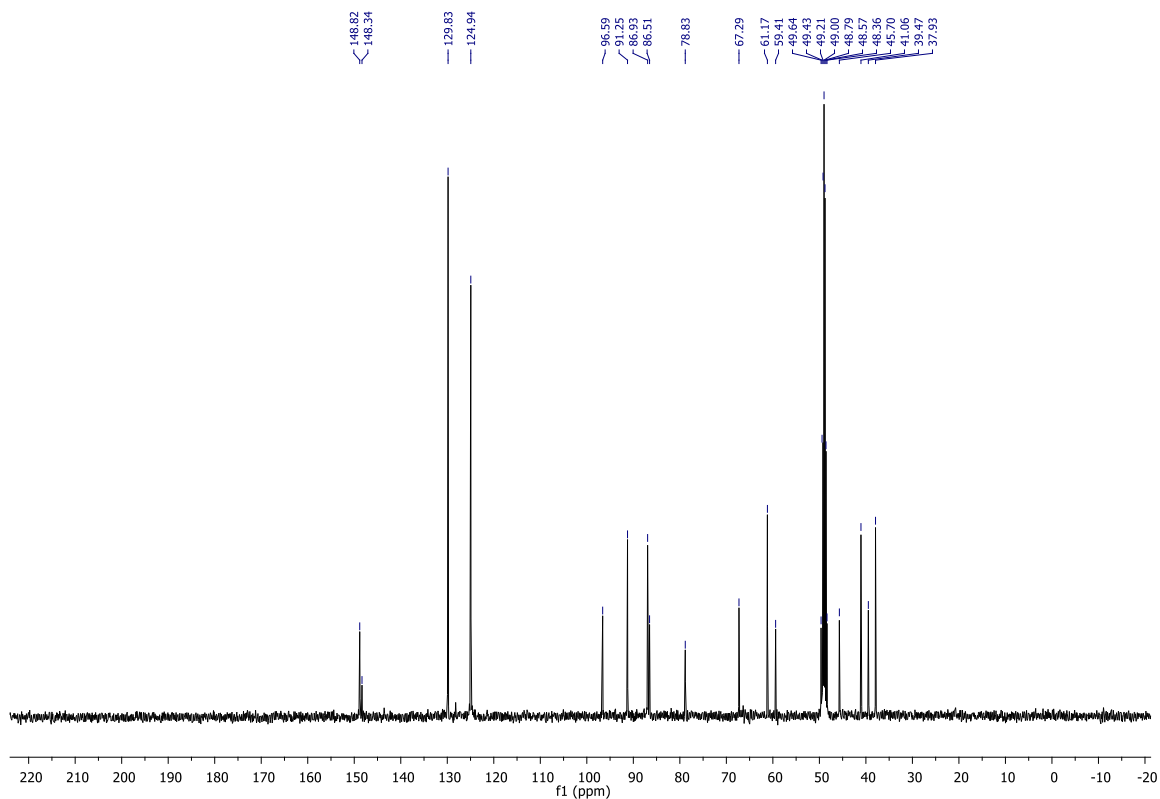
FIGURE 122: 100 MHz ^{13}C NMR spectra in MeOD of 4-(4-nitrophenyl)-5-nitrotetrahydro-2H-pyran-2-ol (**118**).
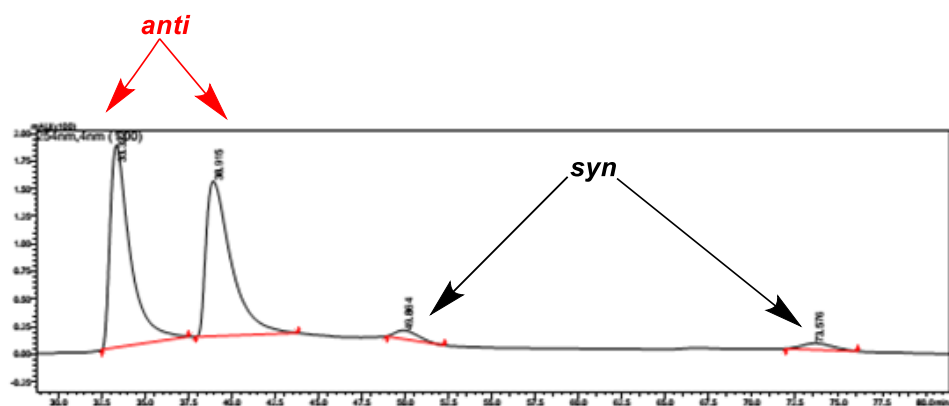
PeakTable

PDA Ch2 254nm 4nm

Peak#	Ret. Time	Area	Height	Area %
1	33.322	14800535	182947	48.588
2	38.915	14201477	140282	46.622
3	49.864	730937	7725	2.400
4	73.576	728243	5831	2.391
Total		30461192	336786	100.000

FIGURE 123: Chiral HPLC analysis of racemic 4-(4-nitrophenyl)-5-nitrotetrahydro-2H-pyran-2-ol (**118**).
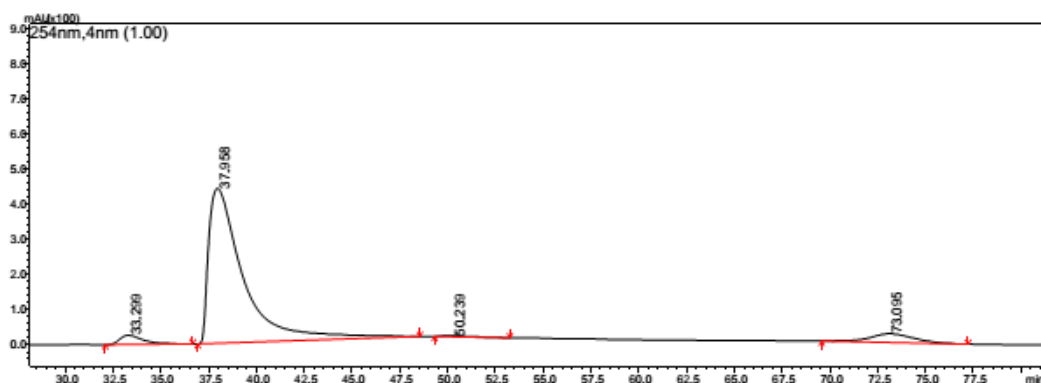
PeakTable

PDA Ch1 254nm 4nm

Peak#	Ret. Time	Area	Height	Area %	Height %
1	33.299	2223491	26102	3.571	5.292
2	37.958	55777419	440121	89.579	89.236
3	50.239	238901	2390	0.384	0.485
4	73.095	4026622	24596	6.467	4.987
Total		62266432	493209	100.000	100.000

FIGURE 124: Chiral HPLC analysis of 4-(4-nitrophenyl)-5-nitrotetrahydro-2H-pyran-2-ol (**118**) obtained by the 1,4-addition reaction catalyzed by **15**. Chiralpak AD-H (n-hexane/i-PrOH 90:10), 25°C at 1.0 ml/min, UV detection at 210 nm.
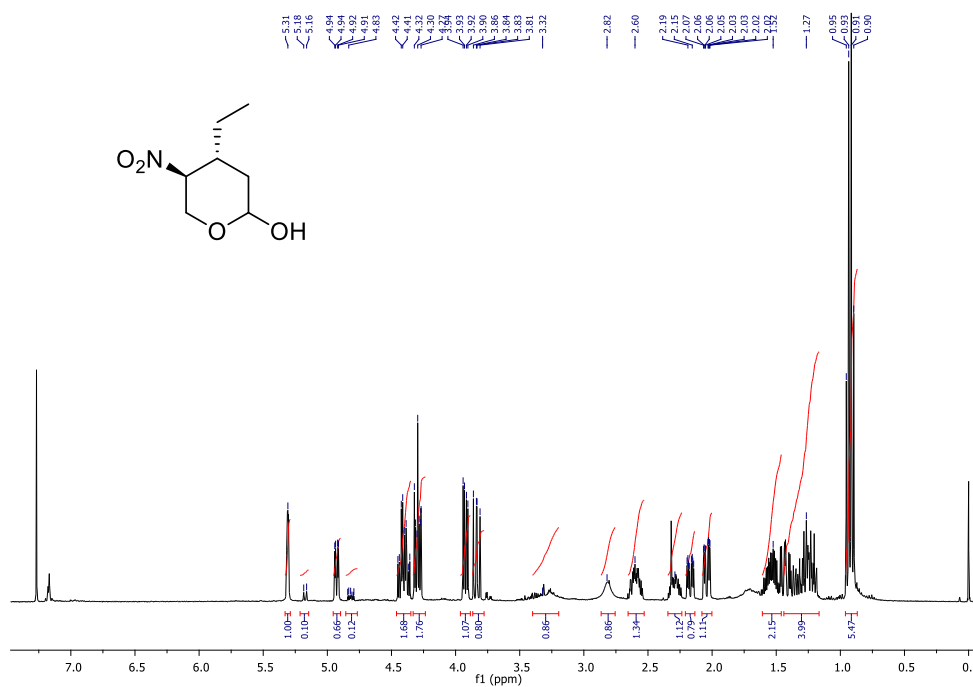
FIGURE 125: 400 MHz ^{1}H NMR spectra in CDCl$_3$ of 4-(4-ethyl)-5-nitrotetrahydro-2H-pyran-2-ol (**119**).
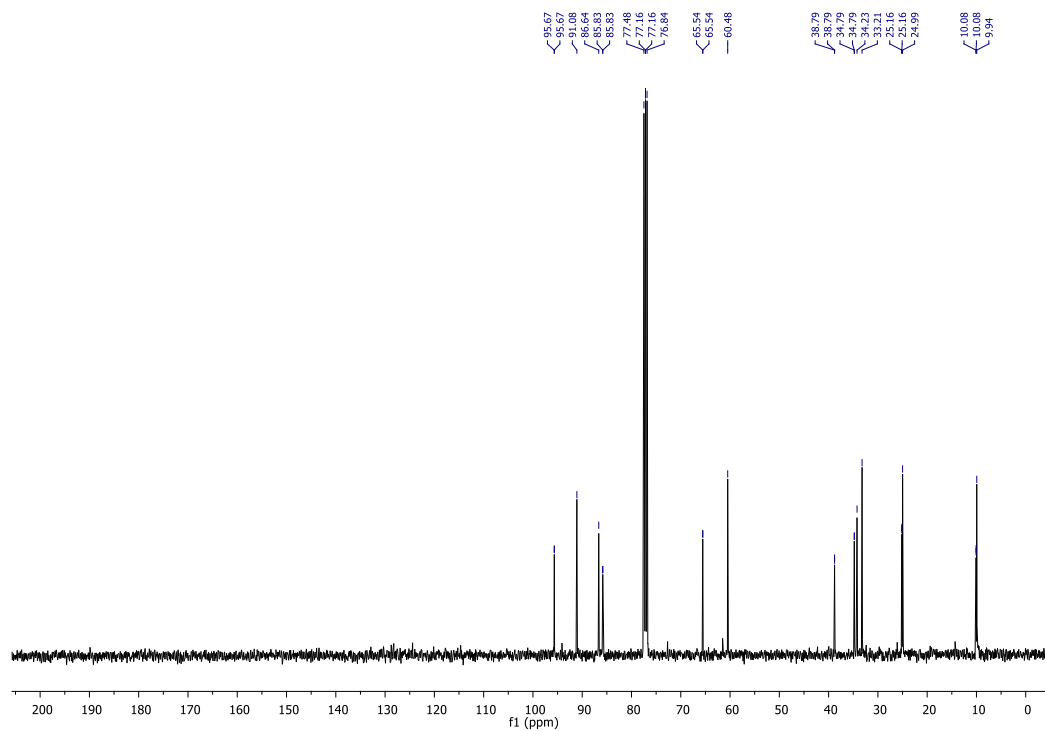
FIGURE 126: 100 MHz ^{13}C NMR spectra in CDCl$_3$ of 4-(4-ethyl)-5-nitrotetrahydro-2H-pyran-2-ol (**119**).
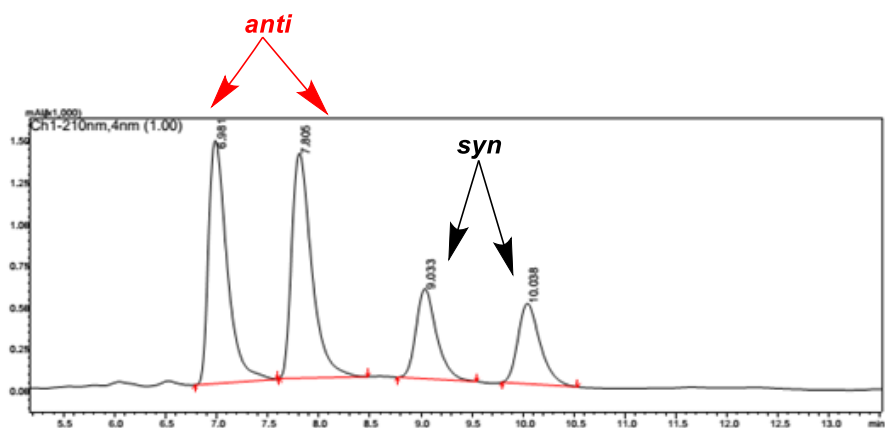
Peak#	Ret. Time	Area	Height	Area %	Height %
1	6.981	18523423	1462413	35.671	38.106
2	7.805	18525755	1352244	35.676	35.235
3	9.033	7537547	540293	14.515	14.078
4	10.038	7341596	482796	14.138	12.580
Total		51928321	3837745	100.000	100.000

FIGURE 127: Chiral HPLC analysis of racemic 4-(4-ethyl)-5-nitrotetrahydro-2H-pyran-2-ol (**119**).
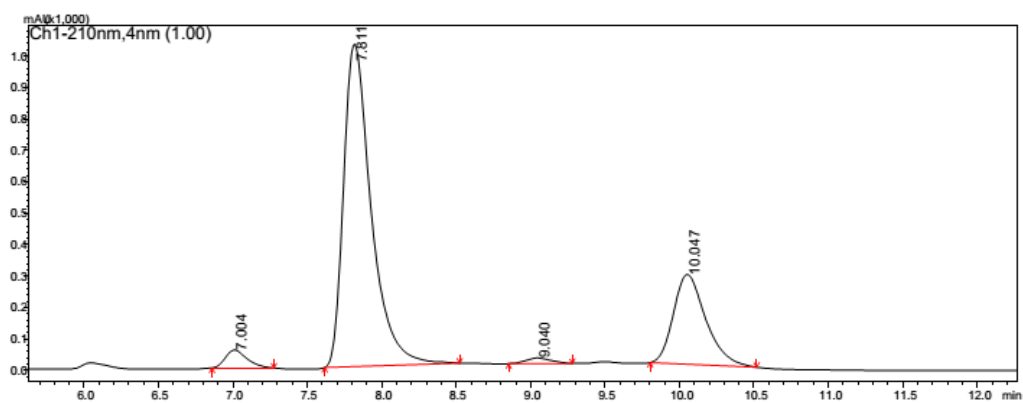
Peak#	Ret. Time	Area	Height	Area %	Height %
1	7.004	577039	57223	3.149	4.129
2	7.811	13227977	1025971	72.191	74.035
3	9.040	208847	17398	1.140	1.255
4	10.047	4309719	285193	23.520	20.580
Total		18323582	1385785	100.000	100.000

FIGURE 128: Chiral HPLC analysis of 4-(4-ethyl)-5-nitrotetrahydro-2H-pyran-2-ol (**119**) obtained by the 1,4-addition reaction catalyzed by **15**. Chiralpak AD-H (n-hexane/i-PrOH 90:10), 25°C at 1.0 ml/min, UV detection at 210 nm.
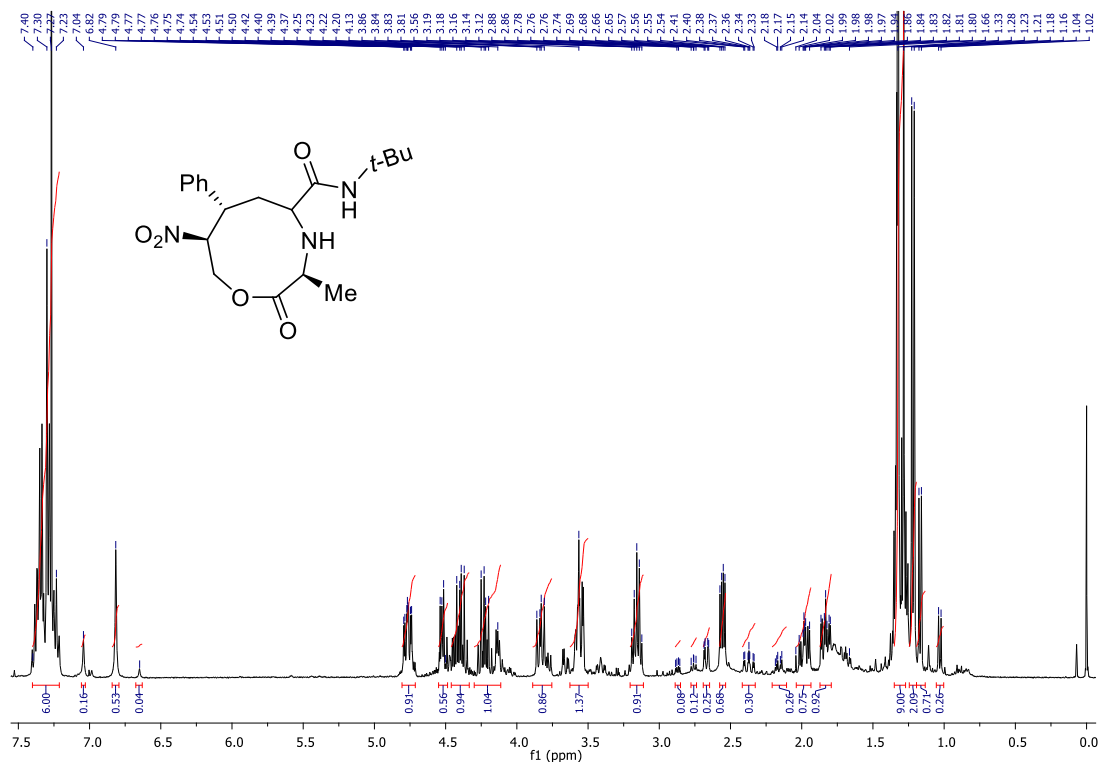
FIGURE 129: 400 MHz ^{1}H NMR spectra in CDCl$_3$ of the mixture of diastereomers of compound **120**.
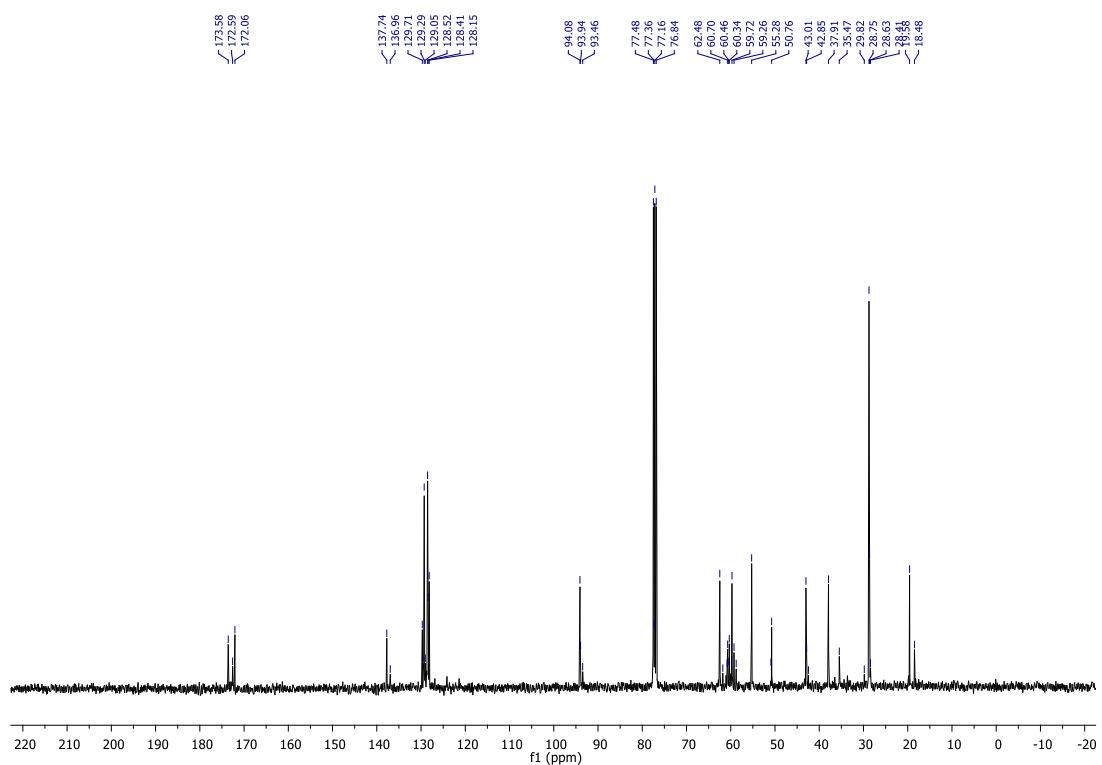
FIGURE 130: 100 MHz ^{13}C NMR spectra in CDCl$_3$ of the mixture of diastereomers of compound **120**.
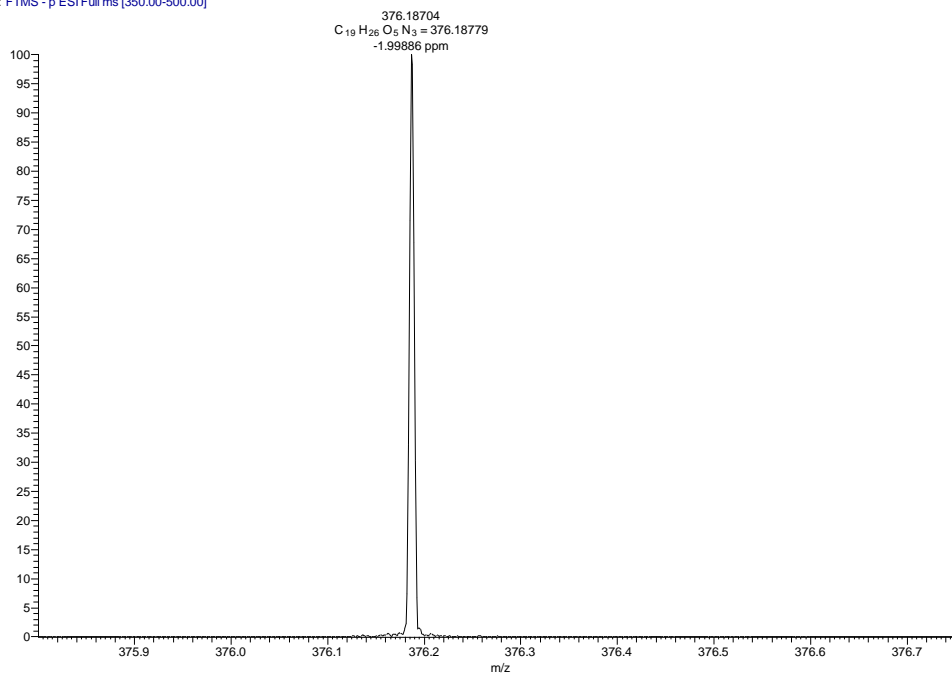
FIGURE 131: HRMS (ESI-FT-ICR) m/z spectra of **120**.
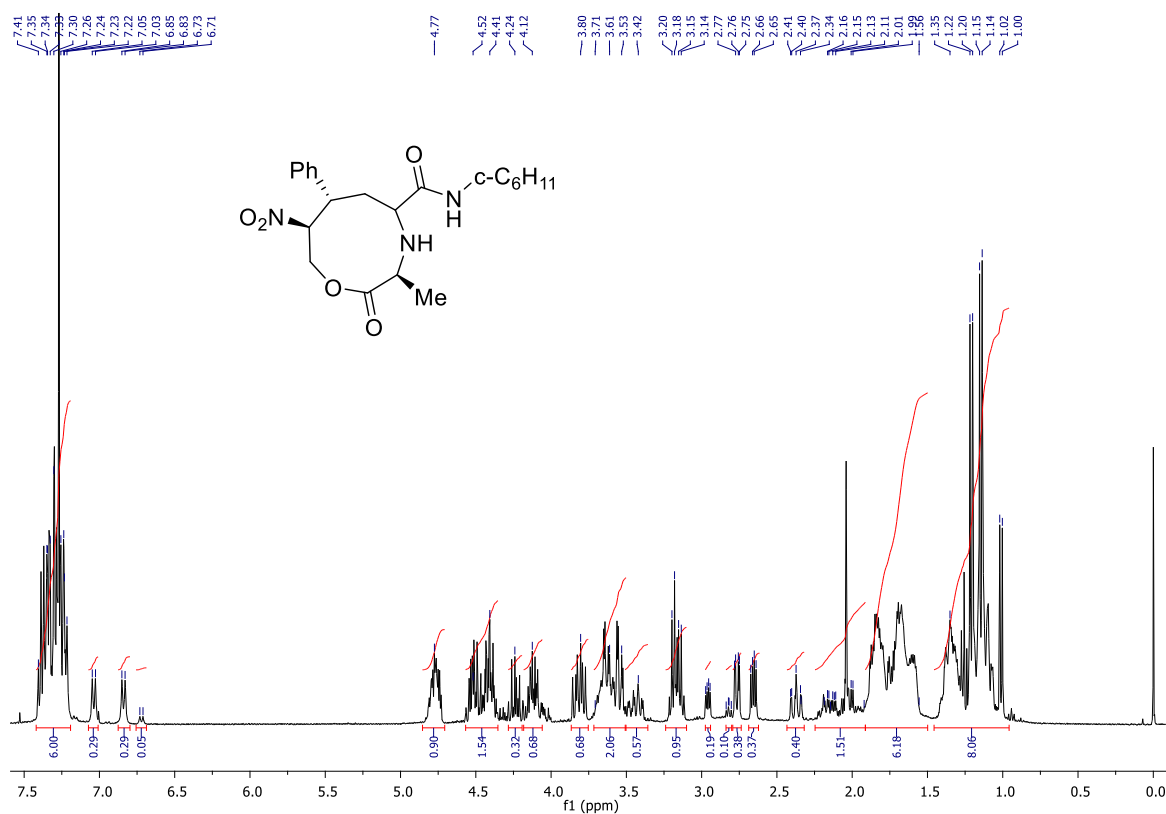
FIGURE 132: 400 MHz ^{1}H NMR spectra in CDCl$_3$ of the mixture of diastereomers of compound **121**.

246
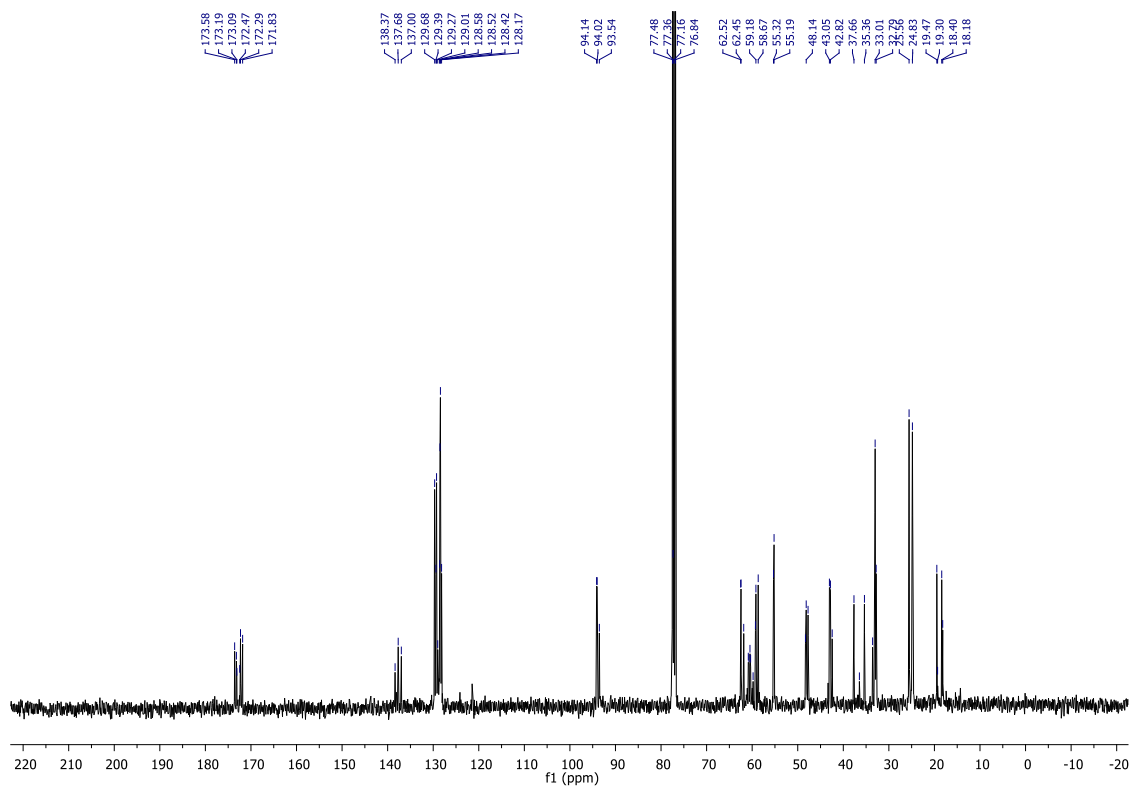
FIGURE 133: 100 MHz ^{13}C NMR spectra in CDCl$_3$ of the mixture of diastereomers of compound **121**.
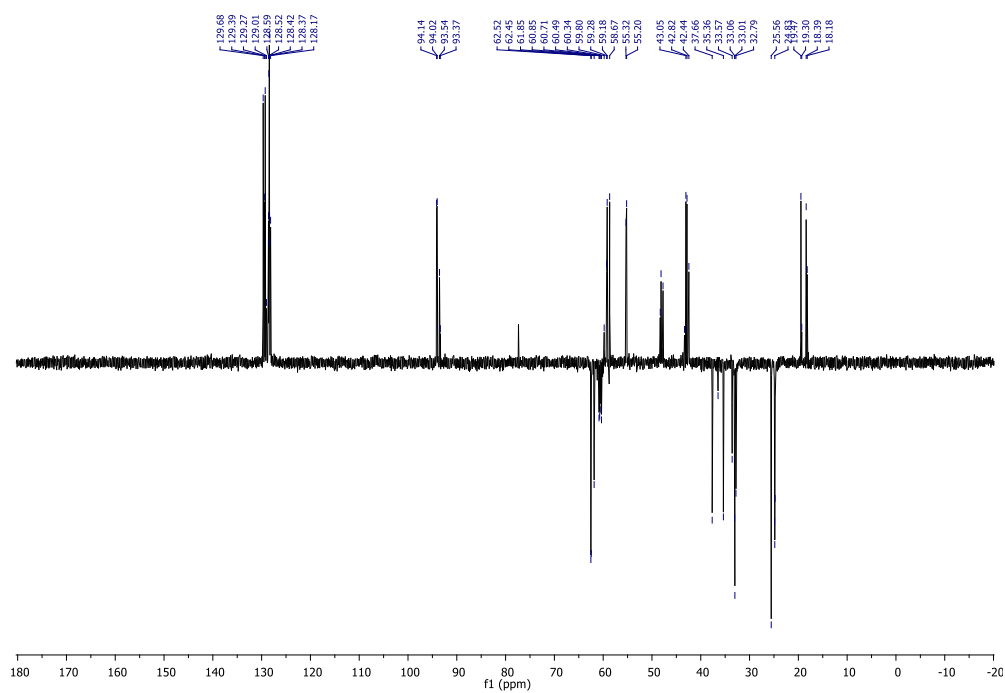
FIGURE 134: DEPT 135° spectra in CDCl$_3$ of the mixture of diastereomers of compound **121**.
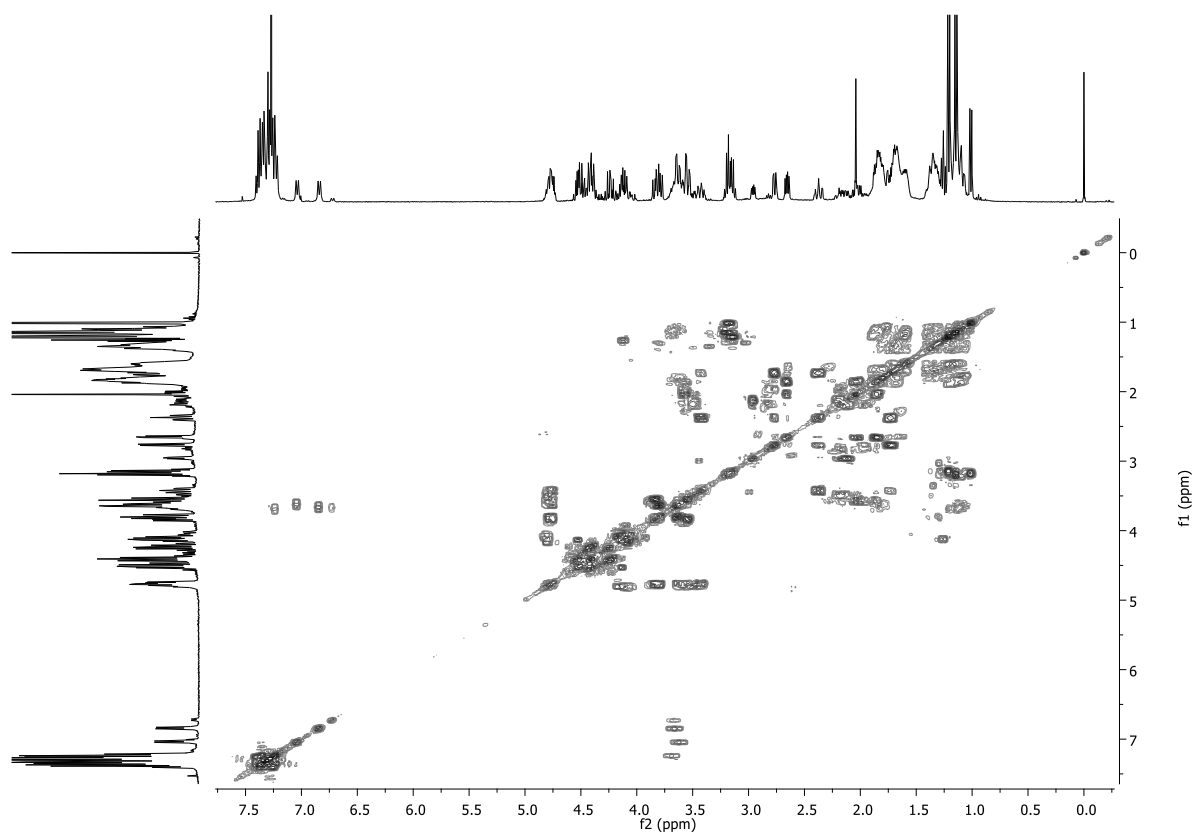
FIGURE 135: COSY spectra in CDCl₃ of the mixture of diastereomers of compound **121**.
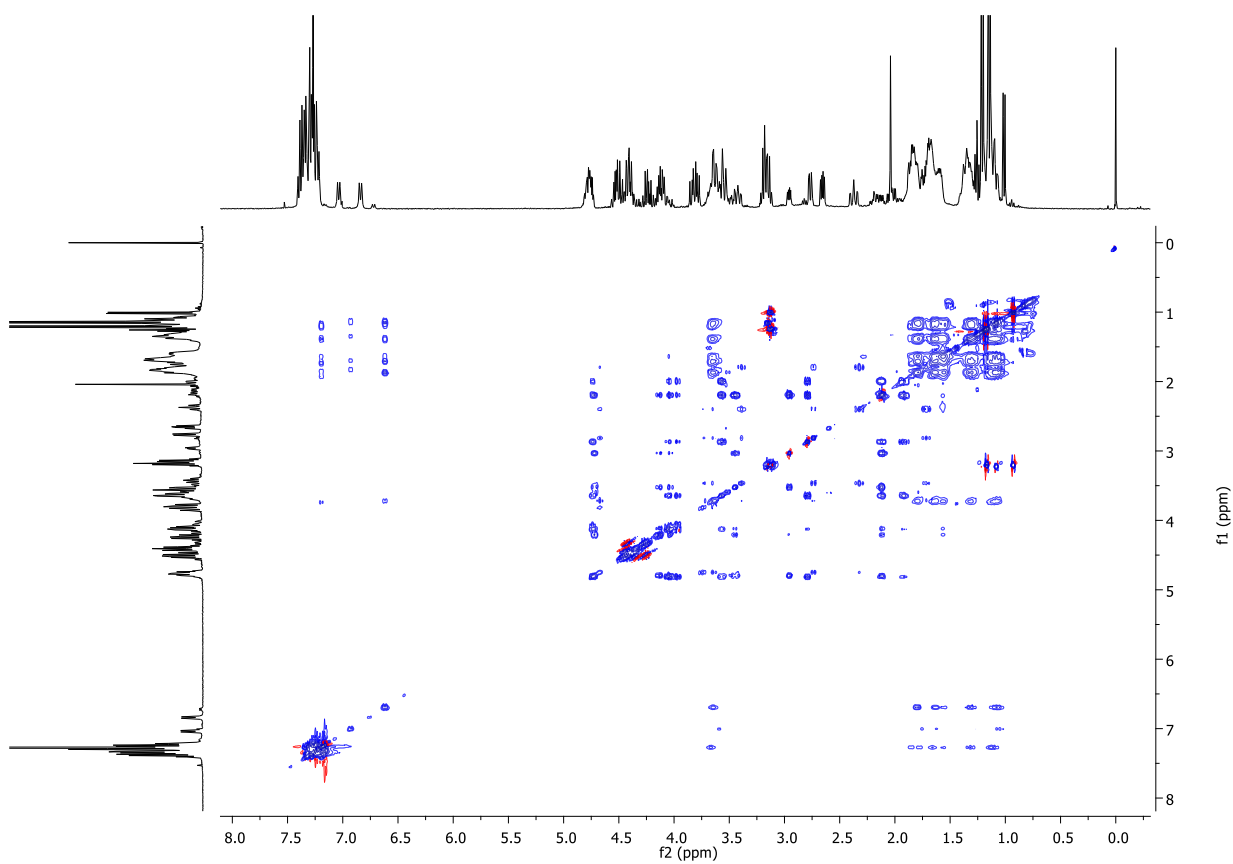
FIGURE 136: ROESY spectra in CDCl₃ of the mixture of diastereomers of compound **121**.
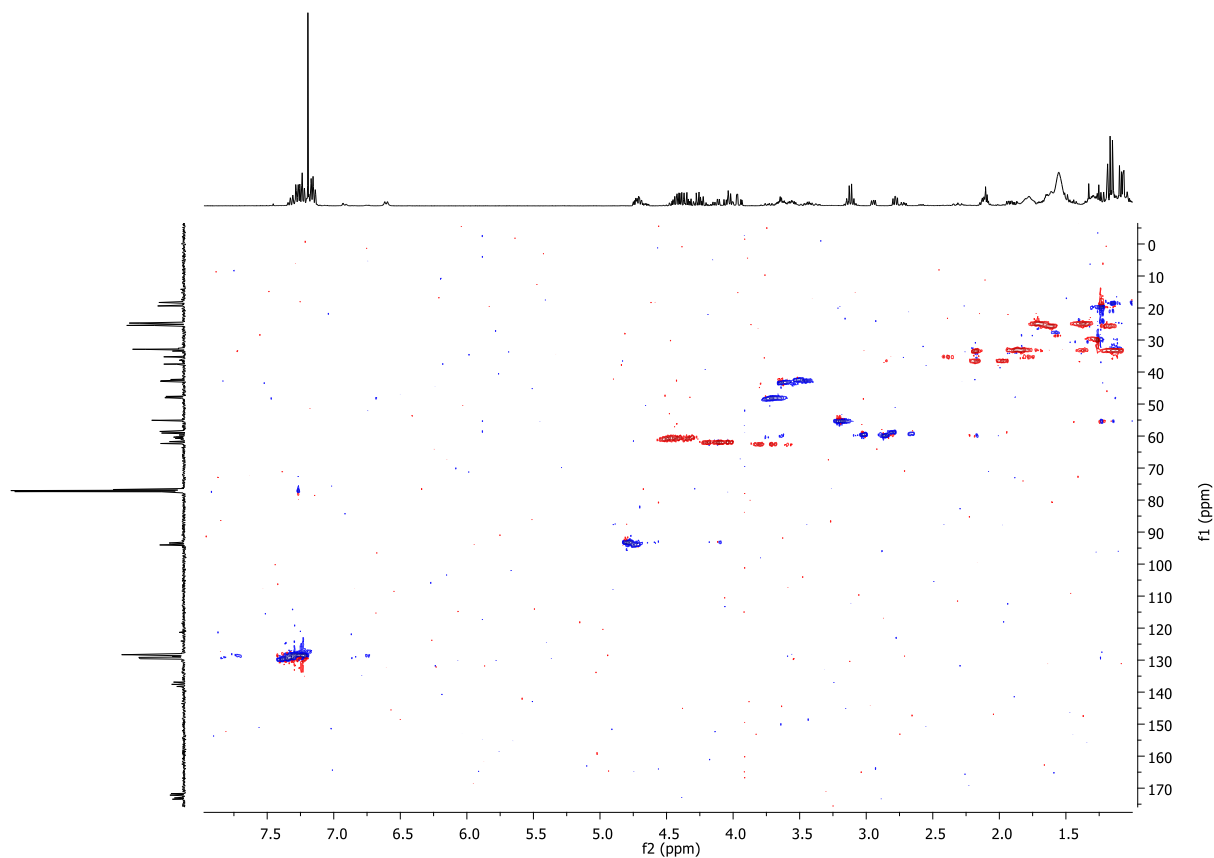
FIGURE 137: HSQC spectra in CDCl₃ of the mixture of diastereomers of compound **121**.
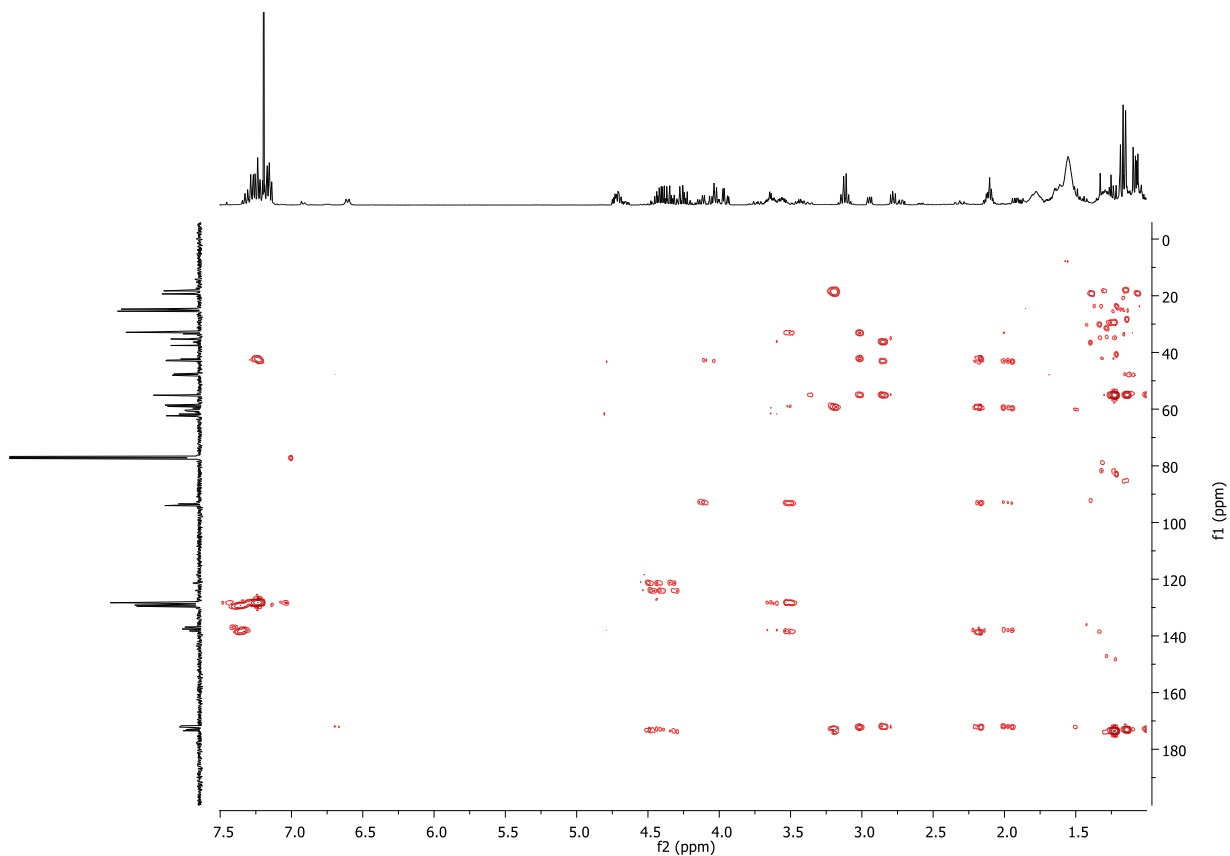
FIGURE 138: HMBC spectra in CDCl₃ of the mixture of diastereomers of compound **121**.

402.20190
C₂₁H₂₈O₅N₃ = 402.20344
-3.82878 ppm
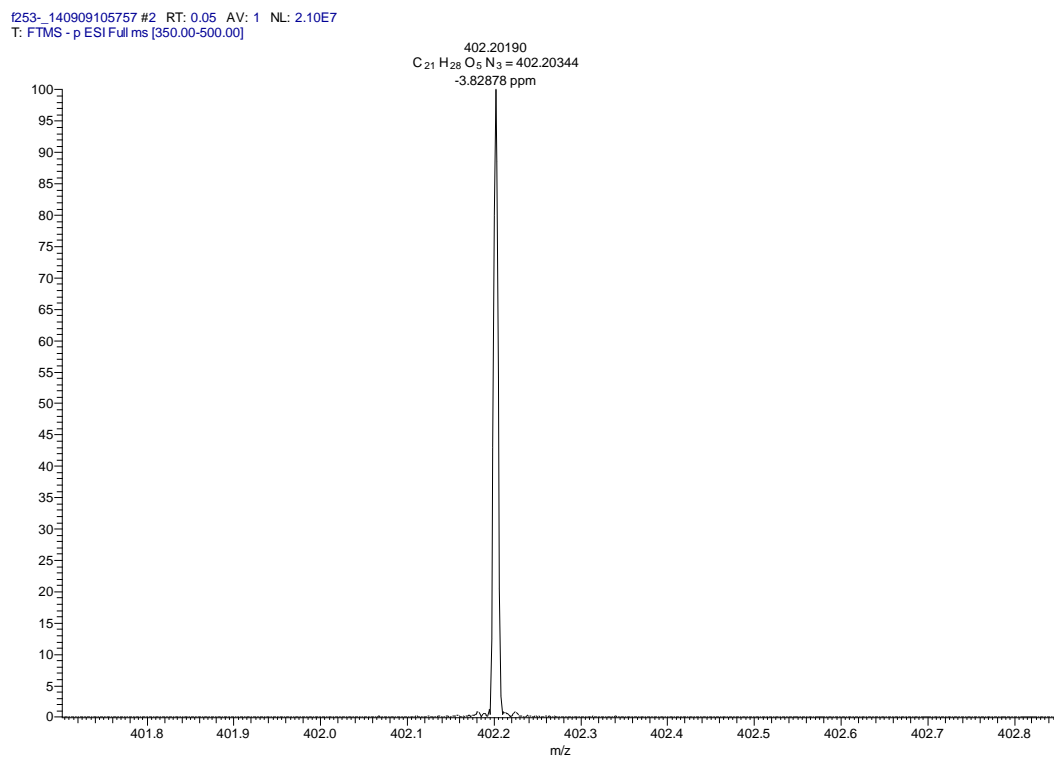
FIGURE 139: HRMS (ESI-FT-ICR) m/z spectra of **121**.
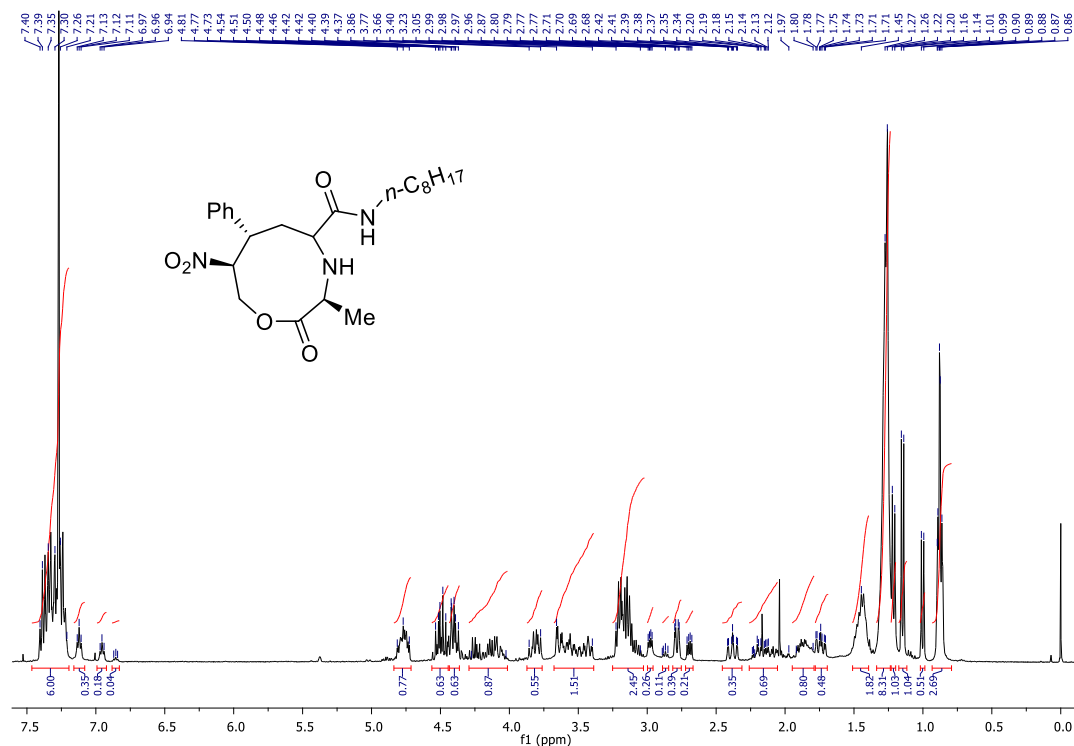
FIGURE 140: 400 MHz ^{1}H NMR spectra in CDCl$_3$ of the mixture of diastereomers of compound **122**.
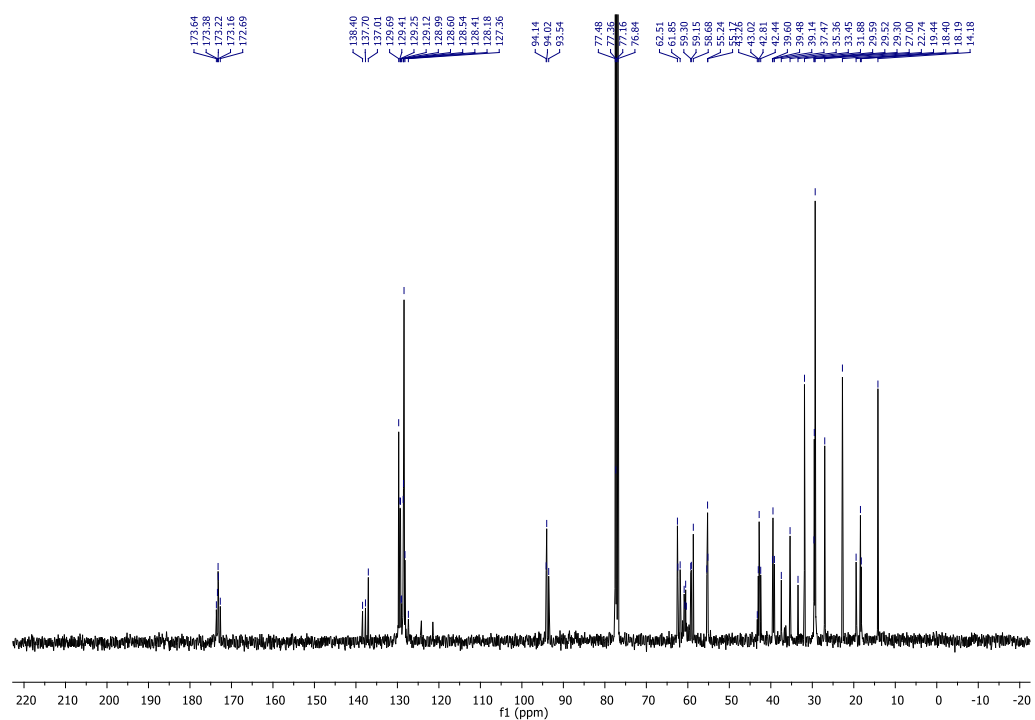
FIGURE 141: 100 MHz ^{13}C NMR spectra in CDCl$_3$ of the mixture of diastereomers of compound **122**.

251
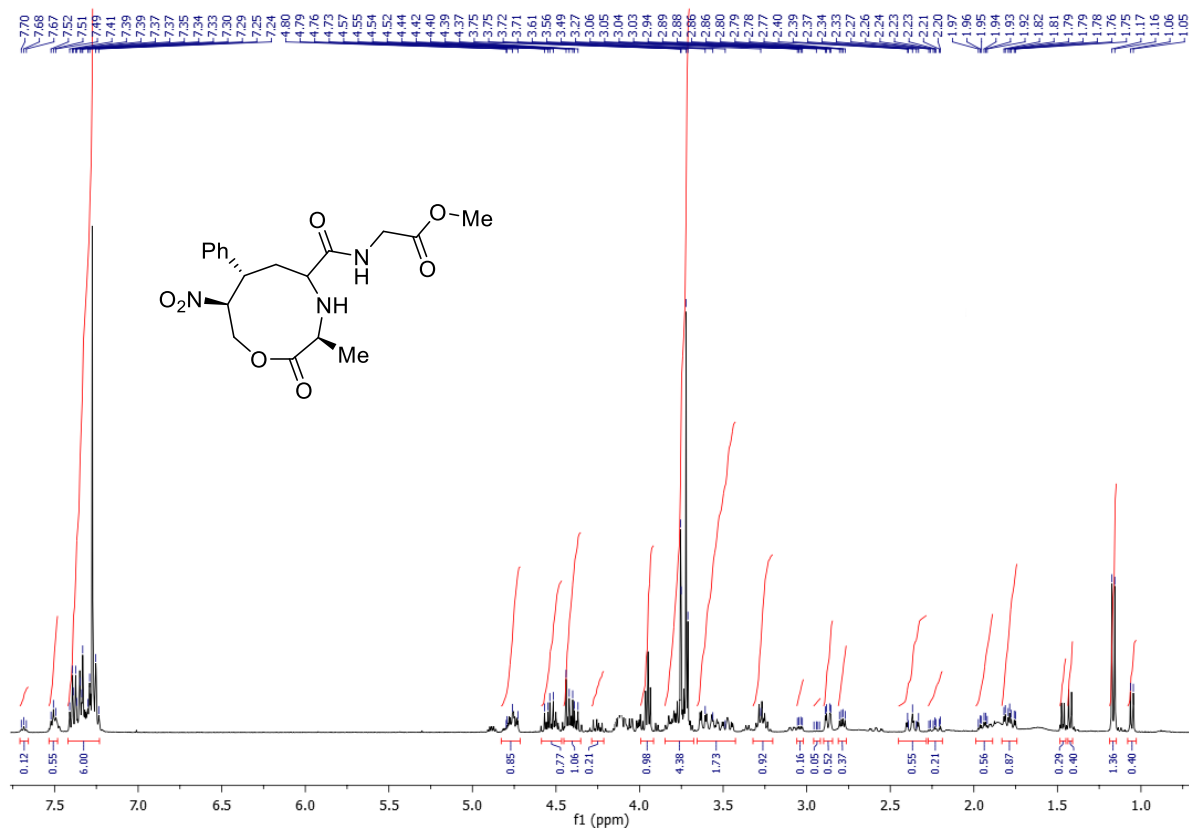
FIGURE 142: 400 MHz ^{1}H NMR spectra in CDCl$_3$ of the mixture of diastereomers of compound **123**.
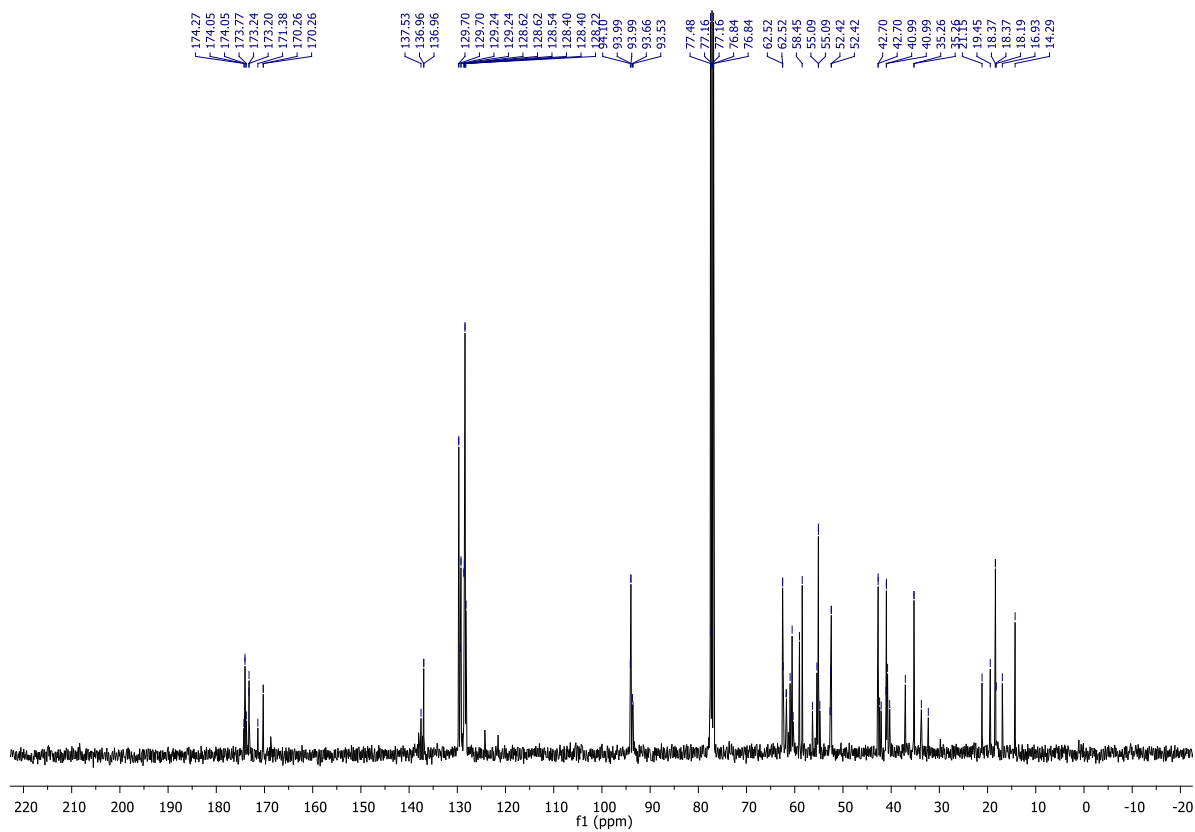
FIGURE 143: 100 MHz ^{13}C NMR spectra in CDCl$_3$ of the mixture of diastereomers of compound **123**.
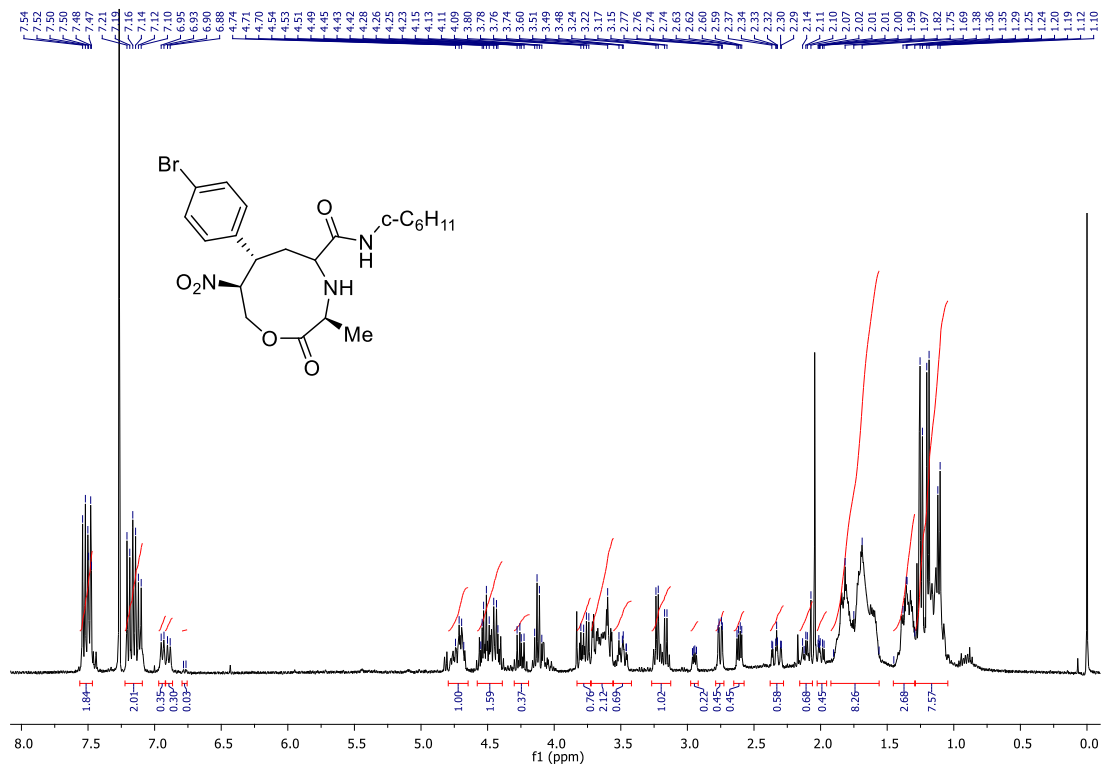
FIGURE 144: 400 MHz ^{1}H NMR spectra in CDCl$_3$ of the mixture of diastereomers of compound **124**.
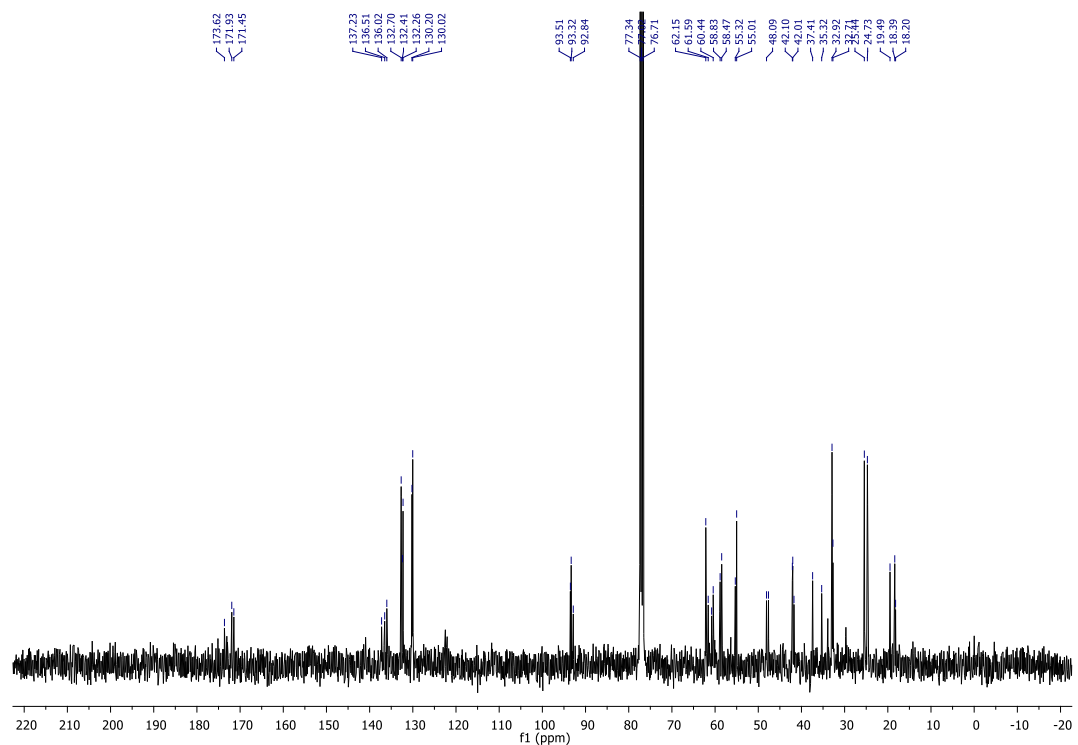
FIGURE 145: 100 MHz ^{13}C NMR spectra in CDCl$_3$ of the mixture of diastereomers of compound **124**.
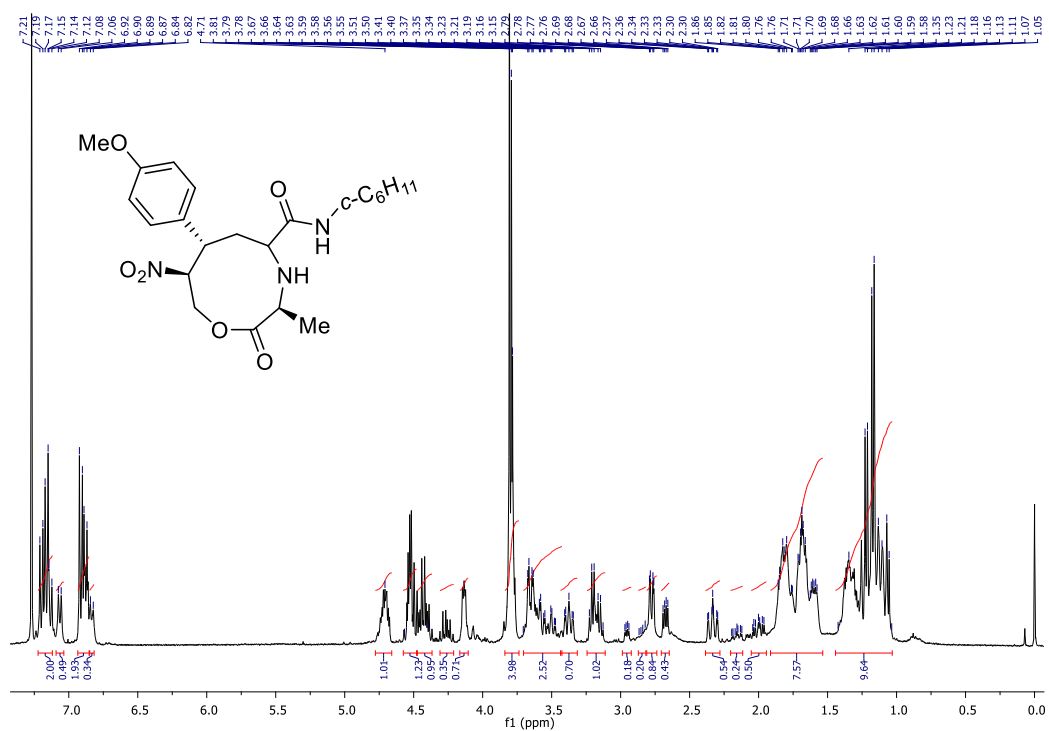
FIGURE 146: 400 MHz ^{1}H NMR spectra in CDCl$_3$ of the mixture of diastereomers of compound **125**.
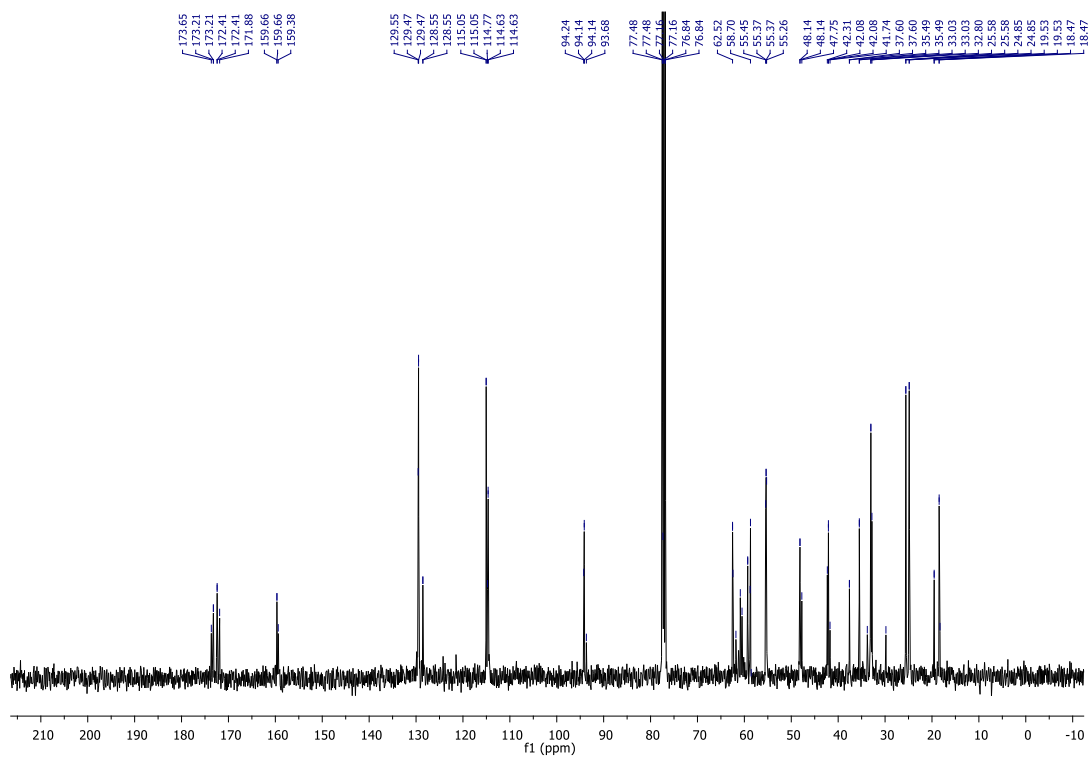
FIGURE 147: 100 MHz ^{13}C NMR spectra in CDCl$_3$ of the mixture of diastereomers of compound **125**.
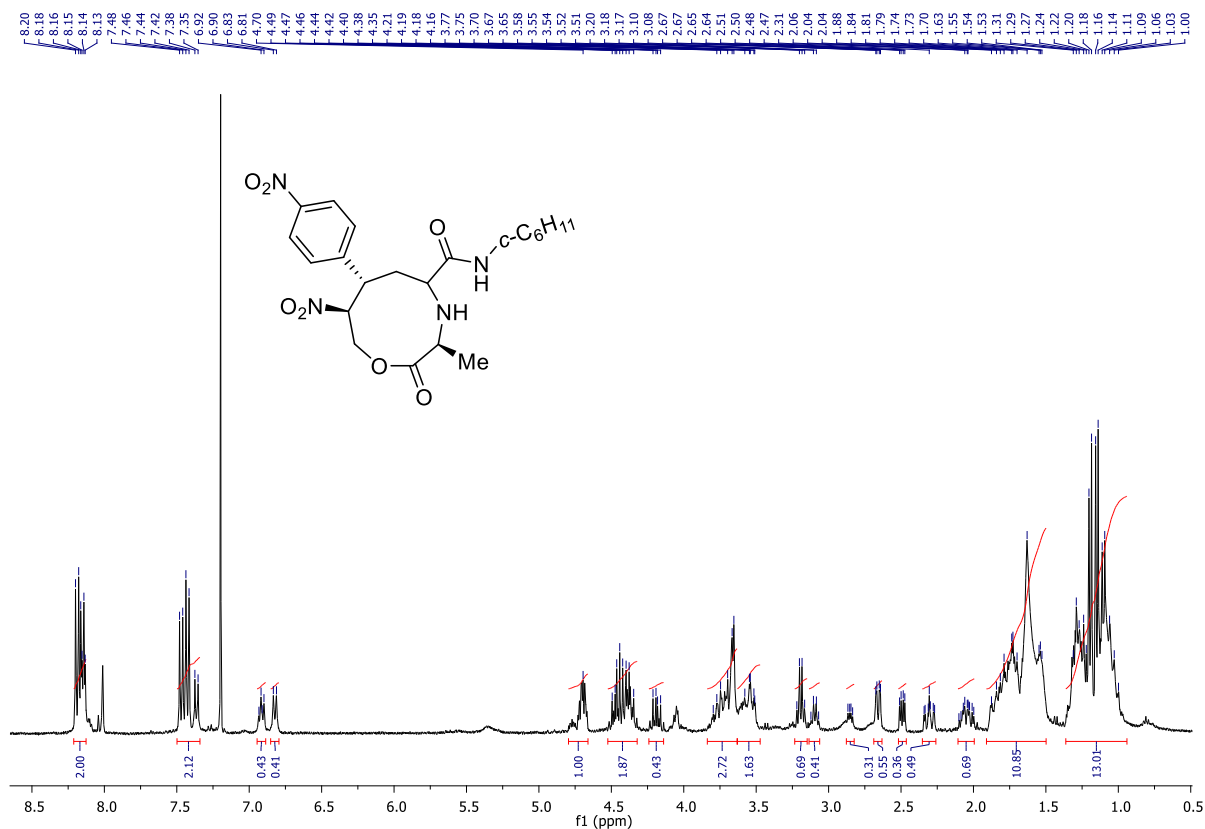
FIGURE 148: 400 MHz ^{1}H NMR spectra in CDCl$_3$ of the mixture of diastereomers of compound **126**.
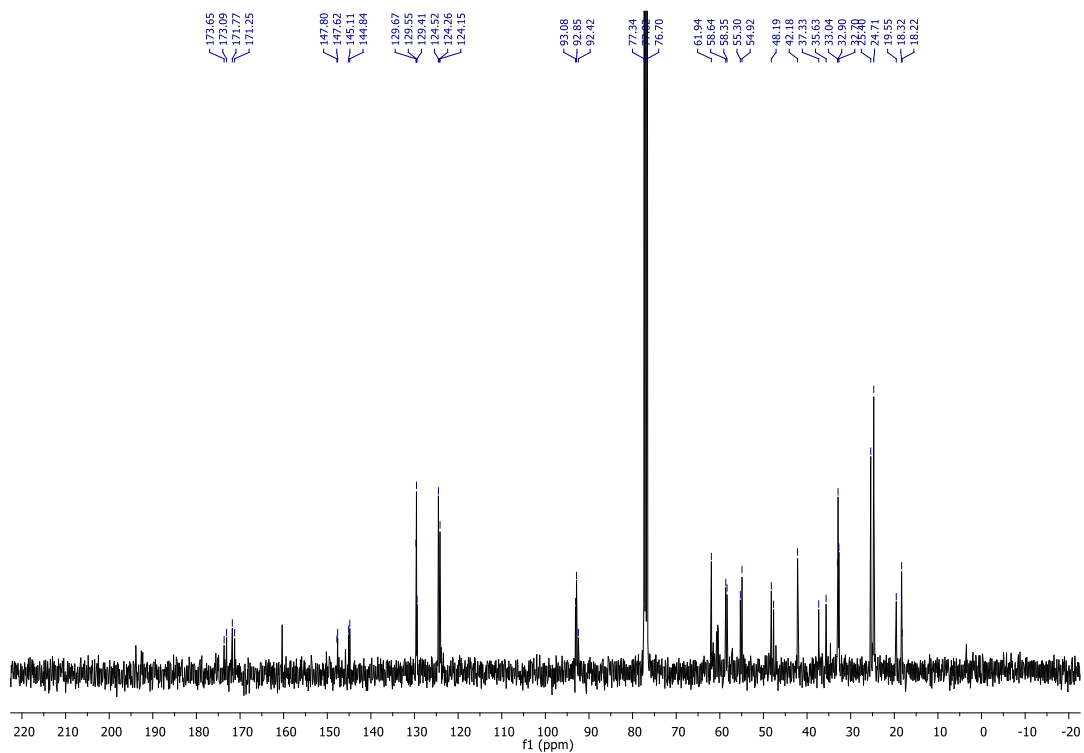
FIGURE 149: 100 MHz ^{13}C NMR spectra in CDCl$_3$ of the mixture of diastereomers of compound **126**.
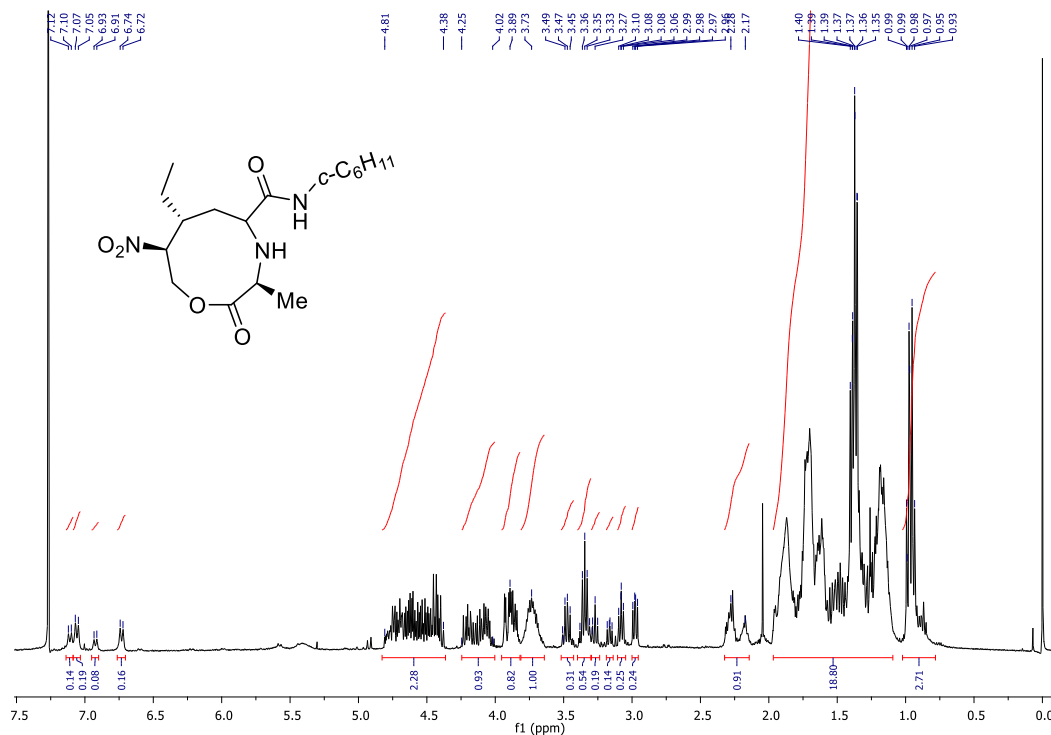
FIGURE 150: 400 MHz ^{1}H NMR spectra in CDCl$_3$ of the mixture of diastereomers of compound **127**.
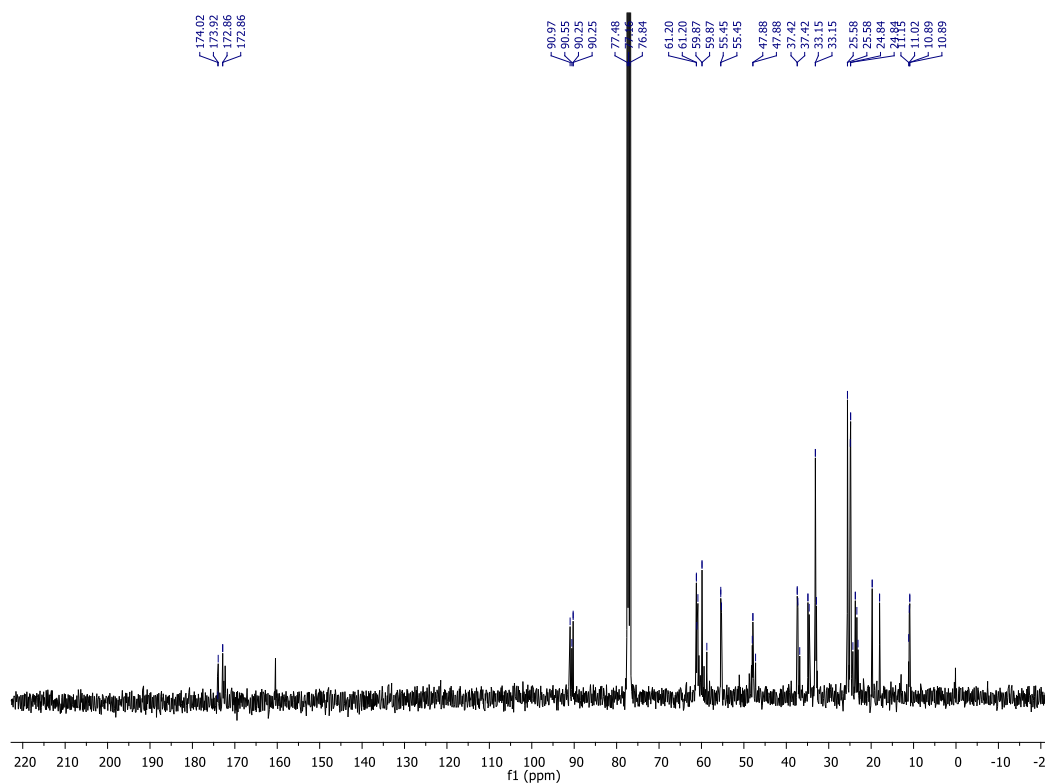
FIGURE 151: 100 MHz ^{13}C NMR spectra in CDCl$_3$ of the mixture of diastereomers of compound **127**.
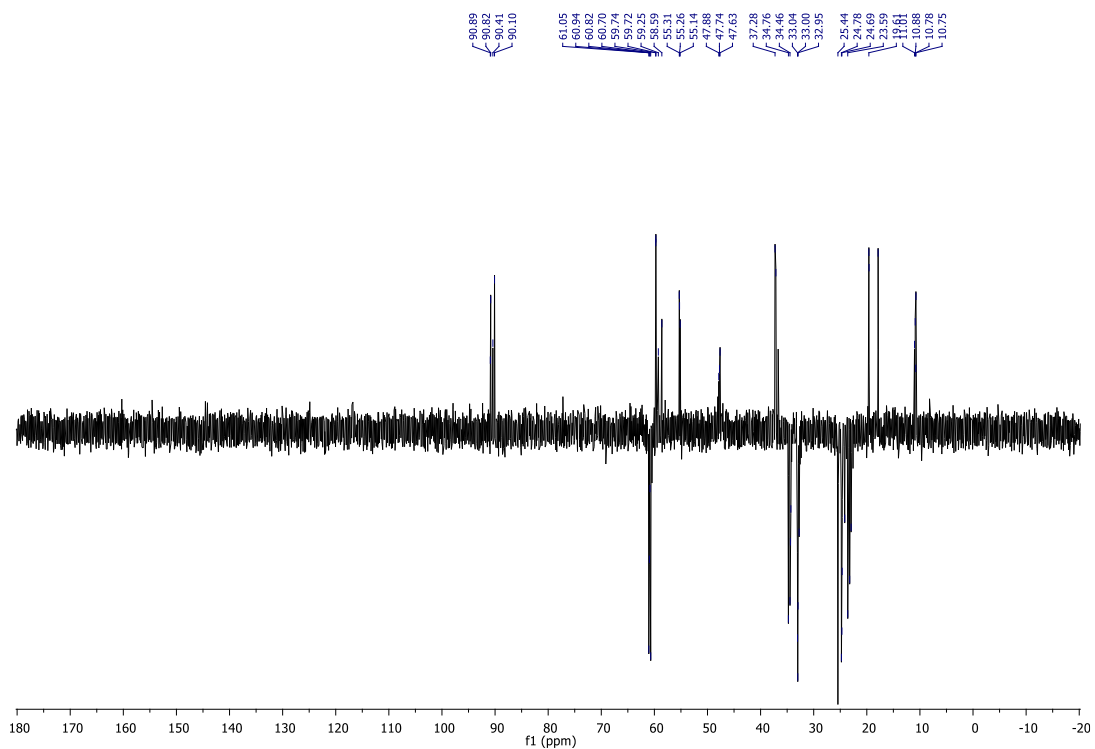
FIGURE 152: DEPT 135° spectra in CDCl$_3$ of the mixture of diastereomers of compound **127**.
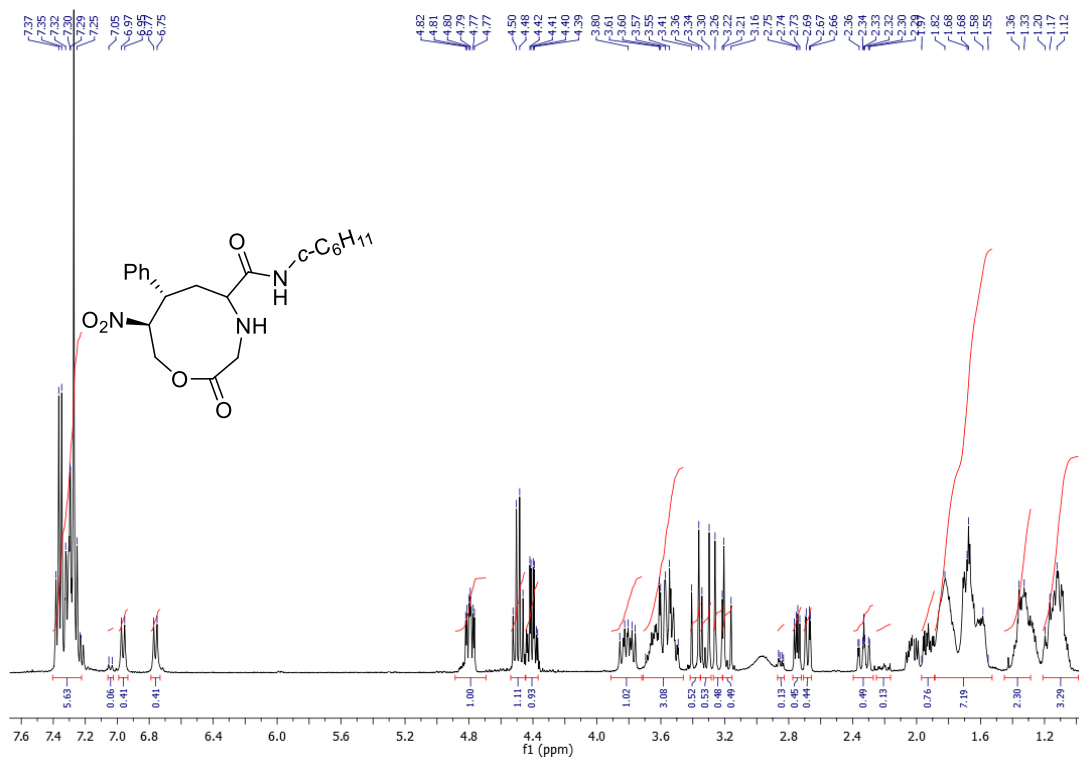
FIGURE 153: 400 MHz ^{1}H NMR spectra in CDCl$_3$ of the mixture of diastereomers of compound **128**.
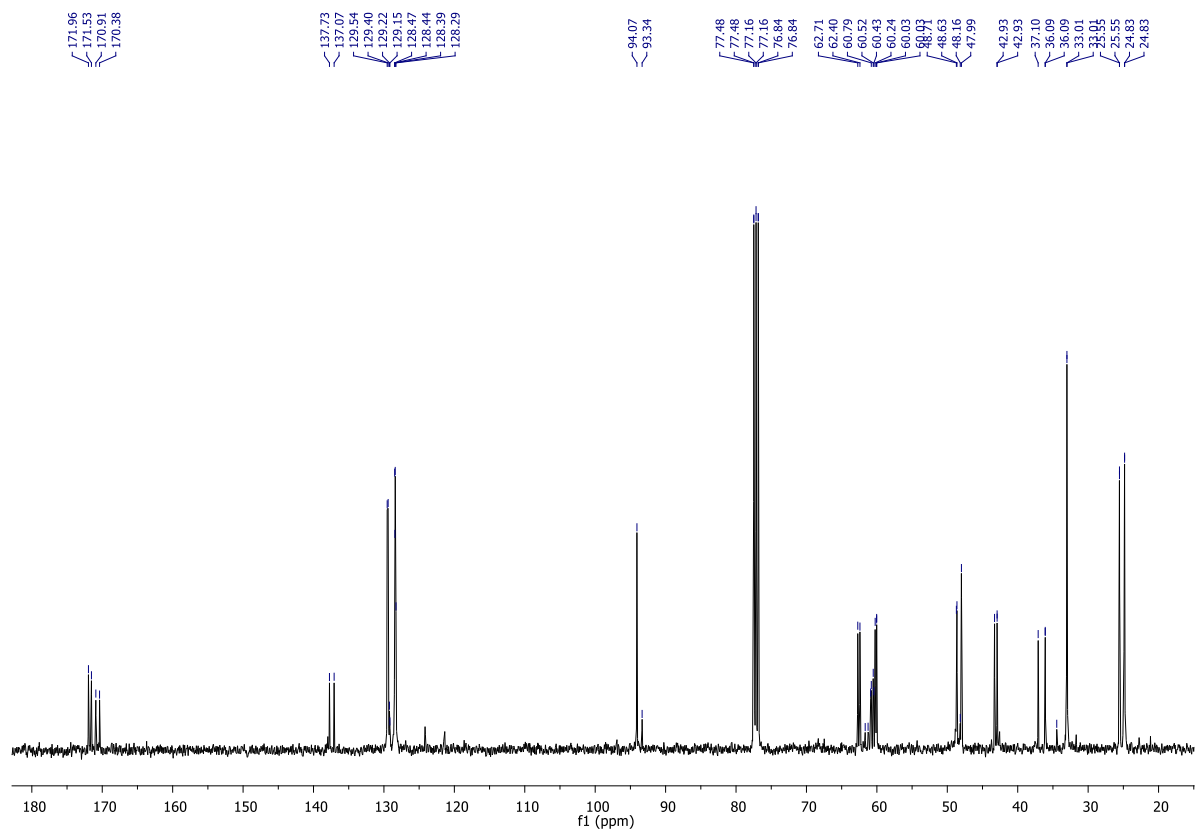
FIGURE 154: 100 MHz ^{13}C NMR spectra in CDCl$_3$ of the mixture of diastereomers of compound **128**.
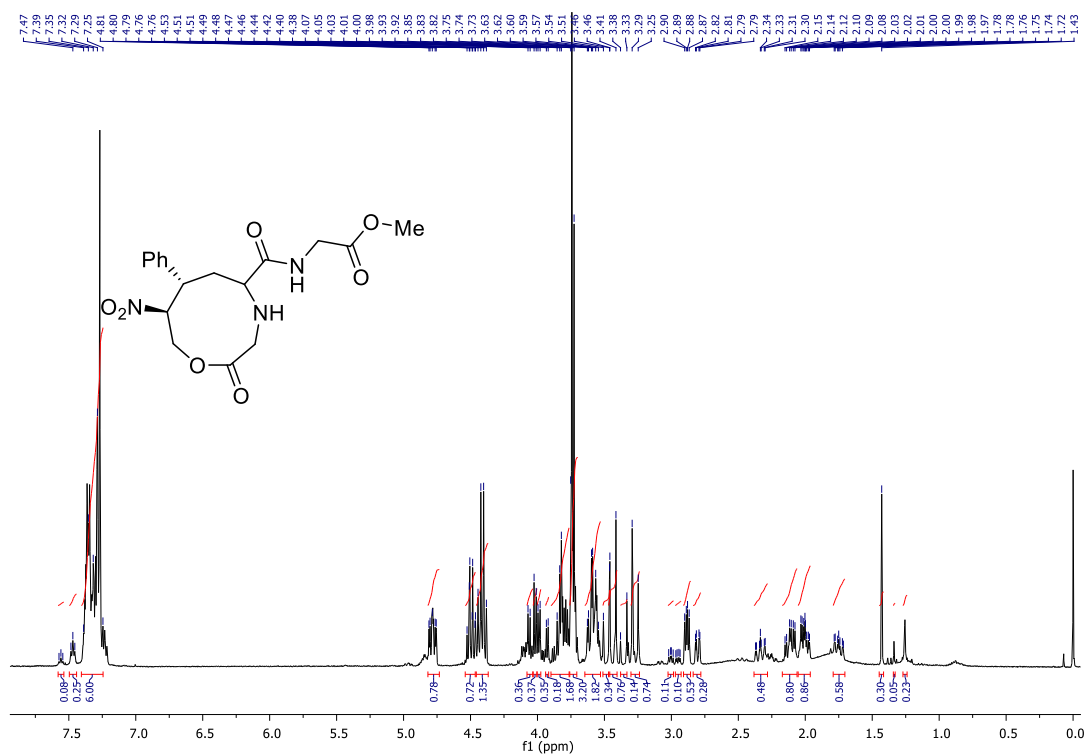
FIGURE 155: 400 MHz ^{1}H NMR spectra in CDCl$_3$ of the mixture of diastereomers of compound **129**.
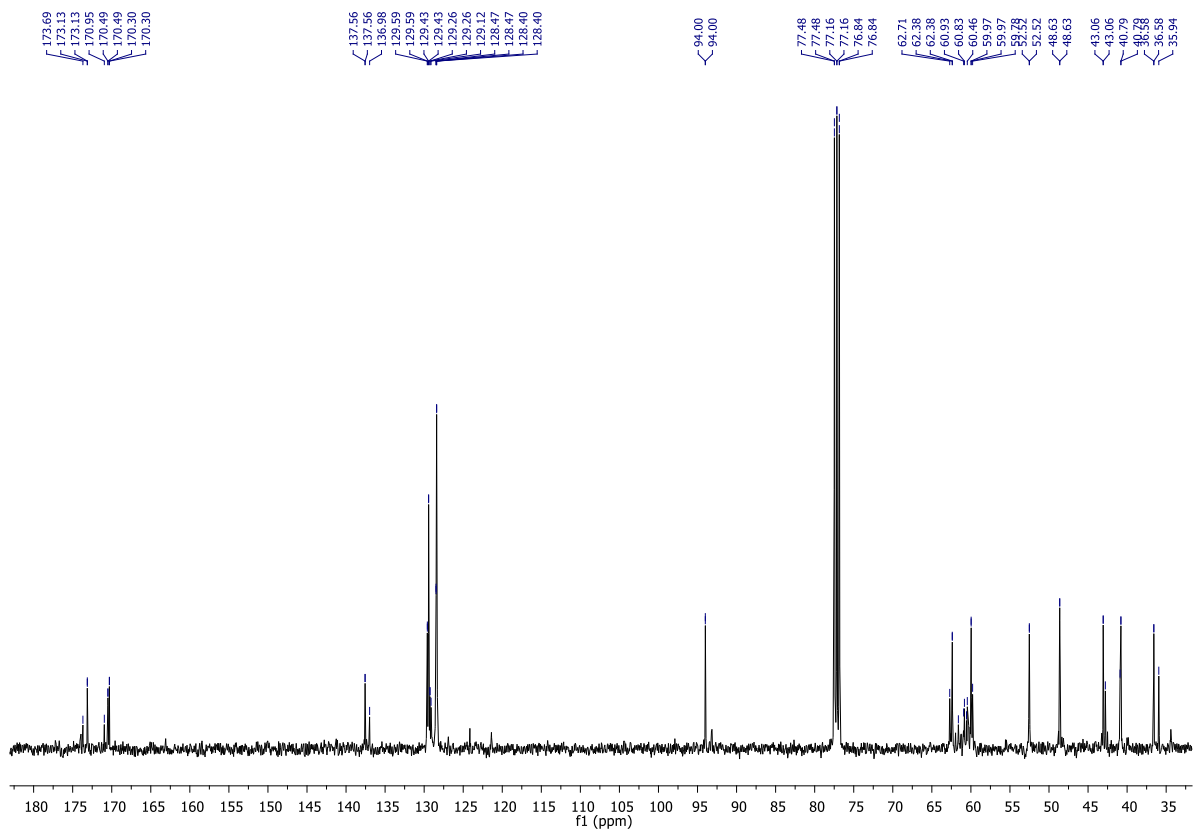
FIGURE 156: 100 MHz ^{13}C NMR spectra in CDCl$_3$ of the mixture of diastereomers of compound **129**.
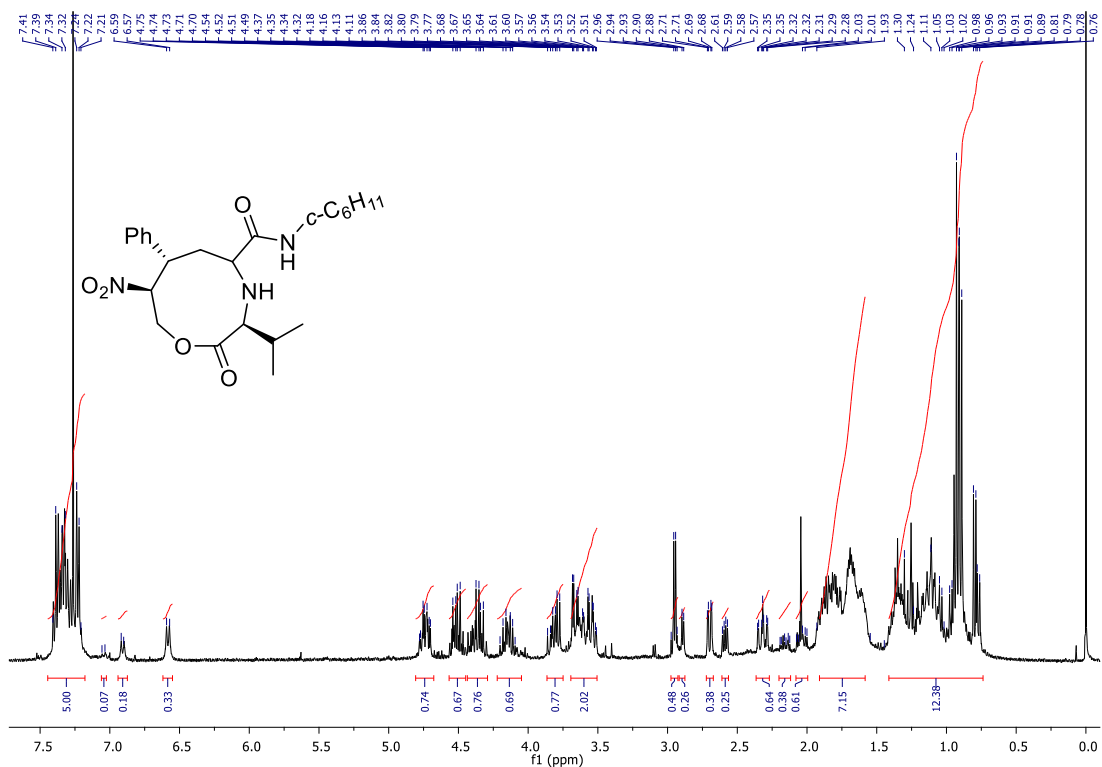
FIGURE 157: 400 MHz ^{1}H NMR spectra in CDCl$_3$ of the mixture of diastereomers of compound **130**.
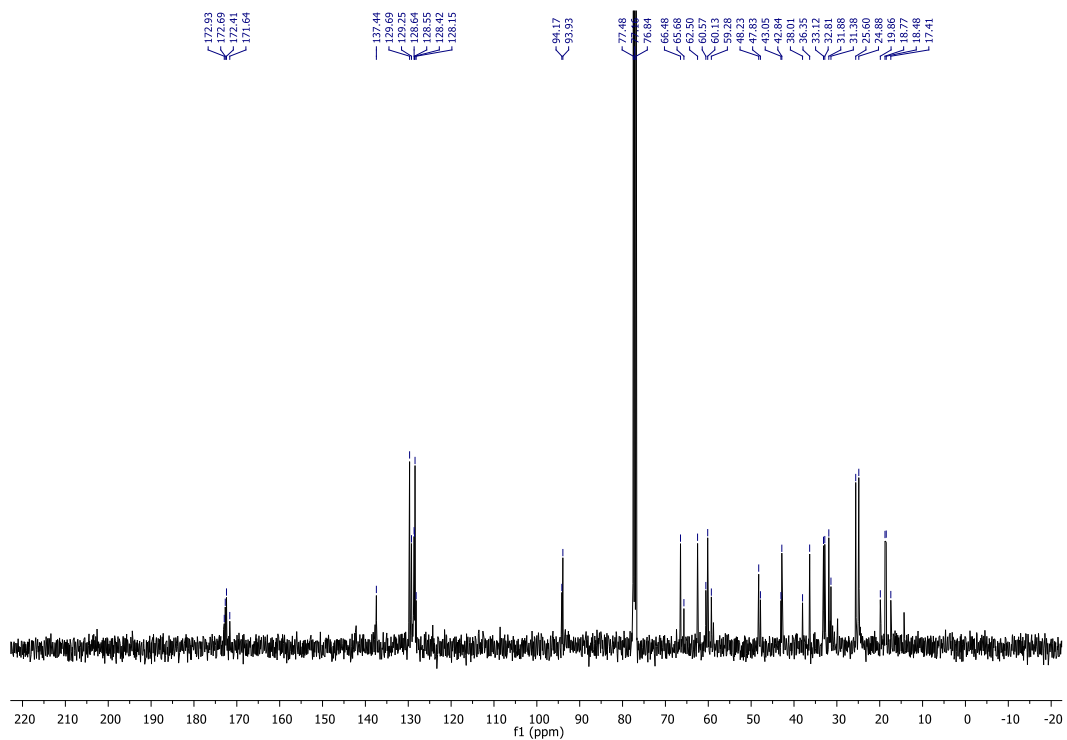
FIGURE 158: 100 MHz ^{13}C NMR spectra in CDCl$_3$ of the mixture of diastereomers of compound **130**.
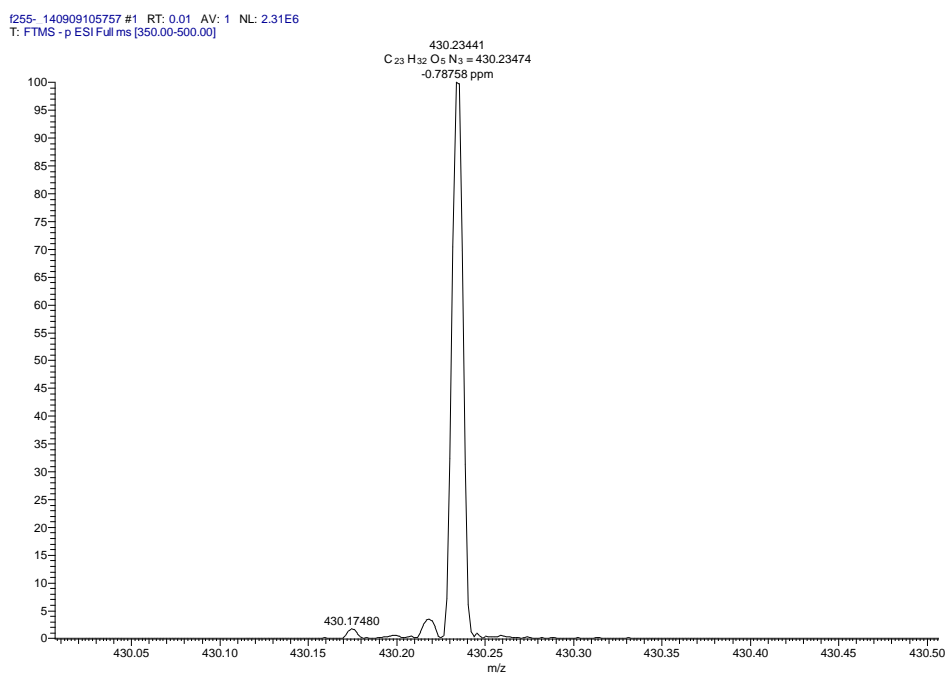
FIGURE 159: HRMS (ESI-FT-ICR) m/z spectra of **130**.
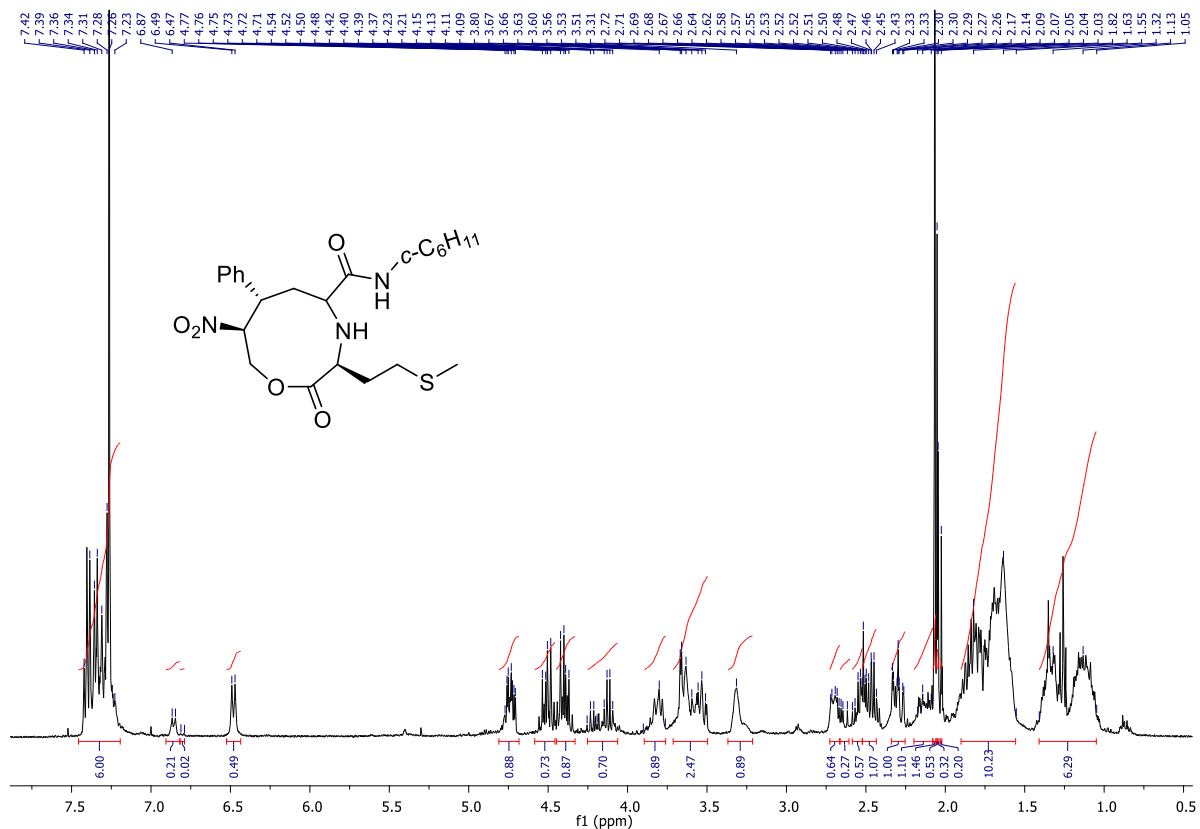
FIGURE 160: 400 MHz ^{1}H NMR spectra in CDCl$_3$ of the mixture of diastereomers of compound **131**.
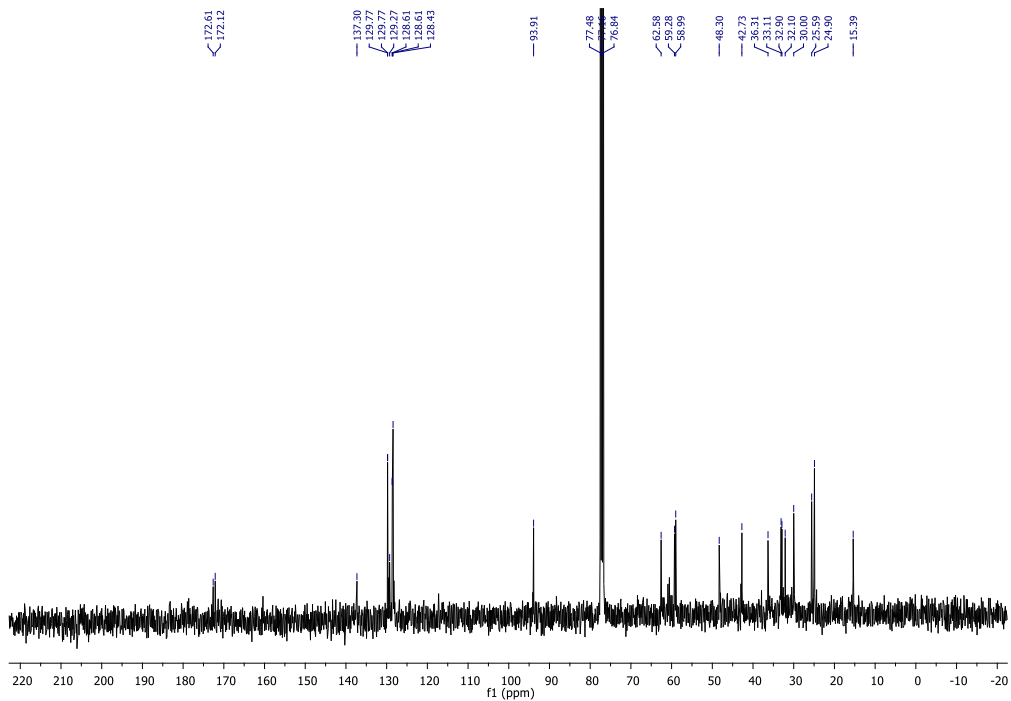
FIGURE 161: 100 MHz ^{13}C NMR spectra in CDCl$_3$ of the mixture of diastereomers of compound **131**.
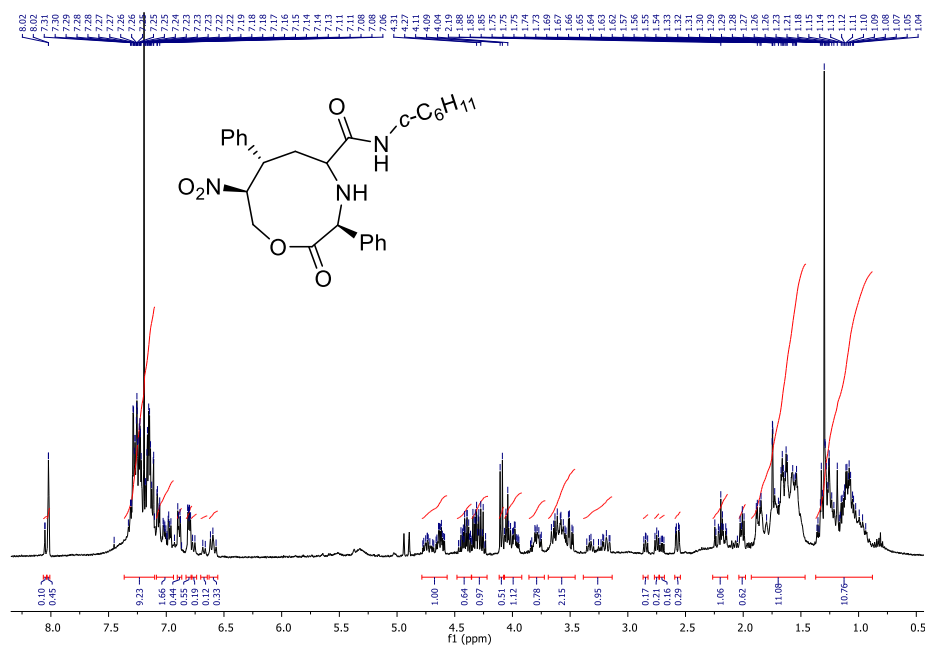
FIGURE 162: 100 MHz ^{13}C NMR spectra in CDCl$_3$ of the mixture of diastereomers of compound **132**.
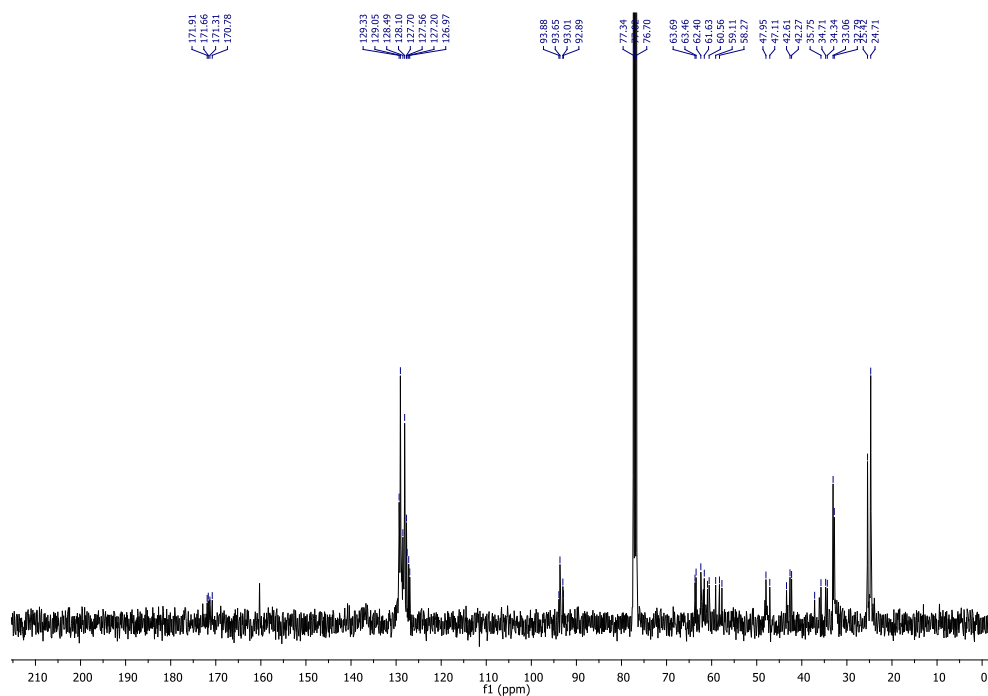
FIGURE 163: 100 MHz ^{13}C NMR spectra in CDCl$_3$ of the mixture of diastereomers of compound **132**.
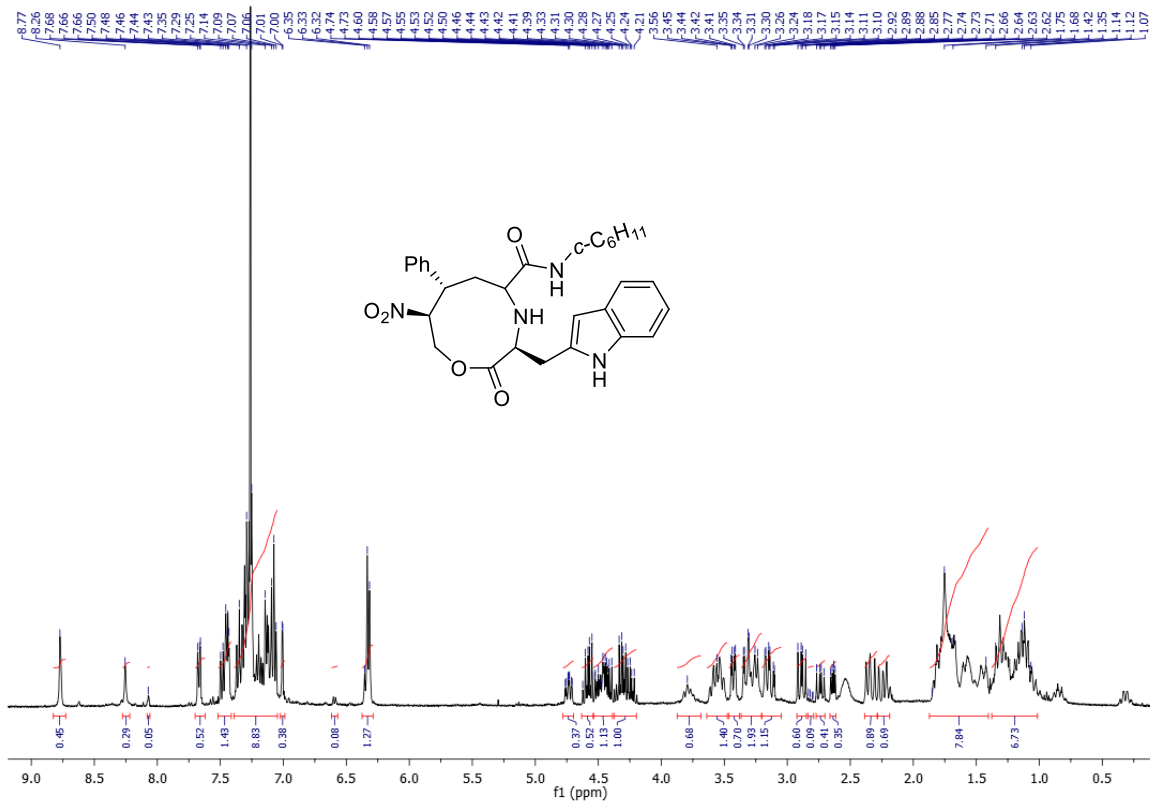
FIGURE 164: 400 MHz ^{1}H NMR spectra in CDCl$_3$ of the mixture of diastereomers of compound **133**.
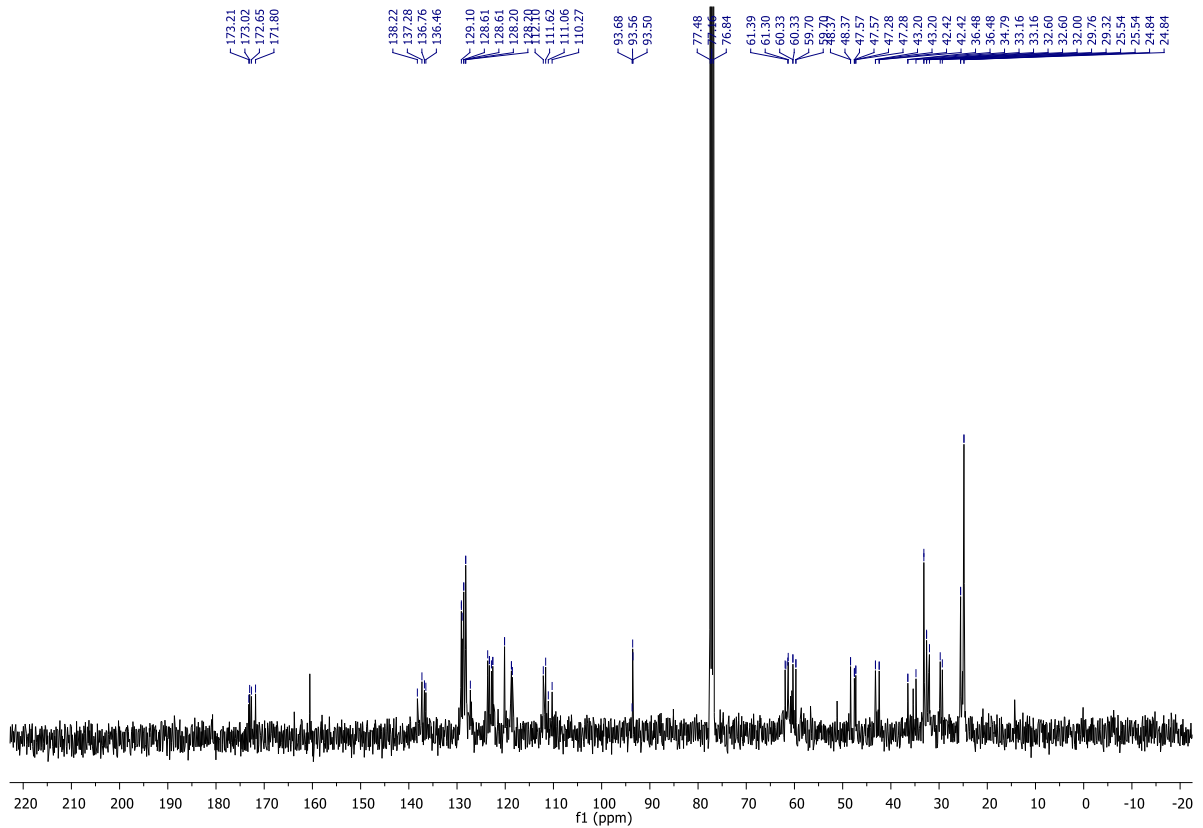
FIGURE 165: 100 MHz ^{13}C NMR spectra in CDCl$_3$ of the mixture of diastereomers of compound **133**.
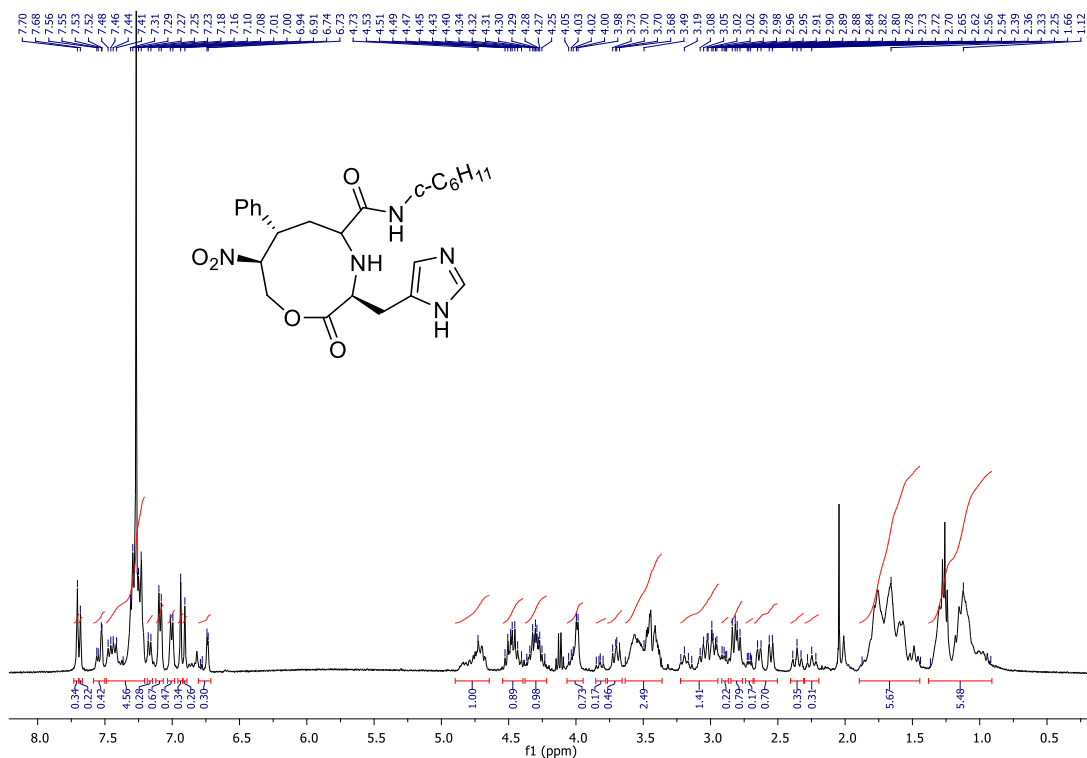
FIGURE 166: 400 MHz ^{1}H NMR spectra in CDCl$_3$ of the mixture of diastereomers of compound **134**.
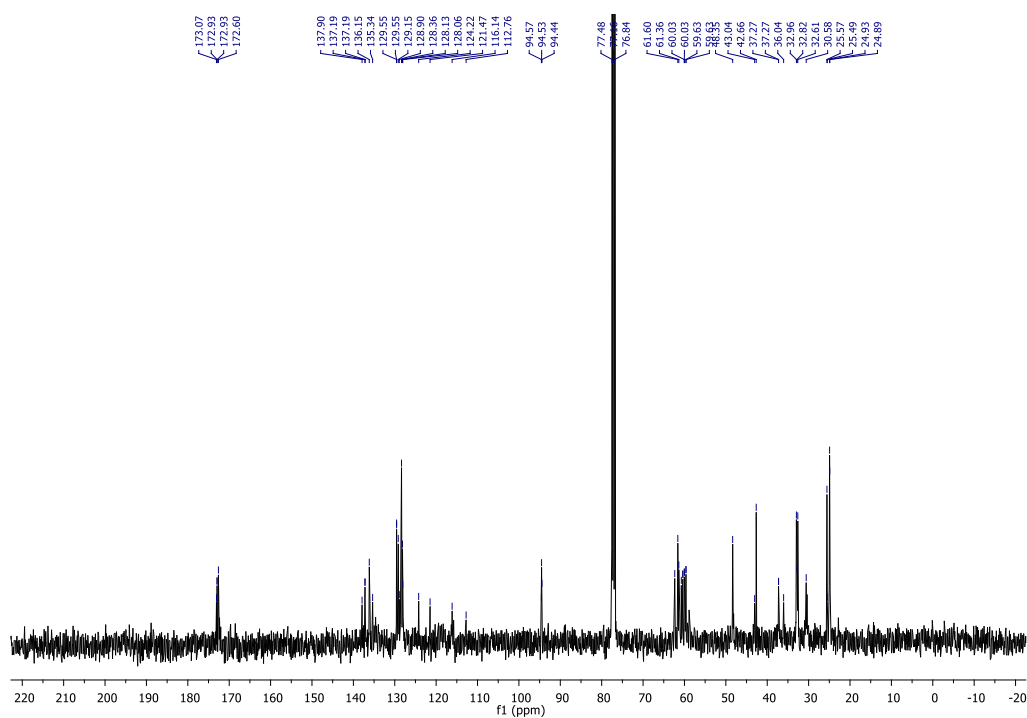
FIGURE 167: 100 MHz ^{13}C NMR spectra in CDCl$_3$ of the mixture of diastereomers of compound **134**.
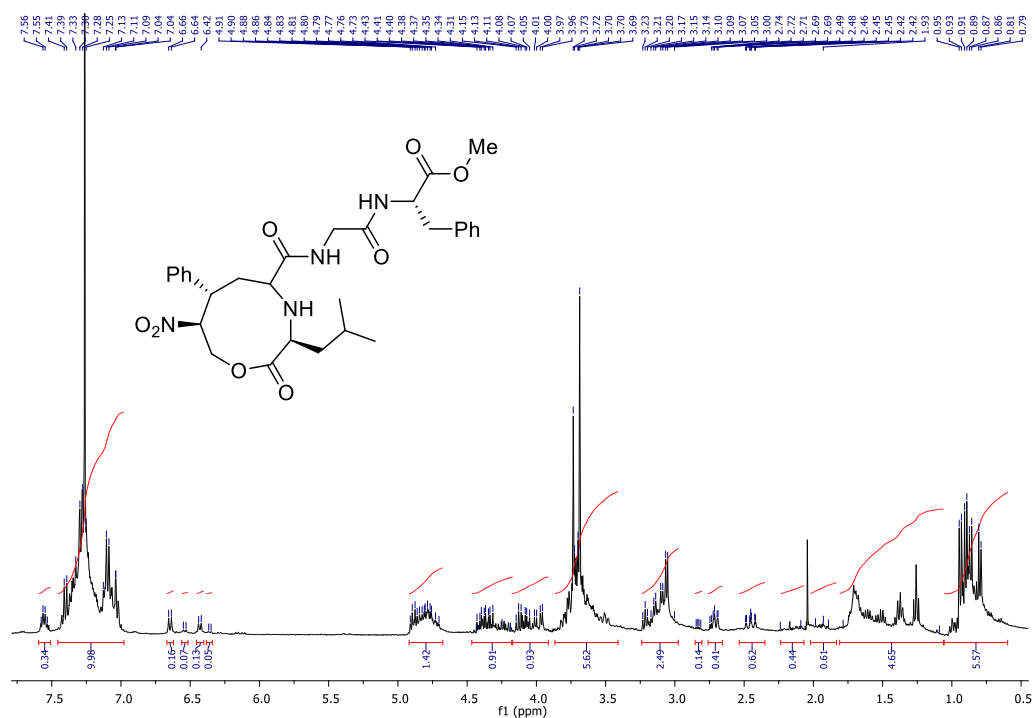
FIGURE 168: 400 MHz ^{1}H NMR spectra in CDCl$_3$ of the mixture of diastereomers of compound **135**.
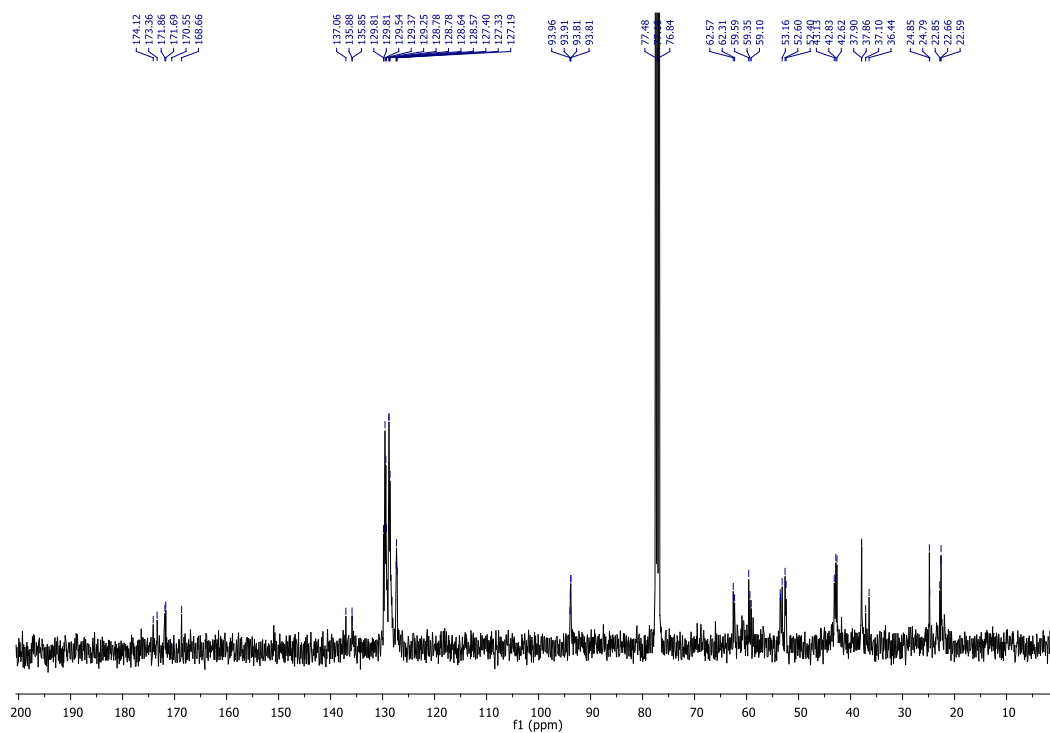
FIGURE 169: 100 MHz ^{13}C NMR spectra in CDCl$_3$ of the mixture of diastereomers of compound **135**.
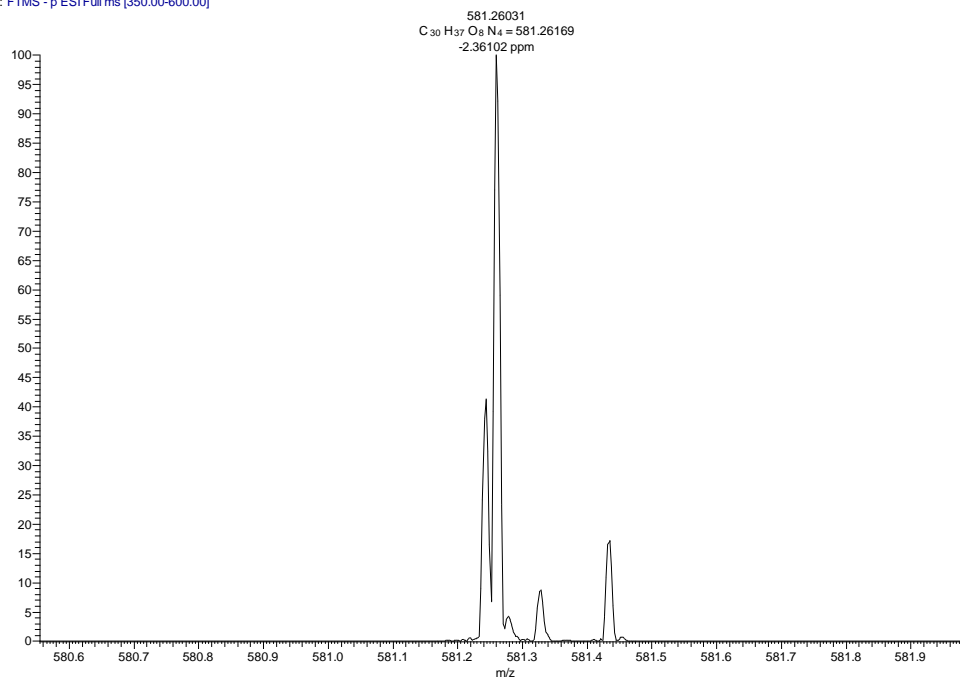
FIGURE 170: HRMS (ESI-FT-ICR) m/z spectra of **135**.
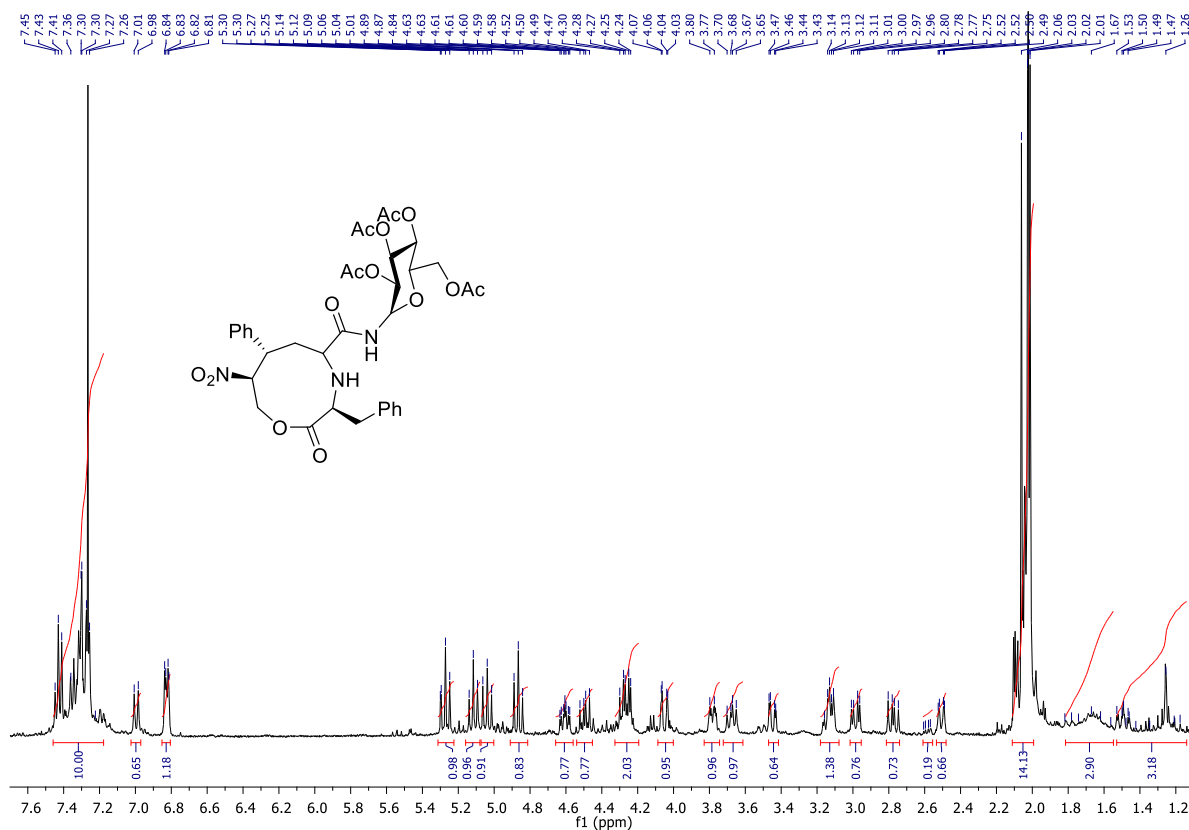
FIGURE 171: 400 MHz ^{1}H NMR spectra in CDCl$_3$ of the mixture of diastereomers of compound **136**.
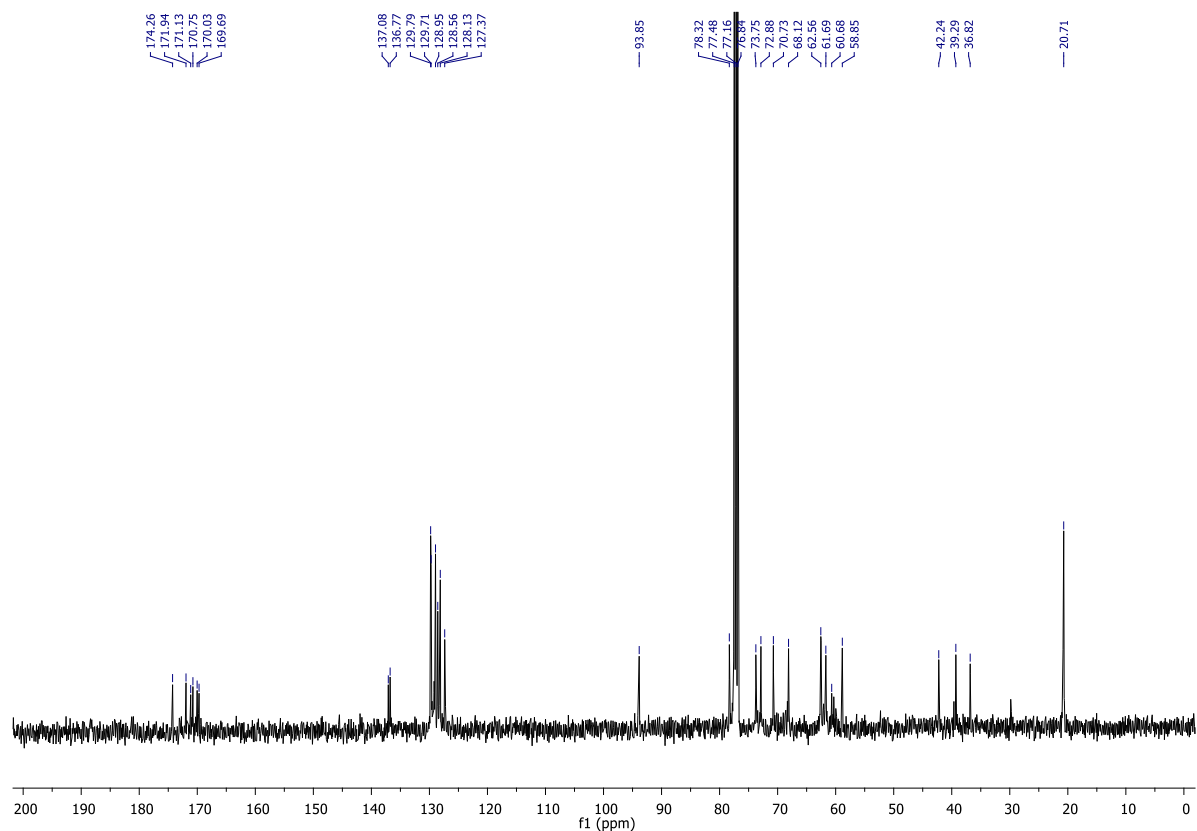
FIGURE 172: 100 MHz ^{13}C NMR spectra in CDCl$_3$ of the mixture of diastereomers of compound **136**.
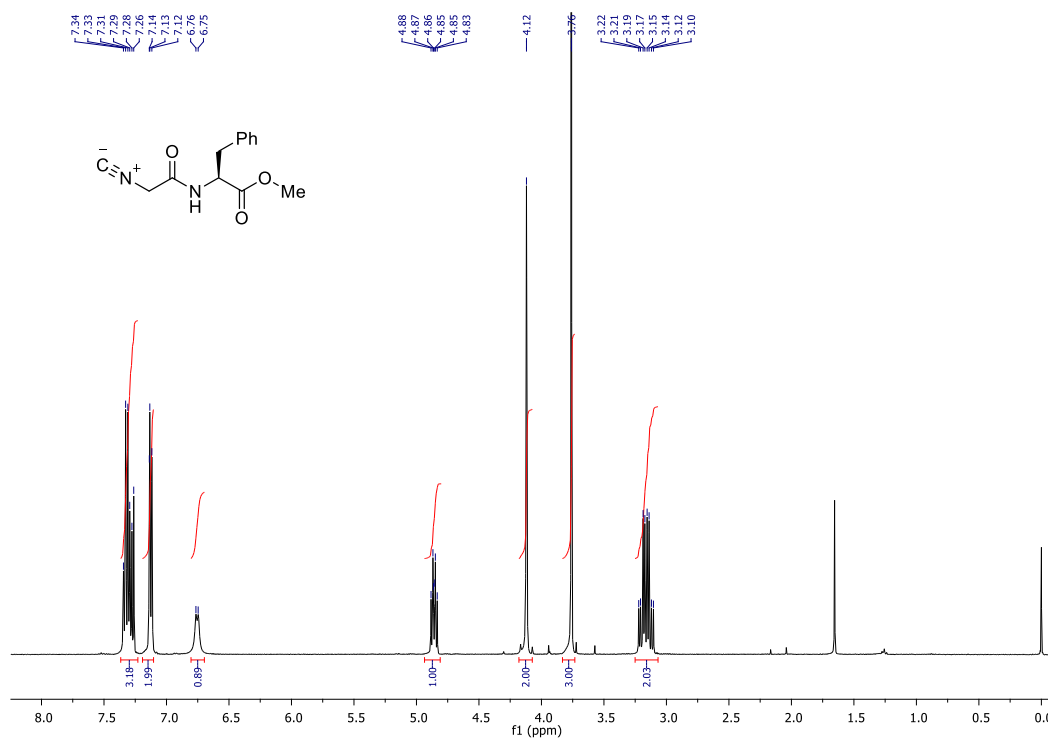
FIGURE 173: 400 MHz ^{1}H NMR spectra in CDCl$_3$ of **138**.
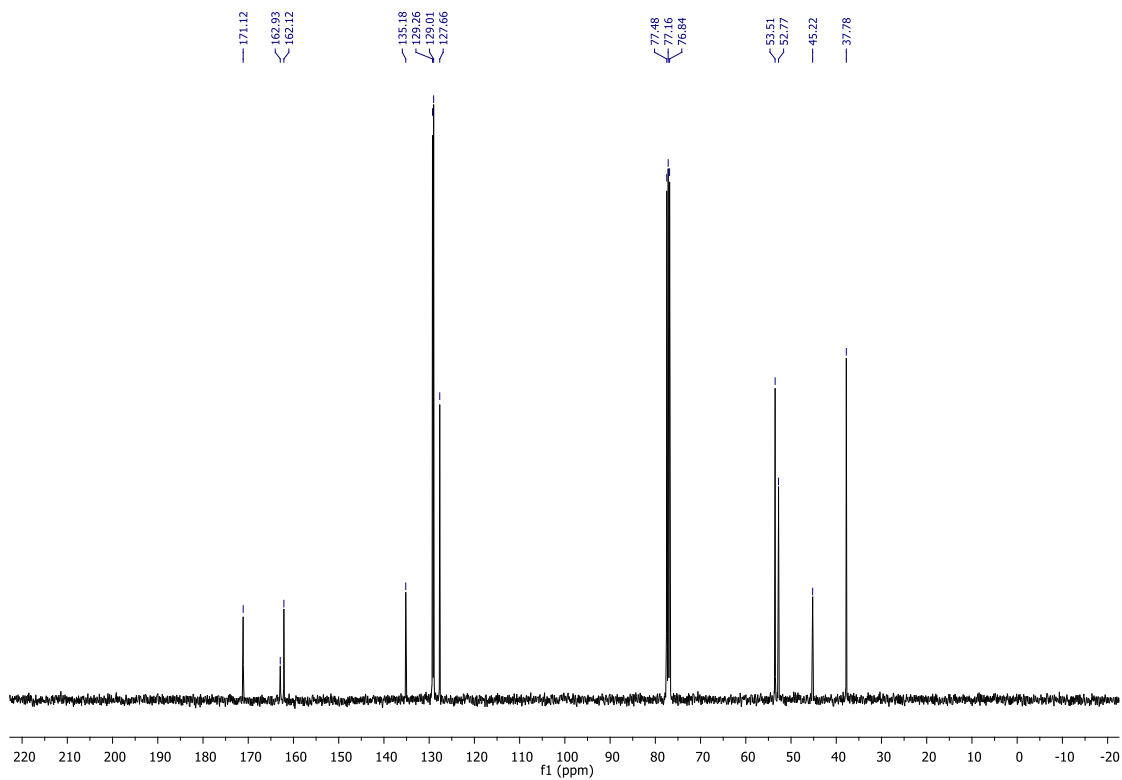
FIGURE 174: 100 MHz ^{13}C NMR spectra in CDCl$_3$ of **138**.
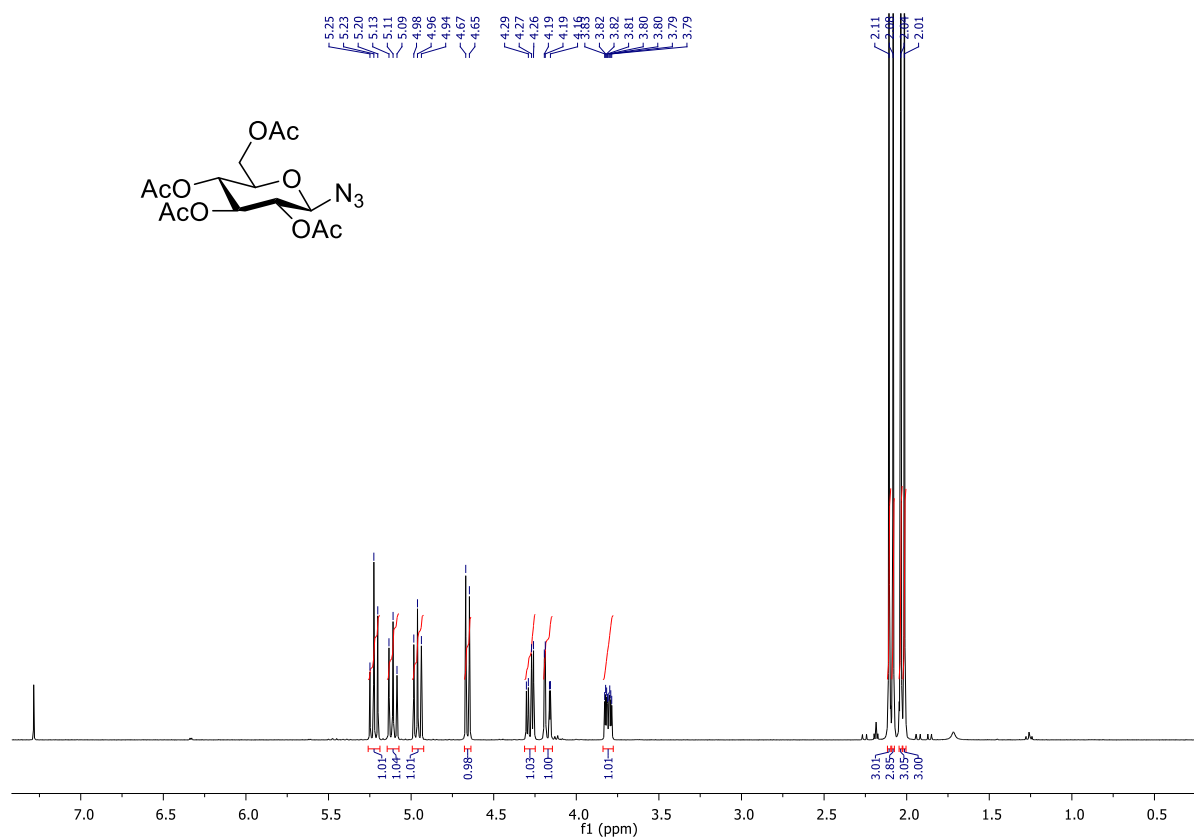
FIGURE 175: 400 MHz ^{1}H NMR spectra in CDCl$_3$ of **139**.
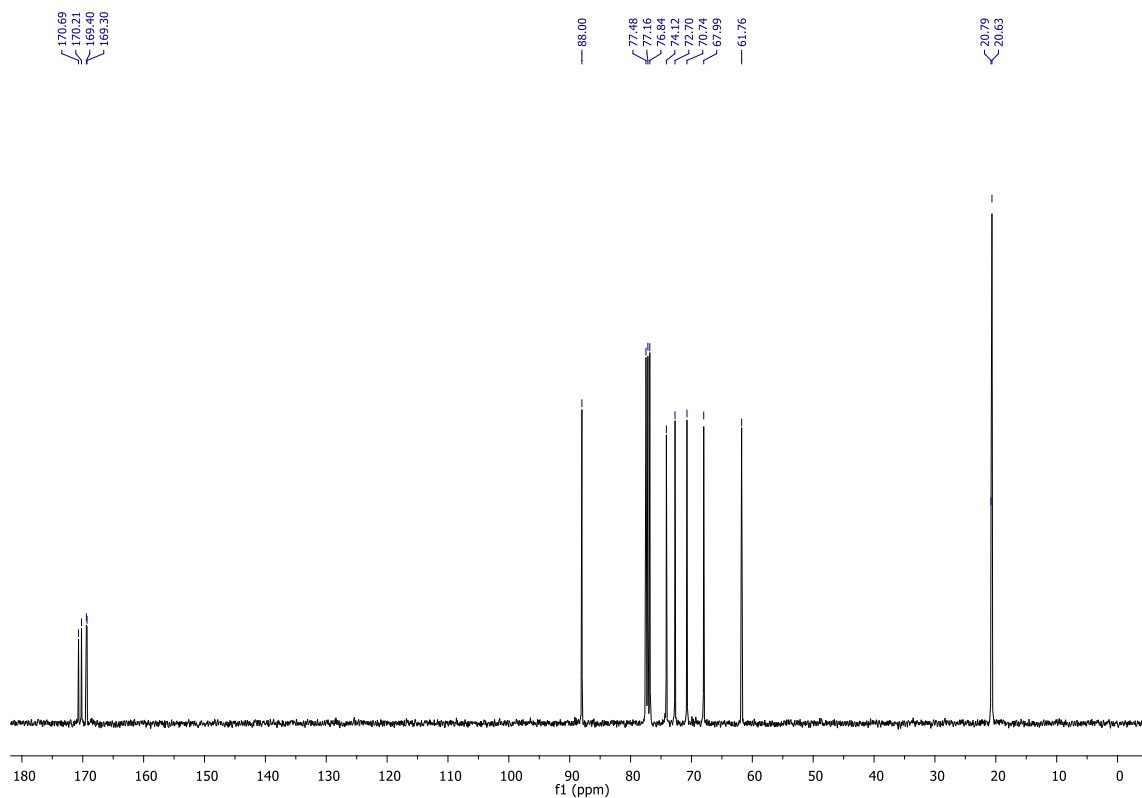
FIGURE 176: 100 MHz ^{13}C NMR spectra in CDCl$_3$ of **139**.
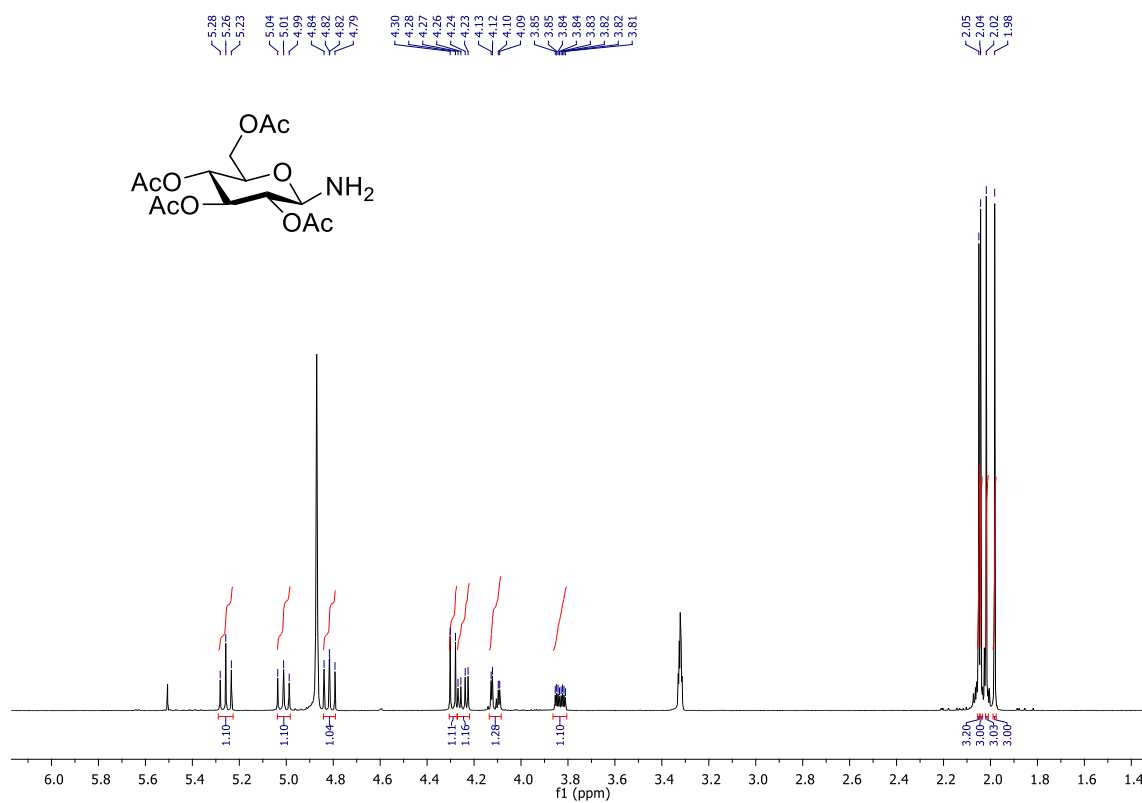
FIGURE 177: 400 MHz ^{1}H NMR spectra in MeOD of **140**.
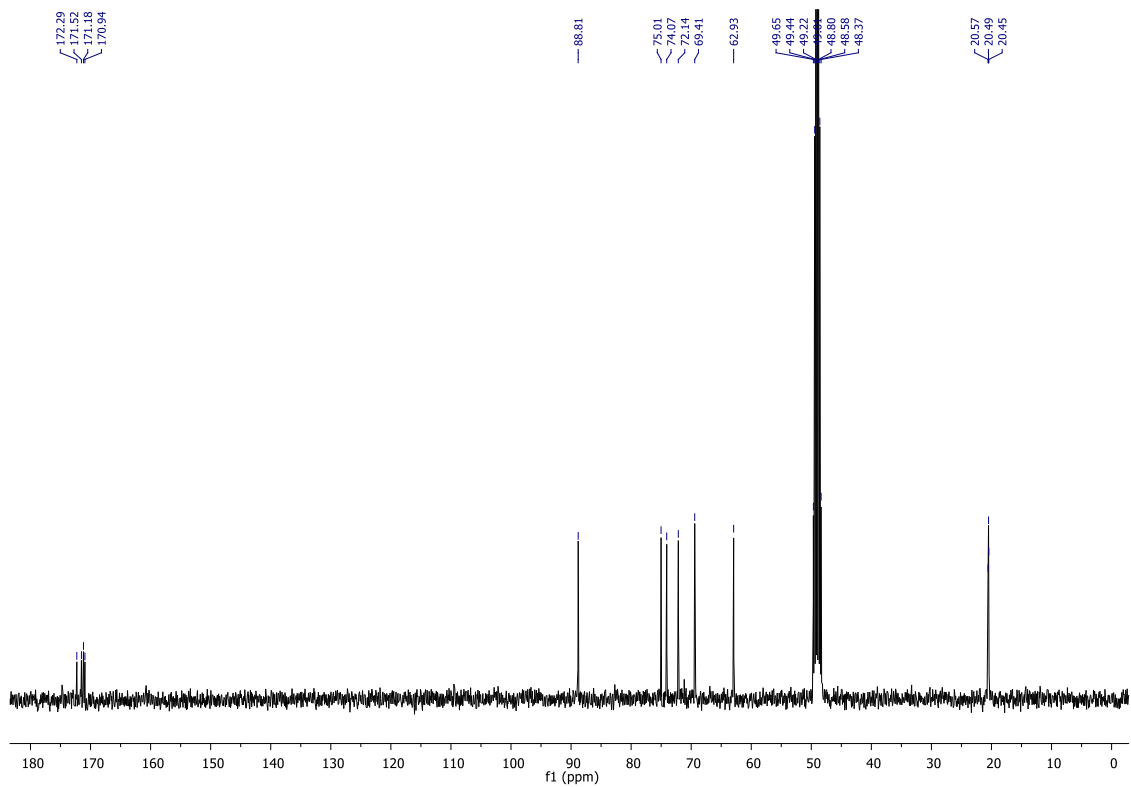
FIGURE 178: 100 MHz ^{13}C NMR spectra in MeOD of **140**.
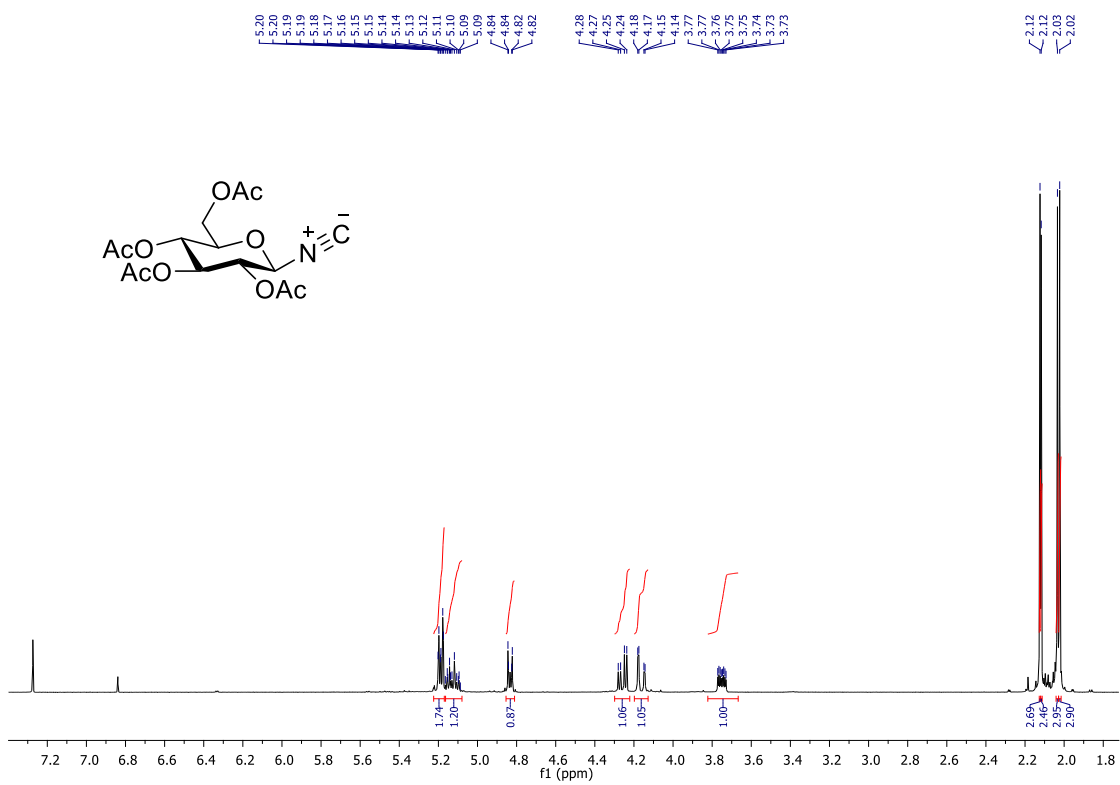
FIGURE 179: 400 MHz ^{1}H NMR spectra in CDCl$_3$ of **142**.
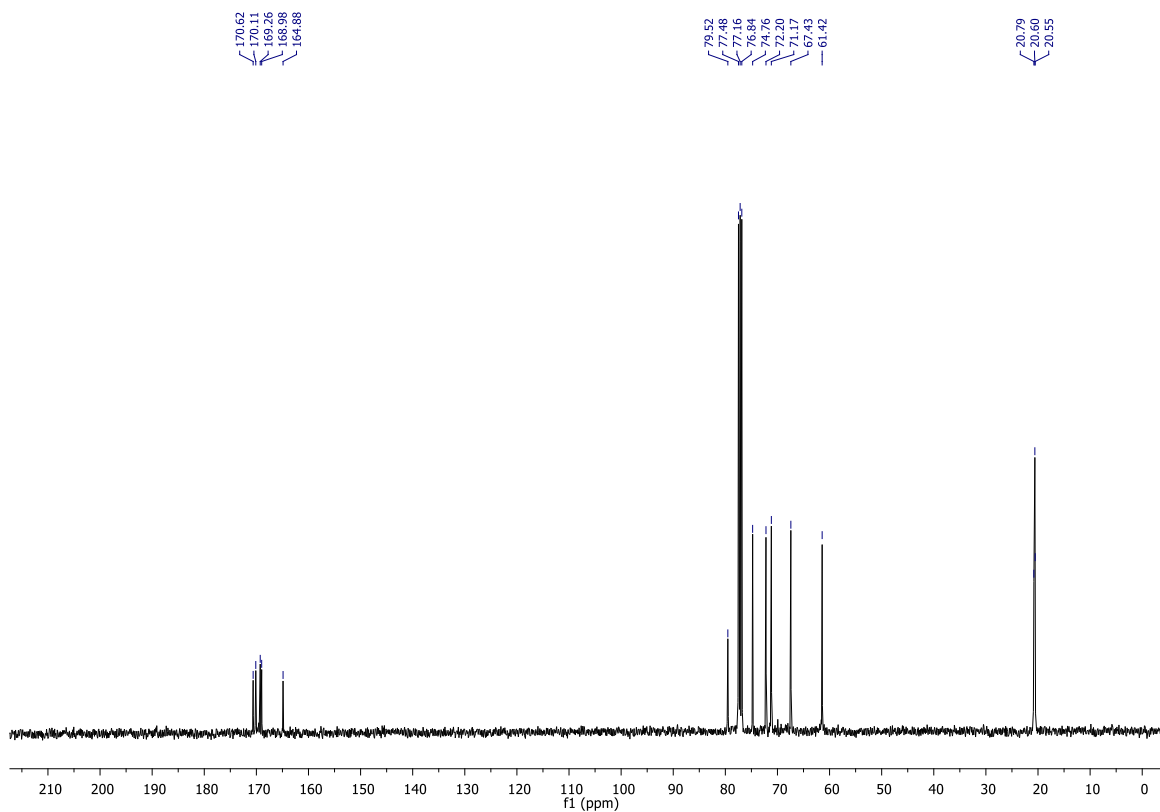
FIGURE 180: 100 MHz ^{13}C NMR spectra in CDCl$_3$ of **142**.
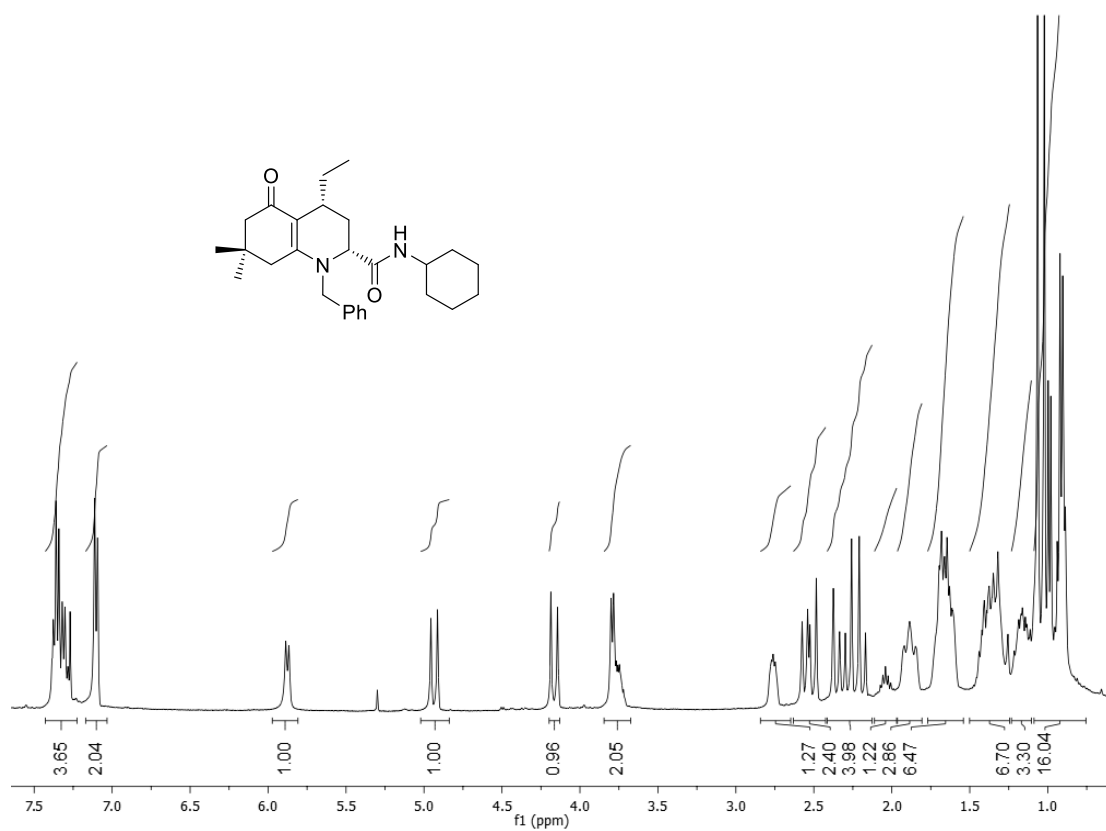
FIGURE 181: 400 MHz ^{1}H NMR spectra in CDCl$_3$ of the diastereomer cis of compound **146**.
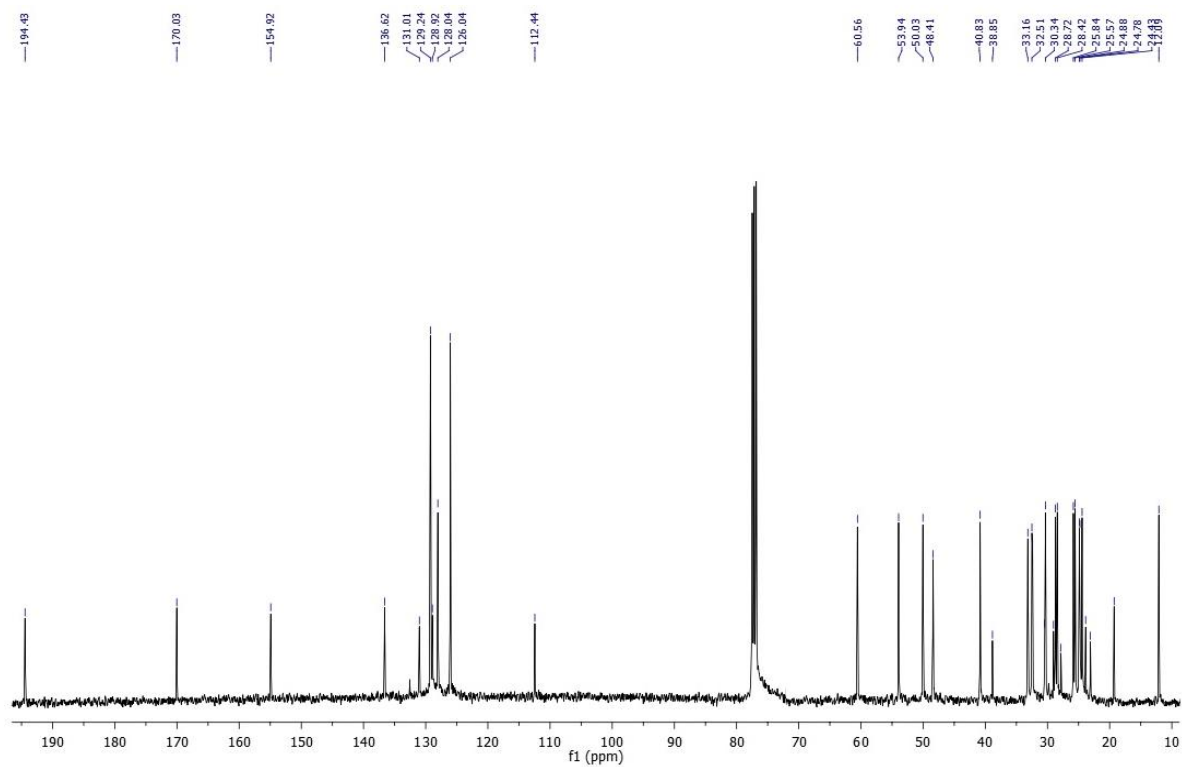
FIGURE 182: 100 MHz ^{13}C NMR spectra in CDCl$_3$ of the diastereomer cis of compound **146**.

272
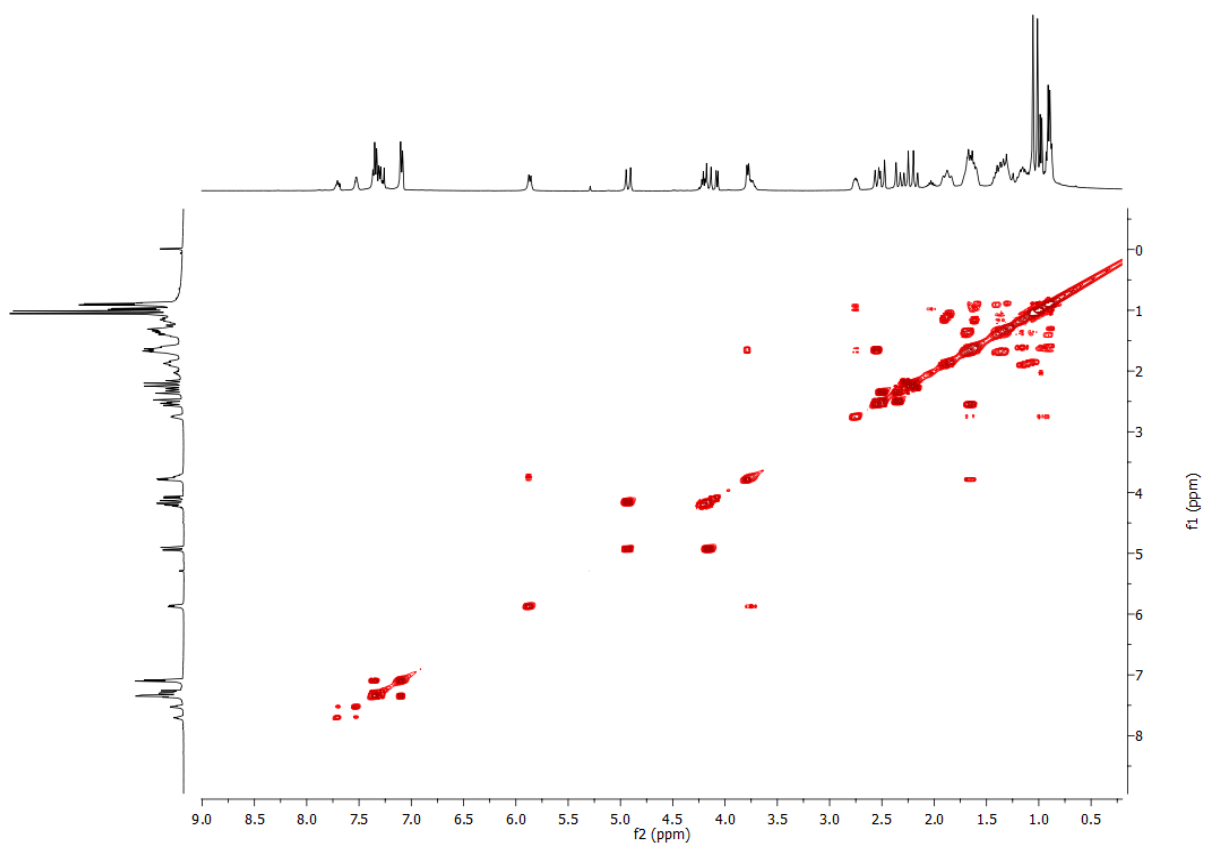
FIGURE 183: COSY spectra in CDCl$_3$ of the diastereomer cis of compound **146**.
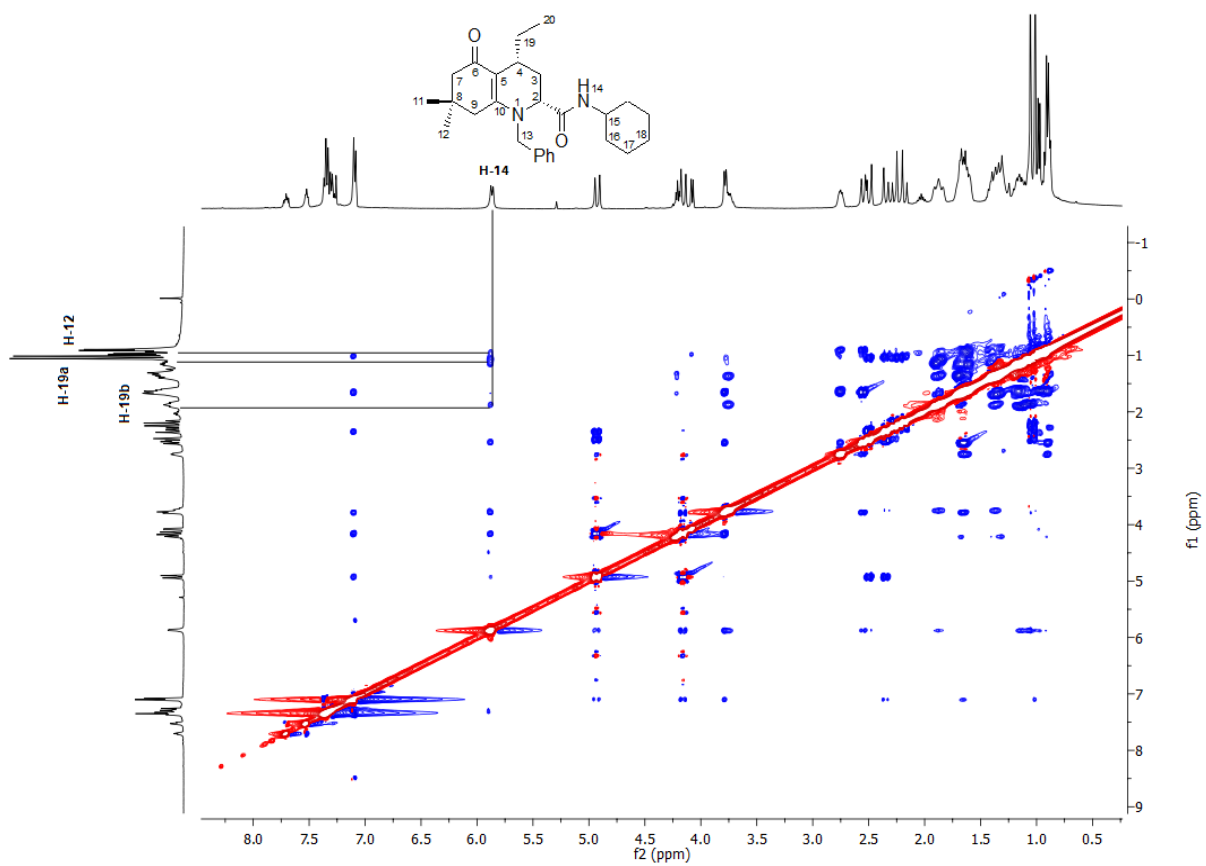
FIGURE 184: NOESY spectra in CDCl$_3$ of the diastereomer cis of compound **146**.
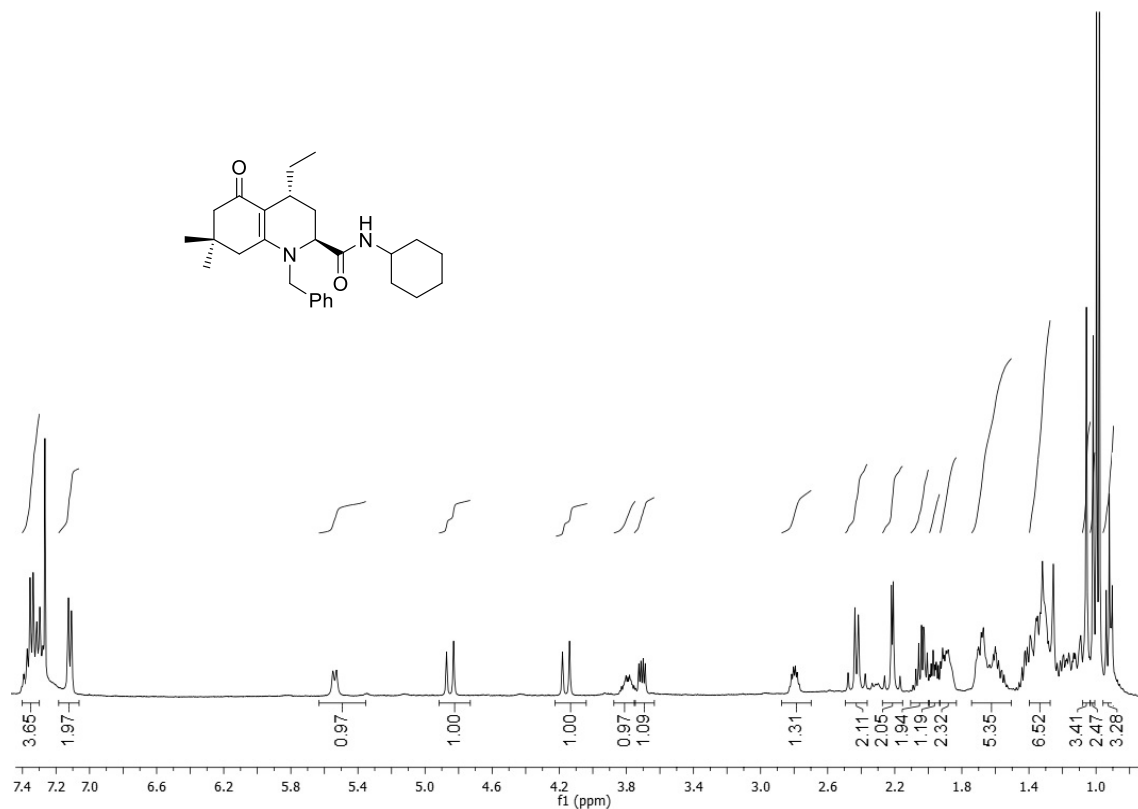
FIGURE 185: 400 MHz ^{1}H NMR spectra in CDCl$_3$ of the diastereomer trans of compound **146**.
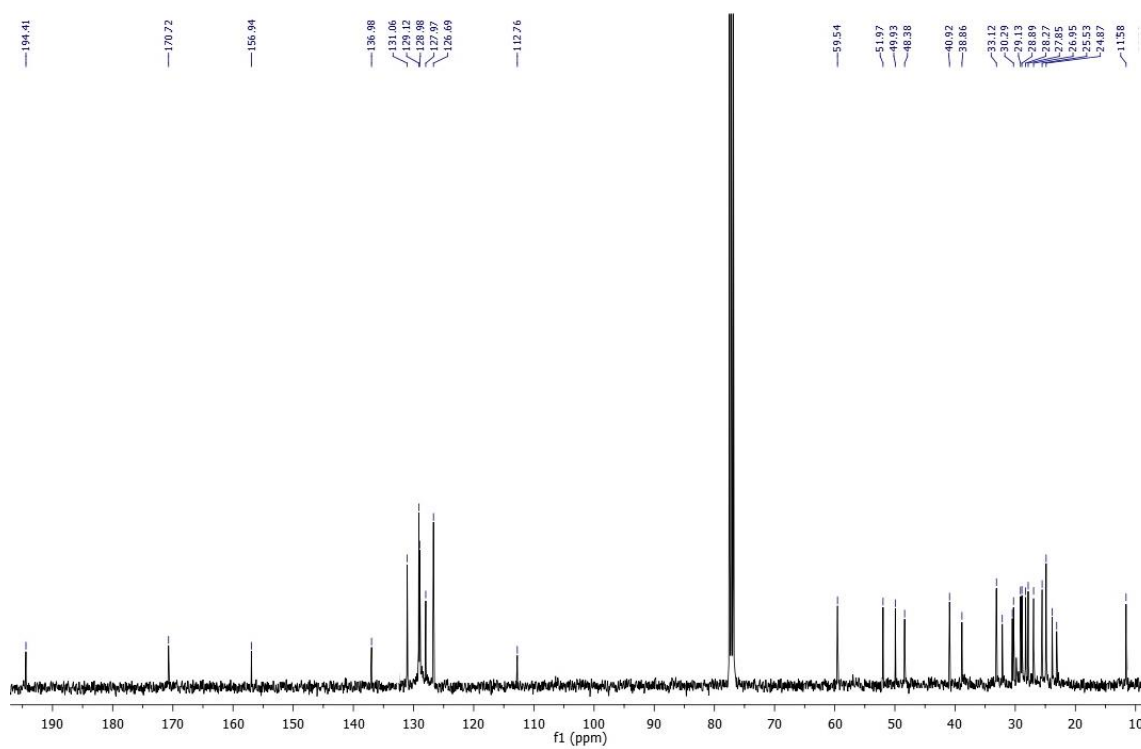
FIGURE 186: 100 MHz ^{13}C NMR spectra in CDCl$_3$ of the diastereomer trans of compound **146**.
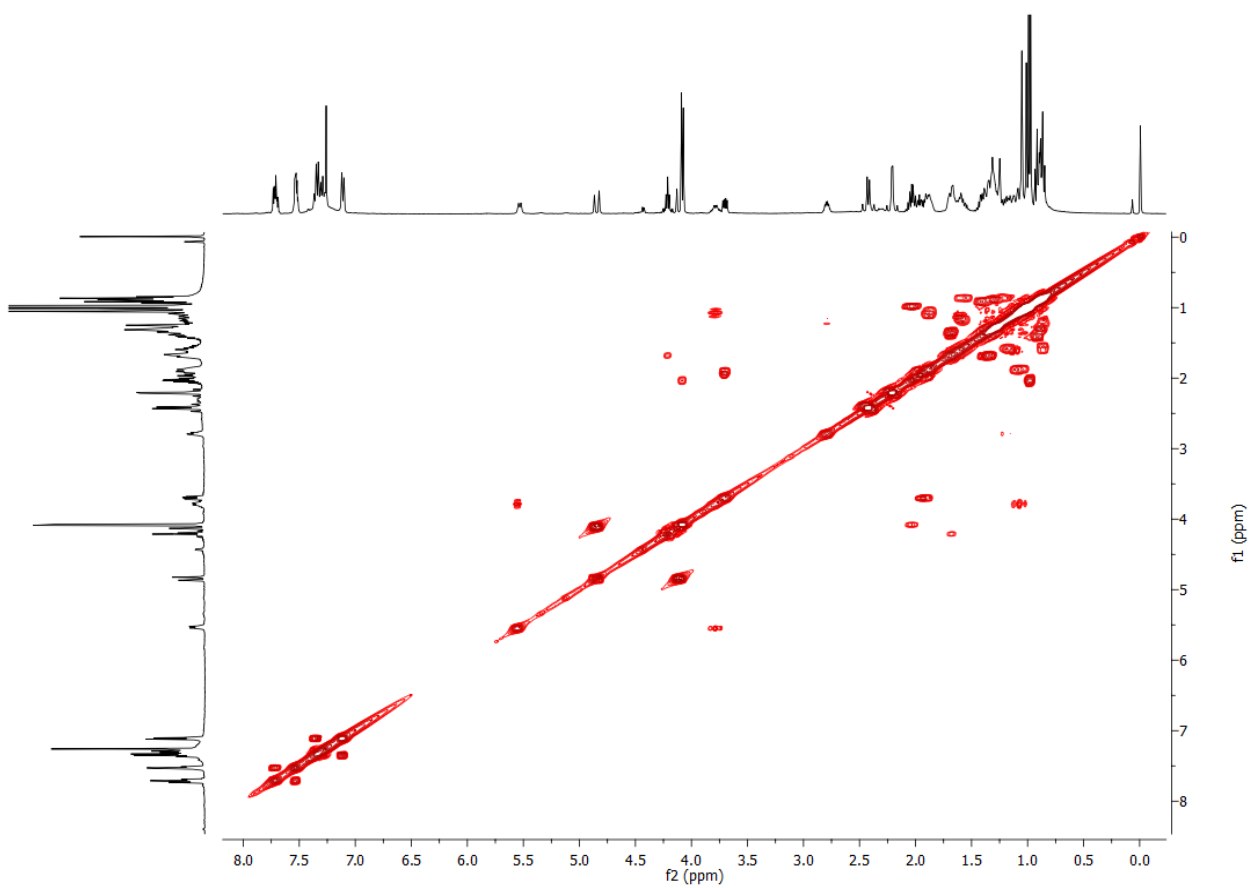
FIGURE 187: COSY spectra in CDCl$_3$ of the diastereomer trans of compound **146**.
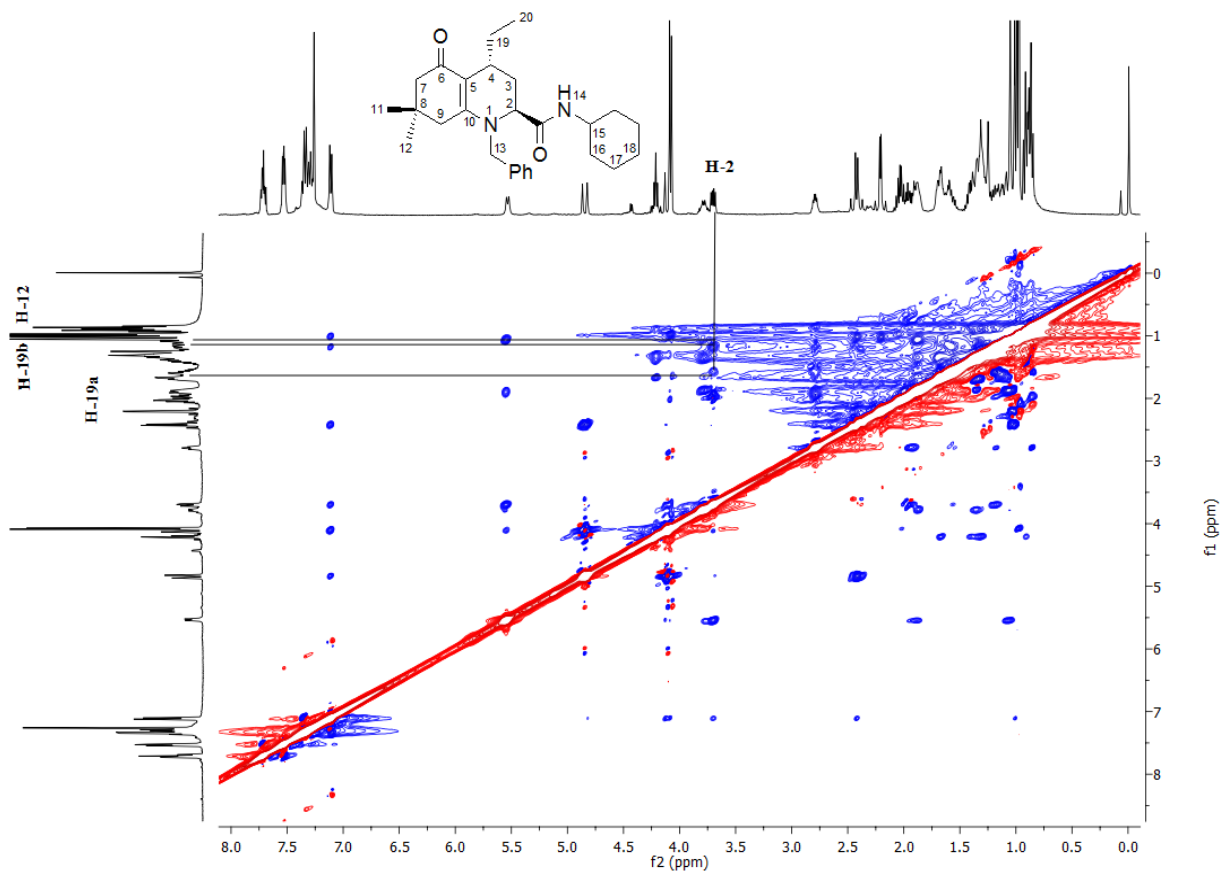
FIGURE 188: NOESY spectra in CDCl$_3$ of the diastereomer trans of compound **146**.
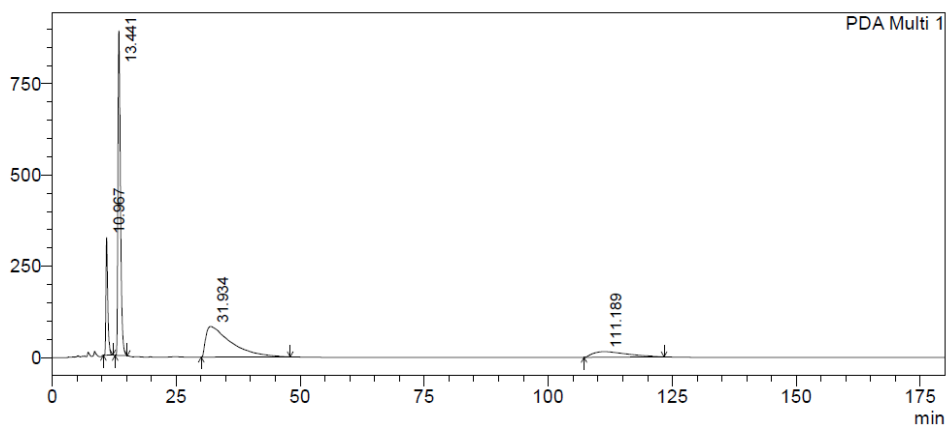
PDA Ch1 300nm 4nm

Peak#	Ret. Time	Area	Height	Area %
1	10.967	8494989	322142	11.148
2	13.441	30903885	888932	40.555
3	31.934	29549949	84019	38.778
4	111.189	7254400	15551	9.520
Total		76203223	1310645	100.000

FIGURE 189: Chiral HPLC analysis of the racemic of compound **146**. Chiralpak AD-H, n-hexane/i-PrOH 90:10, 25°C at 1.0 ml/min, UV detection at 300 nm.
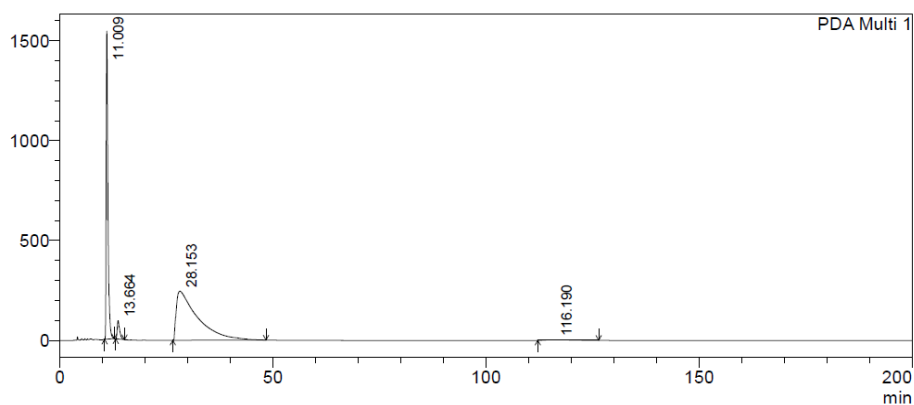
PDA Ch1 300nm 4nm

Peak#	Ret. Time	Area	Height	Area %
1	11.009	45121046	1542300	33.319
2	13.664	3652498	92501	2.697
3	28.153	85163596	245563	62.888
4	116.190	1484218	3402	1.096
Total		135421357	1883766	100.000

FIGURE 190: Chiral HPLC analysis of the mixture of diastereomers of compound **146**. Chiralpak AD-H, n-hexane/i-PrOH 90:10, 25°C at 1.0 ml/min, UV detection at 300 nm.
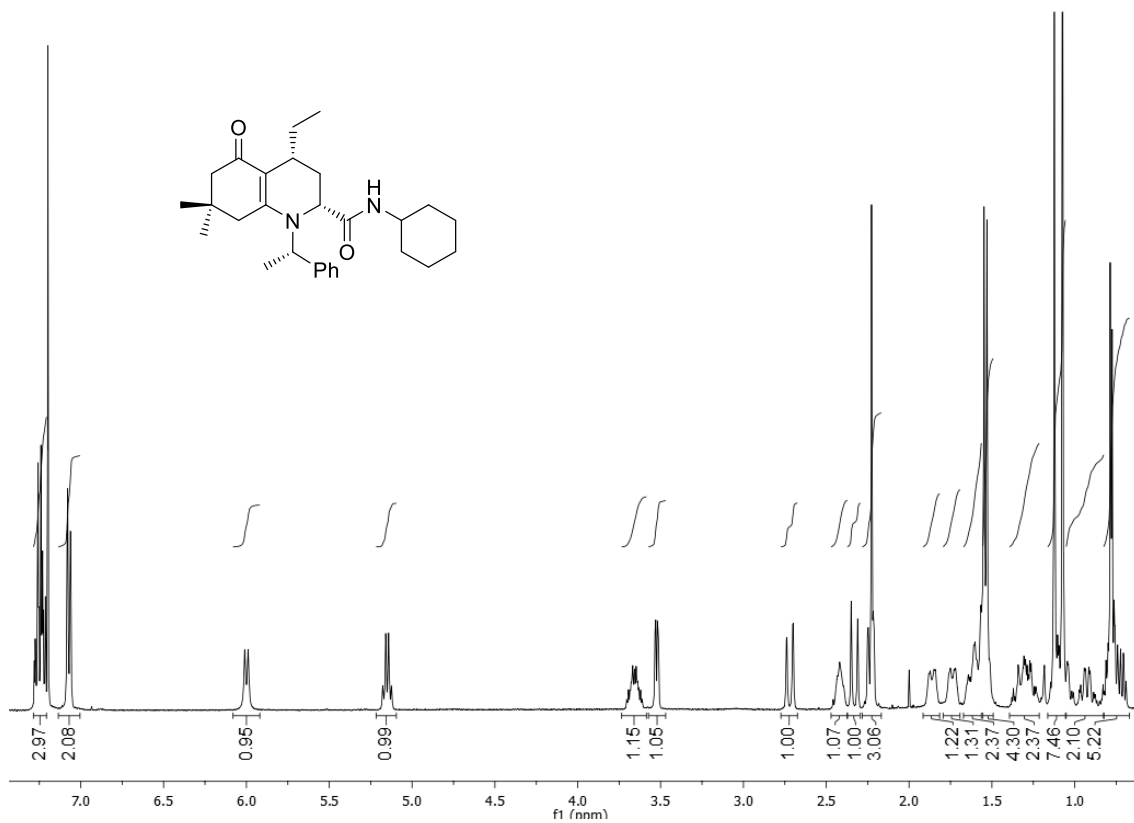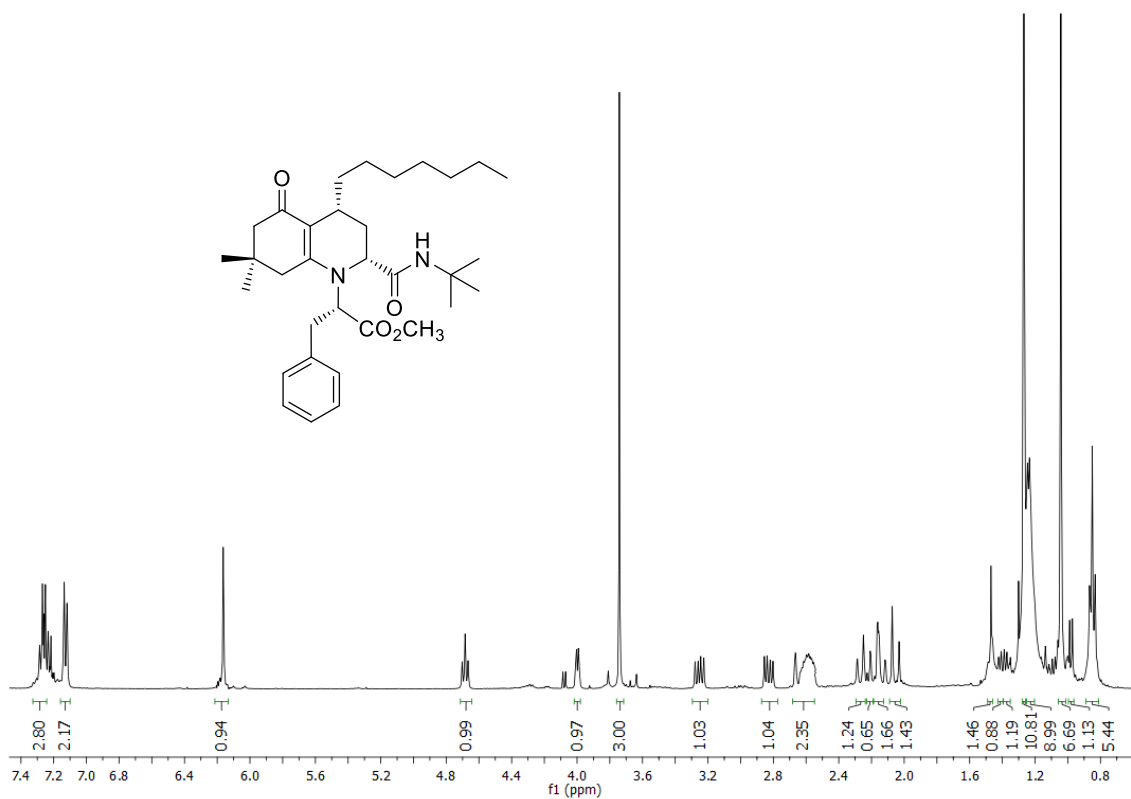
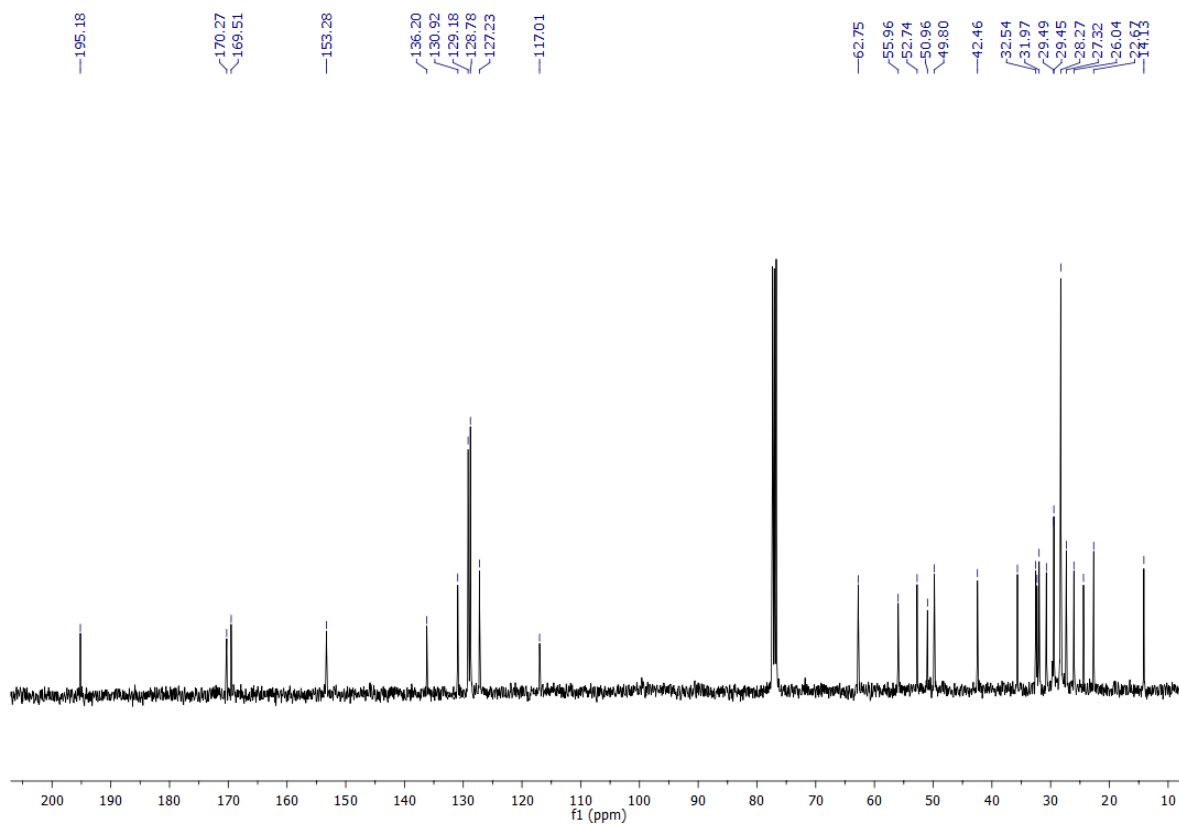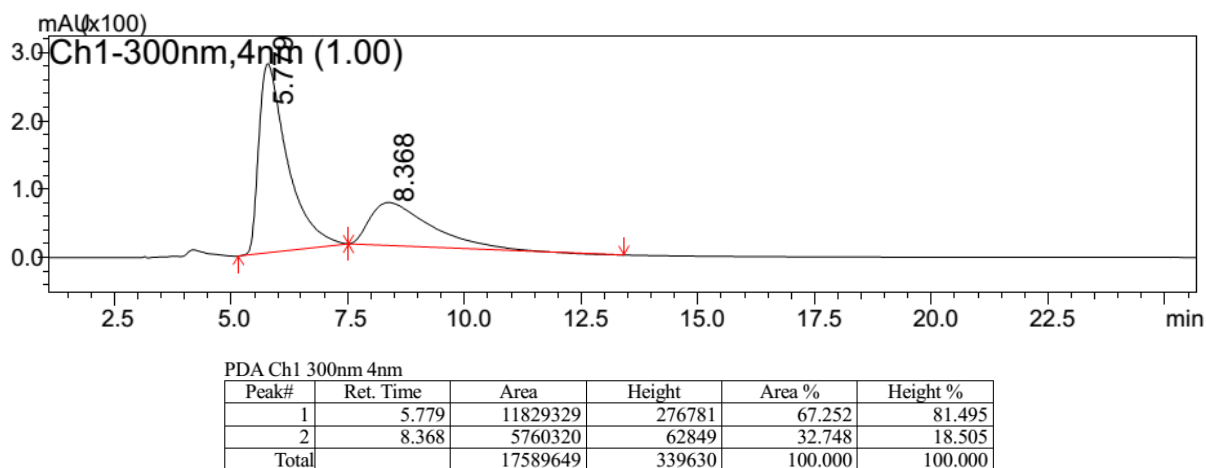FIGURE 191: 400 MHz ^{1}H NMR spectra in CDCl$_3$ of compound **147**.
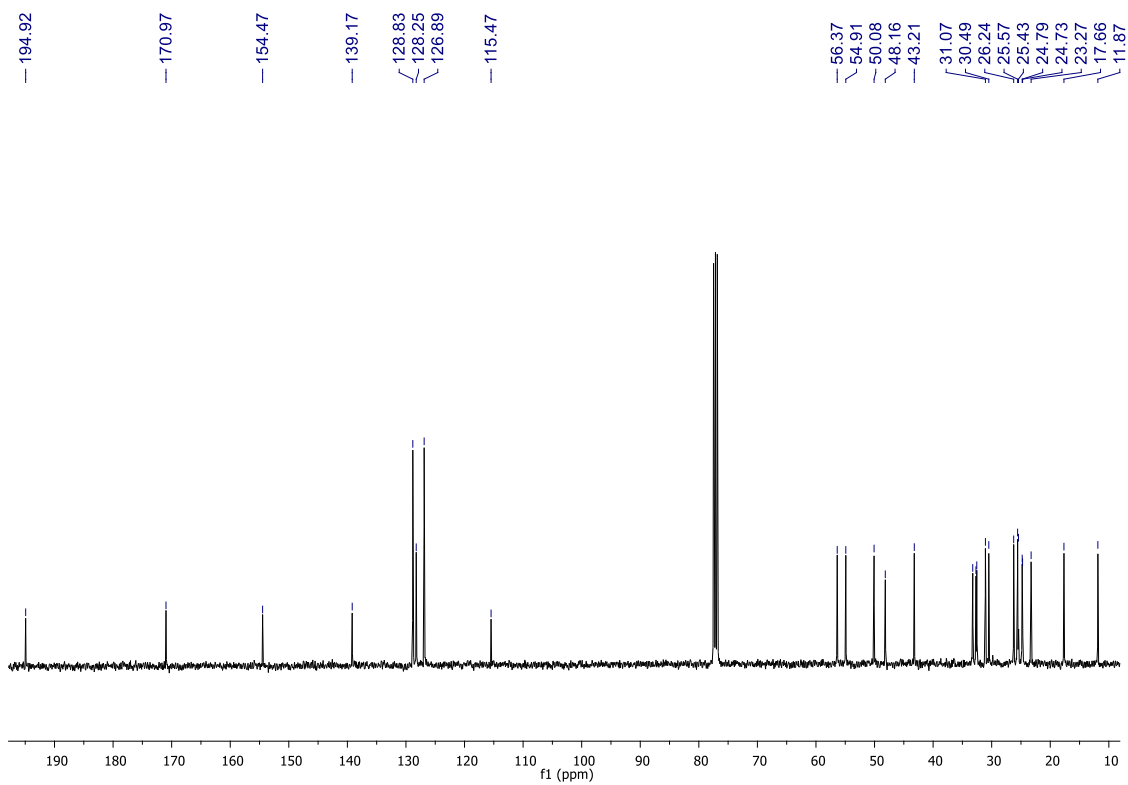
FIGURE 192: 100 MHz ^{13}C NMR spectra in CDCl$_3$ of compound **147**.
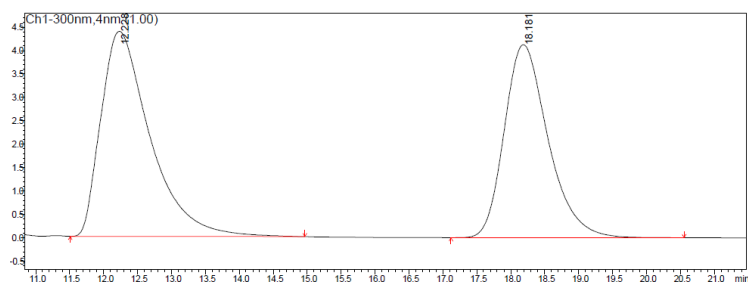
PDA Ch1 300nm 4nm

Peak#	Ret. Time	Area	Height	Area %
1	12.228	22038058	438186	54.376
2	18.181	18490616	412362	45.624
Total		40528674	850549	100.000

FIGURE 193: Chiral HPLC analysis of the racemic of compound **147**. Chiralpak AD-H (n-hexane/i-PrOH 90:10), 25°C at 1.0 ml/min, UV detection at 300 nm.
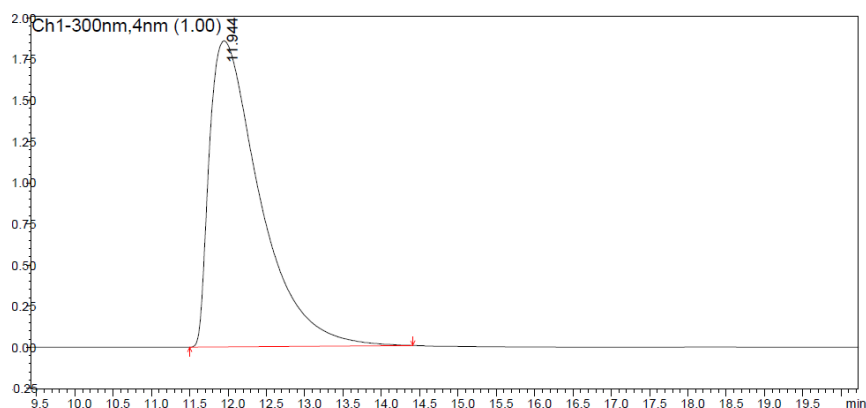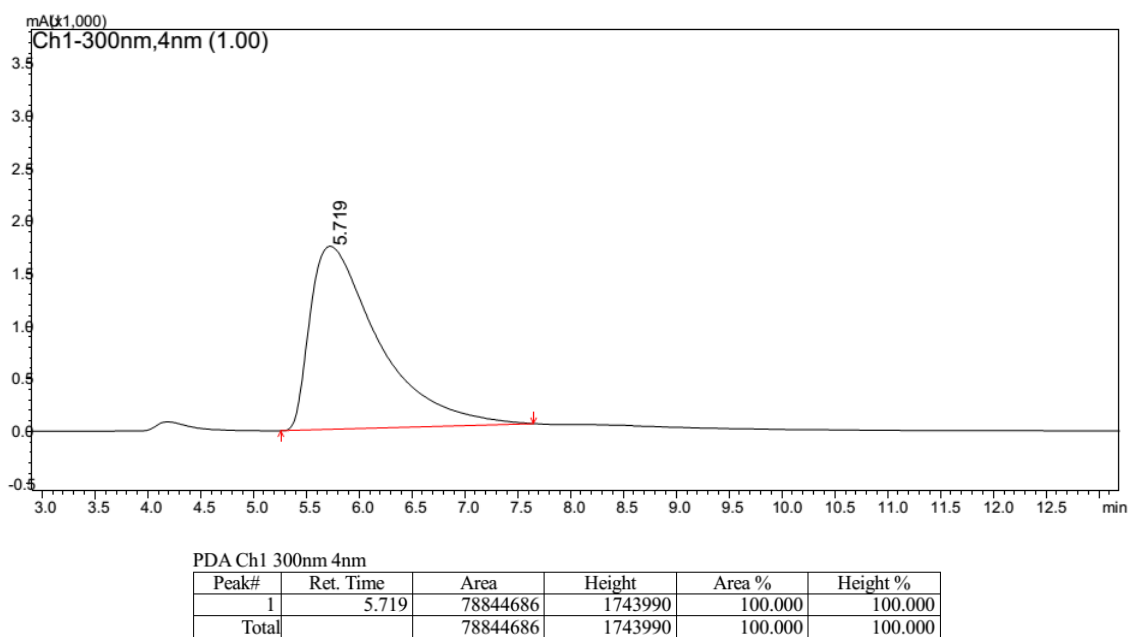

PDA Ch1 300nm 4nm

Peak#	Ret. Time	Area	Height	Area %
1	11.944	85012511	1858220	100.000
Total		85012511	1858220	100.000

FIGURE 194: Chiral HPLC analysis of the mixture of diastereomers of compound **147**. Chiralpak AD-H (n-hexane/i-PrOH 90:10), 25°C at 1.0 ml/min, UV detection at 300 nm.
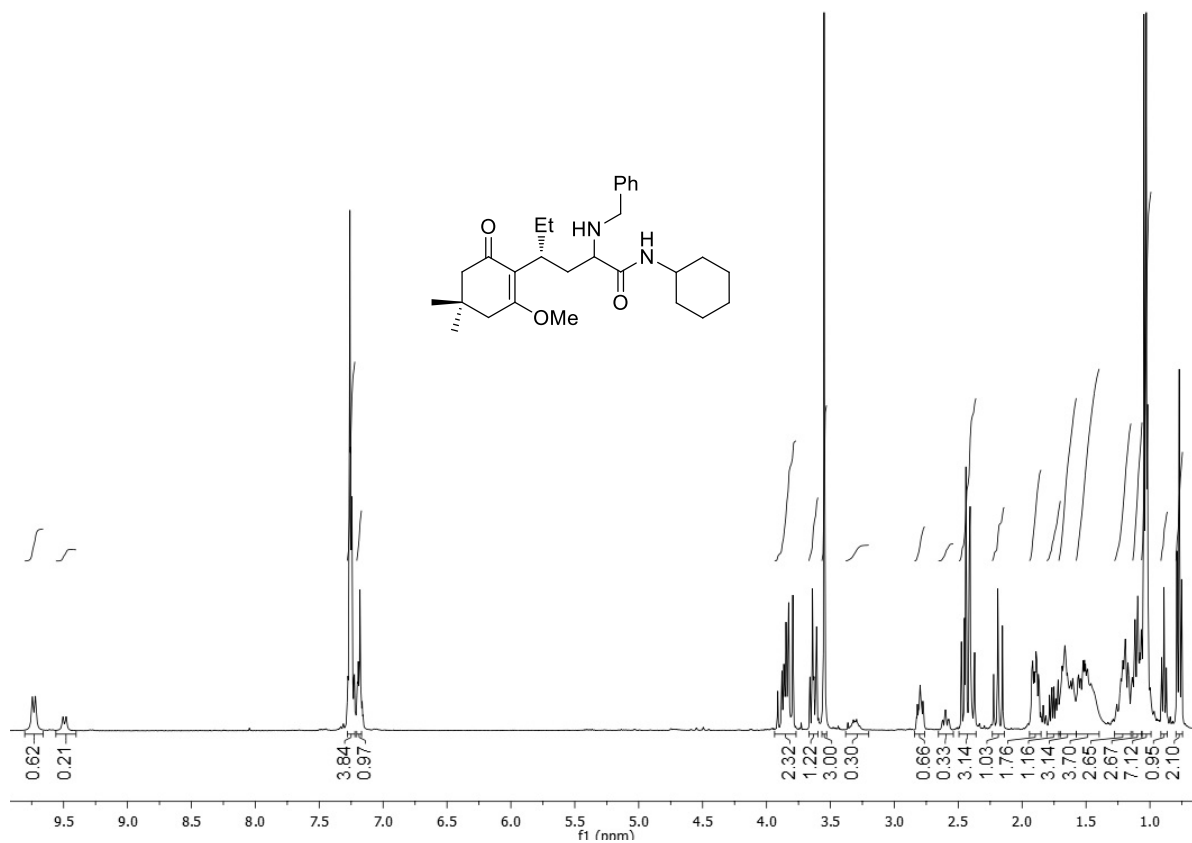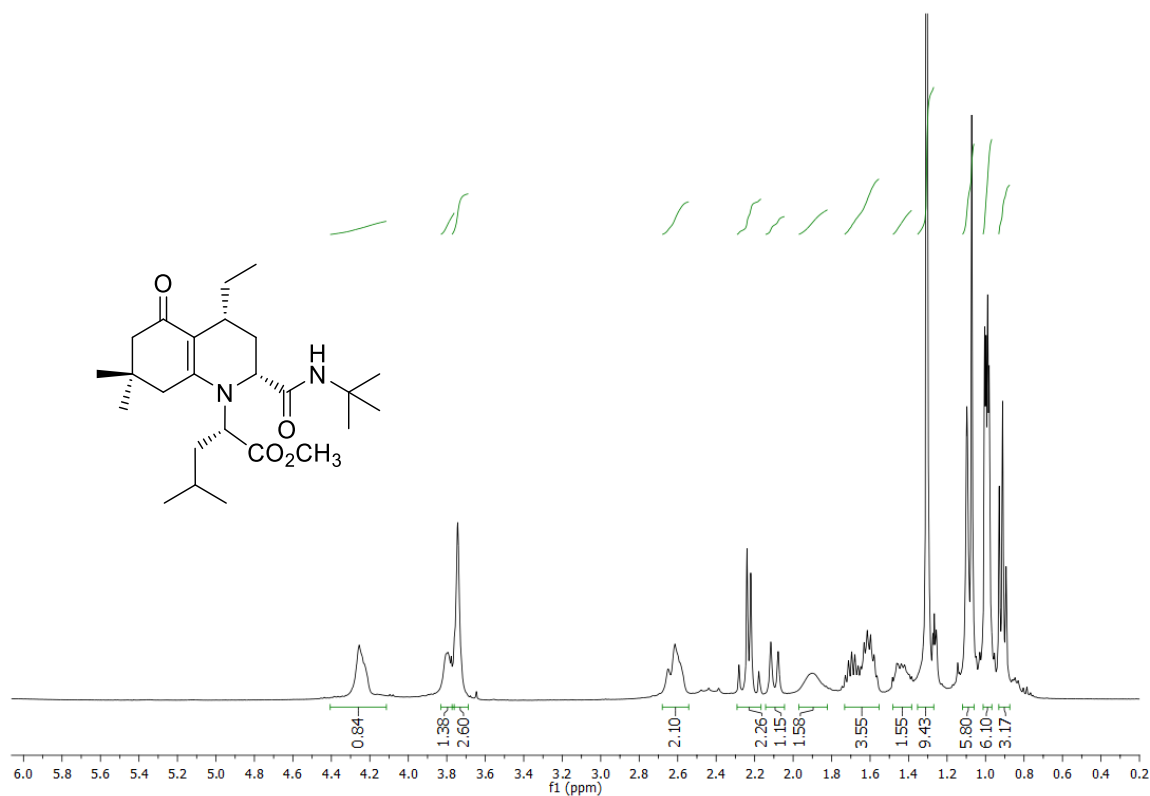
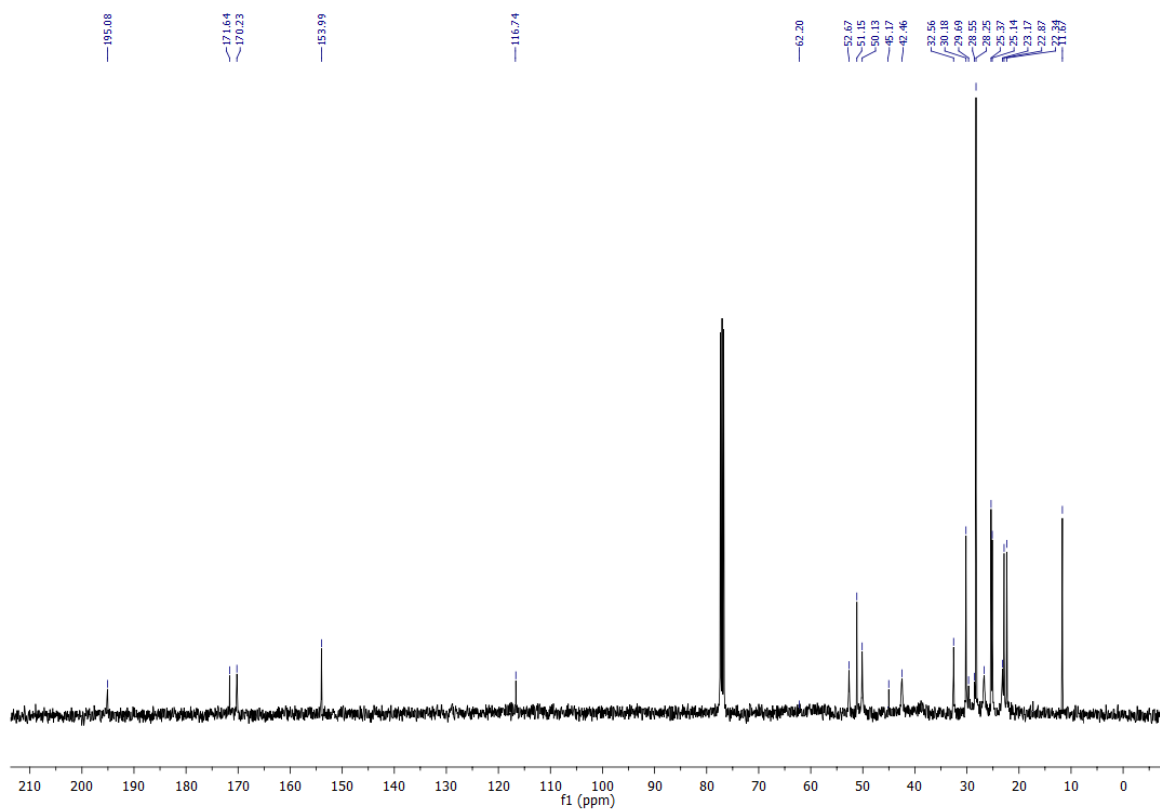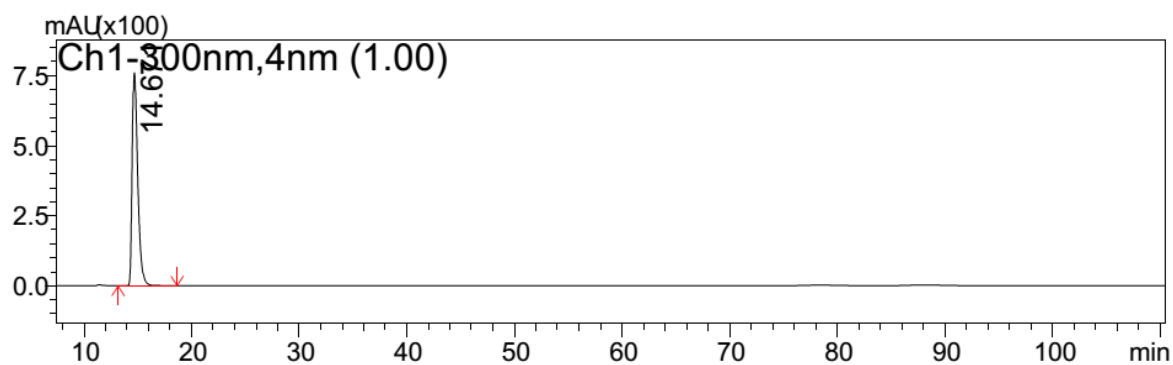FIGURE 195: 400 MHz ^{1}H NMR spectra in CDCl$_3$ of compound **148**.
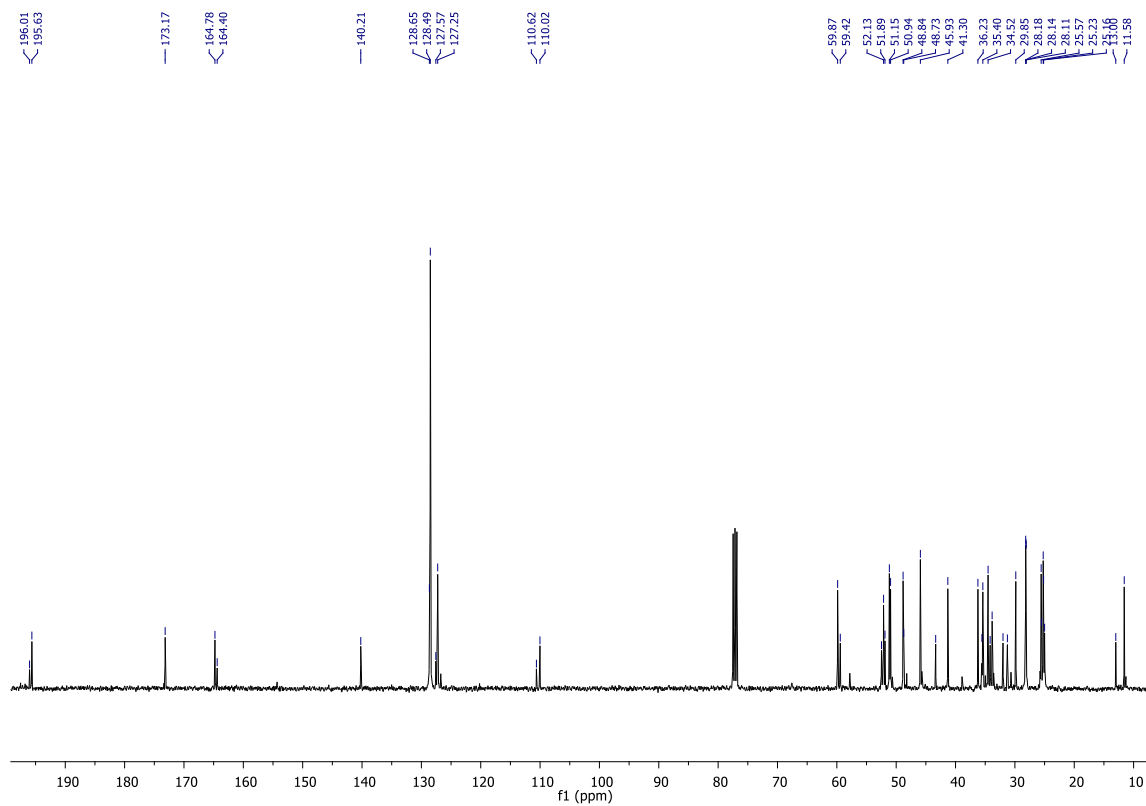
FIGURE 196: 100 MHz ^{13}C NMR spectra in CDCl$_3$ of compound **148**.
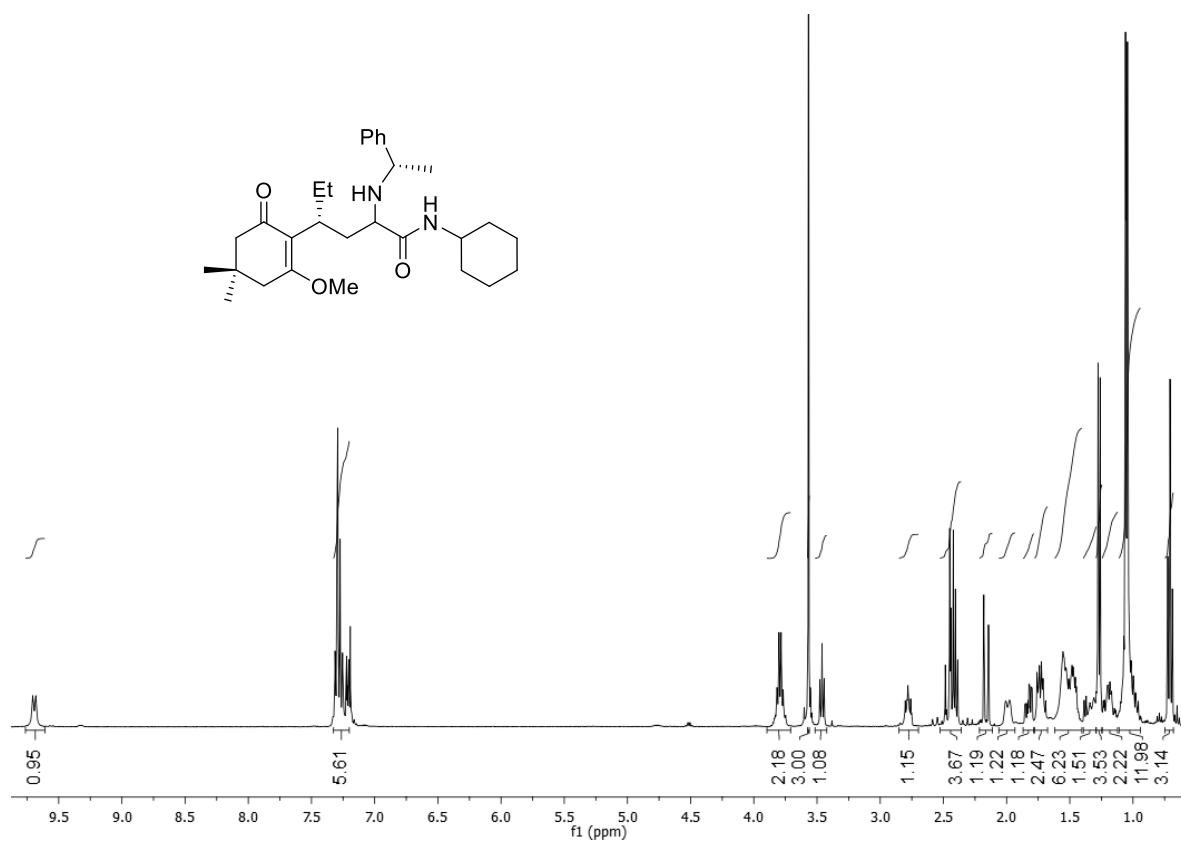
FIGURE 197: 400 MHz ^{1}H NMR spectra in CDCl$_3$ of compound **149**.
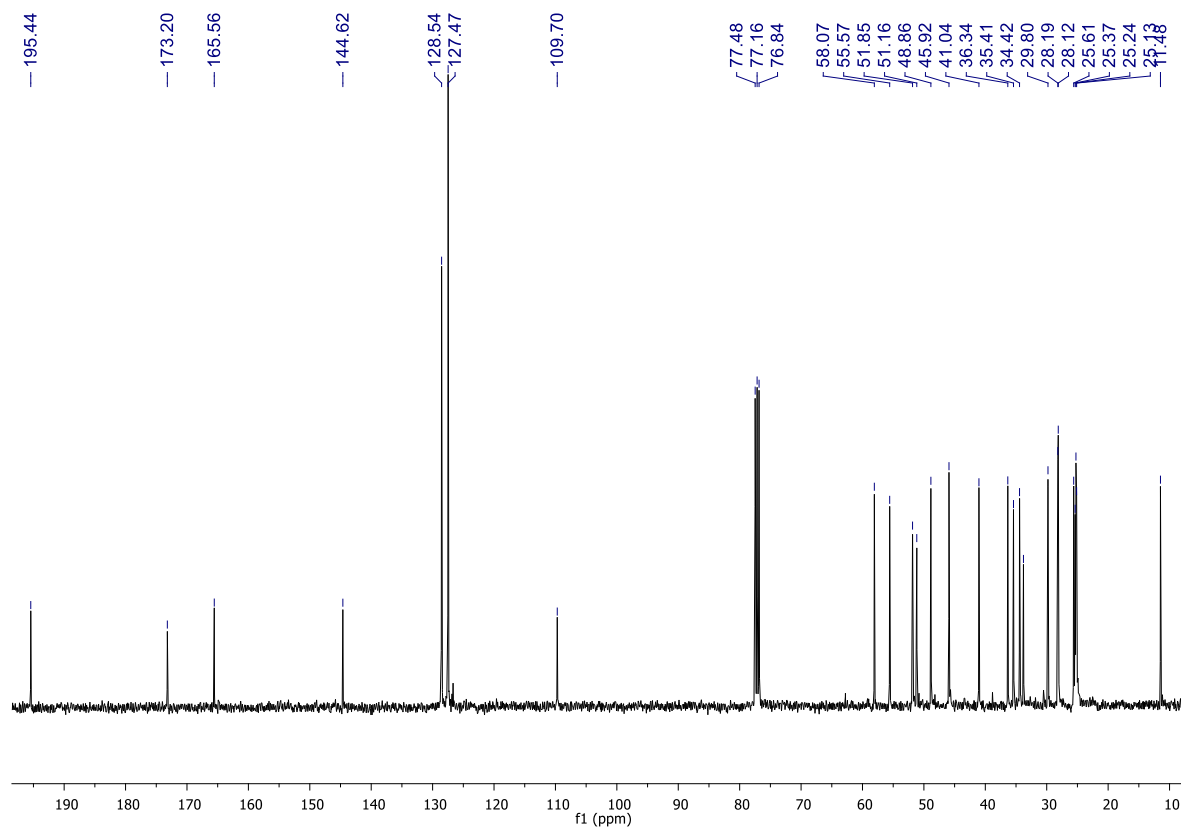
FIGURE 198: 100 MHz ^{13}C NMR spectra in CDCl$_3$ of compound **149**.
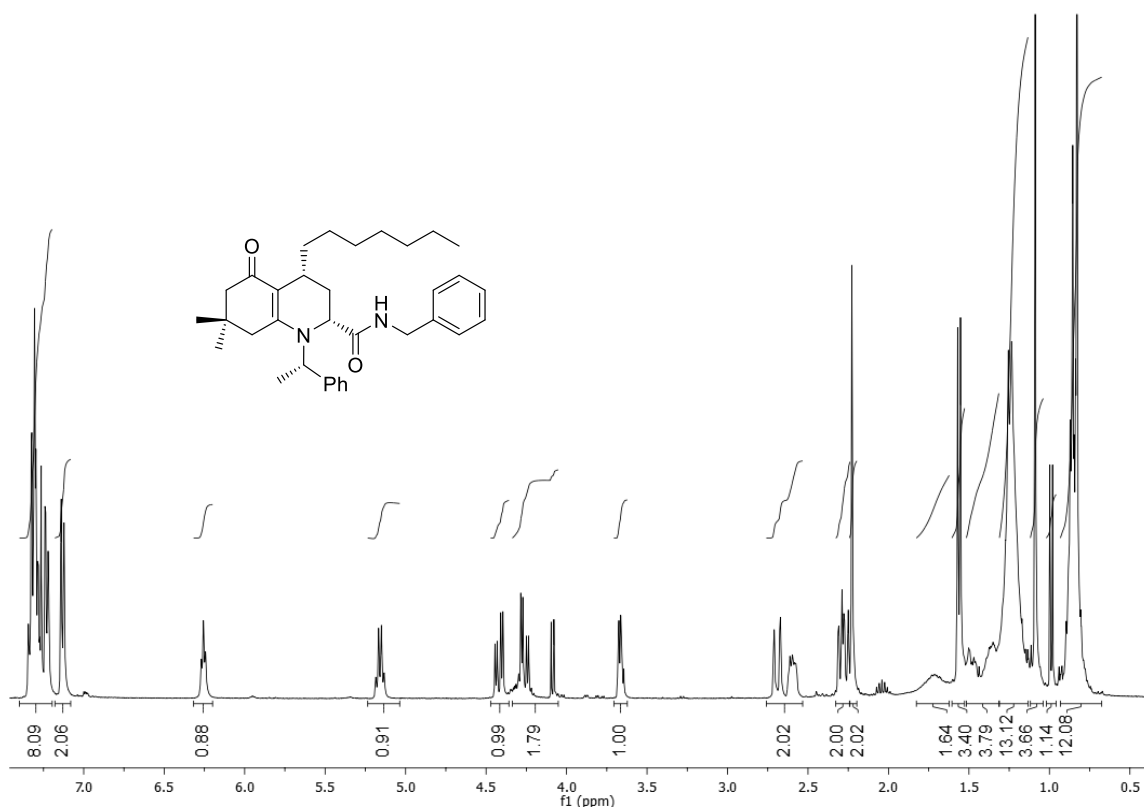
FIGURE 199: 400 MHz ^{1}H NMR spectra in CDCl$_3$ of compound **150**.
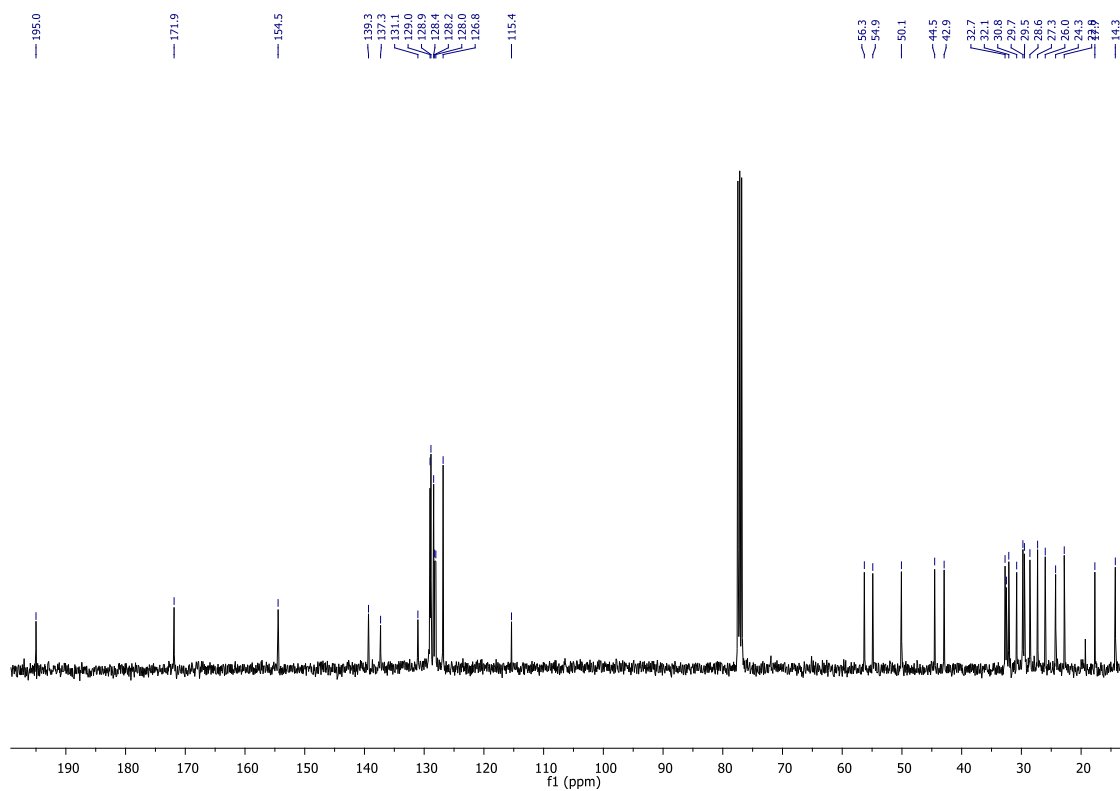
FIGURE 200: 100 MHz ^{13}C NMR spectra in CDCl$_3$ of compound **150**.
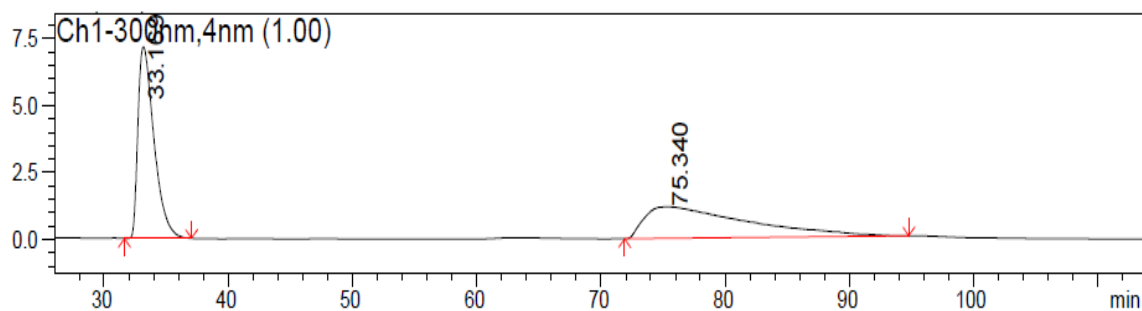
PDA Ch1 300nm 4nm

Peak#	Ret. Time	Area	Height	Area %
1	33.169	64570743	717418	48.748
2	75.340	67886796	119241	51.252
Total		132457538	836660	100.000

FIGURE 201: Chiral HPLC analysis of the racemic of compound **150**. Chiralpak AD-H (n-hexane/i-PrOH 90:10), 25°C at 1.0 ml/min, UV detection at 300 nm.
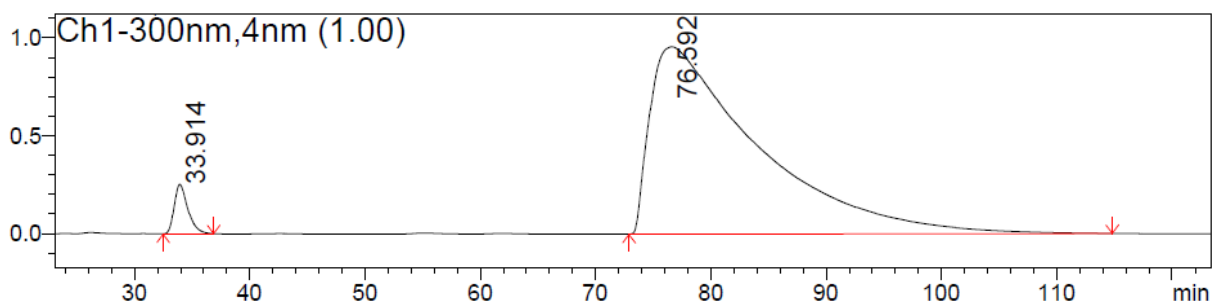
PDA Ch1 300nm 4nm

Peak#	Ret. Time	Area	Height	Area %
1	33.914	2095780	25349	3.254
2	76.592	62319177	95801	96.746
Total		64414957	121150	100.000

FIGURE 202: Chiral HPLC analysis of the mixture of diastereomers of compound **150**. Chiralpak AD-H (n-hexane/i-PrOH 90:10), 25°C at 1.0 ml/min, UV detection at 300 nm.
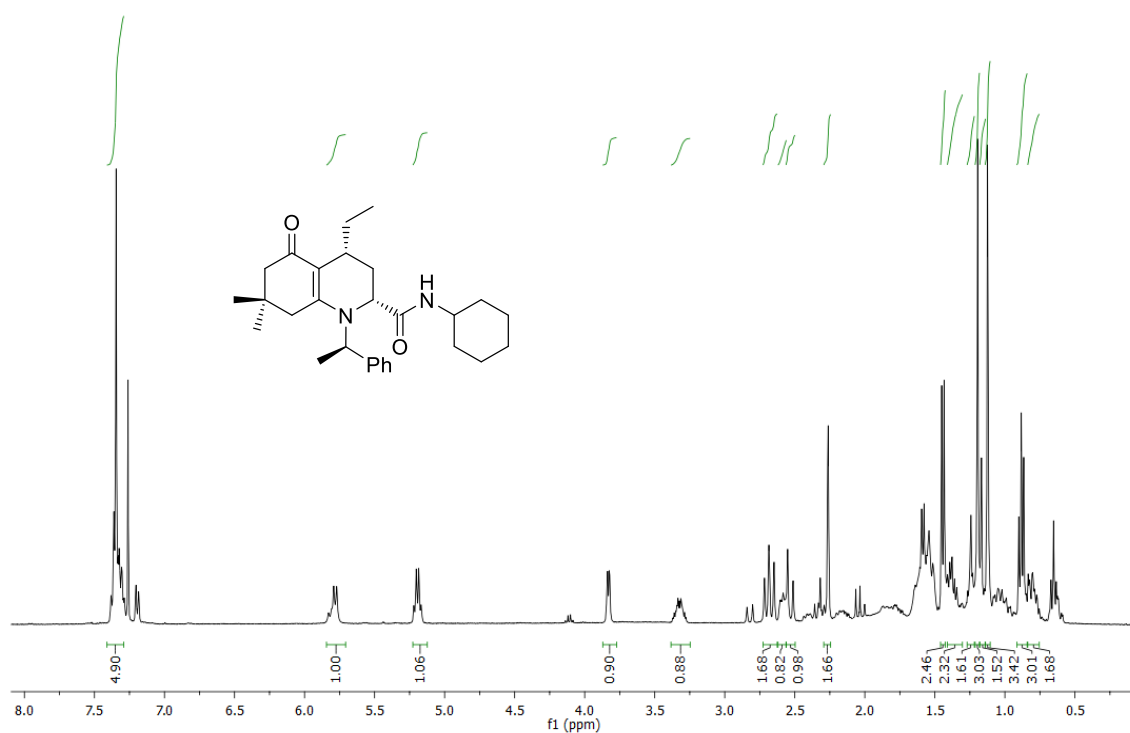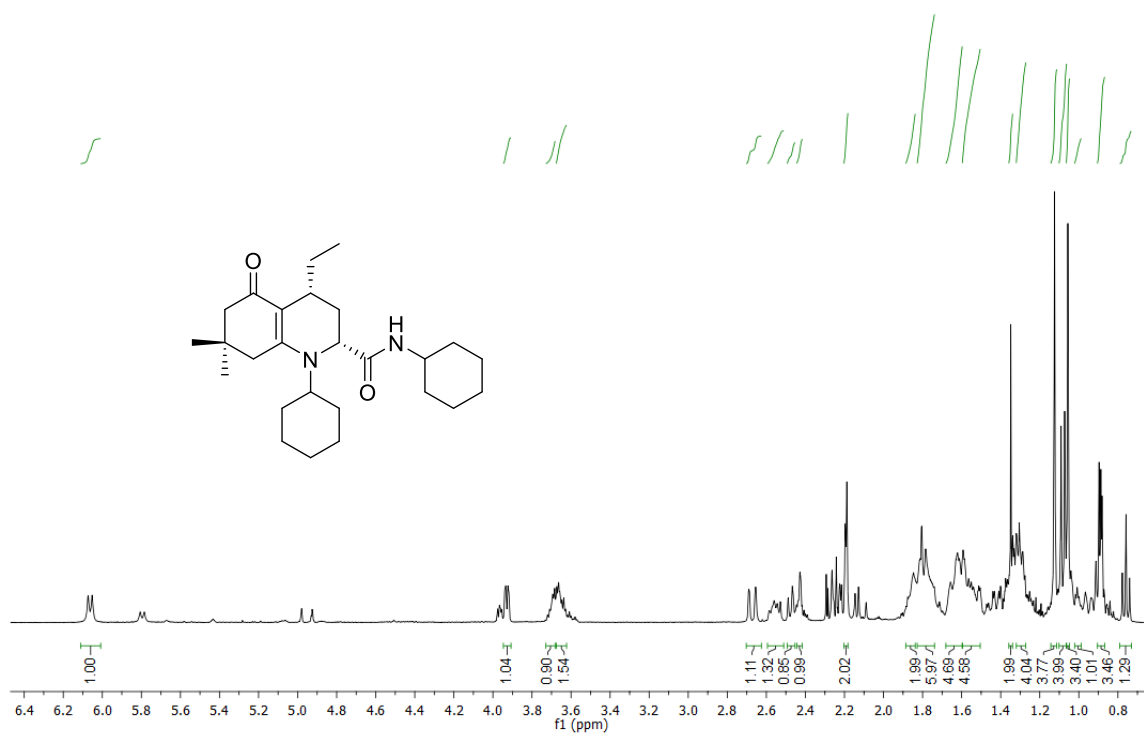
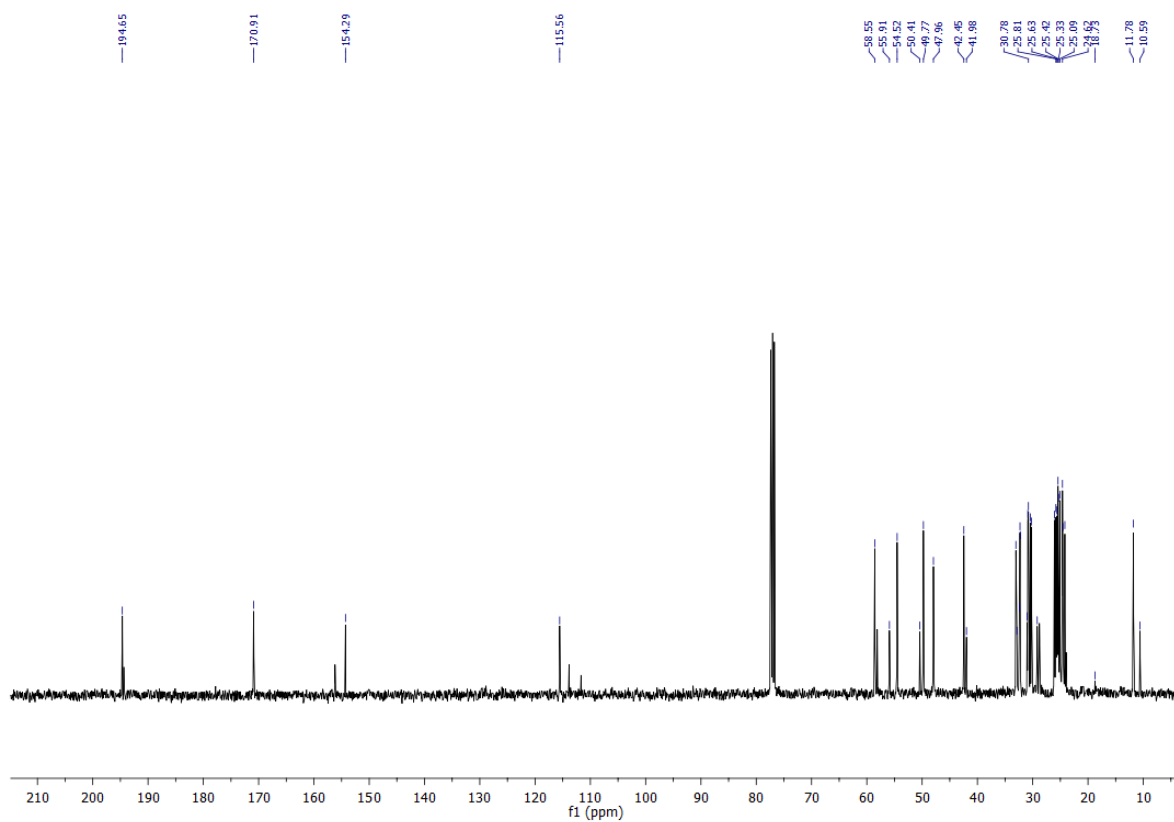FIGURE 203: 400 MHz ^{1}H NMR spectra in CDCl$_3$ of compound **151**.
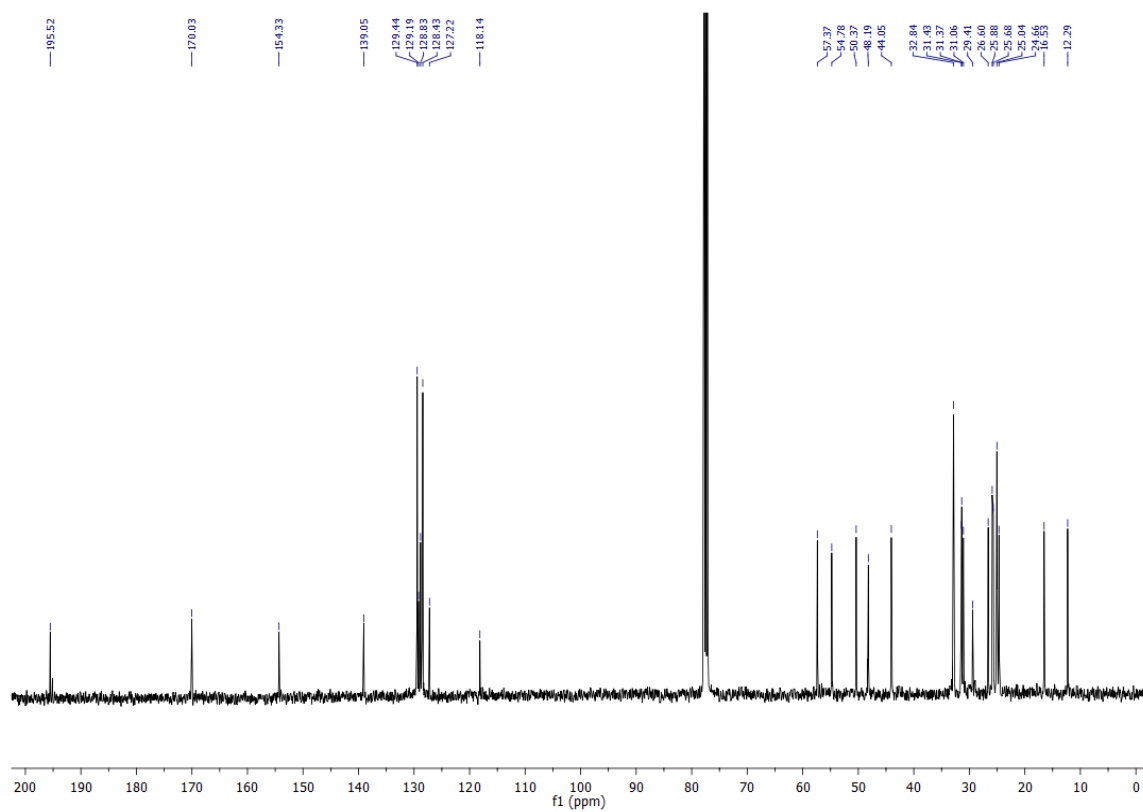
FIGURE 204: 100 MHz ^{13}C NMR spectra in CDCl$_3$ of compound **151**.

FIGURE 205: 400 MHz ^{1}H NMR spectra in CDCl$_3$ of compound **152**.
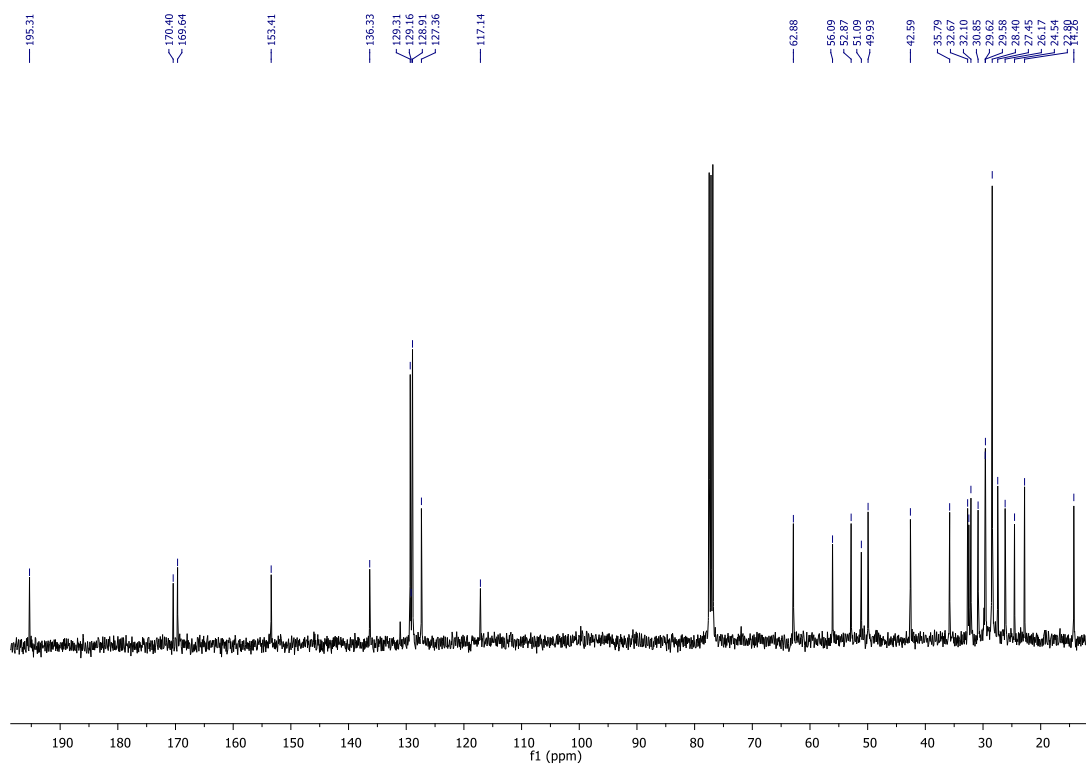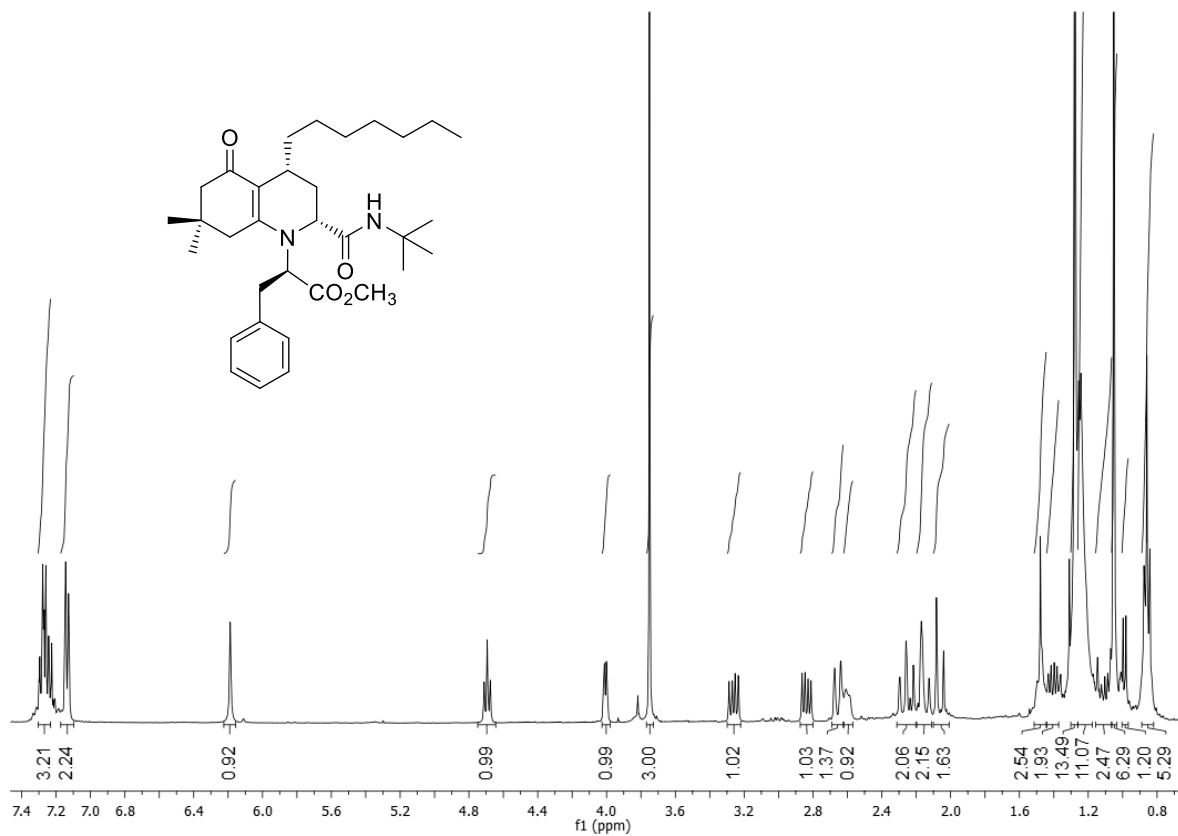
FIGURE 206: 100 MHz ^{13}C NMR spectra in CDCl$_3$ of compound **152**.
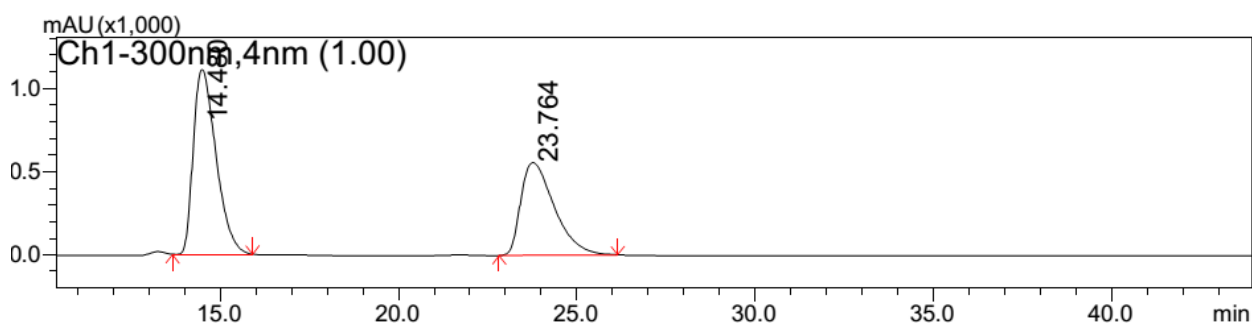
Peak#	Ret. Time	Area	Height	Area %	Height %
1	14.480	49303850	1110013	57.328	66.506
2	23.764	36699587	559037	42.672	33.494
Total		86003438	1669049	100.000	100.000

FIGURE 207: Chiral HPLC analysis of the racemic of compound **152**. Chiralpak AD-H (n-hexane/i-PrOH 95:5), 25°C at 1.0 ml/min, UV detection at 300 nm.
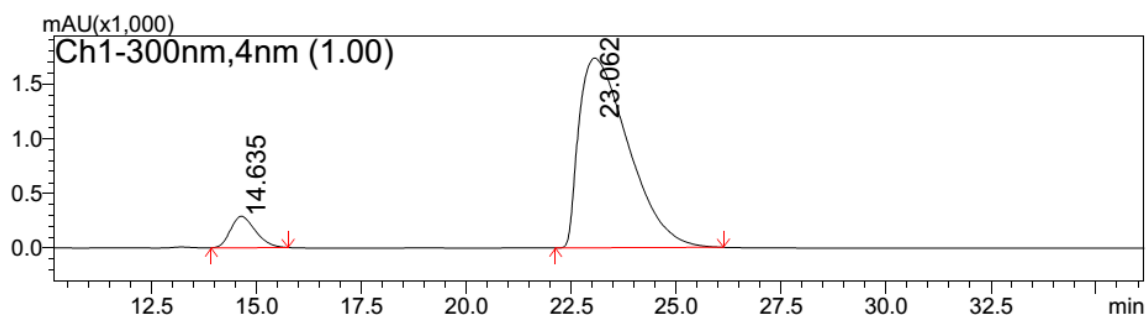
Peak#	Ret. Time	Area	Height	Area %	Height %
1	14.635	11940311	286696	7.750	14.209
2	23.062	142121644	1730991	92.250	85.791
Total		154061955	2017687	100.000	100.000

FIGURE 208: Chiral HPLC analysis of the mixture of diastereomers of compound **152**. Chiralpak AD-H (n-hexane/i-PrOH 95:5), 25°C at 1.0 ml/min, UV detection at 300 nm.
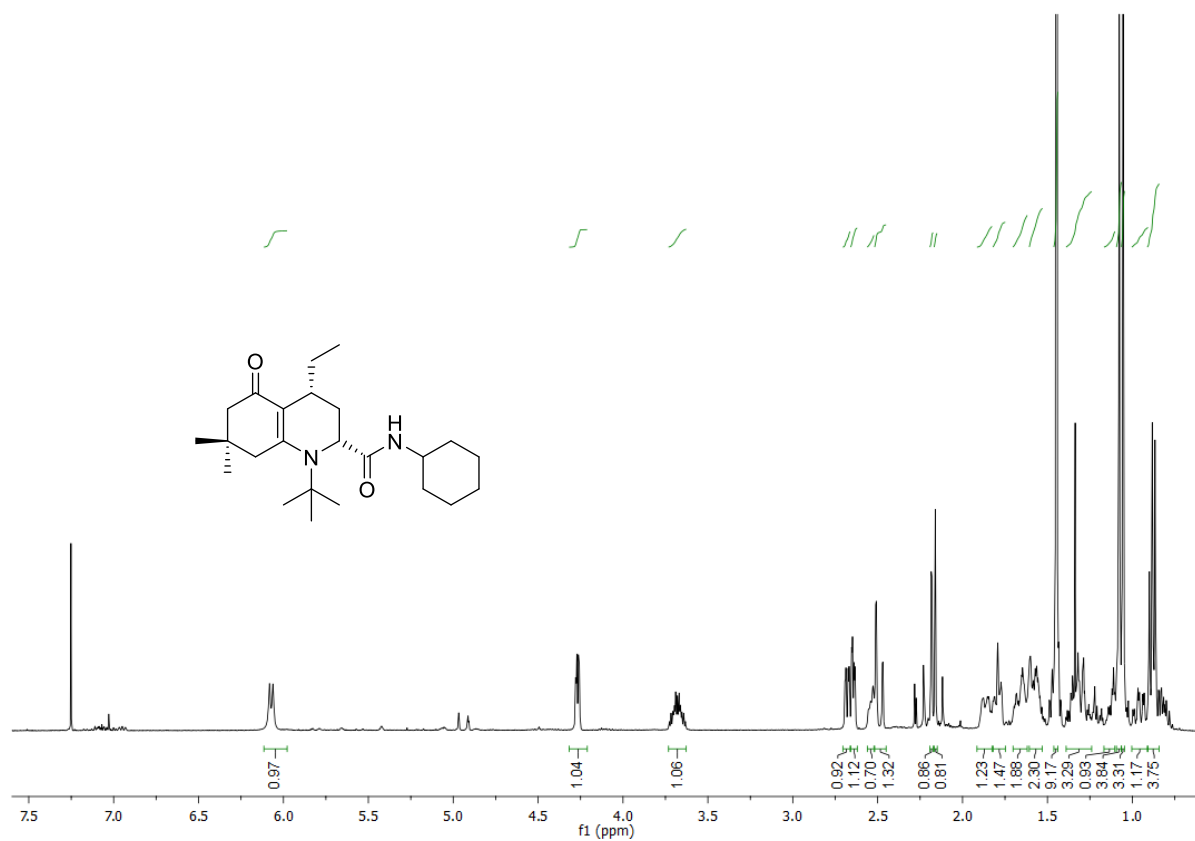
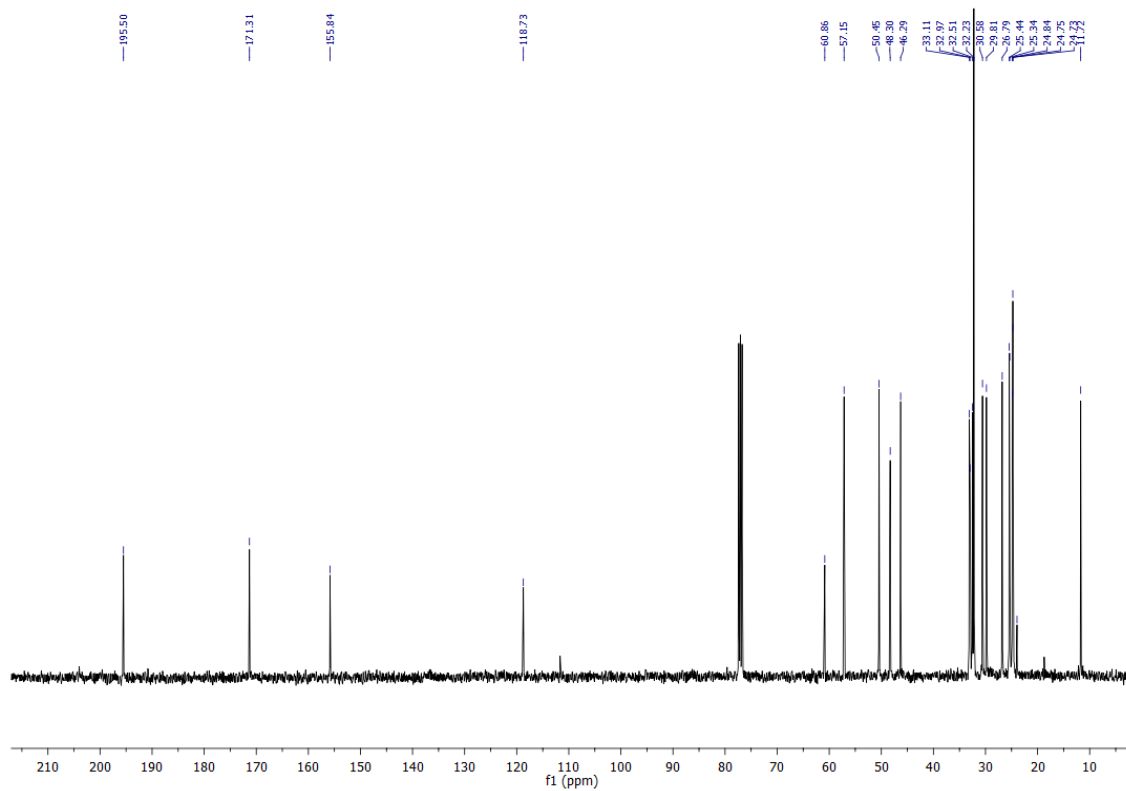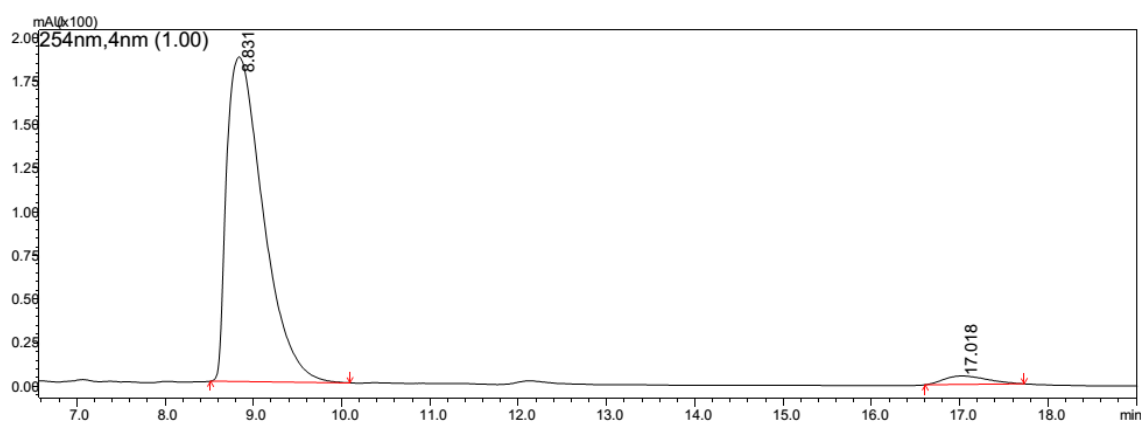FIGURE 209: 400 MHz ^{1}H NMR spectra in CDCl$_3$ of compound **153**.

FIGURE 210: 100 MHz ^{13}C NMR spectra in CDCl$_3$ of compound **153**.

PDA Ch1 300nm 4nm

Peak#	Ret. Time	Area	Height	Area %	Height %
1	5.779	11829329	276781	67.252	81.495
2	8.368	5760320	62849	32.748	18.505
Total		17589649	339630	100.000	100.000

FIGURE 211: Chiral HPLC analysis of the racemic of compound **153**. Chiralpak AD-H (n-hexane/i-PrOH 95:5), 25°C at 1.0 ml/min, UV detection at 300 nm.

PDA Ch1 300nm 4nm

Peak#	Ret. Time	Area	Height	Area %	Height %
1	5.719	78844686	1743990	100.000	100.000
Total		78844686	1743990	100.000	100.000

FIGURE 212: Chiral HPLC analysis of the mixture of diastereomers of compound **153**. Chiralpak AD-H (n-hexane/i-PrOH 95:5), 25°C at 1.0 ml/min, UV detection at 300 nm.
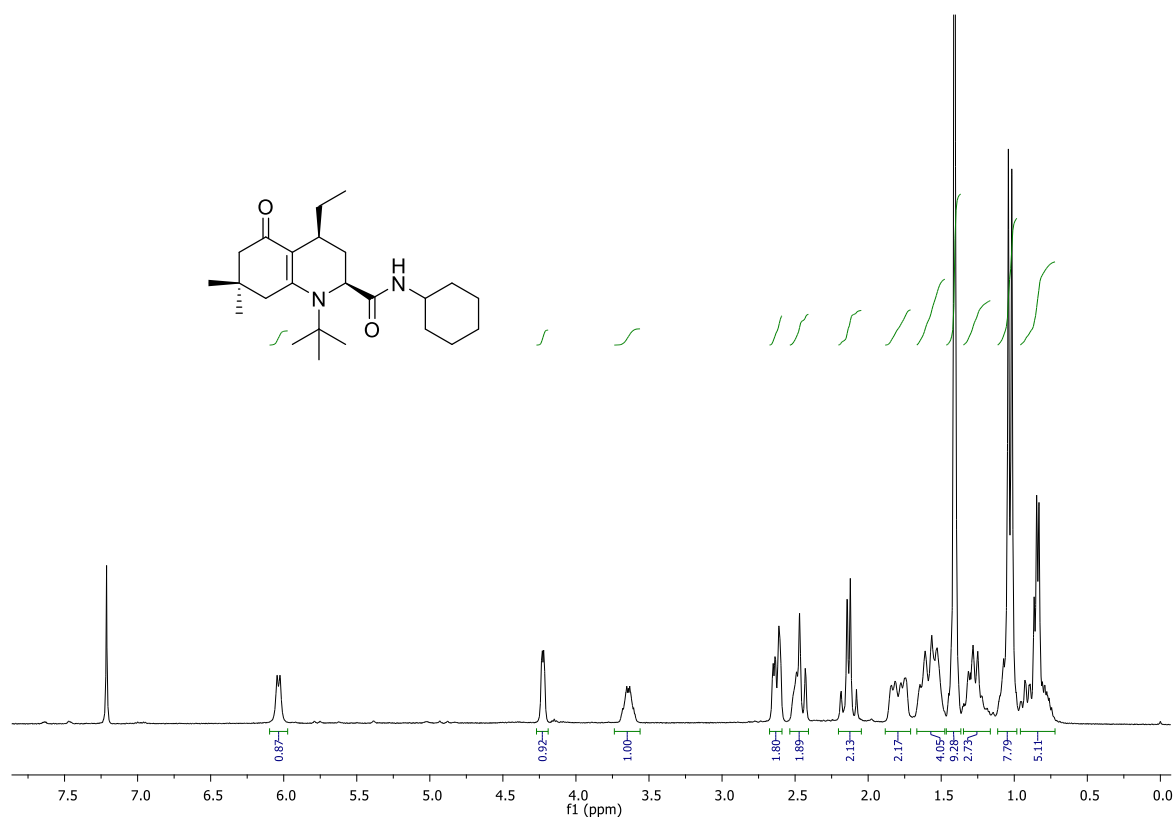
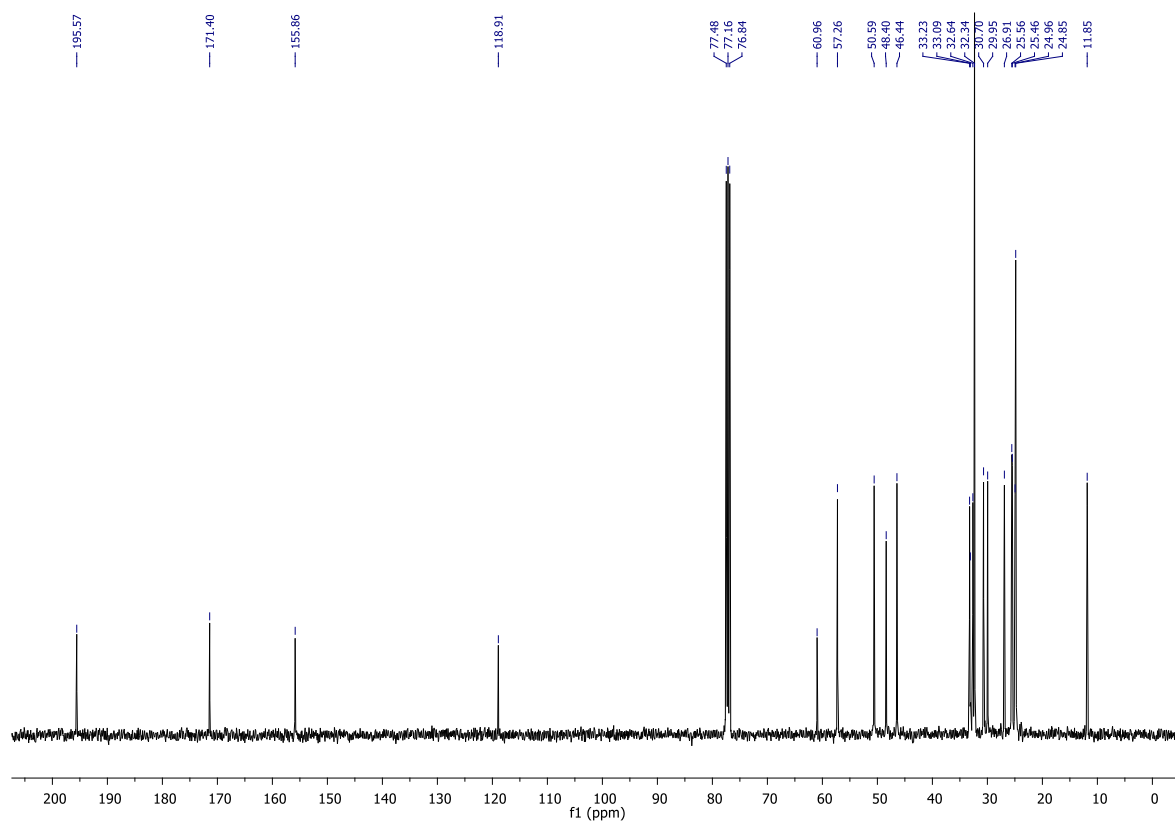FIGURE 213: 400 MHz ^{1}H NMR spectra in CDCl$_3$ of compound **154**.

FIGURE 214: 100 MHz ^{13}C NMR spectra in CDCl$_3$ of compound **154**.
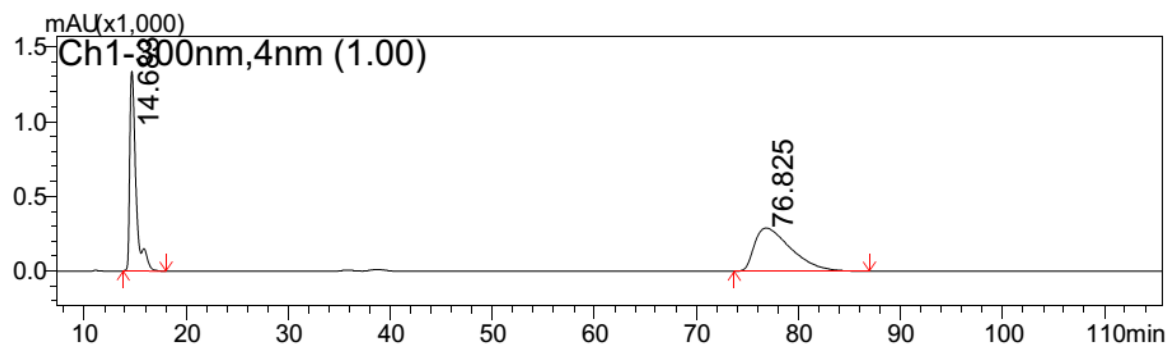
Peak#	Ret. Time	Area	Height	Area %	Height %
1	14.683	56876558	1335259	44.273	82.249
2	76.825	71590958	288184	55.727	17.751
Total		128467516	1623443	100.000	100.000

FIGURE 215: Chiral HPLC analysis of the racemic of compound **154**. Chiralpak AD-H, n-hexane/i-PrOH 95:5, 25°C at 1.0 ml/min, UV detection at 300 nm.

Peak#	Ret. Time	Area	Height	Area %	Height %
1	14.671	27378842	760913	100.000	100.000
Total		27378842	760913	100.000	100.000

FIGURE 216: Chiral HPLC analysis of the mixture of diastereomers of compound **154**. Chiralpak AD-H (n-hexane/i-PrOH 95:5), 25°C at 1.0 ml/min, UV detection at 300 nm.

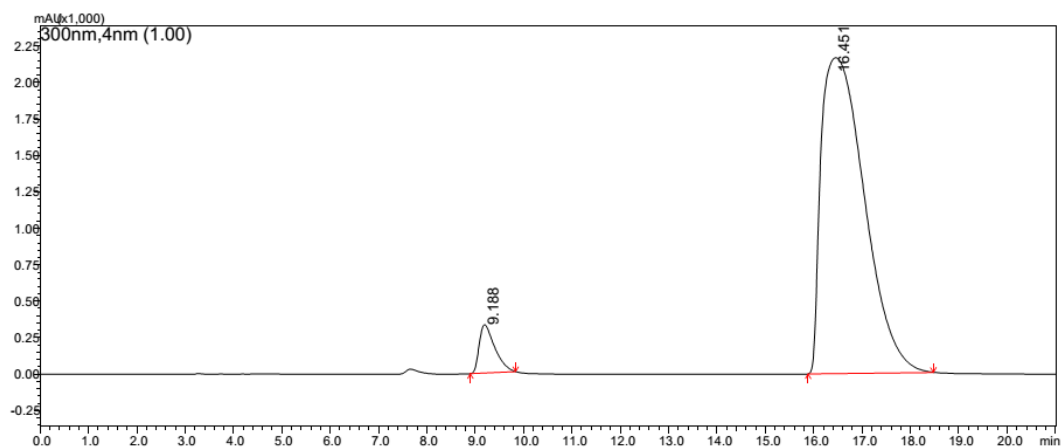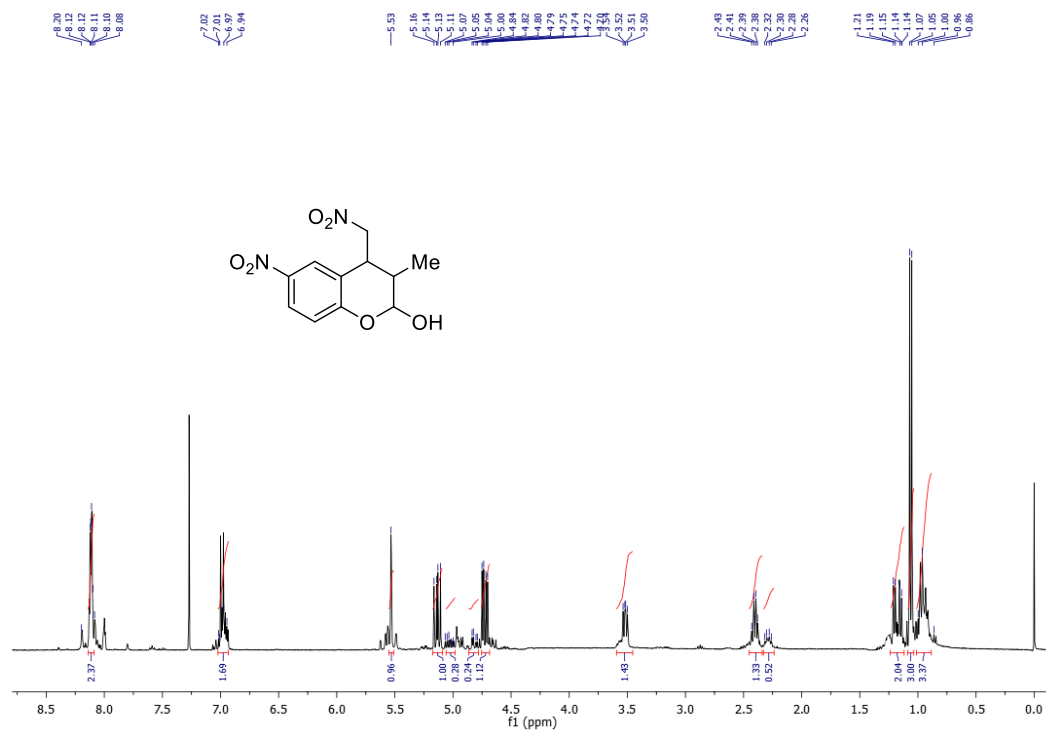FIGURE 217: 400 MHz ^{1}H NMR spectra in CDCl$_3$ of compound **155**.

FIGURE 218: 100 MHz ^{13}C NMR spectra in CDCl$_3$ of compound **155**.
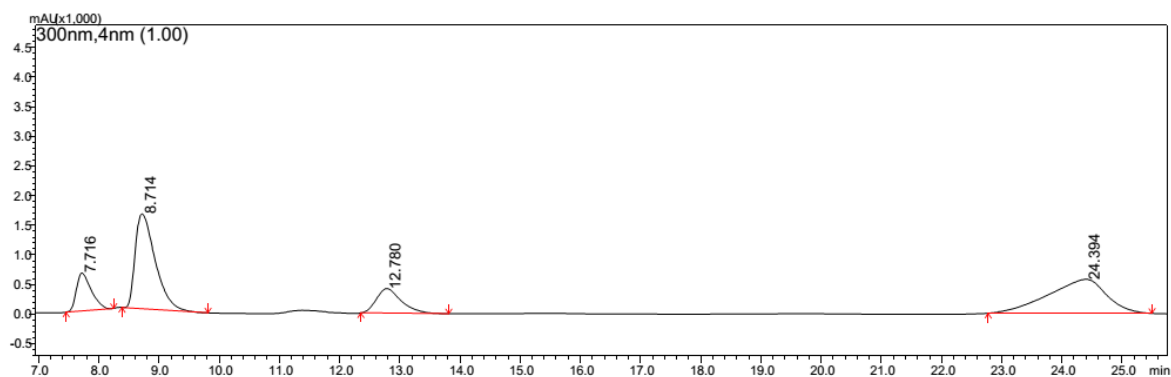
PDA Ch1 300nm 4nm

Peak#	Ret. Time	Area	Height	Area %	Height %
1	7.716	10914310	639213	11.092	19.821
2	8.714	37019109	1599663	37.622	49.602
3	12.780	11932123	413288	12.126	12.815
4	24.394	38532006	572820	39.160	17.762
Total		98397549	3224984	100.000	100.000

FIGURE 219: Chiral HPLC analysis of the racemic of compound **155**. Chiralpak AD-H (n-hexane/i-PrOH 90:10), 25°C at 1.0 ml/min, UV detection at 300 nm.
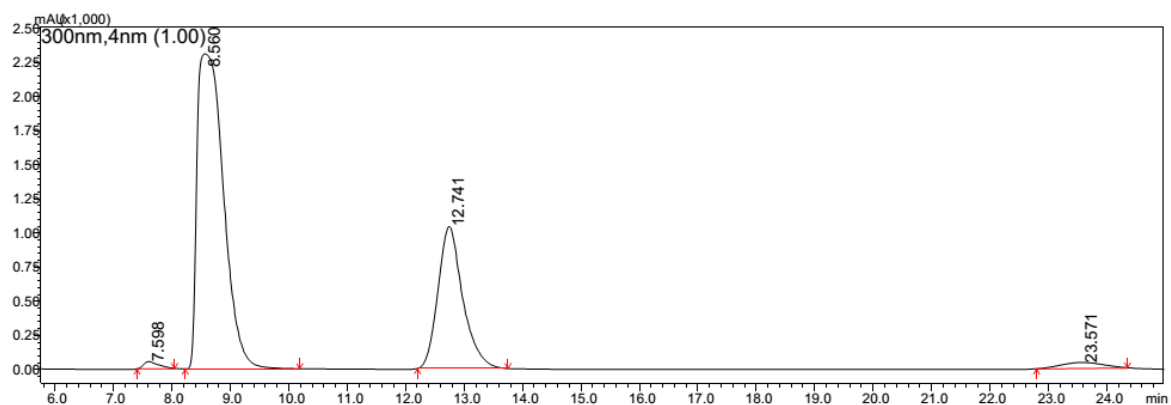
PDA Ch1 300nm 4nm

Peak#	Ret. Time	Area	Height	Area %	Height %
1	7.598	943182	52559	0.887	1.526
2	8.560	72612800	2307800	68.264	66.999
3	12.741	30632945	1040159	28.799	30.197
4	23.571	2180922	44009	2.050	1.278
Total		106369849	3444527	100.000	100.000

FIGURE 220: Chiral HPLC analysis of the mixture of diastereomers of compound **155**. Chiralpak AD-H (n-hexane/i-PrOH 90:10), 25°C at 1.0 ml/min, UV detection at 300 nm.

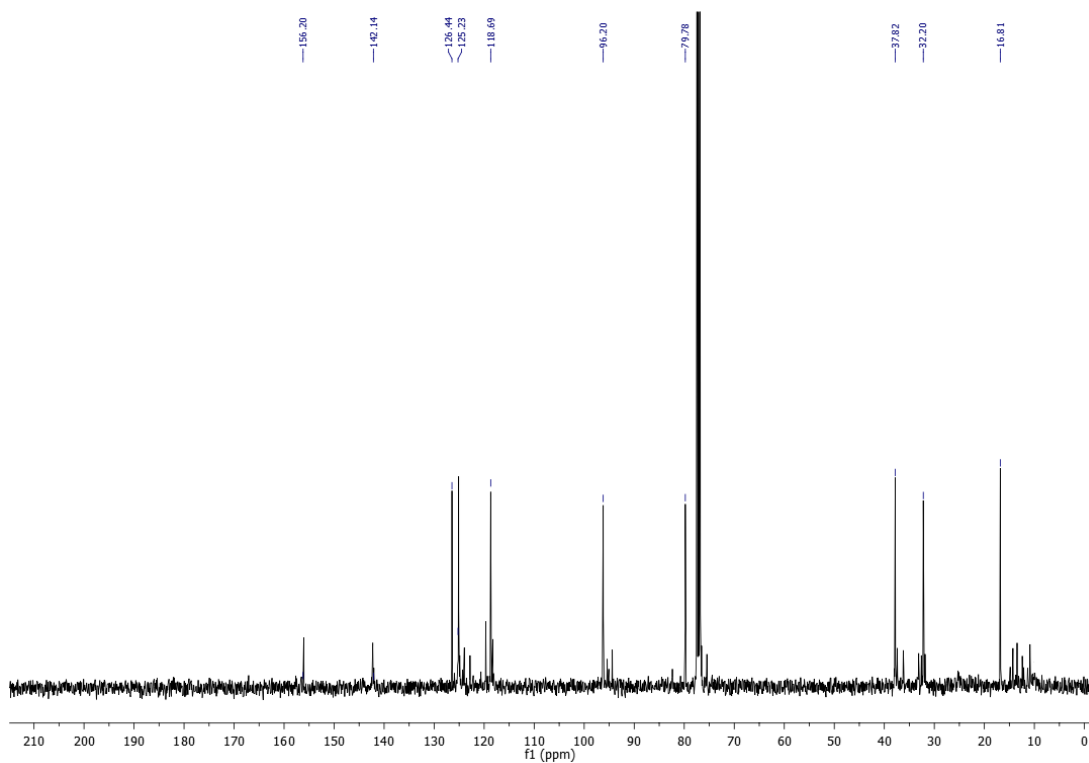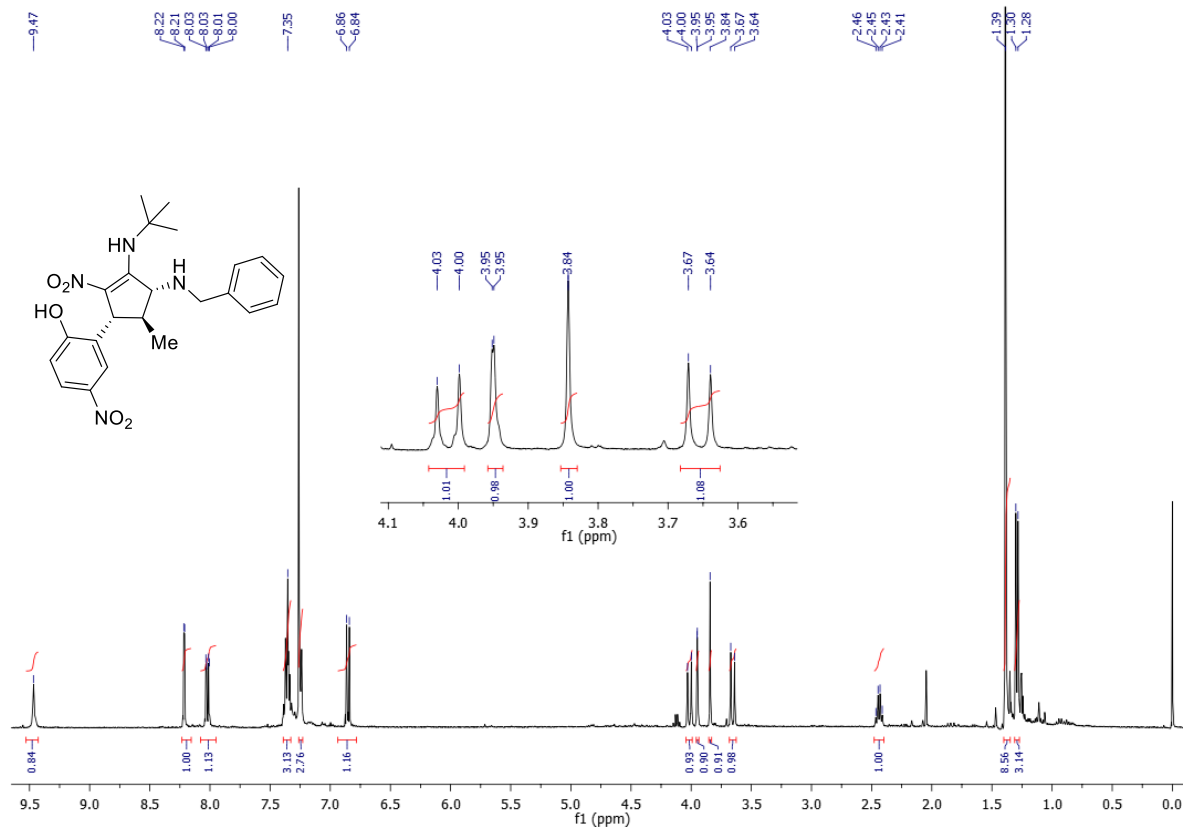FIGURE 221: 400 MHz ^{1}H NMR spectra in CDCl$_3$ of compound **156**.

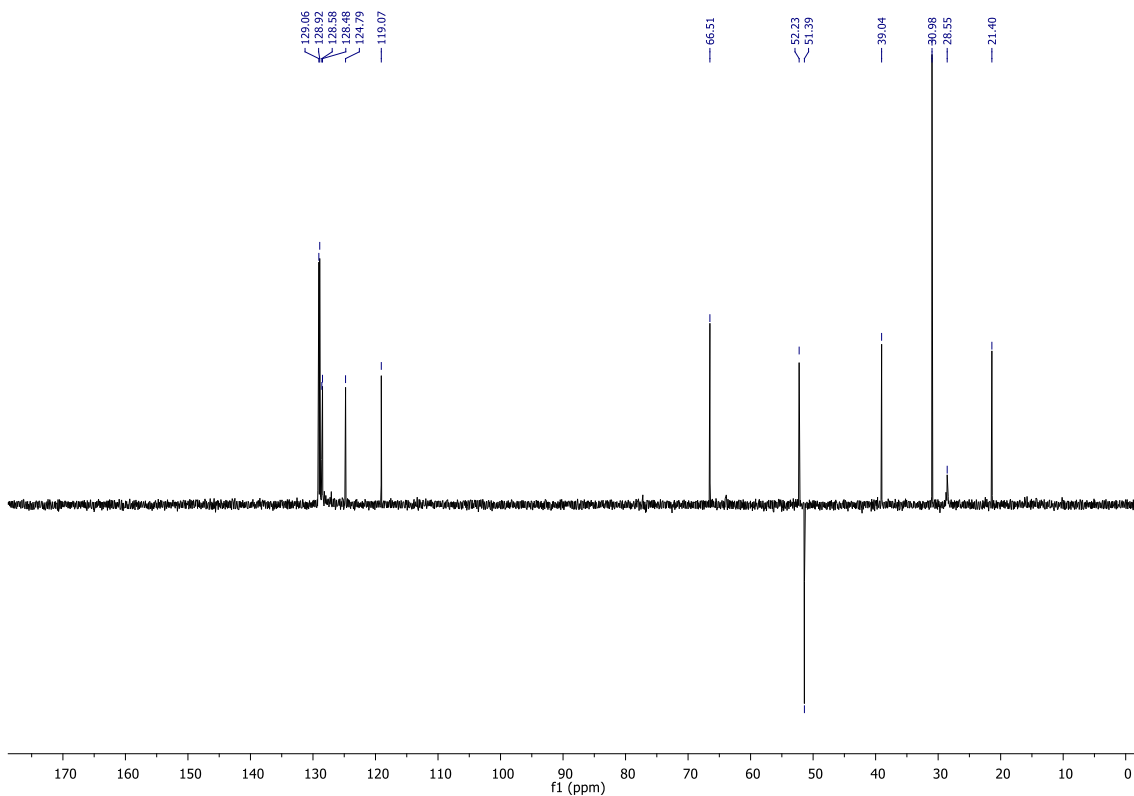FIGURE 222: 100 MHz ^{13}C NMR spectra in CDCl$_3$ of compound **156**.
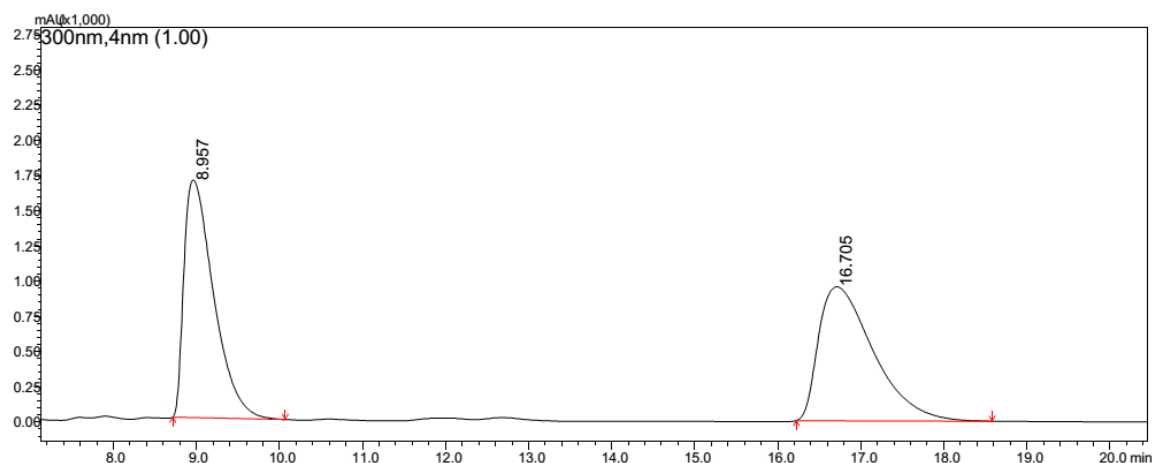
PDA Ch1 300nm 4nm

Peak#	Ret. Time	Area	Height	Area %	Height %
1	8.957	41938213	1688683	50.177	64.197
2	16.705	41642233	941778	49.823	35.803
Total		83580446	2630461	100.000	100.000

FIGURE 223: Chiral HPLC analysis of the racemic of compound **156**. Chiralpak AD-H (n-hexane/i-PrOH 90:10), 25°C at 1.0 ml/min, UV detection at 300 nm.

PDA Ch2 254nm 4nm

Peak#	Ret. Time	Area	Height	Area %	Height %
1	8.831	5342503	185967	96.996	97.443
2	17.018	165464	4879	3.004	2.557
Total		5507967	190847	100.000	100.000

FIGURE 224: Chiral HPLC analysis of the mixture of diastereomers of compound **156**. Chiralpak AD-H (n-hexane/i-PrOH 90:10), 25°C at 1.0 ml/min, UV detection at 300 nm.

FIGURE 225: 400 MHz ^{1}H NMR spectra in CDCl$_3$ of compound **157**.

FIGURE 226: 100 MHz ^{13}C NMR spectra in CDCl$_3$ of compound **157**.
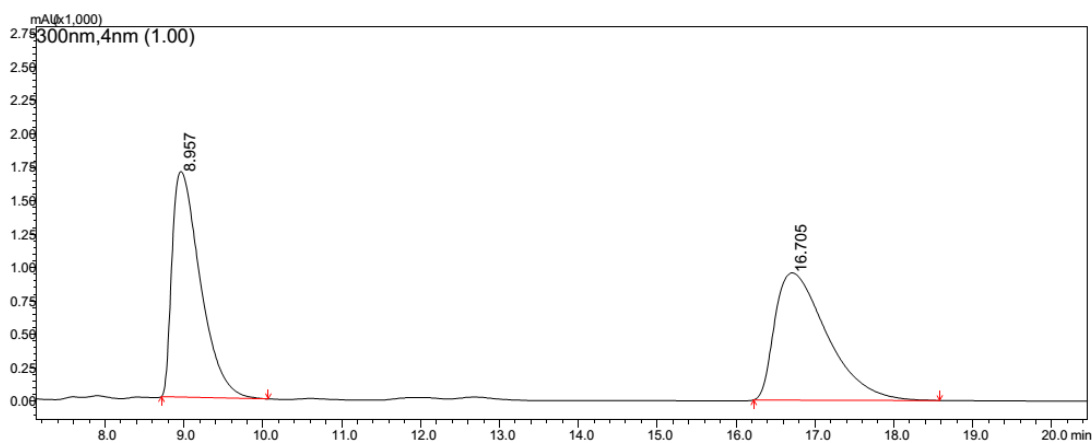
PDA Ch1 300nm 4nm

Peak#	Ret. Time	Area	Height	Area %	Height %
1	8.957	41938213	1688683	50.177	64.197
2	16.705	41642233	941778	49.823	35.803
Total		83580446	2630461	100.000	100.000

FIGURE 227: Chiral HPLC analysis of the racemic of compound **157**. Chiralpak AD-H (n-hexane/i-PrOH 90:10), 25°C at 1.0 ml/min, UV detection at 300 nm.

PeakTable

PDA Ch1 300nm 4nm

Peak#	Ret. Time	Area	Height	Area %	Height %
1	9.188	7438274	332265	5.217	13.305
2	16.451	135136557	2165102	94.783	86.695
Total		142574831	2497368	100.000	100.000

FIGURE 228: Chiral HPLC analysis of the mixture of diastereomers of compound **157**. Chiralpak AD-H (n-hexane/i-PrOH 90:10), 25°C at 1.0 ml/min, UV detection at 300 nm.

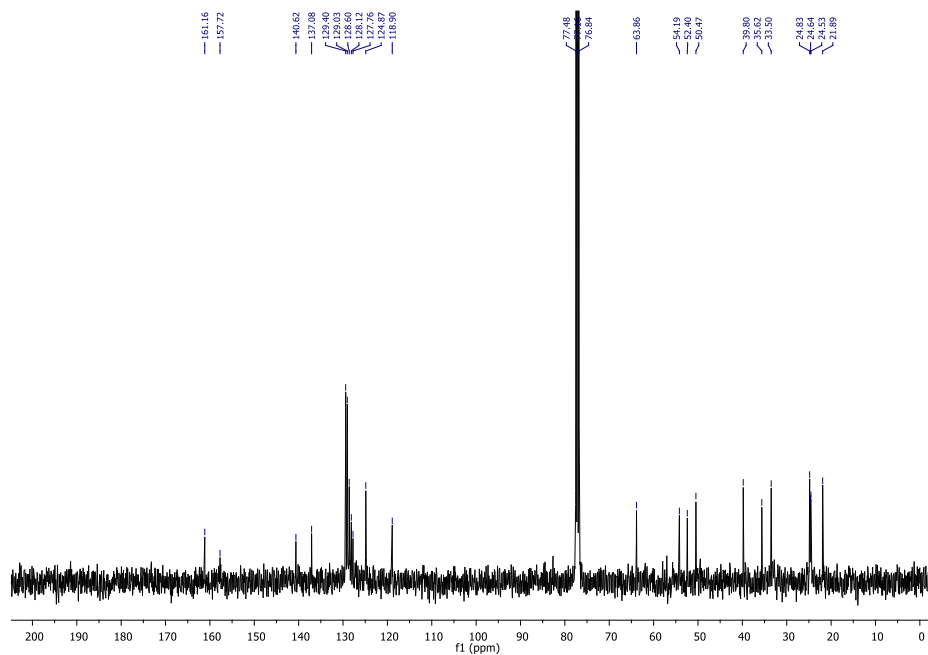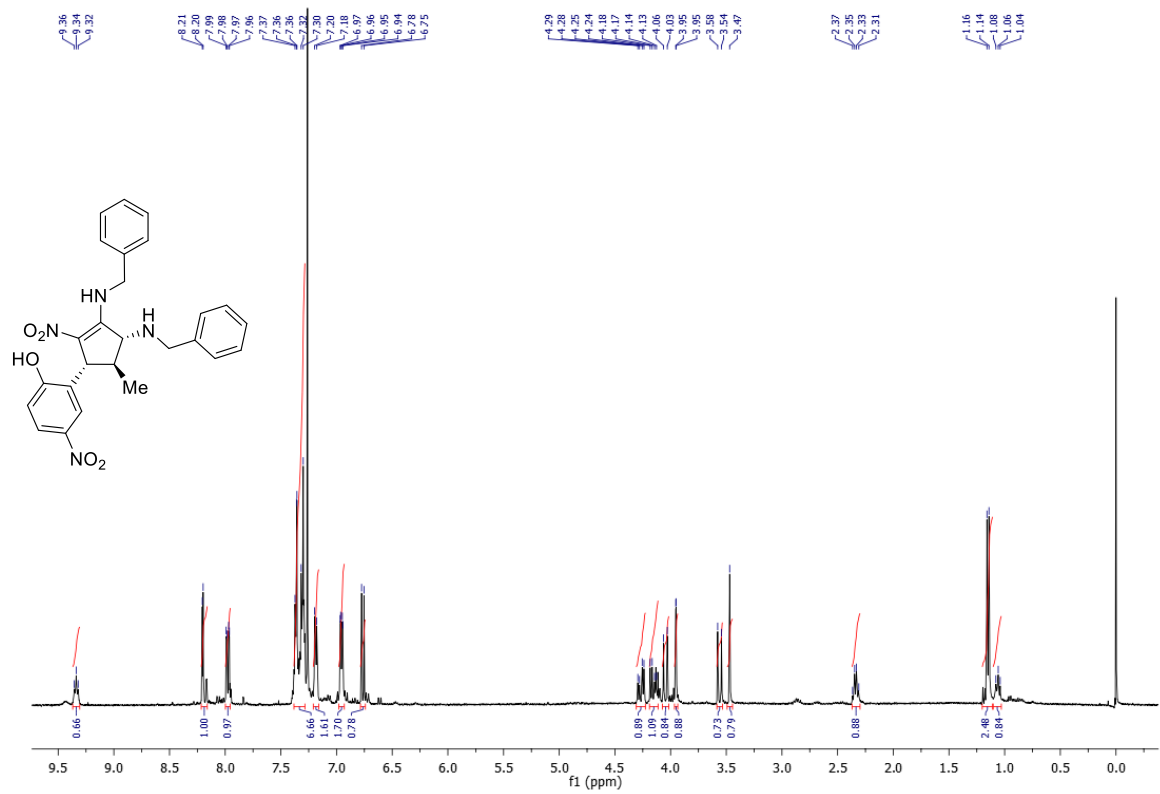FIGURE 229: 400 MHz ^{1}H NMR spectra in CDCl$_3$ of compound **158**.

FIGURE 230: 100 MHz ^{13}C NMR spectra in CDCl$_3$ of compound **158**.

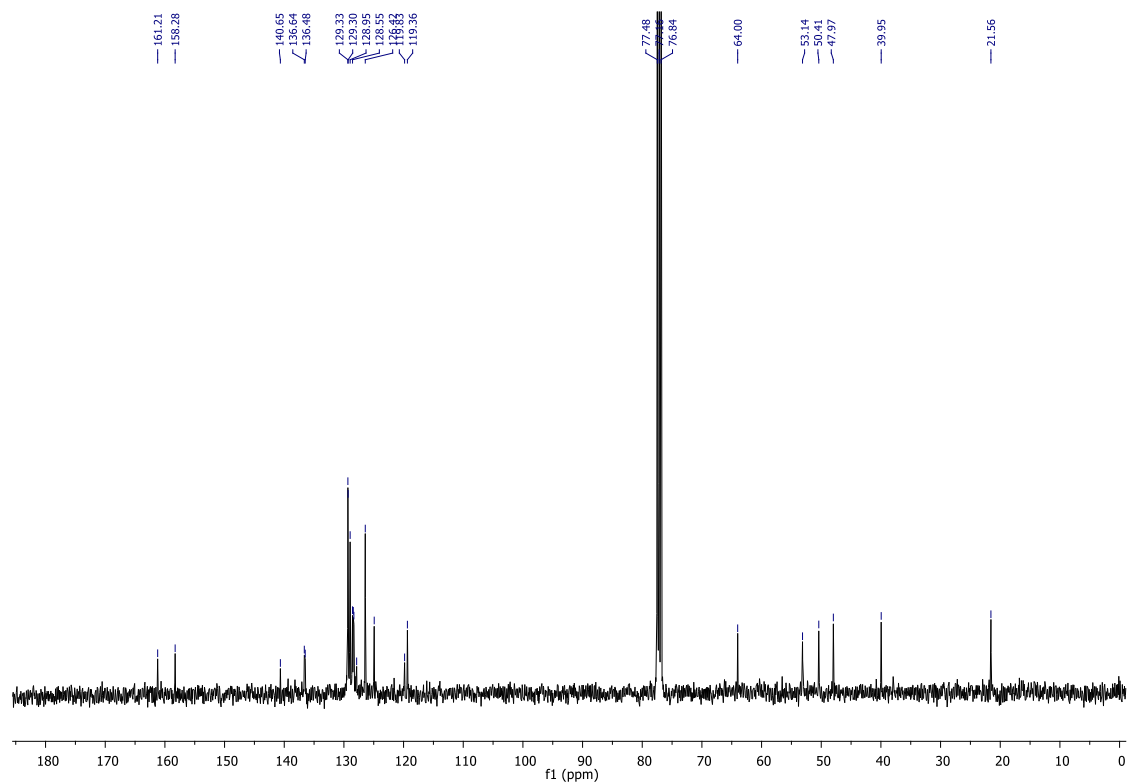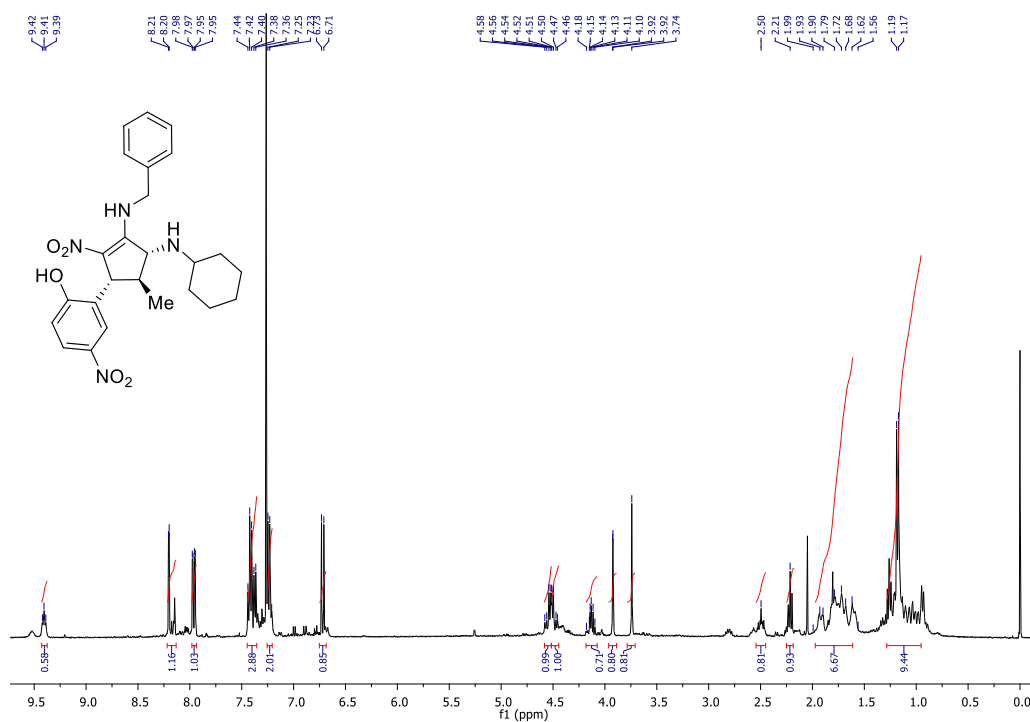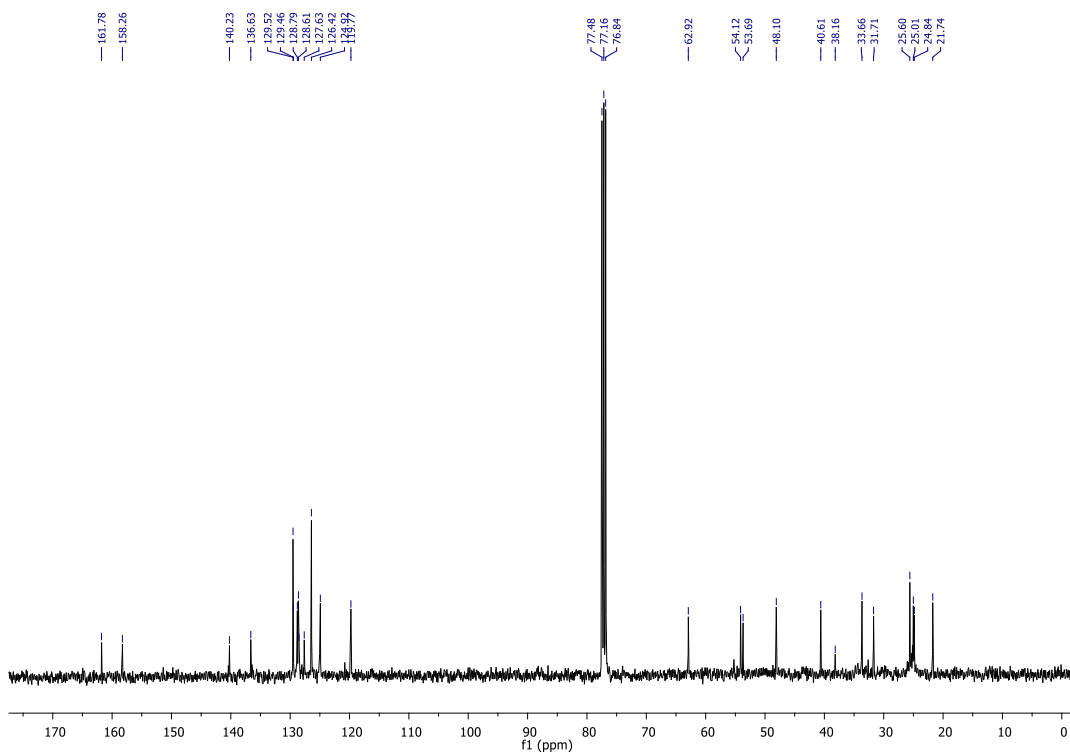FIGURE 231: 400 MHz ^{1}H NMR spectra in CDCl$_3$ of compound **160**.
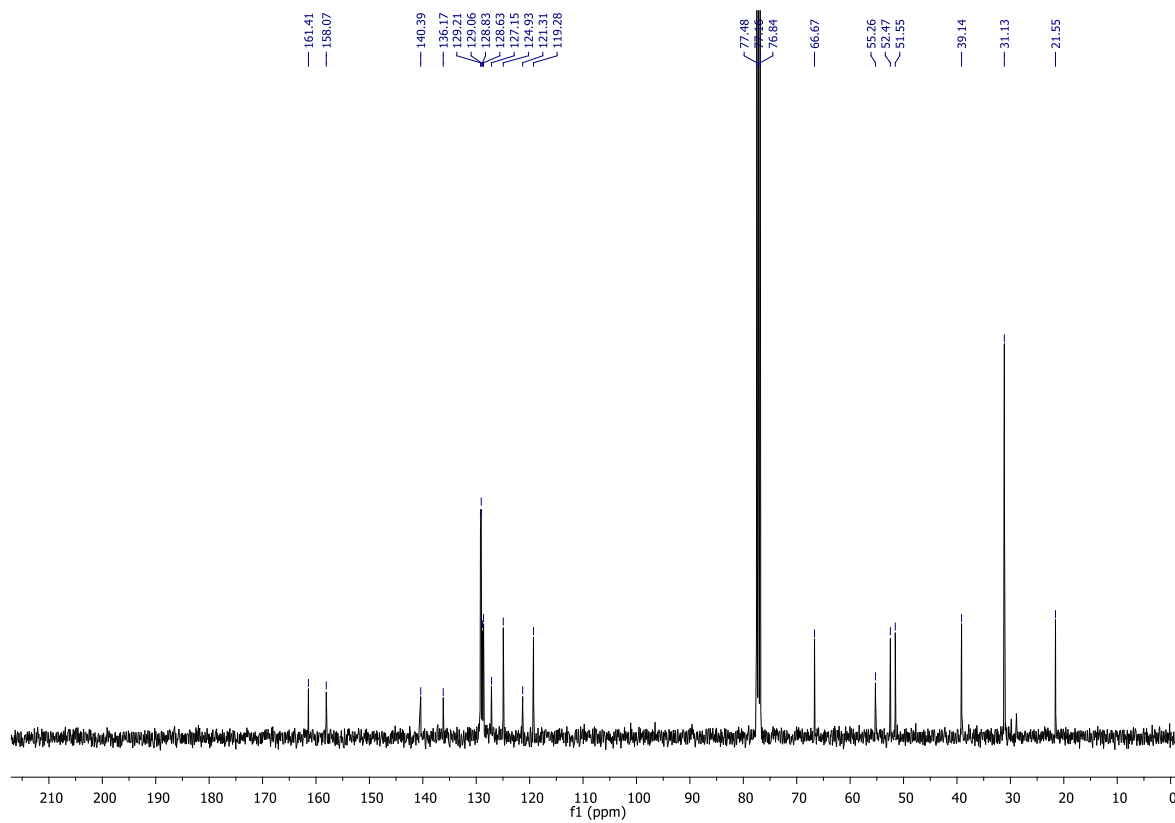
FIGURE 232: 100 MHz ^{13}C NMR spectra in CDCl$_3$ of compound **160**.

FIGURE 233: 100 MHz DEPT 135° spectra in CDCl$_3$ of compound **160**.
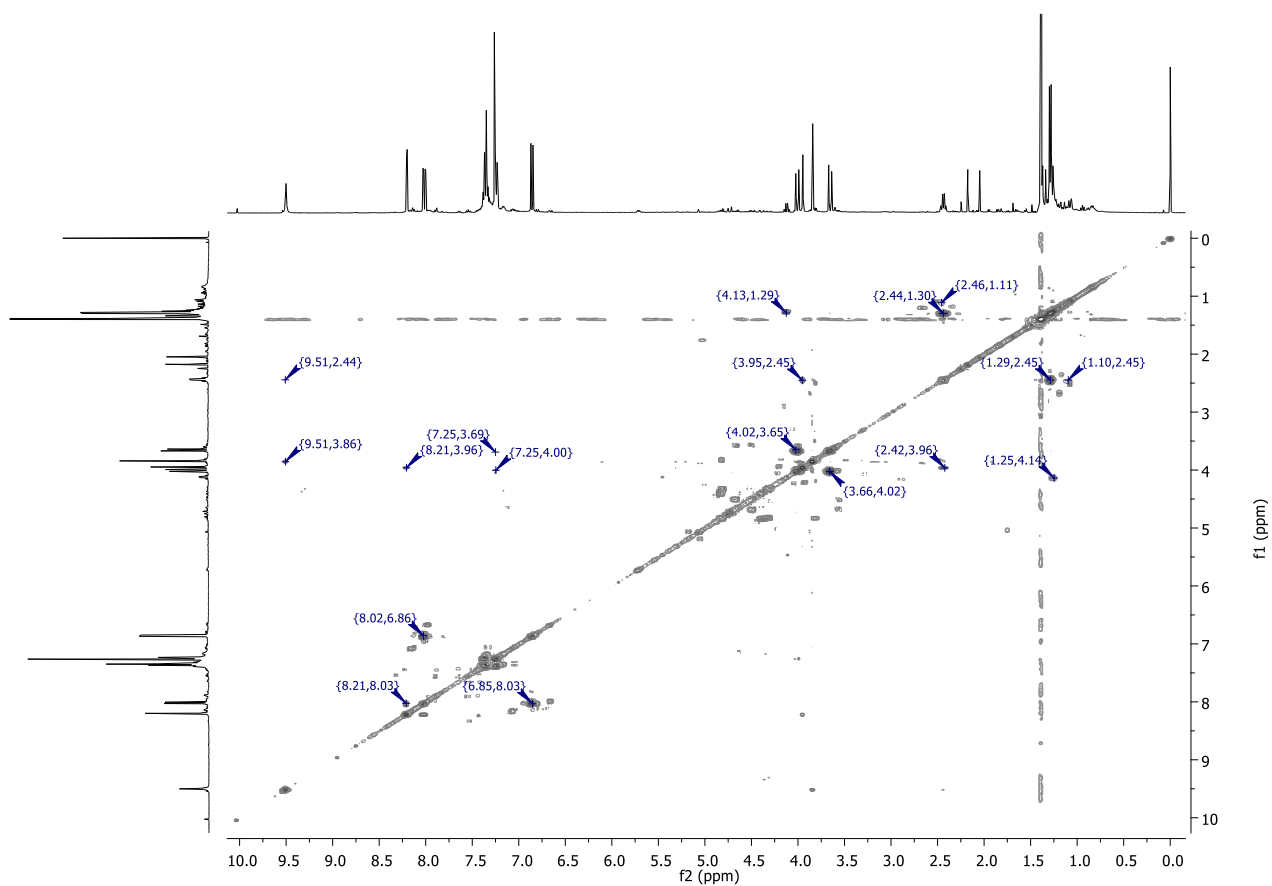
FIGURE 234: COSY spectra in CDCl$_3$ of compound **160**.

300
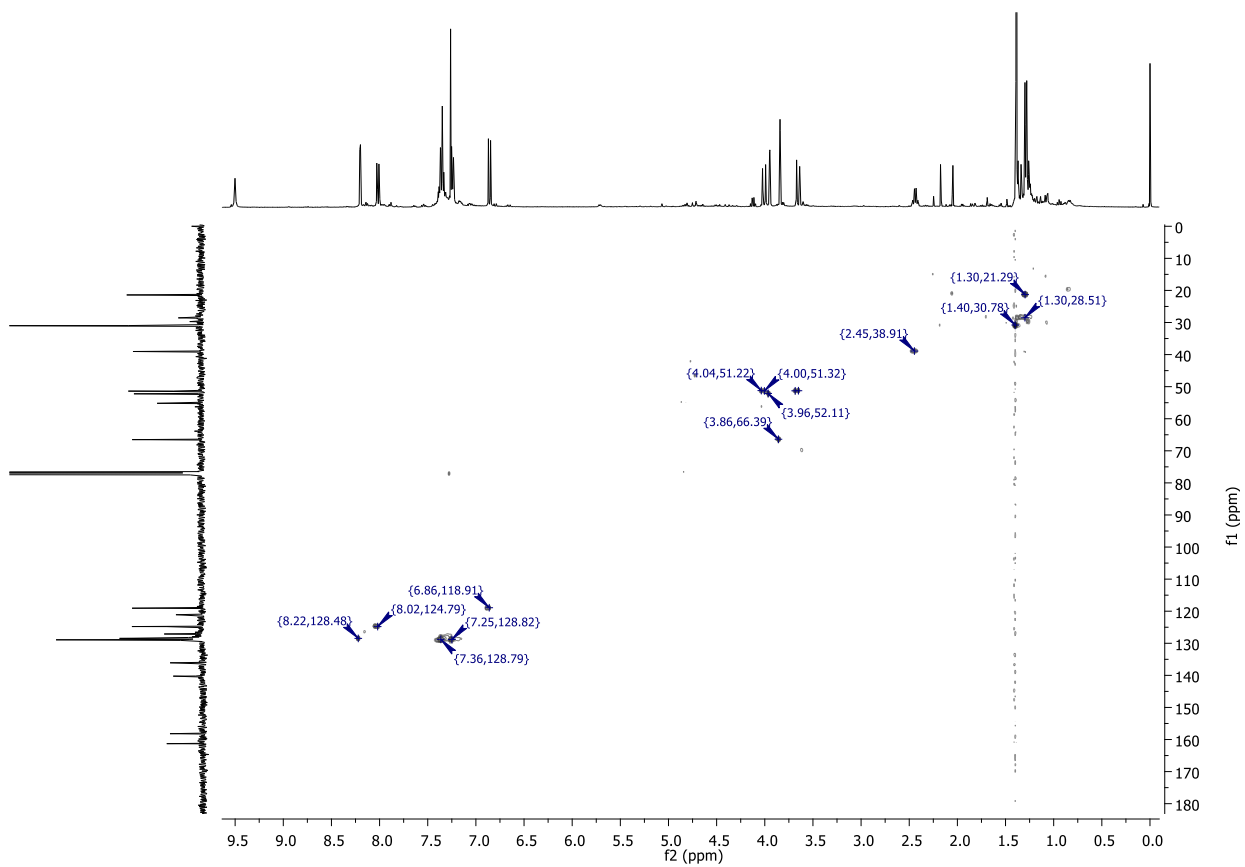
FIGURE 235: HSQC spectra in CDCl$_3$ of compound **160**.
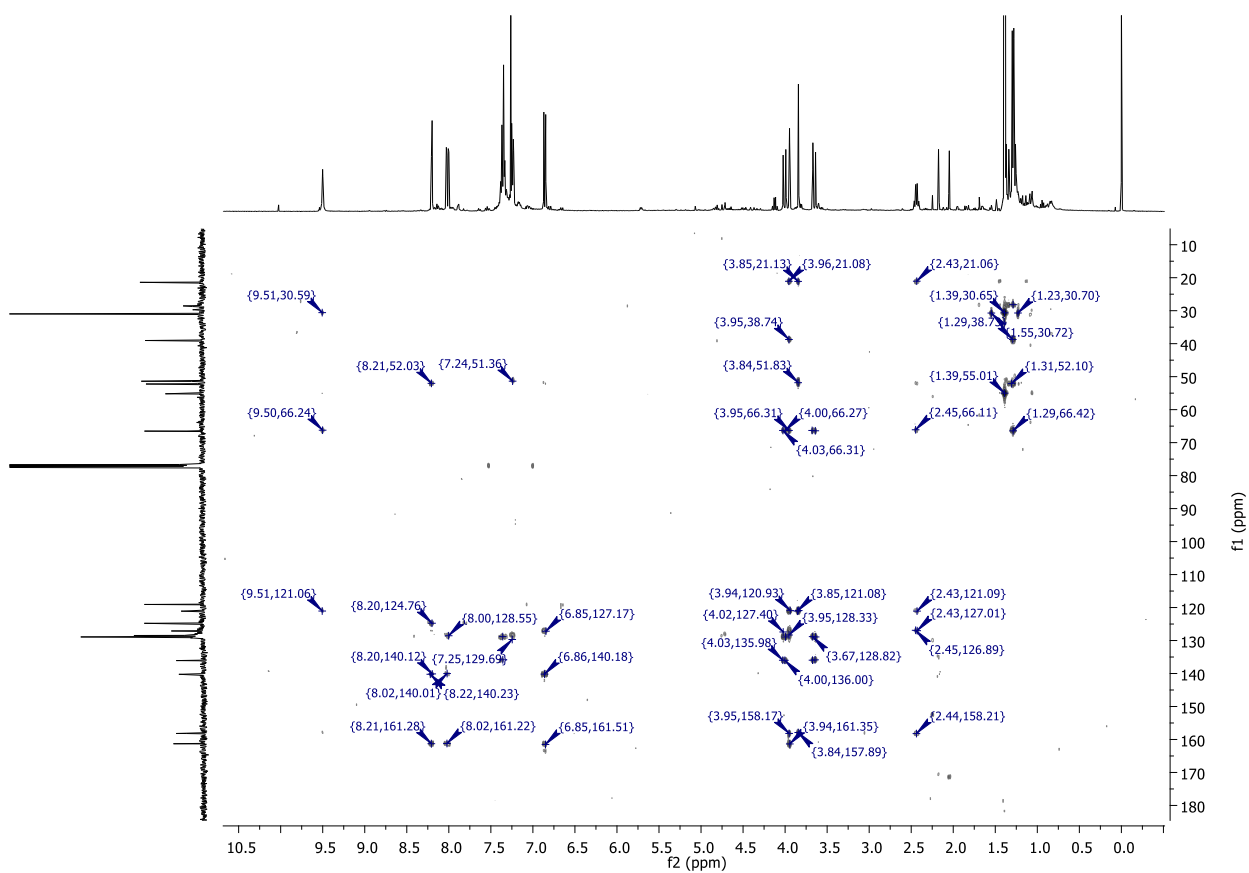
FIGURE 236: HMBC spectra in CDCl₃ of compound **160**.
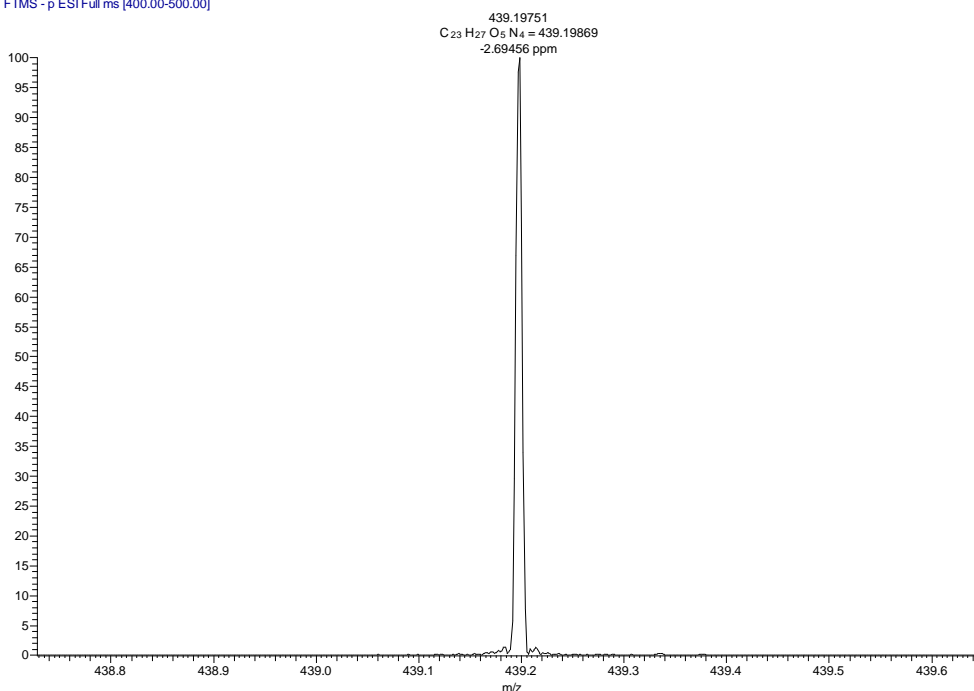
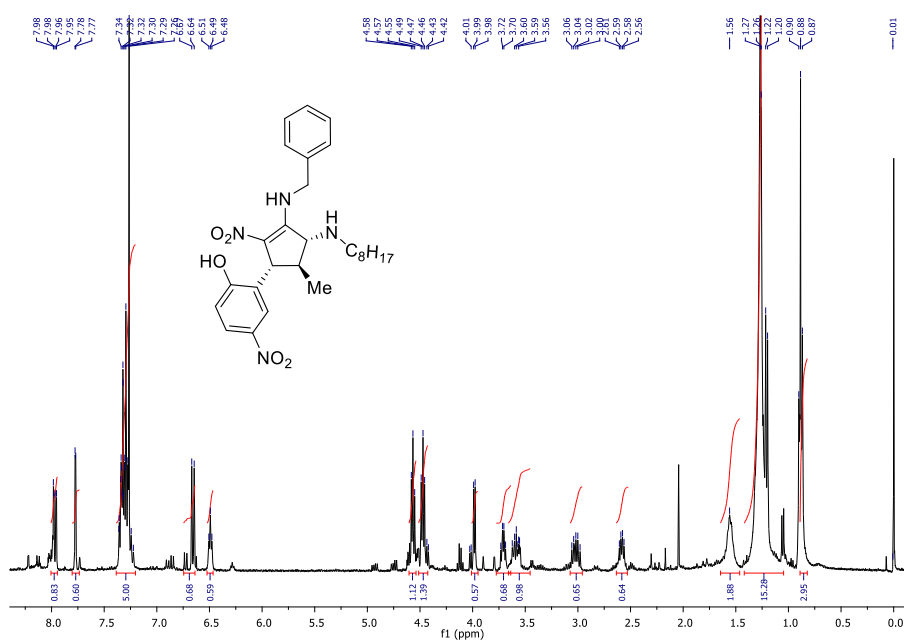FIGURE 237: HRMS (ESI-FT-ICR) m/z spectra of compound **160**.
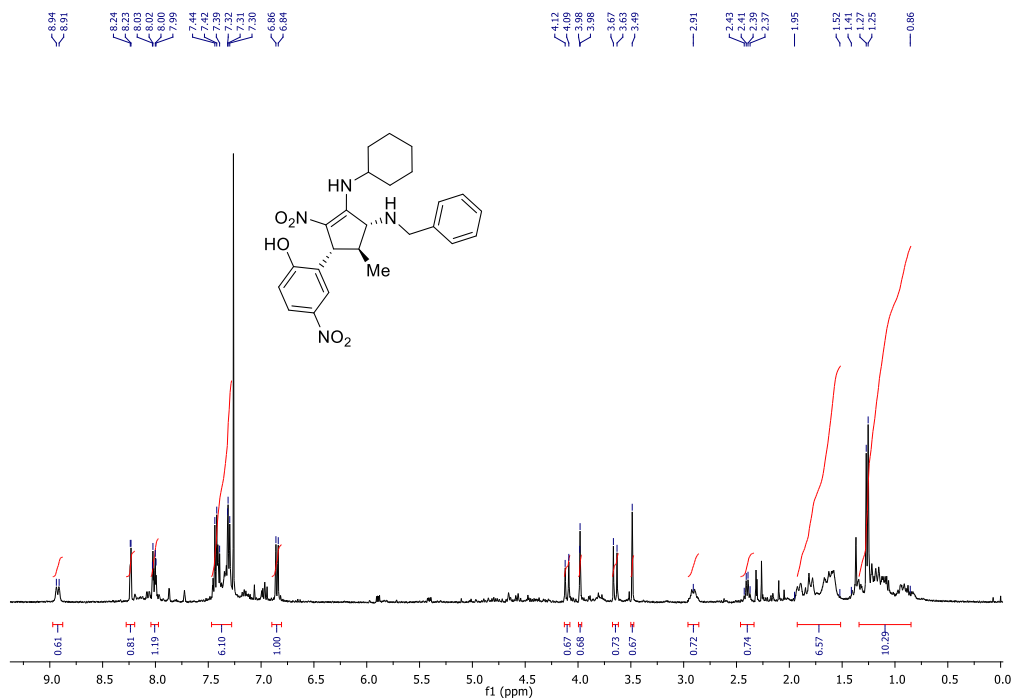
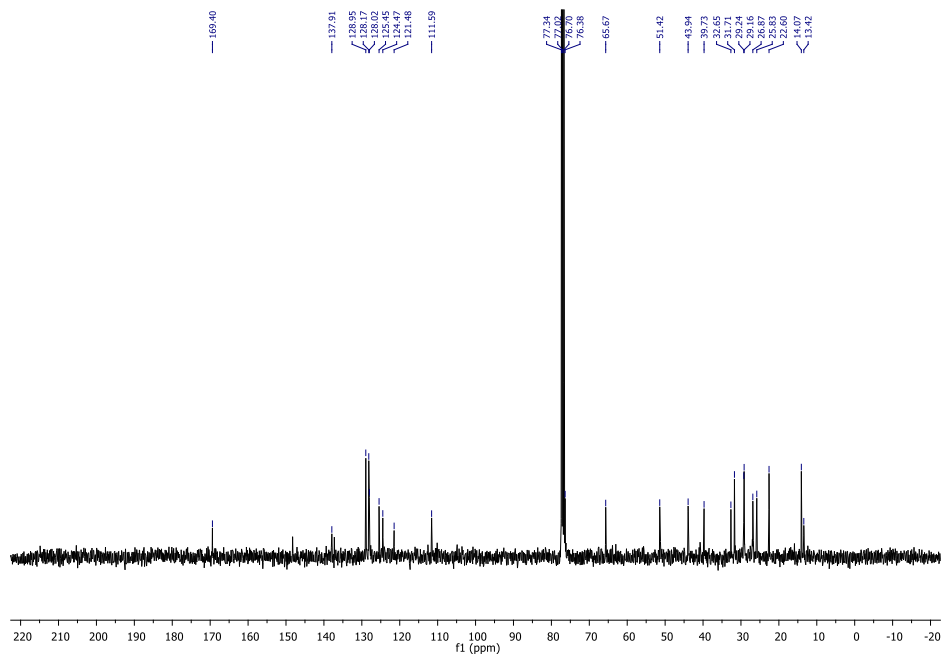FIGURE 238: 400 MHz ^{1}H NMR spectra in CDCl$_3$ of compound **161**.

FIGURE 239: 100 MHz ^{13}C NMR spectra in CDCl$_3$ of compound **161**.

FIGURE 240: 400 MHz ^{1}H NMR spectra in CDCl$_3$ of compound **162**.

FIGURE 241: 100 MHz ^{13}C NMR spectra in CDCl$_3$ of compound **162**.

473.18170
C$_{26}$ H$_{25}$ O$_5$ N$_4$ = 473.18304
-2.83504 ppm
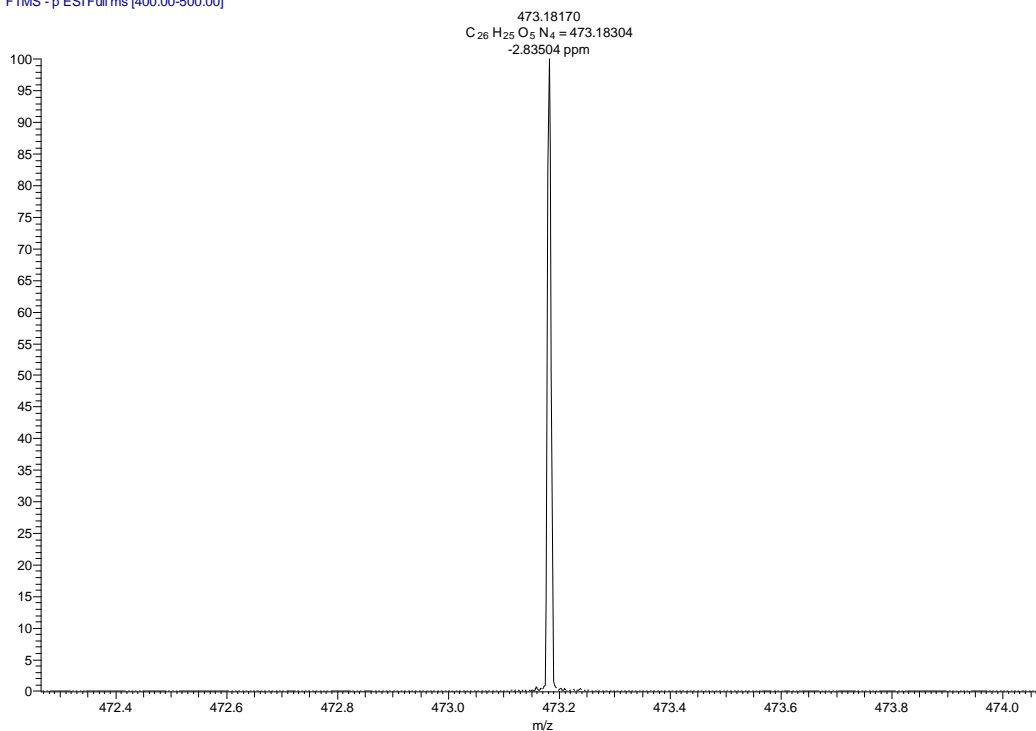
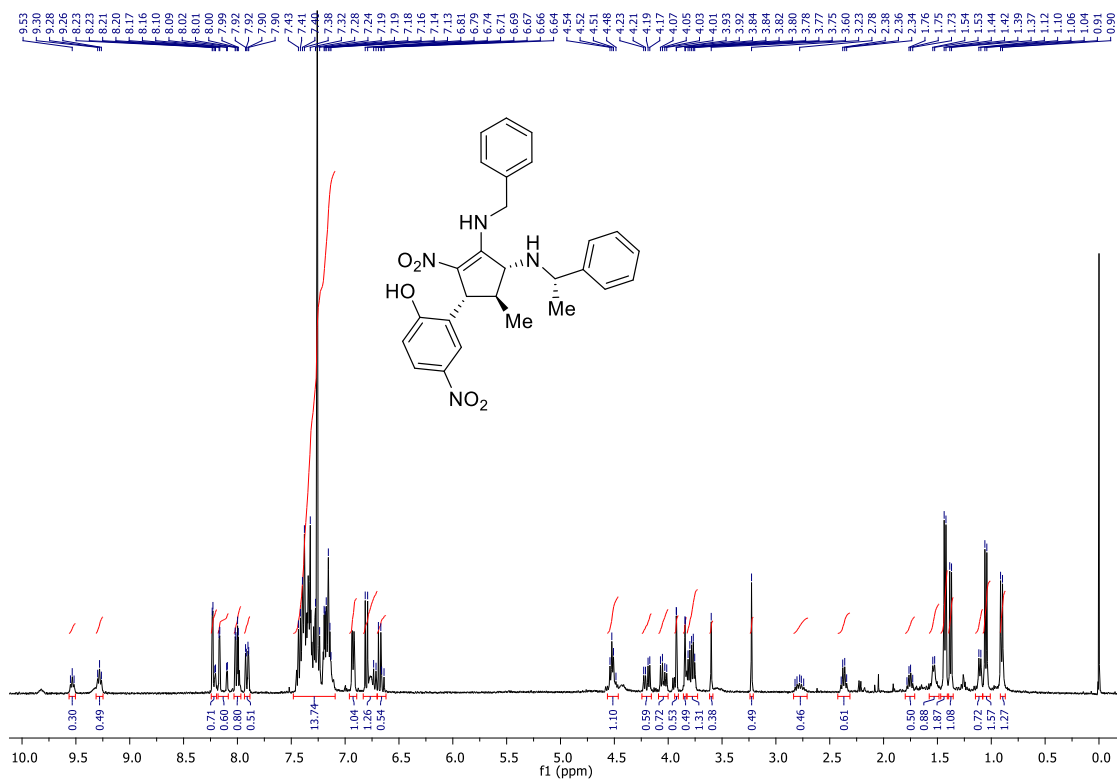FIGURE 242: HRMS (ESI-FT-ICR) m/z spectra of compound **162**.

FIGURE 243: 400 MHz ^{1}H NMR spectra in CDCl$_3$ of compound **163**.

FIGURE 244: 100 MHz ^{13}C NMR spectra in CDCl$_3$ of compound **163**.

FIGURE 245: 400 MHz ^{1}H NMR spectra in CDCl$_3$ of compound **164**.

FIGURE 246: 100 MHz ^{13}C NMR spectra in CDCl$_3$ of compound **164**.

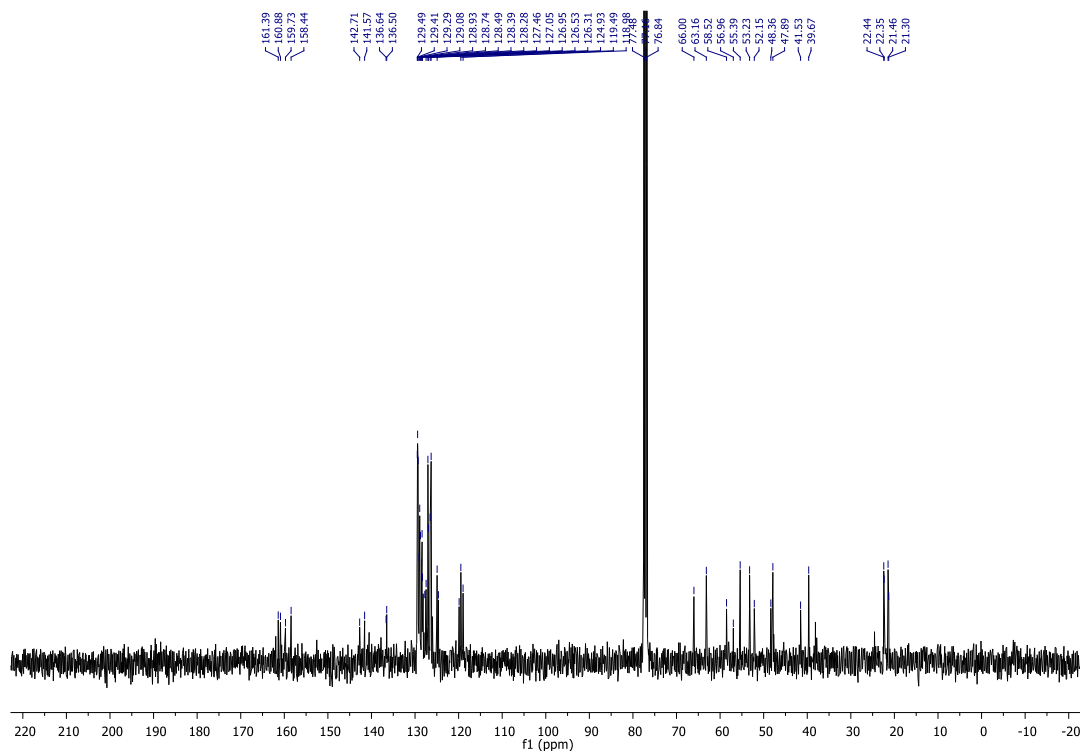FIGURE 247: 400 MHz ^{1}H NMR spectra in CDCl$_3$ of compound **165**.

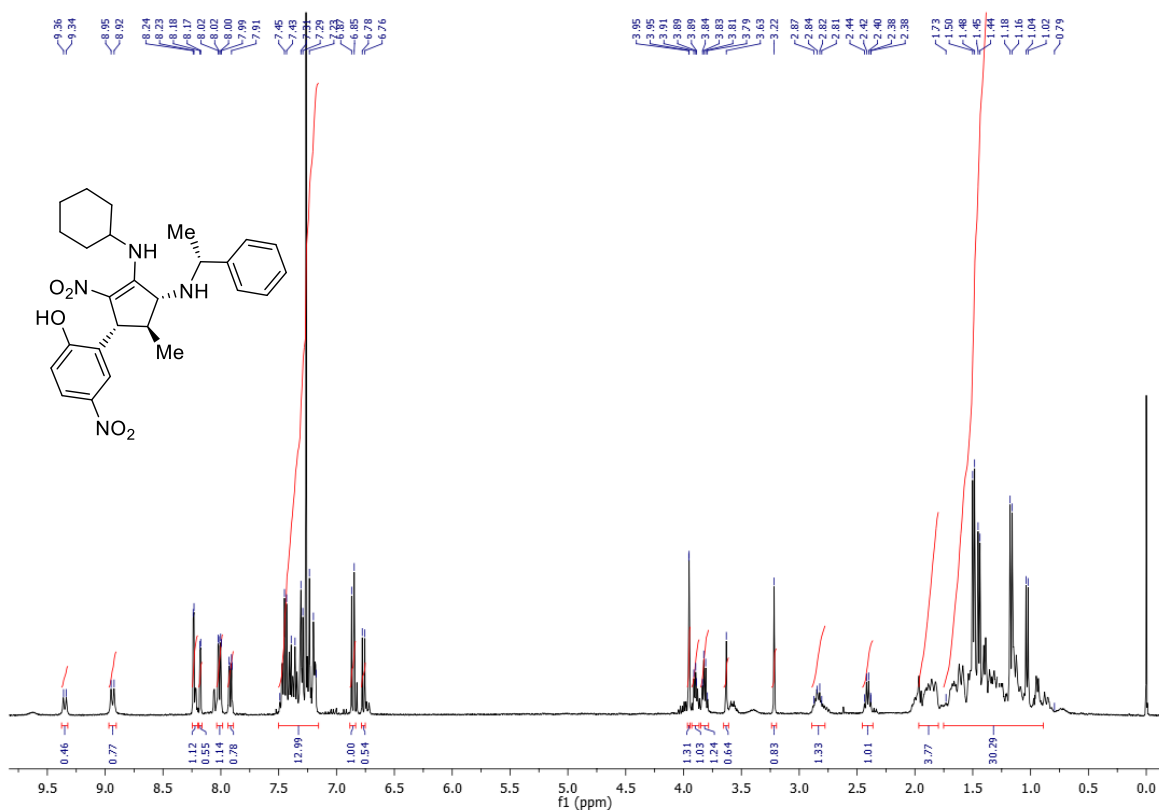FIGURE 248: 100 MHz ^{13}C NMR spectra in CDCl$_3$ of compound **166**.

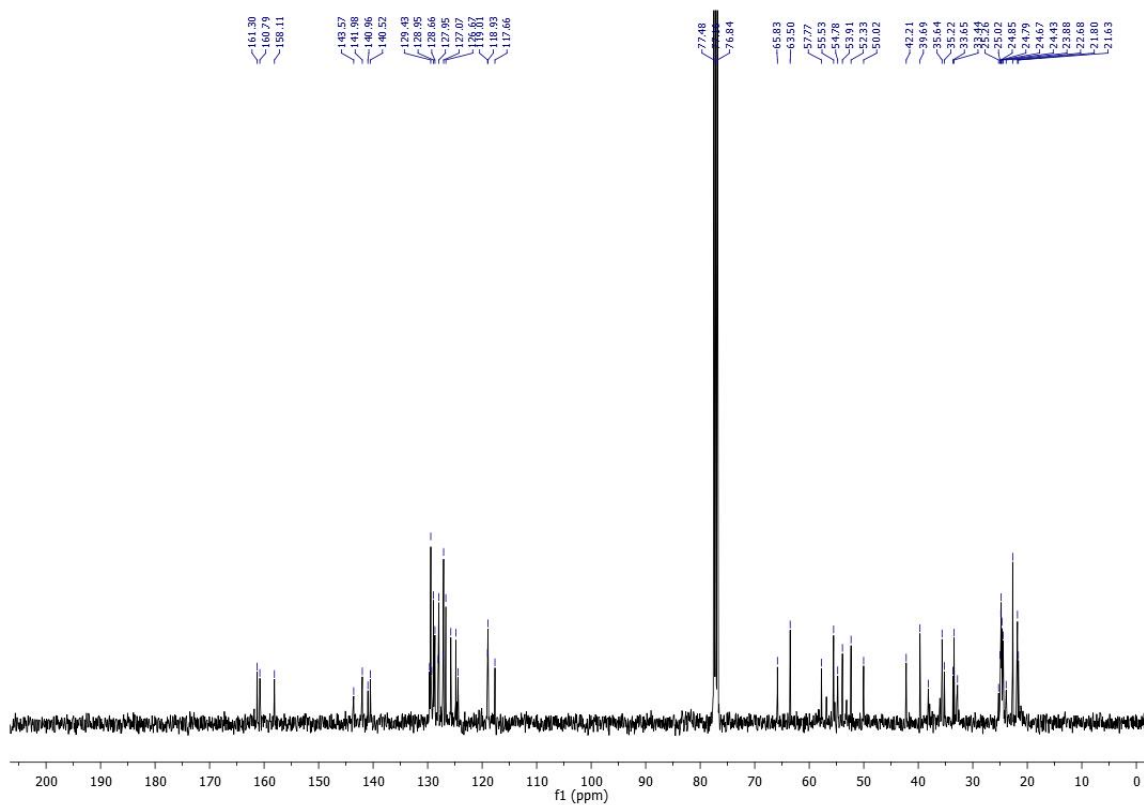FIGURE 249: 400 MHz ^{1}H NMR spectra in CDCl$_3$ of compound **166**.

FIGURE 250: 100 MHz ^{13}C NMR spectra in CDCl$_3$ of compound **166**.